Mechanisms of Rod Photoreceptor Motility in Development and Following Transplantation

Nozie Dominic Aghaizu

UCL INSTITUTE OF OPHTHALMOLOGY

Department of Molecular and Cell Therapy

2016

A thesis submitted to University College London for the degree of Doctor of Philosophy (PhD)

DECLARATION

I, Nozie Dominic Aghaizu, confirm that the work presented in this thesis is my own. Where information has been derived from other sources, I confirm that this has been indicated in the thesis.

Habe nun, ach! Philosophie,
Juristerei und Medizin
Und leider auch Theologie
Durchaus studiert, mit heißem Bemühn.
Da steh ich nun, ich armer Tor!
Und bin so klug als wie zuvor;

– Johann Wolfgang von Goethe, “Faust”

ABSTRACT

To establish the mature neuroepithelial tissue architecture, newborn neurons often migrate from their place of birth, usually at the apical neuroepithelial limit, towards their target destination. Even before neurons are born, the nucleus of the mitotic neuronal progenitor cell migrates within the apico-basal cellular extent in synchrony with the cell cycle (interkinetic nuclear migration or IKNM) – a migratory pattern so far only observed in mitotic epithelial progenitor cells.

Rod photoreceptors, too, are born at the apical limit of the retinal neuroepithelium. They then populate a layer directly adjacent (outer nuclear layer or ONL), but not the more basal retinal layers. How rod photoreceptors become enriched specifically within the ONL is presently ill defined.

Here, it was identified that rod photoreceptor somata of the developing mouse retina are constantly pushed basally (presumably caused by proximal progenitor IKNM events). To become enriched apically within the (presumptive) ONL despite this, the post-mitotic rod photoreceptors utilised an IKNM-like migratory behaviour more typically associated with dividing cells: rod somata actively migrated apically, driven by microtubule-associated dynein I motors. Another microtubule-associated motor protein, KIF1A, acts as a molecular brake during basal displacement, preventing ectopic basal positions. Rod somata oscillate between apical and basal motions at least from P1 up until ~P10. Whether this involves a component of glial-guided migration could not be established beyond reasonable doubt. Nonetheless, this is the first report of an oscillatory, IKNM-like migration behaviour occurring within a post-mitotic neuronal cell population.

Rod photoreceptors have also been assumed to migrate into the adult neural retina following sub-retinal transplantation for cell-replacement therapeutic purposes, although this has not been directly observed. Here, time-lapse footage for the first time showed rod photoreceptors migrating from the sub-retinal space into the host retina. This supports the notion that photoreceptor cell replacement therapy could become a clinically viable treatment option.

ACKNOWLEDGEMENTS

I would like to thank my supervisors Professor Rachael Pearson and Professor Robin Ali for awarding me the opportunity to work on this challenging, yet interesting, project and for creating a highly stimulating research milieu. I am especially grateful to Professor Rachael Pearson for her continuous academic support, the insightful research feedback and guidance throughout my PhD.

My sincerest gratitude also goes to Dr. Katherine Warre-Cornish, who's excellent PhD project set the groundwork for my own project. Helping me reach my full research potential, I must also include special mentions for Dr. Christopher Thrasivoulou, Daniel Ciantar and Tim Robson for their assistance during microscopy image acquisition, Professor Matteo Carandini, Martha Robinson and Paul Waldron for their programming and data analysis expertise, Dr. Alexander Smith and Dr. Anastasios Georgiadis for molecular biology related advice, as well as Professor Rachael Pearson, Yanai Duran, Dr. Ayad Eddaoudi and Robert Sampson for their support during experiments.

I would also like to thank all other colleagues and friends I have made throughout my PhD, both within and outside of this group, who have made the past years a truly unforgettable experience.

I dedicate this thesis to my family, especially my parents, Dominic Nwabugwu and Maria Azucena, who have gone above and beyond themselves to provide me and my sister, Grazia Chidi, with the best opportunities.

TABLE OF CONTENTS

LIST OF FIGURES

CHAPTER V. DEVELOPMENTAL ROD PHOTORECEPTOR MOTILITY AND GLIAL GUIDANCE

CHAPTER VI. THE MIGRATION AND INTEGRATION OF TRANSPLANTED ROD PHOTORECEPTORS INTO THE RECIPIENT RETINA

LIST OF TABLES

Table 2.1.11. Gene specific primer pair and hydrolysis probe (Universal ProbeLibrary, Roche, Swi**t**zerland) combinations used for qPCR relative quantification assays.

Table 2.6.1. List of primary antibodies used in this study.

Table 2.6.2. List of secondary antibodies used in this study.

LIST OF MOVIES

CHAPTER III. ROD PHOTORECEPTOR SOMATA ARE MOTILE DURING DEVELOPMENT

Movie 3.3.1. 3D representation of the rod somal motility detection methodology.

Movie 3.3.2. Time-lapse recording of rod photoreceptor somal motility in the P1 *Nrl.GFP*$^{+/+}$ retina.

Movie 3.3.3. Rod photoreceptors can oscillate between more apical and more basal radial positions (shown here: P1 *Nrl.GFP*$^{+/+}$ retina).

CHAPTER V. DEVELOPMENTAL ROD PHOTORECEPTOR MOTILITY AND GLIAL GUIDANCE

Movie 5.3.1. Rod photoreceptor IKNM-like somal translocation in close proximity to an NRSC in the P3 *Nrl.GFP*$^{+/+}$ retina.

Movie 5.3.2. Rod photoreceptors migrate radially in close proximity to an NRSC in a columnar unit-like arrangement in the P7 *Nrl.GFP*$^{+/+}$ retina.

CHAPTER VI. DEVELOPMENTAL ROD PHOTORECEPTOR MOTILITY AND GLIAL GUIDANCE

Movie 6.3.1. Transplanted rod photoreceptor precursor cells migrate from the IPM into the ONL.

LIST OF COMMON ABBREVIATIONS

AAV	Adeno-associated virus
ATP	Adenosine triphosphate
AvMSD	Average man squared displacement
BDNF	Brain derived neurotrophic factor
bHLH	basic Helix-loop-helix
CC	Connecting cilium
cDNA	complementary Deoxyribonucleic acid
cGMP	cyclic Guanosine monophosphate
CNS	Central nervous system
CRX	Cone-rod homeobox protein
DIV	Days *in vitro*
DMSO	Dimethyl sulfoxide
DNA	Deoxyribonucleic acid
ECM	Extracellular matrix
FACS	Fluorescence-activated cell sorting
GCL	Ganglion cell layer
GDP	Guanosine diphosphate
GFAP	Glial fibrillary acidic protein
GFP	Green fluorescent protein
GOF	Gain-of-function
GS	Glutamine synthetase
GTP	Guanosine triphosphate
IF	Intermediate filament
IKNM	Interkinetic nuclear migration
ILM	Inner limiting membrane
INL	Inner nuclear layer
IPL	Inner plexiform layer
IPM	Interphotoreceptor matrix
iPSC	induced Pluripotent stem cell
IS	Inner segment
KIF	Kinesin family member

LIS1	Lissencephaly 1
LOF	Loss-of-function
mRNA	messenger Ribonucleic acid
MSD	Mean squared displacement
MTOC	Microtubule organising centre
NBL	Neuroblastic layer
NMII	Non-muscle myosin II
NMMHC-IIB	Non-muscle myosin heavy chain IIB
NRL	Neural retina leucine zipper
NRSC	Neural retina spanning cell
n.s.	non-significant
NSC	Neuroepithelial stem cells
OLM	Outer limiting membrane
ONL	Outer nuclear layer
OPL	Outer plexiform layer
OS	Outer segment
PCR	Polymerase chain reaction
qPCR	Quantitative polymerase chain reaction
RGC	Retinal ganglion cell
RLBP	Retinaldehyde binding protein
RNA	Ribonucleic acid
RNAi	Ribonucleic acid interference
ROI	Region of interest
RPC	Retinal progenitor cell
RPE	Retinal pigment epithelium
SRS	Sub-retinal space
TK	Thymidine kinase
XFP	(X = colour) fluorescent protein

CHAPTER I. INTRODUCTION

The focus of this thesis was to provide a detailed characterisation of rod photoreceptor neuronal migration to the correct final location within the retina, which is an important aspect of establishing the retinal architecture required for image-forming vision. While this is important during normal retinogenesis, targeted migration likely re-emerges in the artificial scenario of rod photoreceptor cell replacement therapy to replace those cells that were previously lost due to injury or disease. The following introduction will thus provide information on the general structure, function and development of the retina, and rod photoreceptors in particular, as well as accessory cells perhaps involved in the migration process. Subsequently the presently known modes of neuronal migration will be introduced in detail based on previous characterisations in the retina as well as the brain. Finally, the pre-clinical field of photoreceptor cell replacement therapy will be introduced.

The information provided within this introduction should thus provide the reader with the necessary knowledge required for optimal comprehension of this thesis.

1.1. The mammalian eye

1.1.1. Overview

The processing and computation of sensory visual information is an essential element of how many animals act within and interact with their environment. The eye is a highly specialised sensory organ equipped to detect such visual stimuli coming from the environment and to convert them into electrical signals. Those signals are then partially processed and relayed to higher visual centres of the central nervous system where further visual processing and image formation take place.

The link between the eye and higher visual centres, such as those found in the brains of many vertebrate species, has been postulated long before the advent of modern science. Even though initial descriptions of the eye-brain connection were slightly more esoteric (Cicero, 46BC), it has become clear that the eye, and more specifically the retina, is in fact an extension of the central nervous system (CNS) and hence the brain (see London *et al.*, 2012). This connection is not only anatomic in nature; it is also rooted deeply within embryonic development as eye specifications begin to extend and protrude away from a substructure of the CNS called diencephalon.

The eye is relative easy to access, as opposed to most other areas of the CNS. This has made the eye an interesting organ to study matters of CNS development, injury and disease. This also means that surgical intervention is a feasible option in scenarios where injury and disease have caused damage.

1.1.2. Structure and function of the eye

From outside to inside, the mammalian eye features three distinct layers (Figure 1.1.1): sclera and cornea form the outermost or external layer. The intermediate layer is made up of the iris, ciliary body and the choroid. Lastly, the retina, the light sensing tissue within the eye, forms the internal layer. Furthermore, there are three separate chambers of fluid within the mammalian eye: the anterior chamber is located between the cornea and iris,

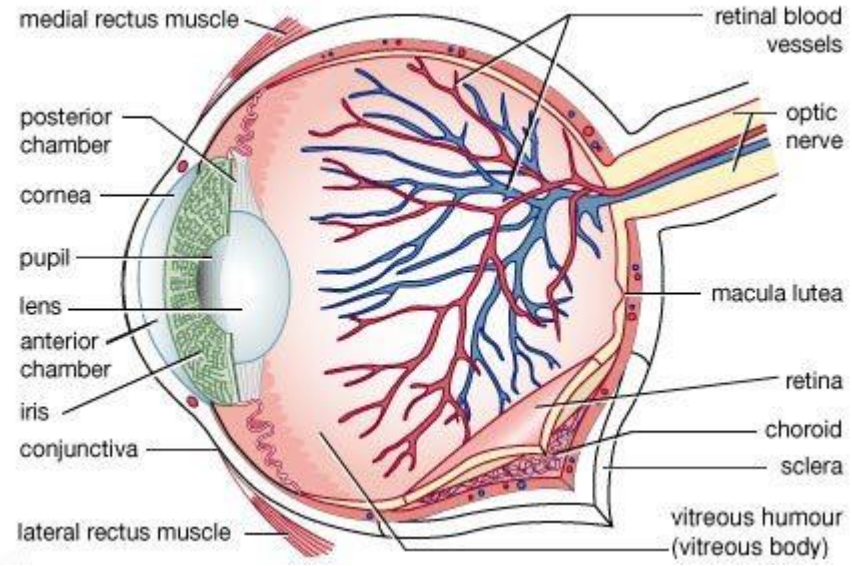

Figure 1.1.1 Schematic representation showing the structure of the eye. With permission from http://www.britannica.com/science/blind-spot.

the posterior chamber is found between iris, zonule fibres and lens, and the vitreous chamber is located between lens and retina. Incoming photons travel through the cornea, anterior chamber, lens and vitreous chamber before reaching the neural retina, which is capable of detecting them.

The external layer consists of sclera and cornea. The cornea is the first element of the eye to face incoming photons and accounts for the majority of the eye's total optical power. Its structural composition is fine tuned for this role. Collagen, one of the key components of the cornea, is shaped, arranged and spaced in such a manner to appear optically translucent and to focus incoming photons onto the lens.

The intermediate layer, consisting of iris, ciliary body and choroid, lines the inside of the external layer from the pupil back to the optic nerve. The choroid is invested with a network of blood vessels and capillaries to supply the metabolically highly active outer layers of the retina with nutrients.

The retina forms the internal layer and is in itself comprised of two sub-layers: the neural retina, which is responsible for photon detection and electrical impulse generation to be relayed into higher visual centres of the CNS, and the retinal pigment epithelium (RPE), which engages in numerous support roles to the adjacent neural retina.

1.1.3. Structure of the retina

The retina can be subdivided into a neural compartment (neural retina) and a non-neuronal compartment (the retinal pigment epithelium or RPE, which engages in numerous support roles towards the neural retina) (Figure 1.1.2A). The neural retina is comprised of a further three distinct cellular layers, which are populated by an array of seven neuronal cell types (rod photoreceptors, cone photoreceptors, bipolar cells, horizontal cells, bipolar cells, amacrine cells and retinal ganglion cells) as well as a single main glial cell type (Müller glia). During development, multipotent retinal progenitor cells (RPCs) give rise to all of these cell types (Turner and Cepko, 1987). In the mature retina, rod and cone photoreceptor somata are located within the cellular layer closest to the RPE, called outer nuclear layer (ONL), which contains around 10 rows of photoreceptor cell bodies along the apico-basal axis of the mouse retina. This side of the neural retina is also referred to as the apical side. The inner nuclear layer (INL) is adjacent to the ONL and is populated

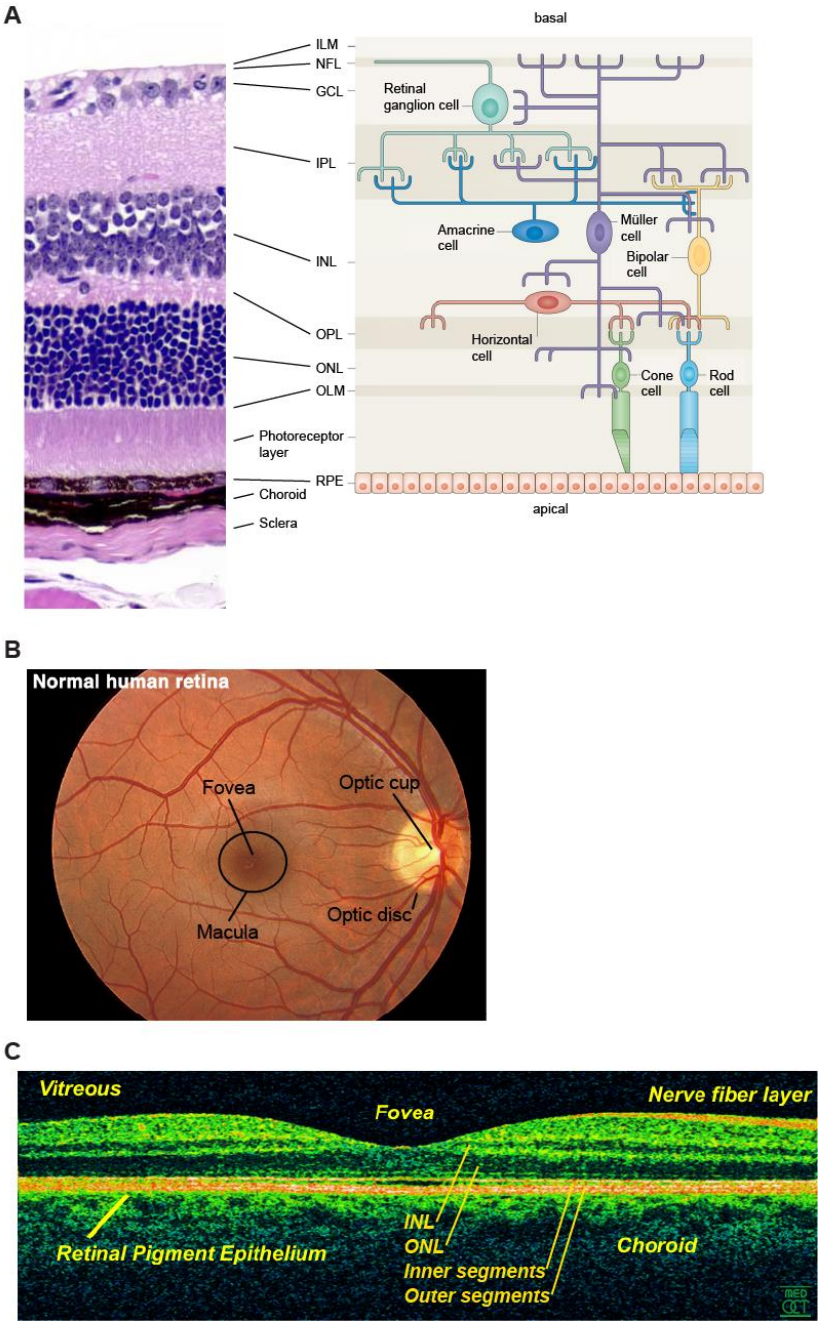

Figure 1.1.2 Structure of the mammalian retina. **(A)** Depicted are a histology cross-section of a retina and external layers and a schematic highlighting the distribution of the different retinal cell types across the neural retina, as well as their synaptic connections. GCL – ganglion cell layer, ILM – inner limiting membrane, INL – inner nuclear layer, IPL – inner plexiform layer, OLM – outer limiting membrane, ONL – outer nuclear layer, OPL – outer plexiform layer, RPE – retinal pigment epithelium (adapted with permission from Goldman, 2014). **(B)** Fundus photograph of the human retina (adapted with permission from http://webvision.med.utah.edu/). **(C)** Optical coherence tomography image of a human retina with the fovea depicted in the centre (adapted with permission from https://commons.wikimedia.org/wiki/File:Retina-OCT800.png).

by the cell bodies of the retinal interneurons (bipolar, amacrine and horizontal cells). Retinal ganglion cell (RGC) somata line up in a single row to form the ganglion cell layer (GCL) located at the basal edge of the neural retina. In-between these three cellular layers are two distinct neuropil layers: firstly, the outer plexiform layer (OPL) where synapses between photoreceptor axons and bipolar as well as horizontal cell dendrites are formed, and secondly, the inner plexiform layer (IPL) containing the synapses between the pre- and post-synaptic termini of bipolar and amacrine cells and RGC dendrites. Perhaps slightly counter-intuitively, the structure of the neural retina is inverted with respect to the influx path of photons into the eye. This means that photons first need to traverse the entire radial extent of the neural retina before reaching the photoreceptor outer segments to initiate the phototransduction cascade, which converts the energy carried by photons into an electrical stimulus. This stimulus is passed on by synaptic transmission first to the secondary interneurons of the INL and then to the RGCs in the GCL, the axons of which fasciculate to form the optic nerve, along which the visual information is relayed to higher visual centres of the CNS.

Müller glia somata are found within the INL much like the cell bodies of the interneurons. However, Müller glia have the unique feature of spanning the entire apico-basal extent of the neural retina by extending radial processes all the way towards the apical and basal edges of the tissue. At their basal-most extent, the end feet of Müller glia form a laterally contacting network in conjunction with basement membrane constituents, which is collectively known as the inner limiting membrane (ILM). At their apical most extent, Müller glia end feet engage in a network of adherens junctions formed by Müller glia and photoreceptors, which is called the outer limiting membrane (OLM). All cellular and neuropil layers of the neural retina are heavily invested by Müller glia processes, which form contacts with neuronal somata, synapses and inner retinal blood vessels. As will be discussed below, this is very important for proper retinal function.

The introduced retinal cells are not evenly distributed across the retina and regional specifications exist. For instance, the axons of all RGCs within the neural retina fasciculate in one single location called the optic disc (Figure 1.1.1 & 1.1.2B). At the optic disc, the bundle of axons (the optic nerve) starts projecting out from the eye ball and towards higher visual centres of the CNS. The optic disc is devoid of any neurons, including photoreceptors, thus forming an anatomical blind spot. In most areas of the mammalian retina, such as the periphery, rod photoreceptors by far outnumber cone photoreceptors within the ONL by a ratio of ~20:1. In humans, the macula, a central

retinal sub-domain, is responsible for providing high acuity central vision (Curcio *et al.*, 1985; Ahnelt, 1998). This is made possible by a sub-structure within the macula, called the fovea (Figure 1.1.2C). Here, cone photoreceptors, which provide high acuity vision, dominate in number over rod photoreceptors.

1.1.4. Photoreceptors

Photoreceptors are the principal photon sensing cells of the retina involved in image forming vision. There are two main photoreceptor cell types in the mammalian eye, called rod and cone photoreceptors, which contribute to vision under dim (scotopic) or bright (photopic) light conditions respectively. Their somata are located in the ONL, where rod photoreceptors are located throughout the entire radial width of the ONL; in most regions of the neural retina on the other hand, cone cell bodies line up in one single row situated at the apical-most part of the ONL adjacent to the OLM.

Photoreceptors are a sub-class of neurons with a highly specialised cell morphology that allows them to convert photons into a chemical and, subsequently, into an electrical signal. The etymology behind the names given to rod and cone photoreceptors is routed within the distinctive rod- or cone-like shapes of their so-called outer segments located in the photoreceptor layer (Figure 1.1.2A). The outer segment plasma membrane enwraps assembly of stacked disc-like structures consisting of folded lipid bilayer (Kennedy and Malicki, 2009; Figure 1.1.3B)). These contain a vast amount of visual pigment molecules, which are composed of an opsin protein, a member of the 7TM receptor family (Unger *et al.*, 1997; Palczewski, 2006), and the chromophore retinal, the principal light sensitive molecule in the visual process (Wald, 1935). Rod photoreceptors contain the visual pigment molecule rhodopsin and they show greatest light spectral sensitivity at a wavelength of 496 nm. In humans, there are three different types of cone photoreceptors that express one of three different types of cone opsins rather than rhodopsin. Differences in the opsin protein primary, and hence secondary and tertiary structure confer the different spectral sensitivities. The cone photoreceptor specific L-, M- and S-opsins show greatest sensitivities at 560, 530 and 430 nm respectively (yellow, green and purple visible light) thus contributing to colour vision (Solomon and Lennie, 2007).

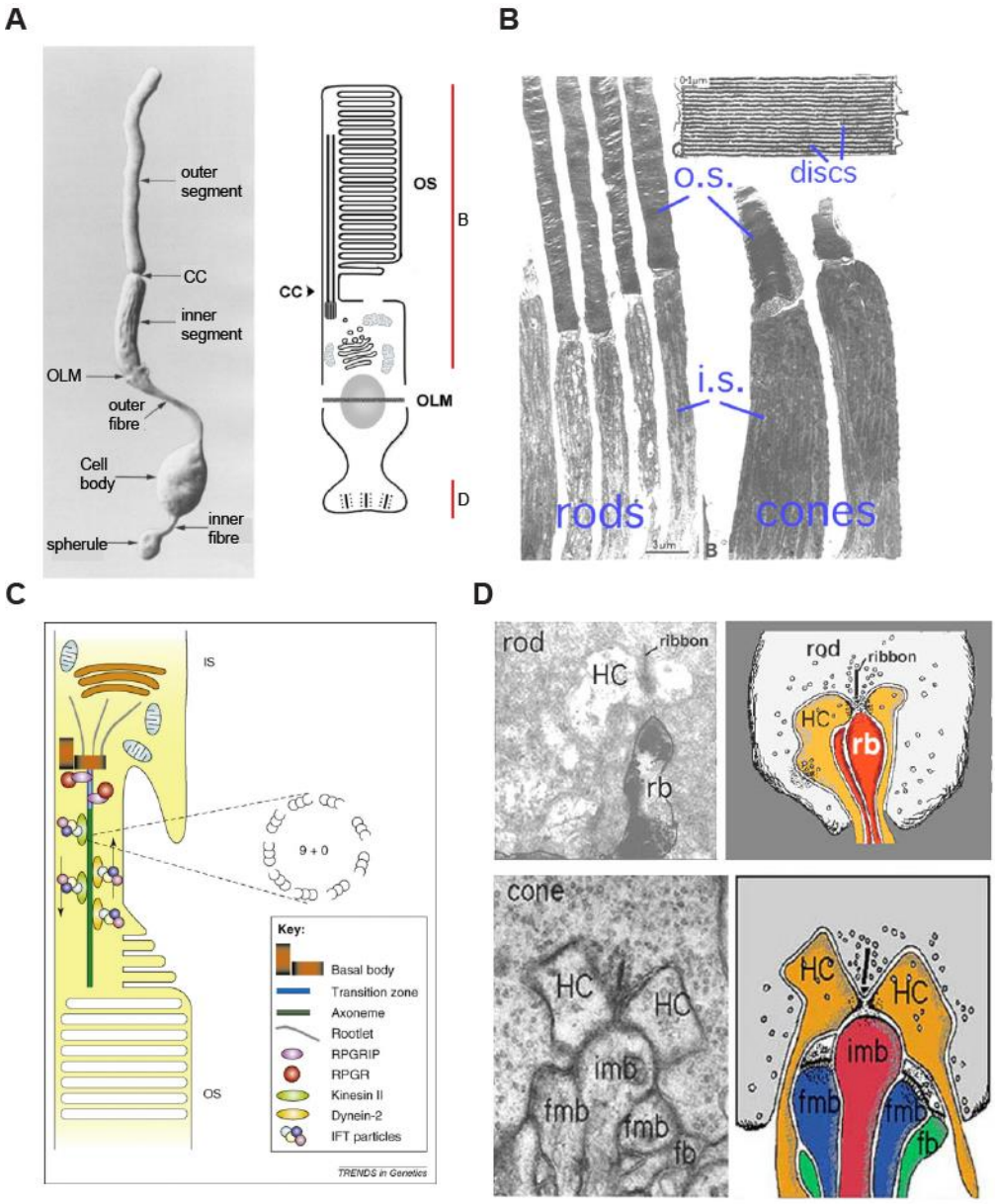

Figure 1.1.3 Photoreceptor structure and morphology. **(A)** Overview of photoreceptor morphology based on an isolated adult rabbit rod photoreceptor cell and adjacent schematic. The location of the structures shown in panels B and D are indicated in the schematic. CC = connecting cilium, OLM = outer limiting membrane, OS = outer segment (reproduced with permission from Townes-Anderson *et al.*, 1988; Kennedy and Malicki, 2009) **(B)** Electron micrograph of monkey rod and cone photoreceptor inner and outer segment structure. i.s. = inner segment, o.s. = outer segment (reproduced with permission from http://webvision.med.utah.edu/) **(C)** Schematic illustration of the connecting cilium between inner and outer segment (reproduced with permission from Smith *et al.*, 2009). **(D)** Electron micrograph of rod and cone ribbon synapses with the post-synaptic dendritic partners: HC (horizontal cell), fmb (flat midget bipolar), imb (invaginating midget bipolar), fb (flat bipolar), rb (rod bipolar) (reproduced with permission from http://webvision.med.utah.edu/).

The connecting cilium bridges the photoreceptor outer segment with the inner segment (Figure 1.1.3C). Inside the cilium is a microtubular structure called the axoneme, which is important for anterograde and retrograde cargo trafficking between inner and outer segment as well as for the membrane folding contributing to outer segment formation. The photoreceptor inner segment is located between the base of the connecting cilium and the OLM. It contains abundant mitochondria, ER and Golgi apparatus structures, which ensure that the high energy, protein, and membrane turnover demand of the outer segments are met.

Each photoreceptor soma extends one basally directed axon, which together with its pre-synaptic axon terminal is responsible for passing on photon-induced electrical stimuli to bipolar cells. Rod and cone photoreceptor axon termini are morphologically different and are referred to as spherules and pedicles respectively. In addition to bipolar cells, photoreceptors also synapse with horizontal cells within the OPL in what is known as a synaptic triad between these three cells. Photoreceptor axon termini contain a characteristic electron-dense pre-synaptic density, called ribbon, which is an important organiser of the pre-synaptic neurotransmitter release machinery (the synapse is thus also called ribbon synapse). The rod spherule typically contains one such ribbon structure, whereas cone pedicles are markedly bigger, containing approximately 30 ribbon structures. (Figure 1.1.3D).

1.1.5. Function of photoreceptors

Photoreceptors are the principal photon detecting cells in the vertebrate retina essential for image forming vision. Rod photoreceptors are remarkably sensitive, being able to detect even one single photon (Hecht *et al.*, 1942; Baylor *et al.*, 1979). They are thus well equipped for scotopic vision (or vision under dim light conditions). Cone photoreceptors on the other hand are less sensitive by comparison and are used for photopic vision (or vision under bright light conditions). They do, however, offer higher temporal resolution as well as colour vision. Photoreceptors are unusual, compared to other neuronal cells, in that they are depolarised in their resting state when no photons are detected (Hagins *et al.*, 1970). This is due to an inward current carried by Na^+ and Ca^{2+} ions (Hodgkin *et al.*, 1985) and driven by the electrochemical gradient of these ions through cyclic nucleotide-

gated (CNG) cationic channels present on the outer segment plasma membrane (Yau, 1994) (Figure 1.1.4A). These channels are gated and kept in an open state in presence of cGMP (Fesenko *et al.*, 1985). At the inner segment membrane, K^+ permeable ion channels allow the efflux of K^+ ions. This circulating current between outer and inner segments is known as the dark current, which keeps photoreceptors at a membrane potential of -40 mV. In this depolarised state, action potentials are generated (Fain *et al.*, 1980; Kawai *et al.*, 2001), leading to the synaptic release of the neurotransmitter glutamate (reviewed by Heidelberger *et al.*, 2006). In order to maintain an overall ionic balance, rod photoreceptors utilise the Na^+/K^+ ATPase at the inner segment membrane to pump Na^+ out and K^+ into the cell as well as the Na^+/Ca^{2+}-K^+ exchanger (NCKX) at the outer segment membrane to remove Ca^{2+} and K^+ in exchange for the import of Na^+.

The phototransduction process has been well characterised in rod photoreceptors but has been found to function in an analogous manner in cone photoreceptors, albeit with some cone specific protein isoforms with different characteristics and kinetics (Kawamura and Tachibanaki, 2008). The chromophore retinal is covalently linked to a 7TM opsin protein (rhodopsin in rod photoreceptors and L-, M- or S-opsin in cone photoreceptors). Together they form the photo pigment, which is a photoinstable molecule that can be isomerised from an 11-cis configuration into an all- trans configuration (Figure 1.1.4B). This process is powered by the absorption of energy carried by an incoming photon according to

$$E = h \times \nu$$

where h is the Planck's constant and ν is the frequency of the photon. The fact that the different opsin proteins that bind retinal have different amino acid sequences, is responsible for shifting the spectral absorption maxima of the individual photo pigments, thus leading to different spectral sensitivities. The structural change associated with the photo-isomerisation of retinal is accompanied by a series of accommodating conformational changes in the opsin protein (Zhou et al., 2012) (Figure 1.1.4B). For rhodopsin, distinct intermediate species called bathorhodopsin, lumirhodopsin, metarhodopsin I are generated first ahead of metarhodopsin II, the active state of rhodopsin (R*), which in turn decays to the inactive metarhodopsin III (Wald et al., 1950). A schematic of the phototransduction cascade is provided in Figure 1.1.4C: Activated rhodopsin causes a conformational change in the heterotrimeric G-protein transducin (Figure 1.1.4C). This causes the α subunit to exchange its bound GDP for GTP (Gα-GTP)

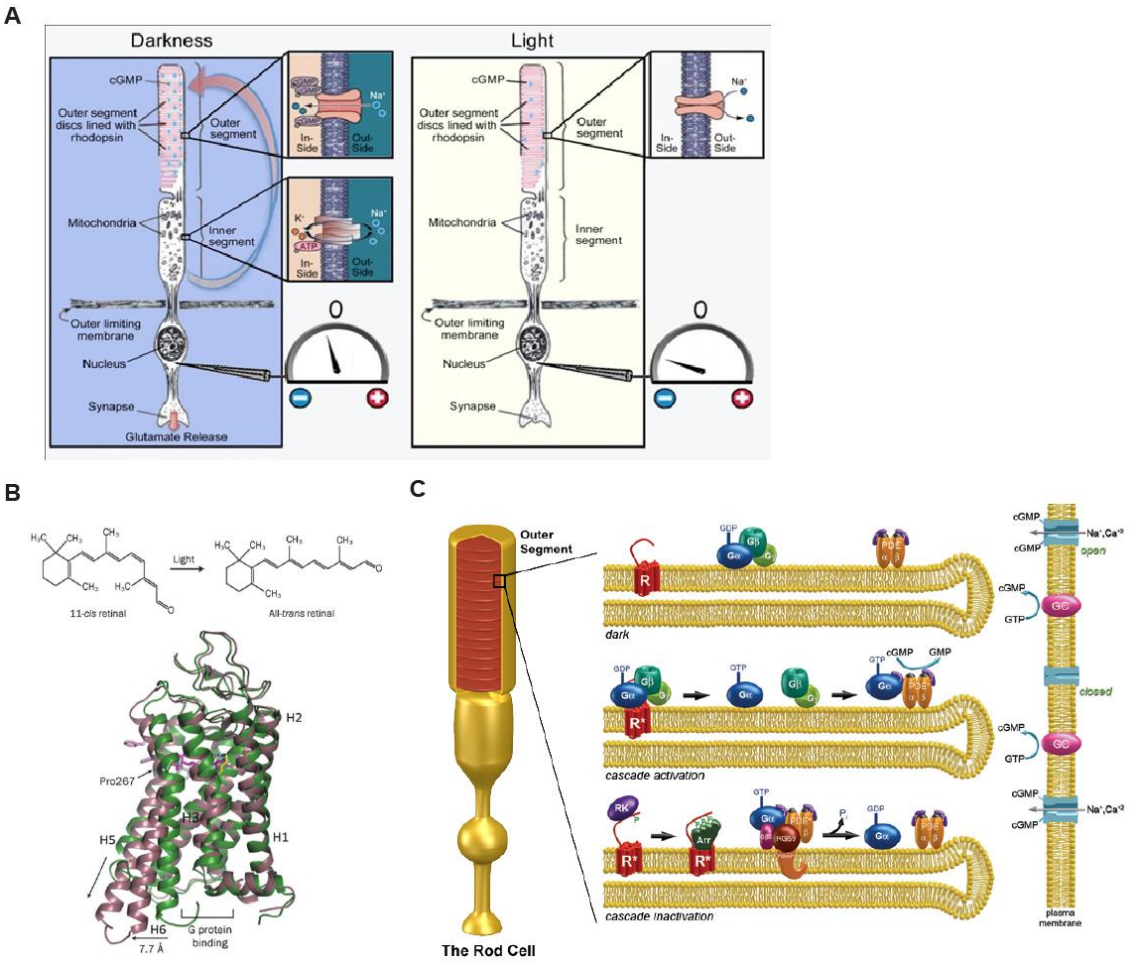

Figure 1.1.4 Photoactivation and phototransduction in photoreceptors. **(A)** Channel current fluxes in photoreceptors in the dark and in the light. Under dark conditions, a circulating (dark) current carried by Na^+ and Ca^{2+} influx at the outer segments and K^+ efflux at the inner segment results in a depolarised membrane potential of -40 mV and neurotransmitter release. Photon detection prevents ion influx at the outer segment, resulting in photoreceptor hyperpolarisation (-70 mV) and cessation of neurotransmitter release. Reproduced with permission from Ramsey and Arden (2015) . **(B)** Structural and conformational changes associated with photon detection in retinal and rhodopsin respectively. X-ray crystallography data depict rhodopsin conformation in ground state (green) and activated state (purple) (adapted with permission from Zhou *et al.*, 2012). **(C)** Phototransduction cascade. Light detection activates rhodopsin (R*) to create the transducin (Gαβγ) binding site, which results in the activation of the Gα subunit (Gα-GDP → Gα-GTP). Gα-GTP releases the catalytic activity of PDE to hydrolyse cGMP to GMP. The reduction in cytoplasmic cGMP results in the closure of cGMP gated CNG cation channels. The cascade is switched off by the inactivation of R* by rhodopsin kinase (RK) and rod arrestin (Arr), the GAP activity of RGS9 resulting in the conversion of Gα-GTP to the inactive Gα-GDP, cessation of cGMP hydrolysis, as well as the restoration of dark cGMP levels by guanylyl cyclase (GC) (reproduced with permission from Arshavsky and Burns, 2012).

and to dissociate from the transducin leaving behind a βγ dimer (Kwok-Keung Fung and Stryer, 1980). Two Gα-GTP molecules are required to activate the phosphodiesterase PDE, which catalyses the hydrolysis of cGMP to GMP (Baehr *et al.*, 1979; Deterre *et al.*, 1988; Heck and Hofmann, 1993; Calvert *et al.*, 2000). The reduction in cGMP levels leads to the closure of cyclic nucleotide-gated cationic channels and cessation of the inward dark current (Fesenko *et al.*, 1985). Consequently, glutamate neurotransmitter release from photoreceptors is reduced. Thus, photoreceptors form an exception to the neuronal action potential paradigm. Neuronal activity stimulates neurotransmitter release in most neurons, whereas transmitter release is attenuated following photoreceptor activation.

Phototransduction is a highly efficient process owing to two different factors: Firstly, the activation of photo pigment occurs at a high quantum efficiency due to the extremely high density of photo pigment molecules spread across a large number of outer segment discs, which in combination act as a proficient photon trap. Secondly, the phototransduction signal is subject to catalytic amplification. The first amplification step occurs at the level of the photo pigment as rhodopsin can activate transducin at a rate of 240 s^{-1} (Krispel *et al.*, 2006). The second amplification step is at the level of the highly catalytic PDE, operating at a rate of 4400 s^{-1} in rod photoreceptors (Baehr *et al.*, 1979; Leskov *et al.*, 2000).

In order to ensure that photoreceptors can respond to subsequent incoming photons, each of the key activated species of the phototransduction cascade needs to be inactivated after light cessation (Kawamura and Tachibanaki, 2008). The activity of R* is quenched initially by phosphorylation by rhodopsin kinase (Chen *et al.*, 1999) and subsequently by becoming bound by arrestin (Xu *et al.*, 1997). Activated transducin α subunit Gα-GTP is inactivated by GTP hydrolysis by its own intrinsic GTPase activity, which is additionally modulated by the GTPase activating protein RGS9 (He *et al.*, 1998). The inactivation of the transducin α subunit in turn leads to the deactivation of PDE and cessation of cGMP hydrolysis. The cGMP levels required to keep the CNG cationic channels open are restored by the guanylyl cyclases GC-1 and GC-2 (Liu *et al.*, 1994; Cooper *et al.*, 1995; Lowe *et al.*, 1995). Finally, the isomerised all-*trans* retinal needs to be re-isomerised to 11-*cis* retinal for a subsequent round of phototransduction (visual cycle of retinal). Rod and cone photoreceptors partially outsource this process to the RPE (rod and cone cells) and Müller glia (cone cells) (Das *et al.*, 1992; Muniz *et al.*, 2007; Wang and Kefalov, 2012). Following the release of all-*trans* retinal from opsin, the chromophore is converted

back into 11-*cis* retinal in a multi-step process taking place in RPE and/or Müller glia and re-supplied back to the photoreceptors (Thompson and Gal, 2003).

1.1.6. Müller glia

Several glial cell types exist in the mature mammalian retina: Müller glia, microglia and, in the vascularised mature retina, astrocytes as well. Among these, only the Müller glia are derived from multipotent RPCs like all retinal neurons (Turner and Cepko, 1987). Müller glia are arranged in a regularly spaced mosaic, surrounded by an ensemble of retinal neurons all the way from the apical to the basal most extent of the neural retina in what has been described as a columnar unit of retinal cells (Reichenbach *et al.*, 1993). The nuclei of Müller glia are located within the INL. However, unlike any other retinal cell type, Müller glia span across the entire radial width of the neural retina by extending processes along the apico-basal axis (Figure 1.1.5A & 5B). At the apical and basal most extents of the neural retina, Müller glia processes form slight cytoplasmic enlargements, known as end feet. Apically, these end feet contribute to the formation of the OLM in conjunction with photoreceptors, with which they form adherens and tight junctions (Figure 1.1.5C). Membranes connected via such junctions form a barrier that is highly impermeable to fluids, thus helping to seal the neural retina from its surroundings and maintain an environment within the tissue conducive to proper retinal function. Basally, the end feet contribute to the production of the acellular ILM basal membrane, consisting of sheets of extracellular matrix (Figure 1.1.5A). At the level of the three cellular and two neuropil layers within the neural retina, Müller glia extend many lateral branches and processes to contact and ensheathe all retinal neuron somata, processes and synapses as well as blood vessels (Magalhães and Coimbra, 1972; Reichenbach and Reichelt, 1986; Prada *et al.*, 1989; Reichenbach *et al.*, 1993).

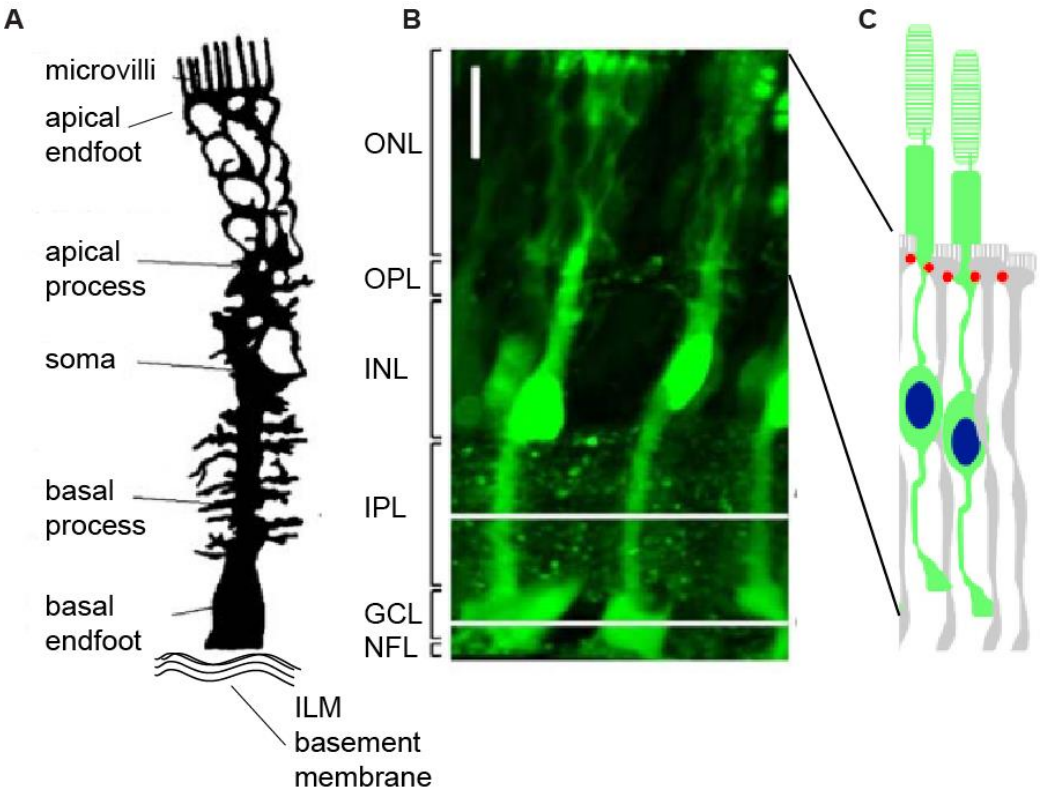

Figure 1.1.5 Morphology of Müller glia. **(A)** Drawing of a Golgi labelled rabbit Müller cell (reproduced with permission from Bringmann *et al.*, 2006). **(B)** Müller glia, selectively labelled with the vital dye Mitotracker Orange, span the entire thickness of the guinea pig neural retina. (reproduced with permission from Uckermann *et al.*, 2004). **(C)** The apical end feet of Müller glia (grey) form adherens and tight junctions (red) with neighbouring end feet and photoreceptor apical processes (green). (reproduced with permission from West et al., 2008)

1.1.7. Functions of Müller glia

Just like astrocytes in the brain and spinal cord, retinal Müller glia have a range of functional responsibilities to ensure the correct function of retina. Müller glia position and structure within the retina are clearly geared towards such activities (see Table 1.1.1 for a list of known Müller glia functions). For instance, they are important for a number of homeostatic and metabolic support roles towards retinal neurons (Bringmann *et al.*, 2006; Reichenbach and Bringmann, 2013). Converting photon stimuli into electrical neuronal impulses is an energetically highly costly process. Neuronal action potential generation requires a large amount of Krebs cycle and electron transport chain activity. To account for this, Müller glia supply glycolytically produced lactate, pyruvate or transaminated alanine to the retinal neurons, which, in return, use it to fuel their Krebs cycle (Poitry-Yamate *et al.*, 1995; Poitry *et al.*, 2000). On top of that Müller glia also contain reservoirs of glycogen and express glycogen phosphorylase, an enzyme required to mobilise those energy reserves in times of very high retinal neuron energy demand (Poitry-yamate and Tsacopoulos, 1991; Poitry-Yamate and Tsacopoulos, 1992; Pfeiffer-Guglielmi *et al.*, 2005).

Müller glia express carbonic anhydrase to buffer CO_2 emerging from the Krebs cycle of retinal neurons (Newman, 1994). At the same time, Müller glia also remove extracellular K^+, a product of neuronal action potential propagation, using Kir2.1 subunit containing K^+ channels to remove local K^+ from the plexiform layers predominantly, and Kir4.1 subunit containing K^+ channels, which are mainly expressed on the basal end feet, to funnel K^+ away to the vitreous body and blood vessels (Newman *et al.*, 1984; Kofuji *et al.*, 2002); this process is also known as K^+ siphoning. Since the highly active electron transport chain produces H_2O as a by-product and additional H_2O influxes also occur due to osmosis via metabolite uptake from the blood as well as due to intraocular pressure, retinal H_2O homeostasis also needs to be tightly regulated (Bringmann *et al.*, 2006). Müller glia express the water channel AQP4; the expression pattern is similar to the combined patterns of Kir2.1 and Kir4.1 containing K^+ channels (Nagelhus *et al.*, 1999; Bringmann *et al.*, 2006). This suggests that K^+ siphoning is at least to some extent coupled to H_2O homeostasis, whereby both K^+ ions and H_2O are taken up by Müller glia and passed on to the vitreous body and blood vessels (Nagelhus *et al.*, 1998, 1999).

Physiological process	Müller cell function	Glia-specific protein/peptide
Metabolic support and nutrition of neurons	• Delivery of lactate/pyruvate/ alanine • Storing of glycogen and glycogenolysis	Lactate dehydrogenase Glycogen phosphorylase
K^+ and H_2O homeostasis	• CO_2 buffering • Removal of external K^+ (K^+ siphoning) • Dehydration of inner retina	Carbonic anhydrase Kir4.1 channel AQP4 H_2O channel
Contribution to neuronal signalling	• Neurotransmitter uptake • Neurotransmitter recycling	GLAST (glutamate) GAT-3 (GABA) Glutamine synthetase
Modulation of neuronal activity by gliotransmitter release	Storage and release of glutamate, GABA, D-serine, ADP/ATP, retinoic acid, NO	
Protection against oxidative stress	Release of free radical scavengers	Glutathione
Neurotrophic support for neurons	Secretion of neurotrophic factors	BDNF, CNTF, bFGF, IGF-1, NGF, neurotrophins-3 and -4, GDNF, LIF, and PEDF
Vascular homeostasis	Secretion of vasoactive factors	PEDF, TSP-1, TGF-β2 and GDNF, VEGF, TNF-α, MMPs
Ensuring continued photoreceptor function	• Aiding photoreceptor outer OS formation • Cone OS phagocytosis • Cone retinal recycling	RLBP
Aiding high acuity vision	Cellular light guidance through the retina	
Mechanical tissue support and homeostasis	• Structural support and tissue organisation • Providing retinal tensile strength • Regulation of extracellular space volume	VEGF, purinergic receptors

Table 1.1.1 Functions and roles of Müller glia in the retina (adapted with permission from Bringmann *et al.*, 2006).

Müller glia are also important for the regulation of synaptic activity by rapidly taking up synaptically released neurotransmitters (mainly glutamate and γ aminobutyric acid or GABA) via the transporters GLAST and GAT-3 before synaptic spill over can occur, thus ensuring a spatio-temporally correct electrical encoding of light stimuli (Brew and Attwell, 1987; Rauen *et al.*, 1998; Biedermann *et al.*, 2002; Bringmann *et al.*, 2009b). The removal of extracellular neurotransmitter (especially glutamate) is also important for the prevention of glutamate-mediated neuronal excitotoxicity (Izumi *et al.*, 1999, 2002). Following glutamate uptake and conversion into the neurotransmitter precursor glutamine, Müller glia re-supply retinal neurons with this precursor molecule to ensure continued synaptic transmission as the neurons convert glutamine back into glutamate or GABA (Pow and Robinson, 1994; Pow and Crook, 1996; Pow *et al.*, 2000).

Müller glia are further able to secrete molecules that can modulate synaptic transmission of retinal neurons (Reichenbach and Bringmann, 2013). These neuroactive factors are collectively known as gliotransmitters and encompass mainly glutamate, D-serine purinergic receptor agonists but also acyl coenzyme A-binding protein, GABA, retinoic acid and nitric oxide (Reichenbach and Bringmann, 2013; Araque *et al.*, 2014). Depending on the neuroactive molecule as well as the context of gliotransmitter release, gliotransmission may have facilitating or depressing effects on synaptic transmission (Newman, 2004a, 2004b). Because of this involvement in retinal synaptic communication, Müller glia, much like astrocytes of the brain and spinal cord, likely contribute to retinal information processing (Newman, 2004a, 2004b; Araque *et al.*, 2014; Sahlender *et al.*, 2014).

Due to the high metabolic activity of retinal neurons these cells are at constant potential risk of oxidative stress. Some of the glutamate taken up by Müller glia is also used to produce glutathione, a scavenger molecule of reactive oxygen species (Pow and Crook, 1995; Reichelt *et al.*, 1997), which is supplied to the retinal neurons to protect against oxidative damage (Schütte and Werner, 1998).

To ensure the continued health and survival of retinal neurons, Müller glia further secrete numerous neurotrophic factors, growth factors and cytokines, including BDNF, CNTF, bFGF, IGF-1, NGF, neurotrophins-3 and -4, GDNF, LIF, and PEDF (reviewed by Bringmann *et al.*, 2009a). Receptors that can recognise these factors have in return been identified on retinal neurons. Müller glia further secrete factors to regulate the blood retinal barrier. Retinal blood vessels are intimately associated with Müller glia processes,

which secrete a cocktail of factors (PEDF, thrombospondin-1, TGF-β2, GDNF, VEGF, TNF-α and MMPs) that control the strength of the tight junctions between the endothelial cells making up the retinal blood vessels, hence regulating retinal vascular permeability (Tout *et al.*, 1993; Eichler *et al.*, 2004a, 2004b).

A specialised support role exists between Müller glia and photoreceptors as Müller glia play an important role in rod and cone photoreceptor outer segment formation (Jablonski and Iannaccone, 2000). Besides that, Müller glia have developed an even more specialised relationship with cone photoreceptors, in particular. Here, Müller glia are responsible for the engulfment (phagocytosis) of shed cone photoreceptor outer segment discs, which is important to keep the outer segment length constant as outer segment genesis continuously progresses due to extreme optical and metabolic demand (Long *et al.*, 1986). Conversely, rod photoreceptor disc phagocytosis is carried out by the RPE. Furthermore, recycling of the visual pigment chromophore retinal – important for continued photon detection – is carried out cone-specifically by Müller glia, whereas RPE cells engage in a canonical rod- and cone-specific visual cycle (Das *et al.*, 1992; Muniz *et al.*, 2007; Wang and Kefalov, 2012).

The vertebrate retina is inverted with respect to the direction of photon flux, as photons first need to traverse the entire radial extent of the neural retina before reaching the photoreceptor outer segments to initiate the phototransduction cascade. Müller glia serve as radial optical fibres, through which photons can travel to the outer segments while at the same time bypassing neuronal and neuropil layers thus avoiding scattering, refraction and reflection aberrations (Franze *et al.*, 2007; Agte *et al.*, 2011). Hence, this Müller glia function is vital for favourable signal/noise ratios, visual sensitivity and contrast. A recent study has also shown that Müller glia radially guide photons as a function of photon spectral wavelength (Labin *et al.*, 2014). Whereas photons in the cone wavelength domain (510/560 nm) were guided by Müller glia, rod wavelength domain photons (450 nm) leaked to the surroundings of Müller glia. Combined with the fact that Müller glia and cone photoreceptors exist at equal retinal densities and are often found along the same radial axis, this suggests that cone photoreceptors receive their photon input from designated Müller cells, thus contributing to high acuity vision (Agte *et al.*, 2011; Labin *et al.*, 2014). Conversely, up to 10 rod photoreceptors may be served with photons by one Müller cell, thus likely enhancing photon sensitivity rather than high acuity and resolution.

Finally, Müller glia are also important for keeping the columnar and laminar structural organisation of the retina intact (Willbold *et al.*, 1995, 2000) and provide important tensile strength to the retina as evidenced by increased retinoschisis in retinae devoid of Müller glia (MacDonald *et al.*, 2015). Müller cells further play a role in retinal mechanical tissue homeostasis. Activation of ionotropic neurotransmitter receptors leads to an influx of Na^+ into post-synaptic neurons, which is accompanied by an osmotic influx of water. This causes neuronal synapses and cell bodies to swell (Uckermann, 2004) and the extracellular space to shrink (Dmitriev *et al.*, 1999). The extracellular space volume is further reduced due to osmotic Müller glia volume increase during glutamate and K^+ uptake following retinal neuron activity. A consequence of that would be increased non-synaptic electric field (ephaptic) coupling of retinal neurons and potentially detrimental neuronal hyperexcitability and excitotoxicity (Dudek *et al.*, 1990; Chebabo *et al.*, 1995; Jefferys, 1995). To prevent this, Müller glia display a thinning and elongation of the basal stem process (Uckermann, 2004), which is mediated by VEGF and activation of purinergic receptors (Wurm *et al.*, 2008, 2010).

1.2. Eye development

1.2.1. Overview

The eye is part of the central nervous system (CNS) and in vertebrates it can be regarded as an extension of the brain. In fact, both originate from the same germ layer, the neuroectoderm. How a complex organ like the vertebrate eye is formed from a defined region of the neuroectoderm has been and continues to be actively investigated. As will be explained in this chapter, eye development consists of a series of morphogenetic movements and rearrangements of cells and tissues that later form the eye (Martinez-Morales and Wittbrodt, 2009). Key events in eye morphogenesis are eye field specification, splitting of the eye field along the midline of the embryo, which is important for the formation of two lateral eyes, and optic pit formation, which constitutes the first visible sign of eye development (Graw, 2010; Sinn and Wittbrodt, 2013). The first major morphogenetic rearrangement occurs during optic vesicle formation, where the neuroectoderm evaginates and becomes sub-specified into the optic stalk, the future retinal pigment epithelium (RPE) and the future neural retina. The optic vesicle remains connected to the developing brain via the optic stalk, which will later accommodate the optic nerve. The second major morphogenetic rearrangement consists of the invagination of the previously established optic vesicle to give rise to the bi-layered optic cup, where the inner cellular layer will develop into the neural retina while the outer layer will develop into the RPE.

The inner layer of the optic cup, the retinal neuroepithelium, consists of retinal progenitor cells (RPCs) arranged in a single cellular layer of cells. Each RPC spans the entire thickness of the retinal neuroepithelium but individual RPC nuclei are scattered throughout the cells' radial extent. This arrangement is called a pseudostratified epithelium. As will be explained in section 1.3.1, this is linked to active RPC proliferation, which leads to the expansion of the neural retina both along the radial as well as along the lateral dimension. Eventually, these proliferating RPCs give rise to all retinal neurons (amacrine cells, bipolar cells, cone photoreceptors, retinal ganglion cells, horizontal cells and rod photoreceptors) as well as the sole retinal glial cell type of RPC origin (Müller glia) (Chow and Lang, 2001). Within the relatively disorganised pseudostratified retinal

neuroepithelium each of these cells needs to find its target stratum (ONL, INL or GCL) via migration mechanisms explained in section 1.3. In addition, each of these cells also needs to differentiate in order to be able to perform tasks related to visual perception.

These processes appear to be regulated by both cell intrinsic transcriptionally controlled mechanisms, as well as by cell extrinsic signalling pathways. Together they orchestrate the formation of retinal neurons and Müller glia from RPCs, details of which shall be provided in this section.

1.2.2. Retinal progenitor cells and proliferation

In the early developing retina, the retinal neuroepithelium is populated exclusively by retinal progenitor cells (RPCs), which are tightly packed within a pseudostratified epithelial tissue. Before the onset of the neurogenic period, during which retinal neurons and Müller glia are born, the sole task performed by RPCs appears to be the expansion of the retinal neuroepithelium by mitotic proliferation. This ensures that adequately sized progenitor pools are present in order to produce all the retinal neurons and glia that later make up the retinal circuitry.

The maintenance of this proliferative state was found to be regulated by several transcription factors, most notably the basic helix-loop-helix (bHLH) or homeobox domain containing transcription factors *Rx1, Pax6, Six6, Six3, Tll (Tlx), Lhx2, ET, Chx10, Sox2, Hes1* and *Hes5* (Ohsawa and Kageyama, 2008; Agathocleous and Harris, 2009). Most of these transcription factors cross-activate each other (Zuber *et al.*, 2003). The bHLH type transcriptional repressors Hes1 and Hes5 are among the key regulators of the progenitor cell state (reviewed by Ohsawa and Kageyama, 2008). In general, Hes type transcription factors act as transcriptional repressors by recruiting the co-repressor protein Groucho to block the bHLH activator type transcription factors such as Mash1 and Math3; these are required for neuronal cell (especially RGC) fate specification (Ohsawa and Kageyama, 2008). Accordingly, over-expression of Hes1 in mice was shown to lead to the accumulation of undifferentiated cells whereas ablation of *Hes1* resulted in premature expression of the proneural genes *Math5*, *Ngn2* and *Mash1* in conjunction with accelerated RGC formation (Takatsuka *et al.*, 2004; Lee *et al.*, 2005). Similar to what has been observed for *Hes1* and *Hes5*, loss of function (LOF) of other transcription factor

genes listed at the beginning of this paragraph often leads to microphthalmia (small eyes) or anophthalmia (complete lack of eyes) mice, as is the case for *Chx10* (Burmeister *et al.*, 1996) or *Sox2* (Taranova *et al.*, 2006).

Hes1 and Hes5 are downstream effectors of the Notch signalling pathway (Ohtsuka *et al.*, 1999), which is known to promote the neuronal progenitor cell state in the CNS (Henrique *et al.*, 1997; Gaiano *et al.*, 2000) and is also known to comprise an extra-cellular signalling component. Herein lies another principle of RPC maintenance: that the retention of the RPC state is not solely governed by cell intrinsic aspects such as transcription factors, but that there are also extensive interactions between cell extrinsic factors and intra-cellular signalling pathways, (Agathocleous and Harris, 2009). While the Notch signalling pathway is cell-cell contact dependent and relies on the presence of the Notch ligand Delta on a neighbouring cell, soluble cell extrinsic factors have also been shown to affect the maintenance of the RPC pool. One of these factors is vascular endothelial growth factor (VEGF). Secreted VEGF binds to its receptor FLK1, expressed on the surface of RPCs, which elicits downstream signalling mechanisms that maintain a proliferative RPC state and suppress neurogenesis (Hashimoto *et al.*, 2006). The fact that signalling mediated by another secreted factor, sonic hedgehog (SHH), also suppresses the RGC fate via Hes1 activation indicates that Hes1 acts as a convergent intra-cellular signalling node in RPCs that is the downstream effector of various extrinsic cues that influence RPC proliferation and neurogenesis (Hashimoto *et al.*, 2006).

Breaking the theme of classic signalling cascades and transcriptional networks, the neuroepithelial stem cell gene *Nes* also deserves a special mention. *Nes* encodes the intermediate filament (IF) protein nestin. IF proteins assemble into IF polymers, which constitute the third major class of cytoplasmic filaments besides actin and microtubule filaments. *Nes* was identified to be specifically expressed in neuroepithelial stem cells (NSCs) but not in post-mitotic neurons or glial cells (Lendahl *et al.*, 1990) and has been widely used as a neuronal stem cell marker since its discovery; however, it is also expressed in skeletal muscle cells during development. Since the neural retina is a neuroepithelial tissue, it is not too surprising that *Nes* is expressed in RPCs during retinogenesis (Lee *et al.*, 2012). Whereas other IF proteins such as vimentin readily homopolymerise, nestin containing filaments are only formed upon heteropolymerisation with other IF proteins like vimentin or α-internexin *in vitro* and *in vivo* within cells, in which they are co-expressed (Marvin *et al.*, 1998; Steinert and *et al.*, 1999). The inability to polymerise on its own unlike most other IF proteins is thought to be due to a markedly

shorter N-terminal domain, a domain known to be essential for IF assembly (Lendahl *et al.*, 1990; Michalczyk and Ziman, 2005). Despite being an IF protein, the actual function of nestin in NSCs has remained rather elusive since its initial identification. Targeted disruption of *Nes* in the *Nes*$^{-/-}$ knock-out mouse resulted in embryonic lethality (Park *et al.*, 2010). The neuroepithelium in the developing neural tube of such animals contained fewer NSCs, most likely due to their increased susceptibility to apoptosis. This observed phenotype does not appear to be directly related to the ability of nestin to be incorporated into IFs because elevated apoptosis levels were not observed in vimentin knock-out mice where nestin does not form filaments due to the absence of its heteropolymerisation partner vimentin. Similar results were obtained in a different study on rats, in which *Nes* RNAi was performed (Xue and Yuan, 2010). However, in addition to increased apoptosis levels, this study also detected that knock-down of *Nes* expression suppressed cortical neurogenesis by blocking the mitogen stimulated proliferation of NSCs and by inducing cell cycle arrest. Although the mechanism of nestin mediated NSC proliferation could not yet be identified, nestin somehow appears to engage in a pro-proliferative signalling cascade via the phosphoinositide 3-kinase (PI3K) pathway.

Despite its ill-defined function in proliferation, nestin remains a useful NSC marker to study RPCs in various different contexts. This has led to the generation of different *Nes* reporters. However, rather than the classical design where reporter gene expression is under transcriptional control of a promoter, NSC specific *Nes* reporters have been successfully generated by combining ubiquitously active promoters with a conserved region within the second intronic enhancer element of the *Nes* gene (Lothian and Lendahl, 1997; Kawaguchi *et al.*, 2001; Mignone *et al.*, 2004; Walker *et al.*, 2010).

1.2.3. Principles of cell fate specification in the developing retina

Following an exclusively proliferative period, the RPCs eventually undergo asymmetric cell division(s) in order to populate the neural retina with retinal neurons and Müller glia. In humans, this occurs between day 47 post gestation until about 8 moths of development (Graw, 2010). In mice, the equivalent process takes from embryonic day (E)10.5 until about postnatal day (P)14. Several clonal analysis studies have shown that single RPCs are often multipotent and can give rise to all retinal neurons as well as Müller glia (Turner

and Cepko, 1987; Holt *et al.*, 1988; Wetts and Fraser, 1988). Birth dating studies suggest that cells of the rodent retina are born in a roughly defined chronologic order with consecutive peak production periods of each cell type (although off-peak production overlaps considerably): RGCs are born first, followed by amacrine cells, cone photoreceptors, horizontal cells, bipolar cells, rod photoreceptors and finally Müller glia (Figure 1.2.1) (Young, 1985; Reh and Kljavin, 1989; Rapaport *et al.*, 2004). The intrinsic competence model was initially proposed (Cepko et al., 1996), according to which RPC neurogenic cell divisions follow an internal clock that dictates the sequential generation of retinal neurons and Müller glia in consecutive rounds of the cell cycle .

That this is not the complete story is most easily exemplified by the existence of single RPC lineage clones that are composed exclusively of one cell type (Turner and Cepko, 1987; Gomes *et al.*, 2011; Cepko, 2015; Wang and Cepko, 2016). This in turn suggests that RPCs might be inherently heterogeneous and may, at least in some cases, only produce a restricted set of retinal cells. Indeed, gene expression (including bHLH transcription factor) profiles in individual RPCs can be heterogeneous even at identical developmental time points (Trimarchi *et al.*, 2008). RPCs in the zebrafish retina that expressed the cone-rod homeobox protein (*Crx*) transcription factor prior to terminal division frequently gave rise to a homotypic cone photoreceptor pair of the L-, M-, S- or UV subtype (Suzuki *et al.*, 2013). Lineage bias is not restricted to terminal mitosis, however, as multi-clonal lineage trees with a biased composition of for instance different amacrine cell subtypes have been reported in *Xenopus laevis* tadpole (Huang and Moody, 1997). Despite lineage bias, the effect of stochasticity should not be discounted. The unequal segregation of competing cell fate determinants between clonally related daughter cells can conceivably lead to different cell fate outcomes in the progeny (Bassett and Wallace, 2012; Cepko, 2014).

The intrinsic competence of an RPC to produce certain retinal cells is also related to its ability to respond to extrinsic instructive cues. Exposure to retinoic acid for instance, produced by RPCs, RGCs and RPE cells, stimulates the production of rod photoreceptors (Hyatt *et al.*, 1996; Kelley *et al.*, 1999). Many other extrinsic cues exist that influence the production of certain retinal cells, although this is beyond the scope of this report.

Following the integration of intrinsic and extrinsic cues, genes related to the morphology/function of the differentiated cell need to be activated while genes typically associated with the RPC state need to be silenced (Agathocleous and Harris, 2009).

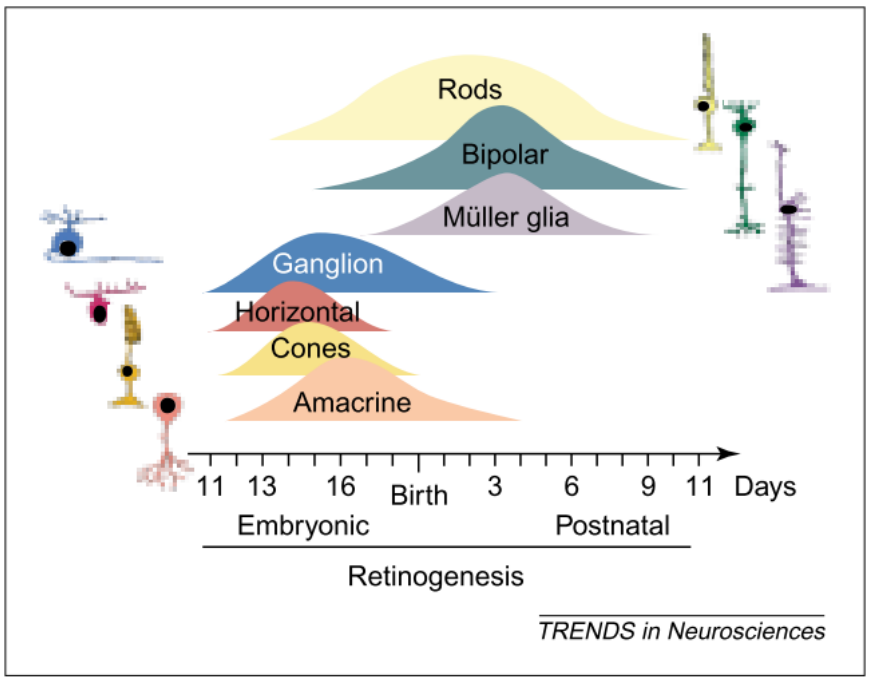

Figure 1.2.1 Retinal neurogenesis and Müller gliogenesis follows a defined histogenic sequence. Individual curves represent relative numbers of cells produced rather than absolute numbers. Schematic is based on data from birth dating studies in the mouse retina (Young, 1985) (reproduced with permission from Marquardt and Gruss, 2002).

Pro-neural bHLH transcription factors are well known regulators of neuronal differentiation (e.g. the key regulator *Ath5* in RGCs) (Liu *et al.*, 2001; Matter-Sadzinski *et al.*, 2001; Logan *et al.*, 2005). Positive feedback loops are then in place to enforce a chosen differentiation route. These routes are quite diverse between the different retinal cell types.

1.2.4. Rod photoreceptor determination and differentiation

In the mouse and the human retina, rod photoreceptors comprise about 70 % of all retinal cells (Young, 1985). In order to be produced in such numbers, rod genesis spans a relatively wide time window compared with other retinal cell types. In mice, this extends from E13 to P7 and peaks around birth (Carter-Dawson and LaVail, 1979). The process of forming an individual photoreceptor cell can be broken down into four steps: 1) restriction of RPC competence, 2) commitment to the photoreceptor lineage during or after neurogenic cell division, 3) expression of photoreceptor genes required e.g. for phototransduction or morphogenesis and 4) axonal growth, synaptogenesis and outer segment formation (Swaroop *et al.*, 2010).

With the advent of modern genetic tools, it has become possible to probe into the complex mechanisms that govern rod photoreceptor determination. In general, a specific gene is thought to be important for photoreceptor determination when the deregulation of its normal function leads to increased/reduced photoreceptor numbers with the concomitant decrease/increase of at least one other retinal cell type (Cepko, 2015). This is to be distinguished from genes that only affect survival; LOF would hence reduce photoreceptor numbers without affecting the production of other retinal cells. It is presently not well understood, which genes and mechanisms are responsible for RPC cell fate restriction in favour of producing rod photoreceptors. There is a better understanding of the molecular mechanisms that regulate full commitment to the rod photoreceptor state, as discussed below.

Photoreceptor determination:

Notch signalling is considered the most upstream determinant of photoreceptor genesis (Figure 1.2.2A and 1.2.2B) and generally functions by repressing neurogenesis and maintaining an RPC state as explained in section 1.2.2. Thus, the birth of a rod photoreceptor cell likely requires a reduction of Notch signalling in asymmetrically dividing RPCs in the correct competence state (Jadhav *et al.*, 2006). Decreased activity of the Notch pathway allows the homeodomain transcription factor Rax to transactivate another homeodomain transcription factor gene (*Otx2*) in the cell cycle immediately prior to photoreceptor birth (Muranishi *et al.*, 2011). *Otx2* is essential for rod and cone photoreceptor genesis as its conditional knockout in mice led to the complete loss of all photoreceptors with concomitantly increased amacrine cell production while its overexpression resulted in ectopic photoreceptors at the expense of amacrine cells (Nishida *et al.*, 2003).

However, *Otx2* is expressed in RPCs that give rise to photoreceptor and bipolar cells as well as their respective progeny. Otx2 transcription factor can transactivate a bipolar differentiation programme, which is prevented in future photoreceptors by the transcriptional repressor Blimp1 (Katoh *et al.*, 2010; Brzezinski *et al.*, 2013). Instead, Otx2 transactivates the pan-photoreceptor transcription factor gene *Crx* in these cells. *Crx* is the earliest photoreceptor marker in the retina and its expression becomes detectable shortly after photoreceptor birth (Nishida *et al.*, 2003; Hennig *et al.*, 2008). In keeping with the timing of its transcriptional transactivation during photoreceptor genesis, Crx is not important for photoreceptor determination but plays a much greater role in orchestrating photoreceptor development and maturation since *Crx*-deficient mice initially produced photoreceptors; however, abnormal outer segment formation eventually led to photoreceptor degeneration (Furukawa *et al.*, 1999). Indeed, $Crx^{-/-}$ mice exhibited down-regulated gene expression levels in a whole range of phototransduction genes.

Rod photoreceptor fate specification:

Crx positive photoreceptor precursor cells can differentiate into cone or rod photoreceptors. In a review by Swaroop and colleagues (2010) it was proposed that photoreceptor differentiation into either rods or the different cone photoreceptor subtypes

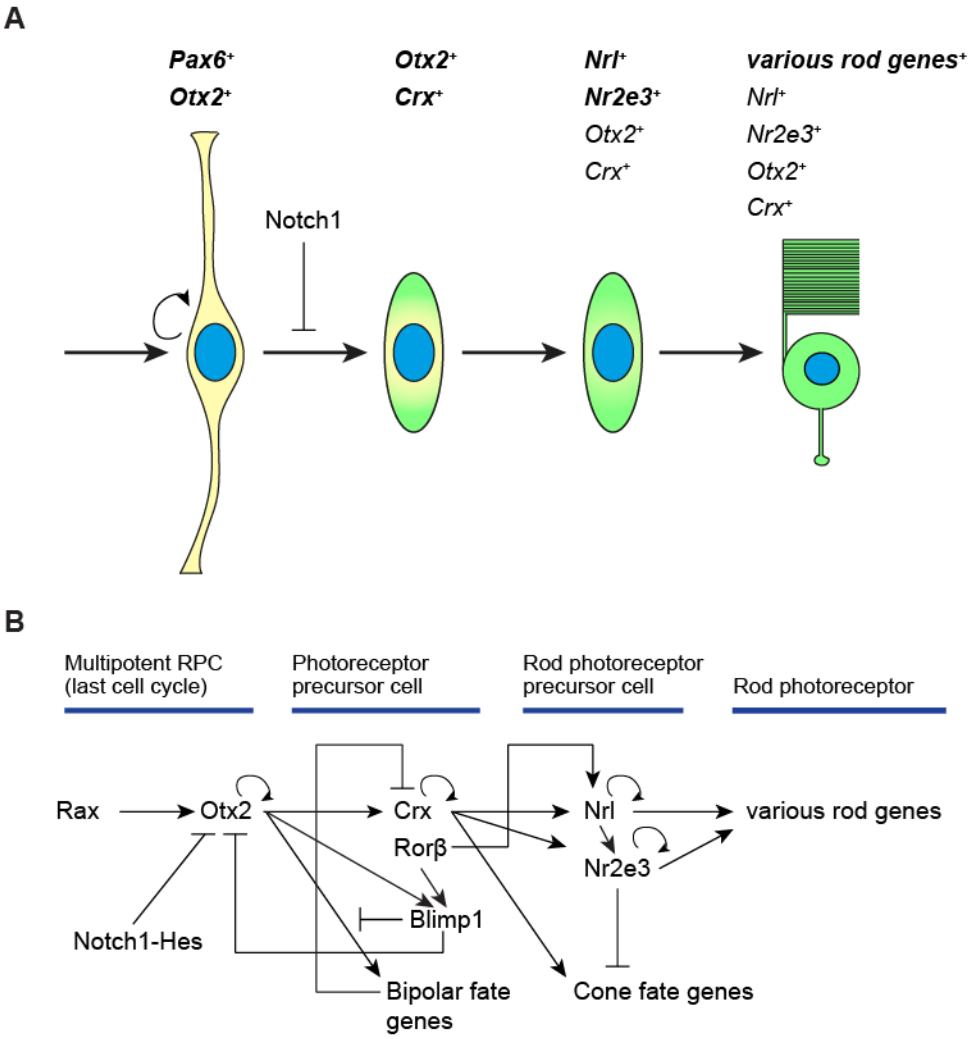

Figure 1.2.2 Rod photoreceptor specification and differentiation. **A)** En route to producing a rod photoreceptor cell, intermediate cellular states (multipotent RPC, photoreceptor precursor cell, rod photoreceptor precursor cell and rod photoreceptor) exhibit characteristic gene expression profiles linked to a step wise acquisition of rod fate. **B)** Overview of the gene regulatory network involved in rod photoreceptor genesis. Arrows indicate transcriptional activation, curly arrows represent self-transactivation, and line terminating in orthogonal bar indicates transcriptional repression.

can be explained by the transcriptional dominance hypothesis: photoreceptors follow a default differentiation pathway that ends in the S-cone fate unless this is transcriptionally overridden in favour of the other photoreceptor fates (Figure 1.2.2B). Which differentiation path is chosen ultimately depends on which transcriptional program becomes dominant, the outcome of which is likely modulated by both cell intrinsic and extrinsic factors. Full commitment to the rod photoreceptor lineage requires the induction of the neural retina leucine zipper transcription factor gene (*Nrl*), which is mediated by retinoid-related orphan nuclear receptor RORβ (Swaroop *et al.*, 1992; Jia *et al.*, 2009). *RORβ*$^{-/-}$ and *Nrl*$^{-/-}$ knockout mice actually have very similar phenotypes in that all rod photoreceptors get diverted towards the S-cone fate (Mears *et al.*, 2001; Jia *et al.*, 2009). *Nrl* is the earliest detectable rod photoreceptor marker and becomes activated soon after the birth of precursors destined to become rod cells. This has been exploited to generate the widely used *Nrl.GFP*$^{+/+}$ rod photoreceptor reporter mouse line, in which *GFP* expression is under transcriptional control of the *Nrl* promoter (Akimoto *et al.*, 2006).

Nrl transcription factor instructs the rod cell fate by transactivating in conjunction with Crx several genes directly related to rod function, but most importantly another master regulatory gene encoding the nuclear orphan receptor Nr2e3 (Oh *et al.*, 2007, 2008). The Nrl and Nr2e3 transcription factors jointly act as transcriptional activators of a set of rod specific genes, overlapping with the Nrl-Crx transcriptional targets (Cheng *et al.*, 2004a, 2006). Together, the activated genes significantly contribute to post-mitotic rod photoreceptor development and maturation. At the same time, Nr2e3 also engages in transcriptional repression of cone related genes in rod photoreceptor precursor cells of the mouse retina thus dually solidifying the rod fate (Chen *et al.*, 2005). Combined, Crx, Nrl and Nr2e3 thus form an alliance of transcription factors that drive rod photoreceptor genesis while preventing cone photoreceptor specification in photoreceptor precursor cells at the correct competence state (Swaroop *et al.*, 2010).

1.2.5. Müller glia determination and differentiation

Müller glia make up approximately 4-5 % of all retinal cells within the mature mouse retina (Young, 1985). The peak of Müller gliogenesis occurs at around P4 in mice, which is thus in chronological terms later than that of any of the retinal neurons. However,

Müller glia are not produced in the mouse retina before E18. Hence, RPCs likely lack gliogenic competence prior to that. Müller glia are not generated from a dedicated glioblast progenitor cell. Instead, lineage analyses have revealed that retinal neurons and Müller glia are all derived from the common RPC lineage (Turner and Cepko, 1987; Wetts and Fraser, 1988).

Notch1 signalling is important for Müller glia determination:

As explained in section 1.2.2, a binary Notch signalling dependent decision point exists during CNS development that either leads to neurogenesis or maintenance of the RPC state (Henrique *et al.*, 1997; Gaiano *et al.*, 2000). While these studies have linked active signalling through Notch to prolongation of the RPC state, other studies have shown that misexpression of constitutively active *Notch1* receptor or the effector negative bHLH transcription factor *Hes5* provides instructive signals to produce Müller glia from RPCs that have reached a suitable state of competence in mouse and zebrafish (Furukawa *et al.*, 2000; Hojo *et al.*, 2000; Scheer *et al.*, 2001). The instruction by Notch1 to produce a Müller glia cell could just as well be the instruction not to produce a retinal neuron, given that signalling through Notch1 represses the transactivation of various pro-neural bHLH transcription factors such as *Mash1, Ngn2, Math3, NeuroD1* and *Math5* by the action of negative bHLH transcriptional repressors such as Hes1 and Hes5 (Ohsawa and Kageyama, 2008). Indeed, mice deficient in pro-neural transcription factors had fewer retinal neurons but had concomitantly overproduced Müller glia (Inoue *et al.*, 2002; Akagi *et al.*, 2004); misexpression of pro-neural bHLH transcription factors on the other hand lead to the ectopic retinal neuron production at the expense of Müller gliogenesis (Brown *et al.*, 1998; Morrow *et al.*, 1999; Bae *et al.*, 2000; Hatakeyama *et al.*, 2001). Following the prevention of neurogenesis via Notch1, RPCs may enter a default pathway ending with either enter gliogenesis or apoptosis (Scheer *et al.*, 2001). In keeping with this notion, misexpression of the homeodomain transcription factor genes *Rax* and *Chx10*, which are known to be linked to RPC status, resulted in the production of ectopic Müller glia in the mouse retina (Furukawa *et al.*, 2000; Hatakeyama *et al.*, 2001).

The Müller glia transcriptional network downstream of Notch1:

The gene regulatory network downstream of the Notch1 pathway responsible for Müller gliogenesis is presently not well understood. What is known is that the high-mobility group box transcription factor Sox9 is required for the production of Müller glia, since Cre recombinase mediated ablation of *Sox9* led to reduced immunohistochemical detection of Müller glia markers in the mouse retina (Poché *et al.*, 2008). However, it was not entirely clear whether *Sox9* was needed for gliogenesis, differentiation or survival. More recent studies have in fact shown that Notch1 signalling stimulates *Sox9* expression in neural stem cells, which was shown to be important for Müller gliogenesis as well as astrogliogenesis, although the underlying transcriptional network is yet to be elucidated (Muto *et al.*, 2009; Martini *et al.*, 2013). *Sox9* is expressed in all RPCs at all stages of retinogenesis even in clones that have produced several retinal neurons before giving rise to a Müller cell, likely due to the presence of active Notch1 signalling (Poché *et al.*, 2008). It seems entirely possible that the scarcity of Müller glia birth events is due to a presently unknown pro-neural factor that antagonises the gliogenic effect of *Sox9*. The consequence of that could be the observed relatively low frequency of Müller gliogenesis and a complete lack thereof before the mouse E18 stage. The Müller glia competence state may only be reached upon overcoming the effects of the Sox9 antagonising factor, after which Sox9 may activate the transcriptional program leading to gliogenesis.

Mammalian Müller glia are differentiated and quiescent RPCs:

Several lines of evidence suggest that RPCs likely become quiescent and differentiate into a Müller glia state rather than giving birth to a Müller cell through mitosis. Investigations of the morphologies of radially spanning cells from early development until adulthood in rabbit and chick strongly suggests that RPCs gradually take on a Müller glia like appearance (Reichenbach and Reichelt, 1986; Prada *et al.*, 1989). Like Müller glia, RPCs exhibit apical and basal processes, which appear to become more elaborate and intricate during retinogenesis. The feature of spanning the entire neuroepithelium is shared with cortical radial glia, which analogously to RPCs give rise to cortical neurons by cell division before also differentiating into a glial cell (astrocyte).

As expected for a subtype of a neural progenitor cell, RPCs express the neuronal stem cell marker and intermediate filament encoding gene *Nes*. During human retinal

development, nestin immunoreactivity in the retina was frequently co-localised with the immunoreactivity of vimentin – an intermediate filament protein also expressed in adult Müller glia (Walcott and Provis, 2003). Based on this finding, it was in fact proposed that the Müller glia state is the end stage phenotype of a differentiating RPC and that during this transition phase *Nes* expression is gradually down-regulated while the expression of mature Müller glia markers is gradually initiated (Figure 1.2.3). Besides *Nes*, a large number of genes expressed in mouse RPCs were also expressed in Müller glia and vice versa, whereas the overlap of either with mature retinal neurons was by far less extensive (Blackshaw *et al.*, 2004; Livesey *et al.*, 2004; Roesch *et al.*, 2008; Trimarchi *et al.*, 2008; Jadhav *et al.*, 2009). While some of the genes expressed in Müller glia are already expressed in early RPCs, a number of genes such as *Rlbp1* (encodes retinaldehyde binding protein 1, which is important for the visual cycle) only start being expressed in late progenitor cells, suggesting that certain Müller glia genes are switched on gradually over time in RPCs (Trimarchi *et al.*, 2008; Jadhav *et al.*, 2009). However, rather than necessarily being an indicator of their functional requirement in RPCs, expression of Müller glia genes in late RPCs may be a manifestation of a Müller glia competence state dictated by underlying transcriptional networks (Jadhav *et al.*, 2009).

Although not all late and glial fate competent RPCs give rise to Müller glia, expression of genes such as *Rlbp1* in late glia competent RPCs and maintenance of their expression in cells, that do eventually differentiate into Müller glia, appears to be a good marker for this encompassing cell population. The potential to transgenically label these cells has in fact been exploited in the shape of reporter animals, such as the *Rlbp1*.*GFP* mouse where *GFP* expression is under transcriptional control of the *Rlbp1* promoter (Vazquez-Chona *et al.*, 2009). A different reporter strategy needs to be employed in order to label a cell population ranging from early to late RPCs/Müller glia. This can be achieved by using *Nes* reporters as discussed in section 1.2.2 (Lothian and Lendahl, 1997).

While RPCs differentiating into Müller glia likely still retain some potential to undergo mitosis, this potential is absent in fully differentiated mature Müller glia in the adult mammalian retina. This state of quiescence seems to be linked to *Sox2* expression; in its absence, Müller glia re-enter the cell cycle effectively depleting them from the mouse retina, which results in retinal lamination defects (Surzenko *et al.*, 2013). Evidence suggests that Müller glia in the mammalian retina can also revert to a RPC-like state following injury or disease as they re-express *Nes* for instance, albeit without re-entering the cell cycle (Xue *et al.*, 2006; Valamanesh *et al.*, 2013). Proliferation can be forced,

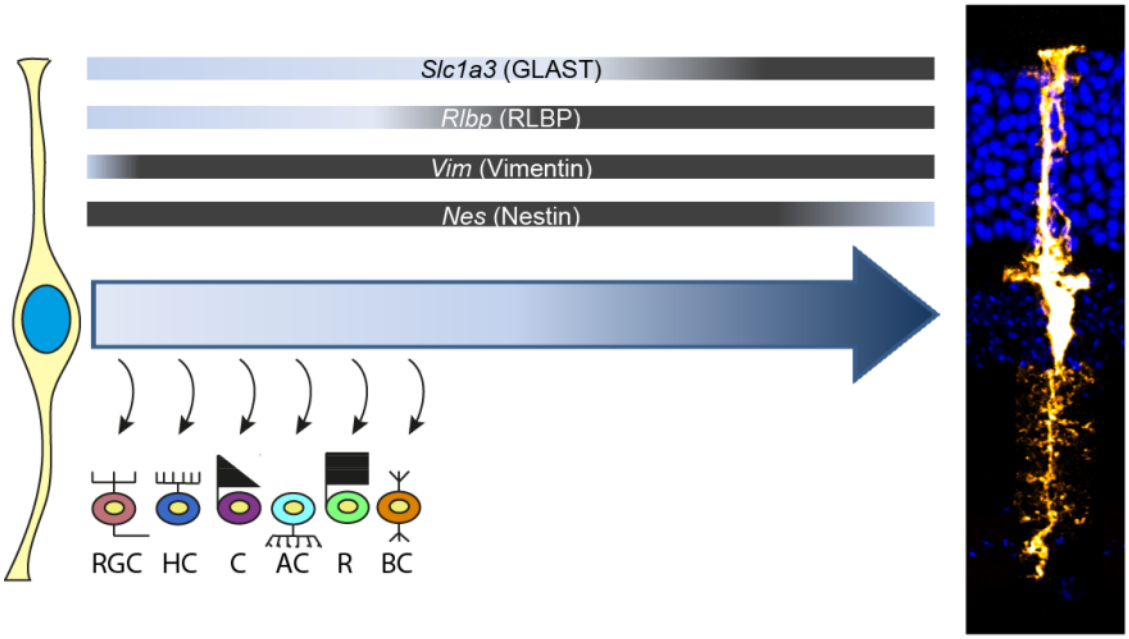

Figure 1.2.3 Retinal progenitor cells (RPCs) give rise to all retinal neurons and Müller glia. Mitotic RPCs undergo neurogenic cell divisions and slowly differentiate into Müller glia. During this transition phase the neural progenitor marker *Nes* (Nestin) is co-expressed with markers usually expressed in mature Müller glia. The onset or cessation of expression of the four depicted genes is indicated in colour gradient transitions from light grey to dark grey and dark grey to light grey respectively. RGC = retinal ganglion cell, HC = horizontal cell, C = cone photoreceptor, AC = amacrine cell, R = rod photoreceptor, BC = bipolar cell.

however, by a combination of injury/disease and mitogenic stimulation or by transgenic cell reprogramming (Das *et al.*, 2006; Del Debbio *et al.*, 2010; Hamon *et al.*, 2015; Ueki *et al.*, 2015). Combined, these studies thus suggest that mature Müller glia in the mammalian retina are quiescent and latent RPCs, the full progenitor potential of which is not usually revealed unless stimulated.

1.3. Migration in the central nervous system

1.3.1. Overview

The majority of the body of work on neuronal migration has focused on migration within the brain – one of the major organs of the central nervous system (CNS) besides the spinal cord. In the developing, as well as in the adult brain, neurons are typically born at the luminal (also referred to as ventricular or apical) side of the neuronal epithelium. From there, these newly born neuronal precursor cells subsequently migrate away from their place of birth towards their target location within the brain using one or more of several previously described mechanisms of neuronal migration. Once at the target destination, these neuronal precursors then engage in setting up the brain neuronal circuitry. CNS neurons exhibit a significant migratory capacity at pre-mitotic as well as at post-mitotic stages. As shall be explained in the following section, pre-mitotic motility involves the intracellular migration of nuclei, which is important to ensure the continued integrity of epithelium; conversely, post-mitotic motility is required for appropriate positioning of the entire neuron within the neuronal tissue. Although fundamentally different, both are essential to establishing the brain tissue architecture and circuitry required for the brain to function properly. The retina is a lateralised CNS region of the brain. Evidence to support this came from explant studies using frog late blastulae: the neuroectoderm, which normally gives rise to the nervous system, was explanted and formed anterior brain structures including eyes (Nieuwkoop, 1963). In addition to their common origin, the retina and brain both exhibit a significant degree of lamination. From that perspective, it is perhaps unsurprising that many of the migratory behaviours of brain neurons are recapitulated by retinal neurons. The following section discusses the principles of neuronal migration based on findings from the retina, as well as the brain, in order to provide a comprehensive overview of CNS neuronal migration.

1.3.2. Interkinetic nuclear migration (IKNM)

The developing retina is a pseudostratified neuroepithelium. This means that each cell spans the entire width of the neuroepithelium by using both an apical and a basal process, but the nuclei can be found at various apico-basal positions within those cells (Miyata, 2008; Randlett *et al.*, 2011a). IKNM describes the migratory behaviour of mitotic, elongated epithelial cells, during which the nuclei migrate (nucleokinesis) along the apico-basal axis of the epithelium through the cell's cytoplasm and in sync with specific stages of the cell cycle (Frade, 2002; Baye and Link, 2007). It was first observed in the 19th and early 20th century that the somata of proliferating *Keimzellen* (neuroepithelial cells) moved closer to the luminal (or apical) surface of the developing CNS during cell division (Schaper, 1897; Sauer, 1935). Thereafter, it took several decades to provide further proof to support this observation: in presence of mitotic inhibitors, metaphase arrested cells accumulated exclusively at the apical surface, whereas microspectrophotometry revealed changes of nuclear DNA content, and hence cell cycle progression, during IKNM (Watterson *et al.*, 1956; Sauer and Chittenden, 1959). Thus, cell cycle and nuclear position are intimately linked and to date IKNM is understood to be a cell behaviour exhibited exclusively by mitotic epithelial progenitor cells. On the other hand, the other modes of cell migration in the central nervous system described later in this section are exhibited by post-mitotic neuronal (precursor) cells.

IKNM seems to be conserved not only in all developing neuroepithelia (Figure 1.3.1A & 1.3.1B), but epithelia in many different non-neuronal tissues as well, such as the Drosophila wing disc or the mouse liver epithelium (Bort *et al.*, 2006; Meyer *et al.*, 2011; Spear and Erickson, 2012a). Cell division occurs almost exclusively when the nucleus is at the apical surface (Figure 1.3.1C; but see also section 1.3.3). During G1 of the cell cycle, the nucleus translocates towards the basal surface where it enters S-phase and DNA replication, before reversing back to the apical surface during G2 (Randlett *et al.*, 2011a). Nucleokinesis during IKNM follows a characteristic motion pattern (Miyata, 2008 with Pearson *et al.*, 2002; Norden *et al.*, 2009; Leung *et al.*, 2011): as exemplified in the developing zebrafish retina with genetically labelled nuclei, time-lapse imaging revealed predominantly random and stochastic nuclear movements during S- and G1-phases in vicinity or approaching the basal surface of the neuroepithelium. G2-phase, on the other

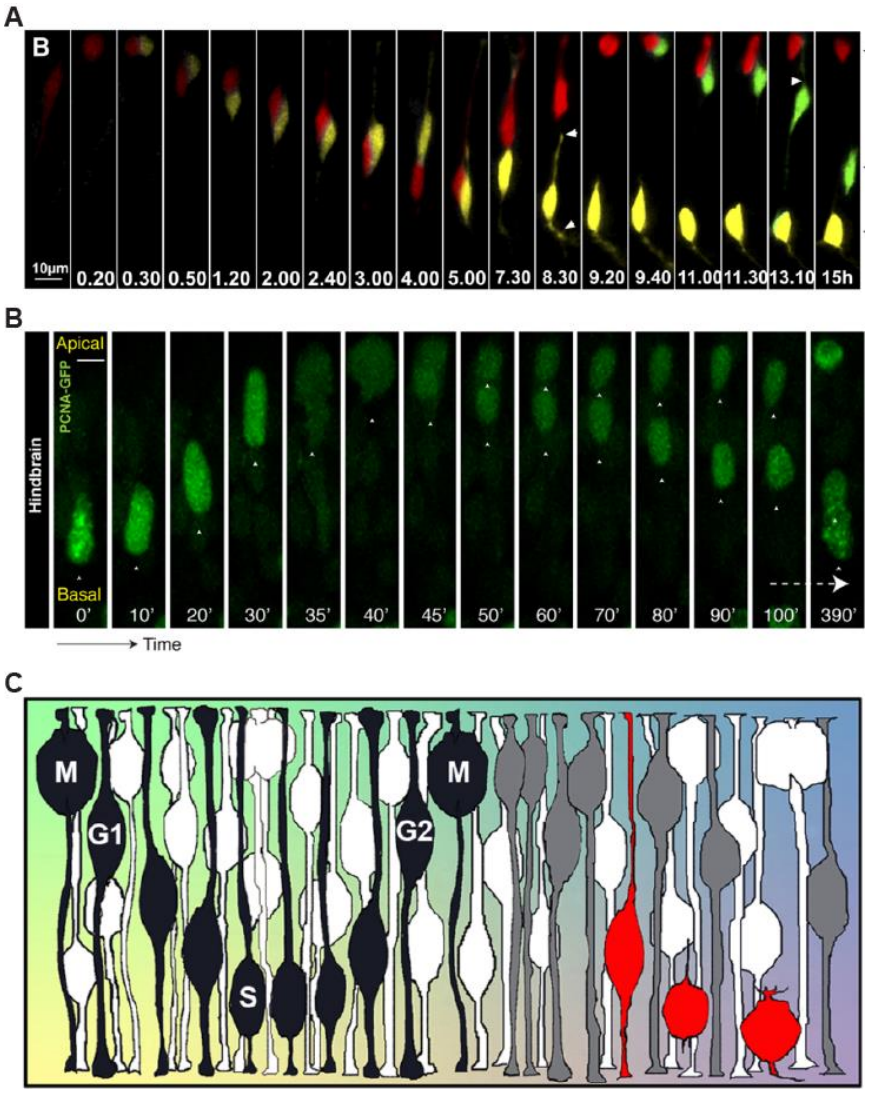

Figure 1.3.1 Interkinetic nuclear migration (IKNM) is conserved in the central nervous system. **(A)** IKNM in the developing zebrafish retina. RPC (*Ath5.GFP* positive; pseudo-coloured in red) undergoing two cell cycles, giving rise to two RGCs (pseudo-coloured in yellow and green). (reproduced with permission from Poggi *et al.*, 2005) **(B)** IKNM in the developing zebrafish hindbrain. Neural progenitor cell nucleus (*PCNA.GFP* positive) dividing and giving rise to two daughter nuclei. Scale bar: 5 µm. (reproduced with permission from Leung *et al.*, 2011). **(C)** Retinal IKNM schematic. RPC (dark grey) going through the cell cycle, undergoing neurogenic cell division and giving rise to a RPC (light grey) and a RGC (red). (reproduced with permission from Baye and Link, 2007).

hand, is much shorter and characterised by high velocity and directed migration of the nucleus towards the apical surface where cell division subsequently takes place.

Neuroepithelial cell divisions occurring during IKNM can be either proliferative or neurogenic; they either expand the pool of progenitor cells or give rise to post-mitotic neuronal daughter cells, respectively. Thus, the mitotic aspect of IKNM clearly serves the purpose to expand the developing retinal tissue and to populate it with retinal neurons. The answer as to why cell cycling is coupled to energy consuming nucleokinesis is less straight forward (as reviewed by Kosodo, 2012). One possible reason could be an increased side-by-side packaging efficiency made possible by having variable apico-basal nuclear positions within the epithelium (Smart, 1972). It has also been proposed that temporal regulation of the individual cell cycle stages could be important for epithelial remodelling (Smith JL, 1987; Spear and Erickson, 2012a). According to this model, extensive proliferation with shortened G1 and/or S-phases may for instance contribute to optic vesicle invagination. Another factor could be the accumulation of cellular components at the apical surface, which need to be distributed to both daughter cells during cell division to ensure the continued function of daughter cells and the whole tissue (Spear and Erickson, 2012a). Tight and adherens junction complexes and their regulators are concentrated at the apical surface. Hence, mitosis at the apical side could allow both daughter cells to inherit junction components and to properly integrate into the existing epithelium, which ensures the continuation of the epithelial polarity (Strzyz et al., 2015). Similarly, centrosomes are found within the tip of the apical process throughout the cell cycle (Norden *et al.*, 2009; Spear and Erickson, 2012b). The centrosome is the major microtubule organising centre (MTOC) of cells. It plays an essential role in the formation of the microtubule based mitotic spindle during M-phase, which segregates sister chromatids into the daughter cells. The return of the nucleus to the apical side of the neuroepithelium is thus important for proper M-phase progression. Moreover, centrosomes also need to be distributed to both daughter cells following centrosomal duplication.

Baye and Link (2007) provide a model for why nuclei migrate away from the apical surface in the first place: based on their observations on fluorescently labelled nuclei in the developing zebrafish retina they proposed that deeper basal migration of the nucleus during G1-/S-phase increases the likelihood of neurogenesis over cell cycle re-entry. It seems plausible that varying apico-basal positions of nuclei allow the cells to react differently to apico-basally polarised signals within the neuroepithelium. Complementary

observations were made in the embryonic mouse cortex where the length of G1 positively correlated with the probability to switch from proliferation to neurogenesis (Calegari and Huttner, 2003; Lange *et al.*, 2009; Pilaz *et al.*, 2009). A consequence of the model proposed by Baye and Link (2007) is that the length of G1 is correlated with the extent of basal migration and hence neurogenesis. It has been suggested that the length of G1 may be proportional to the accumulation of an intracellular neurogenic factor or the competence of an RPC to react to extracellular neurogenic signals (Randlett *et al.*, 2011a).

1.3.3. Somal translocation

Post-mitotic neuronal precursor cells generated by neurogenic cell division need to migrate to their designated strata in order to establish the correct retinal architecture. One way of achieving this is by somal translocation, first described by Morest (1970). In the brain, this mode of migration is especially prevalent during early phases of nervous system development when the neuroepithelium is still relatively thin (Hatanaka *et al.*, 2004; Cooper, 2008). As will be explained later, a different migration mechanism (glial-guided migration) is preferentially utilised in thicker neuroepithelia at later stages of development. However, even in that case the final migratory effort following glial-guided migration is by somal translocation (see Cooper, 2013).

A neuronal precursor cell undergoing somal translocation usually extends a long process towards its target stratum or target site while the nucleus typically still resides within an incorrect location. The tip of the leading process is frequently highly branched. During somal translocation, the nucleus then moves within the previously established process towards its designated target stratum in a grappling hook like manner (Figure 1.3.2A & B) (Nadarajah *et al.*, 2001, 2003; Cooper, 2013). Nucleokinesis was found to be a more or less smooth, continuous process occurring at a relatively high velocity (~ 1 µm/min) in the developing mouse cerebral cortex (Nadarajah *et al.*, 2001, 2003). However, a different study has found that somal translocation in the developing ferret visual cortex can be discontinuous (Borrell *et al.*, 2006). A similar pattern of discontinuous nucleokinesis was also reported in cultured neurons isolated from neonatal rats (Schaar and Mcconnell, 2005).

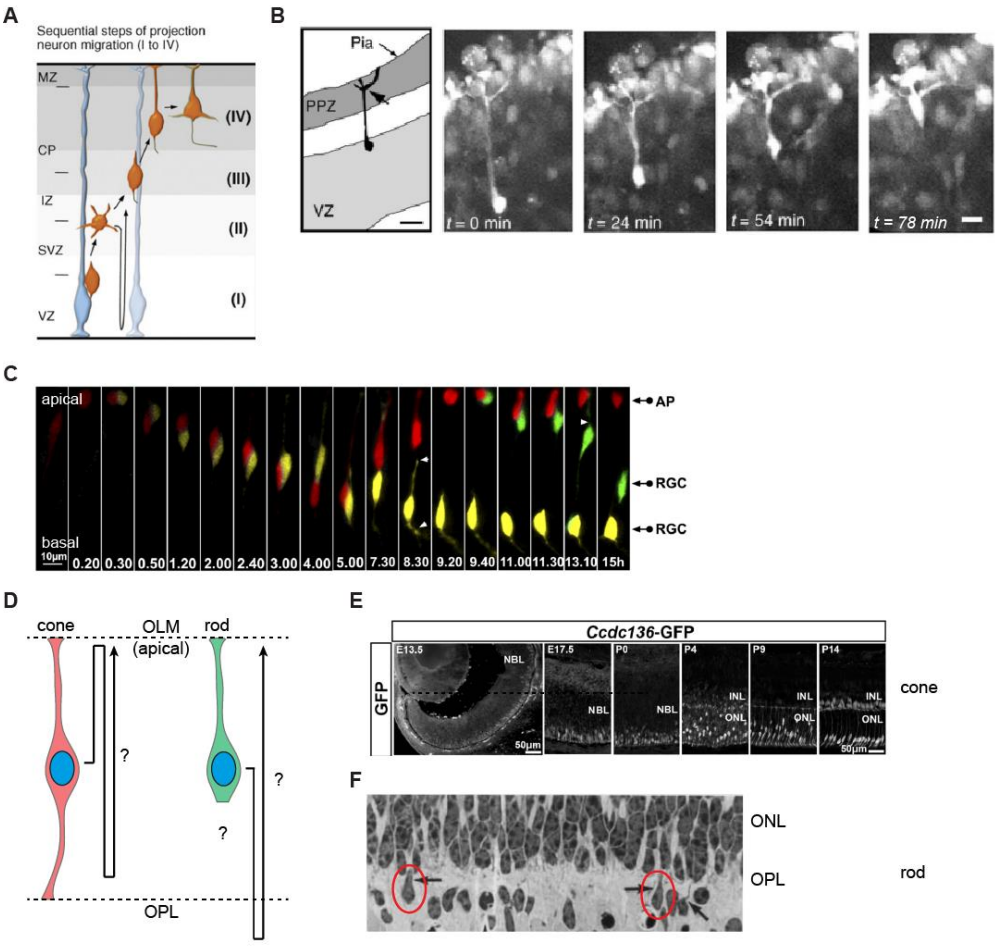

Figure 1.3.2 Somal translocation in the central nervous system – proven and inferred. **(A)** Sequential steps of projection neuron migration. I: bipolar, II: multipolar, III: glial-guided, IV: somal translocation. VZ = ventricular zone, SVZ = subventricular zone, IZ = intermediate zone, CP = cortical plate, MZ = marginal zone (pial surface). (adapted with permission from Heng et al., 2010) **(B)** Neuronal precursor cell in the mouse cerebral cortex undergoing somal translocation towards the pial surface. Fluorescence microscopy time-lapse live imaging of an acute mouse cerebral cortex brain slice (E14). Cell was labelled with Oregon Green BAPTA-1 488 AM. (adapted with permission from Nadarajah *et al.*, 2001). **(C)** RGCs in the developing zebrafish neural retina exhibiting somal translocation. Confocal fluorescence microscopy live imaging time-lapse series of the developing zebrafish retina at 30-32 hours after fertilisation. Newly born RGCs (*Ath5.GFP* positive, but pseudo-coloured in yellow and green) and the mother RPC undergoing IKNM (pseudo-coloured in red) are shown. (adapted with permission from Poggi *et al.*, 2005). **(D)** Photoreceptor somal translocation during retinogenesis has largely remained uncharacterised in terms of morphology, kinetics and directionality. **(E)** Presumptive somal translocation of cone photoreceptors in the developing mouse retina. Cone photoreceptors (and rod bipolar cells) were transgenically labelled in the *Ccdc136*^{GFP} transgenic mouse. Cone somata are found displaced within the ONL between P4 and P9 but are all lined up beneath the OLM at P14, indicative of somal translocation towards the OLM. (reproduced with permission from Smiley *et al.*, 2016). **(F)** Presumptive somal translocation of rod photoreceptors in the developing mouse retina. A P7 mouse retina was stained with toluidine blue, which gave photoreceptor nuclei a characteristically dark staining. Elongated photoreceptors (highlighted with red ellipses) were found in the OPL, morphologically looking like they transited back into the ONL. (reproduced with permission from Young, 1984).

Somal translocation involves nucleokinesis into a pre-existing neuronal process. Identifying the origins of this process is thus an interesting task, as a recently born neuronal precursor cell could either inherit it from its mother progenitor cell or extend a new process altogether. The apical process in contact with the ventricular surface is usually inherited by the neuronal daughter cell of a preceding progenitor cell division, at least in the developing zebrafish neural tube (Alexandre *et al.*, 2010). However, in many cases, it is the basal process that points in the direction of somal translocation. According to Alexandre *et al.* (2010), the basal process is exclusively inherited by the proliferative but not the neurogenic daughter cell. This is in contrast to what has been reported earlier in the E14 mouse cerebral cortex where the basal process is passed on to the neuronal precursor rather than being kept by the mitotic neural progenitor cell (Miyata *et al.*, 2001). A further study reported that, in the retina of embryonic day 17 (E17) mice, both RPCs or neuronal precursor cells can inherit the basal process following cell division (Saito *et al.*, 2003). It is thus possible that the inheritance of the basal process is context, tissue and/or cell type dependent and may have to be formed *de novo* by the neuronal precursor cell prior to somal translocation.

In the developing chick retina, retinal ganglion cells (RGCs) are the first class of neurons to emerge from neurogenic cell divisions at the apical surface and appear to completely lack processes just after their birth (McLoon and Barnes, 1989). In order to reach their target layer at the vitreal surface, post-mitotic RGC precursors first extend both apical and basal processes through the thickness of the epithelium before undergoing basally directed somal translocation (Figure 1.3.2C). The basal process effectively becomes the growing axon containing a terminal growth cone that enters the optic nerve, often even before the onset of nucleokinesis. As somal translocation and axon outgrowth proceed, the apical process is retracted, eventually yielding a differentiated RGC with mature stratal position (Prada *et al.*, 1981; Snow and Robson, 1994, 1995; Poggi *et al.*, 2005; Zolessi *et al.*, 2006). However, in contrast to somal translocation in the cortex, in RGC precursors the centrosome is never positioned ahead of the basally migrating nucleus, but instead remains at the apical-most tip of the cell even during apical process retraction (Zolessi *et al.*, 2006).

Bipolar cells are among the last retinal neurons to be born and their somata have to move from the apical surface into the (presumptive) INL (Vitorino *et al.*, 2009; Reese, 2011).

In mice, this basally directed somal translocation seems to be followed by a short apically directed somal translocation towards the apical limit of the INL, which is the desired bipolar cell position (Morgan *et al.*, 2006). The bipolar precursor cell retains both apical and basal neuroepithelial-like processes throughout somal translocation and these subsequently differentiate into dendrites and axons in the outer and inner plexiform layers respectively (Morest, 1970b; Morgan *et al.*, 2006). In the zebrafish retina, the generation of bipolar cells has been shown to adapt to the maturing retina: at early stages of retinogenesis, they are born through mitosis at the apical most portion of the retinal neuroepithelium (Weber et al., 2014). However, as the ONL consisting of a single layer of photoreceptors starts to emerge, thus preventing RPCs from accessing the apical margin of the retina, the location of bipolar cell birth shifts to the apical margin of the presumptive INL.

Post-mitotic cone photoreceptor precursor cells also seem to migrate to their final position within the retina. Most cone photoreceptor cells are born during early prenatal embryogenesis at the apical surface where they also reside in adults (Figure 1.3.2D & E). However, fixed tissue immunohistochemical analysis of the mouse retina revealed that cone somata become displaced to the entire outer nuclear layer (ONL) between P4-11 (Rich *et al.*, 1997; Smiley *et al.*, 2016). The reasons for this displacement or the mechanisms behind it are currently not well understood. However, this period temporally overlaps with the time window of rod genesis; it is thus possible that the cone somata are displaced by waves of new born rod cells, which vastly outnumber cones in the adult human and mouse retina. In order to return to the designated target location, the cone somata must presumably undergo active somal translocation back to the apical surface by P12. Circumstantial evidence from fixed tissues suggests that post-mitotic rod photoreceptors also somally translocate: their nuclei reside in the ONL in adults but can be found in ectopic positions in the OPL and INL during development (Figure 1.3.2D & F). This is perhaps due to process passive displacement or detachment from the apical surface (Spira *et al.*, 1984; Young, 1984). However, the elongated morphology of some ectopic photoreceptors was indicative of efforts to return to the ONL, almost as if pulled apically along their apical processes (Young, 1984). For both rod and cone photoreceptors, this apparent apically directed movement could perhaps serve the purpose of enriching them within the ONL or at the apical surface respectively.

A more recent study from our group has further investigated the migration of rod photoreceptor precursors in the developing mouse retina (Warre-Cornish, PhD thesis,

2013): within the first post-natal week, *Nrl.GFP*$^{+/+}$ mice, which express *GFP* specifically in post-mitotic rod cells, have been exposed to a BrdU pulse at P1 at the peak of rod genesis. Immunohistochemical analysis of fixed tissue revealed that the average distance of double labelled somata to the apical surface first increased from P2 to P3 and then decreased by P5 and P7. Thus, the somata of rod precursors appear to undergo a bi-directional migration away, and back towards, the apical surface of the developing neural retina, similar to cone photoreceptors. Importantly, when individual Nrl.GFP positive rod precursor cells in live explanted P0-7 retinae were imaged in real time, at least two different types of rod cell somal migration were characterised: stochastic and rapid apically directed (Warre-Cornish, PhD thesis, 2013). The latter is the obvious candidate to account for the reduction of the distance between rod precursor cell somata and the apical surface between P3 and P5/7. Although the mechanisms of this apical motility are currently unknown, the directionality and speed may be indicative of a cell-autonomous and active process (Nadarajah *et al.*, 2001; Franco *et al.*, 2011). Rod precursor cell nuclei frequently migrated stochastically, sometimes simultaneously becoming displaced in the basal direction. This basal movement may be a manifestation of passive displacement caused by neighbouring apically migrating cells (Cooper, 2013). However, the kinetics of this movement would also be in agreement with a mode of neuronal migration that has primarily been described in the developing cortex – glial-guided neuronal migration (Rakic, 1971a, 1971b, 1972). Notwithstanding the above, there are obvious gaps in our current understanding of how photoreceptors reach their target location within the ONL during development.

1.3.4. Multipolar migration

Neurons displaying multipolar migration lack a fixed cell polarity as they do not feature processes that are anchored to either surface of the neuroepithelium; rather they dynamically extend/retract multiple processes during their migration (Tabata and Nakajima, 2003; Huckfeldt et al., 2009). It is thus fundamentally different from IKNM and somal translocation (Randlett *et al.*, 2011a; Reese, 2011). During multipolar migration, the entire, usually multipolar, neuron migrates towards its target location, although this migration may be in a non-directed radial or tangential manner

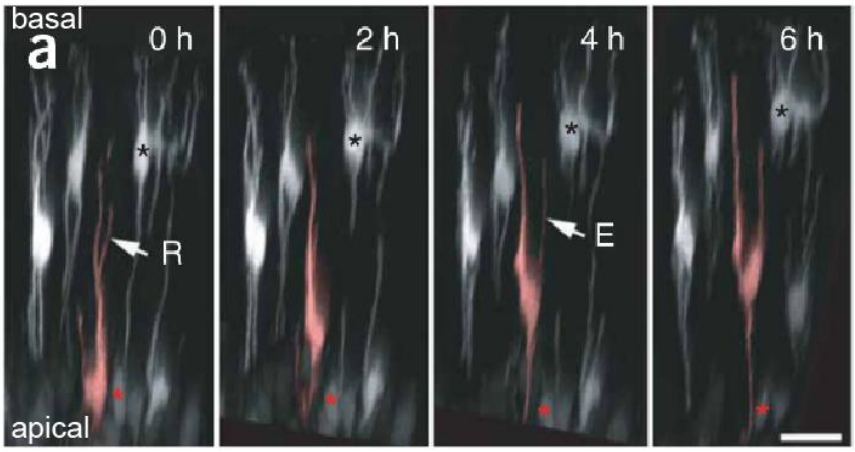

Figure 1.3.3 Time-lapse study of a horizontal progenitor/precursor cell displaying multipolar migration within an E17.5 mouse retina. This study used the G42 transgenic mouse line, in which horizontal cells express GFP. The image series shows the basal movement of a pseudo-coloured migratory horizontal cell relative to a stationary horizontal cell (black asterisk). The starting point of migration is indicated by a red asterisk. Multiple dynamic processes are extended from around the soma. R = retracting process, E = elongating process. Scale bar = 20 µm. (Adapted with permission from Huckfeldt *et al.*, 2009).

(Figure 1.3.3). It has been suggested that the existing processes probe the local environment in search for guidance cues in order to direct the migration (Prada *et al.*, 1987; Tabata and Nakajima, 2003; Godinho *et al.*, 2005). In the developing brain, a large number of multipolar neurons are observed in the subventricular and intermediate zones, which lie between the ventricular zone (where most neurons are born) and the developing cortical plate (where neurons usually migrate by glial-guided migration; see section 1.3.4) (Tabata and Nakajima, 2003). These multipolar neurons exhibit many changes of direction in their migratory paths within the subventricular/intermediate zones, sometimes even reversing towards the ventricular zone or exhibiting mitosis. Eventually, however, these neurons revert to a bipolar morphology as they enter the cortical plate whereupon they migrate only in the radial direction, guided by radial glia fibres (Noctor *et al.*, 2004).

Within the retina, only amacrine and horizontal precursor cells have been described to display multipolar migration (Randlett *et al.*, 2011a; Reese, 2011). Based on fixed tissue analyses of developing mouse and chick retinae, both post-mitotic amacrine and horizontal precursor cells that were in transit to their designated strata assumed a multipolar morphology, extending multiple short and seemingly dynamic processes without clear bias of process directionality (Hinds and Hinds, 1978, 1979; Prada *et al.*, 1987). However, before multipolar migration, both amacrine and horizontal cells undergo a period of bipolar migration, at least in the zebrafish (Chow et al., 2015). The notion that the short undirected processes extended by amacrine and horizontal precursor cells may help their migration towards the appropriate stratum in the INL was strengthened by more recent live imaging studies in mice and zebrafish (Godinho *et al.*, 2005; Huckfeldt *et al.*, 2009; Jusuf and Harris, 2009). Upon arrival, the existing processes become regionally stabilized in a sublamina specific manner, within the inner or outer plexiform layer, and establish the mature synaptic connectivity (Godinho *et al.*, 2005). Interestingly, horizontal precursor cells initially overshoot their target layer at the apical side of the INL and temporarily co-align with amacrine cells at the basal side of the INL of the chick retina. They then migrate retrogradely towards the apical surface to reach their final destination (Edqvist and Hallböök, 2004). Another peculiar event in horizontal cell genesis is that terminal symmetric cell division takes place towards the vitreal side rather than at the apical surface, and either directly before or after retrograde migration in the chick and zebrafish retina respectively (Godinho et al., 2007; Rompani and Cepko, 2008; Weber et al., 2014). This is an interesting exception to classical IKNM, according to which cell

division is restricted to the apical surface (see section 1.3.1). This is likely because the formation of the ONL prevents RPCs from reaching the apical margin of the neural retina, thus shifting mitosis to basal positions. Immunohistochemical detection of the late G2 / M-phase marker phospho-histone H3, horizontal cell reporters with *Prox1*, *Lim1* and *Isl1* as well as EdU labelling experiments in the chick revealed the following: a) some neuroblasts become committed to the horizontal cell lineage before terminal mitosis; b) S-phase takes place during vitreally directed migration in the terminal cell cycle of progenitor cells committed to the horizontal cell lineage; c) horizontal progenitor cells that have migrated vitreally temporarily wait in G2 before carrying out their terminal mitoses (Boije *et al.*, 2009)

1.3.5. Glial-guided migration

Most of our current understanding of glial-guided migration (also known as locomotion) comes from studies on cortical regions of higher mammalian species such as rodents or primates. This mode of migration features neuronal precursors that migrate along extended processes of glial cells (Figure 1.3.2A (III)). During development, the thickness of the neocortex markedly increases over time by the addition of neuronal cell layers in an "inside out" fashion. This means that the inner cortical layers of the adult cortex are populated by early born neurons during development, whereas the layers above are populated by subsequently born neurons, which thus need to migrate through previously established layers of neuropil (intermediate zone) and cell layers (cortical plate). At stages where the cortical plate is still thin, neuronal precursors reach their target strata by somally translocating out of the ventricular zone, the place of their birth, and into the forming cortical plate. However, as radialisation progresses, 80-90% of the neuronal precursors in the mammalian cortex utilise glial-guided migration aided by radial glia (Hatten, 1999). It should be mentioned that glial guidance is often followed by terminal somal translocation to the final apico-basal position within the cortex (Anton *et al.*, 1996; Nadarajah *et al.*, 2001). Radial glia have somata lying close to the ventricular surface and radial fibres spanning the entire width of the neuroepithelium. These are used by migrating neurons as rails to help them reach their increasingly distant designated layers (Nadarajah *et al.*, 2001). Radial glia and the neurons that migrate along them are in the majority of cases clonally related, since the proliferating radial glia divide to produce

daughter neurons thus establishing radial units in the developing cortex (Noctor *et al.*, 2001; Tamamaki *et al.*, 2001).

Glial-guided migration was first observed in fixed neocortical sections of foetal macaque monkeys (Rakic, 1971a, 1971b, 1972). In Rakic's studies it was identified that neuronal precursors that migrate along radial glia possess short leading and trailing processes devoid of contact to either apical or basal surface of the neuroepithelium (Figure 1.3.4A, 1.3.4B). The leading process contains several major cell organelles and a growth cone-like tip, which often wraps around the glial fibre and is larger in volume and length than the trailing process. The soma always remained towards the posterior of the cell and typically displayed a saltatory forward movement during glial-guided migration (Edmondson and Hatten, 1987; Anton *et al.*, 1996; Figure 1.3.4C, adapted from Franco *et al.*, 2011). Two events, which may be cyclically repeated, may contribute to the saltatory type of cell motility observed during glial-guided neuronal migration: first a cytoplasmic swelling is established within the leading process ahead of the nucleus that was proposed to contain a network of cytoskeletal fibres (Zolessi *et al.*, 2006); then the nucleus translocates into the pre-formed swelling, thus effectively shortening the leading process (reviewed, amongst others, in Marín *et al.*, 2006). The nucleus is typically rounded or elongated at the onset of stationary and migratory phases respectively (Schaar and Mcconnell, 2005; Umeshima *et al.*, 2007). Prior to the arrival of the nucleus, the swelling is occupied by several cell organelles such as the centrosome, the Golgi apparatus, mitochondria and the rough endoplasmatic reticulum. Due to the saltatory nature of glial-guided migration, the average velocity exhibited by the migrating neurons is relatively low (0.1-0.25 μm/min; Chen *et al.*, 2008; Franco *et al.*, 2011).

In contrast to somal translocation, the entire neuronal precursor cell (leading process, soma and trailing process) is mobile during glial-guided locomotion (Morest, 1970a; Domesick and Morest, 1977). Somal translocation on the other hand features a grappling hook-like leading process used by the nucleus to translocate into the leading process. Hence, leading process length gradually decreases during somal translocation but remains constant during glial-guided migration.

Like the cortex, the retina also contains a glial cell type (Müller glia) that spans the entire radial width of the tissue. In adult vertebrates, their nuclei locate to the INL and their long thick processes extend to the ILM and OLM. This has made them obvious candidates as mediators of glial-guided migration in the retina (Meller and Tetzlaff, 1976). Given that

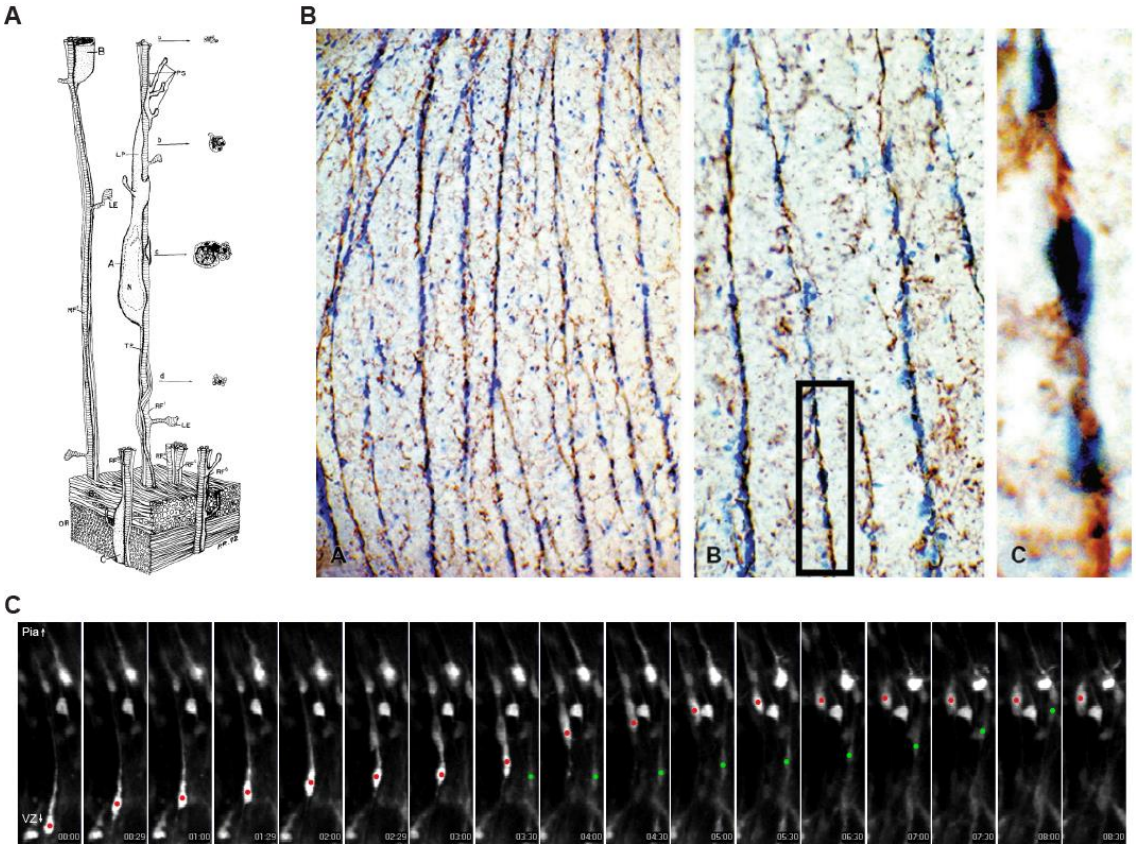

Figure 1.3.4 Glial-guided neuronal migration in the CNS. **(A)** Three-dimensional reconstruction of a neuron migrating along a radial glia fibre in the foetal macaque monkey neocortex. The reconstruction is based on electron micrographs of neocortical sections at the level of the intermediate zone. (reproduced with permission from Sidman and Rakic, 1973). **(B)** Migrating neurons in the 18-week-old human foetus visualised by toluidine blue stain (dark blue) are aligned along immunostained radial glia (brown). Radial glia were stained for GFAP (B-A) and vimentin (B-B and B-C). A high magnification view of the boxed region of interest in B-B is shown in B-C. (reproduced with permission from Rakic, 2003). **(C)** Glial- guided neuronal migration in the mouse neocortex. Neurons were genetically labelled by electroporation with a *Dcx-CRE-iGFP* construct. Two labelled neuronal precursor cells (indicated by red or green dots on soma) were observed to migrate radially along a glial guide (adapted with permission from Franco *et al.*, 2011).

Müller glia have a major organising and stabilising function in the retina, their suggested role as migrational conduits is a very viable possibility (Reichenbach *et al.*, 1993; Willbold *et al.*, 1995, 1996). However, definitive evidence for such a role of Müller glia is still lacking (Godinho and Link, 2012). Birth dating studies suggested that Müller glia are born later than most other retinal neurons, which some see as proof that this mode of migration is unrealistic, at least during earliest retinogenesis (Young, 1985; Rapaport *et al.*, 2004). This is in contrast to the radial glia in the cortex, which emerge before the first neurons are born during corticogenesis (Godinho and Link, 2012). As explained in section 1.2.5, however, mammalian Müller glia are in fact considered to be differentiated and quiescent RPCs – the retinal equivalent of cortical radial glia. For the purpose of describing the spectrum of cells spanning from RPCs to Müller glia, the unifying term neural retina spanning cell (NRSC) shall henceforth be used within this report. Taking into consideration the breath of radially spanning cells that the term 'NRSC' encompasses, scaffolds to support radial migration of neural retinal cells should be present at all times of retinal existence (Young, 1985; Wolburg *et al.*, 1991; Malicki, 2004; Godinho and Link, 2012).

Glial-guidance mechanisms could be utilised by neuronal and non-neuronal cells alike. There is a period of cell death that occurs naturally in the developing retina (see Vecino et al., 2004) that is accompanied by infiltration of microglia into the retinal tissue. The microglia are in close proximity to the vitreal end feet of NRSCs and also migrate radially through the quail retina (Marín-Teva *et al.*, 1999). Although microglia are not neuronal cells (they are derived from the mesoderm), this observation may suggest nonetheless that cells can in principle migrate along NRSCs. A different fixed tissue immunohistochemical study even suggests that photoreceptors born at the apical limit of the adult cichlid fish neural retina can migrate in the basal direction along Müller glia fibres (Mack *et al.*, 2003). The fact that within the adult mammalian retina multiple rod photoreceptors associate with a central Müller cell in what has been called a columnar unit is intriguing (Reichenbach *et al.*, 1993) and suggests that glial guided rod photoreceptor migration may occur at some point during development. Glial-guided neuronal migration in the retina has been brought up time and time again. However, definitive proof is still missing and, in most cases, the provided evidence has been circumstantial and never quite as convincing as in other regions of the CNS such as the cortex.

1.3.6. Tangential migration

In general, clonally related retinal cells are organised in a columnar fashion (Turner and Cepko, 1987; Holt *et al.*, 1988). This led to the general assumption that the lateral position of retinal neurons is set at their time of birth and that tangential migration is negligible (or only artefactual when observed). However, this view was challenged by observations made using the X-inactivation mosaic mouse, in which a reporter construct consisting of the *lacZ* transgene under control of a housekeeping promoter had integrated on the X-chromosome (Figure 1.3.5A). Due to random X-inactivation in females, 50 % of all progenitor cells inactivate the reporter, a trait that is inherited by all clonal daughter cells. While most labelled clonally related cells displayed a columnar organisation, some cells appeared short distances away from their clonal columns (Reese *et al.*, 1999). This phenomenon was attributed to tangential migration, which underlies the formation of adult retinal mosaics where cones, horizontal cells, amacrine cells and RGCs but not rods, bipolar cells or Müller glia become arranged in a regular pattern upon arrival in their respective strata (Reese *et al.*, 1995; reviewed by Reese and Galli-Resta, 2002).

According to simulation studies, the formation of regular mosaics seems to be a by-product of contact repulsion occurring exclusively between cells of the same type and the presence of an appropriate cell density (Eglen *et al.*, 2000). The establishment of an exclusion zone around each mosaic cell even allows later born neurons to become integrated into and dying neurons to be replaced within the mosaic. The end result is a cellular arrangement where the dendritic branches and somata of cells can display quite remarkable non-overlapping boundaries depending on the (sub-)type of retinal neuron. This phenomenon is also known as tiling (Figure 1.3.5B & 1.3.5C). Tiling has previously been observed in Drosophila eyes where homotypic repulsion between dendrites of neighbouring cells creates cellular mosaics before synaptic circuits are established (Ready *et al.*, 1976; Lipshutz *et al.*, 2001). More recently, the same principle was also found to apply to horizontal cells of the mouse retina (Huckfeldt *et al.*, 2009). Thus, even though tangential migration only covers distances much shorter than those covered by radial modes of migration, it is an essential and orchestrated part of retinogenesis. Despite its occurrence in the developing neural retina, tangential neuronal migration during development is more profound in other areas of the CNS, such as the brain. GABA-ergic inhibitory interneurons that eventually form neuronal circuits with the glutamatergic

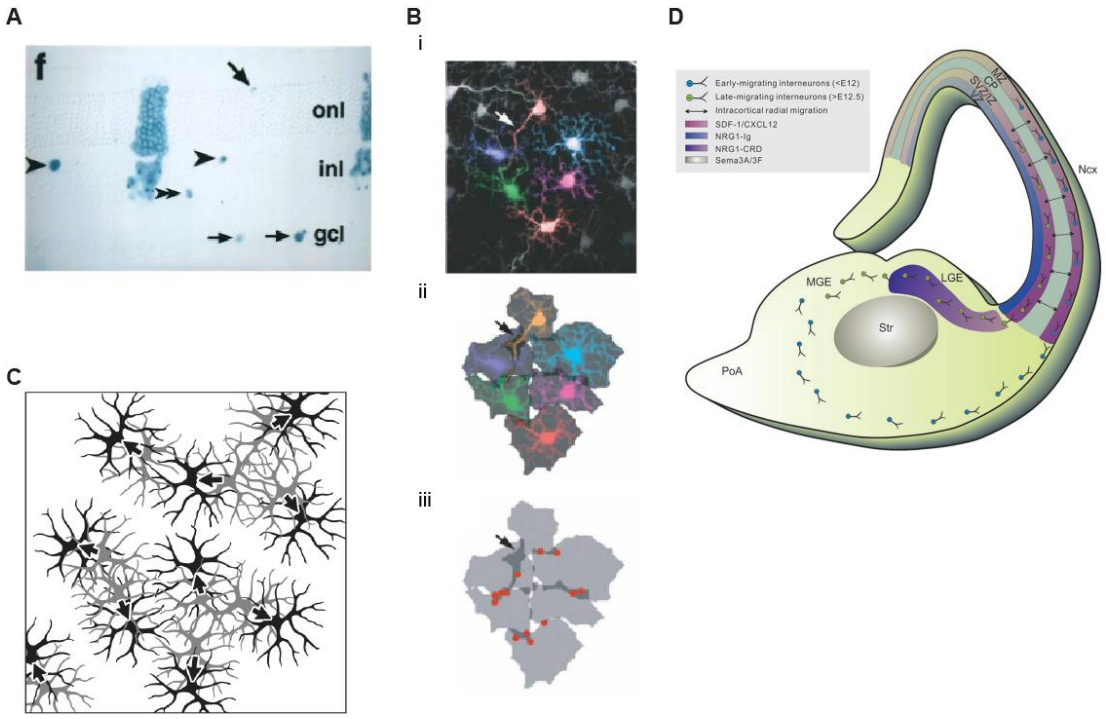

Figure 1.3.5 Tangential migration in the retina. **(A)** Clonally related *LacZ* expressing retinal cells in a X-inactivation chimeric mouse radial section where the transgenic *lacZ* is expressed from the X-chromosome in a small subset of cells. Clonal columns and laterally translated isolated cells (arrows and arrow heads) were observed. ONL = outer nuclear layer, INL = inner nuclear layer, GCL = ganglion cell layer. (reproduced with permission from Reese *et al.*, 1999). **(B)** Horizontal cells form regular mosaics with minimal overlap between cell territories. Transgenic mouse *G42* was used, which provides *GFP* expression in horizontal cells. i) shows the entire P2 horizontal cell field, ii) only shows high-lighted (pseudo-coloured) horizontal cells where each was assigned their own territory, iii) only shows the horizontal cell territories. Light grey regions show territories, medium grey regions indicate overlap between two horizontal cells and dark grey regions show overlap between three horizontal cells. Red dots indicate point of apposition. (reproduced with permission from Huckfeldt *et al.*, 2009). **(C)** Illustration of tangential dispersion between retinal neurons and their processes to establish a regular mosaic. Arrows indicate direction of migration (reproduced with permission from Reese, 2011). **(D)** Tangential migration of interneurons in the developing brain. Interneurons are born in the medial or lateral ganglionic eminence (MGE and LGE) and then undergo long distance migration for instance into the neocortex (Ncx) and striatum (Str) along defined routes (reproduced with permission from Sultan *et al.*, 2013).

neurons originate from the ganglionic eminence, located in the ventral subpallium (reviewed by Marín and Rubenstein, 2001). These interneurons reach their target destination such as the cortex, striatum or the hippocampus by long range glia-independent tangential migration, the direction of which is perpendicular to that of radial migration (Figure 1.3.5D). During this process, the entire neuron migrates and is ususally bi-/multipolar in shape with the leading process(es) pointing in the direction of migration and a typically short trailing process. Tangential neuronal migration continues to be detectable in the adult brain as adult born neurons originating from the subpallium migrate down the rostral migratory stream into the olfactory bulb, where they integrate into the local circuitry as inhibitory interneurons (Altman, 1969). However, in this special case, and unlike its developmental counterpart described in this section, glial tubes composed of astrocytes appear to guide neurons along the rostral migratory stream (reviewed by Sun *et al.*, 2010).

These descriptions demonstrate the complexity and variety of migratory modes used within the developing CNS. There are some obvious differences between the retina and other parts of the CNS with respect to tangential migration, for example. Nonetheless, there are many parralels, for example, with IKNM and somal translocation.

1.3.7. Mechanisms of neuronal migration

It shall be noted that the molecular mechanisms described throughout the following section may not be exclusive to one single mode of migration, even though they are only mentioned within the context of one mode. This applies especially to the mechanisms underlying nucleokinesis, centrosome movement and process/neurite dynamics.

1.3.7.1. Mechanisms of interkinetic nuclear migration

In IKNM, cell cycle progression and nucleokinesis along the apico-basal axis of the epithelial progenitor cell are intimately linked. In fact, this holds true to such large extent that nuclear migration and cell cycle progression can generally not be uncoupled by cell

cycle inhibitors: the use of the cell cycle inhibitors 5-azacytidine (G2- and M-phase arrest) and cyclophosphamide (S-phase arrest) showed that treated neuroepithelial nuclei accumulated in layers of the neuroepithelium that are typically associated with the respective cell cycle stages, at which these drugs were active (Ueno *et al.*, 2006). Furthermore, pharmacological inhibition of cyclin dependent kinase 1, which is essential for the cell cycle G2-/M-phase transition, abolished all rapid apical nuclear motility in the zebrafish neural retina (Leung *et al.*, 2011). Conversely, for reasons currently unknown, perturbing interkinetic movement did not block cell cycle progression and led instead to ectopic cell division events throughout the neuroepithelium (Murciano *et al.*, 2002; Gambello *et al.*, 2003; Carabalona *et al.*, 2016). Thus, nucleokinesis appears to be strongly dependent on cell cycle progression during IKNM, whereas cell cycle progression is not necessarily dependent on nucleokinesis.

The motile behaviour of neuronal epithelial progenitor cell nuclei during IKNM can in principle be a consequence of either active mechanisms or a consequence of passive displacement (reviewed by Cooper, 2013). Past studies have found that the mechanistic blockade of rapid apically-directed somal movements during G2-phase prevented the detection of any radial movements (Smart, 1972; Miyata, 2008; Norden *et al.*, 2009; Kosodo *et al.*, 2011; Leung *et al.*, 2011). These studies thus suggest that the basally directed stochastic somal movements observed during G1- and S-phase are passive in nature and due to rapid apical motility in neighbouring cells. The flux of apically migrating somata of G2-stage RPCs and the apical cell division of M-phase cells creates steric pressure at the apical limit of the neural retina, which is relieved by displacing the somata of other retinal cells in the basal direction (= passive displacement). However, as shall be addressed later in this section, this view is not completely uncontested.

The microtubule cytoskeleton:

Active mechanisms involved in nucleokinesis during IKNM have been shown to rely heavily on the cell cytoskeleton. Microtubule filaments are polarised macromolecules containing a relatively stable end (minus end) often located at MTOCs and a dynamically (de-)polymerising plus end where tubulin monomers are added or removed. Various regulatory factors affect the stability and dynamic behaviour of microtubule filaments. In addition, several motor proteins can transport cargo such as entire cell organelles along microtubule filaments in a highly direction-specific manner – either towards the plus or

the minus end. It is unsurprising, therefore, that microtubules and associated factors are important for nuclear migration in various contexts and in different species ranging from yeast to Drosophila flies and vertebrates (Baye and Link, 2008b; Kosodo *et al.*, 2011). Within neuroepithelial progenitor cells, the microtubule cytoskeleton is highly polarised: the minus end of microtubule filaments is located at the apical surface of the neural epithelium, from where filaments are extended basally to enwrap the nucleus in what is known as a perinuclear cage; the microtubule plus ends thus point in the basal direction past the nucleus (Tsai *et al.*, 2007; Norden *et al.*, 2009).

Evidence suggests that apical migration (towards the microtubule minus ends) of nuclei during G2 is an active process. The microtubule-associated and minus end-directed dynein motor protein complex, which has been shown to bind to nuclei as cargo, is thus an obvious candidate to power such apical migrations. Accordingly, RNA interference (RNAi) of the dynein I subunit *dync1h1* abolished rapid apical migration in neural progenitor cells of the rat neocortex (Tsai *et al.*, 2010). This finding is also complemented by experiments on LIS1, a co-factor of the dynein 1 complex, which regulates its activity and processivity during nuclear translocation: RNAi of the encoding gene *Pafah1b1* perturbed IKNM in rats and stalled mitotic neuroblasts at basal locations away from the apical surface of the neuroepithelium (Tsai *et al.*, 2005). Also associated with the dynein 1 motor complex are NDEL1 and DISC1. NDEL1 aids the interaction between dynein and LIS1 and enhances dynein activity (Shu *et al.*, 2004), whereas DISC1 aids NDEL1 to anchor the dynein complex to the centrosome (Ozeki *et al.*, 2003). Unsurprisingly, perturbations of proteins that anchor the cargo nucleus to the dynein I motor complex (in vertebrates, KASH domain proteins of the nesprin family and SUN domain proteins Sun1/2) have been found to disrupt IKNM in the retina (Yu *et al.*, 2011) and to cause basal displacement of RPC nuclei (Del Bene *et al.*, 2008). Further dynein I recruitment mechanisms for G2-associated apical nucleokinesis are in place, at least in the developing rat brain. Here, dynein I is first recruited to the nuclear pore protein RanBP2 to initiate apical nucleokinesis (Hu et al., 2013); subsequent dynein I recruitment to another nuclear pore protein, Nup133, closer to the apical margin then presumably guarantees the arrival of the neural progenitor cell nucleus at the apical margin of the neuroepithelium such that mitosis can be initiated.

Analogously to dynein I and apically directed nuclear migration, a member of the plus end directed kinesin motor protein family has been shown to drive basally directed nuclear migration. RNAi of the kinesin motor encoding gene *Kif1A* in neural progenitor

cells of the rat neocortex prevented basally directed nuclear motion during IKNM (Tsai et al., 2010; Carabalona et al., 2016). There thus appears to be a cell cycle dependent utilisation of dynein and kinesin motor system that underlies apically and basally directed IKNM in neural progenitor cells. Hence, and in contrast to the findings of another study, basally directed IKNM may not be an entirely passive phenomenon caused by the apical migration of neighbouring cells (Kosodo *et al.*, 2011).

Probably just as important as having intact microtubule associated motor proteins, co-factors and nuclear anchors, is the presence of functional microtubule rails. In a model proposed by Xie *et al.* (2007), the centrosome and microtubule associated proteins Cep120 and TACCs direct the polarised basally directed polymerisation of microtubule plus ends away from the apical centrosome to enwrap the basally located nucleus in a fork like perinuclear cage structure (Tanaka *et al.*, 2004). LOF of Cep120 and TACCs abolished the formation of long, basally directed microtubules required for motors such as dynein I to carry out minus end directed nuclear transport. As a result, nuclei remained at deep basal positions in the mouse neocortex. In a different study, RNAi experiments have shown that Tpx2 organises microtubules in the apical process of G2-phase neural progenitor cells in the mouse neocortex (Kosodo *et al.*, 2011). Following Tpx2 silencing, apical migration was perturbed. Doublecortin (DCX) is a further protein implicated in nucleokinesis by locating to and stabilizing the microtubule filaments between the centrosome and the nucleus (Tanaka *et al.*, 2004). Abnormalities with either of these proteins leads to defects of nuclear and/or centrosome migration, which ultimately results in impaired cortical lamination (Marín *et al.*, 2006).

The actin cytoskeleton:

Another type of cytoskeleton also known to be important for cell motility is the actin cytoskeleton (Fletcher and Mullins, 2010). Similar to microtubule filaments, the actin cytoskeleton is a polymer made up of globular actin monomers (G-actin). These can polymerise into various dynamic filamentous F-actin structures (branched, cross-linked, parallel and antiparallel) with fast and slow polymerisation rates observed at the plus and minus ends, respectively. In conjunction with the associated myosin motor protein complex, which displays motility along actin polymers, the actin cytoskeleton can generate or resist cellular forces (Blanchoin *et al.*, 2014). So-called stress fibres are found in non-muscle cells and consist primarily of antiparallel actin filaments cross-linked by

non-muscle myosin II (NMII) motor protein. In this configuration, NMII activity leads to actin cytoskeleton constriction and exertion of force that is sufficiently strong to drive nuclear motility in some contexts (e.g. Norden *et al.*, 2009).

Recent studies have demonstrated that activated NMII accumulates basal to the nuclei of RPCs in the zebrafish retina (Norden *et al.*, 2009; Leung *et al.*, 2011). These studies suggested that actomyosin constrictions are responsible for pushing nuclei in the apical direction. Indeed, no rapid apical migration events were detected when NMII was pharmacologically inhibited using Blebbistatin or BDM. Conversely, overexpression of the BDM insensitive and constitutively active NMII subunit myosin light chain MRLC2^{T18DS19D}-GFP partially rescued the BDM effect (Norden *et al.*, 2009). In contrast to the observation described above for IKNM in the cortex, Norden and colleagues found that microtubules and their regulators played only a minor role in IKNM, compared with actomyosin. In RPCs expressing a dominant negative dynactin-1 subunit (DNp150) and in cells with pharmacologically compromised or even completely abolished microtubule filaments, the main features of IKNM remained comparable to control values. Hence, these observations suggest that apically directed IKNM in the developing zebrafish retina is primarily driven by actomyosin constrictions. A role for actomyosin constriction forces has also been reported for basally directed IKNM in the developing mouse telencephalon (Schenk *et al.*, 2009). In the developing rat neocortex, on the other hand, NMII inhibition had no effect on either apically- or basally-directed motility, for reasons that are currently not well understood (Tsai *et al.*, 2010). This discrepancy notwithstanding, putative actin binding sites in addition to microtubule binding sites on the KASH domain protein Syne-2/Nesprin-2 could play an important role in linking the nucleus to the actin cytoskeleton in order to mediate actomyosin mediated nuclear movements (Baye and Link, 2008b).

How to reconcile the different IKNM mechanisms?

In this apparent jungle of active versus passive and actomyosin versus microtubule based nuclear IKNM motions, finding a mechanistic consensus is difficult. This challenge has been addressed in reviews by Lee and Norden (2013) and Kosodo (2012), summarised schematically in Figure 1.3.6. IKNM is far from having been exhaustively investigated across all different species, tissues and developmental stages. Quite likely, a complete, over-arching consensus does not exist. However, a potential pattern may be emerging

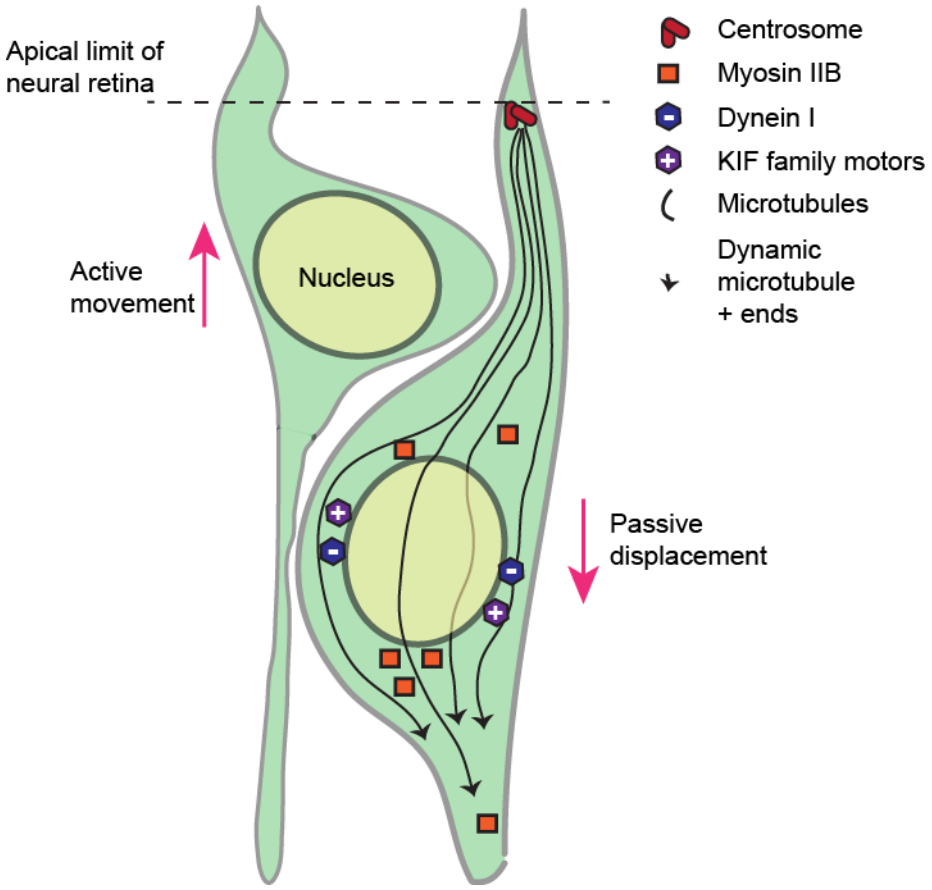

Figure 1.3.6 Schematic representation of the potential active or passive mechanisms involved in apico-basal nucleokinesis during IKNM.

from the available evidence, whereby actomyosin-driven IKNM could be an evolutionarily more ancient trait, whereas microtubule-based IKNM is found in more evolved species and CNS structures, such as the mammalian neocortex. In the zebrafish retinal neuroepithelium (Norden *et al.*, 2009; Leung *et al.*, 2011), the Drosophila imaginal disc and the anemone ectoderm (Meyer *et al.*, 2011), all of which feature actomyosin based IKNM, the nuclei of progenitor cells tend to display radial motility across the entire pseudostratified epithelium, which is typically less than 50 µm thick. These cells further display abundant cytoplasm within the relatively wide radial processes. Conversely, in the evolutionarily more recent mammalian neocortex, which features microtubule based IKNM, neural progenitor cells are much longer and thinner with only little cytoplasm within the radial processes (e.g. Miyata *et al.*, 2001). Although IKNM associated nuclear movements are restricted to the cell segment within the ventricular zone (100 µm), this is still considerably thicker than in the evolutionarily more ancient systems. Thus, different epithelial cell morphologies might favour different cytoskeleton-based nuclear motility mechanisms: short and wide cells may preferentially recruit the actomyosin system, whereas long and thin cells recruit microtubule based systems. Although purely conjecture at this time, it is possible that a mechanistic switch occurs from actomyosin to microtubule based, even within the same higher species, as it progresses from early to later developmental stages, for instance as the neural tube develops into the neocortex.

Whether microtubule or actin filament based, there are several regulatory kinases that participate in various signalling cascades that eventually converge onto the cytoskeleton and thus control IKNM (Baye and Link, 2008b). Two prominent examples are the kinases Cdk5 and FAK, which have been shown to regulate nucleokinesis. In migrating neurons, FAK stabilises the microtubules located between the nucleus and the centrosome. Through phosphorylation by Cdk5, S732-phophorylated FAK locally accumulates on microtubules between the nucleus and the centrosome (Xie *et al.*, 2003). By reorganising the microtubules in this region, Cdk5 and FAK may allow microtubule-based systems to pull the nucleus towards the centrosome or at least to locally loosen the microtubule fork such that actin constriction forces can push the nucleus towards the centrosome from behind (Tsai and Gleeson, 2005; Baye and Link, 2008b). For apical nucleokinesis in the developing rat brain, the previously mentioned, G2 phase-associated recruitment of dynein I to the nuclear pore proteins RanBP2 and Nup133 is regulated by Cdk1 (Baffet et al., 2015). Phosphorylation of RanBP2 by Cdk1 activates binding of the dynein I adapter protein BicD2 and hence also dynein I; Cdk1 also stimulates the export of the

adapter protein CENP-F from the nucleus, which enables dynein I to associate with Nup133. As well as regulating dynein I-/microtubule-dependent rapid apical nuclear migration during IKNM in the rat brain, Cdk1 also controls the acto-myosin-dependent rapid apical nuclear migration during IKNM in the zebrafish retina (Strzyz et al., 2015). This suggests that Cdk1 could be a universal regulator of G2 phase-associated apical nucleokinesis irrespective of species and the cytoskeletal machinery required for this movement.

Cell extrinsic factors and IKNM:

In addition to cell intrinsic events, IKNM is also regulated by extracellular factors. Ca^{2+} and purinergic signalling loops have been demonstrated to influence the timing and kinetics of mitotic events in the developing chick retina (Pearson *et al.*, 2002, 2004, 2005a). Spontaneous Ca^{2+} transients within the retinal pigment epithelium (RPE) led to the efflux of ATP from RPE cells via connexin 43 (Cx43) hemichannels. The released ATP could then act on RPCs by binding purinergic P2Y cell surface receptors, which in return acted as accelerators of mitosis via intracellular Ca^{2+} transients. Ca^{2+} transients within RPCs were often temporally coupled to interkinetic nuclear movements. Consistently, intracellular Ca^{2+} buffering was shown to slow interkinetic migration (Pearson *et al.*, 2005b). Neighbouring RPCs display junctional coupling via Cx43 channels such that Ca^{2+} transients and other signals can locally spread in order to couple and synchronise neighbouring RPCs during IKNM. Consistent with the above, LOF approaches to block Cx43 channel function or gap junction formation acted to slow interkinetic movement. Curiously however, blocking of unopposed Cx43 hemichannels also perturbed the rate of IKNM, which suggests that non-junctional Cx43 roles, such as signal release into the extracellular space or adhesive functions, could influence IKNM as well.

1.3.7.2. Mechanisms of somal translocation

As discussed in section 1.3.2, recently born neurons do not always inherit the leading process required for somal translocation from their mother progenitor cell. In such cases,

a leading process contacting structures in the target stratum has to be established *de novo* prior to the onset of nucleokinesis into the newly formed process. This is dependent on the signalling pathway triggered by the secreted molecule reelin – at least in the neocortex (Franco *et al.*, 2011). Mutations in the reelin signalling pathway can lead to the severe brain development disorders lissencephaly and cerebral hypoplasia (Hong *et al.*, 2000). Mice with mutations in reelin pathway components present with dysfunctional corticogenesis caused by the inability of later-born neocortical neurons to migrate past earlier-born neurons to establish the typical inside-out chronologic architecture of cortical projection neurons (Rice and Curran, 2001). This results in the inversion of the normal cortical architecture. In radially migrating neurons, reelin binds to the cell surface receptors VLDLR and ApoER2, which via the cytoplasmic adaptor protein Dab1 activate the Ras GTPase superfamily member Rap1. In turn, Rap1 regulates the cell surface levels of the cell adhesion molecule N-Cadherin (Rice and Curran, 2001; Jossin and Cooper, 2011). Franco *et al.* (2011) demonstrated that activation of the reelin pathway is required for glia-independent somal translocation but not for glial-guided neuronal migration. Specifically, reelin signalling stabilises the leading process required for the final somal translocation past earlier born neurons in an N-cadherin dependent manner. In addition to leading process stabilisation, the reelin pathway can potentially also influence the nucleokinesis aspect of somal translocation in a more direct manner: activated Dab1 has been shown to recruit the dynein I co-factor LIS1, which in turn may regulate dynein I dependent nucleokinesis along microtubules (towards the pial surface) in somally translocating neuronal precursor cells (Assadi *et al.*, 2003; Zhang *et al.*, 2007; Franco *et al.*, 2011).

Of course, nucleokinesis may be influenced by many factors besides dynein I. In principle, nucleokinesis during somal translocation may also be affected by all the factors that influence nucleokinesis during IKNM, and could be microtubule-based, actomyosin-based or others (see section 1.3.6.1). In addition, somal translocation could also be a more mechanical process, as suggested by Miyata and Ogawa (2007). Their findings show that somal motility in cortical neurons could at least partially be caused by a spring-like twisting of the leading process, the tension of which eventually pulls the soma towards the target site.

In the retina, several of the retinal neurons display somal translocation. RGCs are initially born without any processes (McLoon and Barnes, 1989). Thus, in order for them to somally translocate towards the vitreal surface of the neural retina, a basal process first

needs to be extended. For RGCs, process extension towards the vitreal surface is synonymous with growth cone guided axonal growth (Randlett *et al.*, 2011b), the general mechanisms of which have been reviewed elsewhere (O'Donnell *et al.*, 2009). Briefly, the neurite destined to become the axon establishes a highly motile growth cone at its tip, which serves to probe the local environment for chemotactic signals. Dynamic growth cone behaviour is achieved using actin filament based protrusions called filopodia and lamellipodia, which rapidly grow and retract; this is regulated by Rho GTPases that act on downstream regulatory factors of actin cytoskeleton dynamics (Causeret *et al.*, 2004; Marín *et al.*, 2006). Depending on the nature of the signal and the intracellular competence to react to them, the growth cone grows either towards or away from the source of the chemotactic stimulus by means of dynamic filopodia and lamellipodia. Growth cone advancements then need to be consolidated by the axon, which sends polymerising microtubule filaments to the core of the translocated growth cone. It is thus almost certain that the basal surface of the retinal neural epithelium is the source of a chemoattractant signal that attracts the ingrowth of RGC precursor axons (Halfter *et al.*, 2001). For rod and cone photoreceptors on the other hand, having a process that attaches to the apical surface of the neural retina is expected to be important especially for apically directed nuclear motility, while extension of a basal process might be required for basally directed nuclear motility. As is the case for RGCs, it seems likely that the apical process, and perhaps also the basal process, needs to be assembled *de novo* rather than being inherited from the mother progenitor cells (but see Saito *et al.*, 2003).

Little is presently known about the mechanisms regulating nucleokinesis in retinal neuronal precursor cells. In somally translocating RGCs, the centrosome is maintained at the apical most extent of the apical process (Zolessi *et al.*, 2006). Microtubule filaments emanating from the centrosome are thus likely oriented with their plus ends pointing towards the vitreal surface. This makes members of the plus end directed and microtubule associated kinesin family of motor proteins attractive candidates to mediate nucleokinesis in somally translocating RGCs. The microtubule filaments within the ONL portion of photoreceptors display a similar arrangement where the vast majority of plus ends point towards the vitreal surface and the segment region while the minus ends are located at the base of the connecting cilium where the centrosome resides (Troutt and Burnside, 1988). It may thus be speculated whether dynein and kinesin motors could be powering developmental nucleokinesis towards the minus end (apical direction) and the plus end (basal direction) respectively. In keeping with this speculation, perturbations of the

dynein I motor complex have resulted in abnormal, basal locations of photoreceptor nuclei in the Drosophila dynactin mutant (Whited *et al.*, 2004) as well as the zebrafish cytoplasmic dynein heavy chain 1 (*dync1h1*) mutant (Insinna *et al.*, 2010). In the former study, it was further shown that kinesin acts antagonistically to dynein since the photoreceptor location defect caused by dominant negative dynactin expression was counterbalanced by a reduction in kinesin heavy chain (*khc*) gene product. Genetic disruption of the nuclear anchor complex that binds to the microtubule motors (Sun domain containing Sun1/2 and KASH domain containing nesprins) displaced cone and rod nuclei to the basal edge of the ONL of the mouse retina, although the cone phenotype manifested more strongly (Yu *et al.*, 2011; Razafsky *et al.*, 2012). These studies thus suggest that microtubule associated motor proteins, by binding to the nucleus via nuclear anchor proteins, mediate nuclear motility in photoreceptors. The role of the actin cytoskeleton in photoreceptor precursor nucleokinesis is yet to be established. Push forces may be generated by actomyosin constrictions similar to somally translocating RGC precursors where F-actin has been shown to localise to the apical side of the nucleus (Zolessi *et al.*, 2006), which may contribute to pushing the nucleus towards the vitreal surface of the neural retina.

1.3.7.3. Mechanisms of multipolar migration

Recently born neurons destined to populate the cortical plate leave the ventricular zone with a bipolar cell morphology but transition to a multipolar shape upon entry into the subventricular/intermediate zone. Whether this change is cell autonomously driven or orchestrated by extracellular cues is yet to be determined (Cooper, 2014). What is known is that cyclin-dependent kinase 5 (Cdk5) becomes activated in post-mitotic neurons, leading to the stabilisation of p27, inhibition of the small GTPase RhoA and activation of cofilin, a well-known regulator of actin cytoskeleton dynamics and cell motility (Kawauchi et al., 2006b). *In vivo* RNAi of p27 during cortical development led to an accumulation of neuronal precursor cells in the intermediate zone, where these neurons appeared with either a rounded morphology (lower intermediate zone) or with a bipolar morphology (upper intermediate zone). This suggests that Cdk5 and p27 signalling regulate multipolar migration within the intermediate zone, as well as bipolar emigration from the intermediate zone into the cortical plate. Within the subventricular/intermediate

zone, multipolar migration occurs laterally as well as radially. The amount of lateral motility of multipolar neurons within the intermediate zone was shown to be dependent on signalling through ephrin (Efn) cell surface ligands that bind Eph cell surface receptor tyrosine kinases on other cells. This signalling can either occur in the forward (Efn → Eph) or reverse direction (Eph → Efn). EfnA to EphA forward signalling increases lateral multipolar motility (Torii *et al.*, 2009), whereas reverse signalling from EphBs to EfnB1inhibits lateral movement in the intermediate zone (Dimidschstein *et al.*, 2013).

Much less is known about the mechanisms governing the multipolar migration of amacrine and horizontal cells within the developing neural retina, since the majority of published studies focussed on the morphological aspects of multipolar migration (Godinho *et al.*, 2005; Huckfeldt *et al.*, 2009; Jusuf and Harris, 2009; Vitorino *et al.*, 2009). However, a recent study has reported the existence of a horizontal cell specific and cell autonomously acting transcription factor (Lim1) that instructs horizontal cell migration to the correct stratum within the developing retina (Liu *et al.*, 2000; Poché *et al.*, 2007). Conditional ablation of *Lim1* in Cre-Lox mice led to the ectopic localisation of horizontal cells to the amacrine cell layer concomitant with the adoption of an amacrine cell-like morphology but with retained expression of horizontal cell markers. With this important role in retinogenesis, Lim1 is the first identified retina-specific transcription factor required to target a specific neuronal subtype to its appropriate retinal stratum (Poché *et al.*, 2007). Further such transcription factors may exist for other retinal cells.

1.3.7.4. Mechanisms of glial-guided migration

As glial-guided migration in the retina still lacks definitive proof, most of our knowledge on underlying mechanisms comes from studies on cortical areas of the CNS. Glial-guided neurons possess dynamically extending/retracting leading and trailing processes. However, their motility and that of filopodia and lamellipodia that form along the entire neuronal surface is not coordinated with the saltatory movement of the nucleus. It thus seems unlikely that any potential pull or push forces generated from these processes result in movement of the nucleus (Edmondson and Hatten, 1987). Traction required for motility seems to originate from the contact interface between the neuronal soma and the

glial fibre surface immediately below. Ultrastructural analysis revealed that an interstitial junction is formed along this interface. Within the junction, fibrils, contiguous with cytoskeletal elements of both cells, extend between these cells (Gregory *et al.*, 1988). The release and reformation of this junction seems to be a major contributor to glial-guided migration in its typical saltatory fashion. Numerous cell surface and secreted factors may contribute to the interstitial junction. As such, homo- and/or heterophilic protein-protein interactions between the two cellular partners or between cell and junctional extracellular matrix components likely mediate cell-cell recognition, adhesion, transmembrane signalling and motility (Anton *et al.*, 1996).

ASTN1, a neuronal adhesion molecule, provides such a system for glial-guided neuronal migration (Fishell and Hatten, 1991; Zheng *et al.*, 1996). It is expressed on the surface of the leading process of neurons undergoing glial-guided migration, helping the neuron to attach to its glial guide. Consistent with this role, its expression is developmentally regulated in the mouse cerebellum and coincides with the period of granule cell migration. *Astn1* LOF prevented the adhesion between neuronal membranes and radial glia and slowed the velocity of glial-guided migration *in vitro* and *in vivo* (Fishell and Hatten, 1991; Adams *et al.*, 2002). In order for the neuron to glide along the glial fibre under normal circumstances, it loosens its ASTN1 mediated grip on the glial fibre by clathrin-mediated endocytosis of ASTN1 at the posterior of the cell, which in mice is promoted by ASTN2; as the cell progresses forward, ASTN1 is recycled and exocytosed at the front of the migrating neuron (Wilson *et al.*, 2010). Intracellular cell adhesion molecule trafficking might be a more generally utilised cellular migration strategy: the homophilic cell adhesion molecule N-cadherin is expressed on the cell surfaces of locomoting neurons as well as on radial glia fibres of mouse cerebral cortices (Kawauchi *et al.*, 2010). N-cadherin was in fact shown to be trafficked in locomoting neurons similarly to ASTN1 to help neurons progress along radial glia (Shikanai *et al.*, 2011).

Additionally contributing to the interstitial junction are gap junction proteins, which are known for forming solute permeable channels between neighbouring cells, on which they are expressed (Anton *et al.*, 1996). Acute knock down of *Gja3* (Cx43) and *Gjb2* (Cx26) as well as the conditional knock-out of *Gja3* impaired radial migration along glial fibres in the mouse neocortex (Elias *et al.*, 2007; Cina *et al.*, 2009). However, rather than the gap junction function, it appears to be the adhesive function of gap junction proteins that mediates glial-guided neuronal migration, since LOF experiments could be rescued by

overexpression of dominant negative connexins that lacked channel function but not connexins that lacked cell-cell adhesion function (Elias *et al.*, 2007).

The integrin family of cell surface receptors represents another class of proteins with known functions in cell-cell and cell-extracellular matrix (ECM) interactions (Schmid and Anton, 2003). Integrin receptors are usually composed of α and β subunits at a 1:1 stoichiometry. In the developing cortex, radial glia produce and align ECM molecules such as fibronectin along their radial fibres, which serve as ligands for integrin receptors expressed on radially migrating neurons (Schmid *et al.*, 2004; Stettler and Galileo, 2004). Mouse mutants of the various integrin α and β isoforms display distinct cortical lamination phenotypes (reviewed by Marín and Rubenstein, 2003; Marín *et al.*, 2010). Furthermore, blocking antibodies against α_3 and α_v integrin reduced the speed of neuronal migration along radial glia *in vitro* and even caused neurons to detach from their glial guides (Anton *et al.*, 1999). However, Cre recombinase mediated ablation of β_1 integrin (the binding partner to α_3 and α_v) specifically in migrating neurons did not result in any cell layering defects in the mouse cerebellum (Belvindrah *et al.*, 2007), while β_1 integrin ablation in radial glia did result in abnormal cortical layer formation. The implications of this study are twofold: 1) cortical layer formation defects observed in previous integrin LOF studies may have been due to dysfunctional radial glia rather than dysfunctional neuronal migration along radial glia; 2) integrins may be less important than, or only used redundantly with, other neuron-glia adhesion molecules (ASTN1/2, N-cadherin and connexins) *in vivo*, although their presence might be more important *in vitro* (Anton *et al.*, 1999).

Secreted factors may also influence glial-guided neuronal migration. Glial growth factor (GGF), which is produced by locomoting neurons themselves, and brain derived neurotrophic factor (BDNF) have both been demonstrated to stimulate neuronal migration along glial fibres in mouse and rat respectively (Rio *et al.*, 1997; Borghesani *et al.*, 2002). GGF also aids neuronal locomotion indirectly by acting on the radial glia, promoting their maintenance and elongation (Anton *et al.*, 1997).

All of the extracellular cues mentioned in this section must be integrated and relayed to the different cytoplasmic cytoskeleton components in order to produce neuronal locomotion along the glial fibre. Cx43, N-cadherin, integrin and ASTN1 either directly or indirectly link to the actin and/or microtubule cytoskeleton. Such interactions are important for processes such as leading process extension and trailing process retraction

as well as nucleokinesis (Trivedi and Solecki, 2011). The mechanisms behind leading process extension and nuclear motility during glial-guided migration are likely related to those observed during somal translocation and/or IKNM (see section 1.3.6.1 and 1.3.6.2). Neurons undergoing glial-guided migration display repeated cycles of initial centrosome advancements into the proximal part of the leading process establishing a local cytoplasmic dilation. This is followed by nucleokinesis into the same proximal portion of the leading process (Rivas and Hatten, 1995; Solecki *et al.*, 2004). The centrosome, as the principal MTOC, has a leading function in organising microtubules, which form parallel bundles towards the cell posterior that fasciculate around the nucleus in what is known as a perinuclear fork while also extending into the leading process (Rivas and Hatten, 1995; Xie *et al.*, 2003; Tsai and Gleeson, 2005; Tsai *et al.*, 2007). The centrosome and nucleus are thus coupled, which has led many to believe that microtubule pulling forces originating from the centrosome help the nucleus advance into the leading process towards the centrosome (Rivas and Hatten, 1995). However, the nucleus has been reported to migrate past the centrosome in studies on mouse and zebrafish neurons, which argues against the proposed pulling function of the centrosome (Umeshima *et al.*, 2007; Distel *et al.*, 2010). These results notwithstanding, the dynamic microtubule plus ends extending towards the nucleus need to be captured by the nucleus such that the nucleus can migrate along the microtubules towards the minus end/centrosome with the help of motor proteins. Hence, the previously mentioned nuclear envelope proteins Syne-2/Nesprin-2 and Sun1/2 as well as their binding partner the microtubule minus end directed dynein I motor complex are all required for pulling the nucleus forward during glial-guided neuronal migration (Xie *et al.*, 2003; Solecki *et al.*, 2004; Tsai and Gleeson, 2005; Tsai *et al.*, 2007; Marín *et al.*, 2010b; Valiente and Marín, 2010). Dynein I and its co-factor LIS1 appear to be just as important for centrosomal advancement as they are for nucleokinesis during glial-guided neuronal migration (Tsai *et al.*, 2007). It has been proposed that dynein I mediates nuclear (and centrosomal) advancements in two ways: 1) by accumulating in a cytoplasmic swelling in the leading process even before the arrival of the centrosome, dynein I acts to pull the entire posterior microtubule network with attached nucleus and centrosome forward; 2) dynein I is also found on the nuclear surface, which in combination with the tear drop shape of the nucleus indicates a dynein I mediated force pulling the nucleus into the leading process.

Interestingly, nucleokinesis, but not centrosomal advancement, may be a concerted effort by both microtubule and actomyosin based systems. Pharmacological inhibition and

RNAi of NMII abolished nucleokinesis in embryonic rat brain slices (Tsai *et al.*, 2007), probably because actomyosin constriction forces generated posterior to the nucleus usually push the nucleus into the leading process (Schaar and Mcconnell, 2005). A more recent *in vitro* study on cultured mouse cerebellar granule neurons has further shown that F-actin is actually a lot more abundant within the leading process, where a high actin turnover and anterograde actin flow were detected, compared to the trailing process (Solecki *et al.*, 2009). F-actin accumulated near the centrosome around the time of its forward translocation. Pharmacological inhibition of NMII prevented both centrosome and nuclear advancement into the leading process (note however, that NMII perturbation in the *in vivo* rat study by Tsai *et al.* (2007) only blocked nucleokinesis but not centrosome translocation). Due to this peculiar F-actin activity in the leading process it may be speculated whether actomyosin constrictions forces originating from the leading process may act to pull the centrosome and nucleus into the leading process. Further tests need to be carried out to fully understand the role of actomyosin constrictions in centrosomal and nuclear motility during glial-guided migration

1.3.7.5. Mechanisms of tangential migration

In the retina, tangential migration only covers short distances and is used by a subset of neurons (cone, horizontal, amacrine and retinal ganglion cells). Matching the shift in the plane of motility from radial to tangential, the centrosome and Golgi apparatus become positioned lateral to the nucleus according to ultrastructural data on horizontal cells in the mouse retina (Hinds and Hinds, 1979). The morphology of tangentially migrating neurons in the retina is actually more comparable to that of cortical neuronal precursor cells exhibiting multipolar migration in the intermediate zone of the developing brain. The mechanisms employed by these retinal cells might thus be similar to what was described in section 1.3.6.3 for cortical multipolar migration. As will be discussed towards the end of this section, tangentially migrating neurons within the cortex are morphologically, and perhaps also mechanistically, quite different from that.

Within the retina, tangential migration appears to be primarily used to arrange subsets of neurons into an equally spaced pattern (tiling). The level and stringency of tiling in the retina varies between neuronal (sub-)types. The ability of retinal neurons to recognise

other neurons of the same class and to convert this recognition into tangential migration is very likely due to cell surface identifiers (Fuerst and Burgess, 2009). In Drosophila, Dscam proteins, which are part of the immunoglobulin (Ig) superfamily of cell adhesion molecules, mediate cell recognition by homophilic self-avoidance. The signal generated by homophilic recognition is converted into repulsive cell motility by the Dscam cytoplasmic domain (Matthews *et al.*, 2007). In flies, the number of *Dscam* splice variants is immense and differences in spatio-temporal expression of individual isoforms contribute to the establishment of a precise architecture of cell body and neurite spacing as well as synaptic connectivity. As a simplified example, sister dendrites that express the same *Dscam* isoform will repulse each other, whereas dendrites from neighbouring neurons may not be subjected to the same repulsion unless they express the same isoform (Matthews *et al.*, 2007).

The *Dscam* orthologue in mice seems to play a similar role in self-repulsion within the retina: *Dscam*$^{-/-}$ mice display clumping of amacrine cell somata and hyperfascicularisation of amacrine cell neurites, which suggests perturbations in repulsive motility (Fuerst *et al.*, 2008). However, in contrast to the fly *Dscam* gene, mouse *Dscam* is not subject to extensive alternative splicing. Thus, related Ig-superfamily molecules such as DSCAML1, Sidekicks or other classes of cell adhesion molecules like the cadherins and protocadherins may contribute to the subclass-specific tiling of at least 25 different amacrine cells and 14 different RGC subclasses (Matthews *et al.*, 2007). Regardless of the nature of the cell identifier, the repulsive (or attractive) motion of neurites and the cell soma could potentially deploy actin and microtubule based mechanisms similar to those observed during IKNM, somal translocation and glial-guided migration. However, this still needs to be formally tested.

By comparison, the task of tangential migration within the developing vertebrate brain appears to occur on a much larger scale compared to the retina (reviewed by Marín and Rubenstein, 2001; Marín *et al.*, 2010; Guo and Anton, 2014). Interneurons are born in the ventricular zone of the ganglionic eminence of the subpallium but need to migrate tangentially to distant locations such as the cortex, hippocampus or striatum. Interneurons leave their place of birth via a combination of chemorepulsive and motogenic signals. Forward ephrin signalling (Efn → Eph) through EfnA5 ligand expressed in the ventricular zone of the ganglionic eminence of the mouse brain and EphA4 receptor strongly expressed in the generated interneurons results in chemorepulsive signalling within the interneurons, driving them out of the ventricular zone (Zimmer *et al.*, 2008).

Chemoattraction, for instance via Neurogenin 1, expressed in the striatum and its receptor ErbB4 expressed on striatal interneurons, mediates targeting to the striatum along specific migratory routes in mice (Villar-Cervino *et al.*, 2015), while ephrin and neuropilin/semaphorin signalling prevent mislocalisation to wrong brain areas (Marín *et al.*, 2001; Nóbrega-pereira *et al.*, 2008; Guo and Anton, 2014; Villar-Cervino *et al.*, 2015). Motogenic signalling cues involve the hepatocyte growth factor/scatter factor (HSF/SF) (Powell *et al.*, 2001), BDNF and NT4 (Polleux *et al.*, 2002) as well as GDNF (Pozas and Ibáñez, 2005).

Ultimately, the chemoattractant and -repulsive cues need to be translated into the cellular rearrangements that underlie cell motility. Since this is beyond the scope of this thesis, this issue will only be addressed briefly. Mechanistically, aspects of tangential migration have been likened to neuronal axon guidance. Tangentially migrating cells within the brain have a typical bipolar-like morphology. The leading process behaves similarly to an axonal growth cone in that side branches closest to chemoattractant cues become stabilised and dominant whereas side branches closest to chemorepulsive cues are demoted and retracted (Martini *et al.*, 2009). The rest of the cell follows into the direction of the stabilised leading process. This is iteratively repeated, allowing interneurons to accurately (re-)calibrate the exact route of their migration path. Mechanistically, dynamic growth cone behaviour is dependent on the actin and microtubule cytoskeletons, where the actin filament based filopodia and lamellipodia form dynamic protrusions/retractions in search for chemotaxis signals and where dynamic microtubule (de-)polymerisation within the base of the growth cone to consolidates such behaviour. Thus, regulators of actin and microtubule dynamics, turnover and stability are important in this process (see Kappeler *et al.*, 2006; Liu *et al.*, 2007; Dent *et al.*, 2011; Steinecke *et al.*, 2014; see also section 1.3.6.2). Finally, nucleokinesis is essential for interneuron tangential migration, as the nucleus will need to migrate into the consolidated leading process branch. Thus, non-surprisingly, factors that influence nucleokinesis in other modes of neuronal migration are also expected to be important for tangential migration (the reader is referred to earlier sections on nucleokinesis).

Elaborate long distance tangential migrations like the ones observed in the brain are probably not prevalent within the developing retina, but might exist on a shorter and smaller scale.

1.4. Transplantation

1.4.1. Overview

A significant proportion of how humans perceive their environment is through the detection of visual sensory information via the eyes, the details of which were summarised in section 1.1. Photoreceptors are the principal photon detection cells and as such, their role in the processing of visual stimuli is indispensable. Just how important these cells are to the visual process becomes especially apparent when their function is impaired or absent due to injury or disease. Traumatic injury to the eye, age related diseases and inherited retinal degeneration disease can lead to severe vision impairment or even blindness (Morrow *et al.*, 1998). Many of these scenarios affect the photoreceptors, causing them to deteriorate and degenerate. They can also directly affect cells that are closely associated with photoreceptors such as RPE cells, which in return leads to photoreceptor damage as a secondary effect. In the scenario of inherited retinal degeneration diseases, gene therapy is proving a promising therapeutic strategy (reviewed by Smith *et al.*, 2009). However, intervention by gene therapy is only feasible early in disease, when the majority of the targeted cells are still present. Once retinal cells have been lost, treatment options include replacement of the degenerated cells by transplantation of healthy cells or the introduction of electronic prosthetics.

Significant progress has been made in the field of retinal cell replacement therapy, but substantial optimisations are required in order for it to become a true viable treatment option for human retinal diseases.

1.4.2. Retinal disease

Various environmental factors, traumatic injury, as well as inherited genetic disorders have been reported to lead to retinal degeneration. In industrialised countries, age-related macular degeneration (AMD) is now the leading case of untreatable blindness within the demographic of people of 50+ years (National Eye Institute, 2015). It is worth noting,

however, that in addition to an age related disease aetiology, macular degeneration also occurs as a juvenile onset inherited form (Stargardt disease). The macula is essential to central and high acuity vision, which becomes impaired as its inhabitant photoreceptors (predominantly cone cells) degenerate. AMD is a multifactorial disease with many possible disease aetiologies and risk factors such as age, smoking and genetic predispositions. AMD may manifest as either dry or wet. Dry AMD affects the RPE underlying the macula in first instance before causing secondary photoreceptor degeneration within the macula (Curcio *et al.*, 1996; Jager *et al.*, 2015). Patients with wet AMD additionally present with choroidal neovascularisation. However, the newly formed blood vessels are relatively fragile and prone to become permeabilised, which may lead to the accumulation of subretinal fluid/haemorrhages and retinal detachment (Santos-Ferreira *et al.*, 2014).

As opposed to AMD, many retinal diseases are directly due to an underlying inherited genetic defect. There are presently over 200 genes that have been linked to inherited retinal degeneration diseases, the majority of which are specifically expressed in RPE/photoreceptors or are essential for their function (Hartong *et al.*, 2006; Daiger *et al.*, 2013). The encompassing term for these diseases is retinitis pigmentosa (RP); it is a group of inherited retinal dystrophies that triggers the loss of photoreceptors either directly or as a consequence of RPE damage. RP clinically manifests along a broad spectrum, depending on the nature of the mutation. Some patients become symptomatic during childhood, whereas other patients only develop symptoms in mid adulthood. The rate of disease progression is just as variable, with some patients becoming fully blind within a few years while other patients never reach that state in their life time (Hamel, 2006).

1.4.3. Therapeutic avenues for retinal diseases

The majority of established clinical therapies for retinal degeneration target the symptoms rather than the underlying cause of disease. Hence, most patients can currently only hope for a slowed disease progression (Hamel, 2006; Santos-Ferreira *et al.*, 2014). People suffering from AMD have been subjected to surgical removal of neovascularisations (Hawkins *et al.*, 2004) or even macular repositioning within the retina towards a less affected area (Mruthyunjaya *et al.*, 2004). Another method to combat neovascularisation

in wet AMD consists of administering blocking antibodies against the angiogenesis stimulatory secreted factor vascular endothelial growth factor A (VEGF-A): ranibizumab (brand name: Lucentis, Genentech) or bevacizumab (Avastin, Genentech). Both antibodies were shown to slow disease progression while preserving visual acuity in patients, while in some cases even reversing visual loss (Rosenfeld *et al.*, 2006; Spaide *et al.*, 2006; Tah *et al.*, 2015).

Gene therapy was shown to be effective in the treatment of Leber's congenital amaurosis (LCA), which comprises a family of inherited retinal dystrophies that impair the ability of RPE cells to convert all-trans retinyl esters to 11-cis-retinol (required for the continued function of the visual cycle and hence phototransduction). Patients present with poor vision at birth and complete loss of vision in early adulthood. The *RPE65* gene is specifically expressed in RPE cells and encodes retinoid isomerohydrolase. Subretinal delivery of non-mutant *RPE65* cDNA using adeno-associated virus (AAV) vectors resulted in sustained improvement in subjective and objective measurements of vision in phase I/II clinical trials (Bainbridge *et al.*, 2008; Maguire *et al.*, 2009). Initially, LCA is an RPE disease, which causes secondary degeneration of photoreceptors. Gene therapy options targeting other retinal dystrophies, which affect the photoreceptors in first instance are also at the clinical or pre-clinical stage. Ultimately however, gene therapy has its limits since it requires the presence of the target cells, which are to express the delivered gene at the correct levels (Bainbridge *et al.*, 2015) and in sufficient numbers (Smith *et al.*, 2009; Boye *et al.*, 2013). Gene therapy may thus only be suitable for early disease intervention at stages before marked degeneration has begun.

The mammalian retina lacks the capacity to regenerate photoreceptors, which shifts the focus to methods of replacement. In many cases of retinitis pigmentosa, the retinal/visual circuitry starting from the bipolar or ganglion cells are still present, even when photoreceptors have already died. This has been exploited in a handful of clinical trials carried out by different groups via the implantation of light detecting electrical devices, which generate and pass on electrical stimuli to the remaining retinal circuitry. Patients who received implants were able to produce implant-mediated visual perception in daily life (Stingl *et al.*, 2013), identify letters and short words (da Cruz *et al.*, 2013), and detect motion in visual tasks (Dorn *et al.*, 2013) with long lasting improvements observed sometimes years after the implantation (Ho *et al.*, 2015).

Another way to provide the remaining INL-GCL retinal circuitry with electrically encoded visual stimuli consists of transplanting healthy photoreceptors to replace those that have degenerated. Ideally, transplanted cells will integrate into the recipient retina, form synapses with bipolar/horizontal cells and attain mature photoreceptor morphology. All these aspects are required to detect photons, perform the visual cycle/phototransduction cascade and to pass on electrically encoded signals to the downstream interneurons. Several proof of concept *in vivo* studies carried out in the past decade have demonstrated that the sub-retinal transplantation (injected between recipient neural retina and RPE layer) of donor photoreceptor precursor cells leads to the presence of labelled cells within the retina of the recipient eye (MacLaren *et al.*, 2006; Bartsch *et al.*, 2008; Eberle *et al.*, 2011; Pearson *et al.*, 2012; Gonzalez-Cordero *et al.*, 2013; Homma *et al.*, 2013). These and other studies have shown that treating retinal degeneration diseases by transplanting photoreceptors may become a feasible therapeutic approach in the future (Lakowski *et al.*, 2010; Pearson *et al.*, 2012; Barber *et al.*, 2013).

However, besides solely transplanting a single cell type by injection of a cell suspension, the transplantation of full thickness retinal sheets has also produced promising outcomes. Donor retinal sheets derived from embryonic rats that were transplanted sub-retinally into adult recipient rats have been demonstrated to form outer segments towards the recipient RPE (Seiler and Aramant, 1998), establish synaptic connectivity and restore visual function in higher visual centres such as the superior colliculus of the S334ter-3 retinal degeneration rat (Seiler *et al.*, 2010). Furthermore, patients with retinitis pigmentosa and AMD had improved visual function and visual acuity following retinal sheet transplantation (Radtke *et al.*, 1999, 2008). The establishment of synaptic connectivity between graft retinal sheet and recipient retina is conceivably more complex in comparison to the transplantation of single-cell suspension photoreceptors alone. Both methodologies are promising in their own right. Whether one is to be favoured over the other in terms of visual outcome and transplant survival is yet to be determined in a systematic comparative study (Zarbin, 2016). It was speculated whether cell transplantation could be more effective when intervening during early retinal degeneration, whereas sheet transplants may be more beneficial at advanced stages (Assawachananont *et al.*, 2014). For the purpose of this present study, the exclusive focus shall henceforth be on the single-cell suspension based transplantation of photoreceptors.

1.4.4. The transplantation of donor derived photoreceptor cells

In an effort to replace lost photoreceptors in the degenerating retina, various different studies were carried out within the last decades. Some studies focused on the transplantation of neural stem cells (Banin *et al.*, 2006; McGill *et al.*, 2012) or retinal progenitor cells (Klassen *et al.*, 2004; Luo *et al.*, 2014). However, the beneficial results in these studies in terms of vision performance seemed to stem largely from a trophic effect originating from the transplanted stem cells that protected the pre-existing retinal architecture and slowed down degeneration.

In a series of publications, Gouras and colleagues for the first time performed transplantations using isolated post-natal photoreceptors derived from donor animals into the retinally dystrophic RCS rat or the C3H mouse at disease stages with virtually complete loss of endogenous photoreceptors (Gouras *et al.*, 1991a, 1991b, 1991c, 1992, 1994; Gouras and Tanabe, 2003). Combined, these studies demonstrated that the transplanted photoreceptors were able to extend outer segments towards the RPE and putative pre-synaptic structures towards cells of the INL. However, despite these findings it was still uncertain whether the transplanted photoreceptors could restore visual function in retinal degeneration animal models.

This changed with key proof of concept studies, which demonstrated functional recovery of vision in stationary night blind mice (*Gnat*$^{-/-}$) following sub-retinal transplantation of donor-derived rod photoreceptors (MacLaren & Pearson *et al.*, 2006; Pearson *et al.*, 2012). *Gnat*$^{-/-}$ mice possess a largely intact ONL, populated by non-functional rod photoreceptors, into which transplanted rod photoreceptors could integrate. In terms of morphology, the labelled rod photoreceptors had nuclei that were correctly located within the ONL, single outer processes that terminated in inner and outer segments pointing towards the RPE as well as single inner processes that terminated in the OPL as axon terminals. These harboured the pre-synaptic release machinery opposed by the post-synaptic dendrites of bipolar and horizontal cells (Figure 1.4.4) (MacLaren & Pearson *et al.*, 2006; Bartsch *et al.*, 2008; Lakowski *et al.*, 2010; Pearson *et al.*, 2012).

The improvement in visual function could be detected on several levels in these mice, which usually completely lack the rod transducin alpha subunit Gnat1 (*Gnat1*$^{-/-}$) and,

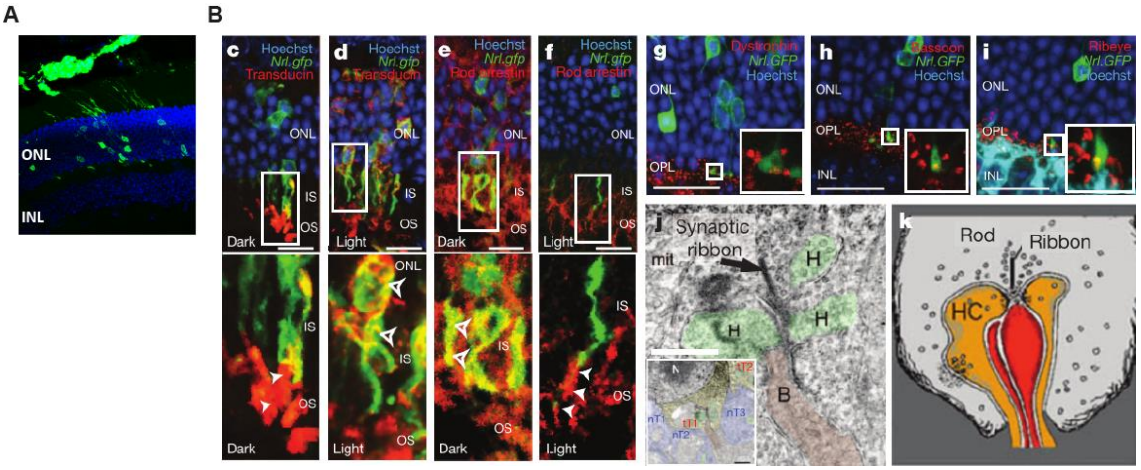

Figure 1.4.4 Transplanted rod photoreceptors functionally integrate into the host retina. Immunohistochemical and ultrastructural analysis of rod photoreceptor functional integration into the recipient retina. **(A)** Following transplantation of *Nrl.GFP*$^{+/+}$ rod photoreceptors into the mouse retina, several cells seem to have emigrated from the photoreceptor cell mass in the SRS and migrated into the ONL of the recipient neural retina. **(B)** Immunohistochemical evidence for the expression of functional components of the phototransduction cascade and pre-synaptic release machinery components (c-i) as well as ultrastructural evidence depicting the presence of the characteristic ribbon synapse involving an integrated rod photoreceptor (j); schematic of the rod ribbon triad-synapse (k), (reproduced with permission from Pearson *et al.*, 2012; Webvision; H. Kolb *et al.*, http://webvision.med.utah.edu/).

therefore, lack rod mediated (scotopic) vision: following transplantation and upon stimulation with scotopic light, GFP positive cells within the recipient retina were responsive to dim light (in contrast to neighbouring GFP negative cells), the scotopic light-evoked pupillary reflex was restored, RGCs as well as the visual cortex showed light dependent responses and lastly, the mice also demonstrated behaviour mediated by scotopic vision in a visual cue based water maze. Crucially, the degree of functional restoration increased with higher numbers of photoreceptor integration (MacLaren & Pearson *et al.*, 2006; Pearson *et al.*, 2012; Warre-Cornish *et al.*, 2014). However, only a small percentage of the sub-retinally transplanted cells were subsequently found within the recipient retina – typically around 5 % out of 200,000 injected cells. In the *Gnat1*$^{-/-}$ mouse, at least 25,000 integrated rod photoreceptor cells were required in order to improve scotopic vision in behavioural tests (Pearson *et al.*, 2012). Thus, although transplanted rod and cone photoreceptors can integrate into various retinal degeneration mouse models (Lakowski *et al.*, 2010; Barber *et al.*, 2013; Singh *et al.*, 2013; Ferreira *et al.*, 2015; Barnea-Cramer *et al.*, 2016; Neves *et al.*, 2016), it is essential to reliably increase current integration efficiencies before future clinical use.

In order to isolate donor derived rod photoreceptors, most of the studies listed in this section used the transgenic *Nrl.GFP*$^{+/+}$ mouse as a source, in which *GFP* expression is under transcriptional control of the neural retinal leucine zipper gene (*Nrl*) promoter, which becomes transcriptionally activated specifically in rod photoreceptors shortly after terminal mitosis (Akimoto *et al.*, 2006). As was collectively demonstrated by MacLaren & Pearson *et al.* (2006), Gust & Reh (2011) and Pearson *et al.* (2012), committed but not fully differentiated rod photoreceptor precursor cells isolated from P8 *Nrl.GFP*$^{+/+}$ donor mice by fluorescence associated cell sorting (FACS) exhibited the best integration capacity. On the other hand, rod photoreceptors derived from mice younger or older than P8 as well as RPCs or a mixture of post-natal retinal cells were significantly less likely to yield rod integration. Integration thus seems to rely on the fact that the donor cell population is specifically enriched for rod photoreceptors that are at the correct stage of development.

1.4.5. The transplantation of stem cell derived photoreceptor cells

As promising as the pre-clinical studies using perinatal, donor-derived rod photoreceptor cells may be, this particular source of cells only holds limited potential for future clinical use in humans. This is because humans reach a developmental stage equivalent to that of the early post-natal donor mouse within the second trimester (Pearson, 2014), which thus imposes significant ethical and logistical barriers.

Stem cells represent a renewable source of readily obtainable photoreceptors that could eliminate the dependence on donor-derived material. Pluripotent embryonic stem cells (ESCs) as well as induced pluripotent stem cells (iPSCs) (Takahashi and Yamanaka, 2006) can be maintained in a mitotic stem cell state or driven to differentiate into virtually any cell type, as was pioneered for telencephalic (neuronal) specification by Watanabe *et al.* (2005). Neural retinal precursor specification was achieved in a similar manner by inhibiting the Wnt and nodal signalling pathways in combination with activin and serum treatment (Ikeda *et al.*, 2005). These neural retinal precursor cells can be further pushed down the photoreceptor lineage by the addition of a cocktail of soluble factors (e.g. fibroblast growth factor, sonic hedgehog, retinoic acid and taurine) as well as by pharmacological inhibition of the Notch signalling (Osakada *et al.*, 2008, 2009; Meyer *et al.*, 2009; Lamba *et al.*, 2010).

However, only after the 2D aggregate culture system was upgraded to a 3D differentiation protocol could stem cells self-aggregate into retinal neuroepithelium optic cup structures that more closely resembled *in vivo* retinogenesis (Eiraku *et al.*, 2011). In contrast to the 2D version, this novel 3D optic cup protocol led to the production of transplantation-competent rod photoreceptors (Gonzalez-Cordero *et al.*, 2013; Decembrini *et al.*, 2014). However, the integration efficiency was markedly lower compared with that of donor mouse derived rod cells (~ 10,000 vs. < 1,000 GFP positive cells per eye out of 200,000 transplanted cells). Future studies will need to improve this efficiency in order for stem cell derived photoreceptors transplantation to become a clinically viable option. Furthermore, iPSCs may eventually have to replace ESCs in order to circumvent the ethical and logistic concerns associated with obtaining ESCs.

1.4.6. Potential mechanisms involved in the integration and migration of transplanted rod photoreceptor cells

Photoreceptor migration in the interphotoreceptor matrix:

Despite the advancements of pre-clinical photoreceptor cell replacement therapy, there is presently no publicly known concept of how transplanted photoreceptors, which were injected into the sub-retinal space, migrate out of the injection cell mass and towards the recipient retina. Sub-retinally transplanted photoreceptors have to navigate through the interphotoreceptor matrix (IPM, the space between the OLM and the RPE layer populated by the inner/outer segments of photoreceptors and RPE processes). It is decorated with high molecular weight hyaluronic acid and chondroitin sulphate proteoglycans that likely exert an inhibitory effect on photoreceptor integration (Hollyfield, 1999; Singhal *et al.*, 2008).

The sub-retinal space, IPM as well as the neural retina itself are rich in further membrane bound and diffusible factors, which may have a chemotactic, cell adhesive or cell repulsive effect on transplanted photoreceptors (Unachukwu *et al.*, 2016). Grafted donor photoreceptors themselves may express cognate migratory, adhesive or repulsive cell surface receptors. However, there are presently no published studies that have investigated the role of chemotactic signalling and cell-adhesion within the context of photoreceptor transplantation. Interestingly though, retinal detachment, which occurs as a by-product of sub-retinal injection of the photoreceptor cell suspension, has been demonstrated to result in increased expression of *Cdh2* (encoding the homophilic cell adhesion molecule N-cadherin) at the level of the OLM, interphotoreceptor matrix and RPE in the rat eye (Chen and Ma, 2007). Although the physiological function of this upregulation is likely the promotion of neural retinal reattachment to the RPE, *Cdh2* is also well known for its role in neuronal migration (see section 1.3). The modulation of *Cdh2* expression levels or function within the sub-retinal space could crucially impact upon photoreceptor integration efficiency in a similar way as the regulation of *Cdh2* expression levels affects the kinetics of glial-guided neuronal migration (Kawauchi *et al.*, 2010; Shikanai *et al.*, 2011, see also section 1.3.6.4).

Whatever the nature of the chemotactic and cell-adhesion/-repulsion signals may be, they then need to be translated into cytoskeletal and nucleokinetic activities intrinsic to the

photoreceptors in order to result in their migration. Thus, similar actin or microtubule filament based mechanisms may be utilised in photoreceptors that migrate following transplantation and motile photoreceptors in the developing retina. The reader is thus referred to section 1.3.6 for a description of cytoskeletal mechanisms involved in neuronal migration.

Photoreceptor penetration through the OLM:

Prior to reaching the host neural retina, sub-retinally transplanted photoreceptors need to penetrate through the OLM. The OLM consists of the apical microvilli of Müller glia as well as their apical end feet, which are interconnected with each other and the apical processes of photoreceptors via tight junctions. It thus presents another barrier to integration. Indeed, the disruption or removal of IPM and OLM components has led to modest increases in the number of integrated cells in mouse studies (West *et al.*, 2008; Pearson *et al.*, 2010; Barber *et al.*, 2013). It has furthermore been shown that these factors can be subject to glial cell hyper- or hypotrophy, the extent of which was variable between different retinal dystrophies (Barber *et al.*, 2013; Hippert *et al.*, 2015). Accordingly, the rod photoreceptor transplantation efficiency following sub-retinal transplantation varied markedly between different retinal disease models. Similar findings have been reported in the laser injured eye, where an improved transplantation outcome was correlated increased metalloproteinase 2 and 9, as well as reduced neurocan proteoglycan, expression, each of which may result in the reduction of barriers inhibitory to integration (Jiang *et al.*, 2010).

Photoreceptor migration within the neural retina:

GFP positive rod photoreceptors found within the recipient retina following transplantation can be found within the entire radial thickness of the ONL (MacLaren & Pearson *et al.*, 2006). This implies that once the cells have penetrated through the OLM they may continue their migration along a radial trajectory to reach their final position within the ONL. An intriguing parallel can be drawn to the cichlid fish. In that species, and in contrast to mammals, retinal neurogenesis is observed even in adulthood. New rod photoreceptors are born at the apical edge of the adult cichlid fish neural retina and then migrate radially in the basal direction and were further in direct proximity to Müller glia

processes (Mack *et al.*, 2003). Upon reaching the OPL, this preferential juxtaposition was lost. Although this study is based on fixed tissue analysis, which has its obvious limitations when investigations cell motility, it arguably still presents one of the strongest pieces of evidence for retinal glial-guided neuronal migration in the published literature.

More recent unpublished works from within the group further corroborate the above finding: in mouse transplantation studies, integrated GFP positive rod photoreceptors were often radially aligned with apical Müller glia fibres within the ONL (Warre-Cornish, PhD thesis, 2013; see Figure 1.4.6). Based on the analysis of many GFP positive cells, this association was significantly closer than would be predicted from a completely random integration within the lateral dimension of the retina. Since this study is also based on fixed tissue analysis, future experiments will need to demonstrate a similar outcome using time-lapse live imaging. As a starting point, Warre-Cornish further performed *in vitro* studies of freshly isolated rod photoreceptor cells, which were co-cultured on previously plated, morphologically elongated Müller glia. The rod cells not only seemed to preferentially associate with Müller glia, they also exhibited elongated somata. Importantly, time-lapse recordings showed that these rod photoreceptors migrated along Müller glia, whereas they remained stationary when co-cultured with RGCs. Thus, although *in vivo/ex vivo* retinal time-lapse live imaging experiments will be required to prove the existence of glial-guided photoreceptor migration following transplantation, the *in vitro* co-culture system may provide a simpler option to study the molecules and mechanisms that are potentially involved.

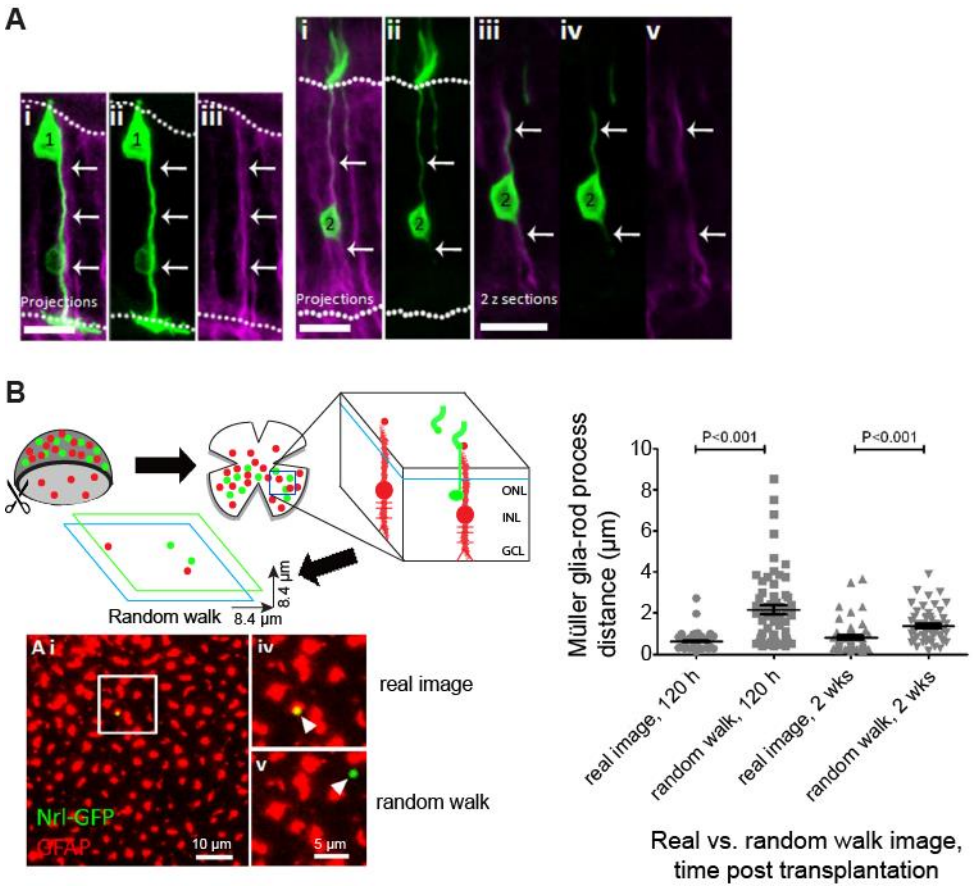

Figure 1.4.6 Transplanted and integrated rod photoreceptors are often closely aligned with Müller glia. **(A)** Cryo-sectioned and confocal imaged mouse eyes that had received sub-retinal rod photoreceptor transplants (Nrl.GFP positive cells) frequently displayed integrated cells juxtaposed to Müller glia (GFAP immuno-staining; magenta). **(B)** Nearest neighbour *in silico* assessment of proximity between integrated rod photoreceptors (GFP positive) and recipient Müller glia (GFAP positive; red). As depicted in the schematic, retinae of transplanted eyes were flat mounted and imaged by confocal microscopy. Green and red channels were then translated in the *xy* dimension relative to each other (random walk) and the distance between rod photoreceptor outer processes and nearest Müller glia fibres were measured and compared to the real image. (Adapted with permission from Warre-Cornish, PhD Thesis, 2013)

AIMS AND OBJECTIVES

The retina is a highly organised and stratified neuronal tissue, within which various retinal neurons and glia are connected and in communication with each other. Neurons and glia assume defined radial and/or lateral positions within the retina and form precise neuronal networks, both of which are required for correct visual function. In the adult retina, rod photoreceptors are exclusively located within the outer nuclear layer (ONL), the apical-most stratum of the neural retina. Like other retinal neurons, rod cells are born in the ventricular zone at the apical edge of the developing neural retina. Since this already places them in the (presumptive) ONL, their target stratum, there appeared to be little need for rod cells to be extensively motile. However, previous studies have provided strong indications that rod photoreceptors are migratory during retinogenesis (Young, 1984; Warre-Cornish, PhD thesis, 2013). Presumably, this rod motility would be linked to their eventual enrichment within the ONL as opposed to ectopic locations in other layers of the neural retina. However, such a connection would need to be demonstrated first.

One of the primary research goals was, thus, to provide a detailed characterisation of the migratory behaviour exhibited by rod photoreceptors during retinogenesis. Within this primary goal, several key aims were defined:

- To provide a detailed characterisation of the kinetics of developmental rod somal motility and to compare and contrast rod motility with known modes of neuronal motility.
- To identify the developmental time window, during which rod photoreceptors are motile.
- To elucidate the mechanisms driving developmental rod photoreceptor motility, be they cell-intrinsic or dependent on cell-cell interactions. Special attention will be on establishing whether rod migration could be subject to guidance by neural retina spanning cells (NRSCs).
- Given the successful mechanistic characterisation of developmental rod photoreceptor motility, to propose a hypothesis as to why rod cells migrate during retinogenesis.

The other primary research goal was concerned with rod photoreceptor transplantation in cell replacement therapy – a method that holds the potential to be put into clinical use to combat the otherwise irreversible loss of photoreceptors suffered by patients of retinitis pigmentosa. Several studies have shown that sub-retinally transplanted rod cells can apparently migrate into the host retina and contribute to improved vision (MacLaren *et al.*, 2006; Bartsch *et al.*, 2008; Eberle *et al.*, 2011; Pearson *et al.*, 2012; Gonzalez-Cordero *et al.*, 2013; Homma *et al.*, 2013). The degree to which vision was functionally restored in these studies depended critically on the integration efficiency. It is proposed that increased integration efficiencies can be achieved via an increased mechanistic understanding of rod migration and integration. To deepen our knowledge of these processes, the following key aims were thus formulated:

- To capture the migration/integration of transplanted rod photoreceptors into the recipient retina in real time.
- To test whether transplanted rod photoreceptors migrate and integrate into the recipient retina with the help of Müller glia guidance, as proposed by Warre-Cornish (PhD thesis, 2013)

CHAPTER II. MATERIALS AND METHODS

2.1. Methods of molecular biology

2.1.1. General cloning techniques

2.1.1.1. Polymerase chain reaction

Polymerase chain reactions (PCR) for cloning experiments were carried out using the Expand^{TM} High Fidelity PCR System (Roche, Switzerland) according to the manufacturer's instructions. Reactions mixes were prepared on ice as summarised in Table 2.1.1:

Reagent	Stock concentration	Volume (µl)	Final concentration
Deoxyribonucleotide mix	10 mM (each NTP)	1	200 µM (each NTP)
Forward primer	10 µM	1.5	300 nM
Reverse primer	10 µM	1.5	300 nM
DNA template	Variable	Variable	0.1 – 15 ng / reaction
Expand High Fidelity buffer (+ $MgCl_2$)	10 x	5	1 x
Expand High Fidelity enzyme mix	3.5 U/µl	0.75	2.6 U/reaction
ddH_2O	-	Added up to 50 µl	-
Final volume		50 µl	

Table 2.1.1 PCR reaction mixes for high fidelity amplification as per the manufacturer's instructions (Expand^{TM} High Fidelity PCR System, Roche, Switzerland).

Reaction mixes were then placed into a Touchgene thermal cycler (Techne, USA) set to perform the following PRC program (Table 2.1.2):

PCR step	Temperature (°C)	Duration	
Initial denaturation	94	2 min	
Denaturation	94	15 sec	10 x
Annealing	Variable	30 sec	
Extension	72	Variable	
Denaturation	94	15 sec	20 x
Annealing	Variable	30 sec	
Extension	72	Variable (+ Δ5s for each cycle)	
Final extension	72	7 min	
Final hold	4	∞	

Table 2.1.2 Thermal cycler settings for PCR amplifications performed using the Expand^{TM} High Fidelity PCR System (Roche, Switzerland). The primer-template annealing temperature was chosen according to recommendations from SnapGene software (GSL Biotech SSL, USA) based on the nucleotide sequences of primer and template DNA strand. The extension duration was set to 1 minute per 1000 bp.

Following completion of the PCR, the amplified DNA was purified using the QIAquick PCR Purification Kit (Qiagen, Germany) according to the manufacturer's instructions.

2.1.1.2. Restriction enzyme digestion

Plasmid DNA or PCR amplified DNA was digested with appropriate restriction enzymes (New England Biolabs, USA or Promega, USA) in designated restriction enzyme buffer mixes according to the manufacturer's instructions. Digestion conditions (temperature and duration) were chosen as per the manufacturer's recommendation (usually 37 °C, 1 hour).

2.1.1.3. DNA agarose gel electrophoresis

Following PCR reaction and/or restriction enzyme digestion, DNA fragments were electrophoresed on 1-2 % (w/v) agarose gels in 0.5 x TBE or 1 x TAE buffer, where the agarose concentration was chosen in order to achieve maximum resolution around the desired band sizes. For the visualisation of DNA bands, 5µl SafeView (NBS biologicals) was added per 100 ml of agarose gel. DNA samples were loaded onto the gel following addition of Blue/Orange Loading dye, 6x (Promega, USA). 1kb or 100bp ladders (Promega, USA) were loaded next to the DNA samples in order to provide DNA band size reference markers. A voltage of 180 V was applied to achieve DNA band separation according to the length of the DNA molecules. Following electrophoresis, agarose gels were photographed on an ultraviolet transilluminator.

2.1.1.4. DNA extraction and purification

For preparative gels, DNA fragments of desired size were excised from agarose gels using sharp blades and the DNA was gel purified using QIAquick™ Gel Extraction Kit (Qiagen, Germany) according to the manufacturer's instructions. The concentration and quality of the extracted DNA was assessed by photospectroscopy using a Nanodop® ND-1000 Spectrophotometer (Labtech Int., UK).

2.1.1.5. DNA cloning ligations

DNA fragments were ligated using T4 DNA ligase (Promega, USA) according to the manufacturer's instructions. Plasmid backbone and DNA insert were added to the ligation mix at a molar ratio of 1:1, 1:3 or 3:1, depending on the size of the nucleic acids, in a final volume of 10 µl. The ligation reaction was allowed to proceed at 25 °C for 3 hours or at 16 °C overnight.

2.1.1.6. Transformation and recovery of plasmid DNA

For the recovery of ligated plasmids and to evaluate whether the ligation was successful, Alpha-Select Gold Efficiency competent *Escherichia coli* cells (Bioline, USA) were transformed with the ligation reaction according to the manufacturer's instructions. Briefly, cells were thawed on ice for 5 minutes, upon which the ligation reaction was added to the thawed bacteria. The transformation mix was then incubated for 15-30 minutes on ice and subsequently heat shock treated at 42 °C for 45 seconds. Bacteria were allowed to recover on ice for 2 minutes. Transformants were usually selected by antibiotic resistance as the plasmid backbones utilised in the ligation step typically harboured either the Ampicillin or Kanamycin resistance gene. This allows bacteria carrying the plasmid to grow in presence of the antibiotics ampicillin or kanamycin. Following the 2 minute recovery period on ice, 150 µl Super Optimal Broth with Catabolite repression (S.O.C.) medium (ThermoFischer Scientific, USA) was added to the transformation mix. To allow the build-up of the antibiotic resistance gene product, the bacteria were incubated for 1 hour at 37 °C, 225 rpm. After that, the bacteria were spread on previously made selective LB agar plates: 15 g/l bacteriological Agar (Sigma, USA) and 25 g/l LB (Millipore, USA) autoclaved in water with either 100 µg/ml ampicillin or 50 µg/ml kanamycin. Plates were incubated overnight at 37 °C to selectively permit the growth of plasmid harbouring bacteria.

For plasmid DNA production, LB medium, 25 g/l LB (Millipore, USA) autoclaved in water, with either 100 µg/ml ampicillin or 50 µg/ml kanamycin was inoculated with individual bacterial colonies from the LB agar plates and incubated overnight at 37 °C to allow bacterial growth and plasmid replication to occur. For small scale and large scale plasmid production, inoculations were performed with 5 ml and 500-1000 ml LB medium respectively. Plasmid was isolated and purified using GenElute^{TM} Plasmid Miniprep Kit (Sigma) and Qiagen Plasmid Mega Kit (Qiagen, Germany) for small and large scale bacterial cultures respectively. Plasmid DNA purity and yield were determined on a Nanodrop ND-1000 spectrophotometer (Thermo Scientific, USA).

2.1.1.7. Plasmid DNA verification

For the verification of cloned DNA plasmids, the plasmid DNA isolated from individual *E. coli* bacterial clones was initially screened by restriction enzyme analysis. Restriction enzymes (New England Biolabs, USA or Promega, USA) were chosen so as to produce a distinctive DNA digestion band pattern upon analytical agarose gel electrophoresis (see sections 2.1.1.2 and 2.1.1.3). As an alternative screening method, colony PCR was also performed using the GoTaq® G2 Green Master Mix kit (Promega, USA) according to the manufacturer's instructions. Briefly, individual bacterial colonies were picked straight from the LB agar (+ antibiotic) plate into the PCR reaction mix, which had a composition as described in Table 2.1.3:

Reagent	Stock concentration	Volume (µl)	Final concentration
Forward primer	10 µM	1.5	600 nM
Reverse primer	10 µM	1.5	600 nM
DNA template (colony)	-	-	-
GoTaq® G2 Green Master Mix	2 x	12.5	1 x
ddH_2O	-	Added up to 25 µl	-
Final volume		25 µl	

Table 2.1.3 PCR reaction mixes for colony PCR as per the manufacturer's instructions (GoTaq® G2 Green Master Mix kit, Promega, USA).

Reaction mixes were loaded into PCR tubes or onto PCR plates, which were placed into a Touchgene thermal cycler (Techne, USA) set to perform a PRC program as per Table 2.1.4:

PCR step	Temperature (°C)	Duration	
Initial denaturation	95	7 min	
Denaturation	95	15 sec	20 x
Annealing	Variable	30 sec	
Extension	72	Variable	
Final extension	72	5 min	
Final hold	4	∞	

Table 2.1.4 Thermal cycler settings for colony PCR performed using the GoTaq® G2 Green Master Mix kit (Promega, USA). The primer-template annealing temperature was chosen according to recommendations from SnapGene software (GSL Biotech SSL, USA) based on the nucleotide sequences of primer and template DNA strand. The extension duration was set to 1 minute per 1000 bp.

Clones that passed the initial screening were subjected to DNA sequencing for ultimate verification. All sequencing reactions were carried out externally at Beckman Coulter Genomics using the Sanger method. Glycerol stocks were subsequently prepared from verified clones by adding glycerol (Sigma, USA) at a final concentration of 25 % to bacterial cultures. Glycerol stocks were kept at -80 °C for long term storage.

2.1.2. Specific plasmid DNA design

pD10 *CAG.DsRed* and pD10 *mU6.shCtrl.CAG.DsRed* constructs were previously cloned by members of the group.

2.1.2.1. pD10 CAG.DsRed.mU6.sh(migration targets)

LOF experiments in order to determine the mechanisms that underlie developmental rod migration were carried out by RNAi mediated gene silencing using short hairpin (sh) constructs. The short hairpin target sequences used in this study were obtained from published works (Table 2.1.5):

Gene target	Gene product	Target sequence	Source
Scrambled control	-	5'-GATCGGACACTCCTCATAA -3'	Internal
Dync1h1	Dynein cytoplasmic 1 heavy chain 1	5'-AGGCTTTAACCAAGCAGATAA-3'	Tsai *et al.*, 2007
Kif1a	Kinesin family member 1A (Kif1a)	5'-ACGCAGTCTTCAACATCATT -3'	Liu *et al.*, 2012
Myh10	Non-muscle myosin heavy chain IIB (NMMHC-IIB)	5'-GGACCGCTACTATTCAGGA -3'	Shajia and Horowits, 2008
Pafah1b1	LIS1	5'-GGATGCTACAATTAAGGTGTG-3'	Tsai *et al.*, 2007

Table 2.1.5 Targets of RNAi mediated gene silencing. Gene targets for shRNA mediated gene silencing, their target sequences and the source publications that successfully demonstrated knock-down of gene expression with these target sequences in mice.

The published target sequences were used to design knock-down cassettes that consisted of the following elements (5' → 3'): AflII restriction enzyme site – mU6 promoter – target sequence – loop (5'- TTCAAGAGA-3') – anti-parallel target sequence – U6 terminator sequence (5'- TTTTT-3') – AvrII restriction enzyme site. The underlined

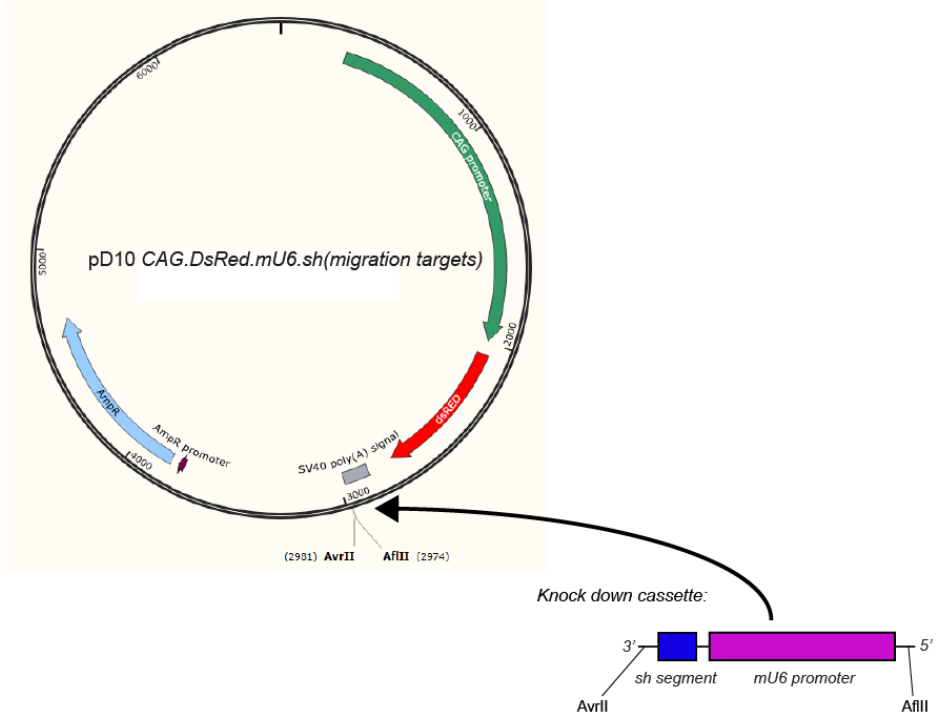

Figure 2.1.1 Summarised cloning approach to produce RNAi constructs. DNA constructs (pD10 *CAG.DsRed.mU6.sh(migration targets)*) harbouring the short hairpin constructs to silence the gene expression of *Dync1h1, Kif1a, Myh10 and Pafah1b1* as well as a scrambled control were produced.

segment represents the short hairpin structure, the expression of which should lead to RNAi. The knock-down cassettes were synthesised by GeneArt® Gene Synthesis (ThermoFisher Scientific, USA). Both the knock-down cassettes as well as the pD10 target plasmid containing the future *CAG.DsRed* reporter module were restriction enzyme digested with AflII and AvrII creating 5'- sticky overhangs. The knock-down cassettes were then ligated into the linearised pD10 CAG.*DsRed* DNA backbone with T4 DNA ligase HC (Promega, USA) using the sticky ends generated in the previous step to yield the pD10 *CAG.DsRed.mU6.sh(migration target)* plasmids (Figure 2.1.1). Following transformation of competent *E. coli* with the ligation reactions, colony PCR was performed to screen clones for the successful insertion of the knock-down cassettes (forward primer: 5'-TAAGCACTTAAGTCACTATAGGGCGAATTGAAGG-3', reverse primer: 5'-TGCTTACCTAGGCTATGACCATGTTAATGCAG-3'). Selected clones displaying the correct ~0.4 kb amplicon band following DNA electrophoresis were further verified by DNA sequencing using the reverse primer 5'-TCCATCACTGATCCTTGAC-3', which primed the sequencing reaction from downstream of the knock-down cassette. One successful clone was then used for this study.

2.1.2.2. pD10 TK.DsRed.eNestin714

The previously described *Nes* reporter construct *Nestin714.TK.lacZ*, consisting of a conserved 714 bp enhancer element within the second intron of the human *Nes* gene, the basic herpes simplex virus thymidine kinase (*TK*) promoter and the *lacZ* open reading frame, was shown to direct reporter gene expression to CNS progenitor cells in transgenic mice (Lothian and Lendahl, 1997; see Figure 2.1.2A). For its desired use in some of the live imaging experiments within this project, the *lacZ* reporter gene had to be replaced by a fluorescent protein reporter gene. The initial cloning strategy consisted of cloning the *eNestin714.TK* element upstream of the *DsRed* reporter gene within the pD10 backbone plasmid. Due to not completely compatible restriction enzyme sites, a cohesive/blunt-end type strategy was designed: the e*Nestin714.TK.lacZ* construct (Figure 2.1.2A) and the pD10 *GNAT1.DsRed* plasmid (Figure 2.1.2B) were digested with NotI and BamHI restriction enzymes respectively and the generated cohesive ends were blunted with the DNA polymerase 1 large (Klenow) fragment (Promega, USA). SphI restriction enzyme

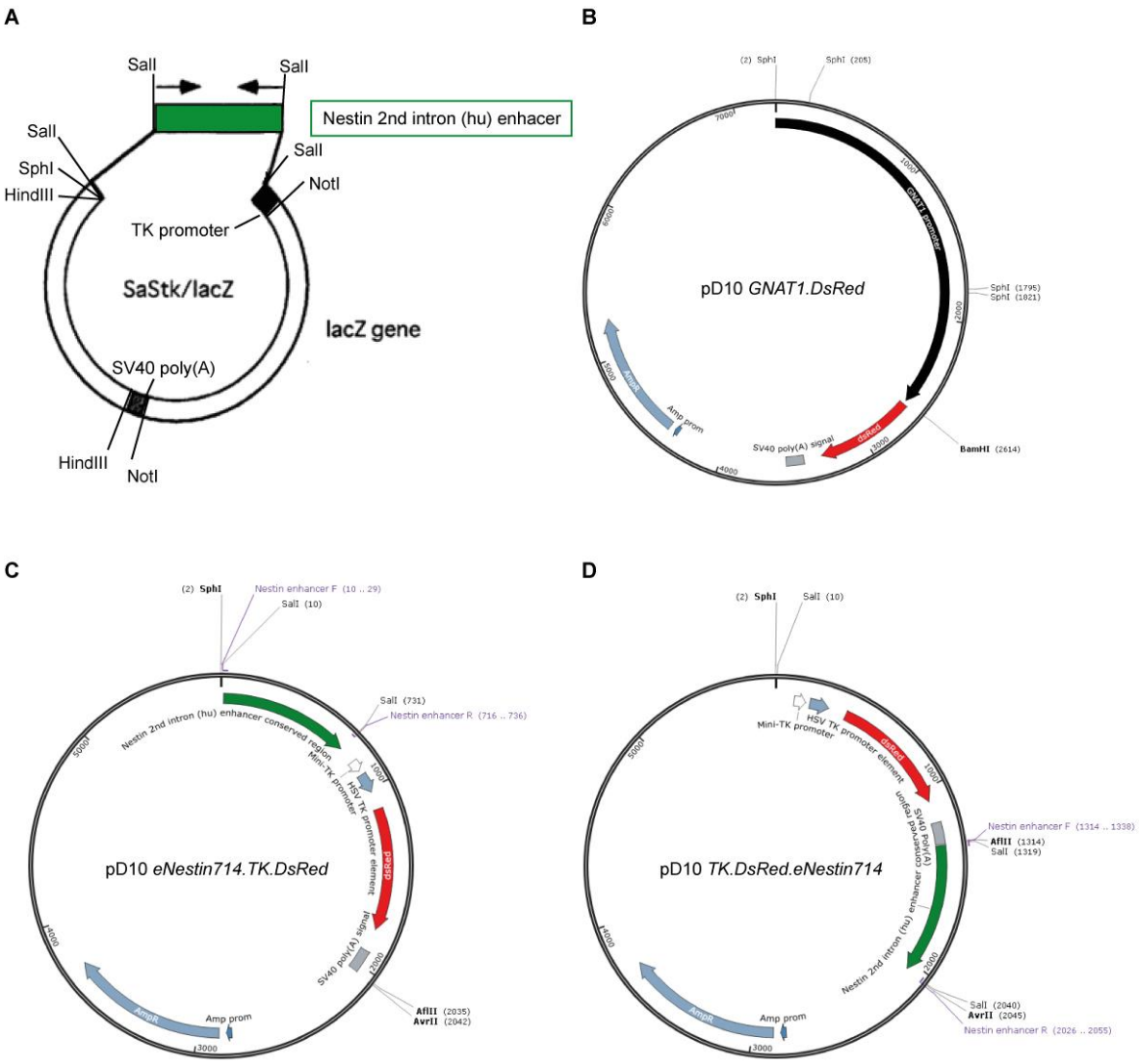

Figure 2.1.2 DNA plasmids utilised and generated during the cloning of the *Nes* reporter pD10 *TK.dsRed.eNestin714*. **(A)** The *Nes* reporter *SaStk/lacZ* designed by Lothian and Lendahl, 1997. *LacZ* reporter gene expression in this plasmid is driven by the HSV thymidine kinase promoter with the consered human 714 bp 2nd intronic *Nes* enancer element (*eNestin714*) placed upstream. **(B)** pD10 *GNAT1.DsRed* reporter plasmid used as a precursor to clone the *Nes* reporter. **(C)** pD10 *eNestin714.TK.DsRed*. The first version of the *Nes* reporter made wihtin this study was cloned by replacing the *GNAT1* promoter in the pD10 *GNAT1.DsRed* plasmid with the *eNestin714.TK* element from the *SaStk/lacZ* plasmid. The reporter module arrangement was 5'- enhancer-promoter-reporter gene-3'. **(D)** pD10 *TK.DsRed.eNestin714*. The second and improved version of the *Nes* reporter made within this study. The conserved 714 bp 2nd intronic *Nes* enhancer element was placed downstream of the repoter gene *DsRed* by PCR cloning, resulting in a reporter module configuration 5'-promoter-reporter gene-enhancer-3'.

was used to generate sticky ends on the opposite ends of the desired DNA fragments. The *Nestin714.TK* element was then ligated into the pD10 *DsRed* DNA backbone with T4 DNA ligase HC (Promega, USA) using the sticky and blunt ends generated in the previous step to yield the pD10 e*Nestin714.TK.DsRed* plasmid (Figure 2.1.2C). Restriction enzyme analysis was performed on successful ligation clones by SalI digestion. Clones displaying the expected band sizes (a 0.7 kb band corresponding to the Nestin714 enhancer element and a 5 kb band corresponding to the pD10 *DsRed* backbone) were validated by DNA sequencing using sets of primers to generate a contig spanning over the e*Nestin714.TK.DsRed* sequence region. One successful clone was then used for this study.

To validate faithful *Nes* reporter expression in retinal progenitor cells, the pD10 e*Nestin714.TK.DsRed* plasmid was introduced by means of AAV viral transduction and/or by electroporation into retinae as well as embryonic stem cell derived *in vitro* 3D neuroretinae (Gonzalez-Cordero *et al.*, 2013) at early developmental stages where retinal progenitor cells should still be present. However, *DsRed* expression was not evident in any of the tested scenarios (data not shown). It was speculated that a configuration that places the enhancer element upstream of the promoter followed by the reporter gene may only work in a genomic context such as in transgenic mice with stable integration of the reporter construct into the genome (Lothian and Lendahl, 1997). Perhaps, an episomally maintained reporter plasmid required a configuration that is more akin to that of the *Nes* gene, with the promoter upstream and the second intronic enhancer element downstream of the transcription start site. To this end, the enhancer element was first PCR amplified (forward primer: 5'-TAAGCACTTAAGTCGACGGATCCAGACTGCT-3', reverse primer: 5'-TGCTTACCTAGGTCGACAAGTCTTGGAGCCAC-3') from the pD10 e*Nestin714.TK.DsRed* plasmid, resulting in an amplicon flanked by the restriction enzyme sites AflII and AvrII (underlined sections in primer sequences); these would be required for later insertion downstream of the *DsRed* open reading frame. Then, a pD10 *TK.DsRed* backbone plasmid was made by excision of the enhancer element from the pD10 e*Nestin714.TK.DsRed* plasmid by SalI digestion and subsequent ligation of the backbone plasmid. Both the *Nes* enhancer amplicon and the pD10 *TK.DsRed* backbone plasmid were then restriction enzyme digested with AflII and AvrII and the enhancer ligated into pD10 *TK.DsRed* downstream of the *DsRed* gene with T4 DNA ligase HC (Promega, USA), resulting in the plasmid pD10 *TK.DsRed.eNestin714* (Figure 2.1.2D). Restriction enzyme analysis was then performed on successful ligation clones by SacI

and SphI digestion. Clones displaying the expected band sizes (3689 bp, 1746 bp and 308 bp) were validated by DNA sequencing using sets of primers to generate a contig spanning over the *Nestin714.TK.DsRed* sequence region. One successful clone was then used for this study.

2.1.3. Recombinant AAV

2.1.3.1. Recombinant AAV production

The *pD10 CAG.DsRed* DNA construct (AAV2 ITRs) was packaged into AAV ShH10 viral capsids to generate AAV ShH10 *CAG.DsRed* viral particles.

Viral particles were produced with a tripartite transfection method in HEK293T cells using polyethylenimine (PEI) as a transfection reagent, as described elsewhere (Gao *et al.*, 2002). Briefly, HEK293T cells were grown to 70-80 % confluence in Ø15 cm cell culture plates or 10-layer cell factories (equivalent to 42 Ø15 cm cell culture plates, Corning, USA) in D10 cell culture medium (DMEM / 10 % fetal calf serum (Gibco, USA) / antibiotic/antimycotic (Gibco, USA)) at 37 °C / 5 % CO_2. For all AAV 2/9 vectors the following transfection mixtures were prepared per Ø15 cm cell culture plate: 10 µg pD10 plasmid, 10 µg pAAV ShH10.Y445F (a kind gift from J. G. Flannery, University of California, Berkeley, USA; it carries the viral genes *rep* and *cap*) and 30 µg pHGTI helper plasmid were allowed to complex to 118 µg PEI (Sigma, USA) in DMEM for 10 minutes at room temperature. Transfection mixtures were then added to the cultures and cells were incubated overnight at 37 °C / 5 % CO_2. On the following day, the medium was replaced with fresh D10 medium. 3 days after transfection, cells were harvested by scraping and centrifuged for 5 minutes at 2000 g. Cell pellets were resuspended in TD buffer (140 mM NaCl / 5 mM KCl / 0.7 mM K_2HPO_4 / 3.5 mM $MgCl_2$ / 25 mM Tris base in ddH_2O, pH 7.5). The cells containing virus were then initially lysed by 4 freeze/thaw/vortex cycles, followed by enzymatic lysis using 50 U/ml benzonase (Sigma, USA) for 30 minutes at 37 °C. Following repeated filtration and centrifugation to remove cell debris, virus particles were purified using affinity chromatography (AVB Sepharose column, GE Healthcare, USA). The final virus preparation was resuspended in PBS-MK

buffer (0.1 M phosphate buffered saline (PBS) / 2.5 mM KCl / 1 mM $MgCl_2$) to yield titres within the range of ~ 10^{12}-10^{13} genome copies/ml.

2.1.3.2. Recombinant AAV characterisation

To assess the purity of viral preparations, analysis by denaturing sodium dodecyl sulphate polyacrylamide gel electrophoresis (SDS-PAGE) was performed. An aliquot of virus preparation was denatured at 95 °C for 10 minutes in Laemmli buffer (2 % SDS / 10 % glycerol / 0.002 % bromophenol blue / 62.5 M Tris HCl pH 6.8 / 0.1 M DTT in ddH_2O, pH6.8). The denatured samples were then loaded onto an SDS-PAGE gel and the gel was run at DC 90 V for 2 hours. The gel was then stained using the SYPRO® Ruby gel staining method (Life technologies, USA) according to the manufacturer's instructions: briefly, gels were exposed to fix solution (50% v/v methanol, 7 % v/v acetic acid in ddH_2O) for 2 x 30 minutes on an orbital shaker at 55 rpm. The gels were then placed in SYPRO® Ruby gel stain solution and incubated overnight under agitation. The following day, gels were washed 2 x 30 minutes using wash solution (10 % v/v methanol, 7 % v/v acetic acid in ddH_2O). Image acquisition was performed on a G:BOX Chemi system (Syngene, UK) and the presence of the 3 AAV capsid proteins VP1, 2 and 3 (87, 72 and 62 kDA respectively) was verified.

Genome copy titres were initially assessed by dot blot until a qPCR-based assay was designed (see below). For dot blot analysis, an aliquot of virus preparation was digested with 0.05 µg/µl proteinase K (Sigma, USA) in proteinase K buffer (100mM Tris pH 8.5 / 5mM EDTA / 200 mM NaCl / 0.4 % w/v SDS in ddH_2O) at 56 °C for 60 minutes. The viral DNA was then precipitated in 126 mM NaOAc / 40 ng/µl glycogen / 52 % ethanol at -20 °C for 30 minutes. Following centrifugation at 14.000 rpm for 10 minutes, a 70 % ethanol wash and a further spin at 14.000 rpm for 2 minutes, the DNA pellet was resuspended in 0.4 M NaOH / 10 mM EDTA in ddH_2O. Following denaturation at 95 °C for 2 minutes, samples and suitable standard plasmid samples containing 10^7-10^{12} molecules were loaded onto a nylon membrane. The membrane was then pre-hybridised in Church's buffer (1% BSA / 1 mM EDTA / 0.5 M $NaPO_4$ pH 7.2 / 7 % SDS in ddH_2O) at 65 °C for 30 minutes in a hybridisation oven, after which biotinylated probes were added for overnight hybridisation at 65 °C. Membranes were then washed 3 x with

33 mM NaPi solution (23 mM Na_2HPO_4 / 12 mM NaH_2PO_4 in ddH_2O) at room temperature, followed by 5 minutes incubation in block solution (5 % SDS / 125 mM NaCl / 25 mM NaPi in ddH_2O pH 7.2). Chemiluminescence signals based on an alkaline phosphatase-mediated colour reaction were then generated using the Phototope®-Star detection kit (New England Biosciences, USA) and imaged on a Fujifilm LAS 500 bio imager. Exported images were analysed using Fiji/ImageJ software (National Institute of Health, USA) and titres were determined by comparing signal intensities of unknown samples to a standard curve generated from the signal intensities of standard samples.

Alternatively, viral genome copy numbers were determined by a qPCR absolute quantification method. For each viral sample, the titre was determined from 4 10-fold serial dilution steps run in triplicates. Amplification reactions were prepared in triplicates for each sample as described in Table 2.1.6:

Reagent	Stock concentration	Volume (µl)	Final concentration
Forward primer	2.5 µM	1	100 nM
Reverse primer	2.5 µM	3.4	340 nM
Probe	2.5 µM	1	100 nM
Virus sample	4x 10-fold serial dilutions	5	variable
PerfeCTa® qPCR FastMix® II, Low ROX™	2 x	12.5	1 x
ddH_2O	-	2.1	-
Final volume		25 µl	

Table 2.1.6 Reaction mix for qPCR absolute quantification assay for the determination of AAV titre.

Primers were designed to create an amplicon from part of the poly(A) SV40 sequence present within the pD10 plasmids that had been packaged into AAV vectors (see Table 2.1.7). The hydrolysis probe was designed to anneal to a nucleotide sequence within the poly(A) SV40 amplicon:

Forward primer sequence (5'→ 3') Reverse primer sequence (5'→ 3')	AGCAATAGCATCACAAATTTCACAA AGATACATTGATGAGTTTGGACAAAC
Amplicon (5'→ 3')	AGCAATAGCATCACAAATTTCACAAATAAAGCATTTTTTTCAC TGCATTCTAGTTGTGGTTTGTCCAAACTCATCAATGTATCT
Probe (5'→ 3')	**6FAM**–AGCATTTTTTTCACTGCATTCTAGTTGTGGTTTGTC– **TAMRA**

Table 2.1.7 Nucleotide sequences of primer pair, created amplicon and hydrolysis probe (6FAM = fluorophore, TAMRA = quencher) used in the qPCR absolute quantification assay to determine AAV titres.

Standard samples were included in parallel in the qPCR run in order to generate a standard curve for absolute titre quantifications. In 10-fold serial dilution steps, 10^2-10^{10} molecules of pre-synthesised poly(A) SV40 amplicon were added to the amplification mixtures instead of virus sample. Reaction mixes were then loaded onto MicroAmp® Optical 96-Well Reaction plates (Applied Biosystems, USA). In turn, these plates were placed into an ABI Prism 7900HT Fast Real-Time PCR Sequence Detection System (Applied Biosystems, USA) that was set to perform the following program (Table 2.1.8):

PCR step	Temperature (°C)	Duration	
Activation of FastStart Taq DNA polymerase	95	10 min	
Denaturation	95	15 sec	40 x
Annealing/Extension	60	30 sec	

Table 2.1.8 PCR settings on the ABI Prism 7900HT Fast Real-Time PCR Sequence Detection System used in the qPCR absolute quantification assay to determine AAV titres.

On the Sequence Detection Systems software 2.2.2 (Applied Biosystems, USA), signal thresholds were manually determined and maintained for each individual experimental run to lie within the linear portion of the exponential amplification curve on a fluorescence intensity vs. cycle number plot. To generate the standard curve, cycle

number at threshold (Ct) values of standard samples were plotted against molecule number. The data points were fitted with a best-fit straight line, the linear equation of which was then used to determine genome copy titres of unknown viral samples from the obtained Ct values.

2.1.4. RNA analysis

2.1.4.1. Total RNA isolation

Total RNA was isolated from cell pellets, FACS sorted cells or whole retinae (previously snap frozen in liquid N_2) using the RNeasy® Mini or Micro Kit (Qiagen, Germany) according to the manufacturer's instructions. The RNA concentration and purity were determined on a Nanodrop ND-1000 spectrophotometer (Thermo Scientific, USA). Total RNA was stored at -80 °C.

2.1.4.2. cDNA synthesis by mRNA reverse transcription

For the generation of cDNA from isolated RNA, the QuantiTect Reverse Transcription Kit (Qiagen, Germany) was used according to the manufacturer's instructions. Briefly, genomic DNA contaminations were removed from the RNA samples with the gDNA Wipeout buffer and incubation at 42 °C for 2 minutes. Subsequently, the reverse transcription reaction was performed following the addition of the Quantiscript Reverse Transcriptase, Quantiscript Reverse Transcription Buffer and Reverse Transcription Primer mix (containing random octamers and dT nucleotide mix) and incubation at 42 °C for 45 minutes. After completion of the reverse transcription reaction and heat inactivation of the reverse transcriptase at 95 °C for 3 minutes, cDNA samples were stored at -20 °C.

2.1.4.3. Quantitative polymerase chain reaction – relative quantification

Quantitative polymerase chain reaction (qPCR) was used to determine relative expression levels of target genes within cDNA samples derived from cell pellets, FACS sorted cells or whole retinae. qPCR assays were performed using the 2x FastStart TaqMan® Probe Mastermix (Roche, Switzerland) in conjunction with the Universal ProbeLibrary system technology (Roche, Switzerland), which is a fluorophore/quencher hydrolysis probe based library system designed for extensive transcript/cDNA coverage. Primers for the target and endogenous reference control markers were designed and probes were chosen according to recommendations by the Universal Probe Library Design Center (Roche, Switzerland) (see Table 2.1.11). The following reaction mixes were prepared (usually in triplicates) (Table 2.1.9):

Reagent	Stock concentration	Volume (µl)	Final concentration
Forward primer	20 µM	0.2	200 nM
Reverse primer	20 µM	0.2	200 nM
Probe	10 µM	0.2	100 nM
cDNA	1:4-1:10 dilution from reverse transcription reaction	5	variable
PerfeCTa® qPCR FastMix® II, Low ROX™	2 x	10	1 x
ddH_2O	-	4.4	-
Final volume		20 µl	

Table 2.1.9 Reaction mix for qPCR relative quantification assays.

Reaction mixes were then loaded onto MicroAmp® Optical 96-Well Reaction Plates (Applied Biosystems, USA), which in turn were placed into an ABI Prism 7900HT Fast Real-Time PCR Sequence Detection System (Applied Biosystems, USA) set to perform the following program (Table 2.1.10):

PCR step	Temperature (°C)	Duration	
Activation of FastStart Taq DNA polymerase	95	10 min	
Denaturation	95	15 sec	40-60 x
Annealing/Extension	60	1 min	

Table 2.1.10 PCR settings for qPCR relative quantification assays. Reactions were performed on the ABI Prism 7900HT Fast Real-Time PCR Sequence Detection System (Applied Biosystems, USA). The number of cycles was adjusted according to the expected expression levels of target genes.

Gene	Protein name	Forward primer sequence (5'→ 3') Reverse primer sequence (5'→ 3')	Probe # (Roche Universal ProbeLibrary)
Actb	β-actin	AAGGCCAACCGTGAAAAGAT GTGGTACGACCAGAGGCATAC	56
Car2	Carbonic anhydrase 2	TTACTGTCAGCAGCGAGCA ACGCCAGTTGTCCACCAT	89
Cd44	CD44	GCATCGCGGTCAATAGTAGG CACCGTTGATCACCAGCTT	29
Clu	Clusterin	AAGTACTACVCTTCGGGTCTCCA AGCTTCACCACCACCTCAGT	6
Glul	Glutamine Synthetase (GS)	CTCGCTCTCCTGACCTGTTC TTCAAGTGGGAACTTGCTGA	31
Nes	Nestin	TCCCTTAGTCTGGAAGTGGCTA GGTGTCTGCAAGCGAGAGTT	67
Rlbp1	RLBP	CCCCTCGGATCTCAAGAAG TTTGAACCTGGCTGGGAAT	1
Sox9	Sox9	GTACCCGCATCTGCACAAC CTCCTCCACGAAGGGTCTCT	66
Vim	Vimentin	TGCGCCAGCAGTATGAAA GCCTCAGAGAGGTCAGCAA	79

Table 2.1.11 Gene specific primer pair and hydrolysis probe (Universal ProbeLibrary, Roche, Switzerland) combinations used for qPCR relative quantification assays.

The following methodology was applied to obtain normalised, relative gene expression levels: signal thresholds were first manually determined and maintained for each individual experimental run on Sequence Detection Systems software 2.2.2. They were chosen such that they lay in the middle of the linear part of log-based fluorescence amplification curves on fluorescence intensity vs. cycle number plots. To normalise target against *Actb* control expression levels, cycle numbers at threshold (C_t) were used to calculate ΔC_t.

$$\Delta C_t = C_t(\text{target}) - C_t(\textit{Actb})$$

To normalise sample (e.g. P0) against control levels of target expression (e.g. adult), $\Delta\Delta C_t$ was calculated:

$$\Delta\Delta C_t = \Delta C_t(\text{sample}) - \Delta C_t(\text{control})$$

Finally, to obtain normalised relative target expression levels in '% of control levels', the following formula was applied:

$$\text{Normalised expression levels (\%)} = (2^{-\Delta\Delta Ct}) \times 100$$

2.2. Animals

All experiments were carried out according to the Policies on the Use of Animals and Humans in Neuroscience Research, revised and approved by the ARVO Statement for the Use of Animals in Ophthalmic Vision Research. The following mouse lines were used within this study: a) *Nrl.GFP*$^{+/+}$ mice (kind gift of A. Swaroop, University of Michigan, USA) (Akimoto *et al.*, 2006), which expresses *EGFP* under control of the rod photoreceptor specific *Nrl* promoter; b) *Rlbp.GFP*$^{+/+}$ mice (kind gift of E. Levine, John A. Moran Eye Centre, USA), which express *EGFP* under control of the Müller glia specific *Rlbp* promoter (Vazquez-Chona *et al.*, 2009); c) *Prph2*$^{rd2/rd2}$ mice (kind gift of G. Travis, University of California) (Travis *et al.*, 1991), which is a slowly degenerating retinitis pigmentosa mouse model; d) wild-type *C57BL/6J* mice (Harlan, UK). For DNA delivery experiments using viral vectors or electroporation the following mouse strains were used: *C57BL/6J, Nrl.GFP*$^{+/+}$, *Prph2*$^{rd2/rd2}$. For the developmental rod migration studies, *Nrl.GFP*$^{+/+}$ mice were used. For the transplantation experiments, *Nrl.GFP*$^{+/+}$ mice served as a source of rod photoreceptor donor cells, while *C57BL/6J* and *Prph2*$^{rd2/rd2}$ served as transplant recipients. *Rlbp.GFP*$^{+/+}$ mice served as a source of Müller glia primary cells. All animals were maintained in the animal facility at University College London. Animals were group-housed wherever possible and provided fresh bedding, nesting material daily and were given food *ad libitum*. They were kept on a standard 12/12 hour light/dark cycle.

2.3. Methods of *in vivo* and *in situ* plasmid DNA delivery

2.3.1. Plasmid DNA delivery into the retina using AAV viral vectors

2.3.1.1. Sub-retinal viral administration into adult mice

Sub-retinal viral administration into adult mice was performed under direct ophthalmoscopy control through a Zeiss operating microscope (Zeiss, Germany). Adult *C57BL/6J* mice aged 6-8 weeks were anaesthetised by intra-peritoneal administration of Domitor anaesthetic: ketamine (Fort Dodge Animal Health, Southampton, UK) and medetomidine hydrochloride (Pfizer Pharmaceuticals, Kent UK) were respectively dosed at 60 and 1 mg/kg. 1 % w/v Minim's Tropicamide (Bausch & Lomb, USA) and Viscotears (Novartis, Switzerland) liquid gel were then applied to the eyes in order to dilate pupils and to keep eyes hydrated. Eyes were gently held in place using a pair of forceps by holding on to a segment of the conjunctiva and extraocular muscle. A glass cover slip was placed on top of the cornea over the layer of Viscotears applied earlier to facilitate visualisation of the retinal fundus through the operating microscope. The sclera was punctured at the level of the anterior chamber with the tip of an 8mm, 34-gauge hypodermic needle (Hamilton, Switzerland) mounted on a 5 µl Hamilton syringe (Hamilton, Switzerland) to avoid excessive intraocular pressure. The same needle was then used to administer a sub-retinal injection of 2 µl of viral preparation by tangential insertion through the sclera into the sub-retinal space, resulting in local retinal detachment. Animals were allowed to recover from surgery following intra-peritoneal administration of Antisedan reversal solution dosed at 1mg/kg (Pfizer, USA). During the injection and during the first post-operation day, mice were placed on heat mats set to 33 °C to help regulate their body temperatures. Upon returning to cages, mice were placed on tissue to reduce the risk of bedding material contacting the eyes and given softened food.

2.3.1.2. Sub-retinal viral administration in early post-natal mice

Viral administration was performed under direct ophthalmoscopy control through a Zeiss operating microscope (Zeiss, Germany). P2/3 *C57BL/6J* pups were subjected to ice anaesthesia for several minutes. After cleaning the eyelids with 70 % ethanol using a cotton swab, a small incision was made along the future edge of the eyelid using a clean pair of dissection scissors and the eyeball was gently prolapsed. 1 % w/v Minim's Tropicamide and Viscotears (Novartis, Switzerland) liquid gel were then applied to the eyes in order to dilate pupils and to keep eyes hydrated. A glass cover slip was placed on top of the cornea over the layer of Viscotears applied earlier to facilitate visualisation of the retinal fundus through the operating microscope. The sclera was punctured at the level of the anterior chamber with the tip of an 8mm, 34-gauge hypodermic needle (Hamilton, Switzerland) mounted on a 5 µl Hamilton syringe (Hamilton, Switzerland) to avoid excessive intraocular pressure. The same needle was then used to deliver a sub-retinal injection of 1 µl of an AAV viral suspension in the superior hemisphere. The prolapsed eye was then gently pushed back into the eye socket. The pups were recovered on a heat mat and returned to their mothers as soon as they were moving and kept with them until donor age was reached.

2.3.1.3. Intra-vitreal viral administration in early post-natal mice

Intra-vitreal viral administration was performed under direct ophthalmoscopy control through a Zeiss operating microscope (Zeiss, Germany). P10 *C57BL/6J or Prph2*$^{rd2/rd2}$ pups were anaesthetised by intra-peritoneal administration of Domitor anaesthetic: ketamine and medetomidine hydrochloride respectively dosed at 60 and 1 mg/kg. After cleaning the eyelids with 70 % ethanol using a cotton swab, a small incision was made along the future edge of the eyelid using a clean pair of dissection scissors and the eyeball was gently prolapsed. Eyes were gently held in place using a pair of forceps by holding on to a segment of the conjunctiva and extraocular muscle 1 % w/v Minim's Tropicamide and Viscotears (Novartis, Switzerland) liquid gel were then applied to the eyes in order to dilate pupils and to keep eyes hydrated. A glass cover slip was placed on top of the cornea over the layer of Viscotears applied earlier to facilitate visualisation of the retinal

fundus through the operating microscope. An 8 mm, 34-gauge hypodermic needle (Hamilton, Switzerland) mounted on a 5 µl Hamilton syringe (Hamilton, Switzerland) was used to deliver an intra-vitreal injection of 1 µl of AAV viral suspension. The prolapsed eye was then gently pushed back into the eye socket and the pups were left to recover from surgery following an intra-peritoneal administration of Antisedan reversal solution dosed at 1mg/kg. The pups were recovered on a heat mat and returned to their mothers as soon as they were moving and allowed to reach adulthood to serve as transplant recipients.

2.3.2. Plasmid DNA delivery into the retina by electroporation

2.3.2.1. In vitro electroporation and explant culture

In vitro electroporation was performed following the retinal electroporation protocols by the Cepko lab (Matsuda and Cepko, 2004; Hsiau *et al.*, 2007). For a schematic illustration see Figure 2.3.1A. The retinae from early postnatal (P0 - P4) *Nrl.GFP*$^{+/+}$ mice were dissected out in serum-free medium (SFM; 1:1 DMEM/F-12 supplemented with L-glutamine and 15 mM HEPES (ThermoFisher Scientific, USA) / 50 units/ml penicillin / 50 µg/ml streptomycin (ThermoFisher Scientific, USA) / 1 mM Taurine (Sigma, USA)); all non-neural retinal tissues, with exception of the lens, which was left in place, were removed. Retinae were then transferred with custom made wide bore pipette tips into an electroporation cuvette with 2 mm gap size (BTX, USA) containing a 1 µg/µl plasmid DNA solution in PBS. The tissue was orientated within the cuvette such that the apical and vitreal sides of the retina were aligned with the cuvette electrodes; the apical surface was juxtaposed to the anode for optimal electroporation efficiency (Matsuda and Cepko, 2004). Using a pulse generator (model ECM 830, BTX, USA), the retinae were then electroporated with 5 x 30 V square pulses of 50 ms duration and with 950 ms intervals. Subsequently, the electroporated retinae were allowed to recover for 5 min in SFM pre-equilibrated at 37 °C / 5 % CO_2. This was followed by an additional 5 min recovery step in pre-equilibrated SFM supplemented with 5 % fetal calf serum (ThermoFisher Scientific, USA). The retinae were then placed lens side down on 0.2 µm polycarbonate transwells (Millipore, USA) and cultured at 37 °C / 5 % CO_2 in SFM / 5 % fetal calf

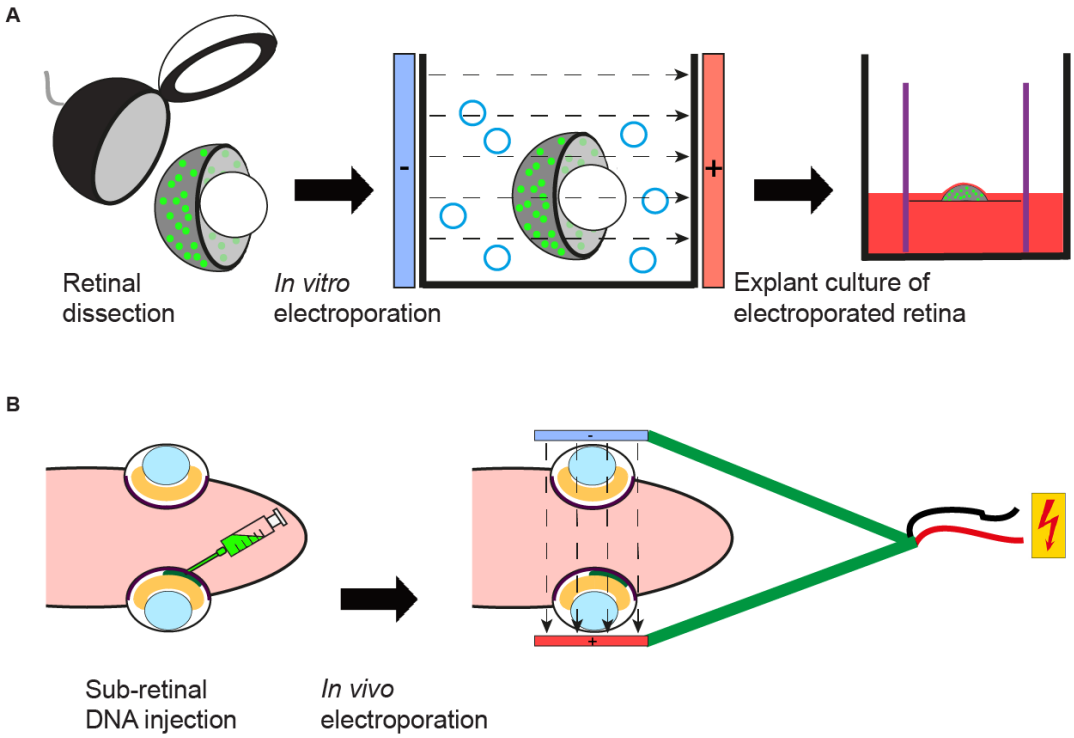

Figure 2.3.1 Schematics of whole retina electroporation protocols utilised in this study. **(A)** *Ex vivo* DNA electroporation. Early post-natal mice (P0-P4) were sacrificed and the retinae explanted together with the lense in place. The tissue was then electroporated in PBS containing DNA plasmid, and subsequently transferred onto a transwell for *in vitro* culturing (protocol adapted from Hsiau *et al.*, 2007). **(B)** *In vivo* early post-natal DNA electroporation. Similary to the *in utero* electroporation protocol, a PBS solution containing plasmid DNA was sub-retinally injected into P0-P1 mice and the electrodes were then placed adjacent to the temples with the cathode next to the injected eye.

serum. Every other day the medium was replaced with a 1:1 mix of old and freshly made SFM / 5 % fetal calf serum.

2.3.2.2. In vivo electroporation of neonatal pups

Neonatal (P0-P1.5) *Nrl.GFP*$^{+/+}$ pups were subjected to ice anaesthesia for several minutes. After cleaning the eyelids with 70 % ethanol using a cotton swab, a small incision was made along the future edge of the eyelid using a clean pair of dissection scissors and the eyeball was gently prolapsed. 1 % w/v Minim's Tropicamide and Viscotears (Novartis, Switzerland) liquid gel were then applied to the eyes in order to dilate pupils and to keep eyes hydrated. As illustrated in Figure 2.3.1C, a blunt 8 mm, 34-gauge hypodermic needle was then used to deliver a sub-retinal injection of 0.4 µl plasmid DNA (2 µg/µl in 1x PBS containing 0.1 % Fast Green FCF (Sigma, USA)) under direct ophthalmoscopy control through a Zeiss operating microscope (Zeiss, Germany) (Matsuda and Cepko, 2004). Fast Green served as a tracer aiding in the assessment of whether or not the sub-retinal delivery of DNA was successful: the tracer dye only spreads locally when administered into the sub-retinal space, whereas it rapidly and uniformly spreads in the eyeball when administered intra-vitreally (de Melo and Blackshaw, 2011). Next, tweezer electrodes (BTX, 5 mm round, platinum, BTX electroporator, USA) were briefly soaked in 1x PBS and used to gently clamp the mouse head such that the electrodes were located directly adjacent to the eyes, with the cathode next to the sub-retinally injected eye. This arrangement allows the polyanionic DNA to traverse from the sub-retinal space into the neural retinal tissue as it is being pulled towards the cathode. With the electrodes in place, five 80 V, 50 ms square pulses with an interval of 950 ms were delivered using an ECM 830 square pulse electroporator (BTX, USA). Prolapsed eyes were then gently pushed back into normal position and the pups were allowed to recover from surgery on a heat mat until they were moving before being returned to their mother.

2.4. Methods of rod photoreceptor precursor cell transplantation

2.4.1. Retinal dissociation

A single cell suspension of retinal cells was prepared from retinae of P8 *Nrl.GFP*$^{+/+}$ mice (see Figure 2.4.1 for a schematic illustration of the entire transplantation workflow). Mice were sacrificed by cervical dislocation and retinae were acutely dissected in Earl's Balanced Salt Solution (EBSS, Sigma) free from surrounding tissues. The retinae were dissociated using a papain enzyme dissociation kit (Worthington Biochemical, Lorne Laboratories, UK) according to the manufacturer's instructions. Briefly, retinae were enzymatically dissociated in EBSS / 20 U/ml papain / 1:100 v/v antibiotic/antimycotic at 37 °C / 5 % CO_2 for 45 minutes. For further mechanical dissociation, the cell suspension was gently triturated with a 200 µl pipette tip, passed through a 70 µm strainer and spun down at 200 g for 5 minutes. Cell pellets were resuspended in EBSS / 1 mg/ml ovomucoid protease inhibitor / 100 U/mL DNase I and incubated for 5-10 minutes at 37 °C / 5 % CO_2. The suspension was subsequently layered over an EBSS / 10 mg/ml ovomucoid protease inhibitor solution and centrifuged at 100 g for 5 minutes. Finally, cell pellets were resuspended in an appropriate buffer solution depending on the downstream use and application of the cells (see sections 2.4.2 and 2.5).

2.4.2. Fluorescence-activated cell sorting

Dissociated retinal cells destined for enrichment by fluorescence-activated cell sorting (FACS) were resuspended in EBSS / 1 % fetal calf serum (FCS) at 2 x 10^7 cells/ml and placed on ice until ready for sorting. Cells were sorted under sterile conditions using either the MoFLO DXP cell sorter (Beckman Coulter; sheath pressure: 60 psi), the FACSAria III (BD Biosciences; sheath pressure: 70 psi) or the BD Influx™ cell sorter (BD Biosciences; sheath pressure: 50 psi) with sample pressures usually 0.1-0.8 psi greater

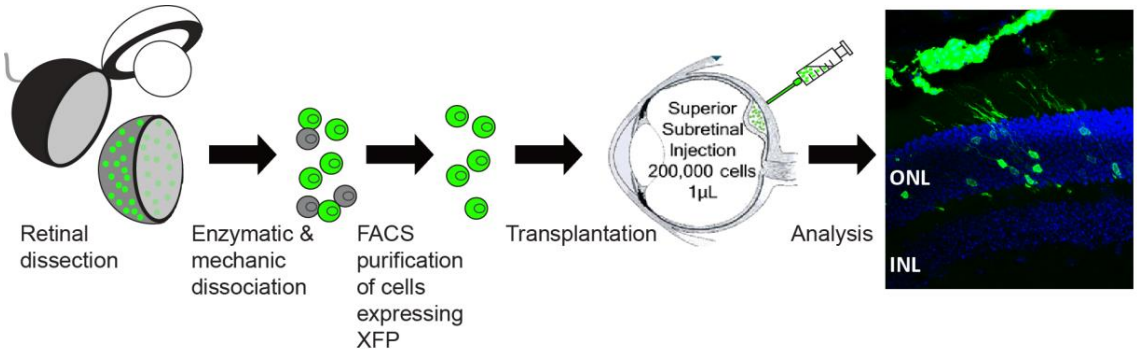

Figure 2.4.1 Transplantation schematic.The eyes of P8 donor mice were harvested and the retinal tissue was enzymatically and mechanically dissociated into a single cell suspension. Photoreceptor cells labelled with a fluorescent protein were then enriched by FACS. The isolated cells were subsequently sub-retinally injected into the eyes of adult recipient mice. Usually, 2 x 10^5 cells in a volume of 1 µl were injected in the superior half of the eye. The transplantation outcome was assessed three weeks post-transplantation by histological analysis.

than sheath pressures. The cell sorters were fitted with 70 µm nozzles. GFP was excited using a 488 nm excitation lasers respectively. Dead cells were excluded from the sorted cell population using the DRAQ7 far-red DNA dye (BD Biosciences), which gains access to the nucleus only in cells with compromised membranes (excitation laser wavelength: 640 nm. Cells were sorted into chilled EBSS / 50 % FCS, after which they were centrifuged at 150 g for 20 minutes. Finally, cells were resuspended in EBSS / 100 U/ml DNase I at a cell density of 2 x 10^5 cells/ml and kept on ice until ready for transplantation.

2.4.3. Rod photoreceptor transplantation

Transplantation surgery was performed under direct ophthalmoscopy control through an operating microscope. Adult *C57BL/6J* or *Prph2*$^{rd2/rd2}$ recipient mice aged 4-8 weeks were anaesthetised by intra-peritoneal administration of Domitor anaesthetic: ketamine and medetomidine hydrochloride dosed at 60 and 1 mg/kg respectively. 1 % w/v Minim's Tropicamide and Viscotears (Novartis, Switzerland) liquid gel were then applied to the eyes in order to dilate the pupils and to keep the eyes hydrated. Eyes were gently and slightly prolapsed and held in place using a pair of forceps by holding on to a segment of the conjunctiva and extraocular muscle. A glass cover slip was placed on top of the cornea over the layer of Viscotears applied earlier to facilitate visualisation of the retinal fundus through the operating microscope. To avoid excessive intraocular pressure, the sclera of recipient eyes was punctured with the tip of an 8 mm, 34-gauge bevelled hypodermic needle mounted on a 5 µl Hamilton syringe (Hamilton). The same needle and syringe were then used to administer a single sub-retinal injection in the superior hemisphere of 1 µl of FAC sorted cell suspension (200,000 cells) by tangential insertion through the sclera into the sub-retinal space, resulting in local retinal detachment due to the injection. Animals were allowed to recover from surgery following intra-peritoneal administration of Antisedan reversal solution at 1mg/kg. During the transplantation and during the first post-operation day, mice were placed on heat mats set to 33 °C to help regulate their body temperatures. Upon returning to cages, mice were placed on tissue to reduce the risk of bedding material contacting the eyes and given softened food.

2.5. Methods of cell culture

2.5.1. Müller glia primary cell culture

A single cell suspension of FAC sorted P7-9 *RLBP.GFP* positive cells was prepared as described in section 2.4.1 and 2.4.2. 1.5 x 10^6 cells were plated out onto 1- or 8-well chamber imaging slides (MoBiTec, Germany) previously coated with 1 mg/ml laminin for 30 min at 37 °C / 5 % CO_2. Cells were cultured in D10 cell culture medium (DMEM / 10 % fetal calf serum (ThermoFisher, USA) / antibiotic/antimycotic (Thermofisher, USA)) at 37 °C / 5 % CO_2 until Müller glia displayed significant levels of process extension, which was interpreted as a sign of Müller glia culture maturity. This was typically observed after 2-3 weeks. The cultures were re-fed once a week with D10 medium pre-equilibrated at 37 °C / 5 % CO_2.

2.5.2. Rod photoreceptor-Müller glia primary cell co-culture

The purpose of the rod photoreceptor-Müller glia co-culture system was to model *in vivo* transplantations where close associations between integrated rod photoreceptor cells and recipient Müller glia were frequently observed (Warre-Cornish, PhD thesis, 2013). *In vivo*, Müller glia assume an elongated morphology, spanning the entire radial extent of the neural retina. *In vitro* on the other hand, Müller glia usually assume a stellate shaped appearance when plated on a laminin coated dish. To ensure that the Müller glia were as close to the *in vivo* morphology possible, single chamber imaging slides with a surface area of 10.84 cm^2 (MoBiTec, Germany) were coated in a striped pattern with 1 mg/ml laminin for 30 min at 37 °C / 5 % CO_2 prior to cell culture. The striped laminin carpets would promote an elongated Müller glia morphology mimicking the *in vivo* situation. The laminin coating was applied using silicone matrices with either 50 or 90 µm wide parallel channels in contact with the culture dish (Knöll *et al.*, 2007). During the coating step the channels were filled with the laminin solution to generate striped laminin carpets. Following the coating step, the silicon matrix was removed and the culture dish was washed once with 1x PBS and subsequently filled with D10 culturing medium.

A single cell suspension of FAC sorted P7-9 *RLBP.GFP* positive cells was prepared as described in the section 2.4.1. 1-1.5 x 10^6 cells were plated out onto the pre-coated culture dish containing pre-equilibrated (37 °C / 5 % CO_2) D10 medium (DMEM / 10 % fetal calf serum (ThermoFisher, USA) / antibiotic/antimycotic (Thermofisher, USA)). The culture medium was replenished with pre-equilibrated D10 medium once a week. After 2-3 weeks in culture, Müller glia typically displayed extensive cell elongation, upon which a single cell suspension of 3x10^5 - 10^6 FAC sorted P7-9 *Nrl.GFP* positive cells was added to the Müller glia culture (Figure 2.5.1).

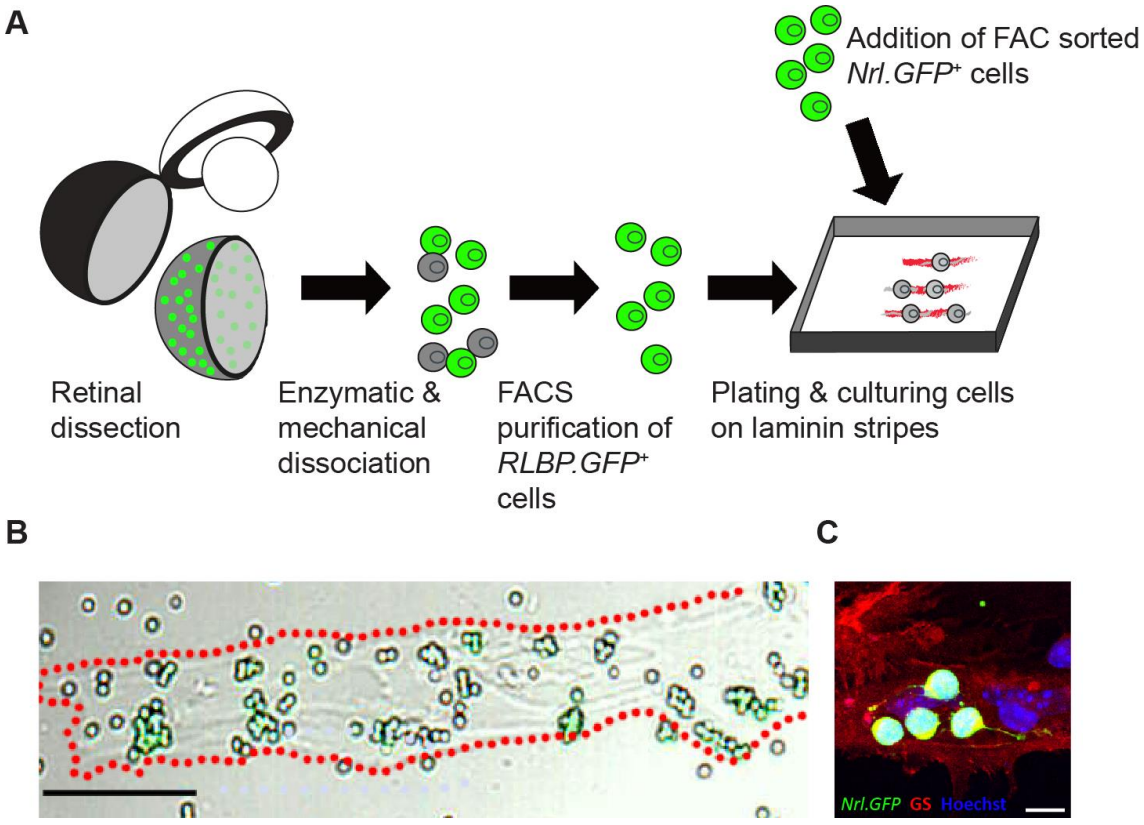

Figure 2.5.1 The Müller glia and rod photoreceptor precursor co-culture model. **(A)** Co-culture schematic. The eyes of P8 *RLBP.GFP*$^{+/+}$ mice were harvested and the retinal tissue was enzymatically and mechanically dissociated into a single cell suspension. GFP labelled Müller glia were enriched by FACS. The isolated cells were subsequently plated onto a glass-bottom tissue culture dish that had been pre-coated with laminin. The laminin coating was applied in stripes using a silicon matrix that contained parallel channels in contact with the culture dish, which could be filled with a coating solution. Following maturation of the Müller glia culture under tissue culture conditions (37 °C, 5 % CO_2), typically after 2-3 weeks, a single cell suspension of FAC sorted P8 *Nrl.GFP* positive cells was added to thus create the co-culture. **(B)** An example single frame image of a Müller glia and rod photoreceptor precursor co-culture time-lapse recording. Comparatively big and elongated Müller glia can be seen within the red dotted lines, while the rod photoreceptor precursor cells are small and spherical by comparison. The co-culture was subjected to time lapse live imaging using a JuLi™ digital fluorescence microscope at 37 °C, 5 % CO_2. **(C)** Confocal microscopy image of Müller glia and rod photoreceptor precursor following one day of co-culture. Rod photoreceptors (green) frequently extended neurites along the Müller glia following over night co-culture (stained for GS (glutamine synthetase), red). Note that such processes were not observable on the JuLi™ digital fluorescence microscope with its relatively basic optical resolving power. Scale bars: 50 µm (B), 10 µm (C).

2.6. Histology, immunohistochemistry and immunocytochemistry

2.6.1. Harvesting of eye and retinal tissue

Animals were sacrificed by cervical dislocation and eyes were enucleated and fixed in 4 % paraformaldehyde (PFA, Sigma, USA) in 1x PBS for 30 minutes at room temperature. For better tissue accessibility of the fixative, the cornea was punctured. After fixation, the tissue was washed three times with 1x PBS. The cornea, iris and lens were carefully removed by dissection. Likewise, retinae maintained as explant cultures were fixed in 4 % PFA (Sigma, USA) in 1x PBS for 30 minutes at room temperature, also followed by three washes with 1x PBS.

The harvested tissues were subsequently subjected to a cryoprotection step in 20 % Sucrose (Sigma, USA) in 1x PBS overnight at 4 °C.

2.6.2. Cell culture fixation

Cell cultures were washed once with 1x PBS pre-equilibrated at 37 °C / 5 % CO_2 to remove cell culture media prior to fixation with pre-warmed (37 °C) 4 % PFA (Sigma, USA) in 1x PBS for 30 minutes. Following incubation in fixative solution, the cell cultures were washed three times with 1x PBS and then stored in 1x PBS at 4 °C until ready for immunocytochemical processing.

2.6.3. Cryosections

Following fixation and cryoprotection, eye or retinal tissue samples were cryo-embedded in O.C.T. medium (Pyramid Innovation, UK) and frozen in 2-methylbutane (Sigma, USA), which had been pre-cooled in liquid nitrogen. After cryo-embedding, the frozen

samples were stored at -20 °C until cryo-sectioning on a Bright OTF5000 cryostat (Bright Instruments Co Ltd, UK) set to produce sections at 18 µm thickness. Sections were transferred onto SuperFrost™ Ultra Plus Adhesion glass slides (ThermoFisher, USA), which were subsequently stored at -20 °C prior to processing for immunohistochemistry.

2.6.4. Immunohistochemistry and immunocytochemistry

For immunohistochemistry, frozen eye sections were air-dried for 15 minutes, rehydrated with two 10-minute washes with 1x PBS and incubated in blocking solution at room temperature for 1 hour. The compositions of the different blocking solutions used are indicated in the table legend of Table 14. They all contained a high concentration of protein or amino acid serving as blocking agents and Triton X-100 (Sigma, USA) as a permeabilisation agent. Subsequently, sections were incubated in primary antibody (Table 2.6.1) diluted in blocking solution overnight at 4 °C. Sections were then washed 6x 5 min with 1x PBS followed by incubation in secondary antibody (Table 2.6.2) for 2 hours at room temperature diluted in the same blocking solution as the primary antibody. Sections were then washed 6x 5 min with 1x PBS and counterstained with 5 µg/ml Hoechst 33342 (Sigma, USA) in 1x PBS for 5 min at room temperature. Following a final 2x 2 min wash with 1x PBS, sections were mounted under coverslips using fluorescence mounting medium (Dako, Denmark) and stored protected from light at 4 °C.

For immunocytochemistry, the same procedure was followed as with the immunohistochemistry from the blocking step onwards.

Primary antibody	Host species	Manufacturer	Dilution	Blocking solution
α CD44 (ICC)	Rat	BD Biosciences (USA)	1:400	A
α CD44 (IHC)	Rat	BD Biosciences (USA)	1:500	B
α Cx43	Rabbit	Sigma (USA)	1:2000	A
α Gamma-tubulin	Mouse	Abcam (UK)	1:100	D
α GS	Mouse	BD Biosciences (USA)	1:500	B
α N-Cadherin	Mouse	BD Biosciences (USA)	1:100	B
α Nestin	Mouse	Abcam (UK)	1:1000	B
α PH3	Rabbit	Millipore (USA)	1:250	B
α Sox9	Rabbit	Millipore (USA)	1:1000	B
α α-Tubulin	Rabbit	Abcam (UK)	1:500	B
α Vimentin	Chicken	Millipore (USA)	1:500	B

Table 2.6.1 List of primary antibodies used in this study. All antibodies were diluted in blocking solution as indicated. A: 1.82 % w/v Lysine / 0.015 % v/v Triton X-100 in 1x PBS, B: 5 % w/v NGS / 1 % w/v BSA / 0.1 % v/v Triton X-100 in 1x PBS, C: 1 % w/v NGS / 1 % w/v BSA / 0.1 % v/v Triton X-100 in 1x PBS, D: 4 % w/v NGS / 2 % w/v BSA / 0.2 % v/v Triton X-100.

Secondary Antibody	Host species	Target species	Manufacturer	Dilution
Alexa Fluor® 488	Goat	As appropriate	Life technologies, USA	1:500
Alexa Fluor® 546	Goat	As appropriate	Life technologies, USA	1:500
Alexa Fluor® 633	Goat	As appropriate	Life technologies, USA	1:500
αGFP-FITC	Goat	-	Abcam, UK	1:500

Table 2.6.2 List of secondary antibodies used in this study. All antibodies were diluted in the same blocking solution as the corresponding primary antibody.

2.7. Microscopy and image analysis

2.7.1. Confocal microscopy

Images of fixed retinal tissue sections or flat mounts were acquired on a Leica TCS SPE upright confocal laser scanning microscope (Leica, Germany) set to a scanning frequency of 400 Hz, fitted with 5x (air, numerical aperture or NA = 0.15), 40x (oil immersion, NA = 1.15) and 63x (oil immersion, NA = 1.3) objectives and photomultiplier tubes to detect fluorescence emission. Hoechst 33342 or DAPI was excited using a 405 nm laser source. For the fluorophores Alexa Fluor® 488, FITC and (e)GFP a 488 nm laser source was used. For Alexa Fluor® 546 and DsRed as well as Alexa Fluor® 633, laser sources of 532 nm and 635 nm respectively were used. When operating in confocal mode, the pinhole size was set to 1 Airy unit (98.4 µm). For image acquisition, *xyz* confocal stacks of representative fields of view were captured at a resolution of 512 x 512 or 1024 x 1024 pixels and at a step size of 1 µm. Where possible, all image acquisitions performed as part of the same experiment were carried out on the same day, with identical laser power as well as detector gain and offset settings.

2.7.2. Time-lapse imaging of rod photoreceptor and Müller glia co-cultures

Rod photoreceptor and Müller glia primary cell co-cultures, each isolated form *Nrl.GFP*$^{+/+}$ and *RLBP.GFP*$^{+/+}$ mice respectively, were live-imaged using a portable JuLi^{TM} Digital Fluorescence Microscope (NanoEnTek, South Korea) inside a tissue culture incubator (37 °C / 5 % CO_2). *xyt* time-lapse recordings were generated by acquiring brightfield and GFP fluorescence images at 10 minute intervals over a period of approximately 24 hours. Despite both being GFP positive at the time of isolation, *RLBP.GFP*$^{+/+}$-derived Müller glia and *Nrl.GFP*$^{+/+}$-derived rod cells could be easily distinguished in the time-lapse recordings: firstly, the Müller glia had lost *GFP* expression during the previous cell culture period and were thus only visible in the brightfield channel, whereas rod photoreceptors could be observed in both brightfield and GFP channels; secondly, rod photoreceptors were morphologically very different from

Müller glia with respect to cell size and shape, with rod cells being roughly spherical with a diameter of ~ 5-7 µm and Müller glia being a lot larger and elongated in comparison (see figure 2.5.1B). When the co-cultures were imaged through the JuLi^{TM} Digital Fluorescence Microscope, the rod photoreceptors appeared to be spherical in shape (Figure 2.5.1B); confocal microscopy imaging, due to its superior optical resolving power, revealed rod neurite extension (Figure 2.5.1C).

2.7.3. 2-photon time-lapse live imaging of retinal explants

Mice were sacrificed by cervical dislocation and eyes were enucleated and placed into ice-cold RPMI 1640 medium (ThermoFisher, USA). While still in RPMI medium, retinal whole mounts were prepared under a dissection microscope by flattening and mounting the retinae with the photoreceptor side up onto a 0.45 µm MF-Millipore™ nitrocellulose membrane (Millipore, USA). For some of the transplantation live imaging experiments, isolated retinae were incubated in 5 µM Mitotracker® Orange CMTMRos (ThermoFisher Scientific, USA) diluted in RPMI 1640 medium at room temperature for 15 min for labelling purposes. Flat mounted retinae were fixed to the bottom of a Ø5.5 cm tissue culture petri dish using vacuum grease and the dish was filled with DMEM^{gfp}-2 live imaging medium (Evrogen, Russia) additionally topped with paraffin oil to prevent medium evaporation. To further prevent tissue drifting, a platinum ring (Warner Instruments, USA) was placed over the membrane, the weight of which contributed to keeping the membrane in place (for a schematic of the imaging set up see Figure 2.7.1). Images were acquired on a Leica SP8 upright confocal laser scanning microscope (Leica, Germany) set to a scanning frequency of 600 Hz and equipped with 25x or 40x water-immersion objectives (NA = 0.95 and 0.8 respectively) as well as Leica photomultiplier tube/avalanche photo diode hybrid HyD detectors (Leica, Germany). The multiphoton laser source was tuned to a wavelength of 900 nm, which managed to sufficiently excite both (e)GFP and DsRed fluorophores. When operating in 2-photon mode, the pinhole was fully dilated. All recordings were made in a temperature controlled imaging chamber set to 37 °C / 5 % CO_2. For image acquisition, *xyzt* image series were captured at a resolution of 512 x 512, at a step size of 1 µm and at 10-20 min intervals, as appropriate. For the pharmacological investigations, 25 µM Blebbistatin (Sigma, USA), 25 µM Ciliobrevin D (Millipore, USA) or 45 nM Demecolcine (Sigma, USA) were added

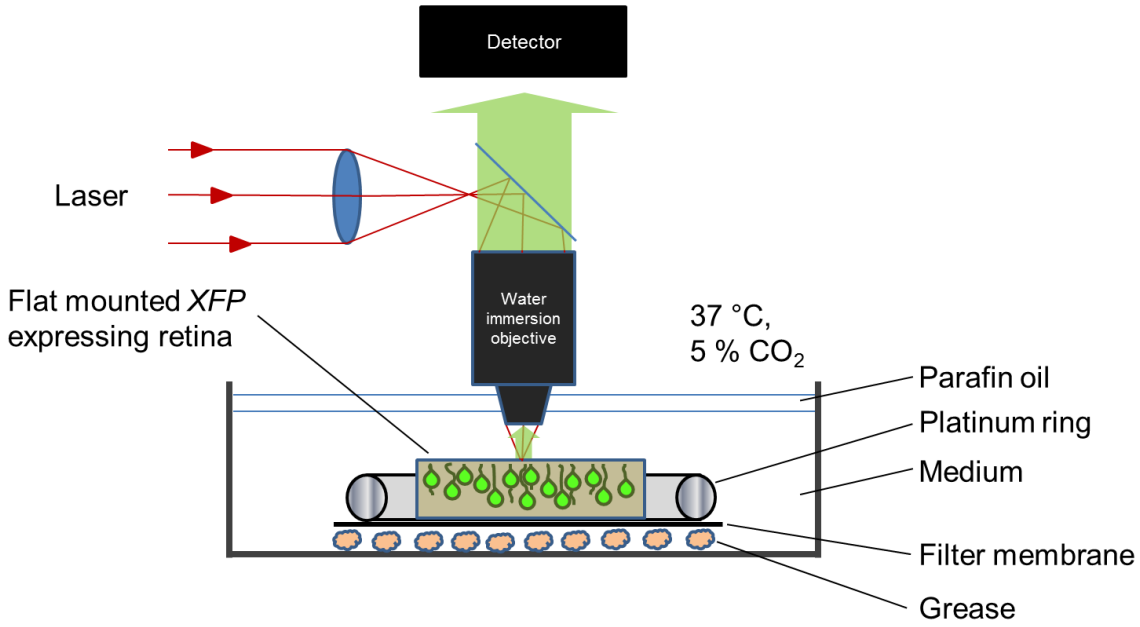

Figure 2.7.1 Schematic depicting the retinal explant live imaging set-up. Retinae harbouring *XFP* expressing cells were flat mounted onto a white filter membrane, typically with the photoreceptor side facing upwards. The tissue was submerged in medium wihtin a petri dish, which was covered by a layer of parafin oil to prevent medium evaporation during the live-imaging session. To reduce the risk of tissue drift in the *x*, *y* or *z* direction, the filter membrane was placed onto a film of grease and the filter was additionally held down by the weight of a platinum ring.The live-imaging was peformed through a water immersion objective dipping into the medium. The whole set-up was placed within an environmental chambre set to 37 °C and 5 % CO_2.

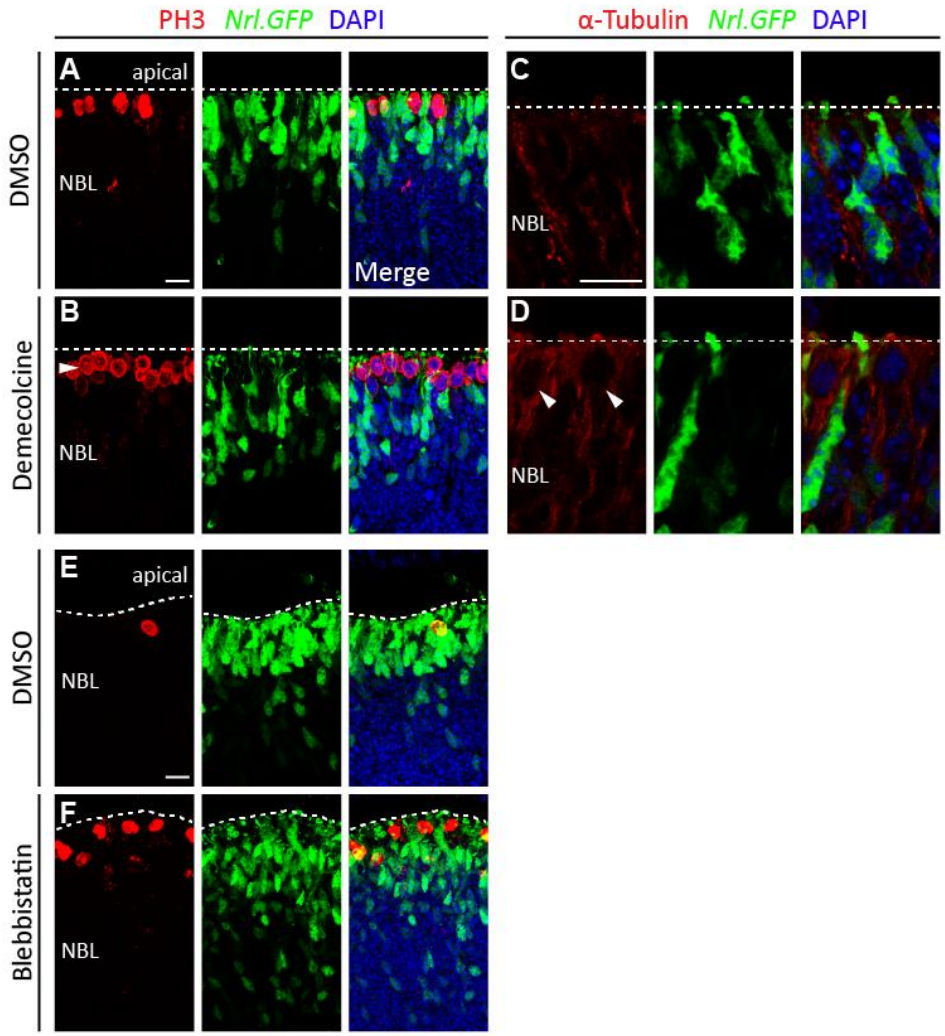

Figure 2.7.2 Characterisation of small molecule pharmacological agents. Eyes from P3 Nrl.GFP$^{+/+}$ mice were explanted and cultured overnight in DMEM^{gfp}-2 live imaging medium and exposed to Demecolcine at a concentration that stabilises microtubule filaments (45 nM) or Blebbistatin (25 µM), with DMSO serving as the control. **(A-D)** In the periphery, a considerable amount of active mitoses were detected, as indicated by immunostaining for the cell cycle M-phase marker PH3 (red) in RPCs, with their somata located adjacent to the apical margin of the neural retina (dotted line) (A). Mitotic cells (PH3 positive, white arrow head)) are arrested in M-phase due to a Demecolcine-mediated arrest in microtubule filament dynamics (B). α-Tubulin immunoreactivity indicates that microtubule filaments are present both in DMSO control (C) and Demecolcine treated neural retinae (D); white arrow head indicates mitotically arrested RPCs. **(E-F)** Central portions of the neural retina exhibit low levels of mitosis (PH3 immunoreactivity) at P3 (E). Blebbistatin treatment leads to a cytokinesis defect in M-phase RPCs resulting in the apical accumulation of their somata (F). Scale bars, 10 µM.

to the imaging medium after a 2-hour control period (0.1 % DMSO was used as vehicle control). Figure 2.7.2 illustrates that the pharmacological agents were effective at the used concentrations. Low concentrations of Demecolcine (45 nM) arrest microtubule filament dynamic behaviour (Panda et al., 1995; Picone et al., 2010), leading to cell cycle arrest during M-phase (Figure 2.7.2A-D). Blebbistatin (25 µM) inhibits actomyosin constrictions, which is required for cytokinesis (the separation of the daughter cells) during M-phase, thus also resulting in the arrest during M-phase (Figure 2.7.2E-F).

2.7.4. Image processing

All acquired images and image series were exported as TIF files and processed in Fiji/ImageJ (National Institutes of Health, USA) (Schindelin *et al.*, 2012) with the standard image processing tools available in order to achieve the maximum possible image quality and signal to noise ratio. All images acquired as part of the same experiment were processed in the exact same way.

For time-lapse recordings, *xyt* and *xyzt* image series were additionally registered to correct for any specimen drift artefacts in the *xy(z)* dimensions that may have occurred during the course of imaging. The Fiji plug-ins used for registration were 'Correct 3D drift' (Parslow *et al.*, 2014) for automated drift correction based on automated landmark recognition and 'Descriptor-based series registration (2D/3D + t)' (Preibisch *et al.*, 2010) in cases where automated registration failed and registration landmarks had to be defined manually. *xyt* time-lapse live imaging recordings of rod photoreceptor and Müller glia co-cultures were additionally signal-enhanced (highlighting specifically rod photoreceptors) and converted from a brightfield type format into a binary format via a series of processing steps, similar to previous descriptions (Chenouard *et al.*, 2014). This was done because GFP signal intensity from individual Nrl.GFP positive rod photoreceptor cells frequently disappeared during the recordings. Thus, rather than relying on the GFP signal for later tracking purposes, only the brightfield signal of individual rod photoreceptors was identified and marked based on size and morphology, to help create a binary image via a custom-made sequence of processing steps performed in Fiji (Figure 2.7.3). Using this methodology, individual rod photoreceptor cells were now coloured white while photoreceptor cell aggregates, cellular debris, Müller glia and the culture dish surface where black. These

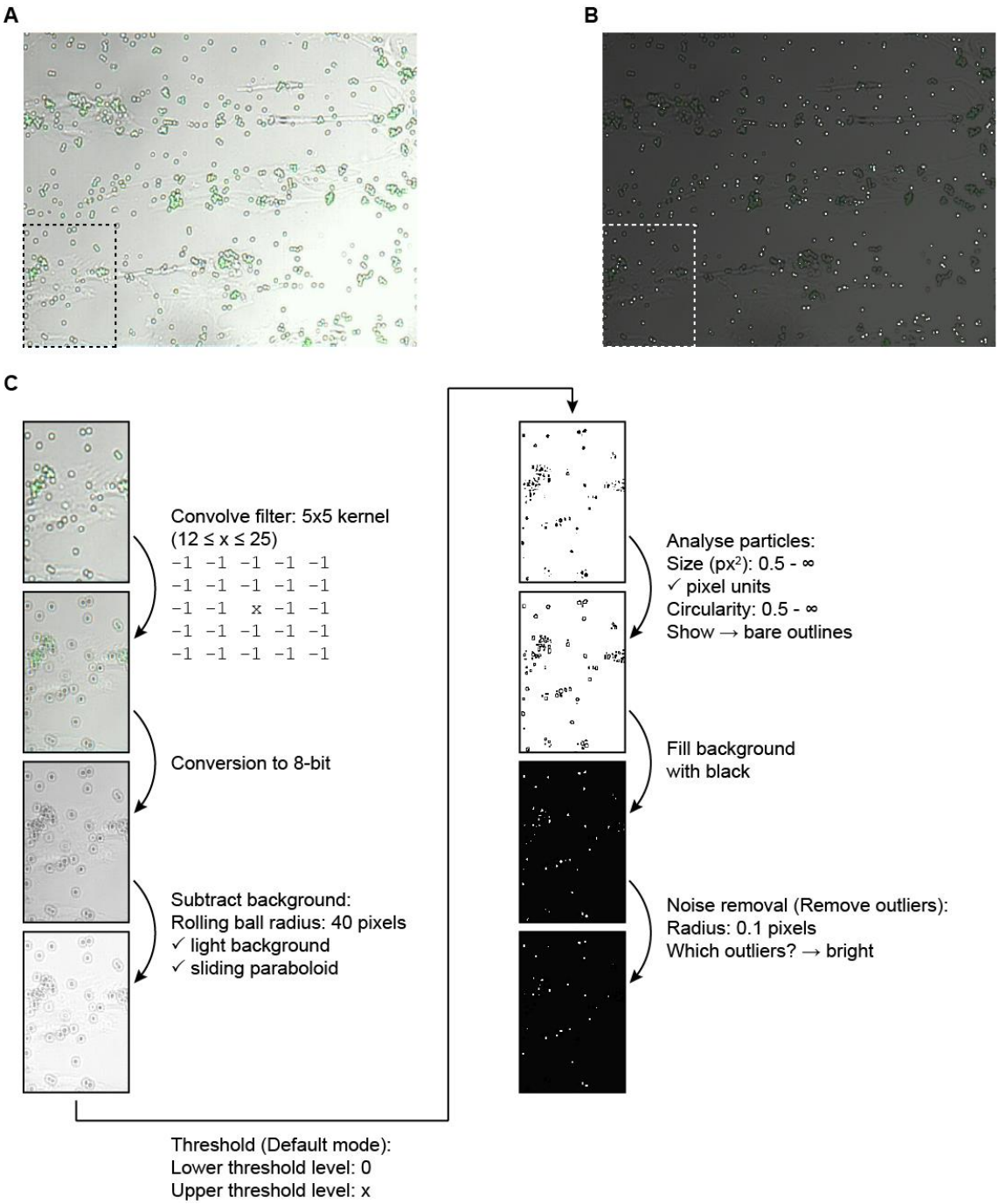

Figure 2.7.3 Image processing of time-lapse live imaging recordings of rod photoreceptor and Müller glia co-cultures. Individual rod photoreceptor somata, as opposed to rod aggregates and Müller glia, were selectively highlighted. **(A)** Overlay of brightfield and GFP fluorescence signal channels. **(B)** Overlay between image shown in A) and processed binary image. The processed binary image depicts mostly individual rod photoreceptor cells (white) but not photoreceptor cell aggregates, cellular debris, Müller glia and the culture dish surface (black). **(C)** Sequence of image processing steps performed in Fiji/ImageJ (National Institutes of Health, USA) based on the boxed region of interest in A) and B).

processed image files were then subjected to cell tracking software analysis (see section 2.7.5).

3D reconstruction of *xyz* or *xyzt* image files was performed using IMARIS software (Bitplane, Switzerland).

2.7.5. Quantitative analysis of rod motility in rod photoreceptor and Müller glia primary cell co-cultures

To track the movement of rod cell bodies in rod photoreceptor-Müller glia co-cultures, the Mosaic Particle Tracker 2D and 3D plugin (Sbalzarini and Koumoutsakos, 2005) in Fiji was applied to registered *xyt* time-lapse image series. Positional information over time (*x*, *y* and *t*) was generated and exported into Microsoft Excel software (Microsoft, USA). Mean squared displacement (MSD) as a function of time was used to quantitatively assess rod cell motility (see Figure 2.7.4A); this was performed with the help of a custom-made code co-developed with Martha Robinson (PhD student with Prof. Robin Ali) and written in MATLAB R2012b (Mathworks, USA). Mean squared displacement values were calculated by taking the average of squared displacements displayed by a cell body between consecutive time steps within a given trajectory followed by further averaging within a population of trajectories; this was repeated for successively increasing time lags. The following equation was applied:

$$MSD(\Delta t) = \frac{1}{N-n}\sum_{i=1}^{N-n}[\Big(x\big((i+n)\delta t\big) - x(i\delta t)\Big) + \Big(y\big((i+n)\delta t\big) - y(i\delta t)\Big)]^2$$

where $(x(i\delta t))$, $(x\big((i+n)\delta t\big)$ and $\big(y(i\delta t)\big)$, $(y\big((i+n)\delta t\big)$ are the *xy* coordinates of a rod cell body at times $i\delta t$ and $(i+n)\delta t$ respectively and where n is an integer representing the data acquisition time interval between those positions; N is the total number of time points within the time-lapse recording. To generate MSD plots, the average MSD values were plotted against time lags Δt (note that the MSD plot will always be positive). The curvature of the produced MSD plot serves as an indicator of the nature of motility displayed (Ruthardt *et al.*, 2011; Figure 2.7.4B). Linear: normal diffusion; positive curvature: active transport; negative curvature: confined/corralled diffusion.

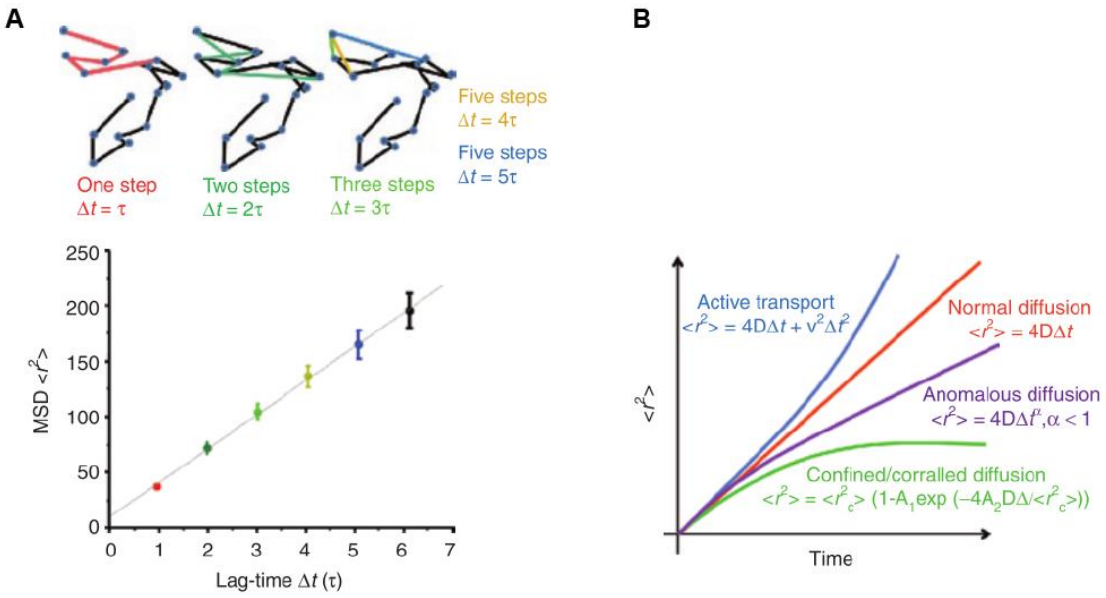

Figure 2.7.4 Principles of mean squared displacement (MSD). **(A)** Schematic trajectory showing the distance travelled between consecutive frames. Within the five initial frames, motions with lag-times from 1-5 frames are indicated. The average of all steps with given lag time contribute to the corresponding point in the MSD plot. **(B)** Interpretation of diffusion coefficient curvature. Linear MSD plot indicates normal diffusion, positive curvature indicates active transport and negative curvature indicates confined/corralled diffusion. (reproduced with permission from Ruthardt *et al.*, 2011).

Diffusion coefficients (D) were calculated from linear MSD plots according to:

$$MSD(\Delta t) = 2D\Delta t$$

The diffusion coefficient of linear MSD plots is thus proportional to the slope of the curve divided by 2. Slopes were obtained from MSD plots in GraphPad Prism® software (Graphpad Software Inc., USA) by fitting a nonlinear regression straight line. As an approximation, the same method was used to derive diffusion coefficients from non-linear MSD plots by fitting a straight line to the relatively linear initial portion of the MSD plots.

2.7.6. Quantitative analysis of rod somatic motility in retinal explant studies

Generally during development, rod cell body migration occurs primarily along the apico-basal axis of the neural retina (Warre-Cornish, PhD thesis, 2013), which translates to the *z* dimension when the time-lapse recording is applied to a Cartesian coordinate system. Lateral movement on the other hand would be in the *xy* dimensions. To track the movement of rod cell bodies, the spot tracking tool within IMARIS software (Bitplane, Switzerland) was applied to registered *xyzt* time-lapse image series. IMARIS software was able to identify rod cell bodies based on the preceding input of size and location parameters. Rod somata were typically ellipsoid in shape, measuring ~ 5µm along the short (lateral) and ~ 7.5 µm along the long (radial) axis, and are typically located deeper within the tissue compared to the developing bulbous segment structures. Positional information over time (*x, y, z* and *t*) was generated and manually verified to ensure faithful tracking of rod cell somata and finally exported into Microsoft Excel software.

Mean squared displacement (MSD) as a function of time was used to quantitatively assess rod cell motility (see Figure 2.7.4A). MSD was used to characterise the different modes of migration with the help of a custom-made code co-developed with Prof. Matteo Carandini, Martha Robinson and Paul Waldron and written in MATLAB R2012b. Mean squared displacement values were calculated by taking the average of squared displacements displayed by a cell body between consecutive time steps within a given trajectory followed by further averaging within a population of trajectories; this was repeated for successively increasing time lags. The following equation was applied:

$$MSD(\Delta t) = \frac{1}{N-n}\sum_{i=1}^{N-n}[z\big((i+n)\delta t\big) - z(i\delta t)]^2$$

where $(z(i\delta t))$ and $(z\big((i+n)\delta t\big)$ are the *z* positions of a rod cell body at times $i\delta t$ and $(i+n)\delta t$ respectively and where n is an integer representing the data acquisition time interval between those positions; N is the total number of time points within the time-lapse recording. To generate MSD plots, the average MSD values were plotted against time lags Δt (note that the MSD plot will always be positive). The curvature of the produced MSD plot serves as an indicator of the nature of motility displayed (Figure 2.7.4B). Linear: normal diffusion; positive curvature: active transport; negative curvature: confined/corralled diffusion.

Diffusion coefficients (D) were calculated from linear MSD plots according to:

$$MSD(\Delta t) = 4D\Delta t$$

The diffusion coefficient of linear MSD plots is thus proportional to the slope of the curve divided by 4. Slopes were obtained from MSD plots in GraphPad Prism® software (Graphpad Software Inc., USA) by fitting a nonlinear regression straight line. As an approximation, the same method was used to derive diffusion coefficients from non-linear MSD plots by fitting a straight line to the relatively linear initial portion of the MSD plots.

Q-Q (quantile-quantile) plot analysis was used to visually assess the normality of measured instantaneous velocities (similar to Warre-Cornish, PhD thesis, 2013; Weir *et al.*, 2004; Clarke *et al.*, 2011). Observed instantaneous velocity values were plotted against their inverse normal values; if the observed values are normally distributed the plotted data points can be fitted with a straight line $y = x$. Where many consecutive observed data points did not fall onto the straight line this was considered a departure from normality. Q-Q plots were made as follows: instantaneous velocity values of a frequency distribution of n data points were ordered in an ascending fashion, ranked ($a = 1, 2, \ldots, n$) and assigned their individual quantile values q. For a given value of a frequency distribution, the quantile describes the proportion of data points below this value ($0 \leq q \leq 1$) and may also be regarded as a measure of probability. It was calculated according to:

$$q = \frac{a}{n+1}$$

where q is the quantile, a is the rank of each data value and n is the total number of data values. The inverse of the standard normal cumulative distribution or probit function (NORMSINV function in Microsoft Excel) was then used to assign values from a standard normal distribution to each quantile (probability) value q. The final inverse normal value was obtained according to:

$$Inverse\ normal = mean(n) + probit \times SD(n)$$

2.8. Statistics

Data are presented as mean ± S.D. (standard deviation) or S.E.M (standard error of the mean). Differences at $p < 0.05$ were assessed for significance based on Student's *t* test or ANOVA as appropriate, in GraphPad Prism® software (GraphPad Software Inc., USA). D'Agostino and Pearson test was used to assess the normality of datasets. For Student's *t* test, data with normal and non-normal distribution were analysed with two-tailed *t* test and Mann-Whitney test respectively. For ANOVA, normally and non-normally distributed datasets were subjected to One-way ANOVA (post test: Tukey) and Kruskal-Wallis test (post test: Dunn's) respectively. Different levels of significance were classified as follows: *, $p < 0.05$; **, $p < 0.01$; ***, $p < 0.001$.

CHAPTER III. ROD PHOTORECEPTOR SOMATA ARE MOTILE DURING DEVELOPMENT

3.1. Introduction

The eye is a highly specialised sensory organ equipped to detect visual inputs and to convert them into electrical signals, which are then partially processed and relayed to higher visual centres of the brain. Essential to this process is an array of diverse neural cells that make up the highly specialised neuronal tissue at the back of the eye known as the retina. The mature retina is stratified in appearance where the different types of neurons are located and synapse with each other in a defined layered organisation. Light detecting rod and cone photoreceptor cells are found in the outermost stratum (ONL) of the retina closest to the retinal pigment epithelium (RPE) whereas retinal ganglion cells (RGCs) locate to the inner layer (GCL) of the retina facing the lens. Between these two classes of cells lies a cohort of secondary neurons that consists of bipolar cells, horizontal cells and amacrine cells as well as Müller glia. Their nuclei populate the INL.

In contrast to this mature stratified architecture, the developing neural retina is arranged in what is known as a pseudostratified neuroepithelium, which is filled with mitotically active retinal progenitor cells (RPCs). These cells span the entire width of the neural retina but their nuclei oscillate between apical and basal positions in synchrony with the different stages of the cell cycle (this is known as interkinetic nuclear migration or IKNM); S- phase is usually carried out basally, while M-phase is restricted to the apical edge of the neural retina, adjacent to the overlying RPE. Consequently, recently born post-mitotic retinal neurons will, in many cases, have to exhibit some form of motility in order to end up in their designated strata. Generally, post-mitotic neuronal precursor cells in the central nervous system (CNS) are known to exhibit one or more of the following modes of migration, depending on cell type: somal translocation, multipolar migration, tangential migration and glial-guided migration. Pre-mitotic neuronal progenitor cells, on the other hand carry out IKNM. Following the birth of RGCs at the apical edge of the neural retina, these cells must traverse the entire radial width of the tissue by somal translocation in order to reach their target layer (GCL). Similarly, amacrine cells, bipolar

cells and horizontal cells need to reach their designated (sub-)layers by migrating in the basal direction, although horizontal cells have been observed to migrate bi-directionally (basally then apically) and in a multipolar fashion towards their target stratum within the INL (Edqvist and Hallböök, 2004).

To date, little attention has been given to photoreceptors. This is most likely due to the fact that, like other retinal neurons, they are born at the apical edge of the neural retina and this already places them in the (presumptive) ONL, their target stratum. Moreover, the majority of studies focussing on retinal neuronal migration and tissue stratification have used the zebrafish as a model vertebrate animal, due to the advantages it offers in terms fluorescence imaging. The zebrafish ONL only features a single layer of photoreceptor cell nuclei, however, making it hard to envision the requirement for any directed photoreceptor migration. The ONL of the mammalian retina, on the other hand, frequently features a larger number of rows of photoreceptors. The mouse ONL, for instance, is approximately 50 µm thick and features ~ 10 rows of rod photoreceptor nuclei, thus providing ample space for migration to occur. Previous fixed tissue immunohistochemical analyses of mammalian retinae have shown that the somata of cone precursors, which are born during early prenatal embryogenesis at the apical surface, become displaced throughout the entire ONL between P4 to P11, before returning back to the apical surface by P12 (Rich *et al.*, 1997), indicating some form of directed movement. Preliminary evidence suggests that rod photoreceptors similarly exhibit somal motility, first in the basal and then in the apical direction (Young, 1984; Warre-Cornish, PhD thesis 2013). This was hypothesised to be analogous to one cycle of IKNM (Warre-Cornish, PhD thesis 2013), a form of migration common to many epithelial tissues but one that is usually only observed in proliferating progenitor cells. Although a preliminary characterisation was presented by Warre-Cornish (PhD thesis, 2013), an in depth characterisation of rod photoreceptor motility has not yet been established.

Understanding the way rod photoreceptors migrate during development is likely to improve our understanding of the establishment of the retinal architecture. Here, it will be important to investigate which of the known modes of neural motility (IKNM, somal translocation, multipolar migration, tangential migration or glial-guided migration) they carry out or whether an entirely novel mode of motility is utilised. Extending beyond the purely developmental domain, a better knowledge of developmental rod photoreceptor somal motility may potentially also contribute towards increasing rod photoreceptor migration and integration into the recipient retina following photoreceptor

transplantation, thereby increasing the clinical prospect of this cell replacement therapeutic approach.

3.2. Aims

The aims of the work carried out in this chapter were:

(1) to investigate and to characterise by 2-photon time-lapse live imaging the migration of genetically labelled rod photoreceptors in the neonatal (P1) explanted *Nrl.GFP*$^{+/+}$ retina

(2) to establish whether rod photoreceptor precursor cells exhibit any of the five known modes of neural motility (IKNM, somal translocation, multipolar migration, tangential migration and glial-guided migration) or whether a novel mode of neural motility is utilised and

(3) to produce a developmental profile of any such motilities occurring between the neonatal stage (P1) and later on in development (P10), by which time cell migrations should have decreased owing to progressive retinal circuit maturation

Combined, these experiments will provide a better insight into how certain aspects of the highly specialised retinal architecture are established with the precision required to enable visual perception.

3.3. Characterisation of rod photoreceptor somal motility

3.3.1. Analysis of rod photoreceptor somal motility at post-natal day 1

3.3.1.1. Rod photoreceptor somal motility occurs mainly along the cell's radial axis

To assess the migratory properties of rod photoreceptor somata in the P1 retina, the eyes of *Nrl.GFP*$^{+/+}$ P1 mice were harvested and the retinae were explanted, flat mounted and time-lapse live imaged by 2-photon fluorescence microscopy at a sampling interval of 10 minutes for a typical duration of 10 hours (Figure 3.3.1A, Movie 3.3.1). The spatial (*xyz*) position of somata over time (*t*) was recorded by an *in silico* tracking method, which was applied to the time-lapse recordings (N = 3 independent retinae). Rod photoreceptor cells all displayed a stereotyped morphology that featured mostly spindle shaped somata measuring ~ 5 µm along the short (lateral) axis and ~ 7.5 µm along the long (radial) axis, dispersed within the apical-most portion of the retinal epithelium. These spindle shaped cell bodies were anchored to the apical limit of the neural retina via an apical process, whereas a basal process could not always be observed. Assuming that the basal process is of similar dimensions as the apical process (this is not an unreasonable assumption based on comparable dimensions in mature photoreceptors), it is unlikely that many basal processes remained undetected due to insufficient imaging resolution. More likely, basal processes may have not been formed by all rod photoreceptors at the time of imaging.

A selection of randomly chosen somal trajectories obtained from the *in silico* tracking was plotted out in a *xyz* Cartesian coordinate system, such that positional changes within the 10-hour recording period are easily observed, albeit without the accompanying time stamps (Figure 3.3.1B). When the coordinate system was viewed from the top (i.e. almost in line with the positive *z* axis), it became immediately apparent that rod somal trajectories displayed very little motility in the *xy* dimensions. In contrast, a rotated, sideways view revealed that these very same trajectories showed a much more pronounced motility along the *z* dimension (compare left and right panels in Figure 3.3.1B).

Thus, the somata of rod photoreceptors display motile behaviour that primarily manifests along the apico-basal axis of the neural retina. The cell morphology and the direction of

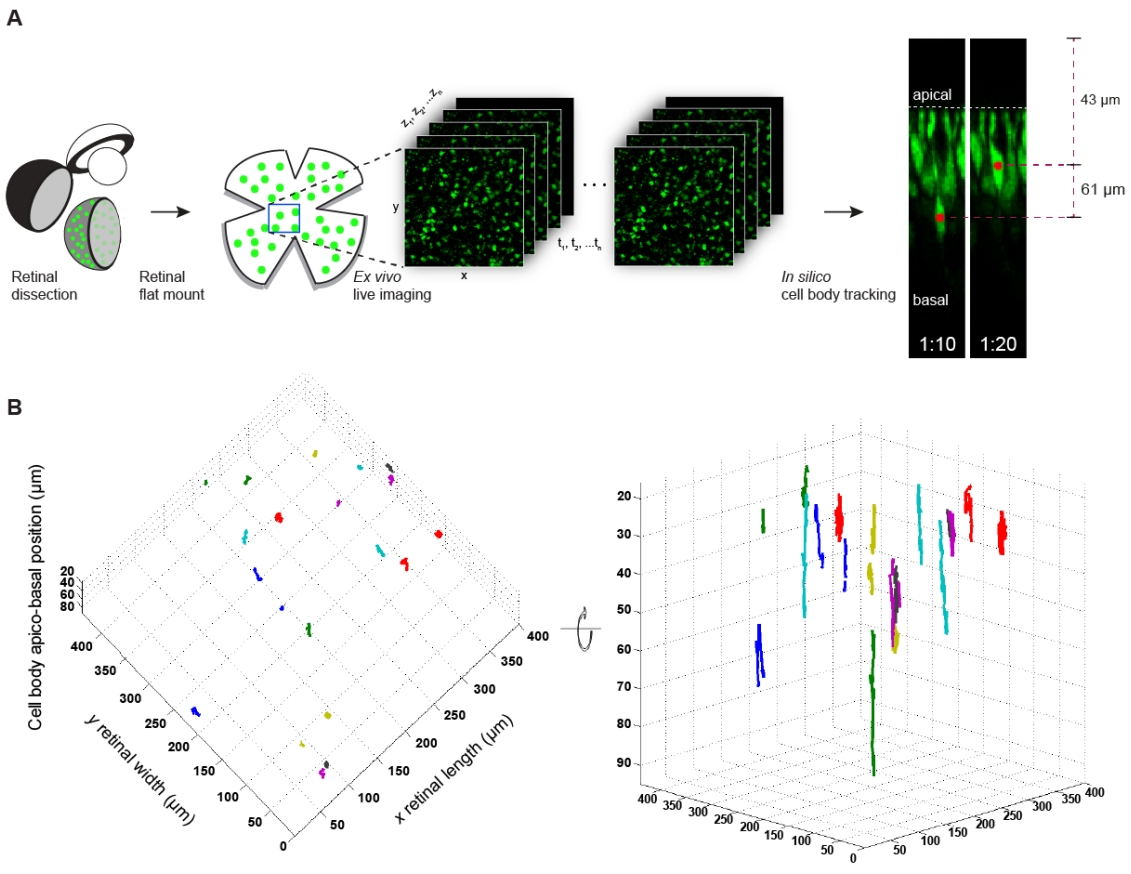

Figure 3.3.1 Assessing rod photoreceptor somal translocation during development. **(A)** Workflow of the investigation of rod photoreceptor somal translocation during development. Retinae were explanted, flat mounted and time-lapse live imaged by 2-photon fluorescence microscopy to produce *xyzt* image stacks. These were then subjected to *in silico* cell body tracking analysis. **(B)** Rod photoreceptor somal translocation occurs preferentially along the apico-basal axis (*z* dimension) rather than laterally within the

movement combined indicate that rod photoreceptor somata do not exhibit multipolar or tangential migration, but rather one (or more) of the radial migration modes.

3.3.1.2. Rod photoreceptors undergo largely stochastic movements interspersed with periods of apically- or basally-directed movement

Due to the pronounced motile behaviour along the radial axis, further analyses were focused on the radial rather than the lateral aspect of rod somal motility. When plotted against time, marked changes in apico-basal position of individual rod photoreceptor somata could be observed from the time-lapse recordings (Figure 3.3.2A & 3.3.2B, Movie 3.3.2). Following initial inspection, somata carried out at least 3 types of movement: cell bodies underwent apically or basally directed migration along the radial axis, together with periods of stochastic positional changes with zero net movement. This section will provide an overview of rod somal motility and gross population-based analyses and the reader is referred to sections 3.3.1.3-3.3.1.5 for a more in depth characterisation of each movement type. Any given individual cell may undergo one or all three of these types of movement in the imaging period. When looking at the frequency distribution of measured instantaneous velocities of all cells (n = 394; N = 3) at all time points, a quasi-Gaussian distribution peaking at 0.0 µm/min could be determined, demonstrating that, over the time frame examined, most of the measured instantaneous velocities were comparatively small (Figure 3.3.2C). In general, somal movements in the apical and basal directions resulted in recorded negative and positive instantaneous velocity values respectively. The recorded peak velocities reached -2.2 µm/min and 1.6 µm/min, which is thus markedly more rapid than the bulk velocities measured. However, those high instantaneous velocities were a lot less common compared to the bulk of low velocity events. This indicates that cell somata are largely stationary but may undergo short periods of movement.

The entire *z* (radial) trajectories of all detected rod photoreceptor precursor somata, irrespective of the types of movements displayed, were then subjected to cumulative mean squared displacement (MSD) analysis, in order to quantify cell body displacement over

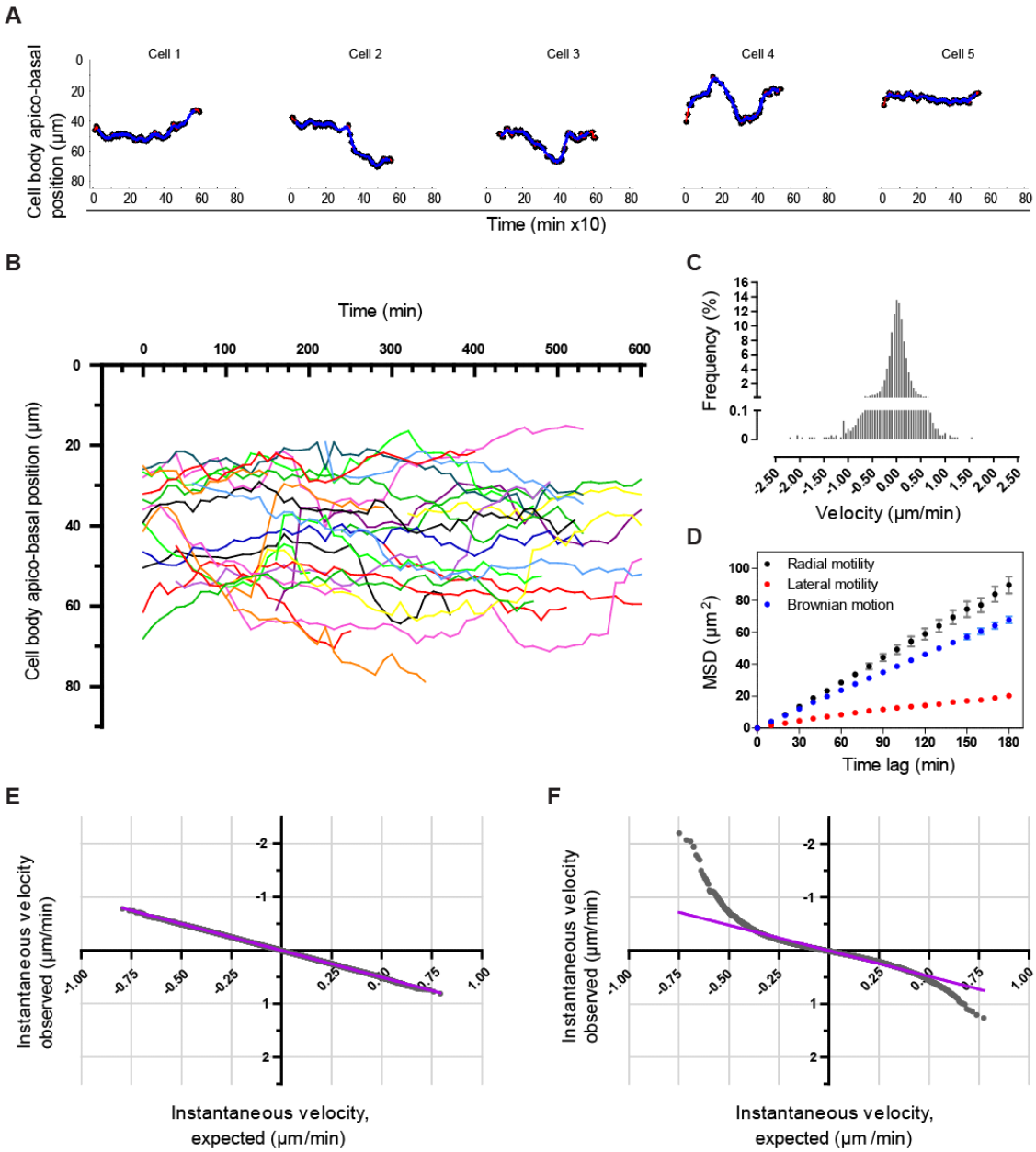

Figure 3.3.2 Global overview of rod photoreceptor somal translocations observed at P1. **(A)** Manually selected, representative example radial trajectories of rod photoreceptor somata. **(B)** Randomly picked rod photoreceptor soma radial trajectories superimposed in a single *zt* plot. 0 µm represents the level of the apical tissue margin. Unfiltered data points are shown in black and are connected by a red line; the blue line shows trajectory data points filtered with a moving average. **(C)** Instantaneous velocity distribution of pooled rod photoreceptor somal translocations. **(D)** Average mean squared displacement (AvMSD) profiles of pooled P1 rod photoreceptor radial (1D) and lateral (2D) translocations. These were additionally compared with the AvMSD profile of 1D Brownian motion trajectories. **(E)** Q-Q plot for 1D Brownian motion trajectories. Instantaneous velocity values were plotted against their inverse normal values. **(F)** Q-Q plot for pooled P1 rod photoreceptor radial somal translocations (1D).

time (Figure 3.3.2D). MSD values were calculated for all time lags within a given trajectory and subsequently averaged within the entire group of trajectories (n = 394 trajectories, N = 3), resulting in average MSD (AvMSD) values at given time lags. The AvMSD for radial somal movements increased linearly with increasing time lag. As mentioned, the overall kinetic profile was dominated by stochastic movements with little to no net displacement (Figure 3.3.2C), thus giving rise to this linear relationship. However, the small but noticeable contribution of directed apico-basal somal motions did likely have a measurable effect on the slope of the AvMSD curve. If movements were purely random and stochastic, then the generated AvMSD curve would appear with a smaller slope similar to the Brownian motion AvMSD curve in Figure 3.3.2D, which was produced from 500 trajectories of Brownian one-dimensional movements; these, by definition, are random but lack consistent, directed apico-basal movements or motility constrains. The fact that the real radial trajectories produced a steeper slope compared with the Brownian trajectories (n.s.) indicates that despite the numerous periods of stochastic zero net displacement movement, there is still a significant positional change of individual cells more profound than Brownian motion. Of note, the slope of the linear AvMSD curve resulting from *xy* lateral movements of rod photoreceptor somata was even more robustly reduced, thus showing quantitatively that rod somata preferentially translocate radially versus laterally (Figure 3.3.1B, 3.3.2D; see also section 3.3.1.1).

To further interrogate the matter of whether the recorded radial rod somal translocations carry an active and directed high velocity migratory component, which would clearly distinguish them from purely Brownian motion, the recorded somal translocations and Brownian movements were compared by Q-Q plot analysis (similar to Warre-Cornish, PhD thesis, 2013; Weir *et al.*, 2004; Clarke *et al.*, 2011). The Brownian motion trajectories were assembled with randomly generated normally distributed positional values. The instantaneous velocity values associated with those trajectories, *ipso facto*, followed the same normal distribution. When these values were plotted against their inverse normal values, all the data points could be fitted with a straight line, thus indicating a normal distribution (Figure 3.3.2E). However, in the case of instantaneous velocity values obtained from real rod photoreceptor somal movements, deviations from normality at negative (apically directed) and positive extremes (basally directed) were apparent (Figure 3.3.2F). Peak velocities in the apical direction were higher compared with basally directed peak velocities (see Figure 3.3.2C). Consequently, the deviation from normality was markedly more pronounced for negative compared with positive

instantaneous velocities, which was accompanied by an earlier onset of deviation from normality at inverse normal values of ~ -0.4 $\mu m^2/min^2$ and ~ 0.5 $\mu m^2/min^2$ respectively (Figure 3.3.2F).

Together, these data demonstrate that rod photoreceptor somal translocation occurs almost exclusively along the apico-basal axis of the neural retina. Although most somal movements appeared to be stochastic with an almost Brownian motion-like character, a small fraction of movements was considerably faster than typical Brownian motion. Hence, the rod photoreceptor somal movements may not be entirely stochastic but could harbour higher velocity, directed somal translocation in the apical and basal directions.

3.3.1.3. Apically directed somal translocation is rapid and highly stereotyped

Among the three modes of rod photoreceptor somal translocation identified, (apically directed, basally directed and stochastic), apically directed translocation is the most striking; although somata can demonstrate a net displacement in the apical direction while undergoing stochastic movement over a prolonged period of time. However, there was a distinct subpopulation of rapid apical translocations. An example of a rod photoreceptor cell undergoing rapid apical somal migration is provided in Figure 3.3.3A and a further fifteen manually selected, example trajectories extracted from the time-lapse live imaging recordings are displayed in Figure 3.3.3B to provide a representative selection of rapid apical translocation events. Initial inspection of manually identified rapid apical translocations revealed that this mode of movement typically displayed a maximum duration of 60-70 minutes. Based on this and the fact that rod photoreceptor somata on average measured 7.5 µm along their radial axes, the threshold for automated rapid apical jump detection was set to 10 µm of apical displacement per 30 minutes. All rapid apical translocations detected with this criterion were normalised with respect to the apico-basal position immediately prior to translocation as well as time and plotted in a single graph (Figure 3.3.3C). The resulting overlay of individual trajectories revealed a highly stereotyped sigmoidal shape consisting of distinct phases of rapid apical translocation: initiation (trajectory displaying positive curvature), principal translocation (linear) and cessation (negative curvature).

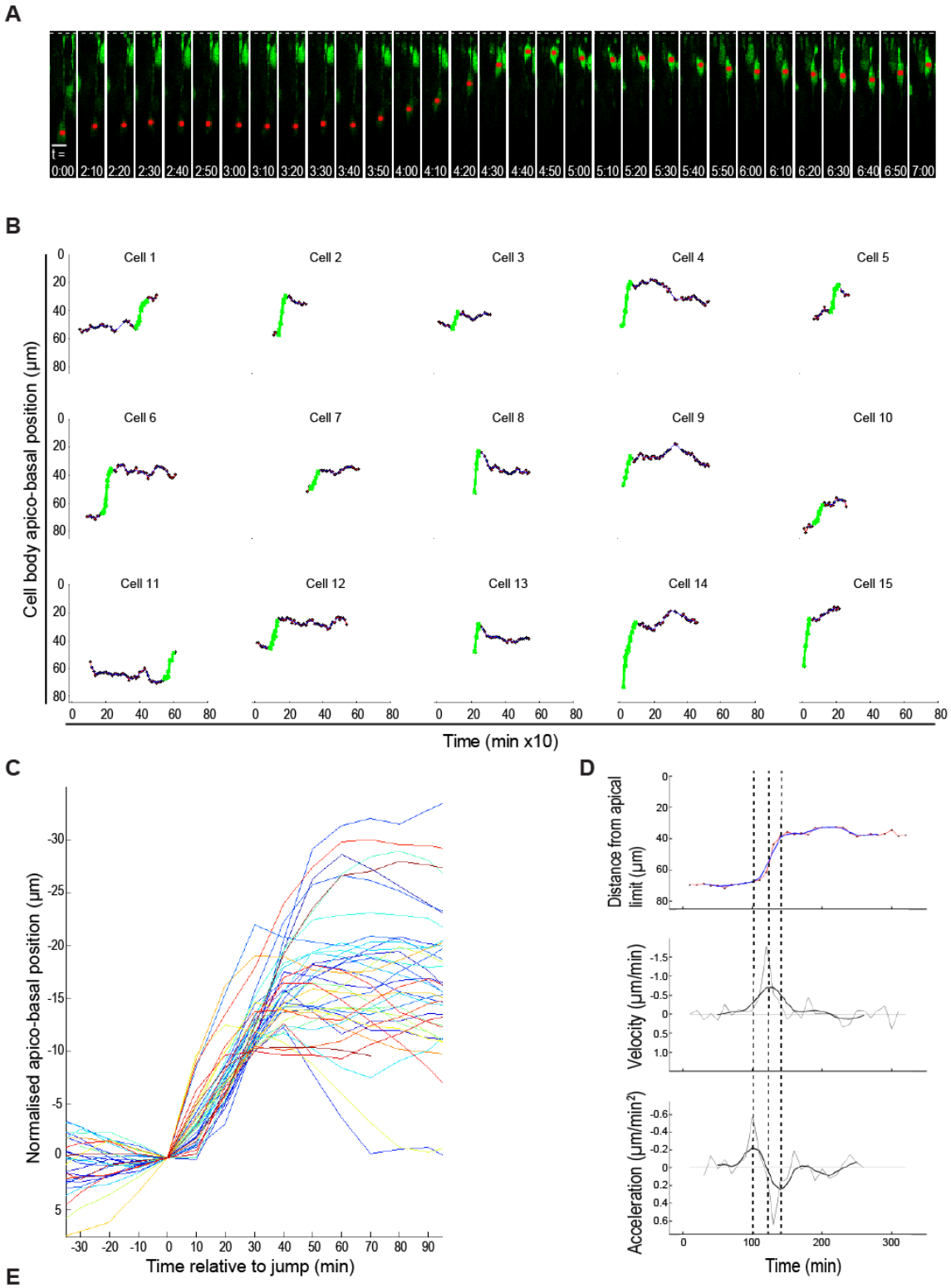

Figure 3.3.3 Characterisation of P1 rod photoreceptor rapid apical somal translocation. **(A)** Representative montage following the apico-basal position of a manually selected rod photoreceptor soma (red dot) displaying rapid apical translocation over time. Scale bar: 10 µm. **(B)** Manually selected, representative example trajectories that featured rod photoreceptor rapid apical somal translocation. (Figure legend continues on following page).

←

(Figure 3.3.3 figure legend continued). 0 µm represents the level of the apical tissue margin. Unfiltered data points are shown in black and are connected by a red line; the blue line shows trajectory data points filtered with a moving average. **(C)** Superimposition of all detected rapid apical somal translocations (threshold: at least 10 µm of apically directed movement in 30 minutes). All rapid apical translocations were normalised with respect to the time and apico-basal position. **(D)** Kinetic profile (position, velocity and acceleration) of an example rapid apical somal translocation. Red or grey lines show raw data recordings while thick blue or black lines show moving average filtered data. **(E)** AvMSD profile of pooled rapid apical translocations of P1 rod photoreceptor somata compared with total radial translocations.

It was next tested whether the occurrence of rapid apical translocations correlated with the depth of the soma within the retina, since apical movement could be triggered upon reaching a certain depth. The *z* (radial) dimension of retinae was split into equally sized 7.5 µm bins, and the probability of finding initiations of apical translocations within these bins was assessed. Under the threshold criteria specified (minimum -10µm in 30 min), very few (1.5 %) of rapid apical translocations were initiated from bins covering a depth up to 18.75 µm away from the apical margin, directly followed by a sharp rise in the

number of initiation events from bins between 18.75 and 48.75 µm (81.3 %), of which the bin centred at 45 µm stood out by contributing 36.5 %. This was followed by a drop off of initiations down to 17.2 % from bins between 48.75 µm to 71.25 µm. While the low probability of finding such jumps at distances less than 18.6 µm is explained by the pre-defined threshold, the low jump probability at depths beyond 48.8 µm correlates well with the fact that most rod photoreceptor somata of the P1 retina were found within 50 µm from the apical limit of the retina. Accordingly, the distance covered by rapid apically translocating somata ranged from 10 to 32 µm. Of note, the cessation phase of rapid apical translocation was not, as might be presumed, dictated by the apical limit of the neural retina, but was observed to occur at a range of depths, much like the initiation depth. Thus, although rapid apical translocation can be initiated from a range of depths, the probability of initiation was highest at a depth of ~ 45 µm. This makes it possible that reaching this pseudo-limit could stimulate rapid apical translocation, although there were exceptions to this rule.

One example trajectory (cell 6 in Figure 3.3.3B) is shown in Figure 3.3.3D to illustrate the kinetic profile of rapid apical translocation, showing tracked somal position, velocity

and acceleration over time. Somal position followed the described stereotypical sigmoidal shape. The velocity and acceleration profiles were found to provide good quantifiable indicators of the three distinct phases of rapid apical translocation: the local velocity minimum (-0.7 µm/min) indicated the peak of the translocation phase (a range of peak velocity values between -0.3-0.7 µm/min was measured for all observed rapid apical translocation events), whereas the local acceleration minimum and maximum (-0.2 µm/min^2 and 0.2 µm/min^2) were indicators of initiation and cessation phases respectively.

Finally, all trajectory fragments corresponding to rapid apical translocation as determined by automated detection were subjected to MSD analysis (Figure 3.3.3E). In comparison to the straight AvMSD curve profile of total radial motility, the AvMSD curve profile of rapid apical translocation was markedly steeper as well as sigmoidal in shape. A positive curvature was identified between time lag values 0 and 30 minutes, which gradually transitioned into a negative curvature with an onset at time lag 60-70 minutes. It is the positive curvature of the AvMSD curve profile that is indicative of a directed, and perhaps active, apical translocation mechanism of rod somata (Qian *et al.*, 1991; Ruthardt *et al.*, 2011).

3.3.1.4. Basally directed somal translocation displays a variable kinetic profile

Next, basally directed translocation of rod photoreceptor somata was investigated. Compared with rapid apical somal translocation, basal somal translocation displayed a slower but, in most cases, more prolonged type of movement. To account for this, a different threshold was applied to the entire group of full-length trajectories in order to select those trajectory fragments that exceeded the threshold of 2 radial cell lengths (or 15 µm) of basal translocation in ≥ 2 hours. In contrast to the highly stereotyped apical movements, there were qualitative differences in the way that cell bodies translocated in the basal direction, as illustrated with the manually selected, representative example trajectories in Figure 3.3.4A and 3.3.4B. Some movements proceeded at a low velocity and in a stochastic manner (e.g. cell 14 in Figure 3.3.4B), while others displayed much higher velocities, in a manner more similar to the directed motions in the apical direction (cell 5). At times, some rod photoreceptor somata were observed to transition from low

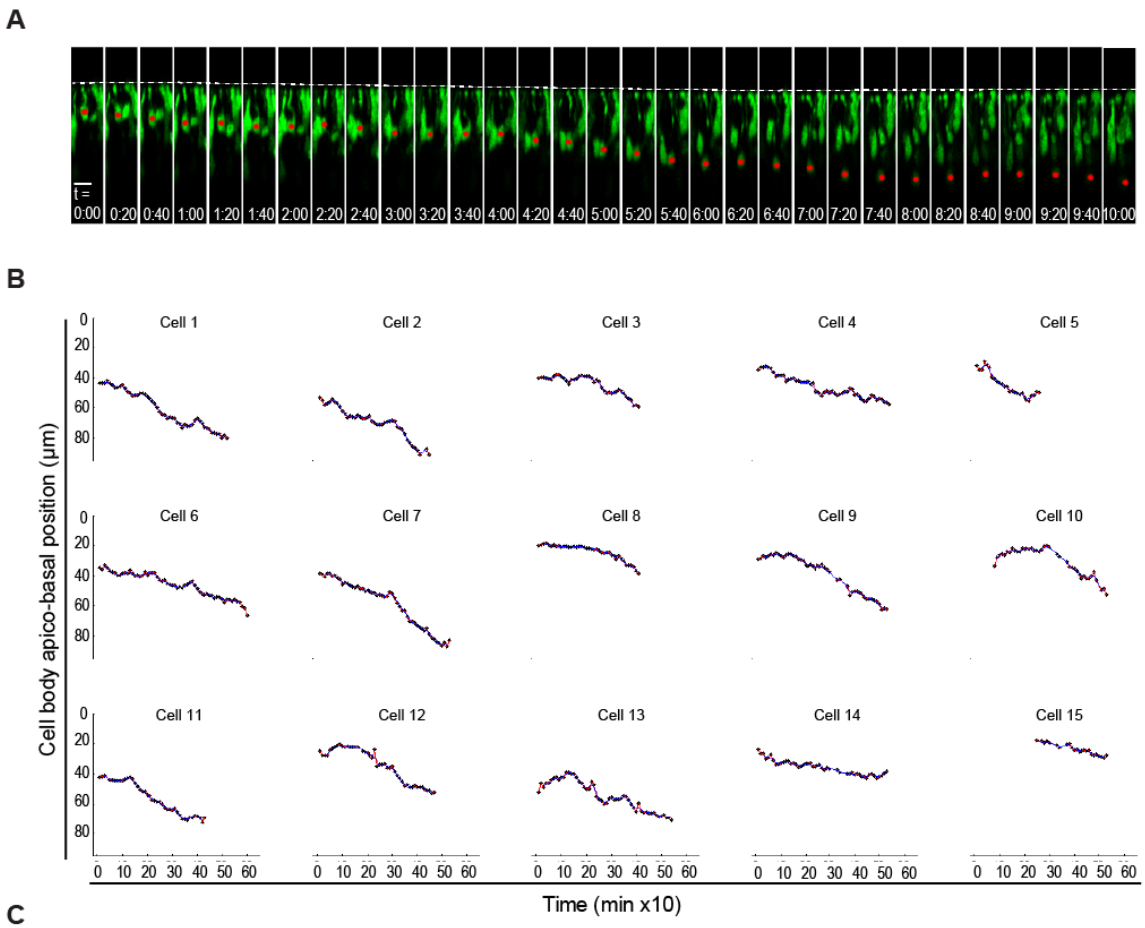

Figure 3.3.4 P1 rod photoreceptor basally directed somal translocation is heterogeneous. **(A)** Representative montage following the apico-basal position of a manually selected rod photoreceptor soma (red dot) displaying basally directed somal translocation over time. The threshold for the detection of basal translocation was set to 15 µm of basally directed translocation in at least 2 hours. Scale bar: 10 µm. **(B)** Manually selected, representative example trajectories that featured rod photoreceptor basally directed somal translocation. 0 µm represents the level of the apical tissue margin. Unfiltered data points are shown in black and are connected by a red line; the blue line shows trajectory data points filtered with a moving average. **(C)** Kinetic profile (position, velocity and acceleration) of an example rapid apical somal translocation. Red or grey lines show raw data recordings while thick blue or black lines show moving-average filtered data.

velocity to higher velocity basal translocation (cell 7). Yet other basal translocations were saltatory with quick bursts of basal movement over relatively short distances, which were interspersed with periods of stochastic movements with little to no net displacement (cells 3, 4 and 6).

The movement kinetics of cell 7 (Figure 3.3.4B) were analysed to illustrate the variable nature of basal somal translocation (Figure 3.3.4C): between 0 and 300 minutes of the imaging period, basally directed somal displacement of this cell proceeded at an almost constant and slow velocity of 0.058 ± 0.007 μm/min. A brief transition phase indicated by the local maximum in the acceleration versus time plot (0.1 μm/min^2), was then

followed by a period of higher constant velocity at an average of 0.155 ± 0.014 μm/min. As exemplified by this cell, there was considerable heterogeneity between basally-directed rod photoreceptor somal translocations. This may point towards the existence of different modes of basal somal translocation, potentially involving different active mechanisms, and/or passive basal displacement caused by the radial translocation of surrounding somata of rod photoreceptors or other retinal cell types.

3.3.1.5. Cells undergoing apical or basal directed movement also display prolonged periods of stochastic motion

The final mode of rod photoreceptor somal translocation described is the stochastic mode. Somata displaying this type of motility typically exhibited many sequential, short distance and short duration movements, which resulted in minimal, if any, net apico-basal displacements. Due to this observation, a threshold was applied to the entire time-lapse recording data set in order to isolate those trajectory fragments that remained below the threshold of 2 radial cell lengths (or 15 μm) of apico-basal translocation for ≥ 2 hours while excluding those that exhibited rapid apical translocation. An example rod photoreceptor cell together with manually selected, representative *z*-dimension trajectories are displayed in Figure 3.3.5A and 3.3.5B. Although the overall net displacement within this group of trajectory segments was mostly negligible, minute net basal (cells 1 & 5, Figure 3.3.5B) and net apical displacements (cells 2 & 4) were occasionally observed

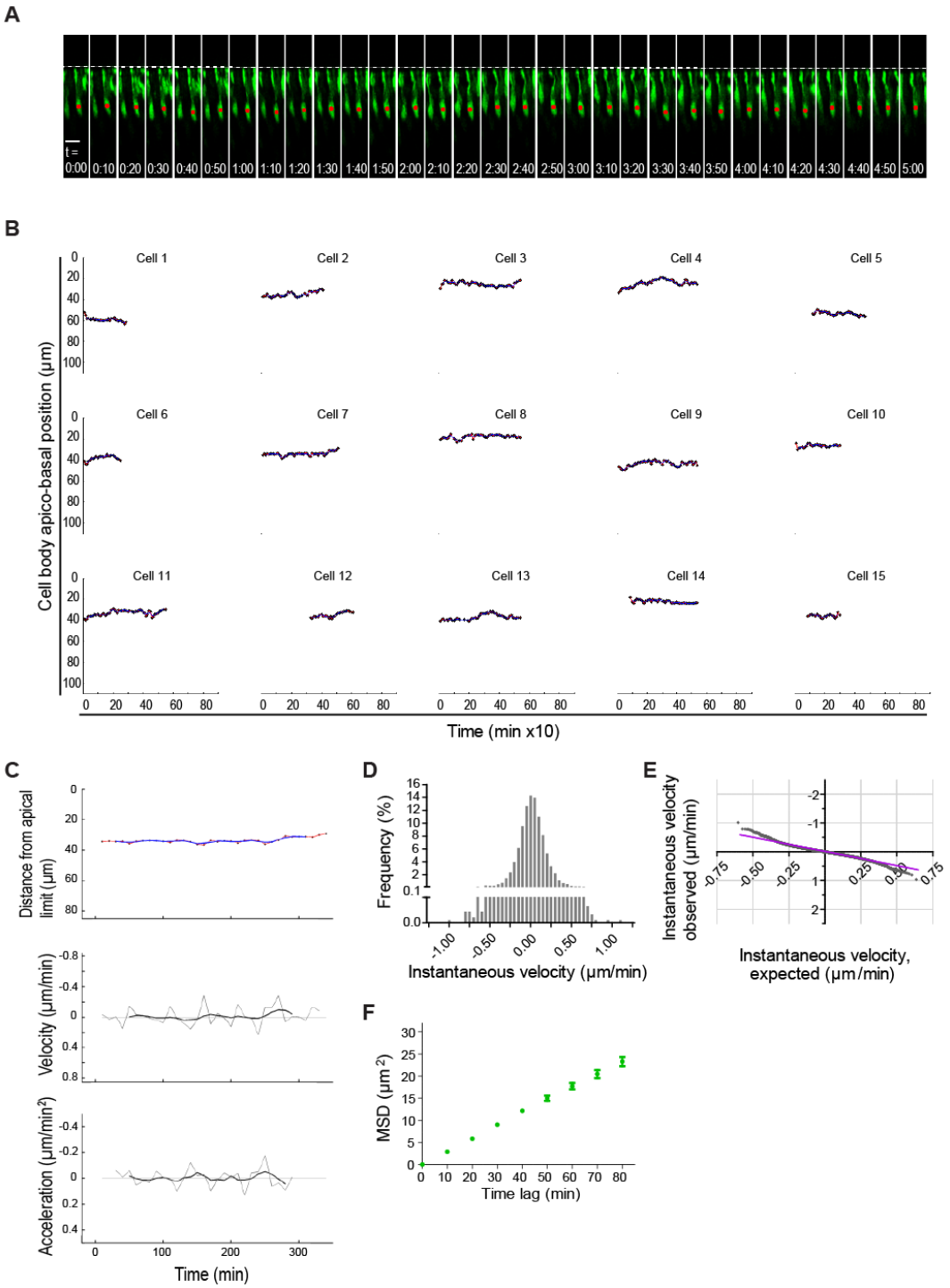

Figure 3.3.5 Characterisation of P1 rod photoreceptor stochastic somal translocation with little to no net displacement. **(A)** Representative montage following the apico-basal position of a manually selected rod photoreceptor soma (red dot) displaying stochastic somal translocation over time. Scale bar: 10 µm. **(B)** Representative example trajectories that featured rod photoreceptor stochastic somal translocation. 0 µm represents the level of the apical tissue margin. Unfiltered data points are shown in black and are connected by a red line; the blue line shows trajectory data points filtered with a moving average. **(C)** Kinetic profile (position, velocity and acceleration) of an example rapid apical somal translocation. Red or grey lines show raw data recordings while thick blue or black lines show moving average filtered data. **(D)** Instantaneous velocity distribution of pooled rod photoreceptor somal translocations. **(E)** Q-Q plot for pooled rod photoreceptor stochastic somal translocations. **(F)** AvMSD profiles of pooled P1 rod photoreceptor stochastic radial translocations.

The stochastic nature of these micro-movements exhibited by rod photoreceptor somata are further highlighted by velocity and acceleration kinetic profiles of an example cell shown in Figure 3.3.5C. Here, the many measured micro changes in velocity and acceleration were detectable only when focusing on the real data points shown in thin grey lines, but not when focusing on the data points created by applying a moving average filter. When the measured instantaneous velocities from all trajectories were placed in a frequency distribution histogram, the velocities displayed a quasi-normal distribution peaking at 0.0 as would be expected from stochastic movement with little to no net somal displacement (Figure 3.3.5D). Accordingly, when these instantaneous velocities were plotted against their inverse normal values, there was only minimal deviation from a linear fit curve that represents perfect normality (Figure 3.3.5E; see also Figure 3.3.2D & 3.3.2E) (Warre-Cornish, PhD thesis, 2013; Weir *et al.*, 2004; Clarke *et al.*, 2011). Finally, the entirety of identified trajectory fragments exhibiting stochastic displacements were subjected to MSD analysis (Figure 3.3.5F). The result was an AvMSD curve profile that could be fit with a straight line, which is usually the case for stochastic motion in general (Qian *et al.,* 1991; Ruthardt *et al.,* 2011). These data are in keeping with the Q-Q plot presented in Figure 3.3.5E. The slope of the AvMSD profile was much shallower compared with the curve profile of rapid apical translocation or total radial motility (see Figure 3.3.3E). This was to be expected since the contributions of apical and basally directed somal translocations likely increase the average in the AvMSD calculations.

3.3.1.6. Rod photoreceptor somata can cycle through all 3 modes of translocation: interkinetic nuclear migration like motility in a post-mitotic neuronal cell population

Following rapid apical translocation, rod photoreceptor somata were often observed to enter a period of either stochastic movement or basally-directed translocation (see Figure 3.3.3A and 3.3.3B). This indicates that any individual rod photoreceptor precursor cell can undergo more than one mode of somal motility. Upon further inspection, it became clear that an individual rod photoreceptor may display all three modes of somal motility and the time lapse recordings even suggest that cells can repeatedly cycle through those three modes (Figure 3.3.6A and 3.3.6B, Movie 3.3.3). Cycling was defined as displaying either a rapid apical-basal-rapid apical or basal-rapid apical-basal type somal motility

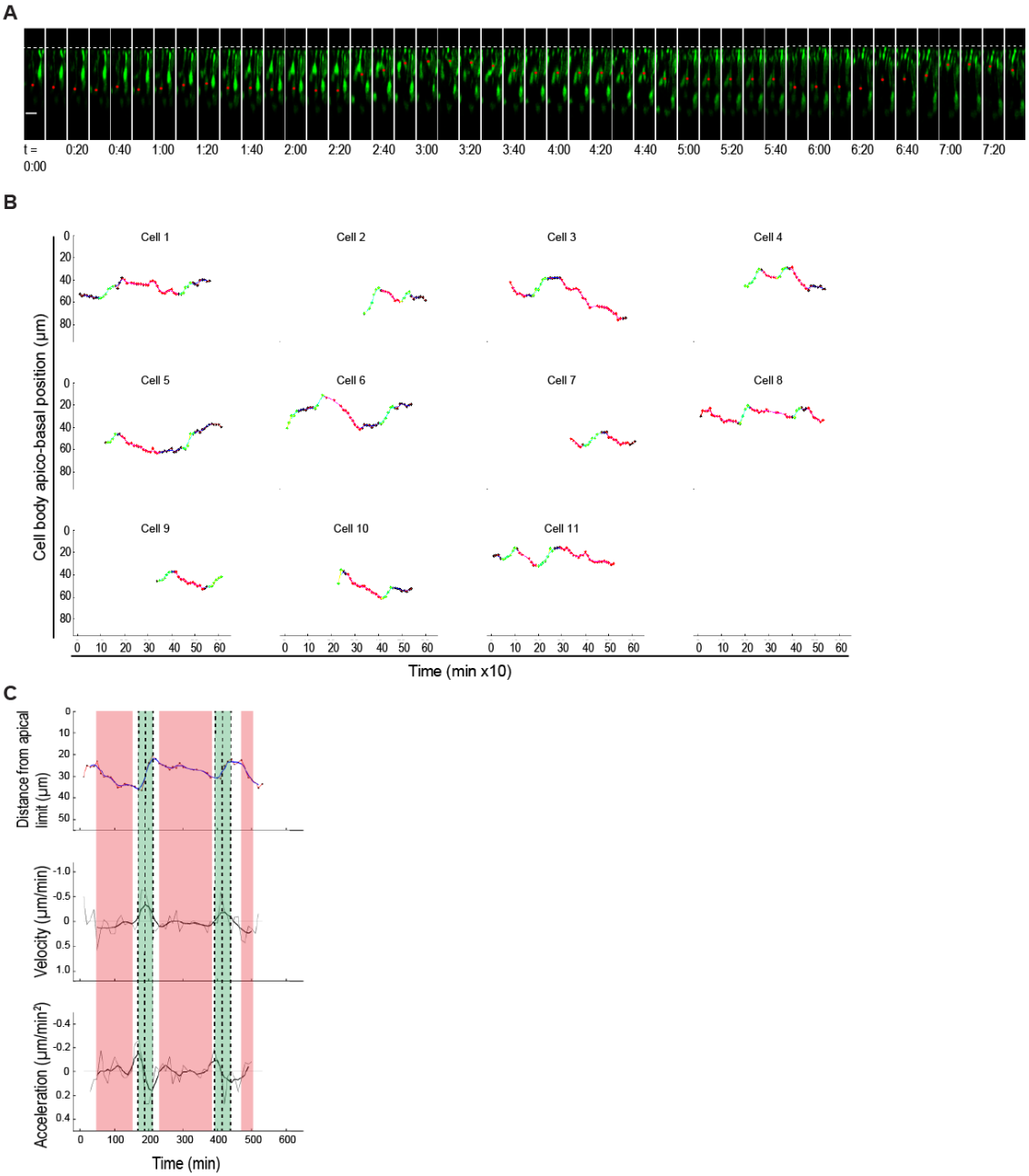

Figure 3.3.6 Rod photoreceptors in the P1 retina can oscillate between more apical and more basal radial positions. **(A)** Representative montage following the apico-basal position of a manually selected rod photoreceptor soma (red dot) displaying apico-basal somal oscillations over time. Scale bar: 10 µm. **(B)** Example trajectories that featured rod photoreceptor somal radial oscillations. Periods featuring rapid apical and basally directed somal translocation were highlighted in green and red respectively. **(C)** Kinetic profile (position, velocity and acceleration) of an example rod photoreceptor exhibiting radial oscillations of the soma. Red or grey lines show raw data recordings while thick blue or black lines show moving average filtered data. Periods featuring rapid apical and basally directed somal translocation were highlighted in green and red respectively.

pattern interspersed with variable periods of stochastic motion. Out of the 394 total trajectories scanned for cycling motion, only 11 exhibited this behaviour (Figure 3.3.6B). This relatively small number most likely reflects the duration of a typical translocation cycle exceeding the imaging duration in this set of experiments (10 hours). A longer time-lapse recording duration would likely permit the detection of more oscillations provided that retinal explants remained viable as well.

The oscillatory apico-basal somal translocation exhibited here by a post-mitotic neuronal precursor cell (rod photoreceptor) has characteristics very similar to the oscillatory apico-basal somal movements, or interkinetic nuclear migration (IKNM), of progenitor cells in pseudostratified epithelia. A hallmark of IKNM is that progenitor somata undergo radial translocation in concert with cell cycle progression; indeed, progression through the cell cycle is thought to be necessary for IKNM (Ueno *et al.*, 2006; Leung *et al.*, 2011). No evidence of cell division was observed in the current study, yet the movement kinetics of post-mitotic rod somata were remarkably reminiscent of IKNM, including the uniformly rapid apical translocation and slow and stochastic basal movements interspersed with soma faster components. This is reflected in the velocity and acceleration profiles of a representative rod photoreceptor soma undergoing oscillatory radial movements (Figure 3.3.6C), which is highly reminiscent of the kinetic profile usually displayed by neural progenitor cells exhibiting IKNM (e.g. Norden *et al.*, 2009; Tsai *et al.*, 2010).

These data demonstrate for the first time that a post-mitotic neuronal cell type can exhibit an oscillatory somal translocation behaviour very similar to IKNM – a type of motility previously only associated with dividing epithelial progenitor cells.

3.3.2. Comparison of rod photoreceptor somal motility between post-natal day 1 and post-natal day 10

3.3.2.1. Rod photoreceptor somal translocation stops by approximately post-natal day 10

Next, retinae from P3, P7 and P10 mice were examined to determine the developmental time period, over which rod somal translocation occurs. Although retinae older than P10 were also investigated, it was difficult to maintain these in a sufficiently viable state (data not shown). In addition, an increase in optical aberrations was noted in P10 and older retinae. For those reasons, kinetic characterisations were restricted to between P1 and P10 (P1: N = 3 independent retinae, n = 394 trajectories; P3: N = 3, n = 324; P7: N = 3, n = 262; P10: N = 3, n = 263).

Figure 3.3.7A shows a side-by-side comparison of superimposed rod somal radial trajectories as observed at P1, P3, P7 and P10. By visual inspection, rod photoreceptor somata in the P1 and P3 retina displayed high apico-basal motility, while those from P7 retinae had fewer translocation events and by P10 the vast majority of rod somata were stationary. Quantitative assessment confirmed this reduction in radial motility during the early post-natal period: When looking at the frequency distribution of all measured instantaneous velocities, quasi-Gaussian distributions peaking at 0.0 µm/min were observed at all four time points (Figure 3.3.7B). However, while the distribution curves were very similarly shaped at P1 and P3, there was a narrowing of the distribution curve at P7 and P10. This narrowing manifests as an increase in zero-to-low velocity events with a concomitant decrease in high velocity events. Similarly, MSD analysis of all full-length trajectories across all developmental stages showed a progressive reduction in rod photoreceptor somal motility during early post-natal development (Figure 3.3.7C). At P1 a coefficient of movement value, which is directly proportional to the slope of a straight line fitted to the initial time lag segment (60 min in this case) of the MSD curve, of 0.234 ± 0.010 $\mu m^2/min^{-1}$ was measured (Figure 3.3.7D). While the coefficient of movement value increased slightly at P3 compared to P1 (0.241 ± 0.017 $\mu m^2/min^{-1}$), the coefficient became considerably smaller at P7 (0.188 ± 0.020 $\mu m^2/min^{-1}$) and even more so at P10 (0.034 ± 0.006 $\mu m^2/min^{-1}$) (P3 vs P10 = 86.1 % reduction, $p < 0.05$).

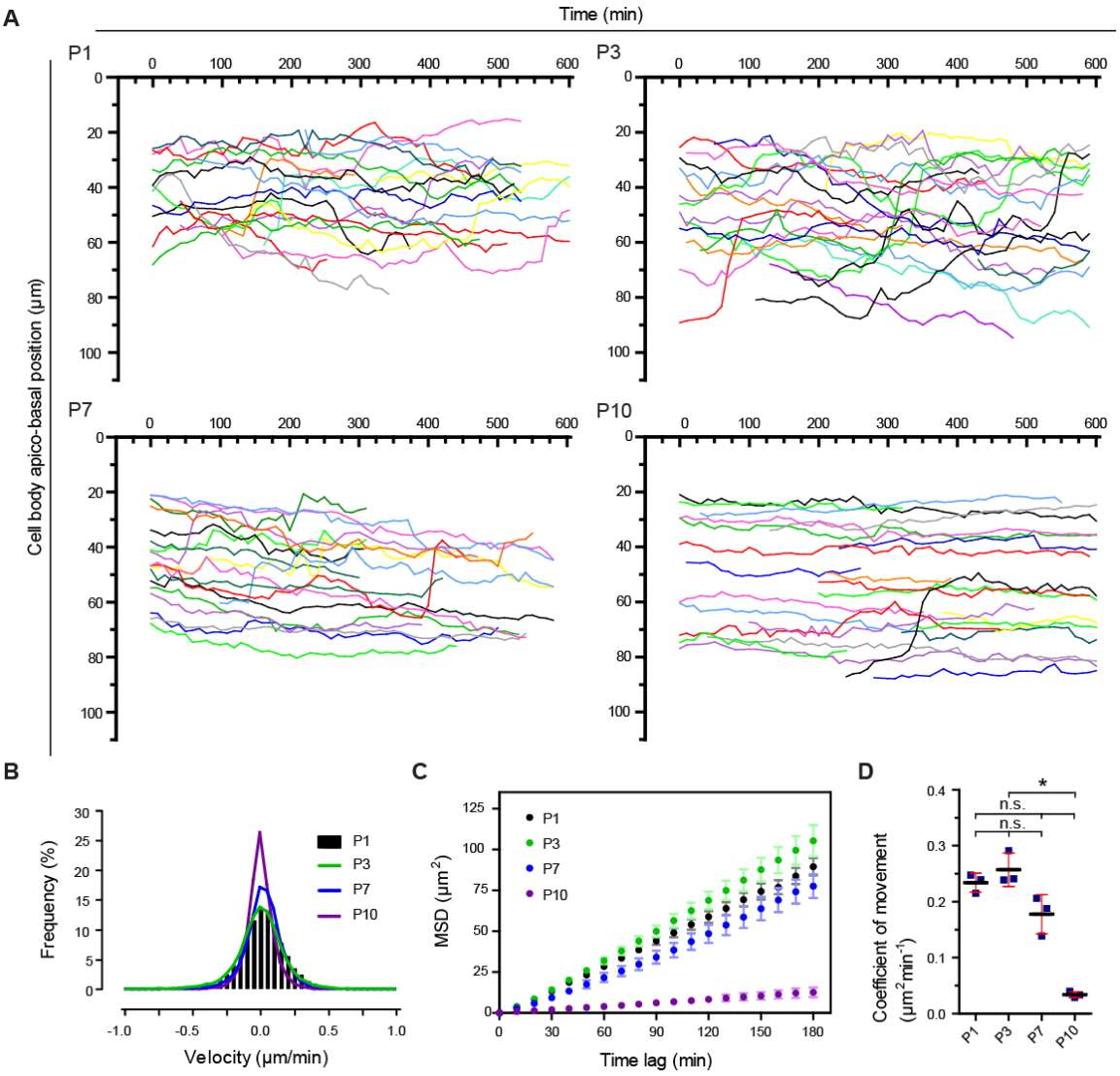

Figure 3.3.7 Characterisation of developmental rod photoreceptor somal motility at P1-P10. **(A)** Randomly picked rod photoreceptor soma radial trajectories observed in P1, P3, P7 and P10 retinae superimposed in a single *zt* plot. **(B)** Instantaneous velocity distribution of pooled rod photoreceptor somal translocations in P1-P10 retinae. **(C)** AvMSD profile of pooled total translocations of P1-P10 rod photoreceptor somata. Data are displayed as mean ± SEM. **(D)** Comparison of coefficient of movement values associated with AvMSD profiles in C. The coefficient of movement is directly proportional to the slope of a straight line fitted to the initial segment (0-60 minutes in this case) of the individual AvMSD profiles. Data are displayed as mean ± SD. Data were compared with 1-way ANOVA. *$p < 0.05$.

Taken together, these data demonstrate that rod photoreceptor somata display high apico-basal oscillatory motility during the first post-natal week, which gradually ceases at or around P10. Moreover, the fact that apico-basal translocations were observed from P1 to P10 supports the notion that individual rod photoreceptor somata can repeatedly oscillate between apical and basal positions in an IKNM-like manner during early post-natal development.

3.3.2.2. Comparing the different modes of rod somal oscillatory motility between P1 and P10

As described in section 3.3.1.6, the oscillatory rod photoreceptor somal translocation observed during P1 retinal development is composed of at least 3 distinct components: rapid apically translocation, basal translocation and stochastic movement. All three modes of somal motility are represented to some extent at P1, P3, P7 and P10, as shown in Figure 3.3.7A. To examine this in greater detail, a side-by-side comparison of all motility components at P1, P3, P7 and P10 was produced.

Rapid apical translocation:

Considering rapid apical somal translocation first, there was no qualitative change between P1 and P10. Figure 3.3.8A-D shows examples of individual motile rod somata taken directly from time-lapse recordings, while Figure 3.3.8E shows superimposed time- and starting position-matched trajectory representations. The three phases of rapid apical translocation (initiation, principal translocation and cessation) were apparent at all time points. However, in accordance with the gradual reduction of overall rod somal motility during post-natal development, there was a noticeable drop in the number of rapid apical translocation events when comparing P7, and especially P10, to P1 and P3 (Figure 3.3.8E; threshold for automatic detection: at least 10 µm of apical translocation covered in 30 minutes). Despite the reduction in frequency of rapid apical translocation events at later time points compared to early time points, the quality of the movement remained relatively constant, at least as assessed by comparing the peak velocity values. The peak

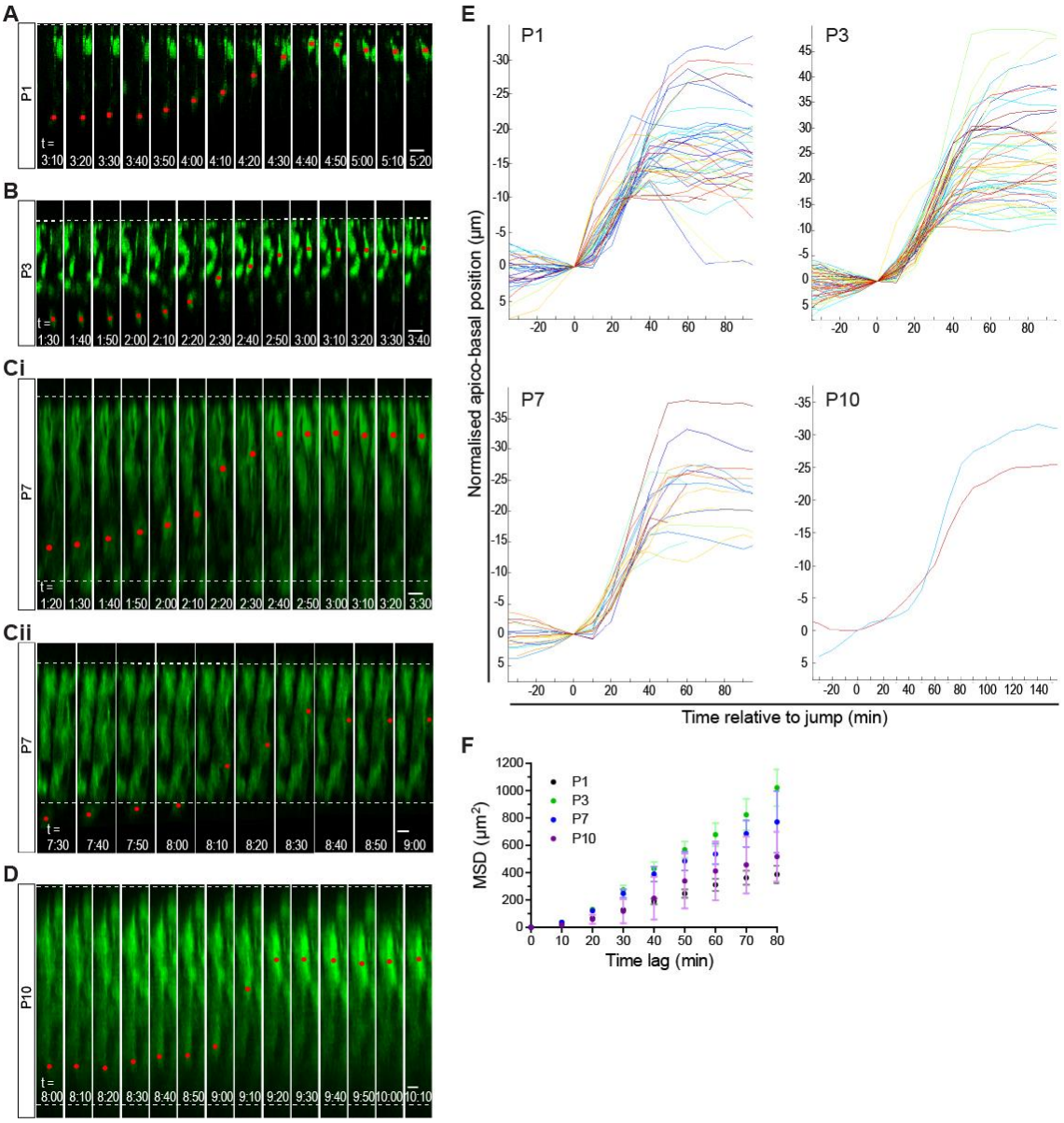

Figure 3.3.8 Characterisation of rod photoreceptor rapid apical somal translocation in the P1, P3, P7 and P10 retina. **(A-D)** Representative montages following the apico-basal position of rod photoreceptor somata (red dot) displaying rapid apical somal translocation over time. Scale bars: 10 µm (A & B), 5 µm (C & D). **(E)** Superimposition of all detected rapid apical somal translocations (threshold: at least 10 µm of apically directed movement in 30 minutes). All rapid apical translocations were normalised with respect to the time and apico-basal position. **(F)** AvMSD profiles of pooled rapid apical translocations of rod photoreceptor somata in P1-P10 retinae. Data are displayed as mean ± SEM.

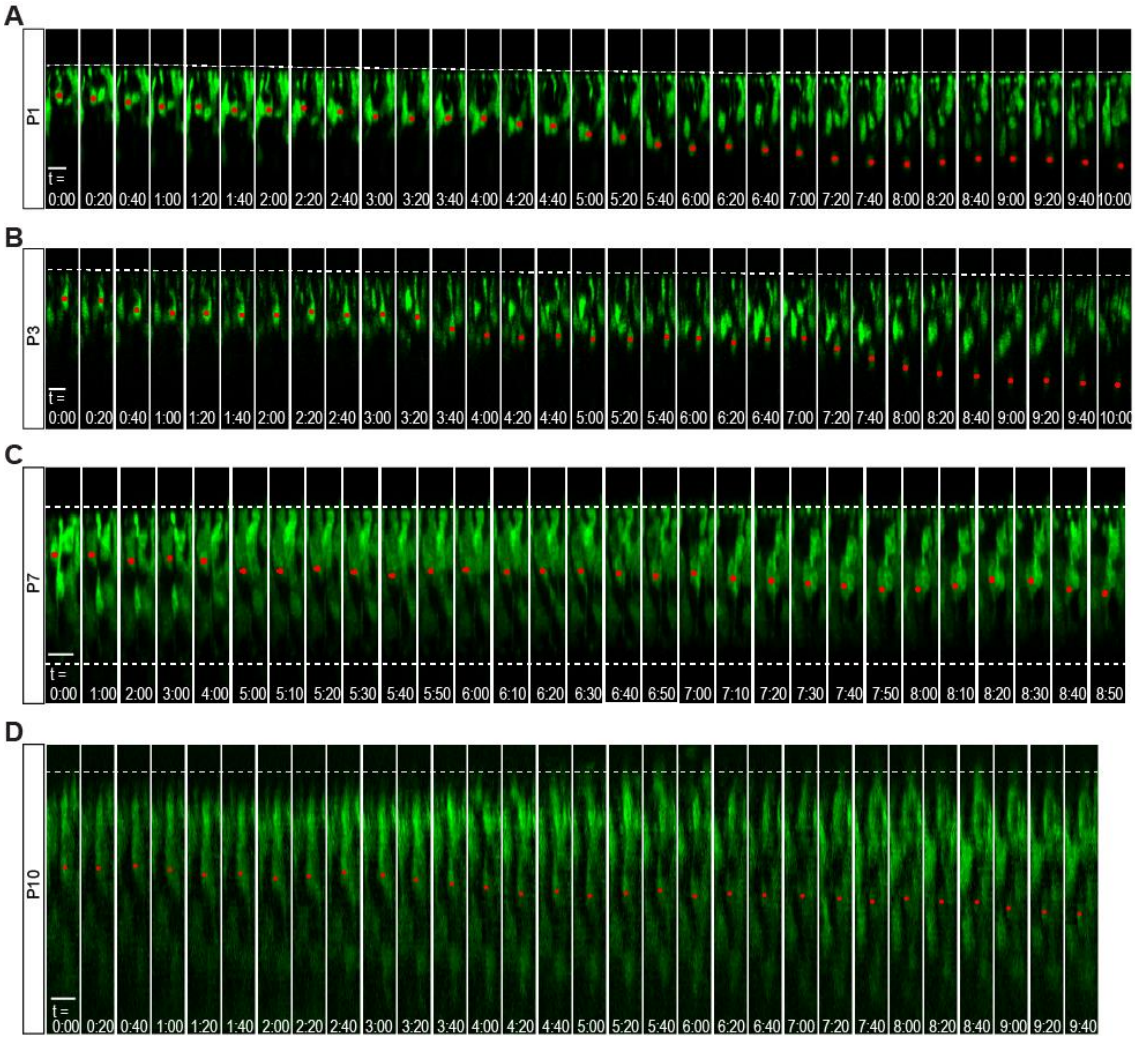

Figure 3.3.9 Rod photoreceptor basally-directed somal translocation in the P1, P3, P7 and P10 retina. **(A-D)** Representative montages following the apico-basal positions of rod photoreceptor somata (red dot) displaying basally-directed somal translocation in the P1-P10 retina over time. Scale bars: 10 µm.

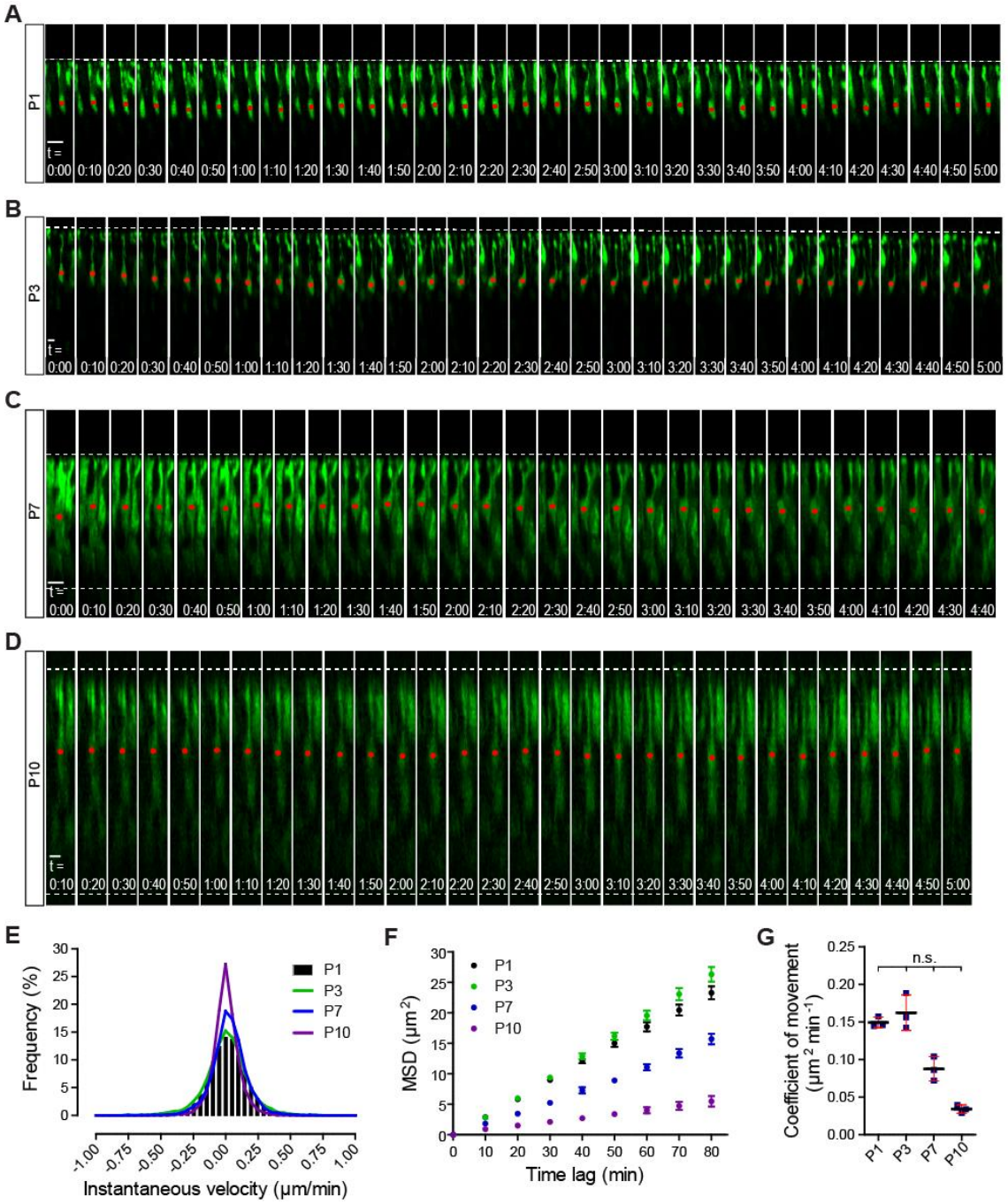

Figure 3.3.10 Rod photoreceptor stochastic somal translocation with little to no net displacement in the P1, P3, P7 and P10 retina. **(A-D)** Representative montages following the apico-basal positions of rod photoreceptor somata (red dot) displaying stochastic somal translocation in the P1-P10 retina over time. Scale bars: 10 µm (A), 5 µm (B-D). **(E)** Instantaneous velocity distribution of pooled rod photoreceptor somal translocations in P1-P10 retinae. **(F)** AvMSD profiles of pooled rapid apical translocations of P1-P10 rod photoreceptor somata. Data are displayed as mean ± SEM. **(G)** Comparison of coefficient of movement values associated with AvMSD profiles in F. The coefficient of movement is directly proportional to the slope of a straight line fitted to the initial segment (0-60 minutes in this case) of the individual AvMSD profiles. Data are displayed as mean ± SD. Data were compared with 1-way ANOVA.

velocities reached during the principal translocation phases were the following: P1: ~ -0.3 to -0.7 µm/min, P3: ~ -0.3 to -1.2 µm/min, P7: ~ -0.3 to -0.9 µm/min, P10: ~ -0.4 to -0.5 µm/min (only two recorded events at P10). There were notable shifts in the steepness of the AvMSD curves with the P3 and P7 AvMSD curves being the steepest and the AvMSD curve at P1 being the shallowest (due to the relatively low number of detected events, the P10 AvMSD curve displayed big error bars making it difficult to interpret this time point). This may be explained by the fact that at P1, the majority of rapid apical events (89.7%) covered a radial distance of up to 20 µm (Figure 3.3.8E). At P3 and P7 on the other hand, there was a larger contribution of rapid apically-directed events ≥ 20 µm, thus producing steeper AvMSD curves. The bias towards short rapid apical translocations at P1 is not too surprising given that at P1 – as opposed to P3 and P7 –, many rod photoreceptors have not been generated yet and that the majority of previously born rod cells remain relatively close to the apical limit of the neural retina.

Finally, the rapid apical translocation event depicted in Figure 3.3.8Cii provides grounds for speculation as to why rod photoreceptors exhibit apically directed somal translocation. As the OPL becomes visibly established form about P5 onwards, it was possible to define the basal limit of the ONL based on where the majority of rod axons terminated. The fact that some rapid apically translocating rod cell somata initiated their motion basal to the basal limit of the presumptive ONL may indicate that rapid apical translocation is a mechanism to avoid ectopic basal rod somal displacement. The ONL of the mature mouse retina is approximately 50 µm thick. In the P1 retina, only 9.4 % of rapid apical translocation initiation events occurred from > 50 µm away from the apical margin and up to a maximum depth of 66.4 µm while the remaining 90.6 % of initiations happened between 13.2 and ≤ 50 µm. At P3, which is shortly after the peak of the neurogenic period in the mouse retina (Young, 1985), 34.3 % of initiation events occurred from > 50 µm and up to a depth of 97.7 µm, while the remaining 65.7 % happened between 24.2 and ≤ 50 µm; in the P7 retina, 31.8 % of initiations happened form > 50 µm and up to a depth of 72.6 µm, while 68.2 % of initiations occurred between 31.4 and ≤ 50 µm. Most of the initiation events across all time points thus occurred proximal to the apical margin of the retina where the density of rod photoreceptors is highest during retinogenesis as opposed to beyond the (presumptive) ONL. Nonetheless, it is still likely that rapid apical translocation is a mechanism employed to avoid ectopically basal rod somal displacement, however, surpassing the depth of the (presumptive) ONL may not be its main trigger. Alternatively, rapid apical translocation may be activated periodically to

reduce the frequency of ectopically basal rod somata by positioning them relatively close to the apical limit of the retina. In this way, the depth of initiation of rapid apical translocation events may just reflect the distribution of rod somata within the retina.

Basal translocation:

As at P1, basally directed somal translocation at P3, P7 and P10 was relatively heterogeneous (Figure 3.3.9A-D; see also section 3.3.1.4). As before, the threshold for this mode of somal movement was set to at least 15 μm of net migration in the basal direction covered in a minimum of 2 hours. However, basal somal translocations were often observed to last for much longer and to consist of periods of low and higher velocity movements. As stated earlier, this heterogeneity may arise from the existence of different basally directed active mechanisms and/or passive basal displacement caused by the radial translocation of surrounding retinal somata.

Stochastic movement:

Finally, stochastic somal translocation with little to no net displacement was assessed and compared across the time points P1-P10 (see also section 3.3.1.5). As before, a threshold of ≤ 15 μm of net apico-basal translocation for a minimum of 2 hours, but excluding all rapid apical translocations, was applied. Somata displaying this type of motility typically exhibited many sequential micromovements of short distance and short duration at all examined time points (Figure 3.3.10A-D). Despite these very minute movements, there appeared to be a quantifiable difference in this type of rod photoreceptor somal translocation, when compared across P1 to P10 (Figure3.3.10E-G). These changes very much mirrored the changes that were observed when globally analysing all trajectories in their entire lengths (see Figure 3.3.7). When all instantaneous velocities associated with stochastic translocation were plotted on a histogram, the Gaussian-like frequency distributions narrowed with age, featuring bigger zero-to-low velocity contributions and smaller high velocity contributions (Figure 3.3.10E). MSD analysis produced linear curves at all four time points highlighting the stochastic, almost random nature of this type of somal movement (Figure 3.3.10F). While the coefficients of movement of the AvMSD curves for P1 and P3 stochastic movements were comparable (0.146 ± 0.004 $\mu m^2/min^{-1}$ and 0.156 ± 0.014 $\mu m^2/min^{-1}$ respectively), this value decreased noticeably by

P7 (0.086 ± 0.009μm^2/min^{-1}) and P10 (0.034 ± 0.003 μm^2/min^{-1}), although the change was not statistically significant (Figure 3.3.10G). Furthermore, some degree of similarity was noticed between the coefficient of movement profile from P1 to P10 between stochastic movements and total movements (see Figure 3.3.7D).

In summary, all three types of rod photoreceptor somal motility were represented at each of the four time points examined here (P1, P3, P7 and P10). In agreement with the finding that rod apico-basal translocation is largely absent by P10 (as determined by MSD analysis; see Figure 3.3.7D & E), there was a concomitant reduction in either the number and/or the magnitude of events attributable to each of the three modes of movement.

3.4. Conclusion

Having photoreceptors in the topographically correct location is important for correct connectivity and retinal function. However, little is known about how photoreceptors end up and remain within the ONL of the retina rather than being found ectopically in a different retinal stratum. This study sought to shed new light onto this matter.

The findings generated within this study elaborate on a previous unpublished, novel finding that rod photoreceptors of the murine retina display motility in both the apical and the basal direction (Warre-Cornish, PhD thesis, 2013). The observed apico-basal motility is unlikely to be just an artefact of the explant culture procedure: BrdU birth dating by *in vivo* administration into P1 mice and subsequent harvesting and fixed tissue analysis at P3, P5 and P7 suggested that rod nuclei/somata, following their presumed birth at the apical edge of the retina, on average moved basally by P3 before returning apically to populate the ONL by P7 (Warre-Cornish, PhD thesis, 2013). Like in the past works, the motile rod photoreceptors observed here displayed a stereotyped morphology that featured a relatively small soma that was permanently attached to the ventricular (apical) side of the neural retina via an apical process as well as a basal process (or axon), which usually only manifested during the later synaptogenic stages of development. While the apical process remained relatively stationary at all times and typically never detached from the apical limit of the tissue, it was the rod photoreceptor soma that underwent translocation along the apico-basal axis. Since the nucleus is the main occupant of the rod photoreceptor cell body, this somal motility is very likely a consequence of nuclear migration within the radial extent of the cell – a process also known as nucleokinesis. The fact that the apical process and its attachment to the apical limit did not exhibit lateral movement contributed to keeping somal translocation relatively confined within the radial axis (Figure 3.3.1 & 3.3.2C). This complements previous reports, which discovered that clonally related rod photoreceptors are organised in columns with no signs of extensive tangential dispersion (Reese *et al.*, 1995, 1999; Reese and Tan, 1998). The morphology of rod photoreceptor precursors and the directionality of their movements are incompatible with multipolar and tangential migration, which shifts the focus onto the remaining modes of neuronal motility.

The most striking component of the rod photoreceptor motile behaviour was the rapid apical somal translocation. This type of movement was reminiscent to cortical projection

neuron precursor cells as they pull themselves towards the pial surface to reach the outermost cortical layers by somal translocation. At the same time, it was also reminiscent of the apical movement component of epithelial progenitor cell IKNM. In this present study, detection of rapid apical translocation events was achieved by applying the following criterion to the trajectory data sets: ≥ 10 μm of apical movement in 30 minutes. This type of motility was strikingly uniform, usually took ~ 60 minutes to run to completion and featured characteristic phases of rapid acceleration (initiation phase), maximum velocity translocation (principal translocation phase) where peak velocities between ~ -0.3 and -1.2 μm/min were reached and deceleration (cessation phase). Moreover, rapid apical translocation could be initiated from virtually any depth within the retina. However, at all developmental stages examined, most of the initiation events occurred proximal to the apical margin of the retina where the density of rod photoreceptors is highest during retinogenesis as opposed to beyond the (presumptive) ONL. However, the fact that rapid apical somal translocations could be initiated from outside the ONL may indicate the purpose of this behaviour: it may be speculated that rod somata undergo apical translocations in order to become enriched within the ONL. Basally directed somal translocation, on the other hand, was a lot less uniform compared to rapid apical translocation. The detection criterion applied was ≥ 15 μm of basal movement in ≥ 2 hours. The duration of translocation was just as variable as the displayed velocities of rod photoreceptor basal somal movement, as some somata even transitioned between slow and fast basal migration almost seamlessly. Occasionally, somata translocated basally in a saltatory manner, where movements with little to no basal migration alternated with short, high velocity basal motions. Finally, rod photoreceptors also underwent stochastic motion, which is characterised by micro-movements yielding mostly zero net displacement, although net apical or basal movement manifested in some cases. Here, the detection criterion was set to ≤ 15 μm (apical or basal) in ≥ 2 hours. Among the three modes of rod somal motility, rapid apical somal translocation was the only mode to occur on an uniformly quick time scale (~ 1 hour). Basal and stochastic rod somal motility, although variable in duration, tended to proceed for several hours. This discrepancy explains why rapid apical rod somal translocation occurred relatively rarely throughout the time lapse recordings.

The apical movement of rod somata alone was reminiscent of neuronal somal translocation in the cortex, especially when considering the kinetics (both around 1 μm/min) and rod cell morphology, particularly at the early post-natal stages. However,

when combined with basally directed and stochastic somal movements, the kinetic profile exhibited by these post-mitotic neuronal precursor cells is remarkably similar to what has been observed previously when describing the apico-basal motions displayed during IKNM of epithelial progenitor cells (Norden *et al.*, 2009). Mitotically active progenitor cells can, of course, go through repeated cycles of IKNM until they leave the cell cycle. One of the novelties of this study is that rod photoreceptor cells also exhibited repeated oscillatory apico-basal somal translocation movements with characteristics and kinetics that were very similar to IKNM. Full oscillations (rapid apical – basal – rapid apical or basal – rapid apical – basal motions) were detected in relatively small numbers. This is most likely due to the fact that one complete apico-basal oscillation took place on a similar (perhaps longer) time scale as the maximum imaging duration achieved in this study (~ 12 hours), which was limited by *ex vivo* tissue viability restrictions. Rapid apical translocation usually took ~ 1 hour, whereas stochastic motion, although quite variable in duration, took 7 hours on average. Assuming that basally-directed somal motion occurred on a similar time scale as stochastic motion (not unlikely, given Figure 3.3.4B), the average full oscillation may take approximately 15 hours. Extending the imaging duration concomitantly with extending the explant viability may thus ensure an increased detection of full rod somal apico-basal oscillations. In contrast, somal translocation exhibited by neuronal precursors in the cortex is thought to be a singular rather than a repeated event (Nadarajah et al., 2001).

The IKNM-like aspect of the described oscillatory rod photoreceptor somal translocation is also novel, since oscillatory apico-basal nuclear/somal motility is a behaviour that was thought to be attributable exclusively to mitotic epithelial progenitor cells, rather than post-mitotic precursor cells such as the rod photoreceptors analysed in this present study. In classic IKNM, cell cycle progression is tightly linked to oscillatory apico-basal nuclear/somal movements; it appears that these have been uncoupled in rod photoreceptors since somal motility was observed in complete absence of mitotic events. It shall be proposed that oscillatory rod photoreceptor somal translocation is a novel mechanism, by which certain recently born neuronal precursor cells, such as rod photoreceptor precursors, can become enriched in their designated target locations. This new hybrid type mechanism, with characteristics of both somal translocation and IKNM, should thus be added to the ranks of previously described mechanisms of neural motility, which are: IKNM, somal translocation, multipolar migration, tangential migration and glial-guided migration.

From all the time points investigated as part of this study (P1, P3, P7 and P10), overall rod photoreceptor apico-basal somal motility was most pronounced at the P1 and P3 stages, reduced by P7 and almost completely absent by P10. This was mirrored at the level of stochastic motions, which transitioned towards smaller micro movements and even towards a complete standstill at P7 and at P10 respectively. The overall rod somal motility also correlated with the quantity, and to some extent also the quality, of detected rapid apical somal translocation events. Whereas many short-distance apical translocations were detected at P1, the later time points exhibited proportionally more long distance movements. At the same time, the number of detected rapid apical translocation events was also reduced at P7 and, even more so, at P10 compared to the earlier time points. Thus, rod photoreceptor somata become progressively less motile, at least from the P7 stage onwards, and were almost completely stationary at or soon after the P10 stage.

In summary, rod photoreceptor somata are motile along their apico-basal axes during retinogenesis. This motility manifests as a novel mode of neuronal migration that appears to have characteristics of both somal translocation and IKNM (oscillatory rod photoreceptor somal translocation), whereby rod somata likely repeatedly migrate rapidly in the apical direction and in a kinetically uniform manner before migrating basally in a much more variable fashion. Whereas somal motility was high at P1 and P3, it was reduced by P7 and almost undetectable by P10. Having investigated the kinetic features of developmental rod photoreceptor somal translocation, the next chapter will focus on determining the mechanisms that underlie this migratory behaviour.

CHAPTER IV. MECHANISMS UNDERLYING ROD PHOTORECEPTOR SOMAL MOTILITY DURING DEVELOPMENT

4.1. Introduction

It was established in chapter III that rod photoreceptors display a novel type of neuronal motility during retinal development, for which the term oscillatory rod photoreceptor somal translocation was coined. Kinetically and in terms of cellular morphology, it combines the features of both somal translocation, known to be exhibited by cortical post-mitotic neuronal precursor cells for instance, and IKNM, which is usually only exhibited by mitotic epithelial progenitor cells (hence, also neuroepithelial retinal progenitor cells). The two other remaining glial-guidance-independent modes of migration (tangential and multipolar migration) are incompatible with the observed rod photoreceptor cellular morphologies and kinetic behaviour. For a complete characterisation of this novel type of neuronal motility shown by rod photoreceptors (oscillatory rod photoreceptor somal translocation), elucidation of the underlying mechanisms, as well as the purpose of this energetically costly process, are required. Addressing these matters will be the focus of this chapter.

To date, IKNM is a type of motile behaviour that has been considered to be an exclusive property of mitotic progenitor cells of various epithelial tissues (Spear and Erickson, 2012a), the most prominent representatives being the several neuroepithelia where IKNM has been observed. Cells undergoing IKNM are bipolar in shape, embedded within a pseudostratified epithelium, with two processes extending radially all the way to the apical and the basal limits of the epithelium. Within the radial extent of the epithelial progenitor cells, the nucleus repeatedly translocates (nucleokinesis) in the apical or basal direction in synchrony with the cell cycle; the nucleus moves basally during G1-, S-phase occurs at a basal position, the nucleus then migrates to the apical surface during G2-phase where M-phase takes place (Schaper, 1897; Sauer, 1935; Watterson *et al.*, 1956; Sauer and Chittenden, 1959). Apical migration is rapid and occurs in a single distinct motion

with uniform kinetics, whereas basal migration tends to be kinetically more heterogeneous.

During somal translocation, neuronal precursor cells that are en route to their target stratum within a multi-layered neuroepithelium extend a radial leading process towards their final destination. This leading process is then used by the cell to pull the trailing soma towards the target location in a grappling hook-like manner (Nadarajah *et al.*, 2001). In terms of kinetics, somal translocation, like the apical movement during IKNM, is rapid, usually occurs in a single distinct motion and is unidirectional.

Given the nature of the observed movements during IKNM as well as somal translocation in various neuroepithelia, it comes to no surprise that they are driven by active mechanisms. It is yet to be shown, however, whether the same mechanisms are also in place during developmental oscillatory rod photoreceptor somal translocation. In principle, actively driven nucleokinesis can for instance be caused by the constriction of antiparallel actin filaments (stress fibres) due to activity of the motor protein non-muscle Myosin II (NMII). Actomyosin constrictions in vicinity of the nucleus can push the nucleus in a certain direction (Norden *et al.*, 2009). Alternatively, nucleokinesis can also be caused by the activities of microtubule filament associated motor proteins, which transport various cargos, including entire nuclei (Tsai and Gleeson, 2005; Tanenbaum *et al.*, 2011; Cooper, 2013). Microtubules are polymeric assemblies containing a relatively stable minus end and a dynamic plus end with active (de-)polymerisation. They consist of polarised tubulin monomers, which, upon polymerisation, makes the whole microtubule filament polarised. This is exploited by different microtubule motor proteins to provide direction-specific cargo transport. While dynein motors possess processivity towards the minus end, kinesin family motors move towards the plus end (Tanenbaum *et al.*, 2011).

Furthermore, microtubule filament polymerisation is usually nucleated from microtubule organising centres (MTOCs) such as centrosomes. Microtubule filaments emanating from centrosomes in migrating neurons often extend towards and enwrap the nucleus in a fork-like perinuclear cage structure (Tanaka *et al.*, 2004). In migrating neurons, centrosomal advancements have been observed to precede nuclear translocation. The perinuclear cage, which is extended from the advancing centrosome, subsequently pulls the nucleus forward (Tanaka *et al.*, 2004; Bellion *et al.*, 2005; Wang *et al.*, 2011). However, this coordination between centrosome and nuclear movement is not universally observed as

the centrosome can also persistently trail the nucleus during somal translocation of retinal ganglion cells (Zolessi *et al.*, 2006), centrosomal and nuclear advancement can be independently regulated such that one may overtake the other during glial-guided neuronal migration (Umeshima *et al.*, 2007) and centrosomes can be almost completely immobile as during IKNM, except for the G2- to M-phase transition where centrosomes migrate basally towards nuclei (Spear and Erickson, 2012b; Strzyz *et al.*, 2015).

Cortical somal translocation in the rodent brain depends on dynein I activity, aided by its co-factor LIS1 (Franco *et al.*, 2011). The well-known reelin signalling pathway operates upstream of dynein I; defects along this pathway were shown to lead to the brain developmental disorders lissencephaly and cerebral hypoplasia (Hong *et al.*, 2000). The reelin signalling pathway acts in two ways: it stabilises the 'grappling hook' leading process required for subsequent nuclear propulsion and activation of the reelin pathway recruits LIS1, an important co-factor of the microtubule associated motor protein complex dynein I (Assadi *et al.*, 2003; Zhang *et al.*, 2007; Franco *et al.*, 2011). This most likely links reelin signalling to dynein I dependent nucleokinesis/somal translocation towards the target location (Shu *et al.*, 2004).

The principles and mechanisms of IKNM have been studied in various different non-neural epithelial tissues and neuroepithelial tissues as well as in different species. Although the kinetics of nucleokinesis are remarkably similar in each case, the underlying mechanisms were not necessarily universally conserved (reviewed by Kosodo, 2012; Lee and Norden, 2013). In the rat neocortex, IKNM is dependent on microtubule associated motor proteins (Tsai *et al.*, 2010; Carabalona *et al.*, 2016): as show by RNAi, dynein I mediates apical translocation during G2 and the kinesin family member KIF1A mediates basal translocation during G1. Pharmacological (Blebbistatin and BDM) and genetic blockade (RNAi) of NMII did not affect IKNM nucleokinesis. In the mouse cerebral cortex on the other hand, basal translocation was mediated by NMII, as shown by Blebbistatin application, while apical movement was assumed to still be dynein I driven (Schenk *et al.*, 2009). In the zebrafish retina, NMII accounts for apical, rather than basal, translocation; furthermore, IKNM movements occurred even in complete absence of microtubules following treatment with the microtubule destabilising drug demecolcine (Norden *et al.*, 2009). Finally, another study on the developing mouse cortex revealed that apical translocation requires microtubule re-organisation in the apical process, most likely to enable dynein I mediated apical nucleokinesis; basal nuclear movements, conversely, appeared to be completely passive, caused by the apical translocation of

neighbouring cells (Kosodo *et al.*, 2011). There are thus marked mechanistic differences between different neuroepithelia, different species and perhaps even developmental stages and no one single mechanism exists. Lee and Norden (2013) proposed, based on various published works, that actomyosin mediated nucleokinesis prevails in neuroepithelia where the progenitor cells are relatively short and wide (e.g. the zebrafish retina), whereas microtubule-based nucleokinesis prevails in long and thin progenitor cells (e.g. the mammalian neocortex). In a wider context, they hypothesised that microtubule-based nucleokinesis, as compared to actomyosin-based nucleokinesis, is an evolutionary more recent mechanism. Hence, actomyosin based nucleokinesis is prevalent in phylogenetically very diverse systems, whereas microtubule-based motility occurs in the more evolved mammalian neocortex for instance.

Given that rod photoreceptor somal motility is presently ill defined, there is a lack in our understanding of the mechanisms that underlie their migratory behaviour. Morphologically and kinetically, mammalian rod somal motility appears to be a hybrid of IKNM and somal translocation. However, as discussed in the above paragraphs, several, partially contradictory, mechanistic options exist that could potentially drive rod migration. Questions to be addressed are as follows: if centrosomes are motile, is their motility coordinated with nucleokinesis? Is apically/basally directed nucleokinesis actively driven by actomyosin- and/or microtubule-based mechanisms? How big is the impact of passive somal displacement due to the influence of the movement of neighbouring cells? Are dynamic microtubules a pre-requisite for somal motility? Finally, investigating the mechanisms underlying rod somal motility may also shed light on the purpose of repeated oscillatory radial movements, which is an energetically very costly process. The kinetic data provided in Chapter III led to the intriguing hypothesis that rod photoreceptor apical somal translocation occurs in order to enrich these cells within the apical-most stratum of the neural retina (ONL). Conversely, it could also serve the purpose to prevent ectopic mislocalisation in the more basal retinal layers, which may trigger apoptosis (Young, 1984). These questions and issues were addressed within this chapter.

4.2. Aims

The aims of the work carried out as part of this chapter were:

(1) to investigate whether the centrosomes of migratory rod photoreceptors are motile and whether their motility was coordinated with somal movements.

(2) to investigate by pharmacology (small molecule antagonists) and via genetic tools (RNAi) whether, and to what extent, actomyosin, the microtubule associated motor proteins dynein I, KIF1A, and microtubule dynamic (de-)polymerisation are required for oscillatory rod photoreceptor somal translocation.

(3) to test the hypothesis that oscillatory rod photoreceptor somal translocation, especially in the apical direction, serves to enrich these cells within the ONL and to reduce the frequency of basally displaced rod photoreceptors.

Combined, these experiments will provide a better insight into how certain ONL aspects of the highly specialised retinal architecture are established with the precision required to enable visual perception. From a translational point of view, the investigation of developmental rod photoreceptor motility might also provide important clues as to what the mechanisms underlying rod photoreceptor migration and integration following photoreceptor transplantation are. However, rod photoreceptor transplantation will formally be addressed in chapter VI.

4.3. Investigating the mechanisms of oscillatory rod somal motility

4.3.1. Analysing the mechanisms of rod somal motility by histochemistry

4.3.1.1. Rod centrosomal motility is not required for somal motility

Nuclear/somal translocation in many types of migrating neurons is preceded by a centrosomal advancement into the leading process (Tsai and Gleeson, 2005; Marín *et al.*, 2006; Cooper, 2013). Centrosomes are the principal microtubule organising centres (MTOC). Microtubule filaments typically emanate from centrosomes, which in turn extend towards and form points of contact with the nucleus. It is, therefore, plausible that motility of the centrosome is linked to motility of the nucleus in developing rod photoreceptors exhibiting somal translocation.

To test this, an immunohistochemical approach was chosen, whereby retinal frozen sections from P2-P14 as well as from adult *Nrl.GFP*$^{+/+}$ mice were immunostained for the centrosomal marker γ-tubulin. If centrosomal motility is important for nuclear motility in somally translocating rod photoreceptors, then one would predict that centrosomes will be in close vicinity of rod nuclei, especially at those developmental time points where high levels of somal motility occurs (~P1-P3 in the present study). However, as revealed by confocal fluorescence microscopy, γ-tubulin immunoreactivity was restricted to the apical edge of the neural retina throughout the first week of post-natal development (blue arrow heads in Figure 4.3.1) This applied to both γ-tubulin puncta that were co-localised with *GFP* expressing rod photoreceptors, as well as to those in GFP negative cells. Mitotic figures were the exception to this general observation, as γ-tubulin puncta (and hence mitotic spindle organising centrosomes) were found slightly basal to the apical limit (purple dots in Figure 4.3.1), which is consistent with the literature (Spear and Erickson, 2012b). From P8 onwards, γ-tubulin immunoreactivity, that was apparently co-localised to GFP positive rod photoreceptors, was increasingly detected throughout the ONL even though some weaker intensity immunoreactivity was retained in the developing rod segments (yellow arrowheads).

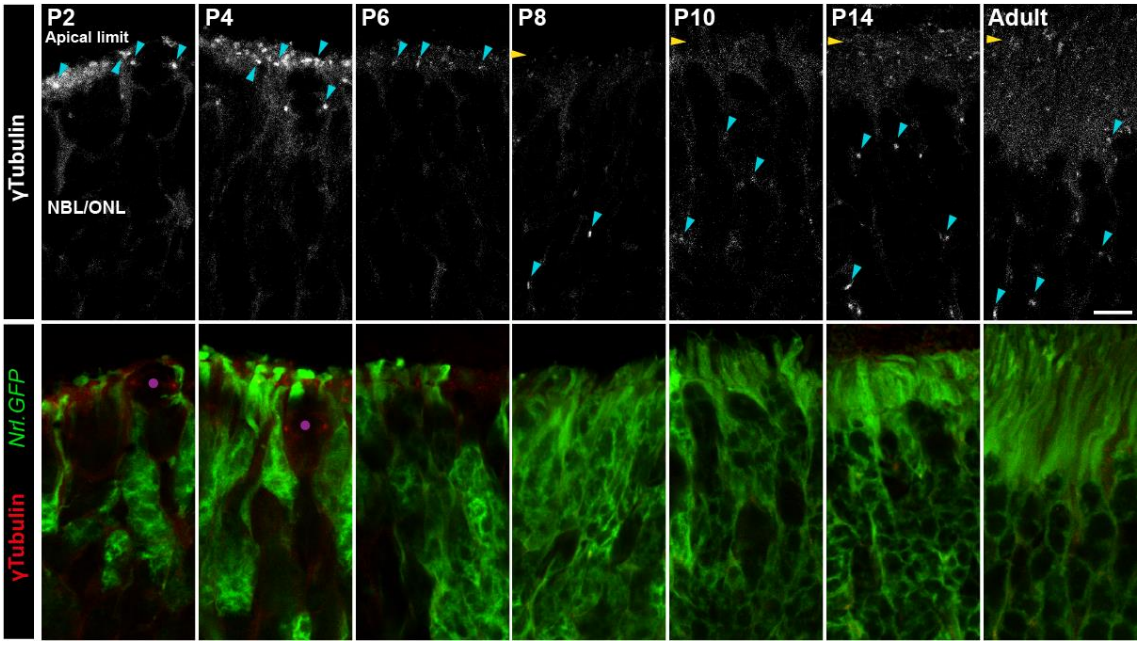

Figure 4.3.1 Rod photoreceptor centrosome motility is not required for somal translocation. Frozen sections from *Nrl.GFP*$^{+/+}$ eye tissues were immunohistochemically stained for the centrosomal marker γ-tubulin. Some of the centrosomal puncta co-localised with Nrl.GFP signal were highlighted with turquois arrowheads. Putative basal bodies located at the apical tips of inner segments were also positive for γ-tubulin (yellow arrowheads). During mitosis, centrosomes form spindle poles at opposite ends of a dividing cell, resulting in the morphologically stereotypical mitotic figures (purple dots). At the earliest time points (P2 & P4), mitotic figures were the only instances were centrosomes were found slightly basal to the apical limit. Scale bar: 10 µm.

The fact that rod photoreceptor centrosomes locate to the apical edge of the neural retina during a period of development, where rod nuclei display high radial motility (P1-P7), suggests that rod nuclear motility does not require centrosomal movements. The basal displacement of centrosomes from P8 onwards is likely to be unrelated to oscillatory somal motility; whether it is relevant for another mode of migration or terminal placement of rod somata would need to be formally tested in a separate experiment.

4.3.2. Analysing the mechanisms of rod somal motility with pharmacology

4.3.2.1. Small molecule antagonist against cytoplasmic dynein I and its effect on rod somal translocation

The dynein I motor protein complex is responsible for minus-end directed cargo transport along microtubule filaments. The microtubule minus-end typically locates to the MTOC (centrosome) whereas the dynamic plus-end is at the opposite end of microtubule filaments. As shown in Figure 4.3.1, the centrosomes of rod photoreceptors are located at the apical limit of P2-P6 retinae (see also Troutt and Burnside, 1988). In combination with the fact that nuclei can be the cargo of dynein I motor proteins, the rapid apically (or minus-end) directed somal/nuclear translocation described in this study could be mediated by dynein I motor proteins. Indeed, the strikingly uniform nature of this mode of somal motility would indicate the involvement of an active, cell-intrinsic mechanism.

To investigate the possible involvement of dynein I motor proteins in rod photoreceptor somal translocation, P3 *Nrl.GFP*$^{+/+}$ retinae were explanted and live-imaged by 2-photon fluorescence microscopy in presence of the dynein I small molecule antagonist ciliobrevin D (25 µM) (N = 3; n = 322) (Firestone *et al.*, 2012). The P3 time point was specifically chosen because a considerable degree of somal motility was detected at this stage and because a substantial number of rod photoreceptors will have already been born following the peak of rod genesis at P1. Ciliobrevin D was usually added to the culture medium at 90 or 120 min into the time-lapse recording, having first established that the retinal tissue was viable on the basis of the kinetics of rod somal translocation observed

during this control period. While rapid apical somal translocation events were reliably detected within the control period, no such movements were observed following addition of ciliobrevin D (Figure 4.3.2A & 4.3.2B). Interestingly, GFP negative retinal cell somata, which were visible when densely surrounded by GFP positive rod photoreceptors, on occasion underwent a type of motion very similar to the rapid apical translocation observed for GFP positive rod photoreceptor cell bodies (Figure 4.3.2C). Nonetheless, when focussing purely on rod photoreceptors, addition of ciliobrevin D showed a remarkable, near instant onset of activity abolishing almost all somal movements (Figure 4.3.2D). Of note, in addition to the loss of rapid apical movements, the faster basal somal translocations were not detectable either.

Quantitatively, rod photoreceptor somal movements that occurred in presence of ciliobrevin D had markedly lower instantaneous velocities, compared with DMSO control (Figure 4.3.2E). As virtually all radial somal movements (apically and basally directed) were blocked, both negative and positive instantaneous velocities appeared to be equally reduced. At the same time, MSD analysis revealed a much shallower AvMSD curve for ciliobrevin D treated retinae compared with DMSO control (Figure 4.3.2F). There was thus a significant, 80.9 % reduction (0.241 ± 0.017 versus 0.046 ± 0.004 μm^2 min^{-1}, $p < 0.05$) in the coefficient of movement, when comparing control and drug treated samples respectively (Figure 4.3.2G).

In order to test whether ciliobrevin D acted by specifically blocking somal translocation rather than by arresting motility due to drug toxicity related cell death, a wash-off assay was designed, as depicted in Figure 4.3.3A. Since the ciliobrevin D effect on rod somal motility had a very rapid onset (see Figure 4.3.2D), the duration of drug exposure was set to 30 minutes, which was followed by four 30-minute wash-off periods. As can be seen in Figure 4.3.3B, rod photoreceptor rapid apical translocation was restored following treatment with ciliobrevin D and subsequent wash-off (N = 2, n = 205). Analysis of the MSD, as well as the associated coefficient of movement, revealed that rod somal motility following wash-off was restored to 71.7 % of DMSO control levels within the 60-minute time lag period (Figure 4.3.3C & 4.3.3D). Complete recovery of motility appeared to be out of reach since even a mock wash-off experiment with DMSO treatment rather than with drug only yielded a restoration of 62.5 % (N = 1, n = 101). There was no statistical difference when comparing the ciliobrevin D and DMSO wash-off groups.

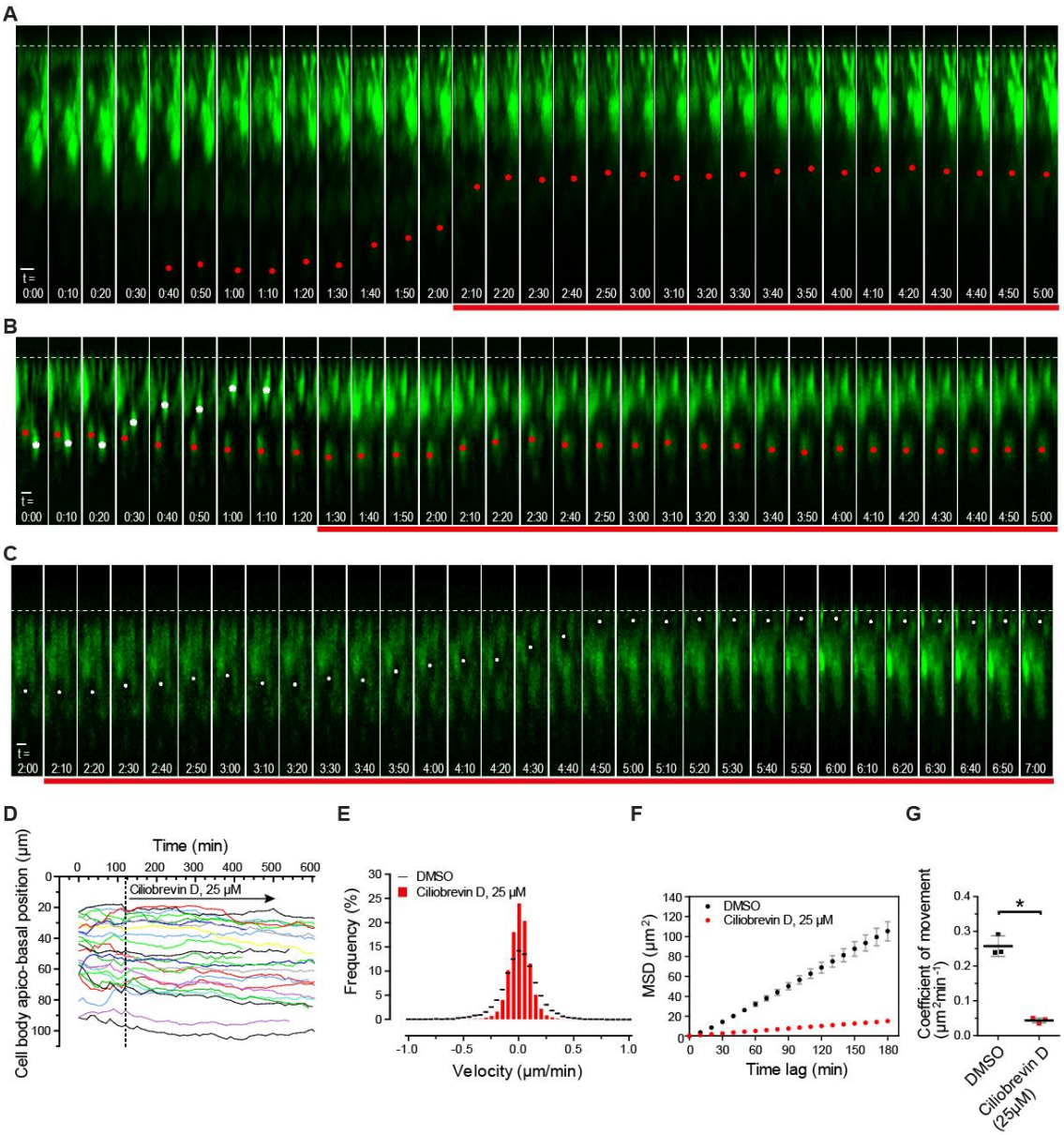

Figure 4.3.2 Pharmacological inhibition of dynein I attenuates rod photoreceptor somal translocation in the P3 retina. Dynein I function was blocked using ciliobrevin D (25 µM). **(A-B)** Representative montages following the apico-basal positions of rod photoreceptor somata (red dot) over time. Addition of 25 µM ciliobrevin D, indicated by the presence of the red bar underneath the montages, arrested rapid apical translocation (A), whereas rapid apical translocation was still observed prior to drug exposure (B). **(C)** Manually selected montage following the apico-basal position of an Nrl.GFP negative cell soma (white dot) over time. Scale bars: 5µm. **(D)** Randomly picked rod photoreceptor soma radial trajectories superimposed in a single *zt* plot. **(E)** Comparison of instantaneous velocity distribution of pooled rod photoreceptor somal translocations in ciliobrevin D vs. DMSO control exposed samples. **(F)** AvMSD profiles of total rod photoreceptor somal translocations in ciliobrevin D vs. DMSO control exposed samples. Data are displayed as mean ± SEM. **(G)** Comparison of coefficient of movement values associated with AvMSD profiles in F. The coefficient of movement is directly proportional to the slope of a straight line fitted to the initial segment (0-60 minutes in this case) of the individual AvMSD profiles. Data are displayed as mean ± SD. Student's t-test was used for statistical analysis. *$p < 0.05$.

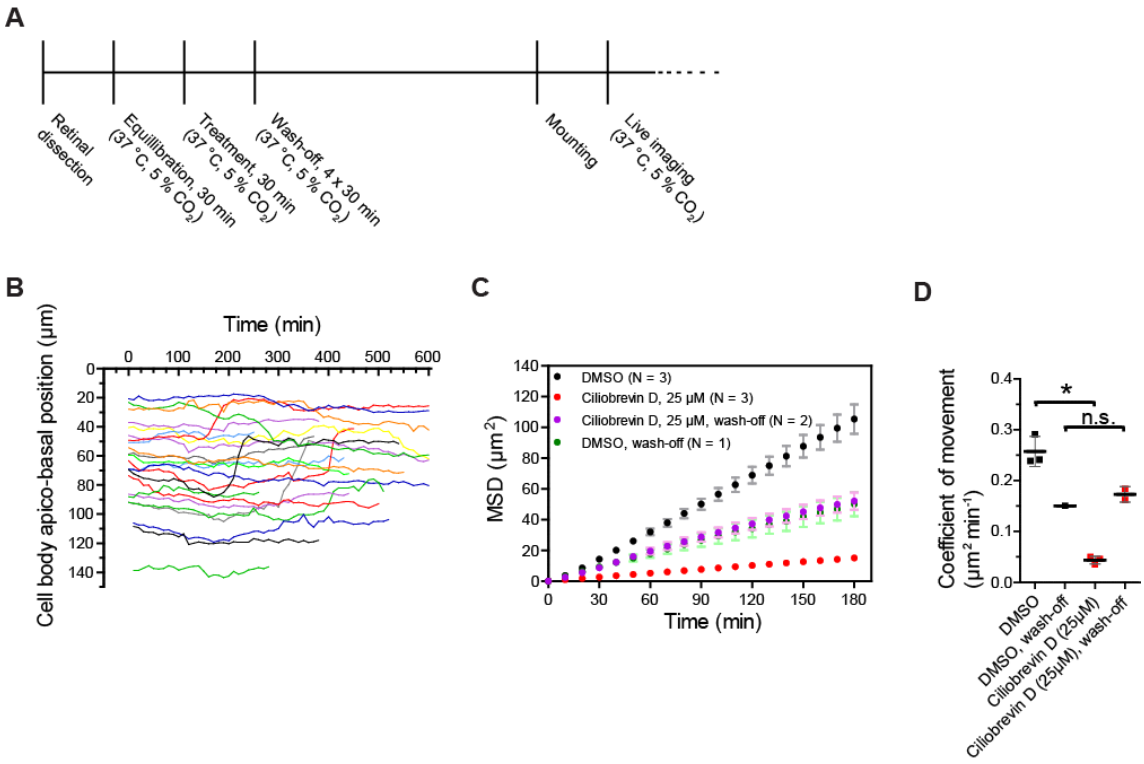

Figure 4.3.3 Rapid apical translocation is restored following ciliobrevin D wash-off. **(A)** Experimental paradigm of the ciliobrevin D wash-off experiment. **(B)** Randomly picked rod photoreceptor radial trajectories of the soma superimposed in a single *zt* plot. **(C)** Comparison of AvMSD profiles of total rod photoreceptor somal translocations in ciliobrevin D wash-off vs. DMSO control wash-off samples additionally compared with ciliobrevin D vs. DMSO control samples from Figure 4.3.2F. Data are displayed as mean ± SEM. **(D)** Comparison of coefficient of movement values associated with AvMSD profiles in C. The coefficient of movement is directly proportional to the slope of a straight line fitted to the initial segment (0-60 minutes in this case) of the individual AvMSD profiles. Data are displayed as mean ± SD. Student's t-test was used for statistical analysis. *$p < 0.05$.

Taken together, these pharmacology data suggest that rod photoreceptor rapid apical somal translocation during early retinal development is a process that is actively driven by the microtubule minus-end directed motor protein dynein I. However, rapid apical translocation in non-rod photoreceptor retinal cells (Figure 4.3.2C; GFP negative cell) may be mediated by a dynein I independent mechanism. Finally, that dynein I inhibition markedly impairs not only apical, but also basally directed, movements lends support to the hypothesis that basal movement is passive and a consequence of rapid apical translocation performed by neighbouring retinal somata.

4.3.2.2. Small molecule antagonist against myosin II and its effect on rod somal translocation

Non-muscle myosin II (NMII) is an actin filament associated motor protein responsible for actin cytoskeletal constriction and force generation. As such, NMII has been heavily implicated as a key molecular component involved in neuronal migration. In order to test whether this motor protein is required for oscillatory rod photoreceptor somal motility during early retinal development, P3 *Nrl.GFP*$^{+/+}$ retinae were explanted and time-lapse live imaged by 2-photon fluorescence microscopy in presence of the NMII selective small molecule antagonist blebbistatin at a concentration that blocks actomyosin constriction (25 µM; see Figure 2.7.2E-F) (N = 3; n = 304).

Similar to the pharmacological investigation with ciliobrevin D, live imaged retinae were only exposed to blebbistatin following a 2 hour control period in absence of the antagonist. This was done to ensure that any observed drug related effects were due to the action of blebbistatin, rather than due to poor tissue. As depicted in Figure 4.3.4A-D, all three modes of rod photoreceptor somal translocation (rapid apical, basal and stochastic) persisted in presence of blebbistatin. These movements were not kinetically different to those observed in the P3 control experiments with DMSO (see Figure 3.3.8-3.3.10). To confirm this quantitatively, the frequency of measured instantaneous velocities was plotted out on a histogram (Figure 4.3.4E). Near identical quasi-Gaussian frequency distributions were detected when comparing blebbistatin with DMSO control samples. Equally, MSD analysis revealed that the AvMSD curve produced from the data set from Blebbistatin-treated retinae was very similar to the AvMSD curve from the DMSO

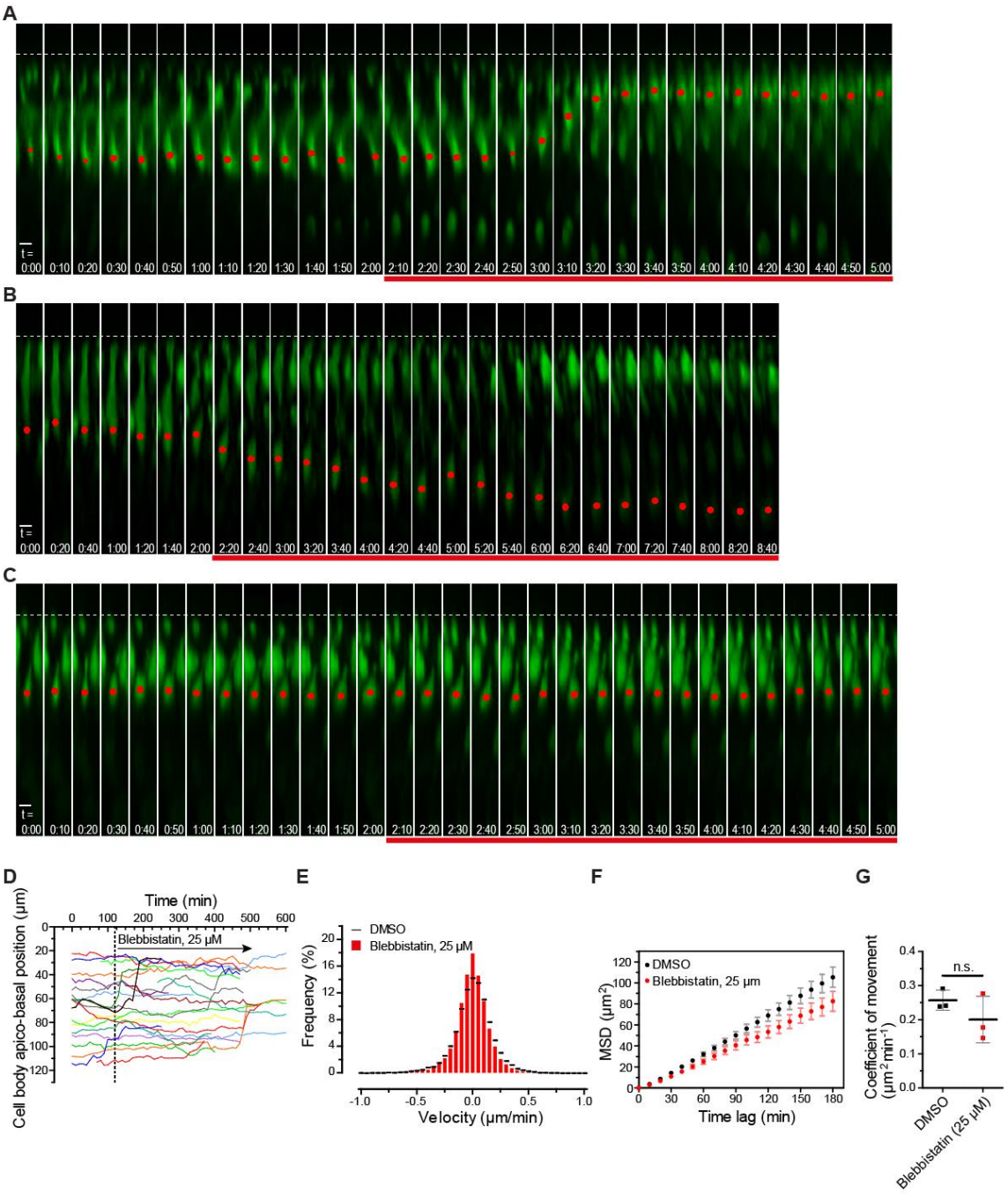

Figure 4.3.4 Inhibition of NMII-mediated actomyosin constriction did not extensively affect rod photoreceptor somal motility. NMII function was blocked using blebbistatin (25 µM; see also Figure 2.7.2E-F). **(A-C)** Representative montages following the apico-basal positions of rod photoreceptor somata (red dot) over time. Presence of 25 µM blebbistatin is indicated by the red bar underneath the montages. Scale bar: 5 µm. **(D)** Randomly picked rod photoreceptor soma radial trajectories superimposed in a single *zt* plot. **(E)** Comparison of instantaneous velocity distribution of pooled rod photoreceptor somal translocations in blebbistatin versus DMSO control exposed samples. **(F)** AvMSD profiles of total rod photoreceptor somal translocations in blebbistatin versus DMSO control exposed samples. Data are displayed as mean ± SEM. **(G)** Comparison of coefficient of movement values associated with AvMSD profiles in F. The coefficient of movement is directly proportional to the slope of a straight line fitted to the initial segment (0-60 minutes in this case) of the individual AvMSD profiles. Data are displayed as mean ± SD. Student's t-test was used for statistical analysis.

control dataset (Figure 4.3.4F). Even though a slight reduction in the slope of the MSD curve was detected for blebbistatin versus DMSO control treated retinae, this reduction proved to be statistically non-significant as demonstrated by the comparison of the coefficient of movement values between these two groups (Figure 4.3.4G): 0.241 ± 0.017 $\mu m^2\ min^{-1}$ (DMSO) versus 0.177 ± 0.039 $\mu m^2\ min^{-1}$ (Blebbistatin).

Thus, pharmacological prevention of actomyosin constrictions using the NMII antagonist blebbistatin does not influence rod photoreceptor somal translocation to any meaningful extent. This suggests that the motor protein NMII is not required for rod somal motility observed during early development.

4.3.2.3. Pharmacological arrest of microtubule dynamic behaviour and its effect on rod somal translocation

Microtubule filaments are polarised macromolecular structures, along which motor proteins, such as minus-end directed dyneins or plus-end directed kinesins, can transport cargo such as the nucleus. Generally in mature photoreceptors, the polarity of the microtubule cytoskeleton is such that the minus-ends of virtually all microtubule filaments locate to the centrosome while the plus-ends extend away towards the segment (apical) or the synaptic domain (basal) (Troutt and Burnside, 1988). During early retinogenesis and before segment formation, the centrosomes of rod photoreceptors were shown to locate to the apical limit of the neural retina (Figure 4.3.1). This in return implies that the microtubule plus ends, which can dynamically extend (polymerise) and retract (depolymerise), are pointing basally. Rod photoreceptor nuclear translocation in the basal direction, be it mediated by active or passive mechanism, would presumably require prior microtubule polymerisation in cases where such a microtubule extension had not previously been established. A lack of microtubule polymerisation could thus potentially result in a reduction of basally directed somal translocation.

To test this hypothesis, P3 *Nrl.GFP*$^{+/+}$ retinae were explanted and time-lapse live imaged by 2-photon fluorescence microscopy in presence of the drug demecolcine at a concentration of 45 nM, at which it stabilises microtubule filaments (Panda *et al.*, 1995; Wilson and Jordan, 1995; Picone *et al.*, 2010; see also Figure 2.7.2A-D) (N = 3; n = 307). However, following exposure to demecolcine after a 2-hour DMSO control period, all

modes of rod photoreceptor somal translocation could still be observed (Figure 4.3.5A-E). Of note, basal somal translocation was detected (Figure 4.3.5B) in addition to individual somata that oscillated between apical and basal positions (Figure 4.3.5D).

The fact that basal somal movements, or other modes of movement for that matter, did not disappear following drug exposure, is reflected in the instantaneous velocity histogram, which bore no significant changes in the distribution of velocities when comparing demecolcine and DMSO exposed retinae (Figure 4.3.5F). Although the MSD curve profile of drug exposed samples was slightly shallower compared with control (Figure 4.3.5G), the reduction in the slope as represented by the coefficient of movement was statistically not significant (Figure 4.3.5H; DMSO: 0.241 ± 0.017 μm^2 min^{-1}, demecolcine: 0.176 ± 0.038 μm^2 min^{-1}).

Thus, exposure of P3 retinae to demecolcine at a concentration that arrests microtubule dynamic behaviour, did not alter the way, in which rod photoreceptor somata translocated to any measurable degree. There is of course the possibility that basally directed somal translocation would have carried on much longer and beyond the extent of pre-existing microtubule filaments were it not for the demecolcine-mediated arrest of microtubule dynamic behaviour. The fact that there was a trend towards stunted motility as indicated by MSD analysis, may acknowledge this – albeit relatively minor – contribution of microtubule dynamic behaviour in rod somal motility.

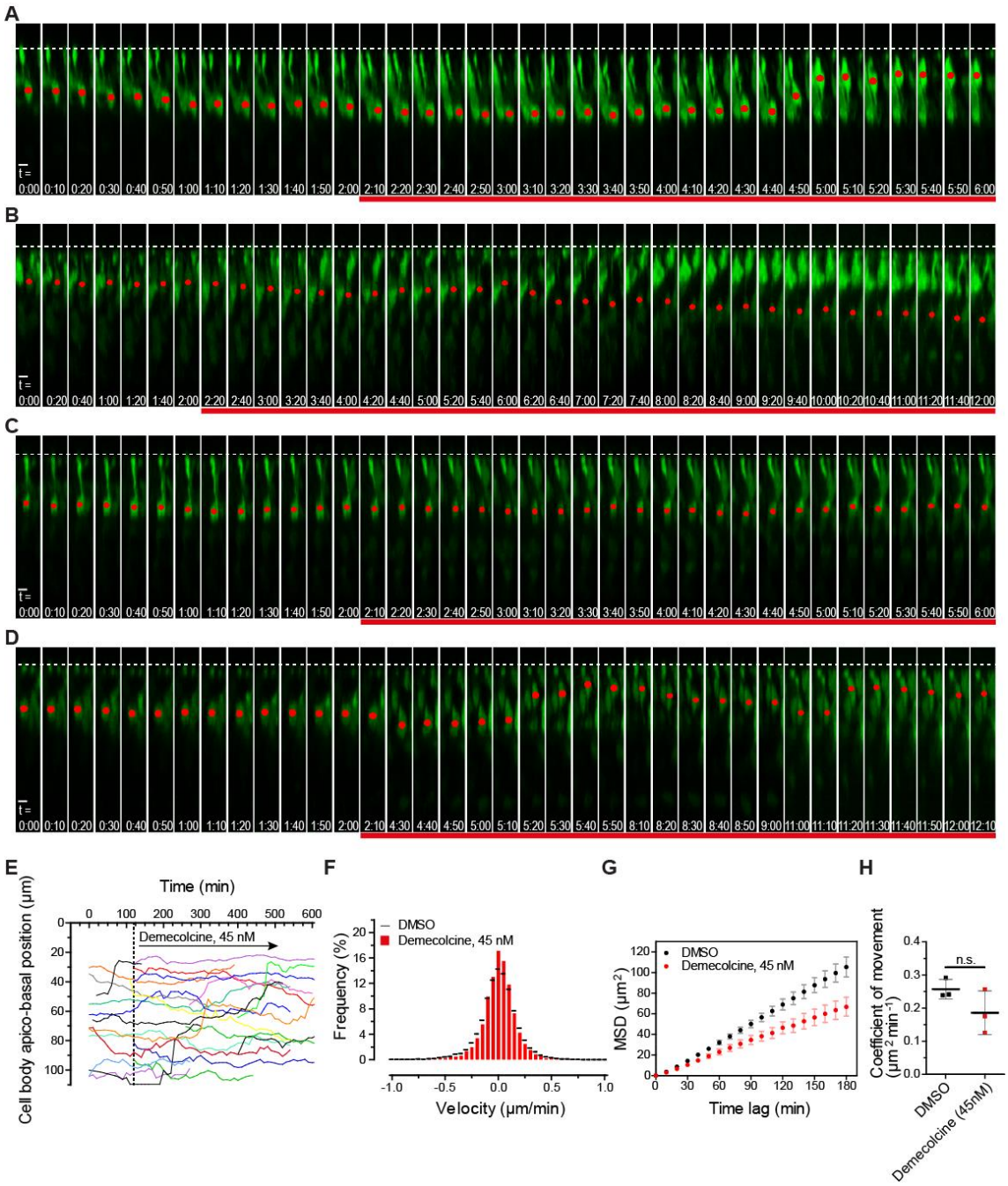

Figure 4.3.5 Arresting microtubule dynamic behaviour did not significantly attenuate rod photoreceptor somal motility. Microtubule dynamic behaviour was blocked using demecolcine (45 nM; see also Figure 2.7.2A-D). **(A-D)** Representative montages following the apico-basal positions of rod photoreceptor somata (red dot) over time. Presence of 45 nM demecolcine is indicated by the red bar underneath the montages. Scale bar: 5 µm. **(E)** Randomly picked rod photoreceptor soma radial trajectories superimposed in a single *zt* plot. **(F)** Comparison of instantaneous velocity distribution of pooled rod photoreceptor somal translocations in demecolcine vs. DMSO control exposed samples. **(G)** AvMSD profiles of total rod photoreceptor somal translocations in demecolcine versus DMSO control exposed samples. Data are displayed as mean ± SEM. **(H)** Comparison of coefficient of movement values associated with AvMSD profiles in F. Data are displayed as mean ± SD. Student's t-test was used for statistical analysis.

4.3.3. Analysing the mechanisms of rod somal motility with RNA interference

4.3.3.1. RNAi based specific gene silencing and its effect on rod somal positioning

In order to further corroborate the finding that the microtubule associated motor protein dynein I is primarily responsible for rapid apically directed (towards the minus end) somal translocation of rod somata, the next step consisted of performing short hairpin (sh)RNAi mediated LOF experiments. Given the proposed roles of dynein I during rod somal motility based on the pharmacology data, rod mislocalisation phenotypes may ensue after dynein I gene silencing. The following gene targets were chosen for this purpose: *Dync1h1* (encoding the dynein I major subunit cytoplasmic dynein I heavy chain 1) and *Pafah1b1* (encoding LIS1, an important dynein I co-factor) (Tsai *et al.*, 2005, 2007). The microtubule associated motor protein and kinesin family member KIF1A was previously shown to be responsible for plus end directed nucleokinesis in cortical neural progenitor cells undergoing IKNM (Tsai *et al.*, 2010). No selective small molecule antagonists against KIF1A presently exist. Its potential involvement in rod somal motility, especially in the basal direction, was thus also assessed by RNAi rather than by a combination of pharmacology and RNAi. Even though small molecule mediated blockade of NMII activity remained without major impact on rod somal motility (section 3.3.3.3), RNAi of the NMII subunit NMMHC-IIB (encoded by *Myh10*) was also included in this screen in order to confirm the earlier pharmacological findings.

A fixed tissue analysis approach was chosen as a first assessment of whether RNAi had led to rod somal mislocalisation. Retinae from P1 *Nrl.GFP*$^{+/+}$ mice were explanted, electroporated with the RNAi plasmids and then cultured. Following retinal harvest, the apico-basal position of rod photoreceptors harbouring the RNAi plasmids was measured on confocal microscopy images. It should be noted that the activity of neither the *mU6* promoter, which drives expression of the short hairpin, nor the *CAG* promoter that drives reporter *DsRed* expression, is restricted to rod photoreceptors. Therefore, only the positions of GFP/DsRed double positive rod photoreceptors, but not those of single positive cells, were formally measured. Representative confocal images of retinae harvested after 4 days (≡ P5) are shown in Figure 4.3.6A-E. As shown in Figure 4.3.6F and 4.3.6G, the somata of rod cells expressing the scrambled RNAi control construct

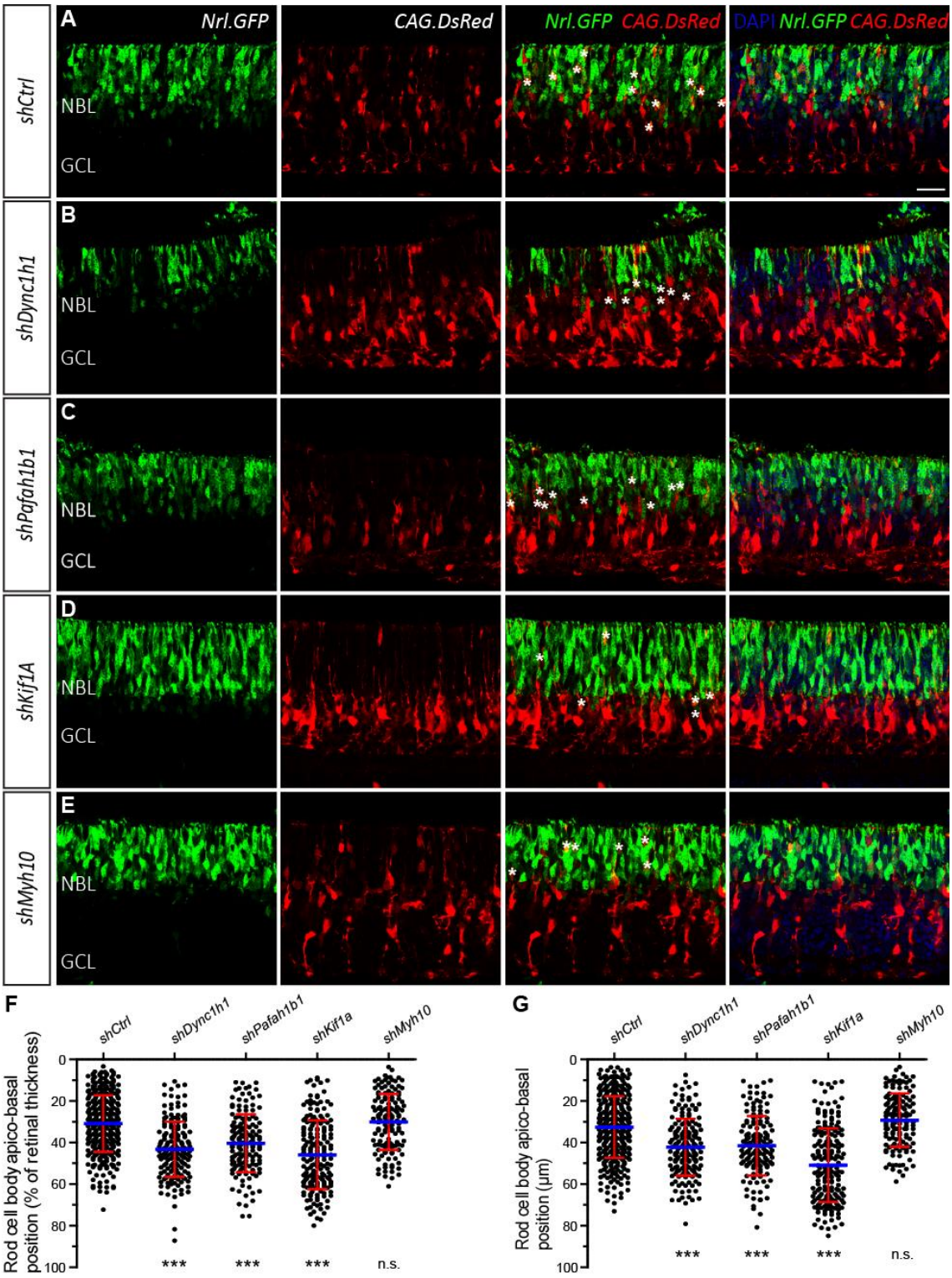

Figure 4.3.6 Functional inhibition of cytoskeletal motor proteins by RNAi for 4 days and its effect on rod somal radial position within the retina. P1 *Nrl.GFP*$^{+/+}$ retinae were explanted, electroporated with shRNA constructs against *Dync1h1*, *Pafah1b1*, *Kif1a* and *Myh10* and cultured for 4 days. **(A-E)** The radial position of rod photoreceptors (green) expressing the shRNA constructs (red) within the retina was assessed by confocal microscopy (yellow/white asterisks). Scale bar: 25 µm. **(F)** Relative and **(G)** absolute quantification of rod somal position within the neural retina. 1-way ANOVA (post test: Dunns) was used for statistical analysis. ***$p < 0.001$. Data are displayed as mean ± SD.

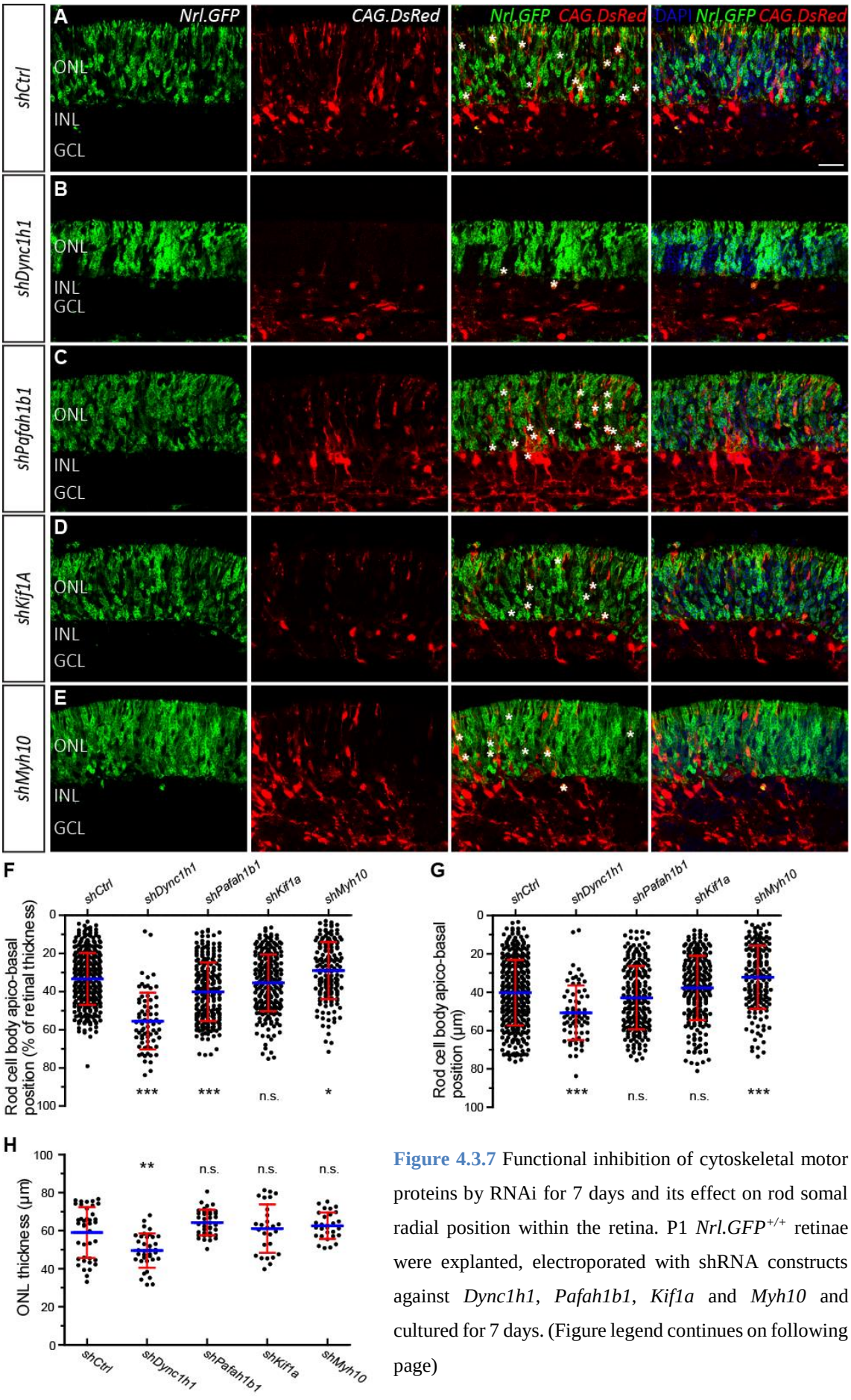

Figure 4.3.7 Functional inhibition of cytoskeletal motor proteins by RNAi for 7 days and its effect on rod somal radial position within the retina. P1 *Nrl.GFP*$^{+/+}$ retinae were explanted, electroporated with shRNA constructs against *Dync1h1*, *Pafah1b1*, *Kif1a* and *Myh10* and cultured for 7 days. (Figure legend continues on following page)

←

(Figure 4.3.7 figure legend continued) **(A-E)** The radial position of rod photoreceptors (green) expressing the shRNA constructs (red) within the retina was assessed by confocal microscopy (yellow/white asterisks). Scale bar: 25 µm. **(F)** Relative and **(G)** absolute quantification of rod somal position within the neural retina. **(H)** ONL thickness measured at 3 different locations in each field of view. 1-way ANOVA (post test: Dunns) was used for statistical analysis. *p<0.05, **p<0.01, ***p < 0.001. Data are displayed as mean ± SD.

(*shCtr*l) were located at an average depth of 32.6 ± 14.8 µm measured form the apical retinal margin, which is equivalent to 30.9 ± 13.6 % of the radial thickness of the retina (N = 2 experimental repeats with 2 retinae each, n = 358 cells). These cells are thus relatively close to the apical margin of the retina, populating the presumptive ONL. By contrast, rod somata with impaired dynein I function were found significantly deeper within the tissue. *shDync1h1*: 42.2 ± 13.7 µm corresponding to 43.2 ± 13.3 % of the tissue thickness (N = 3, n = 174, p < 0.001); *shPafah1b1*: 41.5 ± 14.3 µm or 40.3 ± 14.0 % (N = 2, n = 150, p < 0.001). The motor protein KIF1A acts in the opposite direction to dynein I and hence an apical accumulation of rod somata might have been predicted following *Kif1a* gene silencing. However, *shKifa*, like *shDync1h1*and *shPafah1b1*, resulted in basal somal displacement: 50.9 ± 17.8 µm or 45.9 ± 16.5 % (N = 2, n = 192, p < 0.001). Functional inhibition of NMII by means of *shMyh10* did not produce a radial displacement phenotype: 29.2 ± 12.8 µm or 30.0 ± 13.5 % (N = 2, n = 139, n.s.).

Representative confocal images of retinae harvested after 7 days of RNAi (≡ P8) are shown in Figure 4.3.7A-E. The somata of rod cells expressing *shCtrl* were mostly restricted to the ONL and were located at an average depth of 40.2 ± 17.1 µm or 33.3 ± 13.6 % (N = 2, n = 368; Figure 4.3.7F & 4.3.7G). Functional, RNAi-mediated inhibition of dynein I for 7 days resulted in a basal displacement of rod somata similar to that seen after 4 days of RNAi, although this was more pronounced for *shDync1h1* (50.7 ± 14.3 µm or 55.5 ± 14.9 %; N = 2, n = 71; p < 0.001) compared to *shPafah1b1* (42.9 ± 16.5 µm or 40.0 ± 15.3 %; N = 2, n = 232; p < 0.001 and n.s. respectively). While *shKif1*a produced a rod somal basal displacement phenotype after 4 days of RNAi, rod somata were largely found within the ONL after 7 days of RNAi: 37.8 ± 16.8 µm or 35.4 ± 14.8 % (N = 2, n = 255, n.s.). *shMyh10* did not affect rod somal position after 4 days of RNAi, but, after

7 days of RNAi, an apical accumulation phenotype manifested: 32.2 ± 16.5 µm or 28.9 ± 14.9 % (N = 2, n = 169; $p < 0.05$ and $p < 0.001$ respectively).

After 7 days of RNAi (≡ P8), retinal lamination has already progressed to the extent that the ONL has become separated from the INL (Figure 4.3.7A-E). Thus, the thickness of the presumptive ONL of all electroporated retinae was assessed by performing 3 measurements (taken within the left, middle and right thirds) in each individual field of view (Figure 4.3.7H). Retinae expressing *shCtrl* exhibited an average ONL thickness of 59.0 ± 13.4 µm. Similar values were recorded for *shPafah1b1* (64.3 ± 6.7 µm, n.s.), *shKif1a* (61.1 ± 12.7 µm, n.s.) and *shMyh10* (62.6 ± 6.9 µm, n.s.). By contrast, retinae expressing *shDync1h1* displayed a significantly thinner ONL (49.6 ± 9.1 µm, $p < 0.01$). As mentioned above, the average somal depth of rod photoreceptors expressing *shDync1h1* was 50.7 ± 14.3 µm (or 102.3 % of the average ONL thickness), which placed a large proportion of these somata (56.3 %) into an ectopically basal position, outside the average ONL boundaries. In contrast, the somata of *shCtrl* expressing rod cells were at an average depth of 40.2 ± 17.1µm (68.1 % of the ONL thickness) and only 28.3 % of these somata were basal to the average ONL boundaries.

Taken together, the results generated in this section by means of RNAi lend further support to the theory that dynein I motors are responsible for apical somal translocation in rod photoreceptors of the developing mouse retina. When dynein I function is impaired, rod somata are at greater risk of ending up in ectopically basal positions outside of the ONL. KIF1A and actomyosin constrictions may also be involved in rod somal positioning within the retina, but their exact roles are presently not as clear cut. Based on the results obtained here, KIF1A may act as a molecular brake (rather than a motor) preventing excessively basal rod somal locations, whereas actomyosin constrictions may act to push rod somata basally. As mentioned, however, RNAi was not specifically targeted to rod photoreceptors and off-target effects in other retinal cells may account for some of the experimental outcomes.

4.4. Conclusion

As was demonstrated in chapter III, the somata of rod photoreceptors are motile along the radial axis of the developing retina and they exhibit a movement that has here been named oscillatory rod photoreceptor somal translocation. The name was given to this novel mode of neuronal motility because it combines the morphological and kinetic features of both IKNM and somal translocation. The observed migratory behaviour characteristically featured a kinetically uniform, high velocity apical translocation component, whereas basal translocation was kinetically more heterogeneous. Apical and basal translocation events, in return, were often interspersed with periods of stochastic somal motions where only limited net motility is registered. Given that such a pattern of motility has, to the best of my knowledge, not been observed in any post-mitotic neuronal precursor cells, the mechanisms that underlie developmental rod photoreceptor somal motility are presently ill defined. IKNM and somal translocation have been reportedly driven by diverse, and sometimes contradicting, mechanisms, depending on the model organism, tissue or developmental stage under investigation. The experiments performed as part of this chapter were designed to shed light on the mechanisms that govern the oscillatory rod photoreceptor somal translocation during retinogenesis.

In many instances of neuronal migration, centrosomal motility is tightly linked to nucleokinesis and the two might even be coordinated and co-regulated (Tanaka *et al.*, 2004; Bellion *et al.*, 2005; Wang *et al.*, 2011). However, this is not universally true for all migrating neurons or neuronal progenitors (Zolessi *et al.*, 2006; Umeshima *et al.*, 2007; Spear and Erickson, 2012b; Strzyz *et al.*, 2015). Based on immunohistochemical analysis of the developing retina in this present study, centrosomes (immunoreactive for γ-tubulin) were exclusively found at the apical limit of the neural retina, at least from P0 up until P6 (Figure 4.3.1), whereas varying radial positions would be expected if centrosome motility was required for and/or coordinated with nucleokinesis. Since the P0-P6 period covers a time span where rod somata are motile, it can be concluded that the oscillatory rod somal motility does not require centrosomal motility, at least not during this period of retinal development.

Although there was some suggestion from the fixed tissue sections of centrosomes becoming displaced with increasing developmental age, it is unlikely these belonged to photoreceptors. The centrosomes of photoreceptors, in all likelihood, become the basal

bodies at the base of the connecting cilium located towards the apical tip of the photoreceptor inner segments (Pugacheva *et al.*, 2007; Bornens, 2008). Indeed, weak γ-tubulin immunoreactivities consistent with this location were observed at developmental stages where outer segments are known to be present (Figure 4.3.1). The γ-tubulin positive centrosomes that were dispersed within the ONL from P8 onwards may belong to other migrating late born neurons, such as bipolar cells, or indeed Müller glia, rather than the photoreceptors.

The rapid apically directed aspect of oscillatory somal translocation invariably featured an initiation phase, where somata started accelerating towards the apical margin, a principal translocation phase, during which somata reached peak velocity, and a cessation phase, where somata decelerated. The uniform kinetics of rapid apical somal translocation pointed towards an active and cell intrinsically driven translocation mechanism. According to a previous study, photoreceptors possess a polarised arrangement of their microtubule cytoskeleton, where the microtubule minus ends locate to the apical margin of the retina and the plus ends point towards the vitreal surface and (in the adult) towards the outer segments (Troutt and Burnside, 1988). Dyneins are minus end directed microtubule-associated motor proteins. Accordingly, in this present study, a combination of pharmacological (Ciliobrevin D) and genetic approaches (short hairpin RNAi) showed that apical/minus end-directed somal translocation is mediated by the dynein I microtubule motor protein complex, which encompasses the co-factor LIS1. Ciliobrevin D completely abolished all rapid apical somal translocations when applied to explanted retinae (Figure 4.3.2). This was highly unlikely to be due to drug toxicity related cell death, since rapid apical somal translocation could be restored in wash-off experiments (Figure 4.3.3). RNAi mediated gene silencing of either *Dync1h1* (encoding the heavy chain of dynein I) or *Pafah1b1* (encoding LIS1) led to the basal displacement of transfected rod photoreceptor somata both after short (3-4 days) and long term RNAi exposure (7 days). This is consistent with the idea that rapid apical somal translocation is cell intrinsically regulated by dynein I in individual rod photoreceptors to facilitate their enrichment within the (presumptive) ONL.

After 7 days of *Dync1h1* RNAi, there was a significant reduction in ONL thickness compared with control retinae (although the entire neural retinae appeared thinner as well). Furthermore, markedly fewer RNAi expressing rod photoreceptors (GFP/DsRed double positive) as well as fewer RNAi expressing non-rod retinal cells (DsRed positive) could be identified. It is worth mentioning, that in addition to rod photoreceptor apical

somal translocation, dynein I is likely also required during IKNM of RPCs, especially for G2-phase associated nucleokinesis in the apical direction. The long-term reduction in dynein I function may have thus negatively affected the survival of existing rod and other retinal cells including RPCs, and/or RPC proliferative and neurogenic cell divisions giving rise to future cells of the neural retina. The consistently reduced number in retinal cells transfected with *shDync1h1* versus *shCtrl* retinae points towards a cell survival defect. However, both impaired cell survival and cell cycle dysfunction could potentially invoke a reduction in ONL/neural retinal thickness.

The kinetics of basally directed and stochastic rod photoreceptor somal translocation are much less uniform, compared with rapid apical translocation. Basal somal translocation events were frequently composed of high and low velocity periods, while stochastic somal translocation, although exhibiting an overall zero net displacement, sometimes produced measurable intermittent apical or basal motions. Based on this, it is hard to imagine that these two modes of rod somal motility are subject to similar, mechanistically defined processes as rapid apical translocation. In fact, pharmacological blockade of microtubule dynamic behaviour using Demecolcine or blockade of actomyosin constrictions using Blebbistatin had little demonstrable effect on basal and stochastic somal translocation (nor, indeed, on rapid apical translocation). However, a small, non-significant reduction in the MSD profile was observed in both cases. In the absence of a clear effect of pharmacological NMII blockade (this attenuates actomyosin constrictions) on rod somal kinetics, it is unsurprising that gene silencing of the NMII subunit NMMHC-IIB by RNAi (*shMyh10*) had little effect on the radial positions of transfected rod photoreceptor somata after 3-4 days of RNAi exposure. After 7 days of RNAi exposure, the somata of transfected rod photoreceptors tended to accumulate closer to the apical margin of the retina. It is thus a possibility that actomyosin constrictions mediated by NMII are responsible for active movement of rod somata in the basal direction. It should be noted, however, that RNAi was not exclusively expressed in rod photoreceptors and off-target effects are a possibility. For instance, cytokinesis in dividing RPCs is known to be heavily dependent on actomyosin (reviewed by Heng and Koh, 2010). RNAi-mediated NMII ablation in RPCs may have thus resulted in reduced cell division rates and hence reduced forces pushing rod somata in the basal direction. However, it is unclear how likely this scenario is, given that there was no readily apparent accumulation of M-phase arrested RPCs at the apical limit of the retina and no reduction in neural retinal thickness.

Basally directed and stochastic rod photoreceptor somal translocation may be regulated by microtubule-associated motor proteins just like rapid apical rod somal translocation is regulated by dynein I. As discussed, bath application of the dynein I antagonist Ciliobrevin D completely abolished minus end directed apical translocation of rod somata. In addition to this, virtually all translocations – whether apically or basally directed – came to a more or less complete standstill. This would suggest that non-apically-directed translocations may largely be passive, and secondary to the rapid apical, dynein I mediated translocations of neighbouring cells as they push adjacent cells in the basal direction to reduce steric over-crowding. This in turn suggests that non-apical rod somal translocation is unlikely to be driven by plus end directed microtubule associated motor proteins of the kinesin family. Yet, when expression of the kinesin motor protein gene *Kif1a* was silenced in rod photoreceptors by RNAi for 3-4 days, rod somata did become displaced. However, these somata did not accumulate towards the minus end at the apical limit, as would be expected for a motor protein with plus end processivity. Rather, cells were paradoxically found in ectopically basal positions, similar to photoreceptors with RNAi mediated reduced dynein I function (*shDync1h1, shPafah1b1*). This phenotype was apparently transient, however, since the distribution of rod photoreceptor somata within the neural retina returned to normal with prolonged (7 days) RNAi exposure. Thus, it is presently not entirely clear what mechanisms mediate basal somal translocation; if KIF1A is involved in this process, its exact function will need to be examined more carefully in the future. One possibility appears to be that KIF1A acts as a molecular brake rather than a motor that limits the extent, to which rod somata can move basally.

The results provided by the LOF experiments described in this chapter suggest that oscillatory rod photoreceptor somal translocation is primarily driven by cell-intrinsic processes. However, it would be premature to conclude that the observed motility is, therefore, an entirely cell-autonomous effect. Rod photoreceptor somal motility may be a response to extra-cellular cues. The cell-cell and cell-extracellular matrix interactions that occur during glial-guided neuronal migration in the cortex are known to eventually translate into nucleokinesis by activating the dynein I complex (Solecki *et al.*, 2004; Tsai *et al.*, 2007; Marín *et al.*, 2010a; Valiente and Marín, 2010). What this means in the context of this present study is that the attenuation of dynein I may have not only blocked potentially purely cell-autonomously driven nucleokinesis but also nucleokinesis that resulted from glial-guidance mechanisms. This warrants a careful and separate

examination of the existence and importance glial-guided rod photoreceptor somal motility.

In summary, the experiments and data shown in chapter III and IV provide evidence that the somata of post-mitotic rod photoreceptors engage in oscillatory apico-basal movements during murine retinogenesis. This novel mode of neuronal motility was named oscillatory somal translocation (see chapter III). The experiments carried out as part of chapter IV were designed to shed light onto the mechanisms that underlie this motility. This was an especially intriguing topic to address since IKNM and somal translocation are mechanistically quite heterogeneous, depending on model species, tissue and perhaps even developmental stage (Kosodo, 2012; Lee and Norden, 2013). The obtained results indicate the following: a) centrosomal motility is not required for oscillatory rod photoreceptor somal translocation; b) the most striking aspect of the rod migratory behaviour, rapid apical translocation, is likely powered by the microtubule-associated and minus end-directed (towards the apical tissue margin) dynein I motor protein, assisted by its cofactor LIS1; in absence of dynein I function, rod somata are more likely to end up in ectopically basal positions outside of the ONL; c) non-rapid apical translocation events (including basally-directed translocations) are largely passive in nature and likely caused by the rapid apical translocation of neighbouring cells; d) yet, LOF of *Kif1A*, a kinesin family microtubule-associated motor protein (plus end directed or towards the basal tissue margin), also resulted in a mislocalisation phenotype; unexpectedly, rod somata did not accumulate apically but were transiently displaced basally; e) although somal migration in the basal direction is likely to be overwhelmingly passive, actomyosin constrictions may also be involved; f) rod somal motility does not require the presence of dynamic microtubules. All the results combined provide evidence that rod nucleokinesis is largely mediated by cell intrinsic cytoskeleton-associated mechanisms. However, the experiments carried out within this chapter cannot distinguish between cell-cell contact independent nucleokinesis or nucleokinesis that resulted from cell-cell interactions (i.e. glial-guided migration). For that reason, the role of glial-guidance in rod somal motility will have to be addressed separately.

CHAPTER V. DEVELOPMENTAL ROD PHOTORECEPTOR MOTILITY AND GLIAL GUIDANCE

5.1. Introduction

As part of this present study it was established that rod photoreceptor precursor cells carry out a hybrid motility pattern with characteristics of IKNM and somal translocation (see chapters III and IV). Two other modes of neuronal migration (multipolar and tangential migration) were incompatible with the observed migratory behaviour. Rapid apical translocation of photoreceptor somata was shown to be cell intrinsically driven by the microtubule-associated dynein I motor complex. However, the last remaining mode of neuronal motility, glial-guided migration, also features a dynein I dependent nucleokinesis aspect, at least in the cortex (Tsai *et al.*, 2005, 2007). Perturbation of dynein I function by pharmacology or RNAi thus not only blocked rapid apical translocation, but also prevented movements in the basal direction. This may be due to an indirect effect, if basal movements are passive in nature and resultant from displacement by apically moving cells. Alternatively, a loss of dynein I function may have a direct effect on any glial-guided somal motions.

Glial-guided neuronal migration is firmly established in cortical areas of the brain. Pyramidal projection neurons usually populate the cortical plate in the adult brain. However, these neurons are not born within the cortical layers but in the underlying neurogenic area closest to the ventricles, called the ventricular zone. There, radial glia, the neural progenitor cells of the developing cortex, engage in IKNM, during the course of which neurogenic cell divisions occur at the ventricular zone, which give rise to neuronal precursor cells. Newly born neuronal precursor cells migrate out of the ventricular and neighbouring zones into the quite distant cortical plate. This predominantly occurs by glial-guided radial migration along their mother radial glial cells, which span the entire neuroepithelium (reviewed by Nadarajah and Parnavelas, 2002a). Kinetically, glial-guided neuronal migration exhibits a characteristic saltatory motion, which is due to concerted centrosomal advancement and nucleokinesis into the leading process (Schaar and Mcconnell, 2005; Marín *et al.*, 2006; Umeshima *et al.*, 2007);

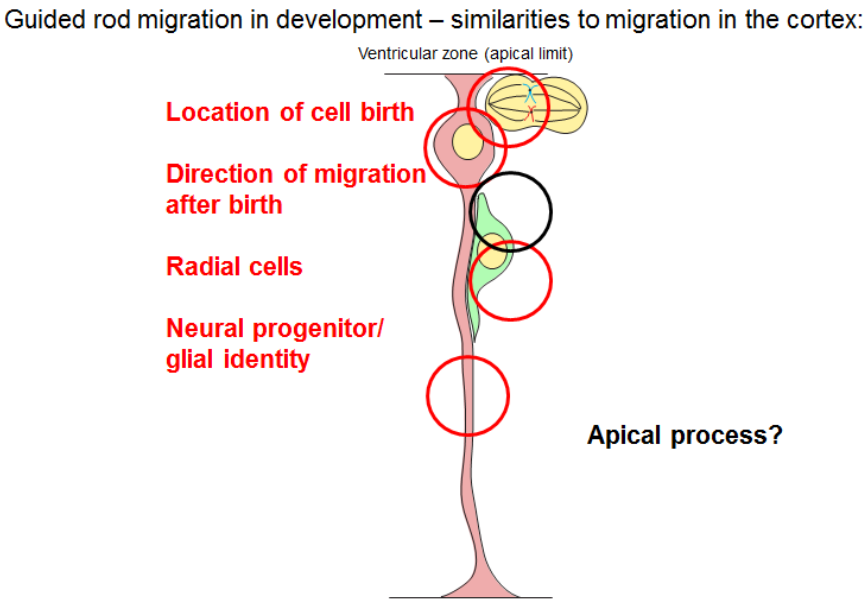

Figure 5.3.1 Similarities and differences between glial-guided neuronal migration in the developing cortex and potentially occurring glial-guided rod photoreceptor migration in the developing retina. Similarities are indicated with red text and circles, differences are indicated with black text/circle.

at the same time, the release and reformation of the interstitial junction (interface of extensive cell-cell contacts between a migrating neuron and its glial-guidance partner) also contributes to the saltatory motion (Gregory *et al.*, 1988; Anton *et al.*, 1996). In combination, this results in a relatively low average velocity of glial-guided neuronal migration (0.1-0.25 µm/min; Chen *et al.*, 2008; Franco *et al.*, 2011). Interestingly, basal movements of rod photoreceptors within the developing retina, although heterogeneous, also largely fell into that velocity range (see Figure 3.3.4C). By contrast, rod photoreceptor rapid apical somal translocation is too fast (~ -0.3 to -1.2 µm/min) to fall within this category.

In the eye, Müller glia also span the entire radial extent of the neural retina and they may thus potentially be used by neurons as glial guides in a similar way as radial glia in the cortex. However, Müller glia are among the last of all retinal cell types to be born. Their genesis peaks at P3 in the mouse retina (Marquardt and Gruss, 2002). It is also around this time that a large part of rod photoreceptor migration occurs during development (Warre-Cornish, unpublished data; section 3.3.1 & 3.3.2). Without the majority of Müller glia present at early stages of post-natal development, it would be difficult to argue that rod somal motility is dependent on Müller glia guidance. However, Walcott and Provis (2003) have proposed that Müller glia are the end stage phenotype of retinal progenitor cells (RPCs), based on the co-localisation of neural progenitor cell marker (nestin) and adult Müller glia marker immunoreactivities in the developing eye. In further support of this, more recent studies have demonstrated similar gene expression profiles in RPCs and Müller glia (Blackshaw *et al.*, 2004; Livesey *et al.*, 2004; Roesch *et al.*, 2008; Jadhav *et al.*, 2009; Nelson *et al.*, 2011). Due to this overlapping identity, the spectrum of cells ranging from RPCs to Müller glia is collectively called neural retina spanning cell (NRSC) within this thesis. Hence, NRSCs, whether they are at the RPC or Müller glia stage, are present at all times when rod cells are and they could thus serve as glial guidance tracks for rod photoreceptors.

The retina and brain share common origins and perhaps, therefore, a list of common features. It is possible that glial-guided neuronal migration will have to be added to the list of features shared between the retina and the brain (Figure 5.3.1). Notably, RPCs, which give rise to all retinal neurons, also span the entire width of the retinal neuroepithelium during retinogenesis, just like the radial glia in the brain. Furthermore, both RPCs and radial glia exhibit hybrid neural progenitor and glial states. Both undergo mitotic cell divisions at the apical margin of their respective neuroepithelia. Most newly

generated retinal neurons subsequently have to move away from the apical margin and in the basal direction to reach their target strata. In the mammalian retina, at least, this can involve traversing distances of 50-100 µm.

Previous speculations and circumstantial evidence have fuelled the debate on whether glial-guided migration occurs to any relevant extent within the retina: Reichenbach and colleagues (1993) coined the term 'columnar unit' in reference to the often clonally related retinal neurons (especially rod photoreceptors) that cluster around a central, related Müller glia cell in the mature retina. These tight associations may have already existed during retinogenesis where rod photoreceptors display marked apico-basally directed somal motility (see chapter III). Furthermore, rod photoreceptors born from adult neurogenesis in the cichlid fish retina appear to move basally along Müller glia following their birth at the apical margin of the retina (Mack *et al.*, 2003). An earlier ultrastructural study also proposed that the proximity between nascent photoreceptors and Müller glia may be indicative of glial-guidance mechanisms as rod cells target into the ONL (Raymond and Rivlin, 1987). Arguing against classical glial-guided (rod) neuronal migration in the retina, like what is observed in the brain, there are critical morphological and structural differences. The most obvious dissimilarity is the fact that rod cells with motile somata always maintained an apical process that anchored them to the apical edge of the neural retina (chapter III & IV; Warre-Cornish, PhD thesis, 2013). Glial-guided neuronal precursor cells of the brain exhibit short leading and trailing processes devoid of contact to the apical or basal limit of the neuroepithelium (Rakic, 1971a, 1971b, 1972). Furthermore, these cells had motile centrosomes that were usually in relatively close proximity to the nucleus, oftentimes leading the nucleus in the direction of migration (Rivas and Hatten, 1995; Umeshima et al., 2007; Distel et al., 2010). Conversely, rod photoreceptors in the developing retina exhibited centrosomes that remained stationary at the apical edge of the retinal neuroepithelium (Figure 4.3.1). Considering these differences, it may be that if glial-guided rod migration truly exists within the retina, then it might mechanistically differ from glial-guided neuronal migration in the brain.

Published works indicating the existence of glial-guided rod migration (Raymond and Rivlin, 1987; Mack et al., 2003) were based on analyses on fixed tissue rather than time-lapse microscopy, a technique that was instrumental to the characterisation of glial-guided migration in the cortex (e.g. Edmondson and Hatten, 1987; Anton *et al.*, 1996; Franco *et al.*, 2011). In order to investigate whether developing rod photoreceptors migrate radially along NRSCs by employing glial-guidance mechanisms, similar time-lapse microscopy

studies will have to be performed. This will require the development of tools to label ideally all NRSCs *in vivo*, while having sparsely labelled rod photoreceptors. NRSC labelling could potentially be achieved by using the *Rlbp.GFP*$^{+/+}$ transgenic reporter mouse line, which was available within the group; sparse rod labelling could be achieved by transfection with an *Nrl* promoter driven rod reporter construct. However, the *Rlbp.GFP*$^{+/+}$ line produced insufficient signal strength during early development while the *Nrl.DsRed* reporter construct, previously cloned within the group, proved to be inactive *in vivo* (personal communication within the group). The most feasible strategy was thus to try to label NRSCs within the *Nrl.GFP*$^{+/+}$ mouse. As opposed to the ideal experimental design, all rod cells, but not necessarily all NRSCs, will be labelled using this strategy. An obvious caveat of this approach is that the lack of NRSC labelling and the lack of the actual NRSC would be indistinguishable; whether rod somal motility was guided by or independent of an NRSC would thus be difficult to tell.

Given all morphological similarities between NRSCs and radial glia, together with the features of rod/glial interactions described above, it is intriguing to speculate whether mammalian photoreceptors could also utilise NRSCs for radial migration towards their final location within the ONL.

5.2. Aims

The aims of the work carried out as part of this chapter were:

(1) to identify a gene with suitable gene expression profile in NRSCs that is active in RPCs as well as nascent Müller glia.

(2) to generate and to validate an NRSC gene expression reporter based on the gene identified in (1) where reporter expression should reflect the expression of said gene in a spatio-temporally accurate manner.

(3) to address by real time fluorescence microscopy live imaging whether rod photoreceptors in the developing, post-natal *Nrl.GFP*$^{+/+}$ mouse retina migrate along NRSCs previously labelled *in vivo* with the NRSC gene expression reporter.

Combined, these experiments aim to address the question of whether rod photoreceptors in the developing neural retina utilise NRSCs to migrate in a manner that is equivalent to glial-guided neuronal migration in the developing cortex. This should provide us with a better insight into how rod photoreceptors reach their final position within the ONL and how aspects of the highly specialised retinal architecture are established with the precision required to enable visual perception. From a translational point of view, the investigation of developmental rod photoreceptor motility might also provide important clues as to what the mechanisms underlying rod photoreceptor migration and integration following photoreceptor transplantation are. However, rod photoreceptor transplantation will formally be addressed in chapter VI.

5.3. Investigating the existence of glial-guided rod photoreceptor migration during development

5.3.1. Identifying a gene suitable for usage as an NRSC reporter

5.3.1.1. Characterisation by qPCR of NRSC marker expression in the developing retina

Besides cell autonomous active mechanisms and passive displacement, rod photoreceptor somal motility may involve cell-cell interactions, including glial-guidance processes. During the phase of retinal development where rod somal translocation has been observed (Warre-Cornish, PhD thesis, 2013; section 3.3.1 & 3.3.2), there is an abundance of NRSCs (the radial glia of the retina), which initially start off as RPCs but slowly transition into Müller glia over time (Walcott and Provis, 2003). In the adult retina, many retinal neurons, especially rod photoreceptors, are closely packed around a single central Müller glia cell in an arrangement that has been termed columnar unit (Reichenbach *et al.*, 1993). This arrangement has various benefits for the correct function of retinal neurons and vision processes in adults (see section 1.1.6), so it is intriguing to speculate whether it arises from the migration of post-mitotic retinal neurons, including rod photoreceptors, along immature NRSCs towards their final position.

Having NRSCs labelled with a fluorescent protein in the same retina as GFP-labelled rod photoreceptors would enable the use of time-lapse live imaging fluorescence microscopy experiments in order to capture any potential glial guidance interactions between NRSCs and rod photoreceptors. To do that, an appropriate NRSC cellular label first needed to be identified. Within the developing and adult retina, the expression of several genes is specifically restricted to the NRSC cell population. Among others, this group of genes includes *Car2* (encoding Carbonic anhydrase 2), *CD44* (CD44), *Clu* (Clusterin), *Glul (Glutamine synthetase or GS), Nes* (Nestin), *Rlbp1* (RLBP), *Sox9* (Sox9) *and Vim* (Vimentin) (Blackshaw *et al.*, 2004; Livesey *et al.*, 2004; Roesch *et al.*, 2008; Jadhav *et al.*, 2009; Nelson *et al.*, 2011). The expression of these markers in the early post-natal

retina, specifically within the first 2 post-natal weeks of murine development, has not yet been investigated in detail.

The expression of these markers in the developing neural retina was investigated by qPCR (Figure 5.3.2) and, in parallel, by immunohistochemistry (see section 5.3.1.2). Expression levels in whole retinal tissue were normalised to the house keeping gene *Actb* and are stated as % relative to adult levels. The expression profiles of the analysed NRSC markers could be placed into three categories: a) increasing levels of expression during development that gradually approached adult levels, as observed for *Car2*, *Cd44*, C*lu*, *Glul*, *Rlbp1* and V*im*; b) already adult levels of expression throughout the early post-natal time point series, S*ox9*; c) decreasing levels of expression that gradually approached adult levels, *Nes*. The NRSC markers placed in category (a) are known to be robustly expressed in adult Müller glia, but between P0 and P8 only *Vim* approached the levels of expression seen in the adult (40.3 ± 4.7 % of adult levels at P0, 90.6 ± 18.8 % at P8). Interestingly, the other NRSC markers that also fall into category (a) can be sub-divided into 3 distinct groups based on the time of expression onset: *Car2* and *Rlbp1* were robustly activated between P4 and P6, while *Cd44* and *Glul* genes only become transcriptionally active between P8 and P10. Finally, the onset of *Clu* gene expression was not detected until after P12. As part of category (b), *Sox9* was expressed at 99.7 ± 4.8 % of adult levels at P0 and 103.5 ± 9.5 % at P8. According to a previous study, *Sox9* is initially expressed in multipotent RPCs and only gradually becomes restricted to Müller glia during development (Poché *et al.*, 2008). This finding would be in agreement with the interpretation that RPCs and Müller glia form part of a continuous spectrum of NRSCs. *Nes* showed a category (c) type expression pattern, with 852.0 ± 226.8 % of adult expression levels at P0 and 334.1 ± 49.7 % at P8. This is in keeping with the developmentally-restricted expression of *Nes* observed previously (Walcott and Provis, 2003).

Based on these qPCR data, *Sox9* and *Nes* display adequate levels of expression during the first post-natal week. These markers may thus be further considered for reporter-based labelling strategies for NRSCs during this time period. A *Vim* reporter could theoretically also be a plausible option; however, a virally delivered vimentin reporter was previously shown to be toxic for the retina (Hippert C., personal communication).

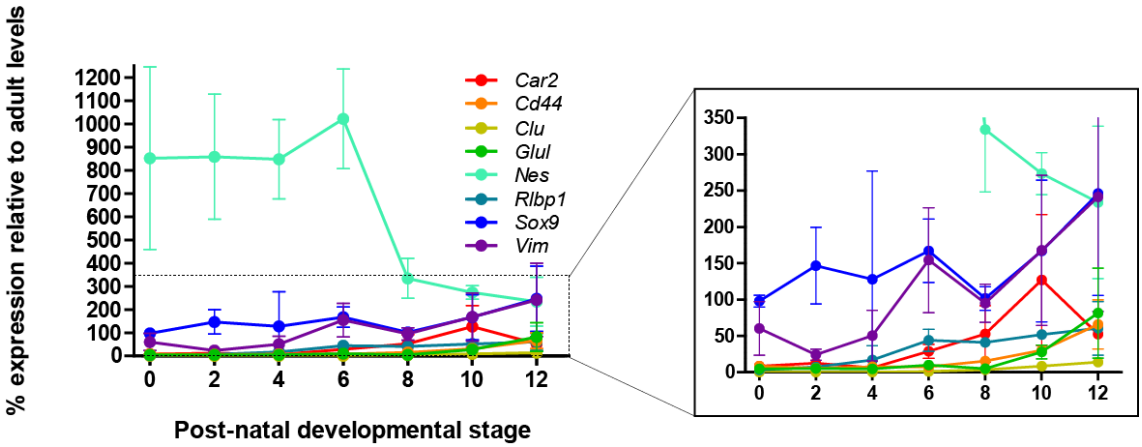

Figure 5.3.2 Expression profiles of several NRSC marker genes in the developing mouse retina as per qPCR. RNA was extracted from total P0-P12 as well as adult neural retinae and then reverse transcribed into cDNA, which was subsequently used for qPCR reactions. Expression levels were normalised to *Actb* levels and stated as % relative to adult levels. The inset to the right shows a magnified version of the boxed field in the left panel. n = 3 for each marker at each time point; all samples were run in triplicates. Data points show mean ± SD.

5.3.1.2. Immunohistochemical characterisation of NRSC marker expression in the developing retina

In parallel to the qPCR screen, the developmental expression of NRSC markers was also investigated by immunohistochemistry in order to identify an appropriate NRSC cellular label for the early developmental period. Besides Sox9 and Nestin, the genes of which have been established as promising candidates by qPCR, the developmental expression of CD44 and Glutamine synthetase (GS) was also analysed. CD44 and GS are both known Müller glia markers in the adult retina; in development, however, there currently only exists an incomplete characterisation of expression although there are some descriptions of their expression within the first postnatal week (Linser *et al.*, 1984; Chaitin *et al.*, 1996; Shinoe *et al.*, 2010). It was thus decided to revisit the characterisation of developmental CD44 and GS expression, in addition to that of Sox9 and Nestin, by immunohistochemistry.

At P2, CD44 and GS immunoreactivities appeared to be relatively weak within the neuroblastic layer (NBL) (Figure 5.3.3A). However, the patterns of expression for each marker were reminiscent of NRSCs, with cell processes that spanned the entire width of the neural retina. GS showed increased immunolabelling in the GCL and the developing inner plexiform layer (IPL). By P7, the previously strong GS labelling in the IPL was absent, whereas expression in the GCL was maintained (Figure 5.3.3B). In the ONL, labelling for both GS and CD44 was weak, but the pattern of expression was consistent with radial NRSC processes. At P10, GS and CD44 labelling appeared in the shape of elongated retinal cells with a morphology highly reminiscent of maturing Müller glia (Figure 5.3.3C). Both markers showed robust expression in the ONL, outer plexiform layer (OPL) and INL. Finally, at P14, both CD44 and GS showed robust and clear labelling almost throughout the radial extent of NRSCs (Figure 5.3.3D).

Cells positive for Nestin immunoreactivity in the P2 retina had morphologies consistent with that of NRSCs, and which spanned the entire thickness of the neural retina (Figure 5.3.34i & 5.3.4Aii). Expression was markedly higher in the IPL and GCL compared to the rest of the NBL. In agreement with its function as a transcription factor, Sox9 labelling was nuclear (note the co-localisation between Sox9 immunoreactivity and Hoechst staining) and restricted to several layers of nuclei within the central portion of

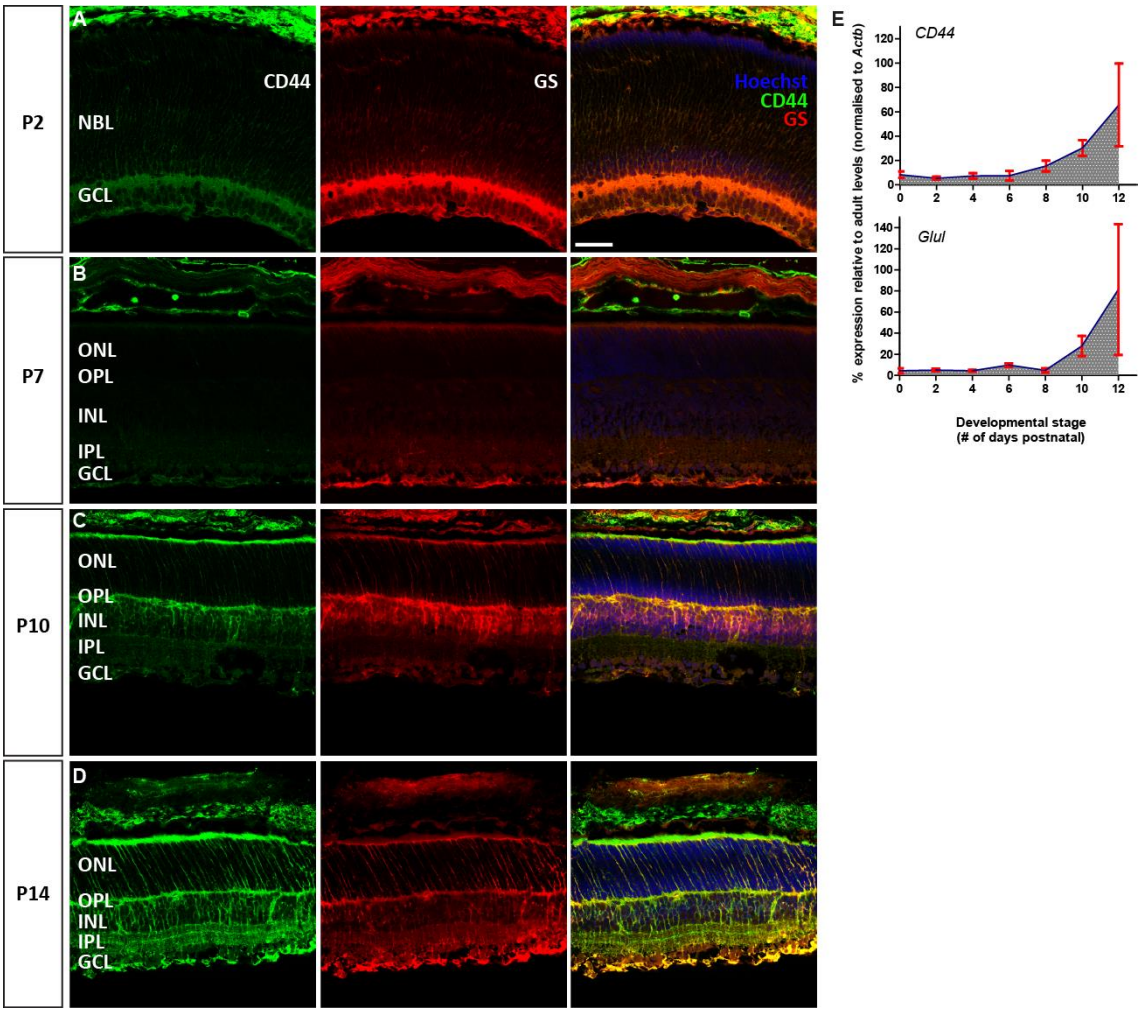

Figure 5.3.3 Immunohistochemical characterisation of the onset of CD44 and GS expression in NRSCs in the developing P2-P14 mouse retina. CD44 (green) and GS immunoreactivities (red) gradually intensified and started to increasingly resemble typical Müller glia cell morphologies in progressing from P2 **(A)**, to P7 **(B)**, P10 **(C)** and P14 **(D)**. GS = glutamine synthetase, NBL = neuroblastic layer, ONL = outer nuclear layer, OPL = outer plexiform layer, INL = inner nuclear layer, IPL = inner plexiform layer, GCL = ganglion cell layer. Scale bars, 25 µm. **(E)** shows the early post-natal expression levels of *CD44* and *Glul* in whole retina at the mRNA level as determined by qPCR and as depicted in Figure 5.3.2. Expression levels were normalised to *Actb* levels and stated as % relative to adult levels. n = 3 for each marker at each time point; all samples were run in triplicates. Data points show mean ± SD.

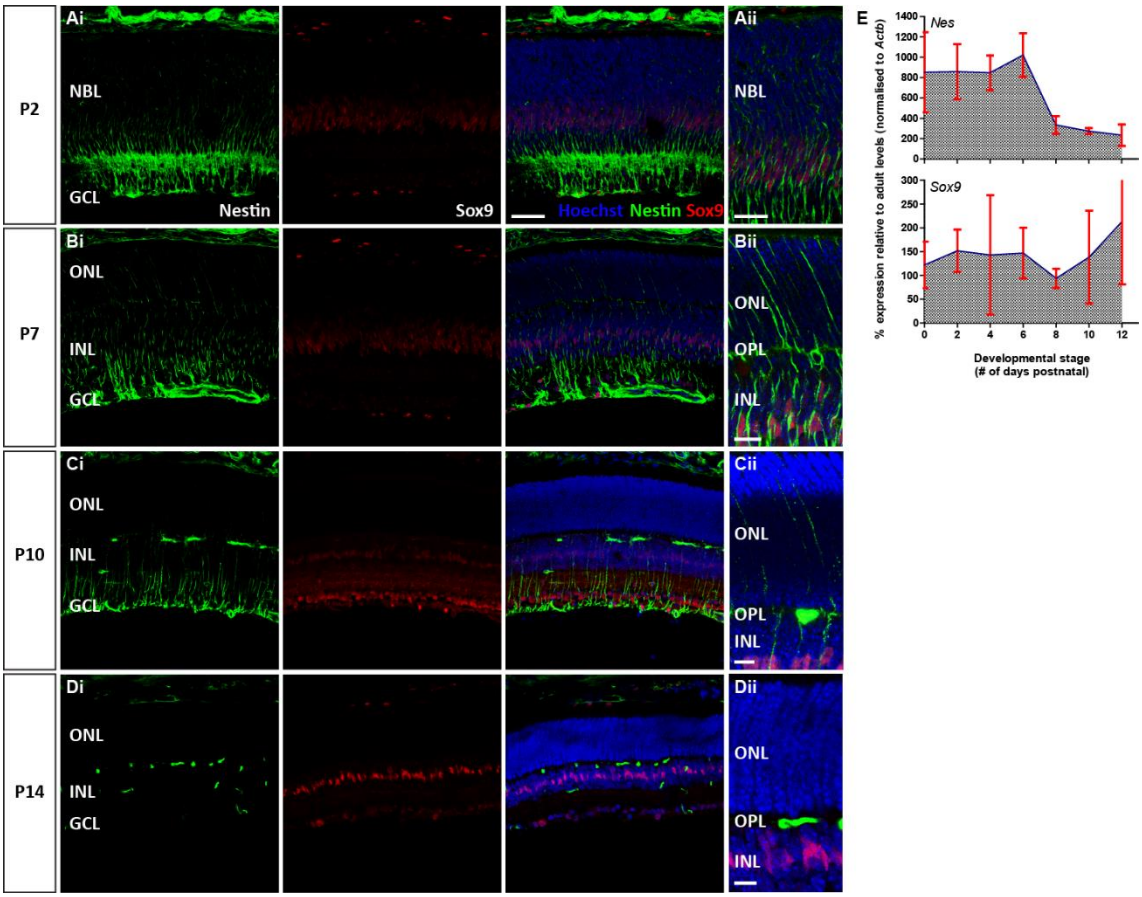

Figure 5.3.4 Immunohistochemical characterisation of Nestin and Sox9 immunoreactivity in the developing P2-P14 mouse retina. Nestin (green) and Sox9 immunoreactivities (red) at P2 **(Ai)** and at higher magnification in **Aii**, P7 (**Bi;** higher magnification in **Bii**), P10 (**Ci**; higher magnification in **Cii**) and at P14 **(Di;** higher magnification in D**ii)** are shown. Note that apparent Nestin immunoreactivity was also evident in the RPE layer. Further, there was non-specific labelling of OPL blood vessels evident at P10 and P14. Sox9 is primarily restricted to the developing (P2, P7) or developed INL (P10, P14). However, Sox9 immunoreactivity was also evident in the RPE layer and GCL as well as the IPL at P10 **(Ci)**. GCL = ganglion cell layer, INL = inner nuclear layer, NBL = neuroblastic layer, ONL = outer nuclear layer, OPL = outer plexiform layer. Scale bars, 25 µm **(Ai, Aii, Bi, Ci & Di)**, 15 µm **(Bii)**, 10 µ **(Cii & Dii)**. **(E)** Early post-natal expression levels of *Nes* and *Sox9* in whole retina at the mRNA level as determined by qPCR and as depicted in Figure 5.3.2. Expression levels were normalised to *Actb* levels and stated as % relative to adult levels. n = 3 for each marker at each time point; all samples were run in triplicates. Data points show mean ± SD.

the NBL as well as to individual cells of the GCL. By P7, the Sox9 immunoreactivity had completely segregated to within the presumptive INL but was additionally still found in the GCL (Figure 5.3.4Bi). Nestin was robustly expressed by NRSCs, particularly in the region of the presumptive IPL and GCL. Robust labelling of Nestin positive fibres was also observed in the ONL (Figure 5.3.4Bi & 5.3.4Bii). At P10, Nestin immunoreactivity was maintained in basally directed radial fibres but had retracted from apically directed radial fibres (Figure 5.3.4Ci). However, higher magnification images still showed the presence of individual, faintly-labelled Nestin positive processes in the ONL (Figure 5.3.4Cii). The Nestin immunolabelling protocol also resulted in non-specific blood vessel labelling in the OPL and IPL, due to the secondary antibody (anti-mouse, produced in goat). By P10, the Sox9 labelling in the INL was restricted to a much narrower band of nuclei compared to earlier stages (Figure 5.3.4Ci). Further, Sox9 was expressed in a larger number of cells in the GCL. By P14, Sox9 immunoreactivity was most robust in a thin layer of nuclei in the INL (Figure 5.3.4D), most likely belonging to Müller glia, given that Sox9 is a known Müller glia-specific nuclear marker in the adult retina (Poché *et al.*, 2008). At this stage, Nestin staining could no longer be detected in radially oriented cells.

Walcott and Provis (2003) have proposed that Müller glia are the end stage phenotype of (at least a subset of) Nestin-positive retinal progenitor cells, based on the co-localisation of Nestin and adult Müller glia marker immunoreactivities in the developing eye. This was further supported by expression profiling studies that revealed overlapping gene expression patterns in RPCs and Müller glia, or NRSC as they are collectively referred to here. In this present study, *Nes* was expressed in NRSCs up until the P10 stage. Thus, appropriate *Nes* reporter strategies could achieve the goal of labelling NRSCs in the developing retina. An equivalent *Sox9* reporter strategy was expected to similarly permit observation of NRSCs. Ultimately, however, efforts were focused on generating a *Nes* reporter because published works have also used *Nes*-based approaches to study glial-guided neuronal migration (Noctor et al., 2001; Tamamaki et al., 2001; Hatanaka et al., 2004; Kawauchi et al., 2006a, 2010; Shikanai et al., 2011). In these past studies, however, preference for *Nes* was presumably related to immunohistochemical labelling strategies, where staining radial glial processes for Nestin was more informative than staining radial glial nuclei for Sox9.

5.3.1.3. Investigating the spatial relationship between Nestin positive fibres and rod photoreceptor somata in the developing retina by immunohistochemistry

As shown in section 5.3.1.2, Nestin immunoreactivity is found in radially oriented cells that span throughout the width of the developing neural retina. Combined with previous reports that Nestin staining was co-localised with Müller glia markers in the early post-natal retina (Walcott and Provis, 2003), this suggests that Nestin is a suitable marker to label Müller glia, or immature forms thereof, in the developing retina (the entire spectrum of which is referred to as NRSCs). An initial analysis on fixed tissue was performed to investigate whether rod photoreceptor precursors can be found closely aligned with NRSCs, stained for Nestin, during development. This could serve as an indicator for the potential existence of glial-guided rod photoreceptor migration.

Nestin immunohistochemistry was performed on fixed eye frozen sections from *Nrl.GFP*$^{+/+}$ mice aged P2 to P8, a period during which *Nes* expression is robust (see Figure 5.3.2 & 5.3.4). At P2, a considerable number of brightly labelled Nrl.GFP positive rod photoreceptor precursors were already visible, most of which were relatively close to the apical surface of the neural epithelium (Figure 5.3.5Ai). Nestin immunoreactivity was comparable to that observed in section 5.3.1.2 and appeared in the shape of progenitor stage NRSCs (Figure 5.3.5Ai, 5.3.5Aii). As can be seen at higher magnification, several Nrl.GFP positive somata were in close proximity to Nestin positive fibres at this stage, which could indicate the presence of an interstitial junction similar to what exists between cortical neurons migrating along radial glia. Many of these rod cell bodies were elongated. This close relationship was continued at P4 and P6, although the Nestin signal had considerably withdrawn from the apical half of the neural retina at P6 (Figure 5.3.5Bi, 5.3.5Bii, 5.3.5Ci, 5.3.5Cii). Indeed, the intensity and distribution of Nestin immunoreactivity in the P6 *Nrl.GFP*$^{+/+}$ retina was notably different from the wild type retina, where many apically directed Nestin positive fibres were still visible at P7 (Figure 5.3.4Bii). In the P8 *Nrl.GFP*$^{+/+}$ retina, Nestin immunoreactivity was almost undetectable within the ONL (Figure 5.3.5Di, 5.3.5Dii). This, together with the vast number of Nrl.GFP positive cells, made it difficult to assess with any degree of confidence the proximity relationships between Nrl.GFP positive cells and Nestin positive NRSC fibres at this stage of development.

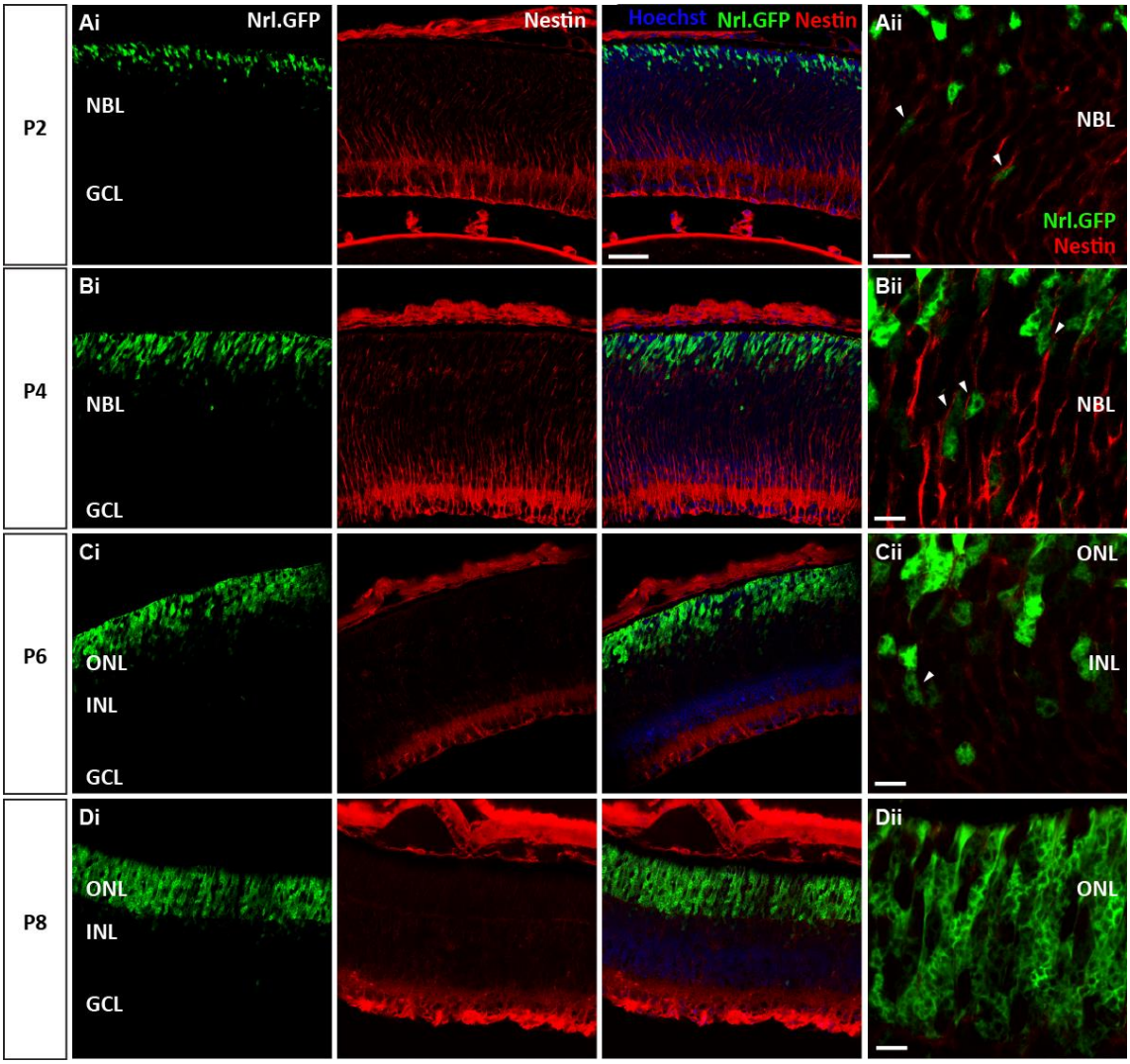

Figure 5.3.5 Nrl.GFP positive rod cells show close apposition to Nestin positive radial fibres in the developing postnatal mouse retina. In the *Nrl.GFP*$^{+/+}$ mouse eye, GFP positive (green) cells were observed in close proximity to Nestin immunoreactive fibres (red) at P2 (**Ai** and **Aii** at higher magnification), P4 (**Bi** and **Bii** at higher magnification) and P6 (**Ci** and C**ii** at higher magnification). Arrowheads indicate examples of direct contact between Nrl.GFP positive cells and Nestin positive fibres. **(Di & Dii)** By P8, most of the Nestin immunoreactivity had retracted from ONL and INL and only remained within the GCL. This thus precluded proximity analyses at this developmental stage. NBL = neuroblastic layer, ONL = outer nuclear layer, INL = inner nuclear layer, GCL = ganglion cell layer. Scale bars, 25 µm (Ai, Bi, Ci, Di), 10 µm (Aii, Bii, Cii, Dii).

Nonetheless, given these findings, *Nes* is a useful marker for labelling NRSCs in the postnatal retina. The next step will thus be to generate a *Nes* reporter that allows NRSCs to be labelled *in vivo*.

5.3.2. Generation and testing of the NRSC reporter

5.3.2.1. Cloning of a Nes reporter

To further investigate whether the radial somal translocation displayed by rod photoreceptor precursors in the developing retina is NRSC-dependent, the next goal was to generate a *Nes* promoter driven reporter construct. GFP labelled rod photoreceptor precursor cells in the living *Nrl.GFP*$^{+/+}$ mouse retina might then be co-imaged in real time with reporter labelled NRSCs. Reporter constructs are typically generated by placing the promoter of the gene of interest upstream of a reporter gene within an expression plasmid. However, the *Nes* promoter has been reported to demonstrate a degree of non-specific activity in various different cell lines, including fibroblast cells, despite activity of the *Nes* gene being usually restricted to neuronal progenitor cells and developing muscle (Cheng *et al.*, 2004b). Neuronal progenitor-specific expression was found to be conferred by cis regulatory enhancer elements within the second intron of the *Nes* gene (Lothian and Lendahl, 1997). This specificity is tied to the enhancer element to such an extent that reliable reporters active only within neuronal progenitor cells have been designed by combining the second intronic enhancer element with ubiquitous promoters (Lothian and Lendahl, 1997; Aoki *et al.*, 2000; Kawaguchi *et al.*, 2001; Walker *et al.*, 2010).

Lothian and Lendahl (1997) have designed a *Nes* reporter that features a 714 bp conserved region within the second intron of the *Nes* gene (*eNestin714*) placed upstream of a modified herpes simplex virus thymidine kinase (*TK*) promoter (Figure 5.3.6A). In their construct (*SaStk/lacZ*), these two elements drive *lacZ* reporter gene expression. Here, it was decided to emulate this design with the modification of replacing the *lacZ* reporter gene with the *DsRed* gene for compatibility with future fluorescence microscopy ambitions. The cloning strategy consisted of replacing the promoter in the

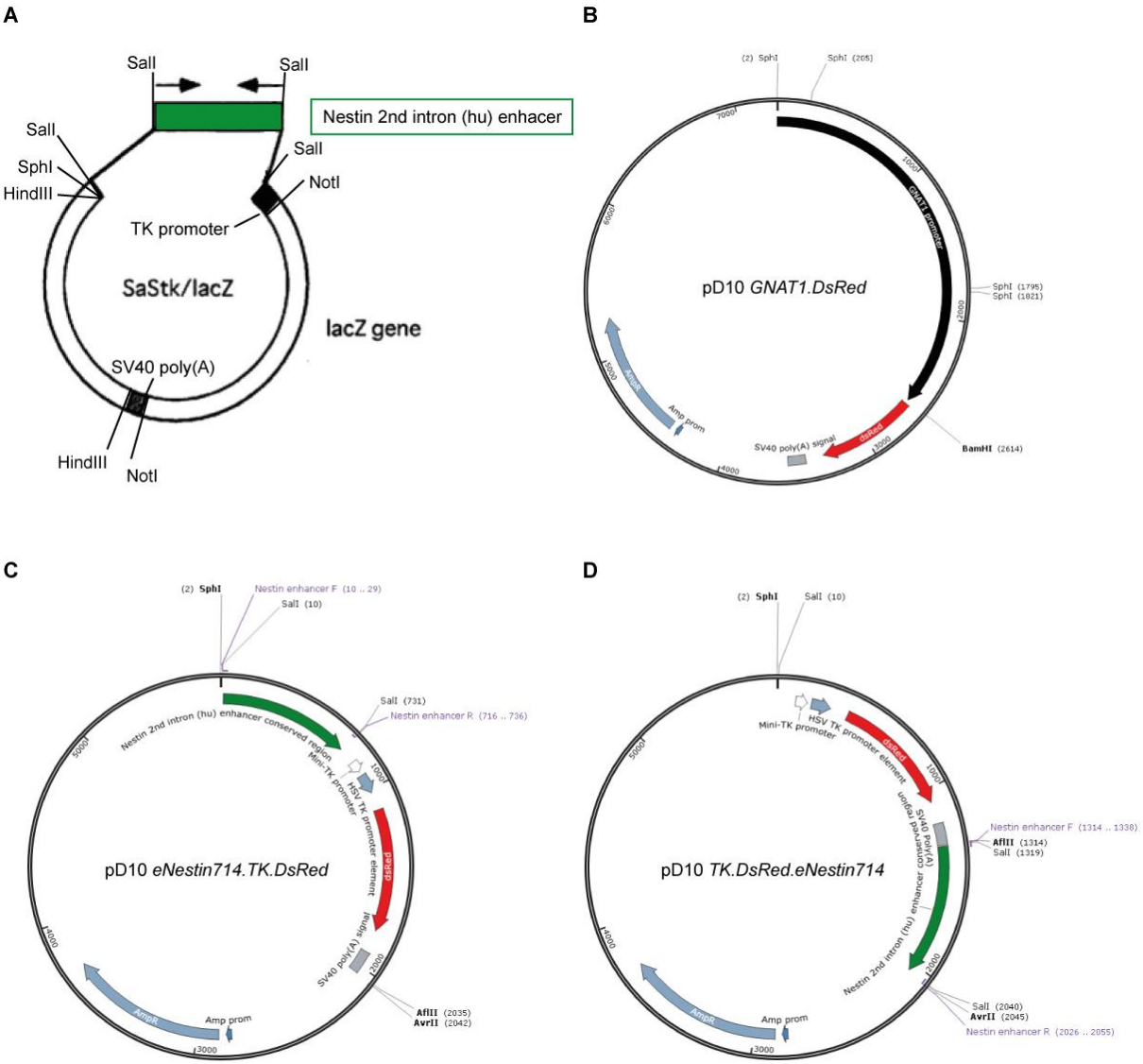

Figure 5.3.6 DNA plasmids utilised and generated during the cloning of the *Nes* reporter pD10 *TK.dsRed.eNestin714*. **(A)** The *Nes* reporter *SaStk/lacZ* designed by Lothian and Lendahl, 1997. L*acZ* reporter gene expression in this plasmid is driven by the HSV thymidine kinase promoter with the consered human 714 bp 2nd intronic *Nes* enancer element (*eNestin714*) placed upstream. **(B)** pD10 *GNAT1.DsRed* reporter plasmid used as a precursor to clone the *Nes* reporter. **(C)** pD10 *eNestin714.TK.DsRed*. The first version of the *Nes* reporter made wihtin this study was cloned by replacing the *GNAT1* promoter in the pD10 *GNAT1.DsRed* plasmid with the *eNestin714.TK* element from the *SaStk/lacZ* plasmid. The reporter module arrangement was 5'- enhancer-promoter-reporter gene-3'. **(D)** pD10 *TK.DsRed.eNestin714*. The second and improved version of the *Nes* reporter made within this study. The conserved 714 bp 2nd intronic *Nes* enhancer element was placed downstream of the repoter gene *DsRed* by PCR cloning, resulting in a reporter module configuration 5'-promoter-reporter gene-enhancer-3'.

pD10 *GNAT1.DsRed* target plasmid (Figure 3.3.20B) with the *eNestin714.TK* element from the *SaStk/lacZ* parent plasmid. Due to partially incompatible restriction enzyme sites in target and parent plasmids, a cohesive/blunt-end type strategy was designed. The *eNestin714.TK* element was excised from the *SaStk/lacZ* parent plasmid by sequential restriction enzyme digestion with NotI, followed by an overhang fill-in step with DNA polymerase 1 large (Klenow) fragment, and subsequent digestion with SphI. The pD10 *GNAT1.DsRed* plasmid was digested with BamHI, blunted and then digested with SphI. Ligation of the SphI/blunt *eNestin714.TK* insert into the SphI/blunt pD10 *DsRed* backbone finally completed the pD10 *eNestin714.TK.DsRed* reporter (Figure 5.3.6C).

5.3.2.2. Testing the Nes reporter

To test the functionality of the *Nes* reporter plasmid, pD10 *eNestin714.TK.DsRed*, and to assess whether reporter expression was spatio-temporarily correct, the reporter construct was electroporated into explanted P1 *Nrl.GFP*$^{+/+}$ retinae (Figure 5.3.7A). Based on the qPCR and immunohistochemistry data shown in Figures 5.3.2, 5.3.4 & 5.3.5, the *Nes* reporter was expected to display good activity within the first post-natal week. Hence, electroporated retinae were cultured for a period of up to 1 week, after which *DsRed* reporter expression was assessed by fluorescence microscopy. Previously, explanted neonatal murine retinae cultured *in vitro* have been shown to develop and mature relatively normally for up to 4 weeks (Ogilvie *et al.*, 1999). The electroporation and *in vitro* culturing protocol was adapted from previously published literature (Hsiau *et al.*, 2007; Matsuda *et al.*, 2009). The relative speed and ease of this procedure, compared to *in vivo* assessments, makes this an ideal assay to test new DNA constructs. However, it should be noted that damage arising from tissue handling may result in retinal folding and rosette formation (Ogilvie *et al.*, 1999); the more severe the original damage, the more exacerbated and apparent those effects become, especially during prolonged culturing periods.

DsRed reporter expression after electroporation was assessed following *in vitro* organ culture for 3, 5 and 7 days. After culturing for 3 days *in vitro* (DIV), which corresponds roughly to a P4 retina *in vivo*, the control plasmid pD10 *CAG.DsRed* drove robust

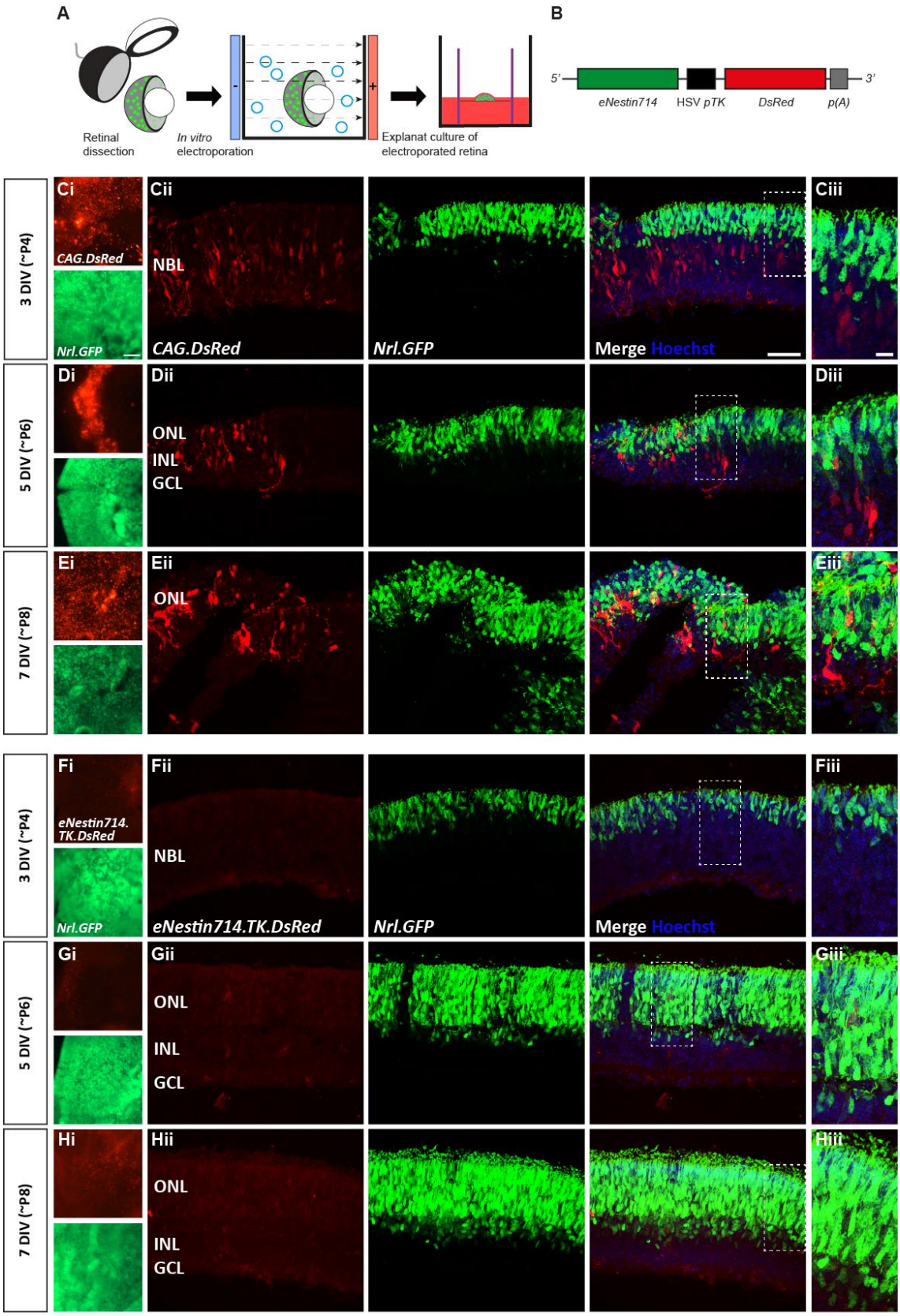

Figure 5.3.7 The original *Nes* reporter construct (pD10 *eNestin714.TK.DsRed*) does not produce *DsRed* reporter expression in electroporated retinae. (Figure legend continues on following page).

←

(Figure 5.3.7 figure legend continued). **(A)** Workflow of *ex vivo* DNA electroporation into P1 *Nrl.GFP*$^{+/+}$ retinae and organ culture on transwells. **(B)** *Nes* reporter construct (pD10 *eNestin714.TK.DsRed*). **(C-E)** *Nrl.GFP*$^{+/+}$ retinae (green) were electroporated with a control plasmid pD10 *CAG.DsRed* (red) at P1 and cultured for 3 (C), 5 (D) or 7 DIV (E). (i) shows epifluorescence images of flat mounted retinae while (ii) and (iii) depict confocal images of frozen sections counterstained with Hoechst (blue). **(F-H)** *Nrl.GFP*$^{+/+}$ retinae were electroporated with pD10 *eNestin714.TK.DsRed* at P1 and cultured for 3 (F), 5 (G) or 7 DIV (H). (i) shows epifluorescence images of flat mounted retinae, (ii) depicts confocal images of frozen sections, (iii) depicts higher magnification views of boxed regions of interest in (ii). Scale bars: 100 µm (i), 50 µm (ii), 10 µm (iii).

DsRed expression in most examined retinae. Figure 5.3.7Ci shows an epifluorescence top-view of a flat mounted *Nrl.GFP*$^{+/+}$ retina (approximately ¼ of the total retinal surface area is depicted). The majority of *DsRed* expressing cells had their nuclei positioned within the middle portion of the NBL, as shown in a cross-section view in Figure 5.3.7Cii. Based on location and morphology, those cells are most likely RPCs and immature inner retinal neurons. Only a small number of *Nrl.GFP* expressing rod photoreceptor precursor cells co-expressed *DsRed*, whereas ganglion cells never exhibited any *DsRed* expression. This pattern of expression was largely maintained at 5 DIV (≡ P6) and 7 DIV (≡ P8) (Figure 5.3.7Di, 5.3.7Dii, 5.3.7Ei & 5.3.7Eii). Of note, the retina depicted in Figure 5.3.7Di & 5.3.7Dii showed a quite regionalised pattern of *DsRed* expression, probably due to a sub-optimal tissue orientation during electroporation, while Figure 5.3.6Eii shows severe tissue folding artefacts, most likely because of imperfect tissue handling.

In contrast to the control plasmid, electroporation with the *Nes* reporter construct pD10 *eNestin714.TK.DsRed* (Figure 4.3.7B) did not result in any verifiable reporter expression in electroporated retinae after 3, 5 and 7 DIV (Figure 5.3.7Fi, 5.3.7Fii, 5.3.7Gi, 5.3.7Gii, 5.3.7Hi & 5.3.7Hii). Thus, the *Nes* reporter in its current format did not appear to be functional and had to be re-designed.

5.3.2.3. Re-designing and testing of the modified Nes reporter

To address the lack of *Nes* reporter activity, the previously generated *Nes* reporter construct was re-designed. In the pD10 *eNestin714.TK.RFP* reporter construct, the *Nes* enhancer element is located upstream of the reporter gene transcription start site as well as the thymidine kinase promoter; this arrangement was previously shown to result in good *Nes* reporter expression in transgenic mice (Lothian and Lendahl, 1997; Kawaguchi *et al.*, 2001; Walker *et al.*, 2010). However, in the mammalian *Nes* gene, this specific enhancer element is located downstream of the transcription start site within the second intron (Lothian and Lendahl, 1997). Other published works have described the generation of *Nes* reporter constructs more akin to the gene arrangement where the enhancer element was placed downstream of the reporter gene (Yamaguchi *et al.*, 2000; Mignone *et al.*, 2004). To replicate this here, the *Nes* enhancer element was placed downstream of the *DsRed* reporter gene and the SV40 poly(A) element by means of PCR cloning to generate the pD10 *TK.DsRed.eNestin714* construct (Figure 5.3.6D). The re-designed *Nes* reporter was then tested by electroporation into explanted P2 *Nrl.GFP*$^{+/+}$ retinae and harvesting of the tissue after 2 DIV, which roughly corresponds to a P4 retina *in vivo*.

Similar, to that shown in Figure 5.3.6Cii, the control plasmid pD10 *CAG.DsRed* drove *DsRed* expression across the entire NBL, with the exception of the GCL (Figure 5.3.8Ai & 5.3.8Aii). The majority of DsRed positive cell bodies were located within the central portion of the NBL. Based on location and morphology, these cells are therefore most likely RPCs and immature amacrine, horizontal, bipolar or Müller glial cells. Albeit at relatively low frequency, Nrl.GFP and CAG.DsRed double positive rod photoreceptor cells were also observed (Figure 5.3.8B-D). Interestingly, a number of DsRed labelled cells that morphologically resemble NRSCs were in close apposition with Nrl.GFP positive rod photoreceptor precursor cells (Figure 5.3.8E-G).

The *Nes* reporter pD10 *TK.DsRed.eNestin714* (Figure 5.3.6D & 5.3.9A) was designed to be able to visualise similarly juxtaposed Nrl.GFP positive rod photoreceptor cells and NRSCs labelled with *DsRed* from the reporter construct. When retinae electroporated with this construct were examined, *DsRed* expression was indeed detected (Figure 5.3.9Bi & 5.3.9Bii). The morphology of *DsRed* expressing cells was typical of NRSCs, with processes extending radially to the apical and basal edges of the neural retina and

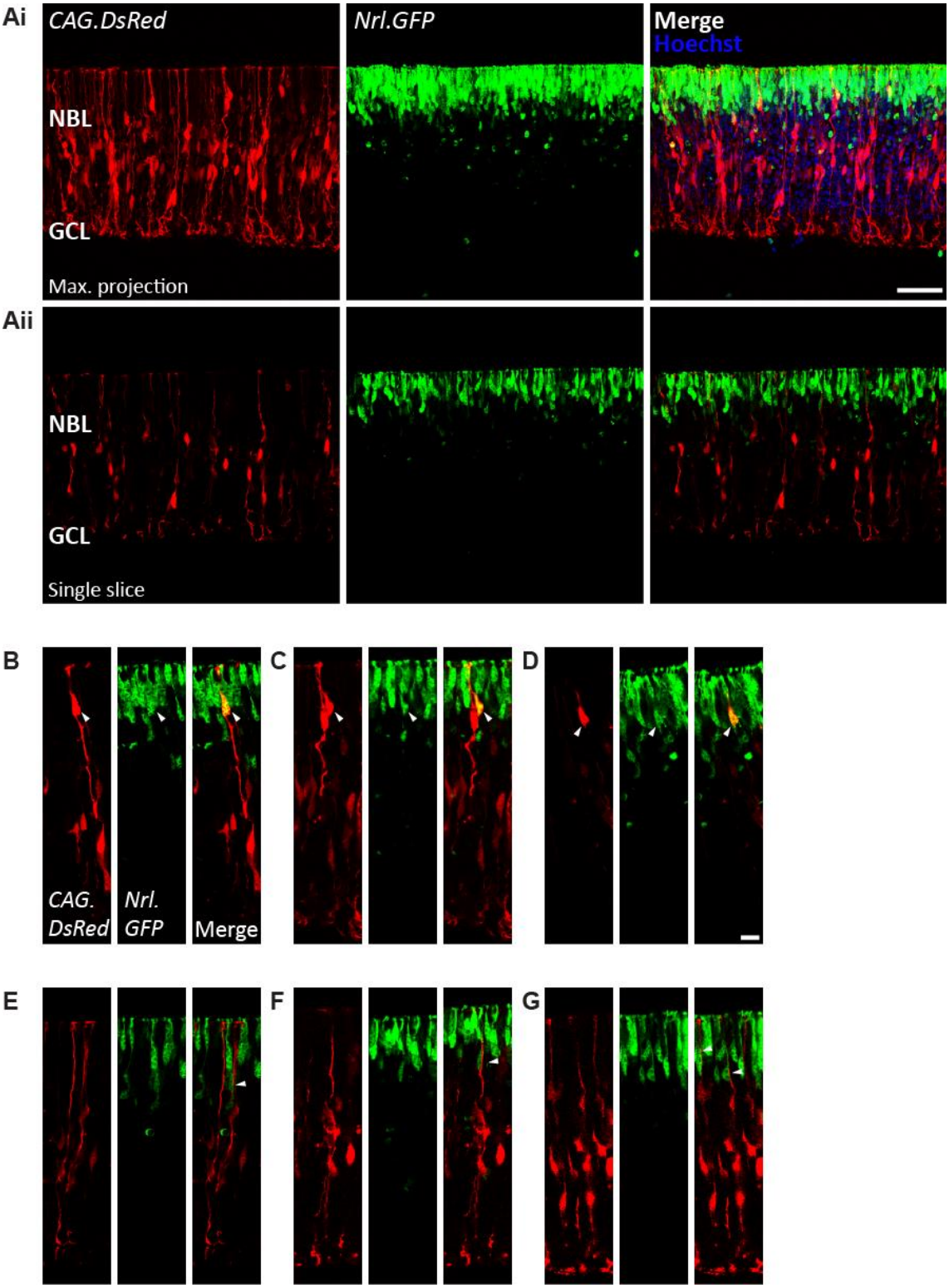

Figure 5.3.8 Widespread *DsRed* expression in different retinal cells with the control plasmid pD10 *CAG.DsRed*. P2 *Nrl.GFP*$^{+/+}$ retinae were electroporated and cultured for 2 DIV. Maximum projection **(Ai)** and single slice view **(Aii)** of a field of view with high transduction efficiency and hence widespread *DsRed* expression. **(B-D)** Regions of interest depicting Nrl.GFP positive rod photoreceptors transduced with pD10 *CAG.DsRed* and hence co-expression of *GFP* and *DsRed*. **(E-G)** Regions of interest showing juxtaposition of Nrl.GFP positive rod photoreceptors with radially elongated DsRed positive cells. Scale bars: 50 µm (A), 10 µm (B-G)

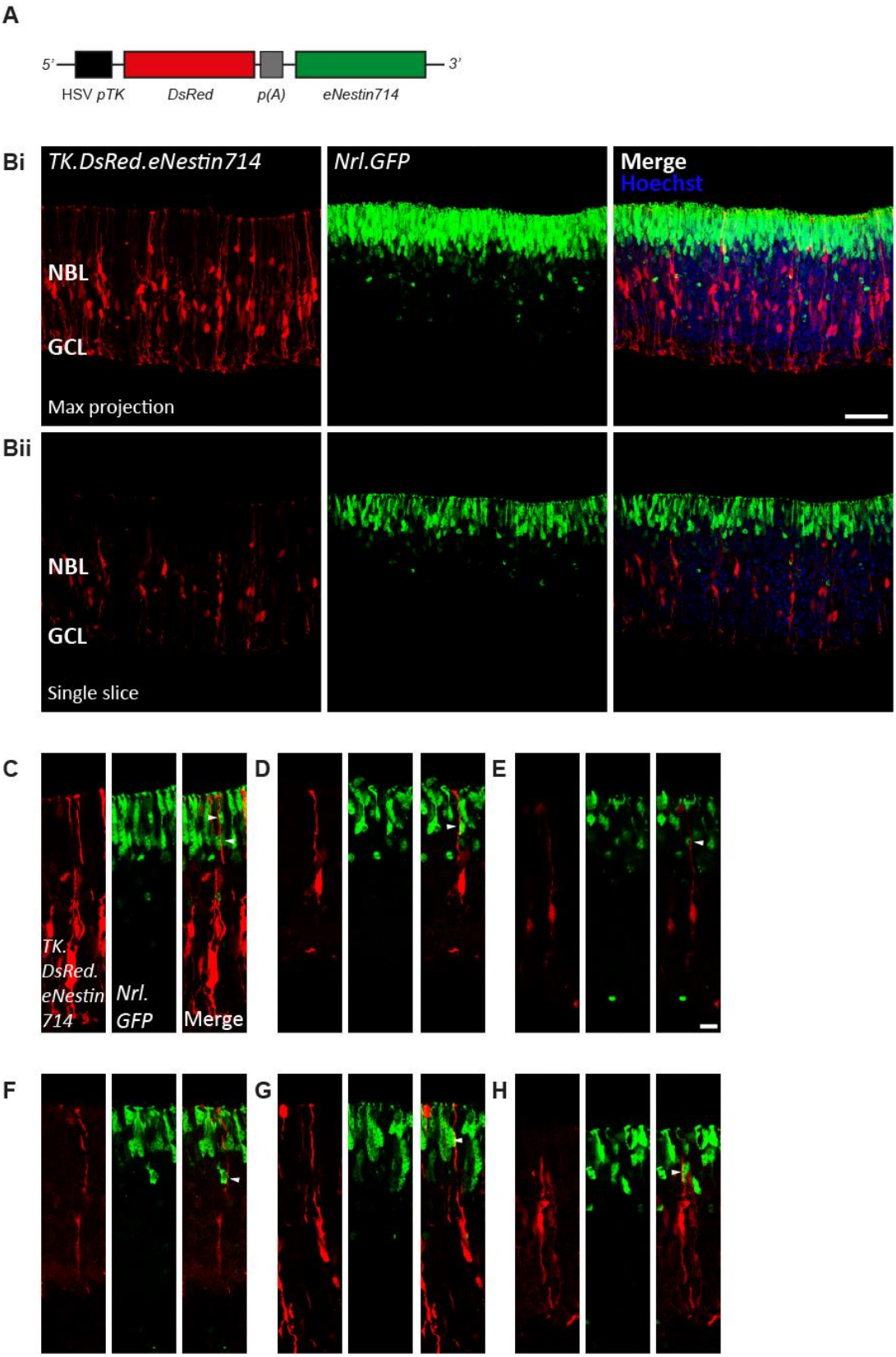

Figure 5.3.9 The modified *Nes* reporter construct (pD10 *TK.DsRed.eNestin714*) produces *DsRed* reporter expression in *Nrl.GFP*$^{+/+}$ retinae. P2 *Nrl.GFP*$^{+/+}$ retinae were electroporated and cultured for 2 DIV. **(A)** *Nes* reporter construct (pD10 *TK.DsRed.eNestin714*). Maximum projection **(Bi)** and single slice view **(Bii)** of a field of view with high transduction efficiency and hence widespread *DsRed* expression. **(C-H)** Regions of interest showing juxtaposition of Nrl.GFP positive rod photoreceptors with radially elongated DsRed positive cells. Scale bars: 50 µm (B), 10 µm (C-H)

with the majority of cell bodies located within the central portion of the NBL. A closer examination revealed that a number of Nrl.GFP positive rod photoreceptor cells were closely aligned with, and extended along, the apical process of a DsRed labelled cell of presumptive NRSC identity (Figure 5.3.9C-H). In agreement with the data shown in chapters III and IV (as well as Warre-Cornish, PhD thesis, 2013), all rod photoreceptors maintained an apical process that anchored them to the apical edge of the retinal neuroepithelium. This is a striking discrepancy to glial-guided neuronal migration in the cortex, where neurons only display a short leading and trailing process devoid of contact to the apical and basal limit of the neuroepithelium (Rakic, 1971a, 1971b, 1972).

Nonetheless, these data thus demonstrate that the re-designed *Nes* reporter construct pD10 *TK.DsRed.eNestin714* was capable of driving *DsRed* expression in retinal cells that morphologically resembled NRSCs. Since *Nes* is a marker for RPCs, the *Nes* reporter should only be active within the immature neural retina where RPCs are still prevalent (Xue *et al.*, 2006; Lee *et al.*, 2012); as the retina matures, RPCs are gradually lost as they transition towards the differentiated Müller glia state (Turner and Cepko, 1987; Walcott and Provis, 2003). In order to verify the temporal specificity of the *Nes* reporter construct (active in the immature retina but inactive in the mature retina), it was first administered by sub-retinal DNA injection and then electroporated *in vivo* into the retinae of live P0-P1 *Nrl.GFP*$^{+/+}$ mice (Figure 5.3.10A). Retinae were then harvested at the P4 stage where reporter activity was expected to be present as well as at the adult stage (P28) where reporter activity should be absent under normal circumstances. To assess whether the *in vivo* electroporation approach was viable in the first place, *DsRed* expression from the control plasmid pD10 *CAG.DsRed* at the P4 stage was first evaluated. As shown in Figure 5.3.10B & 5.3.10C, transduction and *DsRed* expression have primarily occurred within a patch of retinal tissue in close proximity to the presumed site of sub-retinal injection; the injection site was often identifiable by signs of local neural retinal invagination. Similar to that observed for the *ex vivo* electroporation and retinal organ culture model, *DsRed* was expressed in all cell types except for RGCs, based on morphological assessment (Figure 5.3.10Di & 5.3.10Dii).

In vivo electroporation of the *Nes* reporter resulted in regional *DsRed* reporter expression at the P4 stage, comparable to the pD10 *CAG.DsRed* control plasmid (compare Figure 5.3.10B-C & Figure 5.3.11A). At higher magnification, the elongated, radially spanning morphology of transduced cells, which was highly reminiscent of NRSCs, was clear (close to injection site: Figure 5.3.11B & more distant from the injection site: Figure

5.3.11C). One of the hallmarks of RPCs is that they undergo cell division. Interestingly, a small number of *DsRed* expressing cells presented as mitotic figures, as indicated by the white arrowhead in Figure 5.3.11C. In contrast to electroporated eyes harvested at the P4 stage, little to no *DsRed* expression was detected at the P28 stage, neither in close

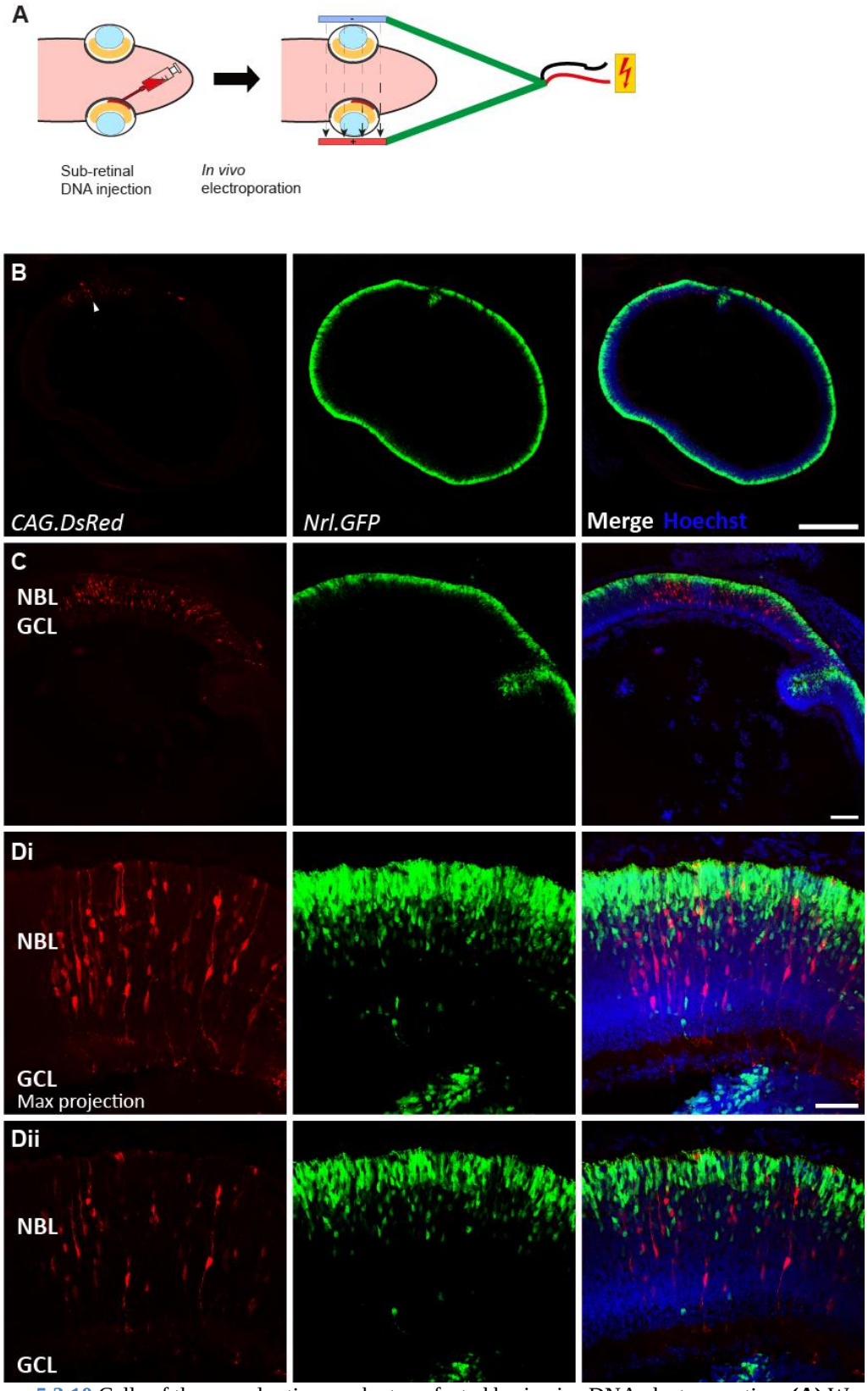

Figure 5.3.10 Cells of the neural retina can be transfected by *in vivo* DNA electroporation. **(A)** Workflow of the *in vivo* DNA electroporation method. Electroporation of *Nrl.GFP*$^{+/+}$ mice was performed at P1 and tissue was harvested at P4. **(B & C)** Low magnification views of transduced areas of the neural retina expressing *DsRed* under transcriptional control of the ubiquitous *CAG* promoter. Maximum projection **(Di)** and single slice view **(Dii)** of a high magnification field of view with high transduction efficiency. Scale bars: 500 µm (B), 100 µm (C), 50 µm (D).

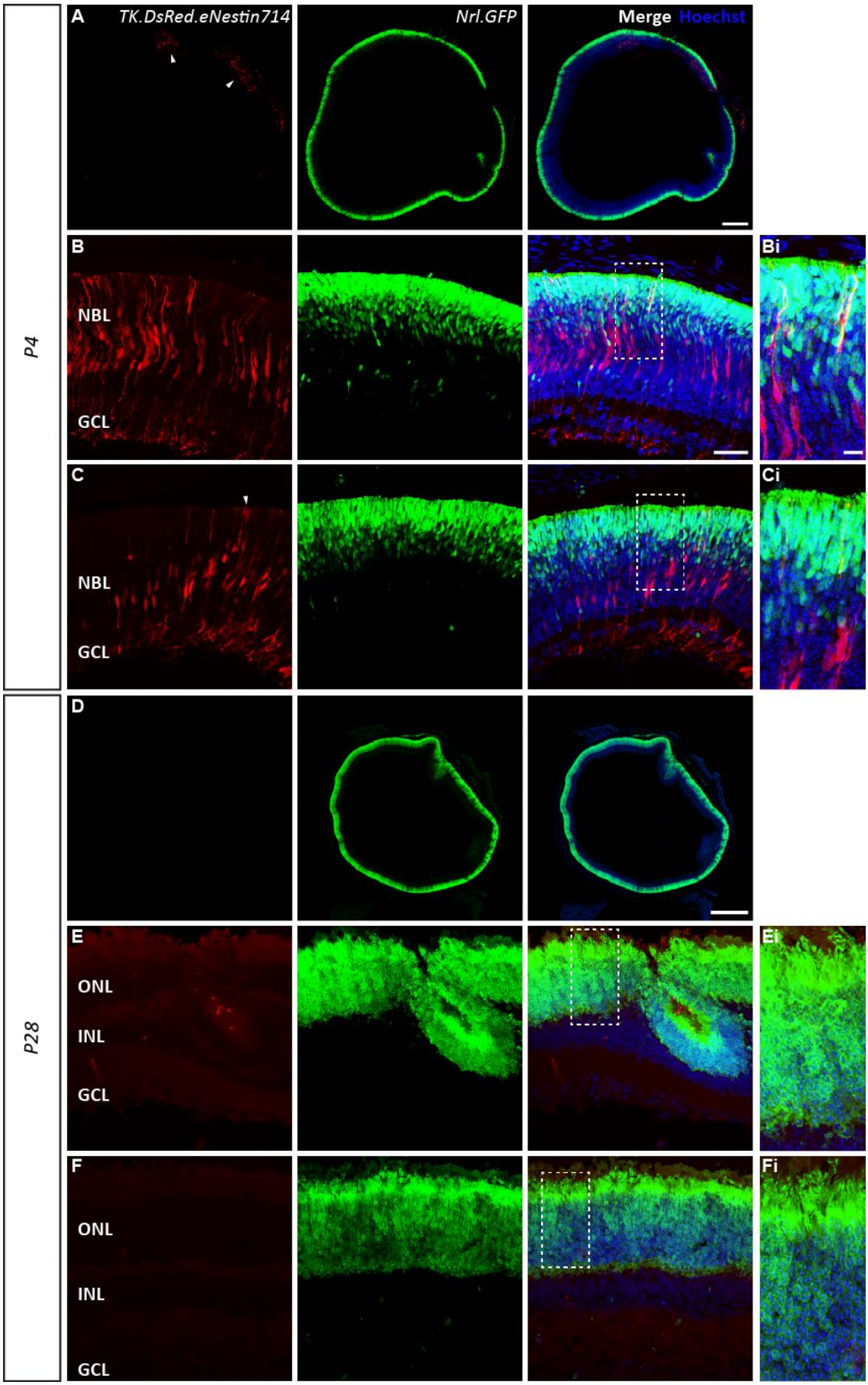

Figure 5.3.11 The *Nes* reporter operates in a temporally specific manner. (Figure legend continues on following page).

←

(Figure 5.3.11 figure legend continued). P1 *Nrl.GFP*$^{+/+}$ retinae were electroporated *in vivo* and retinae were harvested at P4 and P28. **(A-C)** *Nes* reporter expression 3 days post electroporation in the P4 retina. Depicted are a low magnification, maximum projection view of an entire eye section (A) and higher magnification maximum projection views close to or at a distance to the injection site (B & C respectively). Arrowheads indicate regions of transduction (A) and a possible mitotic figure (C). **(D-F)** *Nes* reporter expression 27 days post electroporation in the P28 retina. Shown are a low magnification, maximum projection view of an entire eye section (D) and high magnification, maximum projection views close to (E) or at a distance to the injection site (F); higher magnification views are depicted in (i) Scale bars: 250 µm (A), 500 µm (D), 50 µm (B, C, E, F), 10 µm (i).

proximity to the sub-retinal injection site, nor anywhere else across the explant (Figure 5.3.11D). Even at higher magnification, no *Nes* reporter activity was detected in cells with a clearly identifiable NRSC morphology (Figure 5.3.11E & 5.3.11F). Of note, sparse signals of red fluorescence could occasionally be observed close to the site of sub-retinal injection (Figure5.3.11E), but not at more distant sites (Figure 5.3.11F). However, none of these signals were clearly attributable to any cellular entity. These findings demonstrate that the *Nes* reporter pD10 *TK.DsRed.eNestin714* demonstrates temporal specificity of expression in the developing neural retina.

5.3.3. Real time analysis of developmental rod photoreceptor somal translocation in relation to NRSCs

5.3.3.1. Real time analysis of rod photoreceptor somal translocation in relation to NRSCs in the P3 retina

The focus next shifted towards time lapse microscopy in order to test whether rod photoreceptors of the developing mouse retina can migrate along NRSCs using glial guidance mechanisms. As was discussed in chapter III and IV, the cell bodies of rod photoreceptor precursors engage in somal translocation along the apico-basal axis of the neural retina during early development. It was speculated whether some of these motions may rely on guided migration, dependent on adhesive interactions with neighbouring cells, as exhibited by immature neurons in the cortex, which undergo glial-guided

migration along radial glia (Cooper, 2013; Evsyukova *et al.*, 2013). At least two main criteria that apply in the cortex will have to be fulfilled in order for a given observed motion to qualify as glial-guided rod migration: 1) the soma displays saltatory and overall slow advancements (both apical and basal movements were considered here) between 0.1 and 0.25 µm/min (Chen *et al.*, 2008; Franco *et al.*, 2011); 2) the soma remains closely associated with an NRSC throughout the duration of the translocation event, which may serve as an indicator for the presence of an interstitial junction (Fishell and Hatten, 1991).

Following the development and characterisation of the molecular tool to label NRSCs *in vivo* (the *Nes* reporter pD10 *TK.DsRed.eNestin714*), the subsequent step was to investigate whether somal motility of rod photoreceptors could be guided by NRSCs. To do this, the *Nes* reporter was electroporated *in vivo* into the retinae of P1 *Nrl.GFP*$^{+/+}$ mice (Figure 5.3.12A). 2 days post-electroporation, the retinae were explanted, flat-mounted with the apical side facing upwards and subjected to single-photon confocal fluorescence time-lapse live imaging (Figure 5.3.12B). The ability of single-photon laser light to penetrate into tissues is limited. Hence, in the upright microscope set-up used, the fluorescence emission from *DsRed* expressing NRSCs could be resolved only from the tip of the apical process to just beyond the cell body, corresponding to a depth of approximately 100 µm (Figure 5.3.12B). This incomplete tissue penetration was not considered problematic since photoreceptors are located within these limits.

The cells labelled by the *Nes* reporter displayed typical NRSC morphology, with an apical process extending to the apical limit and with most of the cell bodies located within the central portion of the neural retina. In many cases, the initial segment of a basal process was also visible just before DsRed fluorescence became undetectable upon imaging at greater tissue depths (Figure 5.3.12B). Using time-lapse live imaging, it was also possible to capture a small number of *Nes* reporter-labelled NRSCs undergoing cell division – a behaviour characteristic of progenitor cells (Figure 5.3.13A & 5.3.13B). The two examples in Figure 5.3.13 show DsRed labelled NRSCs (highlighted with light blue dots) with relatively large cell bodies near the apical limit of the neural retina. This location and appearance is usually associated with an RPC in the late G2- or early M-phase of the cell cycle (Pearson *et al.*, 2005b; Norden *et al.*, 2009; Randlett *et al.*, 2011a). In fact, both NRSCs generated a second cell body at the 1:10 (Figure 5.3.13A) and 0:20 hour time points respectively (Figure 5.3.13B). Soon after, the soma of one of the two daughter cells, now presumably in G1- or G_0- phase, then proceeded to move basally. The cell body of the second daughter cell remained, at least initially, at the apical limit of the neural

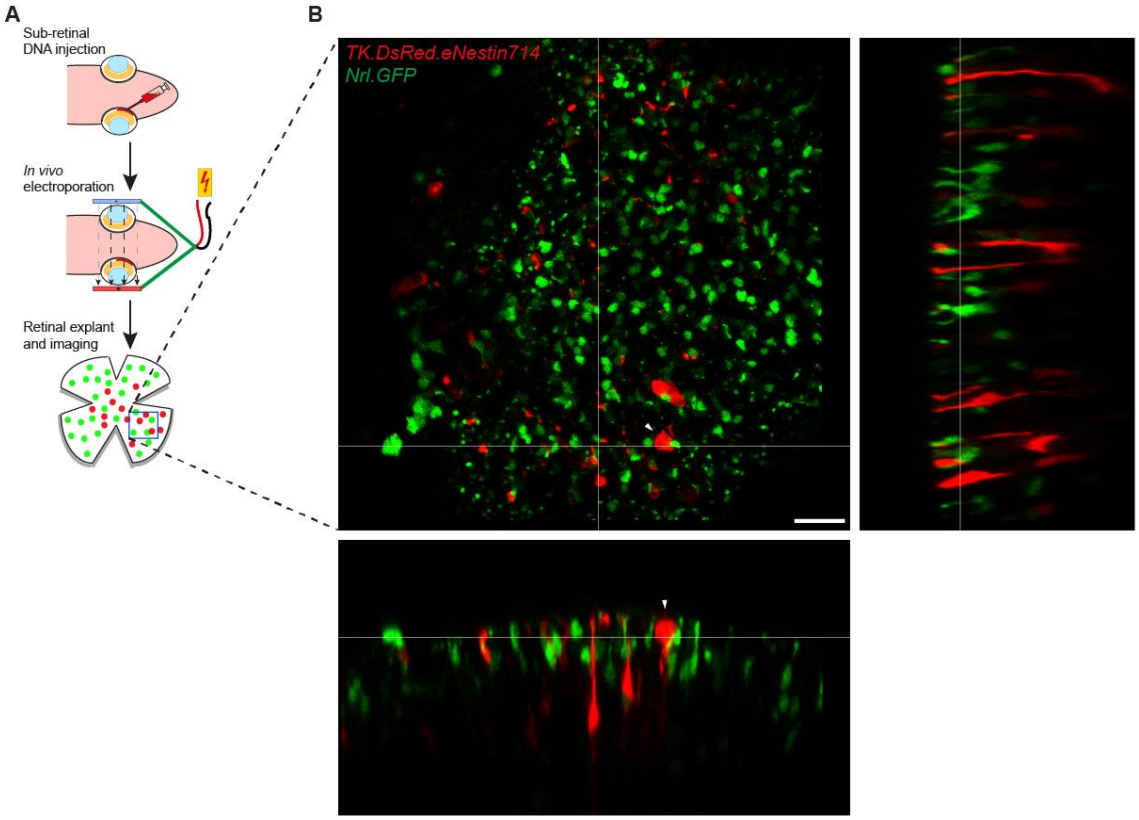

Figure 5.3.12 *In vivo* labelling of NRSCs in P1 *Nrl.GFP*$^{+/+}$ mice and subsequent time-lapse live imaging by fluorescence microscopy at P4. NRSCs were labelled by electroporation with the *Nes* reporter pD10 *TK.DsRed.eNestin714*. **(A)** Experimental workflow depicting sub-retinal DNA injection at P1, subsequent electroporation and retinal explant preparation for the live imaging set up. **(B)** Live image recording of a field of view within the explanted *Nrl.GFP*$^{+/+}$ retina with good *Nes* reporter transduction efficiency. *xy*, *xz* and *yz* views were taken at the levels of the white horizontal/vertical lines and show only the first time point of the time-lapse recording. White arrowheads highlight the presence of a presumptive mitotic figure. Scale bar: 25 µm.

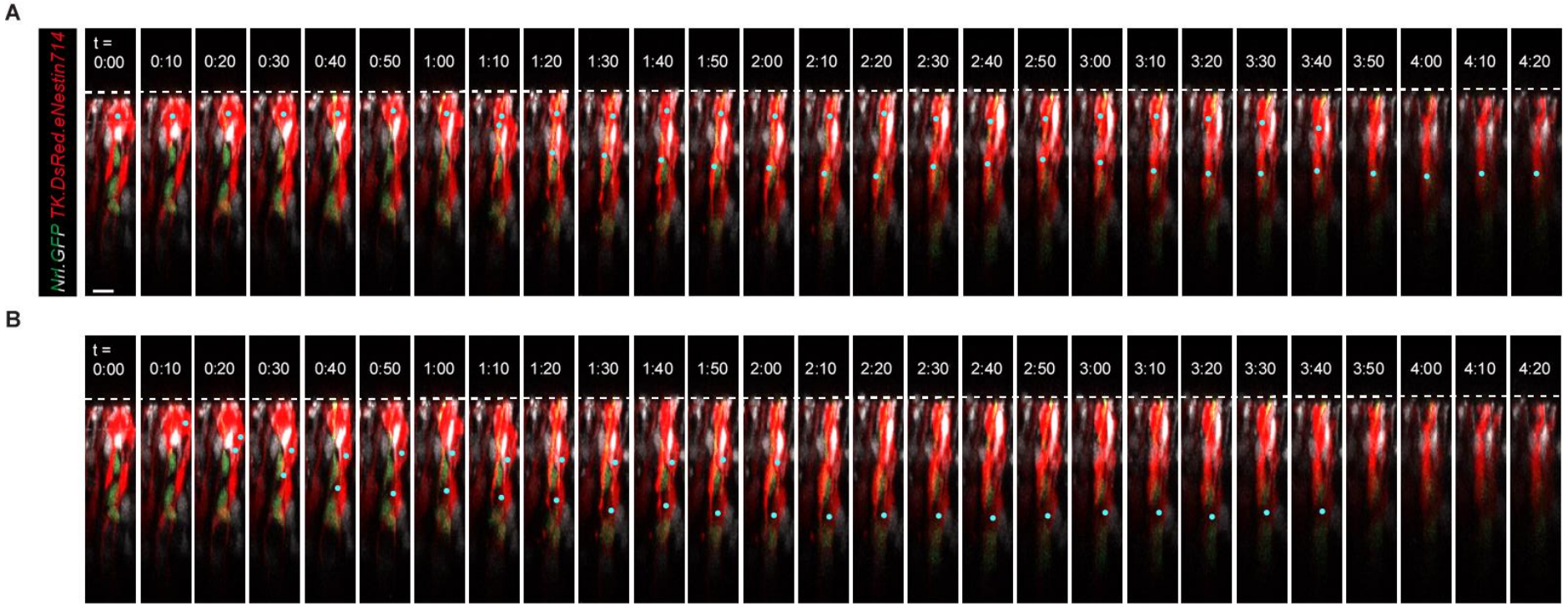

Figure 5.3.13 Retinal cells labelled by the *Nes* reporter show signs of mitosis. pD10 *TK.DsRed.eNestin714* was electroporated into the P1 *Nrl.GFP* $^{+/+}$ retina and time lapse imaging followed at P4. Region of interest derived from the field of view shown in Figure 5.3.12. **(A & B)** Montages following the apico-basal somal positions of DsRed labelled NRSCs (light blue dots) over time. Note how apparent cell division produced 2 daughter cells in both examples. Nrl.GFP positive rod photoreceptors in close proximity to the NRSCs were highlighted by manual segmentation (green) whereas the remaining Nrl.GFP signal is shown in grayscale. Scale bar: 10 µm

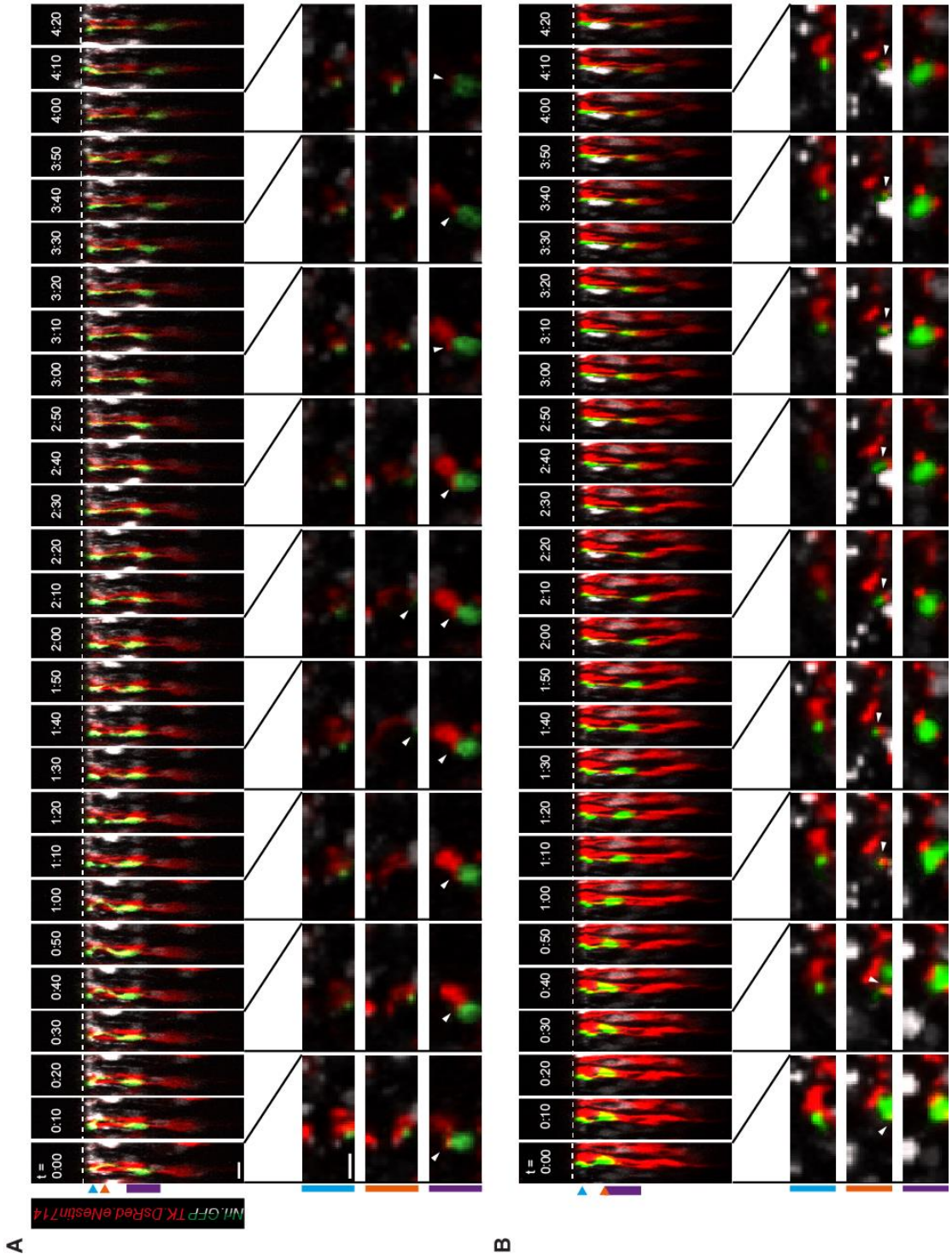

Figure 5.3.14 Low velocity rod photoreceptor somal translocation in close proximity to NRSCs. Region of interest taken from the field of view shown in Figure 5.3.12. P1 *Nrl.GFP*$^{+/+}$ retinae were electroporated with pD10 *TK.DsRed.eNestin714* and time lapse imaged at P4. **(A & B)** Montages following the apico-basal positions of manually segmented rod photoreceptors (green) closely aligned with DsRed positive NRSCs (red) over time. Surrounding rod photoreceptors are shown in grayscale. Cross section and top-down slice views are shown. Slice views were taken at the level of the tip of the apical process (blue), more basally along the apical process (orange) and at the translocating rod soma (purple). Where putative rod-NRSC points of contact may not be immediately obvious, such points were highlighted with white arrowheads. Scale bars: 10 µm (cross section view), 5 µm (top-down slice view).

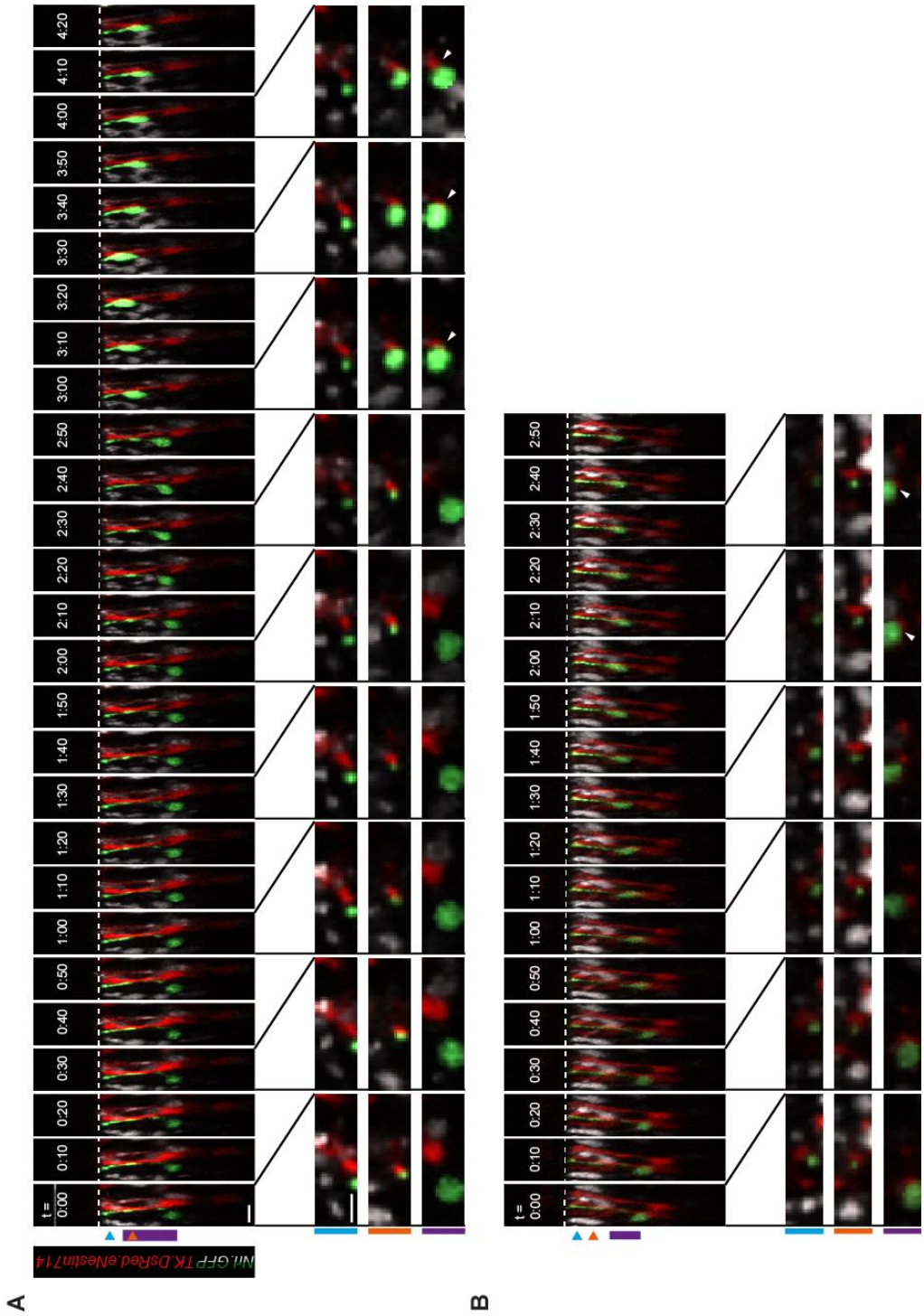

Figure 5.3.15 Rod photoreceptor apical somal translocation in close proximity to NRSCs. Region of interest derived from the field of view shown in Figure 5.3.12. P1 *Nrl.GFP*$^{+/+}$ retinae were electroporated with pD10 *TK.DsRed.eNestin714* and time lapse recorded at P4. **(A & B)** Montages following the apico-basal positions of manually segmented rod photoreceptors (green) closely aligned with DsRed positive NRSCs (red) over time. Rapid (A) and slow apical translocation (B) are shown. Surrounding rod photoreceptors are shown in grayscale. Cross section and top-down slice views are shown. Slice views were taken at the level of the tip of the apical process (blue), more basally along the apical process (orange) and at the translocating rod soma (purple). Where putative rod-NRSC points of contact may not be immediately obvious, such points were highlighted with white arrowheads. Scale bars: 10 µm (cross section view), 5 µm (top-down slice view).

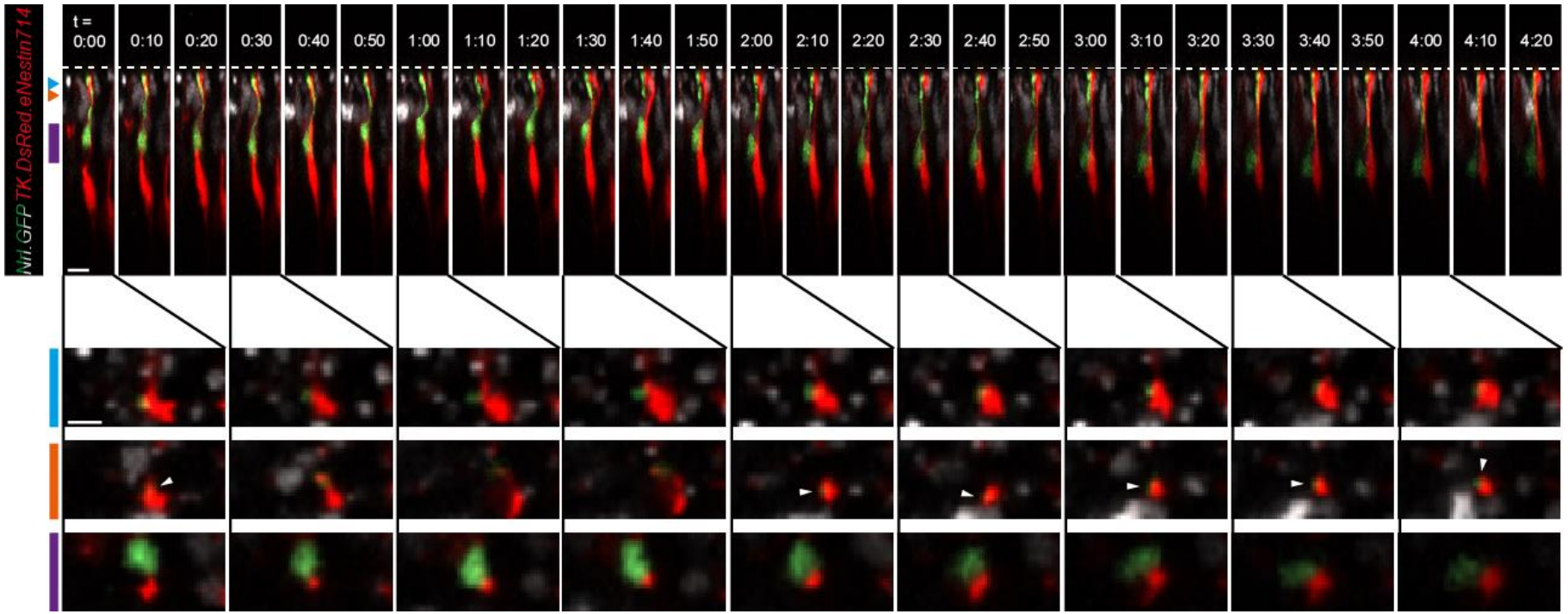

Figure 5.3.16 Oscillatory rod photoreceptor somal translocation in close proximity to an NRSC. Region of interest derived from the field of view shown in Figure 5.3.12. P1 *Nrl.GFP*$^{+/+}$ retinae were electroporated with pD10 *TK.DsRed.eNestin714* and time lapse imaged at P4. Montages following the apico-basal positions of manually segmented rod photoreceptors (green) closely aligned with DsRed positive NRSCs (red) over time. Surrounding rod photoreceptors are shown in grayscale. Cross section and top-down slice views are shown. Slice views were taken at the level of the tip of the apical process (blue), more basally along the apical process (orange) and at the translocating rod soma (purple). Where putative rod-NRSC points of contact may not be immediately obvious, such points were highlighted with white arrow heads. Scale bars: 10 µm (cross section view), 5 µm

retina. This somatic motility in combination with the presence of mitotic events is highly reminiscent of IKNM.

For the detection of putative glial-guided rod photoreceptor somal translocation events, all assessments were based on 22 selected regions of interest obtained from the same 221 x 221 µm field of view (see Figure 5.3.12; N = 1). Note that it was difficult for all elements of this experiment to work according to plan (electroporation of P1 mice, survival of electroporated mice, tissue processing for live imaging, imaging a field of view with good transfection efficiency and tissue health) and hence only one successful experimental repeat was performed prior to completion of this thesis. The mentioned 22 regions were specifically chosen to contain at least one central NRSC and, given the abundance of rod photoreceptors, NRSCs were always surrounded by several rod photoreceptors. Needless to say, rod somal apico-basal movements were also detected in areas without apparent NRSC labelling. The somata of Nrl.GFP positive rod photoreceptor cells were often observed in close proximity to the apical processes of reporter-labelled NRSCs. Figures 5.3.14-5.3.16 show examples of rod somal apico-basal movements that occurred near a labelled NRSC, displayed as cross-section montages. In addition, a top-down view at 3 different depths into the tissue is shown at 30 minute intervals: 1) at the level of the tip of apical process (blue), 2) 5-10 µm basal to the apical tip (orange), and 3) at the level of the widest extent of the migrating rod photoreceptor precursor soma of interest (purple). A small number of rod somata undergoing basally directed translocation in direct juxtaposition to an NRSC were observed (n = 4 rod cells; N = 1 time lapse recording). As defined in section 3.3.1.4, the threshold of detection of such movements was set to ≥ 15 µm of basal translocation in ≥ 2 hours; kinetically, this falls into the same range as cortical glial-guided neuronal migration, which is reported to occur at velocities between 0.1 and 0.25 µm/min (Chen *et al.*, 2008; Franco *et al.*, 2011). Figure 5.3.14A & 5.3.14B display two examples of such a rod somal translocation in the basal direction that occurred in apparent juxtaposition to neighbouring NRSCs. The distances covered between the time points of apical-most and basal-most somal positions are 20 µm (Figure 5.3.14A; time points 1:00 h to 3:40 h) and 15 µm (Figure 5.3.14B, time points 0:30 h to 2:10 h) respectively. The tip of the apical process, the apical process itself and the somata of both rod photoreceptor cells remained in close contact with the respective NRSC apical fibre throughout the imaging period. In all cases where a rod photoreceptor cell undergoing basal somal translocation was associated at the level of the apical process with an NRSC, the rod soma was also found to be directly adjacent to the NRSC rather than at a slight

distance from it. However, given the small number of observed events, this will need to be further re-examined on a bigger scale.

Apically-directed somal translocation in vicinity of an NRSC occurred in similarly small numbers as basally-directed somal translocation. As defined in section 3.3.1.3, the threshold of detection of rapid apical somal translocation was set to ≥ 10 µm of apical translocation per 30 minutes. A total of 5 apical translocation events, that occurred adjacent to an NRSC, were observed. In the representative example shown in Figure 5.3.15A and similar to the data presented in chapter III, rapid apical migration occurred within a relatively short time frame of 1 hour between the 2:20 h and 3:20 h time points. During this period, the soma migrated a distance of 26 µm, reaching a peak instantaneous velocity of -1.6 µm/min (average velocity -0.3 µm/min). The tip of the apical process and the apical process itself were directly adjacent to the nearest neighbouring NRSC before, during and after the rapid apical migration took place (see top down views in Figure 5.3.15A). However, the soma maintained a distance off approximately 5 µm from the same NRSC. A close juxtaposition between the two was only established following rapid apical translocation (this was observed for 2 out of the 6 apically migrating rod somata). Interestingly, this close proximity between the two cells was then maintained as the rod soma moved basally. It is worth noting at this point that DNA electroporation does not guarantee the transduction of every single cell. For that reason, the possibility of an unlabelled NRSC in contact with a rod cell body that appeared to be devoid of initial NRSC contact cannot be excluded.

Indeed, rod photoreceptors that maintained NRSC contact throughout the apical translocation event, even at the level of the soma, were also observed (n = 2). Regardless of whether the soma was in constant contact with the NRSC, the radial depth trajectory profiles and movement kinetics were remarkably similar and in full agreement with the characterisation of rapid apical somal translocation according to section 3.3.1.3. Besides rapid apically translocating cells, an isolated case of slow apically-directed somal translocation next to an NRSC was also detected (Figure 5.3.15B). Markedly slower kinetics of translocation were measured compared with rapid apical translocation, as it took approximately 2:30 h for the soma to migrate a distance of 19 µm (average instantaneous velocity: -0.1 µm/min). This rate of motility falls into the domain of cortical glial-guided neuronal migration. All parts of the rod photoreceptor, including the soma, were seemingly in close contact to the neighbouring NRSC throughout the duration of

the apical migration. Clearly, however, more examples will need to be detected in future experiments to be able to fully attribute this finding to glial-guidance.

In contrast to apical and basal translocation, stochastic rod somal motions that took place adjacent to an NRSC were detected a lot more frequently (n = 53). As defined in section 3.3.1.6, the threshold for stochastic somal translocation was set to ≤ 15 µm in ≥ 2 hours. 48 out of the 53 cells maintained direct contact with the neighbouring labelled NRSC from the tip of their apical processes all the way down to their somata (see for instance Figure 5.3.14B: 2:20 – 2:40 h or 5.3.15A: 0:00 – 2:00 h); the 5 remaining cells on the other hand lacked contact between the rod soma and the neighbouring labelled NRSC even though their apical processes were in close juxtaposition. In addition, there was also compelling evidence that basal displacement of rod photoreceptor somata can be caused by movements of neighbouring cells. In fact, in some instances where NRSCs that underwent IKNM (either apically during G2 or basally during G1), their somal movements seemingly dragged along and/or pushed rod somata in the basal direction (n = 16; example shown in Figure 5.3.13). Apical movements that were clearly attributable to passive displacement were not observed.

As discussed in chapter III, the somata of the rod photoreceptors exhibit an oscillatory translocation pattern during early postnatal development. This behaviour was also observed in retinae electroporated with the *Nes* reporter, albeit at very low frequencies due to a relatively short imaging period of 5 hours (n = 1). Figure 5.3.16 (Movie 5.3.1) depicts an identified cell where the cell body of the highlighted rod photoreceptor translocated rapidly in the apical direction between the 0:30 h and the 1:10 h time points. Over the subsequent 3 hours, the same cell body then moved in the basal direction, covering a distance of 20 µm. All parts of the rod photoreceptor cell, including the soma, were in close contact with a neighbouring NRSC apical process throughout the period of movement.

Taken together, several examples were identified where rod photoreceptor somal translocation occurred directly adjacent to an NRSC within the P3 retina and at a velocity that is in agreement with previous observations on cortical glial-guided neuronal migration (Chen *et al.*, 2008; Franco *et al.*, 2011). During most of these events, large portions of the observable rod photoreceptor cell, from the tip of the apical process down to the soma, were closely aligned with an NRSC. It may thus be speculated whether rod somata moved with the help of glial guidance in these instances. In some cases, rod

somata moved in the apical direction even when they were at a slight distance from the NRSC while simultaneously having juxtaposed apical processes. More generally, many rod somal translocation events will have happened without direct and visible cell-cell contact to a reporter-labelled NRSC, be it due to the actual absence of an NRSC at certain positions or be it because some NRSCs were not labelled by the *Nes* reporter.

5.3.3.2. Real time analysis of rod photoreceptor somal translocation in relation to NRSCs in the P7 retina

Glial-guided migration is typically found in regions where the immature neuron must traverse distances that cannot be readily accomplished by cell intrinsic mechanisms. In the cortex, neuronal precursors migrate along radial glia through the entire thickness of the intermediate zone and most of the cortical plate; only at the end of this journey do these neurons switch from glial-guided migration to the cell intrinsic somal translocation to reach the outermost layer of the cortical plate (Cooper, 2013). To investigate whether glial guidance mechanisms are more apparent in later development, when the ONL is thicker, P1 *Nrl.GFP*$^{+/+}$ retinae were electroporated with the *Nes* reporter and imaged by 2-photon fluorescence microscopy at P7 (see Figure 5.3.17 for a schematic of the experimental work flow).

As shown in Figure 5.3.17B, sparse transduction labelling with the reporter plasmid pD10 *TK.DsRed.eNestin714* was seen at P7. In keeping with NRSCs being a continuum of cells between RPCs and Müller glia, the cells that were labelled with the *Nes* reporter construct were all elongated along the radial axis. Interestingly, when looking at the apical end feet, some displayed a much larger extent of mature Müller glia-like defasciculation than others. When focussing on individual NRSCs, cellular units reminiscent of the columnar units described by Reichenbach *et al.* (1993) could be identified: these columnar units featured a central NRSC, along which were aligned multiple rod photoreceptors within the layer of the presumptive ONL. 12 such columnar units were identified within a field of view of 68 x 68 µm (see Figure 5.3.17B; N = 1 time lapse recording). All rod somal motility assessments were based on the regions of interests defined by those columnar units. As in chapter III, the following thresholds were used for the classification of somal somal motions: rapid apical translocation: ≥ 10 µm of apical translocation per 30 minutes;

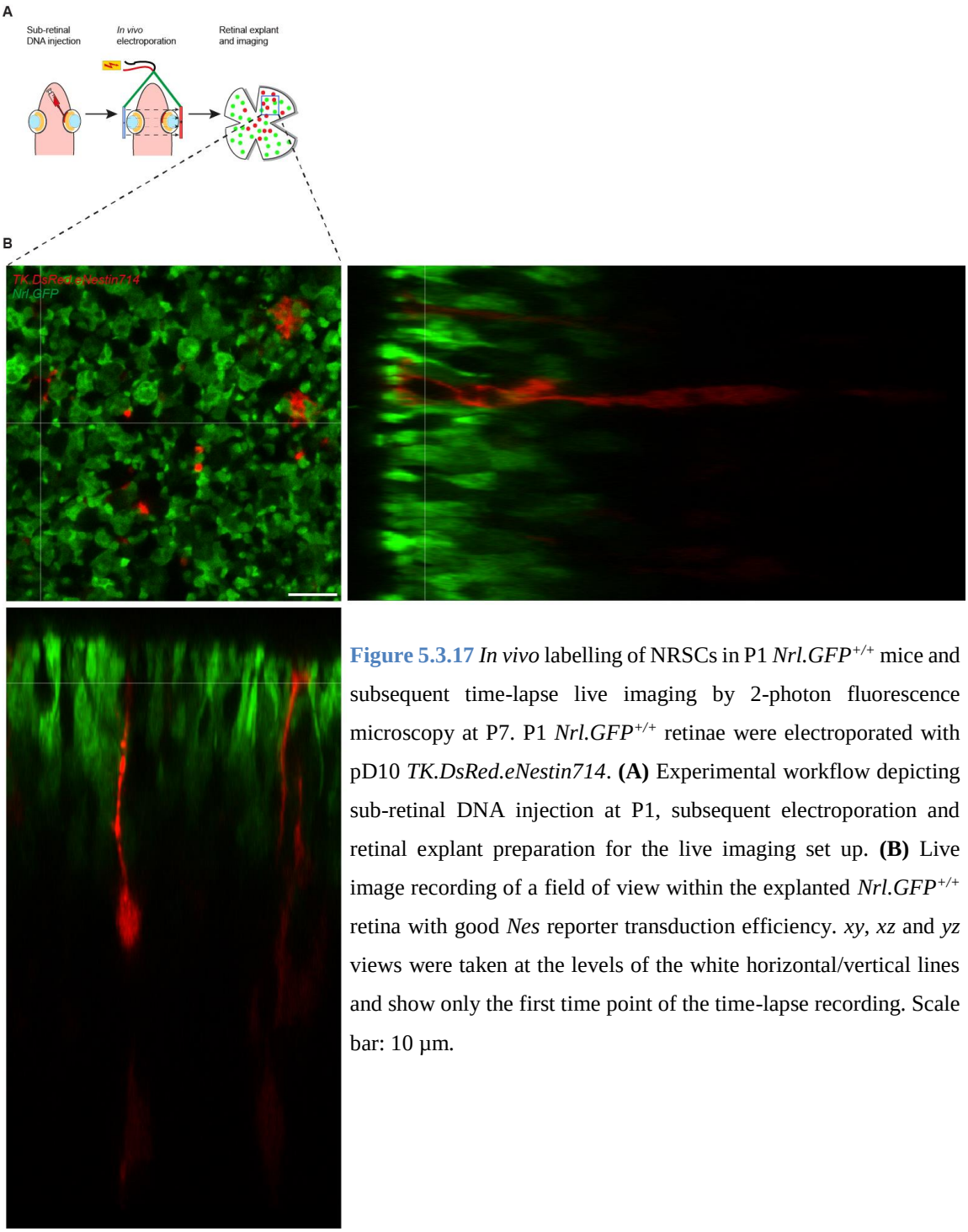

Figure 5.3.17 *In vivo* labelling of NRSCs in P1 *Nrl.GFP*$^{+/+}$ mice and subsequent time-lapse live imaging by 2-photon fluorescence microscopy at P7. P1 *Nrl.GFP*$^{+/+}$ retinae were electroporated with pD10 *TK.DsRed.eNestin714*. **(A)** Experimental workflow depicting sub-retinal DNA injection at P1, subsequent electroporation and retinal explant preparation for the live imaging set up. **(B)** Live image recording of a field of view within the explanted *Nrl.GFP*$^{+/+}$ retina with good *Nes* reporter transduction efficiency. *xy*, *xz* and *yz* views were taken at the levels of the white horizontal/vertical lines and show only the first time point of the time-lapse recording. Scale bar: 10 µm.

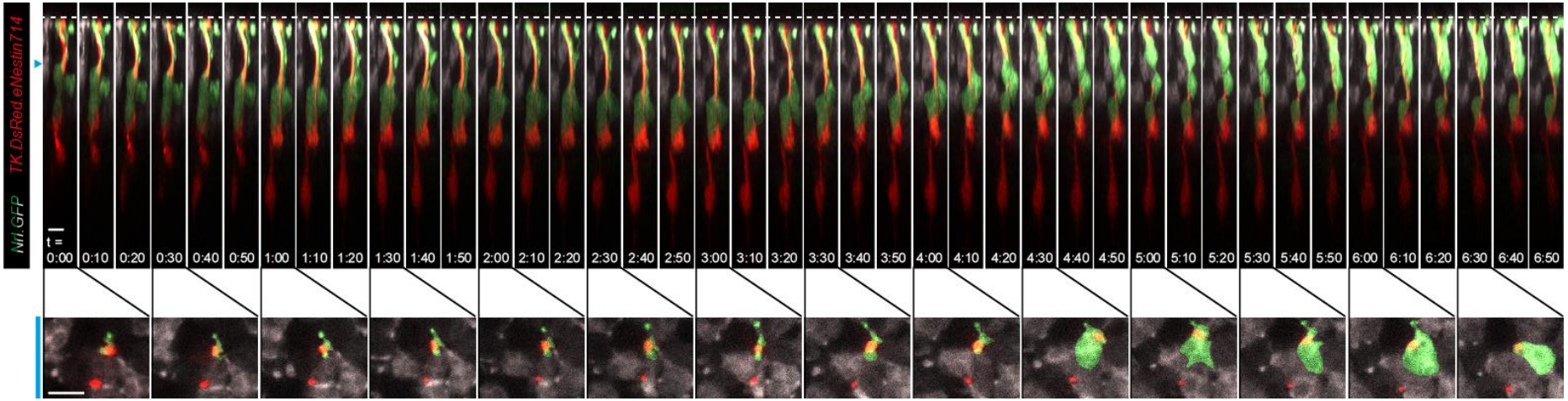

Figure 5.3.18 Columnar unit consisting of an NRSC and closely associated rod photoreceptors undergoing apical somal translocation. Region of interest derived from the field of view shown in Figure 5.3.17B. P1 *Nrl.GFP*$^{+/+}$ retinae were electroporated with pD10 *TK.DsRed.eNestin714* and time lapse imaged at P7. The montage follows the apico-basal positions of manually segmented rod photoreceptors (green) closely aligned with DsRed positive NRSCs (red) over time. The rod somata exhibited rapid apical translocation (from 4:00), stochastic apically directed translocation (from 3:20) and stochastic motion with little to no net displacement. Surrounding rod photoreceptors are shown in grayscale. Cross section and top-down slice views are shown. The slice view was taken at the level of the apical process (blue) such that transiting rod somata are visible (compare slice views at 4:00 and 4:30) Scale bars: 5 µm.

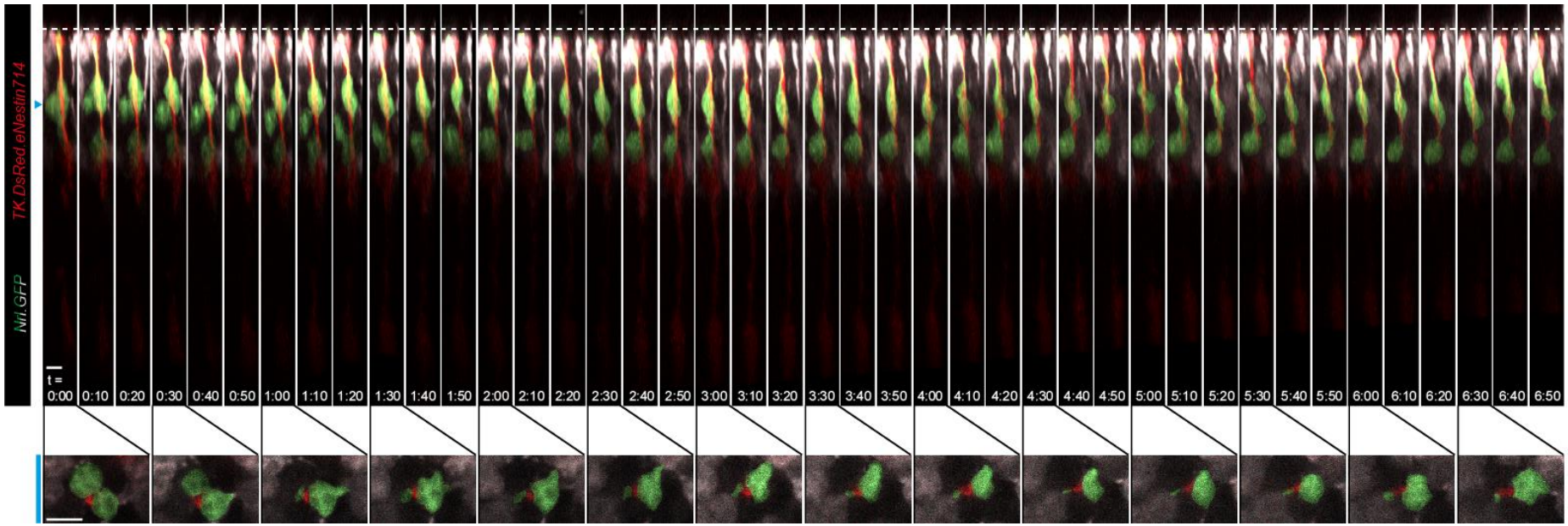

Figure 5.3.19 Columnar unit consisting of an NRSC and closely associated rod photoreceptors undergoing radial somal translocation. Region of interest derived from the field of view shown in Figure 5.3.17B. P1 *Nrl.GFP*$^{+/+}$ retinae were electroporated with pD10 *TK.DsRed.eNestin714* and time lapse imaged at P7. The montage follows the apico-basal positions of manually segmented rod photoreceptors (green) closely aligned with DsRed positive NRSCs (red) over time. The rod somata exhibited basally directed somal translocation (from 0:00), rapid apical somal translocation (from 6:00) and stochastic motion with little to no net displacement. Surrounding rod photoreceptors are shown in grayscale. Cross section and top-down slice views are shown. The slice view was taken at the level of the apical process (blue) such that transiting rod somata are visible (compare slice views at 0:00 and 1:00) Scale bars: 5 µm.

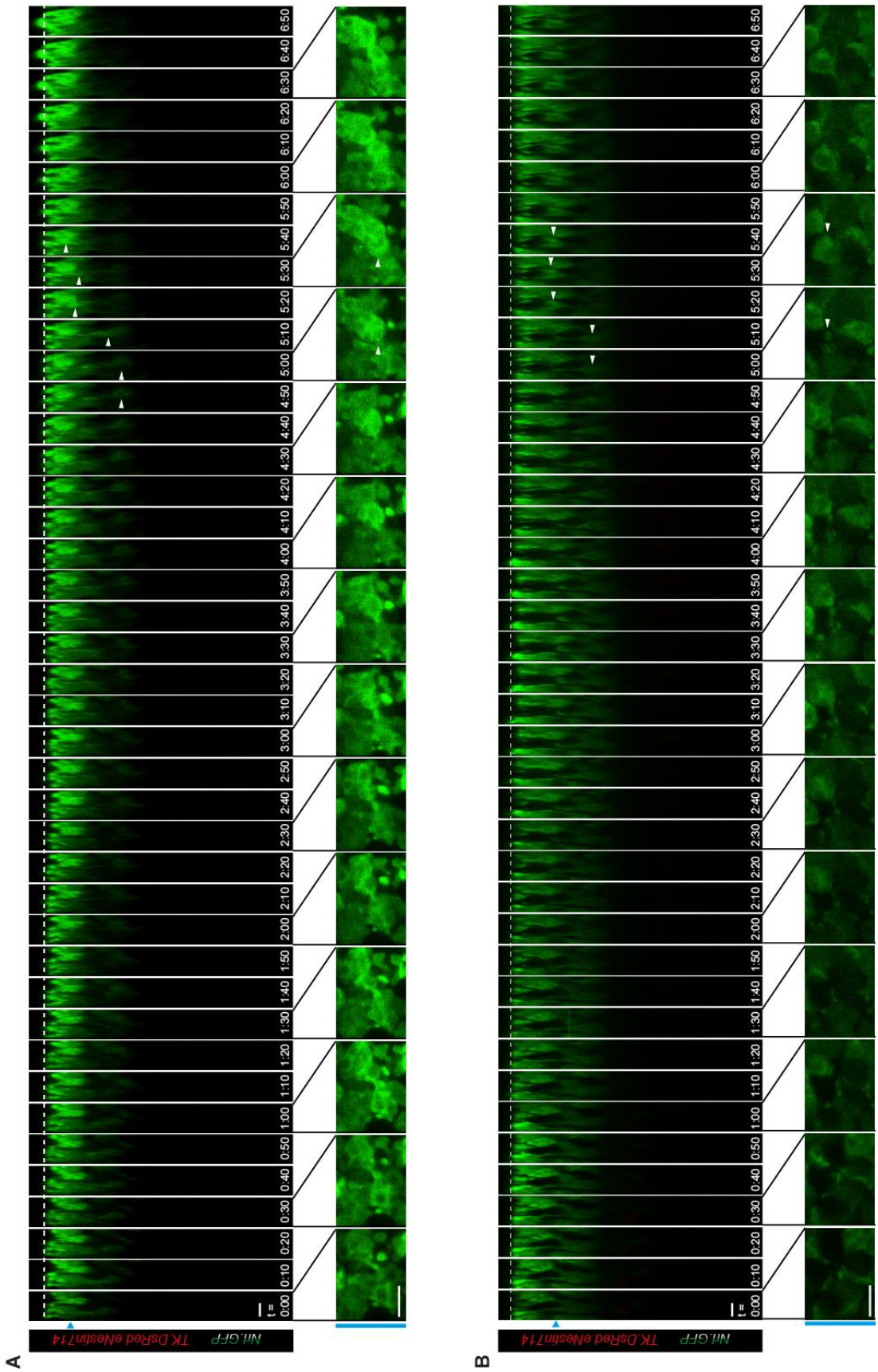

Figure 5.3.20 Evidence of rod photoreceptor (Nrl.GFP positive) somal translocations occurring in absence of labelled NRSCs. (Figure legend continues on following page).

←

(Figure 5.3.20 figure legend continued). Regions of interest derived from the field of view shown in Figure 5.3.17B. P1 *Nrl.GFP*$^{+/+}$ retinae were electroporated with pD10 *TK.DsRed.eNestin714* and time lapse imaged at P7. **(A & B)** The montages follow the apico-basal positions of several rod photoreceptors (green) over time. The rod somata exhibited mostly stochastic somal translocation with little to no net displacement, rare rapid apical somal translocation events (e.g. at 5:00 in A & B) as well as basally directed somal translocation (B). Cross section and top-down slice views are shown. The slice view was taken at the level of the apical process (blue) such that transiting rod somata are visible (compare slice views at 5:00 and 5:30) Scale bars: 5 µm.

basal: ≥ 15 µm of basal translocation in ≥ 2 hours; stochastic: ≤ 15 µm of basal translocation in ≥ 2 hours. The columnar unit depicted in Figure 5.3.18 (Movie 5.3.2) included the somata of three rod cells, which underwent stochastic somal translocation with little to no net displacement for the first 4 hours of the imaging period. As shown in the accompanying slice top views, the apical processes of these three rod photoreceptors cells were all in close proximity to the central NRSC process. One soma subsequently displayed rapid apical translocation, while the other two continued to translocate stochastically, one of them with net apical displacement and the other with zero net displacement. In the second provided example of a columnar unit (Figure 5.3.19), the central NRSC was surrounded by four radially aligned rod photoreceptors. Here, the majority of rod somal translocations were also stochastic in nature, with one rod cell body translocating basally until the 1:40 hour time point and another rod cell body undergoing rapid apical translocation from the 6:00 hour time point. Overall, a small number of rapid apical somal translocation events exhibited by different rod photoreceptors were identified in direct juxtaposition to an NRSC (n = 5). 4 of these cells were aligned with the NRSC from the tip of the apical process down to the soma, whereas the soma of the remaining cell was at a slight distance to the NRSC fibre. Although not formally fulfilling the criteria for rapid apical translocation, there was also a single case of slower apical somal translocation (similar to the P3 retina; section 5.3.3.1, Figure 5.3.15) where it took 4:00 h for the soma to cover a distance of 16.1 µm (Figure 5.3.18).

Basally directed somal translocation events were detected at a similarly low frequency as rapid apical translocation (n = 6); in all of these cases, the rod photoreceptors were aligned with an NRSC at the level of the apical process down to the level of the soma. Like in the P3 retina, stochastic rod photoreceptor somal movements were the predominant detected

type of movement along NRSCs (n = 34; one of these cells had an aligned apical process but distant soma). Finally, there were also recorded instances where rod somata were apparently passively displaced in the basal direction (n = 4); passive displacement in the apical direction was not observed.

While these apparent associations suggest some form of physical interaction between rods and NRSCs, proximity between a translocating rod photoreceptor soma and an NRSC does not necessarily prove the involvement of glial guidance in the translocation event. The neural retina is a densely-packed tissue and it is thus hard to tell whether proximity between two cells is due to specific cell-cell interactions or due to the limited availability of space within the pseudostratified developing retina. Conversely, absence of a transduced *TK.DsRed.eNestin714* positive NRSC adjacent to somally translocating rod photoreceptors does not automatically rule out glial guidance at such an event. This is because electroporation cannot guarantee the transduction of every single NRSC. To demonstrate this, Figure 5.3.20A & 5.3.20B depict rod photoreceptors that somally translocated apically and basally in absence of any apparent *TK.DsRed.eNestin714* reporter labelling.

5.4. Conclusion

Glial-guided neuronal migration has long been known to be essential for cortical layer formation (reviewed by Nadarajah and Parnavelas, 2002). Cortical neuronal progenitor cells appear in the shape of radial glia that span the entire radial width of the developing cortex. They undergo mitosis close to the apical surface in the ventricular zone and their neuronal offspring migrate radially along the radial process of the radial glia cell towards the pial surface in a saltatory manner. Evidence for glial-guided migration occurring within the retina, while seemingly supportive, has been circumstantial. With the experiments carried out as part of this chapter, the goal was to test whether rod photoreceptor precursor cells engage in glial-guided migration within the developing retina.

The retina does not contain radial glia per se, but instead hosts a close relative, which also spans the entire width of the developing retina – the retinal progenitor cell (RPC). Among the list of common features is the dual neural progenitor/glial character during early phases of development, after which a slow transition towards a purely glial fate is made. In the cortex, the end point of this transition is an astrocyte, whereas in the retina the end point is a Müller glia cell. The spectrum of retinal cells ranging from RPCs to differentiated Müller glia was termed neural retina spanning cell (NRSC) within this study. It was anticipated that the most straightforward way to observe glial-guided migration would be by fluorescence microscopy time-lapse live imaging. For that reason, a tool to label NRSCs *in vivo* had to be developed first. The reporter labelling approach was chosen to fit this task. The ideal experimental design was thought to consist of labelling all NRSCs, at least within a certain region of the retina, while having sparsely labelled rod photoreceptors. This would allow potential glial-guidance relationships between rod cells and NRSCs to be resolved most clearly. However, no NRSC reporter mouse lines with appropriate labelling during retinogenesis (such as the *Hes5-GFP* line (Basak and Taylor, 2007; Nelson et al., 2011)) were readily available within the group. Equally, the reporter construct previously cloned by other members of the group, which would have been used to sparsely label rod cells (*Nrl.DsRed*), lacked *in vivo* activity (personal communication within the group). Due to these limitations, an alternative strategy was pursued, consisting of labelling NRSCs with an NRSC reporter construct within the *Nrl.GFP*$^{+/+}$ rod reporter mouse line. An obvious caveat of this approach is that

the lack of NRSC labelling and the lack of the actual NRSC would be indistinguishable; whether rod somal motility was guided by or independent of an NRSC would be difficult to tell.

In order to label NRSCs, a suitable reporter construct had to be generated first. The gene expression profile of several candidate genes was analysed by qPCR and by immunohistochemistry in order to identify those genes that are spatio-temporally correctly expressed within NRSCs (section 5.3.1.1 & 5.3.1.2). Based on the gene expression profile at the mRNA (qPCR) and at the protein level (immunohistochemistry), different expression patterns were identified: a) increasing levels of expression during development that gradually approached adult levels, as observed for *Car2*, *Cd44*, C*lu*, *Glul*, *Rlbp1* and V*im*; b) already adult levels of expression throughout the early post-natal time point series: S*ox9*; c) decreasing levels of expression that gradually approached adult levels: *Nes*. The genes found within group a) were switched on in sequential waves, but were not expressed at significant levels within the first four post-natal days. As this covered a developmental period, during which glial-guided rod migration was to be investigated, none of the group a) genes were further considered. Between *Sox9* and *Nes*, it was determined that the neural progenitor marker gene *Nes* (encoding the intermediate filament protein nestin) would be a good candidate to be used in the format of an NRSC reporter, due to it displaying a very compelling gene expression pattern especially during early post-natal stages: whereas *Nes* expression was not detected in adult retinae, it was highly expressed during the first week of post-natal development in cells that morphologically resembled NRSCs. This was followed by a rapid decline in expression towards adult levels. The finding that *Nes* is expressed in NRSCs from the early RPC stage likely up until they completely differentiate into Müller glia is in agreement with a previous study (Walcott and Provis, 2003) and efforts were thus undertaken to generate a *Nes*-based NRSC reporter.

As demonstrated in several published works, *Nes* reporters do not follow the classical promoter-reporter gene design, but rather contain a *Nes* 2nd intronic enhancer element, a ubiquitous promoter and a reporter gene, the assembly of which appears to be specifically active in neural progenitor cells (Lothian and Lendahl, 1997; Kawaguchi *et al.*, 2001; Mignone *et al.*, 2004; Walker *et al.*, 2010). The *Nes* reporter construct generated in this study was based on the construct designed by Lothian and Lendahl (1997) who used a conserved 714 bp enhancer element in the second intron of the *Nes* gene (*eNestin714*), downstream of which they placed the herpes simplex virus thymidine kinase promoter

(*TK*) and the *lacZ* reporter gene. For compatibility with fluorescence microscopy in conjunction with Nrl.GFP positive rod photoreceptors, the *lacZ* gene was replaced with the *DsRed* open reading frame (ORF). The whole reporter module was further cloned into the AAV2 based pD10 plasmid backbone, should future experiments warrant viral transduction based delivery. However, following electroporation of the original *Nes* reporter construct pD10 *eNestin714.TK.DsRed* into neo-natal *Nrl.GFP*$^{+/+}$ mouse derived retinal explants, no *DsRed* reporter expression was detected in cultured tissue explants. On the other hand, control electroporation with pD10 *CAG.DsRed* (*CAG* is a ubiquitous promoter) resulted in wide-spread *DsRed* expression in morphologically diverse cells throughout the neural retina except for the GCL.

It was noted that the second intronic *Nes* enhancer element was upstream of the reporter gene transcription start site in the reporter designed by Lothian and Lendahl (1997) and hence also the original pD10 *eNestin714.TK.DsRed Nes* reporter generated in this present study. This configuration successfully drove *lacZ* expression upon genomic insertion in the transgenic reporter mice generated by Lothian and Lendahl (1997) but not following retinal electroporation in the present study. It was thought to be possible that the transcriptional machinery involved in *Nes* reporter expression from episomal plasmids, required the *eNestin714* element to be downstream of the transcription start site, as is the case for the *Nes* gene. Indeed, *Nes* reporter expression was unlocked in retinal cells with NRSC morphology, upon placing the *eNestin714* element downstream of the *DsRed* ORF (pD10 *TK.DsRed.eNestin714).* Not only was the re-designed *Nes* reporter active in cells that morphologically resembled NRSCs at early developmental stages, reporter expression was also completely absent in the mature retina, which is in agreement with published (Xue *et al.*, 2006; Lee *et al.*, 2012) and present findings (section 5.3.1.1 & 5.3.1.2). Thus a functional *Nes* reporter construct, suitable for fluorescently labelling NRSCs *in vivo*, was generated as part of this study. However, due to the way that the *Nes* reporter was introduced into the retina (by sub-retinal injection followed by electroporation), the transfection of every single NRSC, even in vicinity of just the injection site, cannot be guaranteed.

Following *in vivo* electroporation of the pD10 *TK.DsRed.eNestin714* reporter into neo-natal *Nrl.GFP*$^{+/+}$ retinae and subsequent examination of live retinae by real time fluorescence microscopy at P4 and P7, rod photoreceptors that migrated radially in close alignment with labelled NRSCs could be observed. In many such instances, several cellular aspects of rod photoreceptors, such as the tip of the apical process, most of the

radial extent of the apical process as well as the soma, were juxtaposed to a labelled NRSC fibre. While this close association between neuronal precursor and radial glial fibre is in agreement with observations from the developing cortex, it is worth reiterating that rod cells have apical processes extending to the apical edge of the retina (chapters III and IV, Warre-Cornish, PhD thesis, 2013), while glial-guided brain neuronal precursor cells have short leading and trailing processes that do not extend to apical or basal edge of the neuroepithelium (Rakic, 1971a, 1971b, 1972). Examples of rods exhibiting this close apposition with NRSCs were seen to migrate both in the apical and/or the basal direction, in both the P4 as well as in the P7 retina. According to previous observations in the cortex, glial guided neuronal migration features saltatory motions at a relatively low average velocity where the neurons alternate between adhering to and gliding along radial glial fibres (Edmondson and Hatten, 1987; Anton *et al.*, 1996). There are thus two key criteria that will likely have to be met in order for any specific rod motility event to be classified as being guided by NRSCs: 1) the soma displays saltatory and overall slow advancements (both apical and basal movements were considered here); 2) the soma remains closely associated with an NRSC throughout the duration of the translocation event. Kinetically slow rod photoreceptor somal translocation events that were arguably saltatory in nature, and which occurred in direct contact with an NRSC, were indeed observed within this study. However, the number of events that fit the proposed criteria was relatively low (n = 5 at P3; n = 7 at P7; see Figure 5.3.15, 5.3.16, 5.3.18 & 5.3.19). This low number could have been due to the low number of experimental repeats (N = 1 at P4 and at P7) as well as the relatively small field of view that was imaged (221 x 221 µm at P4 and 68 x 68 µm at P7). It shall be pointed out again that it was difficult for all elements of this experiment to work according to plan (electroporation of P1 mice, survival of electroporated mice, tissue processing for live imaging, imaging a field of view with good transfection efficiency and tissue health) and hence only one successful experimental repeat was performed prior to completion of this thesis. It may also be that only a small proportion of the somal movements within a given area of the retina are guided by NRSCs.

By contrast, rapid apical somal translocation, according to the characterisations provided in sections 3.3.1.3 and 3.3.2.2, displays much faster kinetics than glial-guided migration. Based on these kinetics, rod photoreceptor rapid apical somal translocation appears to be in the same range as the apical migration exhibited by G2-phase progenitor cells during IKNM rather than the saltatory motion by neuronal precursor cells undergoing glial guidance. In the former case, apically directed nuclear/somal translocation is a cell

intrinsic and glial guidance-independent process. Given the kinetic as well as mechanistic similarities, the rapid apical translocation of rod photoreceptor somata is likely a cell intrinsic and glial-guidance independent as well (see chapters III and IV). Occasionally however, rod photoreceptor rapid apical somal translocations were observed in close alignment with an NRSC (n = 4 at P3; n = 5 at P7). In some of the observed cases, the rod somata of the rapid apically translocating cells were at a slight distance to the neighbouring NRSC while the apical process was closely aligned; in others, the somata, in addition to the apical processes, appeared to be fully aligned with the NRSC. Kinetically, both scenarios were indistinguishable and it is thus unlikely that one was subject to glial-guidance and the other was not. The most likely explanation is that the rapid apical somal translocation of rod photoreceptors is independent of glial-guidance, but due to the nature of the tightly packed pseudostratified retinal neuroepithelium, some rapid apical translocation events will inevitably occur next to an NRSC.

This has profound implications for the utilised experimental assay, which was designed to image rod photoreceptor somal translocations that are potentially subject to glial-guidance. While some of the provided time lapse examples argue in favour of the existence of glial-guided rod photoreceptor somal translocation, a case for migration that is independent of glial guidance can be made just as easily. To name a few examples, during some rod somal movements that fit the kinetic criterion of glial-guided migration, the somata were observed at a slight distance to the nearest reporter labelled NRSC even though the rod apical process appeared to be closely aligned with that NRSC; conversely, some somal movements that did not fit the kinetic criterion of glial-guided migration nonetheless occurred in close alignment to an NRSC; rod cell bodies that are passively displaced by an unlabelled cell may just happen to be pushed along an NRSC process; cell intrinsic mechanisms that resulted in slow rod somal translocations that fit the kinetic criterion of glial-guided migration may appear to be glial-guided; finally, potentially glial-guided rod somal translocation events may be masked by incomplete NRSC transfection. Together, these examples demonstrate the complexities of determining whether rod photoreceptor motility encompasses a glial-guidance component: the developing neural retina is pseudostratified where various somata perform different apico-basal or sometimes lateral motions; secondly, there is uncertainty regarding the completeness of NRSC transfection within the imaged fields of view.

Further experiments are thus needed in order to settle the debate over the relevance of glial-guided neuronal migration within the retina. The issue of incomplete NRSC

labelling can be circumvented by utilising the *Hes5-GFP* transgenic reporter mouse, in which all NRSCs (from RPCs to Müller glia) are labelled during the entire mouse life span (Basak and Taylor, 2007; Nelson *et al.*, 2011). A functional rod reporter DNA construct (using the *Nrl* or an equivalent promoter, becoming active soon after terminal cell division) could be sparsely introduced into the retinae of these mice. Alternatively, one could also attempt to sparsely label RPCs and their progeny cells using a lentivirus approach, which could be combined with an additional rod reporter module to label the rod progeny. This would have the added advantage that potential glial-guidance mechanisms would only be visualised within a given clonally related columnar unit (based on studies in the cortex, glial-guidance frequently occurs between clonally related radial glia and neuronal precursor cells (Noctor *et al.*, 2004)). Nonetheless, both of these alternative experimental strategies would still be confronted with the complex nature of the pseudostratified developing neural retina. To address whether the movement of a rod soma is passive and caused by radial motions of a neighbouring cell, one could perhaps use correlation analysis to determine whether the movements of these cells could be causally related. To address whether physical proximity between a rod cell and the nearest neighbouring NRSC is due to glial-guidance mechanisms rather than due to space limitation, it might be necessary to utilise supra-resolution or ultrastructure microscopy in order to identify a putative interstitial junction, which has been reported to occur between cortical neuronal precursor cells and their glial-guidance partners, the radial glia (Gregory *et al.*, 1988).

CHAPTER VI. THE MIGRATION AND INTEGRATION OF TRANSPLANTED ROD PHOTORECEPTORS INTO THE RECIPIENT RETINA

6.1. Introduction

A multitude of environmental factors, traumatic injury, as well as inherited genetic disorders lead to retinal degeneration, which typically involves the loss of photoreceptors and vision. Unlike the amphibian or the fish retina, the mammalian retina generally lacks the capacity for adult neurogenesis, which permits the production of new photoreceptors to replace those that have been lost. One way to repair the compromised retinal circuitry consists of providing it with an exogenous source of photoreceptors. Several proof of concept *in vivo* studies carried out in the past decade have demonstrated that sub-retinally transplanted (injected between recipient neural retina and RPE layer) photoreceptors apparently migrate and integrate into the retina of the recipient eye (MacLaren *et al.*, 2006; Bartsch *et al.*, 2008; Eberle *et al.*, 2011; Pearson *et al.*, 2012; Gonzalez-Cordero *et al.*, 2013; Homma *et al.*, 2013). These and other studies have shown that transplanting exogenously derived photoreceptors may become a feasible therapeutic approach in the future for medical conditions that lead to the loss of endogenous photoreceptors (Lakowski *et al.*, 2010; Pearson *et al.*, 2012; Barber *et al.*, 2013).

All photoreceptor transplantation studies performed to date exhibit similar experimental designs: pre-labelled (typically with transgenically generated GFP or DsRed) photoreceptor cells are sub-retinally transplanted and (usually around three) weeks later the transplantation outcome is assessed visually by microscopy analysis on fixed tissues. When pre-labelled photoreceptor cells were located within the host retina, it was inferred that these cells must have migrated from the injection site (sub-retinal space) into the neural retina to then become integrated within the existing neural circuitry. Most of the grafted rod photoreceptors appear to have migrated into the recipient eye within the first week following transplantation, based on a time-point analysis on fixed tissue (Warre-Cornish *et al.*, 2014). However, neither photoreceptor migration nor the process of photoreceptor integration and maturation have ever been directly observed or

characterised. Hence, the underlying mechanisms are presently ill-defined. A better understanding of these processes offers the prospect of being able to increase the integration efficiency of transplanted cells, which is crucial for the functional restoration of vision to a meaningful degree.

In terms of the migration of transplanted rod photoreceptors, three principal hurdles will need to be overcome by the transplanted cells in order to allow correct integration within the recipient neural retina to occur: 1) migration out of the transplantation subretinal cell-mass through the interphotoreceptor matrix (IPM) and towards the apical limit of the neural retina; 2) penetration through the outer limiting membrane (OLM) and into the outer nuclear layer (ONL); 3) radial migration through the ONL towards the final position within the recipient retina.

The IPM consists of RPE processes and the inner/outer segments of photoreceptors and is further highly decorated with hyaluronic acid and chondroitin sulphate proteoglycans (CSPGs), which likely exert an inhibitory effect on rod photoreceptor migration and integration (Hollyfield, 1999; Singhal *et al.*, 2008). These inhibitory factors will likely have to be overcome by chemoattractant and cell adhesion forces that stimulate transplanted rod photoreceptors to migrate out of the transplantation cell mass, through the IPM and towards the OLM. Indeed, studies have shown that combining the transplantation with administration of ChABC, a bacteria-derived enzyme that breaks down CSPGs, leads to significantly higher numbers of donor reporter labelled cells within the recipient retina (Suzuki *et al.*, 2007; Singhal *et al.*, 2008; Barber *et al.*, 2013). However, the mechanisms that underlie the chemotaxis of transplanted photoreceptors towards the recipient neural retina are unknown. A recent *in silico* and *in vitro* study delivered indications that the ligand-chemokine receptor pair SDF-1α–CXCR4 could be important for photoreceptor chemotaxis (Unachukwu *et al.*, 2016). Despite this single report, there remains a large gap in our understanding of the mechanisms of rod photoreceptor migration through the IPM.

Following migration through the IPM, penetration through the OLM is the next hurdle that has to be overcome by transplanted rod photoreceptors. The OLM consists of the apical microvilli of Müller glia as well as their apical end feet, which are interconnected via tight junctions with each other and the apical processes of resident photoreceptors (Bunr-Milam *et al.*, 1985; Omri *et al.*, 2010). The OLM thus presents a physical barrier to transplanted rod photoreceptors. It follows that disruption of the OLM may allow more

photoreceptor cells to penetrate through the OLM to reach the ONL. Indeed, the disruption or removal of these components has led to modest increases in the number of integrated cells in various end point studies (West *et al.*, 2008; Pearson *et al.*, 2010; Barber *et al.*, 2013). Similar to the migration of transplanted rod photoreceptors through the IPM, however, the kinetics and mechanisms that underlie the migration of grafted rod cells past the OLM are unknown.

Stage three of migration of transplanted rod photoreceptors consists of radial migration within the ONL. A previous study has shown that those photoreceptors that appeared integrated within the recipient retina were frequently closely aligned with the apical process of resident Müller glia cells (Warre-Cornish, PhD thesis, 2013). Based on the analysis of many integrated cells, this association was significantly closer than would be predicted from a completely random integration within the lateral dimension of the retina. This finding led to the hypothesis that sub-retinally transplanted rod photoreceptors might move into and/or through the recipient ONL by migrating along the apical processes of Müller glia. Müller glia are immensely important for the correct function of the retina, as summarised in Table 1.1.1; a multitude of responsibilities are covered by this cell type, including ionic and osmotic homeostasis, supply of nutrients and neurotrophic factors to the retinal neurons, protection against oxidative stress, neurotransmitter recycling, outer segment phagocytosis, as well as operating as an optic fibre guiding photons from the vitreal to the scleral side of the retina towards the photoreceptor outer segments. It is now a possibility that this already extensive list of duties is to be expanded by the addition of glial-guided neuronal migration. In further support of this, freshly isolated rod photoreceptors co-cultured with pre-established Müller glia primary cells were previously shown to migrate along the glial substrate (Warre-Cornish, PhD thesis, 2013). Migrating rod cells exhibited elongated somata, a characteristic often observed for migrating neurons (Altman, 1969). In the same context, it is interesting to note that rod somata in the developing retina were extended along their apico-basal axes at developmental stages where rod motility was observed (see chapter III; Warre-Cornish, PhD thesis, 2013), whereas the stationary rod somata in the adult retina were more spherical. The rod photoreceptors located on the Müller glia substrate cells frequently extended neurites. Morphologically identifiable inner and outer segment structures were not observed, but this may have been because the rod cells were isolated at a developmental stage (P8) before full inner and outer segment elaboration occurs *in vivo*. In cichlid fish, and in contrast to mammals, retinal neurogenesis is observed even in adulthood. The new rod

photoreceptor cells are born at the apical edge of the adult neural retina and then migrate in the basal direction until they reach the OPL where repulsive signals are proposed to prevent further basally-directed motility (Mack *et al.*, 2003). Photoreceptors that migrated basally through the ONL had spindle shaped somata, indicative of migratory behaviour; crucially, these photoreceptors were in direct proximity to Müller glia processes. Upon reaching the OPL, this preferential juxtaposition was lost. Although the study by Mack and colleagues (2003) was based on fixed tissue analysis, which has its obvious limitations when investigating cell motility, it still presents one of the strongest pieces of evidence for retinal glial-guided neuronal migration in the published literature. A parallel can be drawn to the photoreceptor transplantation scenario, where the basally directed migration of rod cells was also proposed to be initiated from the apical edge of the neural retina (Warre-Cornish *et al.*, 2014).

In addition to real rod photoreceptor integration events, apparent photoreceptor integration can also arise via material transfer. Very recent findings from our group (Pearson *et al.*, 2016), and others (Santos-Ferreira *et al.*, 2016), have found that donor cells transplanted into the subretinal space of recipient animals can engage in the robust exchange of cellular products with photoreceptors in the host retina. This process has been termed material transfer. While the precise cellular mechanism underlying this process remain to be determined, it appears to involve the exchange of RNA and/or protein (but not DNA or nuclei) and results in the host photoreceptors acquiring a wide range of proteins including those missing from the host cells, in the cases of inherited degenerations. The process is sufficiently robust that it is likely to play a significant role in the functional restoration of vision, previously observed in models of retinal degeneration (Pearson *et al.*, 2012; Barber *et al.*, 2013).

In the light of these issues, monitoring, by time-lapse live imaging, the processes that occur following photoreceptor transplantation into the recipient eye could provide valuable new information of how transplanted rod photoreceptors migrate into the recipient neural retina following transplantation, or, indeed, how material transfer between non-integrated and resident photoreceptor cells is achieved. In order for such processes to be imaged, not only do the transplanted photoreceptors need to be clearly identifiable via a cellular label, structures of the recipient neural retina will have to be labelled as well. The *Nrl.GFP*$^{+/+}$ transgenic mouse line, in which *GFP* expression is specifically driven in rod photoreceptors under transcriptional control of the *Nrl* promoter, is a good source of labelled rod photoreceptors. For the labelling of the

recipient retina, two potential avenues will be explored: 1) mitochondria targeting vital dyes (Mitotracker®) have been shown to selectively label Müller glia in the rabbit, rat, guinea pig and human retina (Uckermann *et al.*, 2004). Labelling the recipient retina with such dyes may thus potentially help with the visualisation of the OLM and Müller glia, both of which may be crucially involved in rod photoreceptor migration. Why exactly Mitotracker® dyes are taken up preferentially by Müller glia rather than the other retinal cells is not entirely clear but it was speculated to be related to the thiol reactivity of such dyes and the large amounts of thiol group-containing glutathione produced by and contained within Müller glia (Pow and Crook, 1995; Uckermann et al., 2004). In addition, these vital dyes also label the outer segments of photoreceptors (Bianchini *et al.*, 2014), which should make it possible to observe rod migration through the IPM. 2) Alternatively, Müller glia can also be selectively labelled using an adeno associated virus (AAV) approach. A recombinant AAV serotype (ShH10) exists, which possesses tropism for Müller glia (Klimczak *et al.*, 2009; Pellissier *et al.*, 2014). By encapsidating an XFP-encoding expression construct, AAV ShH10 viral particles can thus specifically label Müller glia of the recipient retina. Using this combination of Mitotracker® and AAV ShH10, rod photoreceptor migration (or material transfer) can be imaged at all possible stages within the IPM, through the OLM and within the ONL. Furthermore, the presence of labelled Müller glia allows for the assessment of their potential involvement in donor cell migration/integration.

Additionally, glial-guidance in the context of the rod photoreceptor transplantation process will also be addressed using the more reductionist Müller glia & rod photoreceptor co-culture model established by a previous member of the group (Warre-Cornish, PhD thesis, 2013). Rod photoreceptors appeared to be motile on Müller glia based on the manual tracking of rod somata. However, the underlying mechanisms are presently unknown. The co-culture model lends itself to loss and/or gain of function studies due to the relative ease of manipulation *in vitro* as opposed to *in vivo*. To prevent potential user bias due to manual tracking, the manual *in silico* tracking method of rod photoreceptors over time used previously will have to be replaced by a more objective, at least semi-automated, tracking methodology. The development of such a tracking tool will be crucial before proceeding with gain/loss of function experiments.

6.2. Aims

The aims of the work carried out as part of this chapter were:

(1) to identify suitable ways to label the neural retina *in vivo* or *ex vivo* with focus on specifically labelling the IPM, OLM and ONL, but also Müller glia.

(2) to optimise the live imaging set-up to such an extent that the processes that follow the *in vivo* transplantation of rod photoreceptors into the recipient retina (be it migration/integration and/or material transfer) can be observed by real time 2-photon fluorescence live imaging

(3) to subject retinae of eyes that were suitably labelled according to (1), and which received rod photoreceptor transplants, to time-lapse live imaging by 2-photon microscopy in order to follow the processes that occur after the transplantation of rod photoreceptors by real time 2-photon fluorescence live imaging. The aim will also be to provide a kinetic and mechanistic description of migration/integration and/or material transfer

(4) to develop a semi-automated *in silico* tracking methodology that can be applied to real time recordings of Müller glia & rod photoreceptor *in vitro* co-cultures. This shall replace the previously used manual tracking method and should make the characterisation of rod kinetic properties more objective.

(5) assuming successful completion of (4), gain/loss of function studies will be performed to investigate the mechanisms that underlie this migratory behaviour

Originally, these experiments were intended to produce time-lapse recordings to bridge the gap in our knowledge of what happens between the sub-retinal transplantation of rod photoreceptors into the recipient eye and their integration into the host retina. Whereas the past has seen many independent studies assuming that transplanted photoreceptors must have migrated and integrated into the host retina, very recent findings from our group (Pearson *et al.*, 2016), and from the group of Marius Ader (Santos-Ferreira *et al.*, 2016), have provided evidence that material transfer between extra-retinal and host photoreceptors may account for a number of observations previously attributed to cell integration. These experiments will shed new light on this issue and provide important

clues as to what the mechanisms underlying rod photoreceptor migration/integration and/or material transfer following photoreceptor transplantation are.

6.3. Characterisation of rod photoreceptor motility following transplantation – an *in vivo* approach

6.3.1. Labelling Müller glia and the live recipient retina

6.3.1.1. Labelling the retina with a mitochondrial vital dye

In order to investigate the migration of sub-retinally transplanted rod photoreceptor precursor cells into and within the recipient retina in real time and to find out whether migration is guided by Müller glia, a strategy was required for robustly labelling various components of the live neural retina, such as the interphotoreceptor matrix (IPM) as well as Müller glia themselves. Previous studies have shown that Mitotracker® mitochondrial vital dyes selectively label Müller glia in explanted retinae originating from a range of vertebrate species such as human, cow, guinea pig and rat. This preferential accumulation within Müller glia was speculated to be due to the thiol reactivity of such dyes and the large amounts of thiol group-containing glutathione produced by and contained within Müller glia (Pow and Crook, 1995; Uckermann et al., 2004). Different studies have further demonstrated that rod outer segments (i.e. part of the IPM) of the bovine retina are efficiently labelled by Mitotracker® (Panfoli *et al.*, 2009; Bianchini *et al.*, 2014).

To assess whether, and in what ways, mitochondrial vital dyes label the mouse retina in this present study, acutely explanted and live adult wild-type retinae were treated with 5 µM Mitotracker® Orange CMTMRos diluted in RPMI 1640 medium for 15 minutes at room temperature. Retinae were subsequently fixated, whole mounted and imaged by confocal microscopy. As shown in Figure 6.3.1Ai and 6.3.1Aii, photoreceptor outer segments were intensely labelled. Furthermore, inner segments as well as photoreceptor somata within the ONL also exhibited Mitotracker® Orange CMTMRos labelling although the signal intensity appeared to be weaker compared to the outer segment region (Figure 6.3.1A & 6.3.1B). However, starting from a depth of approximately 30 µm into the *z* stacks, the labelling intensity gradually decreased (Figure 6.3.1Ai). As will be shown

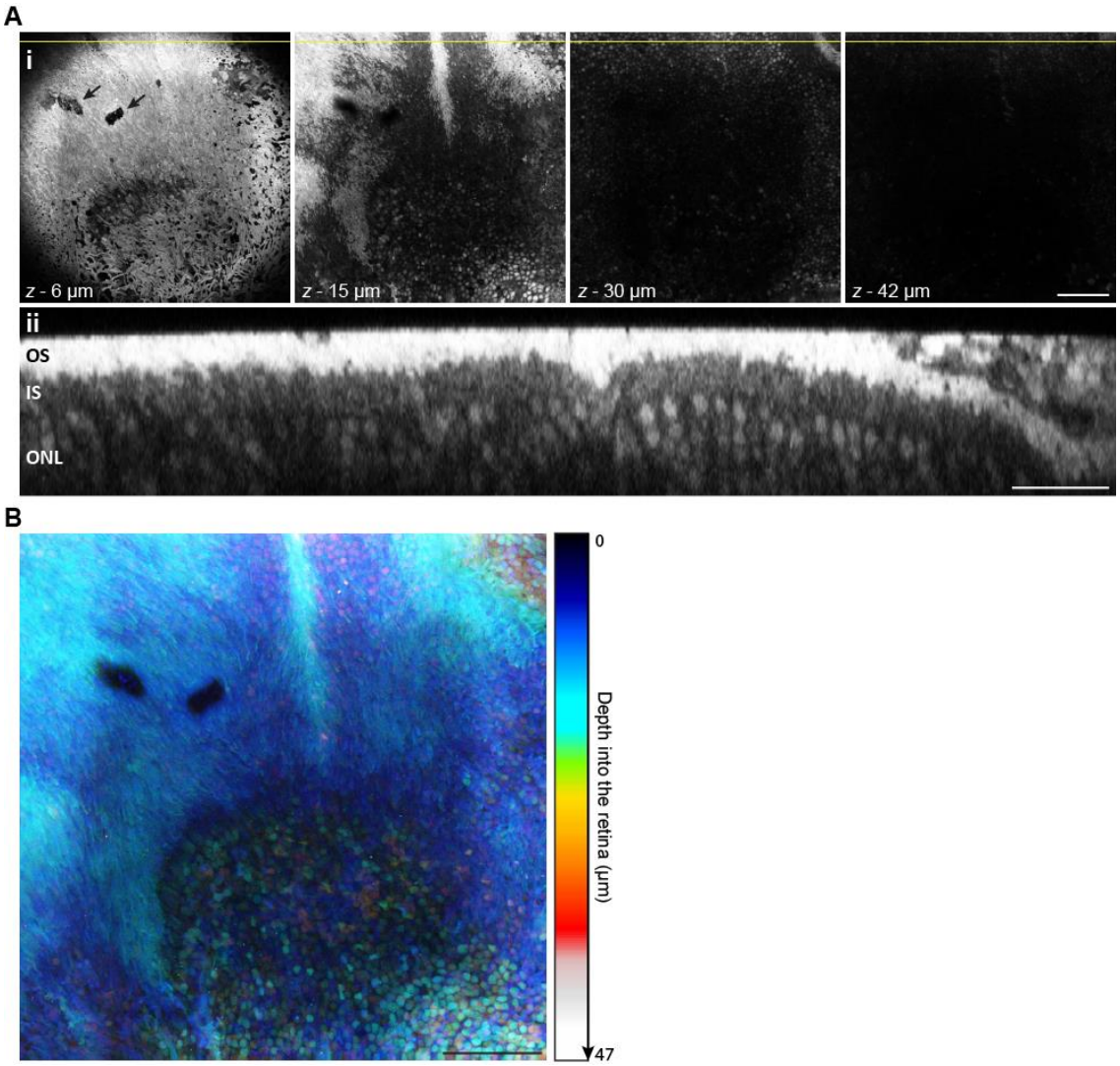

Figure 6.3.1 The mitochondrial vital dye Mitotracker Orange CMTMRos labels various retinal structures. Adult wild-type retinae were acutely explanted, exposed to 5 µM Mitotracker Orange CMTMRos, fixated, whole-mounted and subsequently imaged by confocal microscopy. Labelling was apparent at differnent cellular and acellular layers of the neural retina. **(Ai)** *xy* top view of a whole-mounted retina at different *z*-depths of the acquired image stack. Rod outer segments and ONL cell bodies were distinctively labelled. Mitotracker fluorescence was not detected in RPE cells (black arrows). **(Aii)** *xz* slice view of the same stack depicted in (Ai) taken at the level of the yellow line. **(B)** Colour coded *z* projection of the same image stack as in (Ai) and (Aii). IS = inner segment, ONL = outer nuclear layer, OS = outer segment. Scale bars, 50 µm (Ai, B) and 25 µm (Aii).

in a later section (6.3.2.2), this was likely due to insufficient single-photon laser penetration rather than due to insufficient dye penetration through the whole mounted tissue. Mitotracker labelling was not detected in RPE cells, at least two small patches of which had remained attached to the retinal preparation shown in Figure 6.3.1 following dissection (black arrows in Figure 6.3.1A). More crucially however, no specific labelling of Müller glia was detected in any of the investigated retinae (N = 2, n = 8 individual retinae).

Thus, the mitochondrial dye Mitotracker® Orange CMTMRos efficiently labels the IPM as well as the ONL, which makes it possible to follow the migration of sub-retinally transplanted rod photoreceptors into the recipient neural retina in time-lapse live imaging experiments. Since it was not possible to label Müller glia using mitochondrial vital dyes, a different methodology had to be applied in order to visualise any Müller glia guided aspects that may potentially occur during the photoreceptor integration process.

6.3.1.2. AAV ShH10 CAG.DsRed transduces and labels Müller glia in the adult retina

In order to find out whether the migration/integration of transplanted rod photoreceptors is guided by Müller glia and to investigate any such events in real time, efforts were made to label Müller glia *in vivo*. The AAV ShH10 viral capsid serotype has been shown to possess tropism for Müller glia in the rodent retina (Klimczak *et al.*, 2009). Hence, to label Müller glia in the present study, AAV ShH10 viral particles encapsidating a pD10 *CAG.DsRed* expression construct were used.

Others in the lab have previously established that the most efficient labelling of Müller glia was achieved upon intra-vitreal AAV ShH10 vector administration in P10 mice (Hippert C., personal communication). This administration regimen was followed in the present study. At one week post intra-vitreal injection into the wild type P10 eye (i.e. in the P17 eye) there was wide spread transduction and *CAG.DsRed* expression apparent within neural retinal cells that possessed Müller glia-like morphology (Figure 6.3.2A). The observed features of typical Müller glia included somata lined up in the centre of the INL, radially extending apical/basal processes, as well as end feet located in the OLM and ILM. In further support of the Müller glia identity of DsRed labelled cells, DsRed and the Müller glia marker glutamine synthetase were expressed by the same cells

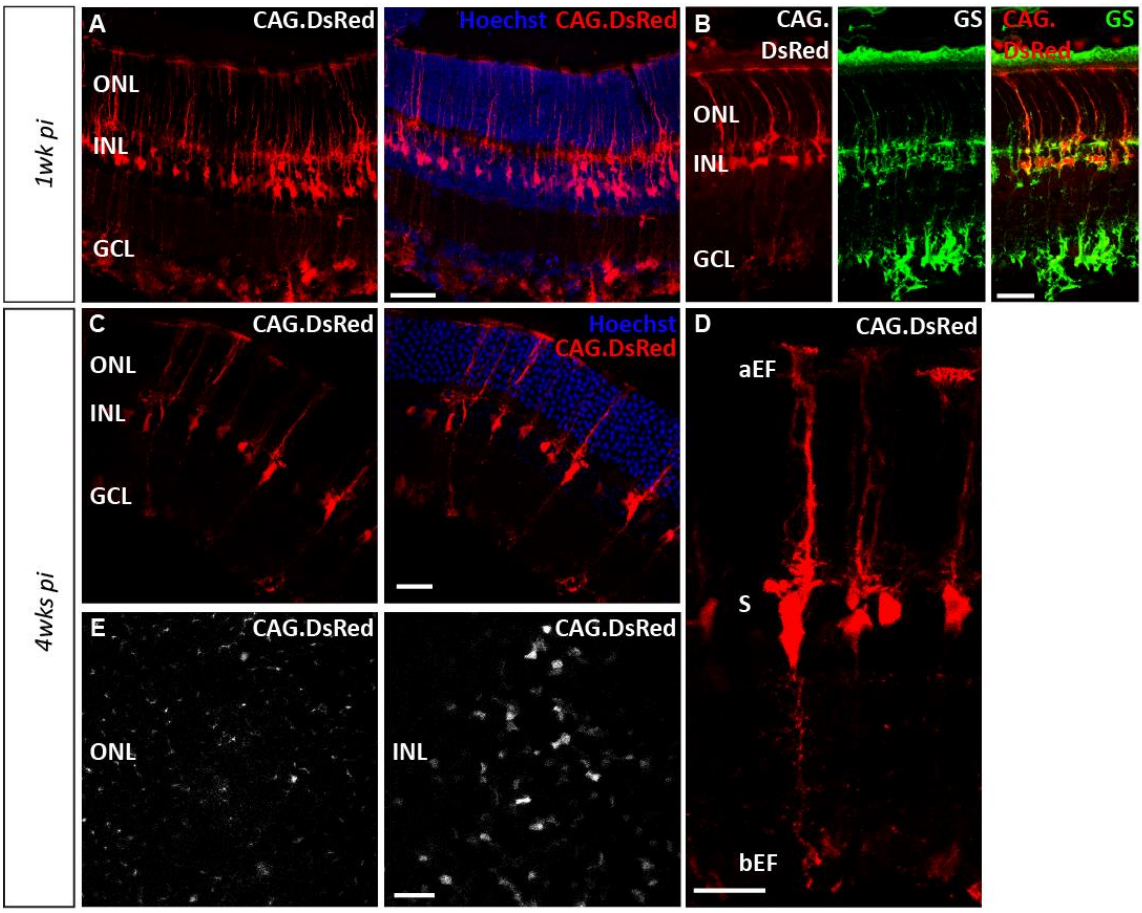

Figure 6.3.2 AAV ShH10 *CAG.DsRed* possesses tropism for and labels Müller glia in the mouse retina with DsRed. AAV ShH10 viral particles encapsidating the pD10 *CAG.DsRed* expression construct were administered into P10 mice by intra-vitreal injection. **(A)** 1 week post injection, *CAG.DsRed* expression (red) was observed across the entire retina in cells that had the morphological appearance of Müller glia. **(B)** *CAG.DsRed* expression (red) in transduced retinal cells was co-localised with the immunoreactivity of the Müller glia marker GS (green). **(C, D & E)** *CAG.DsRed* continued to be expressed in Müller cells 4 weeks post injection. **(C)** Neural retina featuring CAG.DsRed-labelled Müller glia; an enlarged view is shown in **(D)**. **(E)** A whole mounted retina imaged at the level of the ONL and INL exhibited *CAG.DsRed* expression (greyscale) in both layers. ONL = outer nuclear layer, INL = inner nuclear layer, GCL = ganglion cell layer, aEF = apical end foot, bEF = basal end foot, S = soma. Scale bars, 25 µm.

according to immunohistochemical evidence (Figure 6.3.2B). *DsRed* expression persisted in Müller glia at least up until four weeks post vector administration (Figure 6.3.2C), labelling of the entire Müller glia cell from the apical end foot down to the basal end foot (Figure 6.3.2D). Flat mounted retinae from virally injected eyes were also imaged at thelevel of the ONL and INL, where DsRed was detected in the apical processes and somata of Müller glia, respectively (Figure 6.3.2E).

It was noted that viral transduction of retinal Müller glia with intra-vitreally administered AAV ShH10 vector was not necessarily completely uniform across the entire neural retina (compare Figures 6.3.2A and 6.3.2B); this finding may have implications on transplantation experiments where the exact location of sub-retinal photoreceptor injection should ideally coincide with areas where Müller glia were previously efficiently transduced and labelled. A good regional overlap between the two is essential for investigating any potential glial-guidance mechanisms involved in rod migration/integration by time-lapse microscopy.

6.3.1.3. Investigating potential associations between Müller glia and transplanted rod precursor cells by fixed tissue analysis

Having established that intra-vitreal administration of AAV ShH10 *CAG.DsRed* robustly labels adult Müller glia *in vivo*, the next step consisted of transplanting rod photoreceptor precursor cells derived from *Nrl.GFP*$^{+/+}$ mice into adult wild type mice that had earlier been administered an intra-vitreal injection of AAV ShH10 *CAG.DsRed* vector. Previous analyses on fixed retinae from transplanted eyes have demonstrated a statistically significant association between integrated rod photoreceptors and immunohistochemically labelled (GFAP positive) Müller glia fibres (Warre-Cornish, PhD thesis, 2013). The aim here was to determine if these findings could be replicated with virally labelled Müller glia.

The intra-vitreal administration of AAV ShH10 *CAG.DsRed* was performed on P10 wild type mice, which were allowed to age to at least for weeks before receiving a sub-retinal transplantation of *Nrl.GFP*$^{+/+}$ derived cells. The main period during which rod photoreceptor integration occurs following transplantation is the first week post-transplantation (Warre-Cornish *et al.*, 2014). Indeed, confocal analysis of fixed and flat

mounted retinae five days post transplantation clearly showed the somata of grafted Nrl.GFP positive cells at a range of depths spanning from the apical edge of the neural retina at the OLM to deeper within the ONL. These cells were likely at different stages of integration into the ONL of the recipient retina (Figure 6.3.3A).

Further, confocal analysis of fixed eye sections at three weeks post transplantation has shown areas with both good Müller glia labelling and donor-labelled rod photoreceptors in the recipient retina (Figure 6.3.3B). The somata of integrated Nrl.GFP positive cells were found throughout the entire thickness of the ONL, where rods usually reside. Furthermore, basally and apically directed processes could be identified, the latter of which usually terminated in structures that morphologically looked like inner and outer segments. Analysis of a single *xz* plane within the image stack shown in Figure 6.3.3Bi further verified that integrated rod cells were often proximal to at least one Müller glia process (Figure 6.3.3Bii), which is in agreement with previous results (Warre-Cornish, PhD thesis, 2013). To highlight this finding, a *z* image stack of a whole mounted retina, individual slices of which are shown in Figure 6.3.3Ci-Civ, was 3D reconstructed (Figure 6.3.3D). Combined, these panels show a close association between two integrated rod photoreceptor cells and a single Müller glia fibre at the level of the OLM (Figure 6.3.3Ci), the ONL (Figure 6.3.3Cii & Figure 6.3.3Ciii) and the OPL (Figure 6.3.3Civ).

These, and previous (Warre-Cornish, PhD thesis, 2013), fixed tissue data thus suggest that transplanted rod photoreceptors that migrate into and within the recipient neural retina may, to some extent, utilise glial guidance mechanisms. It is also a possibility that axonogenesis and apical process formation are dependent on cell-cell interactions with Müller glia. These aspects shall be addressed by time-lapse live imaging experiments as described in the following sections.

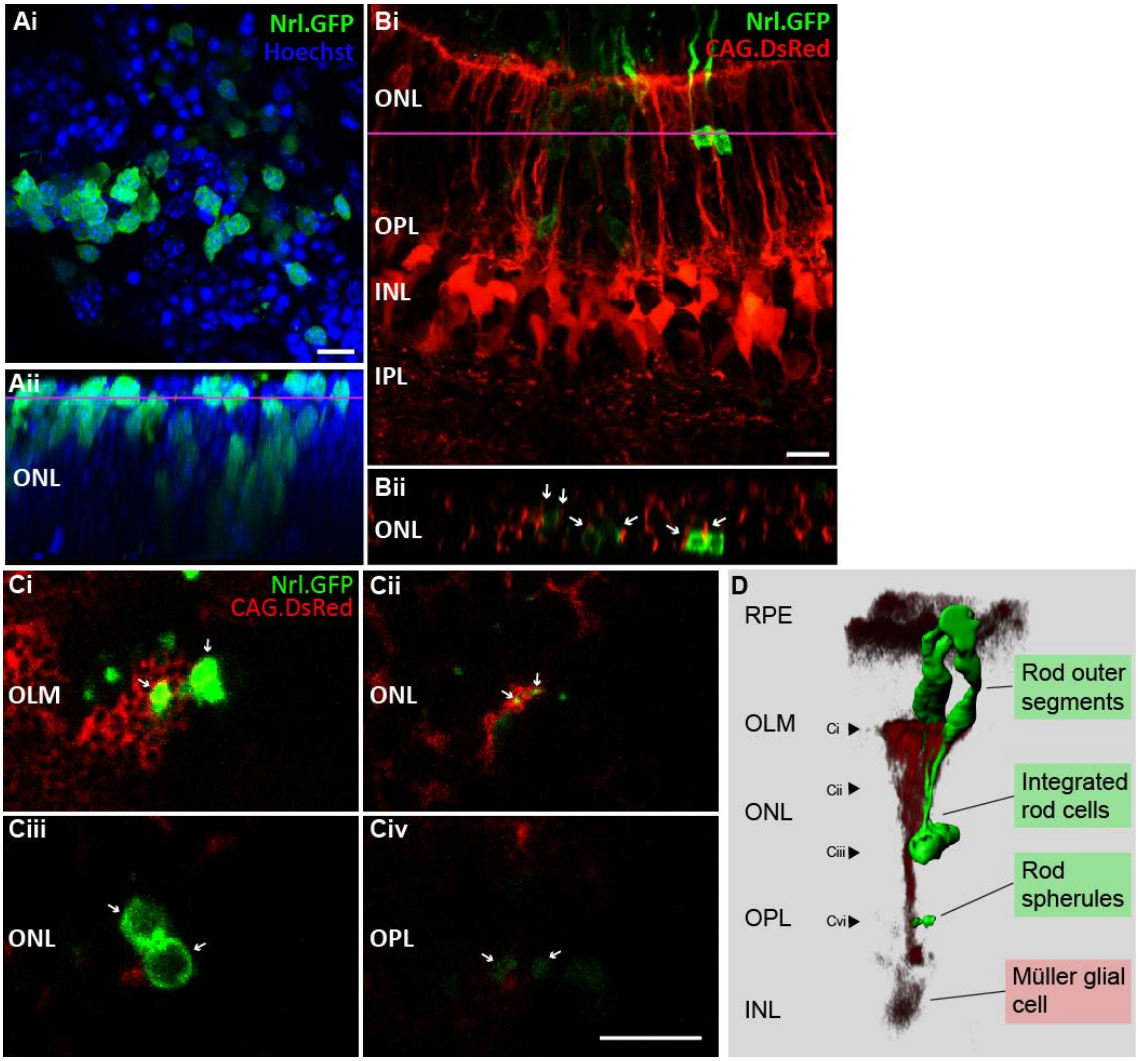

Figure 6.3.3 Fixed tissue analysis of adult wild type eyes sub-retinally transplanted with rod precursor cells. **(Ai)** Top view (*xy*) of a whole-mounted retina at five days post transplantation with Nrl.GFP positive rod precursor cells (green). The orientation of the 3D projection is such that the photoreceptors project towards the reader. **(Aii)** *xz* projection of the same field of view shown in (Ai). Integration of rod precursor cells was already evident 5 days post transplantation. The magenta line indicates the level, at which the top view in (Ai) is shown. **(Bi)** Fixed section maximum projection image obtained from eyes that were harvested three weeks post transplantation. Prior to transplantation, Müller glia of recipient eyes were fluorescently labelled with AAV ShH10 *CAG.DsRed* (red). Good AAV ShH10 *CAG.DsRed* transduction of Müller glia as well as integration of rod photoreceptor cells is evident within the shown field of view. Most of the integrated rod cells were found in close proximity to Müller glia fibres. **(Bii)** *xz* reconstruction of the same image stack used to obtain the maximum projection in (Bi). The level of the *xz* plane is indicated by the magenta line in (Bi). White arrows indicate areas of close cell-cell contacts. **(Ci-Civ)** Selected top views (*xy*) of an *xyz* image stack of a whole-mounted retina at various depths from the OLM to the OPL harvested three weeks post transplantation. A close association between two rod cells (green) and a single Müller glia fibre (red) was apparent (white arrows). **(D)** 3D reconstruction of the image stack shown in (Ci-Civ). ONL = outer nuclear layer, OPL = outer plexiform layer, INL = inner nuclear layer, IPL = inner plexiform layer, GCL = ganglion cell layer. Scale bars, 10 µm.

6.3.1.4. *Investigating the migration of transplanted rod precursor cells by time-lapse live imaging – troubleshooting the experimental protocol*

Analyses of fixed retinae indicated that donor-reporter labelled rod photoreceptors within the recipient retina are often found closely aligned with Müller glia fibres (Warre-Cornish, PhD thesis, 2013). Assuming these events arise as a result of migration/integration, this suggests that the process of integration may involve Müller glia guidance. As a first step to determine whether this is the case, transplanted retinae were subjected to time-lapse live imaging using 2-photon fluorescence microscopy on an upright imaging system.

Adult wild type recipient mice that had received an intra-vitreal injection of AAV ShH10 *CAG.DsRed* at P10 to label the Müller glia subsequently received a sub-retinal injection of Nrl.GFP positive rod photoreceptor cells at 6-8 weeks of age. Eyes were harvested and processed for time-lapse live imaging between three to seven days post transplantation. Initially, the same approach was taken as with the time-lapse experiments on rod photoreceptor migration during early post-natal development (see chapter III and IV). Briefly, retinae were isolated free of surrounding tissues including RPE, whole mounted with the photoreceptor cells facing upwards and subsequently time-lapse live imaged (Figure 6.3.4A). However, during these attempts, a high degree of optical aberration was observed, which prevented the transplanted retina from being imaged with sufficient image quality (representative image shown in Figure 6.3.4B; N = 7 experimental repeats). When observing whole mounted retinae from virally labelled, non-transplanted eyes through the microscope eye piece, it was extremely difficult to focus on the fluorescently labelled cells when the retina was mounted with the photoreceptor cells facing upwards (Figure 6.3.4Cai). At best, isolated small regions could be brought into (poor) focus (Figure 6.3.4Cbi). Focussing of the labelled cells was improved when the retina was mounted with the RGCs facing upwards (Figure 6.3.4Cci). These different focussing potentials translated into marked differences in the quality of recorded images: while it was almost impossible to produce high quality images when retinae where mounted with the photoreceptor cells facing upwards (Figure 6.3.4B, 6.3.4Caii & 6.3.4Cbii), high quality images could be produced when retinae were mounted with RGCs facing upwards (Figure 6.3.4Ccii). In the latter case, however, the 2-photon laser could only

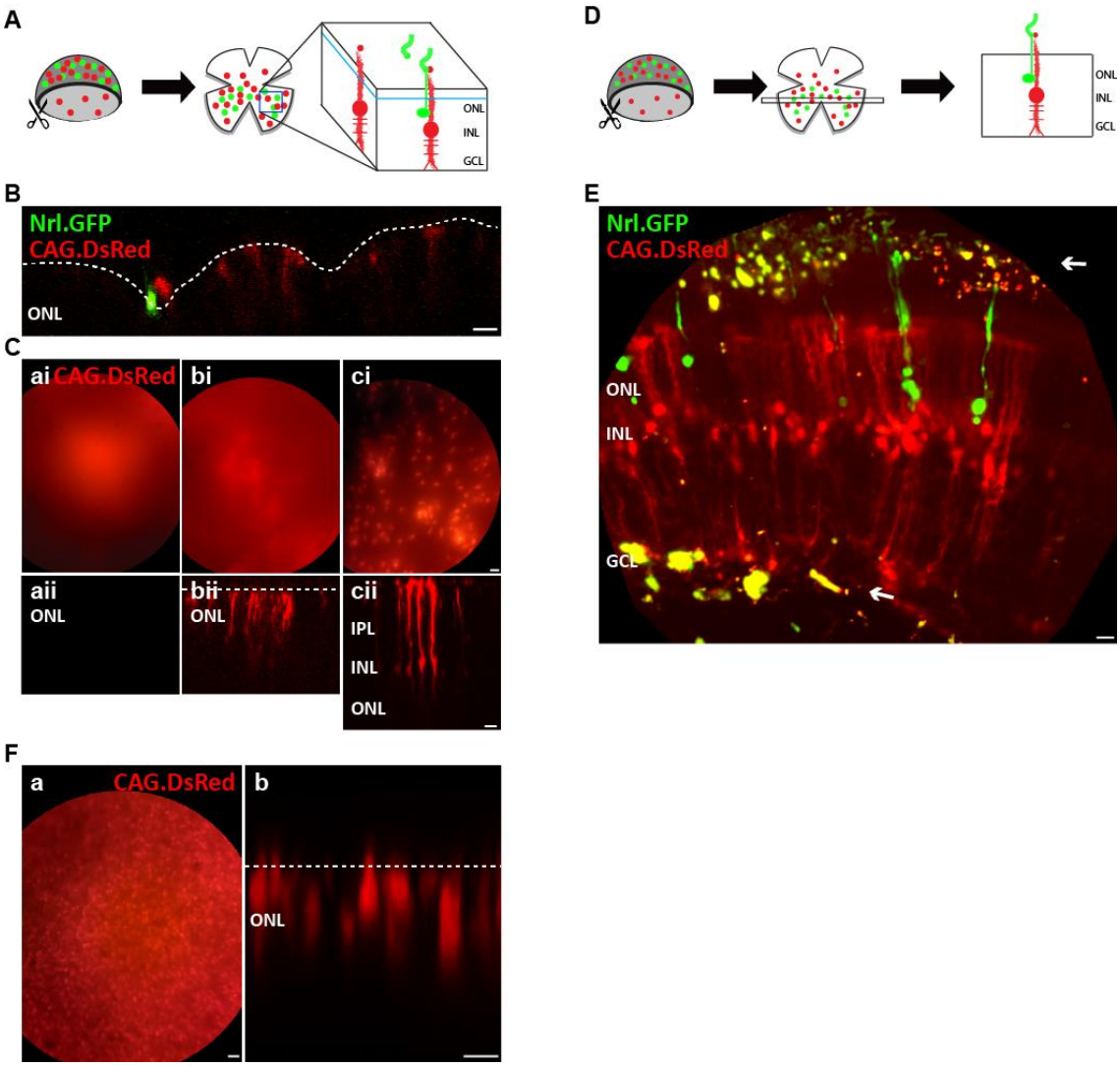

Figure 6.3.4 Strategies to image the migration of transplanted rod photoreceptor precursor cells into and within the recipient retina in real time. Recordings were carried out by time-lapse 2-photon fluorescence live imaging. **(A)** Schematic overview of the retinal whole mount approach. Here retinae were harvested, flat mounted, and suitable regions of interested were imaged. **(B)** Poor image quality when retinae transplanted with Nrl.GFP positive rod photoreceptors (green) were imaged using the retinal whole mount approach. Müller glia had been previously labelled using AAV ShH10 *CAG.DsRed* vector (red). White dashed line represents the presumptive OLM. **(C)** Image quality varied between regions of interests and upon changing the retinal orientation. **(Cai-ci)** Appearance of whole mounted retinae through the microscope eye piece captured on a LG Nexus 5 mobile phone; retinae were either mounted with the photoreceptor side facing upwards (Cai, Cbi) or with the RGCs facing upwards (ci). **(Caii-Ccii)** Corresponding 2-photon fluorescence images. **(D)** Schematic overview of the retinal slice culture approach. Here retinae were harvested and suitable retinal slice preparations were imaged. **(E)** Superb image quality when wild type retinae were imaged using the slice culture approach. However, tissue boiling (white arrows) quickly irreversibly damaged the tissue during time-lapse attempts. **(F)** *Prph2*$^{rd2/rd2}$ mouse previously injected sub-retinally with AAV 2/9 *CAG*.DsRed and imaged using the whole mount approach; appearance through the eye piece (Fa); corresponding 2-photon fluorescence image (Fb). ONL = outer nuclear layer, OPL = outer plexiform layer, INL = inner nuclear layer, IPL = inner plexiform layer, GCL = ganglion cell layer. Scale bars, 10 µm.

achieve a tissue penetration of approximately 120 µm measured from the ILM, which is just slightly beyond the INL and thus insufficiently deep to observe photoreceptor integration and migration at the level of the IPM, OLM and ONL.

Since the orientation of the retina heavily impacted upon the ability to image the tissue, it was considered that an apically located structure may cause the observed optical aberration. Adherent RPE was unlikely to be the reason, as pigmented cells were removed during dissection. Rather, it was suspected that the membrane rich photoreceptor outer segments caused a high degree of light scattering that precluded the formation of focused images when retinae were mounted with the photoreceptor cells facing upwards.

To circumvent this problem, a slice culture approach was next attempted (Figure 6.3.4D). Briefly, explanted retinae were embedded in 1% agarose and cut into thin slices using a vibratome. Selected slices containing both virally labelled Müller glia and transplanted rod photoreceptors were then oriented laid on their sides such that the photoreceptor outer segments were no longer directly obstructing the laser light path to the remainder of the neural retina. The obtained image quality by far surpassed that of the previously attempted whole mount approach, as DsRed labelled Müller glia spanning the entire radial thickness were observed (N = 3; example field of view shown in Figure 6.3.4E). Furthermore, several key cellular features of GFP positive rod photoreceptor cells located within the host retina were apparent, such as the soma, axon, rod spherule, apical process, inner segment and outer segment. Even though the slice culture approach was initially promising, other technical difficulties prevented long term image acquisition. The slice preparation retained the RPE and this resulted in it absorbing energy from the stimulating laser and subsequent tissue destruction (Figure 6.3.4E). The mechanical damage incurred during the slicing process also contributed to a more rapid deterioration in tissue health, preventing sufficiently robust data acquisition.

Due to the technical difficulties with the slice culture approach, further consideration was given to the whole mount method. Since it was thought that the optical aberration observed might arise from the photoreceptor outer segments, a model that lacked outer segments was sought: The *Prph2*$^{rd2/rd2}$ mutant mouse, which exhibits impaired outer segment formation linked to slow retinal degeneration (Travis *et al.*, 1991), was trialled. *Prph2* encodes a structural protein required for the stabilisation and compaction of photoreceptor outer segment discs. As such it is important for the morphogenesis of rod and cone discs. Two months old *Prph2*$^{rd2/rd2}$ mice received a sub-retinal administration

of AAV 2/9 *CAG.DsRed* vector and were imaged by 2-photon fluorescence microscopy (photoreceptors uppermost) 6 days later. This was done in order to test whether the ONL can be imaged through the overlying (remaining) IPM with sufficient resolution, since it is this layer that is of primary interest for the purpose of examining donor cell migration and integration. Individual *DsRed* expressing photoreceptors were clearly identifiable across the entire retina both through the eye piece (Figure 6.3.4Fa) and when images were recorded (Figure 6.3.4Fb) (N= 1). As expected for this model, segment stumps, rather than properly formed inner and outer segments, were observed. Furthermore, only two to three photoreceptor rows are visible, in keeping with the degeneration exhibited by this model at this stage (Travis *et al.*, 1991; Hippert *et al.*, 2015) compared with around 10-12 rows exhibited by wild type mice of similar age. The *Prph2*$^{rd2/rd2}$ mutant mouse has previously been shown to support robust transplantation outcomes with rod photoreceptor integration at similar or higher levels compared to wild-type recipients, perhaps due to a compromised OLM (Barber *et al.*, 2013). The improved image quality seen here makes this model compatible with time-lapse 2-photon fluorescence microscopy for the purpose of following donor cell migration and integration into the host ONL in real time. Since complete ONL loss will eventually occur in this slowly degenerating mouse model, transplantation experiments should be restricted to early adult stages where a sufficiently thick ONL is still present.

6.3.2. Capturing the migration and integration of transplanted rod photoreceptor cells in real time

6.3.2.1. Investigating the motility of transplanted rod precursor cells by time-lapse live imaging – virally labelled Müller glia in the recipient retina

Having established the *Prph2*$^{rd2/rd2}$ mouse as a suitable transplantation model to follow the migration and integration of grafted photoreceptor cells in real time, the next step consisted of investigating whether these processes involved Müller glia. To this end, mice destined to receive rod photoreceptor transplants first received an intra-vitreal injection of AAV ShH10 *CAG.DsRed* vector at P10 in order to label Müller glia. Rod photoreceptor transplantation was then performed in mice aged between one to three months. After

another three days, their retinae were harvested, whole mounted with the photoreceptor side facing upwards and time-lapse live imaged by 2-photon microscopy at a 10 or 15-minute interval (N = 2).

Several transplanted photoreceptors that had been injected into the sub-retinal space could be observed adhering to the apical side of the neural retina (examples shown in Figure 6.3.5A & 6.3.5B). In the provided time-lapse examples, the photoreceptor cell bodies were not observed to penetrate through the OLM, which could be visualised based on the location of the end feet of DsRed labelled Müller glia. However, short dynamic processes a few µm in length were extended by some photoreceptors towards the OLM and perhaps even into the neural retina. This behaviour is indicative of chemoattractant signalling (reviewed for instance by Mortimer *et al.*, 2008), possibly occurring between the recipient retina and transplanted rod photoreceptors. Similar host OLM-directed process extension have been reported previously in fixed tissue analyses (Barber *et al.*, 2013; Warre-Cornish *et al.*, 2014).

It was also noted that, on occasion, DsRed labelled Müller glia, as well as GFP labelled transplanted rod photoreceptors, disappeared between consecutive time frames during the time-lapse recordings, as indicated by the asterisks in Figure 6.3.5A & 6.3.5B. The rate at which fluorescent protein signals disappeared (within 15 minutes) is more compatible with cell death, whereby the cellular contents of the dying cell are potentially released into and diluted within the surrounding, rather than down-regulation of *DsRed* or *GFP* expression, since fluorescent proteins are usually relatively stable with half-lives of around 24 hours (Corish and Tyler-Smith, 1999). This progressive loss of a number of fluorescent protein labelled cells likely reduced the ability to image potential photoreceptor migration and integration events.

Thus, although a platform has now been established for the real time observation of dynamic cellular behaviours of transplanted photoreceptors in explanted recipient retinae, extending tissue life span *ex vivo* will be a key factor influencing the success rate, with which such behaviours can be witnessed.

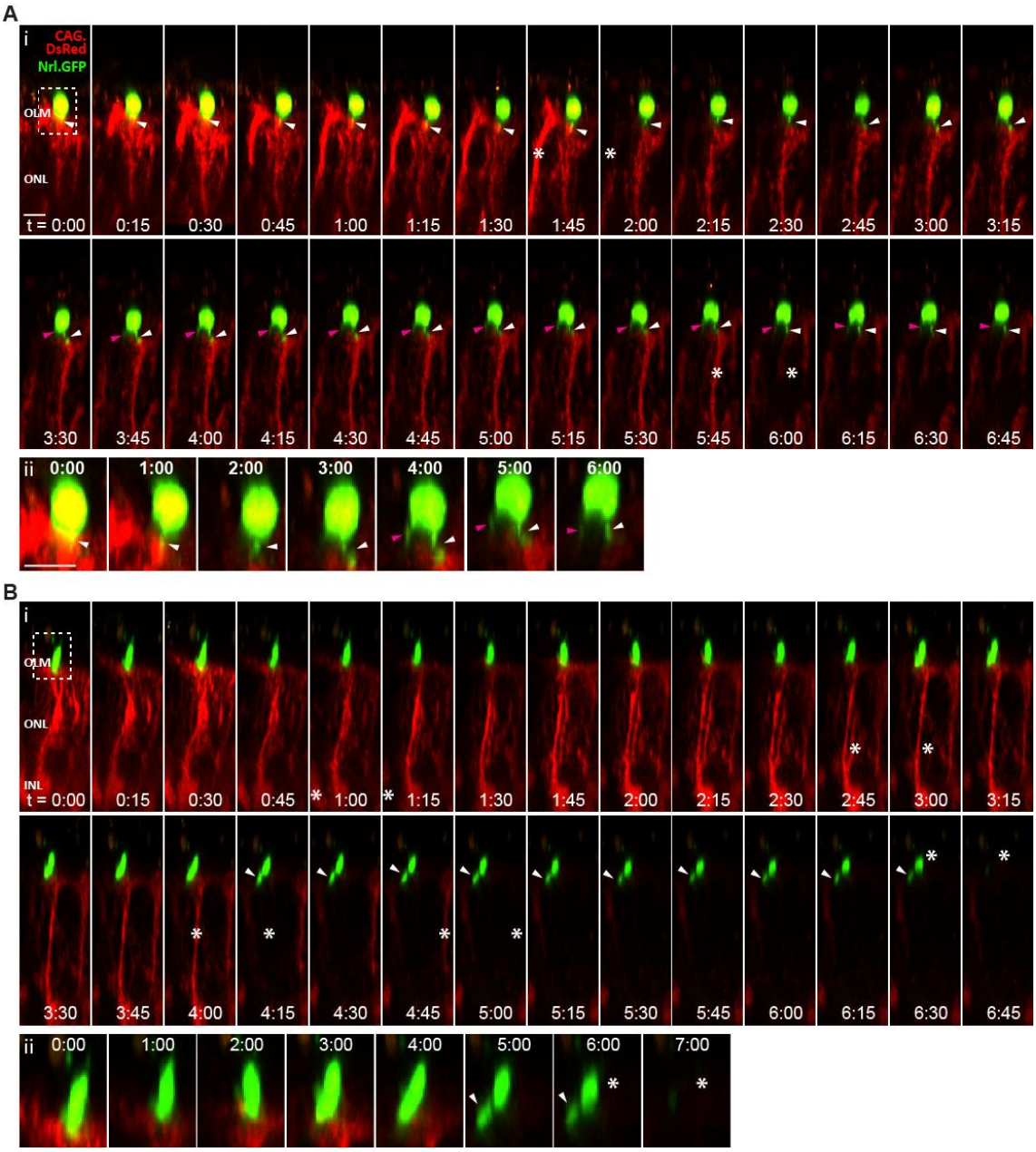

Figure 6.3.5 Transplanted rod photoreceptor precursor cells located within the subretinal space exhibit dynamic process extension towards the OLM. *Prph2*$^{rd2/rd2}$ mice previously injected intra-vitreally with AAV ShH10 *CAG.DsRed* at P10 to label Müller glia (red), received a sub-retinal injection of *Nrl.GFP*$^{+/+}$ rod precursor cells (green) at two to three months of age. Three days post transplantation harvested retinae were whole mounted and time-lapse live imaged by 2-photon microscopy at 15 min intervals. **(Ai, Bi)** Grafted rod photoreceptor precursor cells were found apical to the neural retina, from where they extended dynamic processes towards the neural retina (white and magenta arrow heads). **(Aii, Bii)** Higher magnification views of boxed regions of interest in (Ai) and (Bi). It was noted that both transplanted photoreceptors and Müller glia of the recipient eye often vanished between consecutive time frames (white asterisks). OLM = outer limiting membrane, ONL = outer nuclear layer, INL = inner nuclear layer, Scale bars, 10 µm.

6.3.2.2. *Investigating the motility of transplanted rod precursor cells by time-lapse live imaging – efforts to increase tissue viability and labelling the retina using a mitochondrial vital dye*

The disappearance of DsRed labelled Müller glia, as well as GFP labelled rod photoreceptor cells, in the time-lapse recordings performed up to this point was hypothesised to be attributable to deteriorating tissue health in the *ex vivo* environment. In order to extend the life span of explanted retinae and grafted photoreceptors in the time-lapse live imaging experiments, the imaging medium was supplemented with 5 % FCS. Furthermore, the image stack recording interval between time frames was increased from 10-15 minutes to 20 minutes in order to reduce the frequency and total duration of exposure to the laser light source, in order to reduce phototoxicity.

As previously, rod photoreceptor transplantation was performed in adult Prph2$^{rd2/rd2}$ mice at up to three months of age. Their retinae were harvested 3 days following surgery, whole mounted with the photoreceptor side facing upwards and time-lapse live imaged by 2-photon microscopy. Rather than labelling the Müller glia of the recipient retinae virally using AAV ShH10 *CAG.DsRed,* harvested retinae were acutely treated with 5 µM Mitotracker® Orange CMTMRos as described in section 6.3.1.1, in order to label retinal structures, most importantly the IPM and the ONL (N = 1). Note that it was difficult for all elements of this experiment to work according to plan (correctly aged donor and recipient mice, success of the transplantation, tissue processing for live imaging, imaging a field of view where integration occurs) and hence only one successful experimental repeat was performed prior to completion of this thesis. As shown in Figure 6.3.6A, Mitotracker ® Orange CMTMRos clearly labelled the entire neural retina from the IPM to the GCL at the opposite limit of the tissue, although the ONL appeared to have been labelled most intensely. As expected, vital dye labelling was also detected in transplanted *Nrl.GFP*$^{+/+}$ derived rod photoreceptor cells, which were often located apical to the retinal tissue and adjacent to the IPM at the beginning of the recording period. In agreement with previous findings, grafted rod photoreceptor cells frequently extended processes towards the OLM (Warre-Cornish *et al.*, 2014; section 6.3.2.1)**.** During the time-lapse recording, grafted rod photoreceptor cells located apical to the IPM were on occasion observed to dynamically move through the IPM and mostly towards or in parallel to the OLM

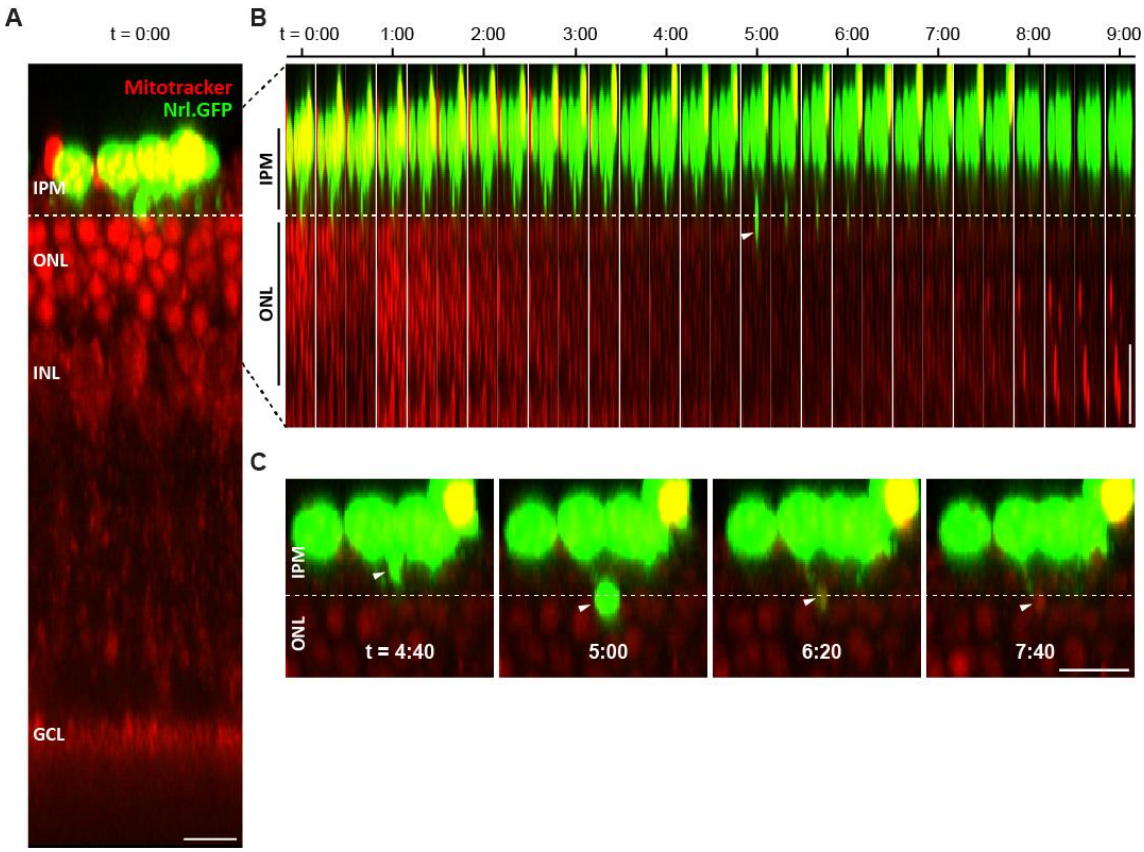

Figure 6.3.6 Transplanted rod photoreceptor precursor cells migrate through the IPM towards the OLM. *Prph2*$^{rd2/rd2}$ mice were administered a sub-retinal injection of Nrl.GFP positive rod precursor cells (green) at two to three months of age. Three days post transplantation, harvested retinae were acutely labelled with Mitotracker Orange CMTMRos (red), whole mounted and time-lapse live imaged by 2-photon microscopy at 20 min intervals and in presence of 5 % FCS. **(A)** A group of grafted rod cells on top of the neural retina directly adjacent to the IPM at the very beginning of the time-lapse recording. Photoreceptor processes had previously been extended towards the OLM (white dashed line). **(B)** Time-lapse montage of the same field of view as depicted in (A) but shown as a series of narrow strips. One grafted photoreceptor soma was observed to traverse the IPM between time points 4:40 and 5:00 h (white arrow head). **(C)** High magnification view of selected time points taken from the time-lapse series in (B). White arrowhead indicates the position of the motile rod photoreceptor. IPM = interphotoreceptor matrix, ONL = outer nuclear layer, INL = inner nuclear layer, GCL = ganglion cell layer. Scale bar, 10 µm.

(n = 4 cells). In the representative time-lapse series shown in Figure 6.3.6B (and at higher magnification and with selected time points in Figure 6.3.6C), an individual rod photoreceptor precursor cell can be seen to migrate from the donor cell mass located in the subretinal space, through the IPM towards the OLM between time points 4:40 and 5:00 h. All of the observed movements happened rapidly, between time frames and spanned a relatively short distance of up to approximately 5 µm. For reasons currently not well understood, *GFP* expression disappeared from some of the migrating rod photoreceptors, especially those that quite closely approached the OLM, at least under the pre-set GFP detection parameters. One possible explanation for this could be the leakage of GFP from the grafted photoreceptor into cells of the recipient neural retina by a presently unknown material transfer mechanism (Pearson *et al.*, 2016). However, there were no concomitant changes (increase) in GFP signal in cells of the recipient neural retina that were proximal to those grafted rod photoreceptor cells that exhibited reductions in GFP signal levels. More generally, it can be stated that there was no detectable transfer of GFP from transplanted to recipient photoreceptor cells at all during this experiment.

In addition to migration within the IPM, transplanted rod photoreceptor cells were sometimes observed to penetrate through the OLM and into the ONL (n = 4 cells). Two representative example cells are displayed within the same region of interested shown in Figure 6.3.7 (Movie 6.3.1). Here, both rod photoreceptors were initially located within the IPM and in close proximity to the OLM (Figure 6.3.7A). However, during the course of the time-lapse recordings, first the cell to the right and, subsequently, the cell to the left moved from the IPM into the ONL (Figure 6.3.7B; between time points 1:40 - 2:00 h and 6:40 - 7:00 h, respectively). The movement of the rod photoreceptor soma was often preceded by the extension of a short process towards the future site of entry into the recipient retina (examples shown in Figure 6.3.7Ci & Figure 6.3.7Cii). In each case, the somal movement occurred abruptly, usually within a relatively short period of up to 20 minutes and with a high degree of directionality. Future repeat experiments will need to demonstrate whether these kinetics hold across all integration events. Within this experiment, rod photoreceptor cell penetration into the ONL of the recipient retina was restricted to the first row of photoreceptors. Although purely speculative at this stage, it is entirely possible that migration past the first photoreceptor row occurs over a period that exceeds the maximum imaging duration (~ 12 h), which is limited by how long the retinal explants can be kept viable.

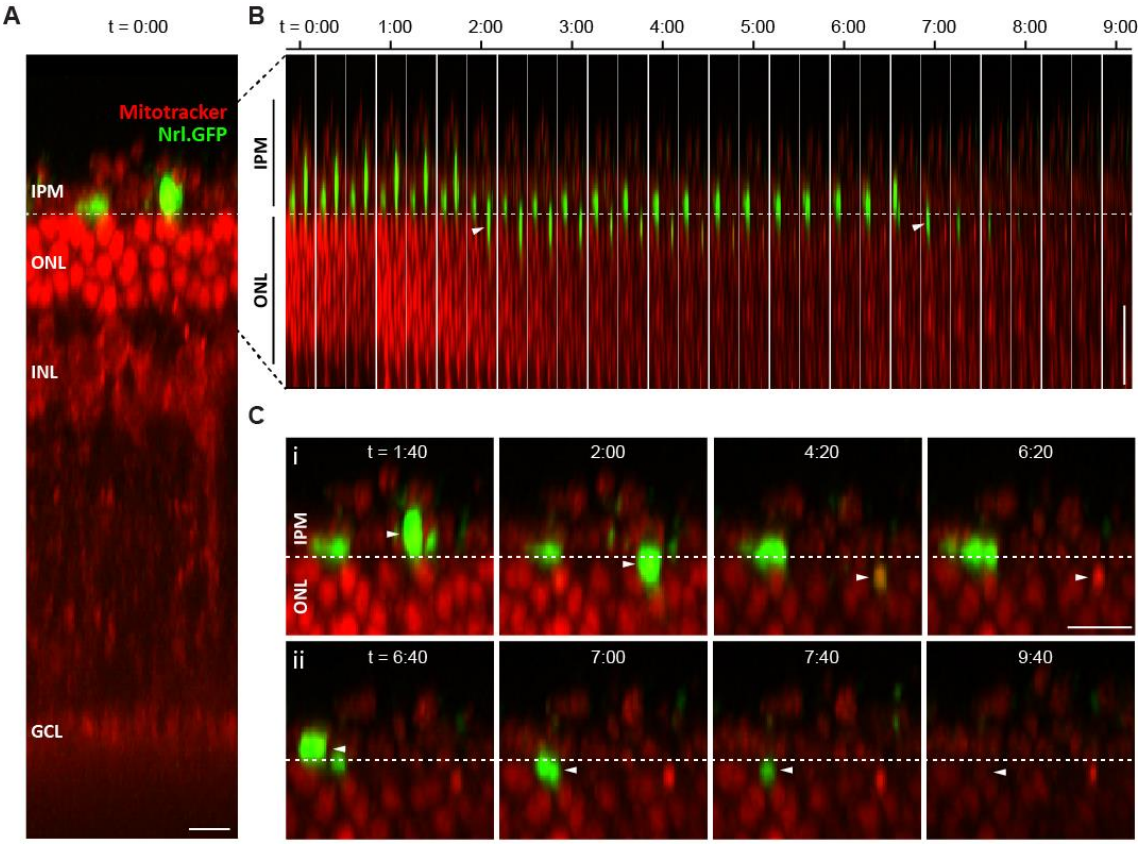

Figure 6.3.7 Transplanted rod photoreceptor precursor cells migrate from the IPM into the ONL. *Prph2*$^{rd2/rd2}$ mouse were administered a sub-retinal injection of Nrl.GFP positive rod precursor cells (green) at two to three months of age. Three days post transplantation, harvested retinae were acutely labelled with Mitotracker Orange CMTMRos (red), whole mounted and time-lapse live imaged by 2-photon microscopy at 20 min intervals and in presence of 5 % FCS. **(A)** Two rod photoreceptor cells within the IPM and apical to the OLM (white dashed line) at the very beginning of the time-lapse recording. **(B)** Time-lapse montage of the same field of view as depicted in (A) but shown as a series of narrow strips. Both grafted photoreceptor somata penetrated through the OLM and into the ONL at the 2:00 and 7:00 time points following initial process extension (white arrow head). **(C)** High magnification view of selected time points taken from the time-lapse series in (B), focussing on the right cell **(Ci)** and on the left cell **(Cii)**. White arrowheads indicate the position of the motile rod photoreceptor. IPM = interphotoreceptor matrix, ONL = outer nuclear layer, INL = inner nuclear layer, GCL = ganglion cell layer. Scale bar, 10 µm.

As described earlier within this section, transplanted rod photoreceptor cells that migrated into the ONL of the recipient retina gradually lost detectable GFP signal ~ 3 hours after penetrating through the OLM (Figure 6.3.7B & 6.3.7C). However, Mitotracker® Orange CMTMRos labelling was maintained in those cells, and served as a placeholder, showing the continued presence of the rod photoreceptor cell within the ONL. As before, GFP was not observed moving from donor rod photoreceptor cells that had migrated into the recipient ONL into neighbouring host cells.

Taken together, these data provide the first real time evidence that grafted photoreceptor cells can indeed migrate and integrate into the neural retina of mouse transplantation recipients, as was suggested previously based on fixed tissue analyses (Warre-Cornish *et al.*, 2014). Within the limitations of the experimental set-up used, evidence of material transfer of GFP between transplanted and resident photoreceptor cells was not observed.

6.4. Characterisation of rod photoreceptor motility following transplantation – an *in vitro* approach

6.4.1. Rod photoreceptors migrate along Müller glia in vitro

Following the *in vivo* sub-retinal transplantation of freshly isolated *Nrl.GFP*$^{+/+}$ rod photoreceptors, those cells that appeared to have integrated into the ONL of the recipient mouse retina were frequently found closely aligned with the apical process of a resident Müller glia cell (Warre-Cornish, PhD thesis, 2013; see also section 6.3). This led to the hypothesis that donor photoreceptors utilised the radial processes of Müller glia to migrate within the ONL following penetration through the OLM. The migration of rod photoreceptors along Müller glia was then also investigated in a more reductionist *in vitro* transplantation model. It consisted of culturing freshly isolated rod photoreceptors obtained from P8 *Nrl.GFP*$^{+/+}$ mice (identified as the ideal donor cell developmental stage; Pearson, unpublished data) onto pre-established Müller glia primary cultures (Warre-Cornish, PhD thesis, 2013). The Müller cells were plated onto a cell culture dish previously coated with stripes of laminin, which enforces an elongated cell morphology thought to best resemble the *in vivo* state. Müller glia cells were obtained from *Rlbp.GFP*$^{+/+}$ reporter mice, in which *GFP* expression is under transcriptional control of the Müller glia specific *Rlbp1* promoter (Vazquez-Chona *et al.,* 2009). The co-cultures were subjected to real time live imaging in epifluorescence and brightfield mode using the portable JuLi^{TM} Digital Fluorescence Microscope to generate time-lapse movies.

Rlbp.GFP$^{+/+}$ mouse derived Müller glia and *Nrl.GFP*$^{+/+}$ derived rod photoreceptors both express *GFP* at the time of their respective isolations by FACS. However, at the time when rod photoreceptors were added to the pre-established Müller glia cultures (usually after 2-3 weeks), *GFP* expression levels had become undetectable in the Müller glia. In combination with the fact that cultured Müller glia develop long, extended morphologies, whereas rod photoreceptor somata are small and almost spherical in shape, distinguishing between the two cell types was relatively easy (Figure 6.4.1A). Furthermore, rod photoreceptors frequently extended fine neurites on the Müller glia substrate cells, which were, however, only visible using confocal microscopy (Figure 2.5.1C). As demonstrated previously, rod photoreceptors located on Müller glia were motile (Figure 6.4.1Bi),

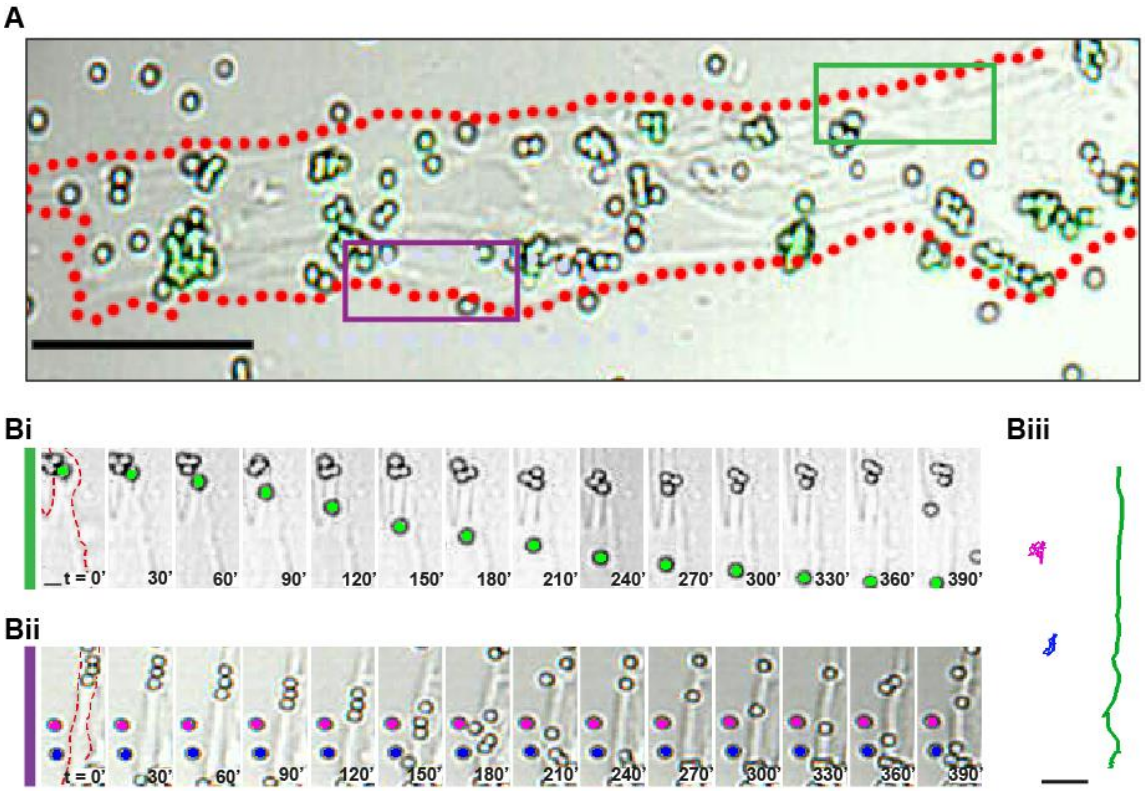

Figure 6.4.1 Isolated rod photoreceptors obtained from P8 *Nrl.GFP*$^{+/+}$ mice migrate on pre-established *Rlbp.GFP*$^{+/+}$ mouse derived Müller glia cultures. **(A)** Müller glia (cell(s) within the red dotted line) form long extended morphologies when plated onto laminin substrate and when cultured for 2-3 weeks. Freshly isolated rod photoreceptors, are small and largely spherical in appearance. Furthermore, the rod photoreceptors are GFP positive, whereas the Müller glia have lost *GFP* expression during the culturing period. **(Bi-Biii)** Co-cultures were subjected to time-lapse live imaging. The motility of few selected, pseudo-coloured rod photoreceptors was manually tracked *in silico*. Bi shows a rod cell (green pseudo-colour) migrating on a Müller cell process (red dotted line). Bii shows two stationary rod photoreceptors (magenta and blue) next to a Müller cell process. Biii depicts the trajectories of the selected rod cells in Bi and Bii. Scale bars, 50 µm (A) and 5 µm (B).

whereas those found on the culture dish were stationary (Figure 6.4.1Bii). According to Warre-Cornish (PhD thesis, 2013) motile rod cells exhibited elongated somata, whereas stationary rod cells displayed rounder somata. Manually tracked example cells and their trajectories (Figure 6.4.1Biii) are shown here just to verify the previous finding that rod photoreceptors migrate along cultured Müller glia (Warre-Cornish, PhD thesis, 2013). In that previous study, a full description of the kinetic properties of this movement, based on the manual tracking of selected rod photoreceptors, was provided. However, the purpose here was to use this *in vitro* co-culture transplantation model to identify molecular mechanisms that underlie Müller glial-guided rod photoreceptor migration by screening various gain/loss of function approaches that could potentially affect rod motility. This necessitated the development of a faster, more objective, and user friendly rod photoreceptor tracking methodology, that was ideally at least semi-automated.

The following section discusses the development of this new tracking methodology.

6.4.2. Development of a semi-automated tracking methodology

As depicted in Figure 6.4.1A, cultured rod photoreceptors, when imaged through the JuLi^{TM} Digital Fluorescence Microscope, had a small, spherical morphology and expressed *GFP*. The GFP signal from each individual cell appeared as a single punctum, which should be easily traceable using one of the many tracking methods available.

However, it was noted that a large proportion of cultured rod photoreceptors were unable to retain *GFP* expression during the course of the time-lapse recordings (Figure 6.4.2). Although the reason for this behaviour could not be elucidated, it was speculated that rod photoreceptors, like the *in vitro* Müller glia, may down-regulate the expression of *GFP* during extended culturing periods. What remained following the loss of rod photoreceptor *GFP* expression was a soma with seemingly normal spherical morphology. Thus, rather than tracking the *xyt* coordinates of GFP puncta to monitor the change in rod photoreceptor location over time, the spherical brightfield signal (circular in 2D) was used to follow the movements of rod photoreceptors. The brightfield signal of all cultured rod photoreceptors was uniform: the cell border appeared as a dark rim while the cytosol was bright in appearance by comparison. However, local and temporal differences in light scattering, diffraction and/or absorption led to small variations in the brightfield signal

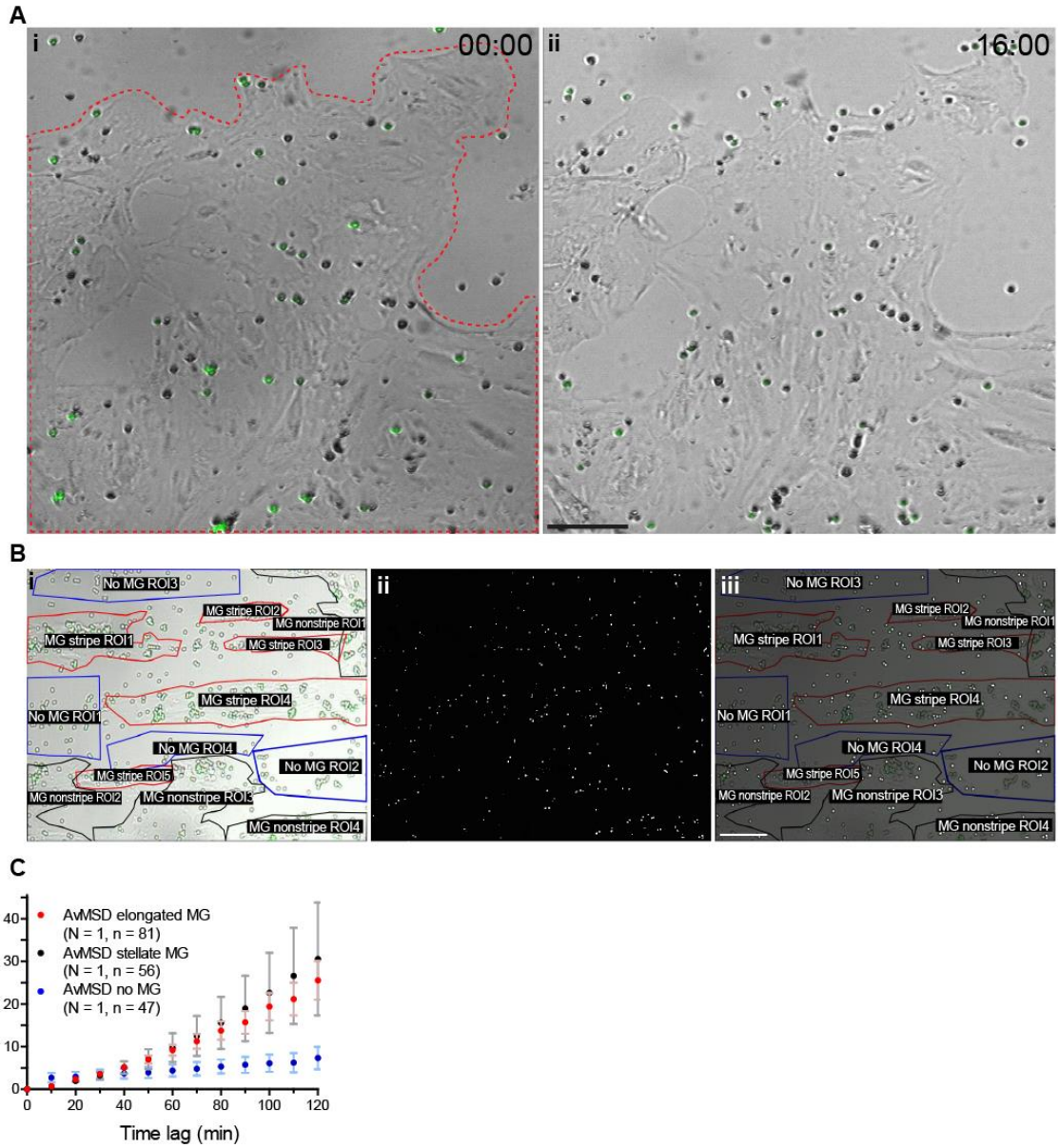

Figure 6.4.2 Semi-automated tracking of rod photoreceptors in rod-Müller glia co-cultures. Nrl.GFP positive rod photoreceptors isolated from P8 *Nrl.GFP*$^{+/+}$ mice were co-cultured with a pre-established Müller glia primary culture (13DIV); co-cultures were live imaged by time-lapse microscopy. **(A)** GFP signal vanished from many rod photoreceptors during the time-lapse recording. Note: the panels shown in (A) were taken from a different co-culture time-lapse recording to B and C. **(B)** Conversion of the brightfield image (i) into a binary image where only isolated rod photoreceptors are selectively shown (ii & iii). **(C)** Mean squared displacement (MSD) analysis of rod photoreceptor motilities as observed within defined regions of interest (ROIs) within the imaged field of view (see Bi): red = ROIs containing elongated/striped Müller glia, blue = stellate-shaped Müller glia, black = no Müller glia. Data are displayed as mean ± SEM. Scale bars, 50 µm.

produced by rod photoreceptors (data not shown). This would make it difficult to define optimal tracking parameters to specifically monitor the movement of rod photoreceptors, since chosen parameters would have to account for these variations. Instead, a simple binary field of view was generated from the original brightfield time-lapse recordings, whereby the brightfield signals produced by rod photoreceptors, but not by Müller glia or the cell culture dish, were converted into white puncta over a black background (Figure 6.4.2B). This was accomplished using a series of image processing steps in Fiji (Schindelin *et al.*, 2012), which progressively highlighted individual rod photoreceptor somata, while ignoring what remained within the field of view (see Chapter II, section 2.7.4 and Figure 2.7.3).

The white rod photoreceptor puncta of the binary time-lapse recordings were tracked using the Mosaic Particle Tracker 2D and 3D plugin (Sbalzarini and Koumoutsakos, 2005) in Fiji in order to extract *xyt* parameters of individual rod photoreceptors. Based on the brightfield time-lapse recording, regions of interest were generated to define whether rod photoreceptors were located on the culture dish or on Müller glia; in the latter case, a qualitative distinction between stellate and elongated cells was made in order to investigate whether elongated Müller cells are the preferred substrate for rod migration (Figure 6.4.2Bi). As depicted in figure 6.4.2C, the mean squared displacement (MSD) profile of rod photoreceptors on Müller glia was markedly steeper compared with the MSD profile of rod cells found on the culture dish (N = 1 independent co-culture; n = 81 rod cell trajectories on elongated, n = 56 for stellate Müller glia; n = 47 for culture dish; note that the newly developed rod tracking methodology was initially tested only on this single co-culture, but then also verified on and expanded to all other co-culture time lapse recordings (see section 6.4.3)). In addition, there was also a slight positive curvature of the MSD profiles produced by rod photoreceptors located on Müller glia, which is indicative of a directed motion regulated by active motility mechanism(s) (see Figure 6.4.1Bi & Bii for representative examples) (Ruthardt *et al.*, 2011). The MSD profiles of rod cells located on elongated and stellate shaped Müller glia were similar. Hence, the shape of the Müller glia substrate cells does not influence the kinetics of rod photoreceptor movement.

Taken together, a semi-automated tracking methodology was successfully developed, which is capable of quantifying the rod photoreceptor motile behaviour when co-cultured with pre-established Müller glia primary cells.

6.4.3. Characterisation of the putative Müller glial guided rod photoreceptor migration in vitro

6.4.3.1. Rod photoreceptor migration on different substrates

Having established that the semi-automated rod photoreceptor tracking methodology developed here is capable of quantifying *in vitro* rod motility, the next issue to tackle was the specificity of the rod-Müller glia interaction within the *in vitro* transplantation model. Within the intact neural retina, the somata of rod photoreceptors are exclusively located within the ONL. Hence, rod cell bodies should only ever come in contact with Müller glia, cone photoreceptors or other rod photoreceptors, but not with other retinal neurons. Thus, to test whether rod migration along Müller glia is a cell type specific interaction, the motility of rod photoreceptors on Müller glia was compared to the motility displayed on other retinal neurons, on the Müller glia culture dish but away from the glia, as well as on laminin coated dishes (Figure 6.4.3A-C). Retrospective analysis using the new semi-automated tracking methodology was performed on time-lapse recordings of retinal neuron containing co-cultures or laminin-only cultures previously acquired by Warre-Cornish (PhD thesis, 2013).

As demonstrated by the steepness of the produced MSD curves, the motility of rod photoreceptors, when co-cultured with Müller glia, is more pronounced on the glia (N = 4 independent co-cultures, n = 739 trajectories) compared with areas of the culture dish devoid of glial substrate (N = 3, n = 395) (referred to as 'Non-Müller glia substrate' in Figure 6.4.3). Similar to that shown in Figure 6.4.2C, the MSD profile of rod photoreceptors located on Müller glia exhibited a slight positive curvature, which is indicative of directed, rather than random or attenuated, cellular motions (Ruthardt *et al.*, 2011). Primary cultures of retinal neurons were produced by isolating GFP negative cells from a preparation of dissociated retinae from *Rlbp.GFP*$^{+/+}$ mice and by exposing these cells to a medium that favours neuronal survival and is biased to RGC differentiation (Heng *et al.*, 1999; Khan *et al.*, 2012). The MSD profile produced by rod photoreceptors added to such cultures was less steep than the profile produced on the Müller glia substrate (N = 2, n = 110). Furthermore, the MSD curve had negative curvature, which is indicative

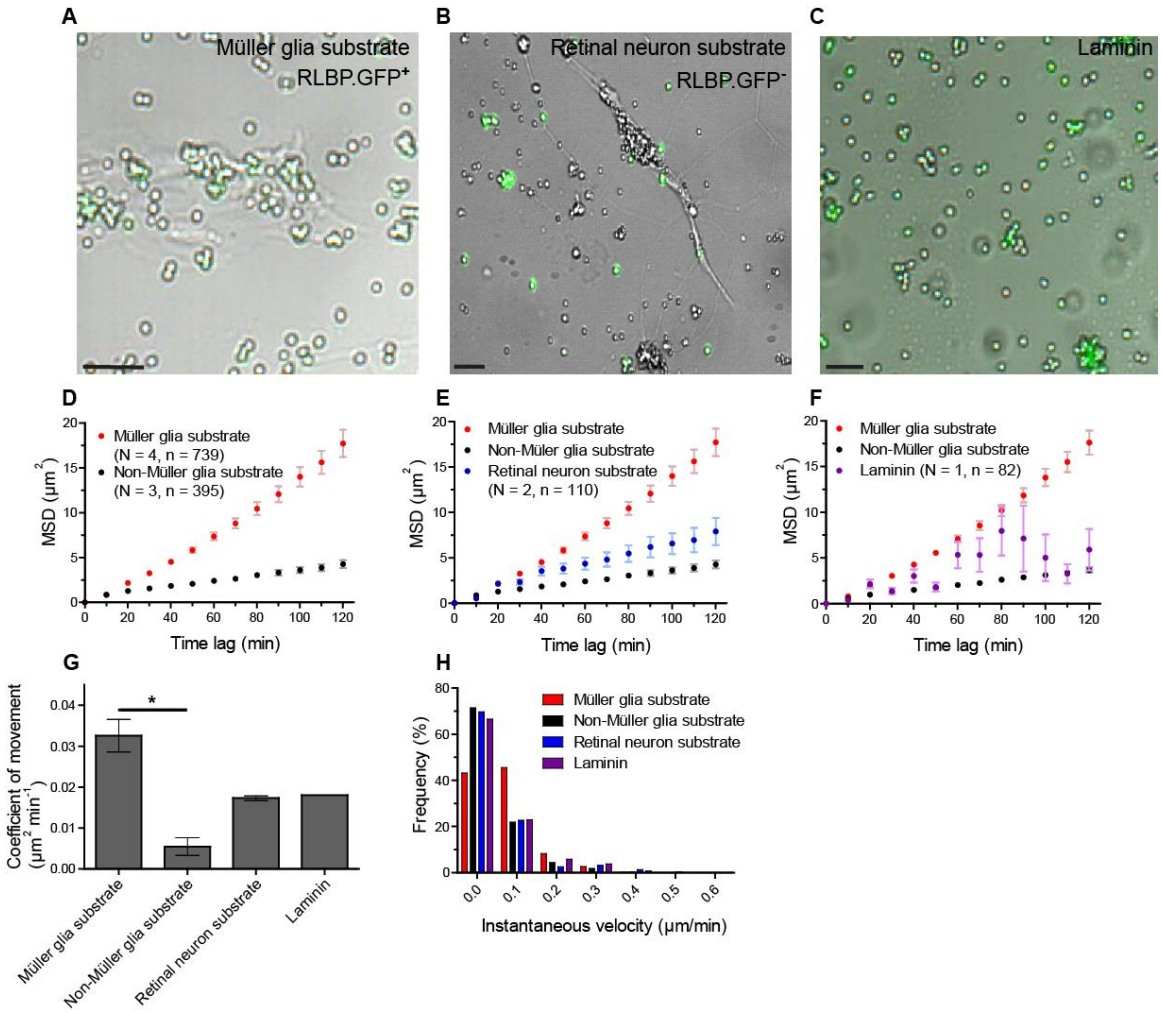

Figure 6.4.3 Rod photoreceptor motility on different substrates. Nrl.GFP positive rod photoreceptors isolated from P8 mice were co-cultured either with **(A)** pre-established Müller glia primary cultures from *RLBP.GFP*$^{+/+}$ mice (GFP positive cell population), **(B)** pre-established retinal neuron primary cultures from *RLBP.GFP*$^{+/+}$ mice (GFP negative cell population, or **(C)** plated out on a laminin pre-coated dish without additional cellular substrate; co-cultures were live imaged by time-lapse microscopy. **(D-F)** The motility of rod photoreceptors was assessed by mean squared displacement (MSD) analysis for rod cells that were on top of or adjacent to Müller glia (i.e. on the culture dish) (D), on retinal neurons (E), or on the laminin coated dish (F). Data are displayed as mean ± SEM. **(G)** Comparison of coefficient of movement values associated with AvMSD profiles in D-F. Data are displayed as mean ± SD. 1-way ANOVA (post test: Dunn's) was used for statistical analysis. *$p < 0.05$. **(H)** Instantaneous velocities displayed by rod photoreceptors on different substrates. Scale bars, 25µm.

of attenuated motion. Rod photoreceptors that were plated on laminin in absence of other substrate cells frequently alternated between settling down on the dish and moving rapidly with what appeared to be convection currents (N = 1, n = 82) (see also, Warre-Cornish, PhD thesis, 2013). This presumably resulted in the inconsistent MSD profile depicted in Figure 6.4.3F.

The MSD data points were fitted with straight lines between time lag 0 and 100 minutes (acknowledging that the MSD curves were not all straight lines). The slopes of these lines were used to derive coefficient of movement values, enabling a comparison of the motilities of rod photoreceptors cultured on the different substrates. Rod cells on the culture dish had a significantly reduced coefficient of movement compared with rod photoreceptors found on Müller glia (0.033 ± 0.008 vs. 0.005 ± 0.002 $\mu m^2 min^{-1}$; $p < 0.05$, 1-way ANOVA with Dunn's post test). Rod migration on retinal neurons (0.017 ± 0.001 $\mu m^2 min^{-1}$), as well as on laminin alone (0.018 $\mu m^2 min^{-1}$; N = 1), was markedly, but not significantly, reduced in comparison to rod migration on Müller glia.

Next, the instantaneous velocity of rod somal movements was assessed. All recorded velocity values were placed into a histogram divided into equally sized 0.1 µm/min wide bins (Figure 6.4.3H). 60-70% of instantaneous velocity measurements for rod photoreceptors on non-Müller glia substrate (on the dish of Müller glia cultures), retinal neuron substrate and on laminin could be placed into the 0.0 µm/min bin; progressively smaller contributions were then recorded in the higher velocity bins. By contrast, only 43.2 % of the instantaneous velocities displayed by rod photoreceptors located on Müller glia fell into the 0.0 µm/min bin, while 45.6 % fell within the 0.1 µm/min bin, which represents a more than a 2-fold increase compared with the other three categories. I*n vitro* rod migration along Müller glia thus proceeds at velocities within the same range as cortical glial-guided neuronal migration (0.1-0.25 µm/min; Chen *et al.*, 2008 & Franco *et al.*, 2011).

In sum, the data shown in this section demonstrate that freshly isolated rod photoreceptors are motile specifically when they are located on Müller glia primary cells, but less so when they are located on other retinal neurons or just on laminin alone. Furthermore, the kinetic parameters of rod motility on Müller glia as determined using the semi-automated tracking methodology were remarkably similar to the previously described manual tracking method (Warre-Cornish, PhD thesis, 2013). This *in vitro* transplantation model thus continues to lend support to the hypothesis that rod photoreceptors transplanted *in*

vivo migrate along resident Müller glia of the recipient neural retina en route to becoming integrated (Warre-Cornish, PhD thesis, 2013).

6.4.3.2. *Migratory capacity of rod photoreceptors isolated at different early post-natal stages*

Rod photoreceptors to be used in pre-clinical mouse transplantation studies have been routinely obtained from donor animals (MacLaren *et al.*, 2006; Pearson *et al.*, 2012). Transplantation of rod cells isolated from P8 mice resulted in the highest number of donor reporter labelled cells in the recipient retina, while cells obtained from younger or older animals integrated into the recipient retina in markedly lower numbers (MacLaren *et al.*, 2006; Pearson, unpublished works). This indicates a requirement for transplanted photoreceptors to be at the correct ontogenetic stage to achieve the best possible grafting outcome (Pearson *et al.*, 2012). The integration, and the presumed preceding migration, of transplanted rod photoreceptors, once within the host retina, were proposed to be dependent on Müller glia guidance (Warre-Cornish, PhD thesis, 2013). It should be noted, however, that the apparent integration outcome is heavily influenced by material transfer, the potency of which may also depend on the ontogenetic stage of the rod donor cells (Pearson *et al.*, 2016). Thus, rod cells isolated at different post-natal developmental stages might be expected to display different kinetics of migration on cultured Müller glia. To test this, the migratory parameters of P8 rod photoreceptors on Müller glia within the co-culture model was compared to those of P4, P10-11 and P14 cells.

As shown in Figure 6.4.4A, the MSD profiles produced by the P4, P8 and P10-11 rod photoreceptor populations were similar; positive curvatures were detected for all three MSD curves (P4: N = 2 independent co-cultures, n = 141 trajectories, P8: N = 4, n = 739; P10-11: N = 2, n = 116). This suggests that all three rod populations are capable of directed, rather than random, cellular motions along Müller glia. By contrast, the MSD curve produced by P14 rod cells was noticeably shallower as well as more linear, indicating their migration was attenuated and more stochastic in nature (N = 1, n = 127). In keeping, the coefficient of movement values associated with P4, P8 and P10-11 rod photoreceptors, which were obtained by fitting straight lines between time lags 0 and 100, were similar (P4: 0.035 ± 0.012 $\mu m^2 min^{-1}$, P8: 0.033 ± 0.008 $\mu m^2 min^{-1}$, P10-11:

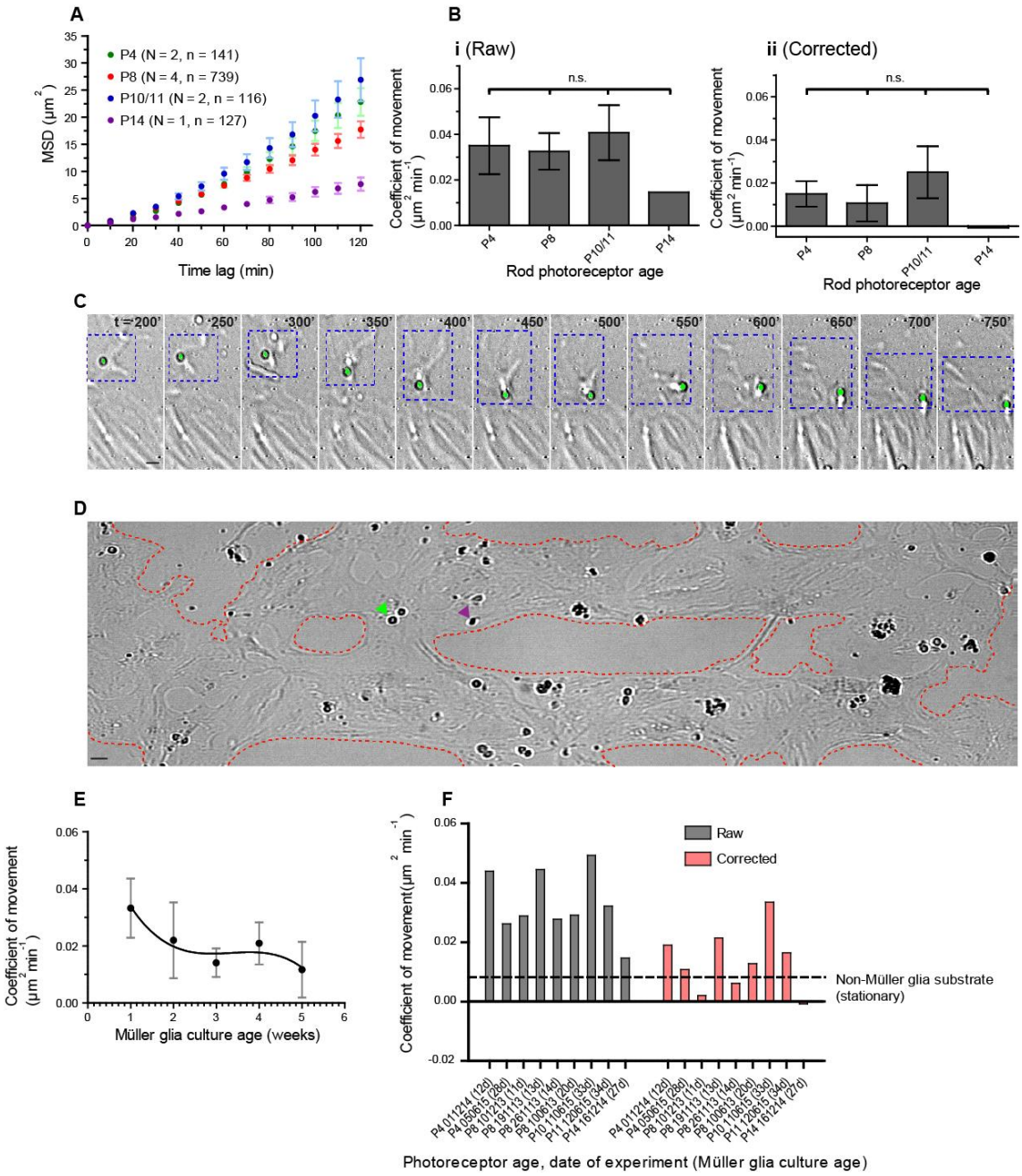

Figure 6.4.4 Motility of rod photoreceptors obtained from *Nrl.GFP*$^{+/+}$ mice at different post-natal stages and co-cultured with pre-established Müller glia primary cultures. Quantification of Müller glia morphological plasticity vs. rod photoreceptor (P4-P14) motility. **(A)** Mean squared displacement (MSD) analysis for rod cells isolated at different stages of post-natal development, which were on top of Müller glia. Data are displayed as mean ± SEM. **(B)** Comparison of coefficient of movement values associated with AvMSD profiles in A (1-way ANOVA; post test: Dunn's). i and ii show pooled raw data and baseline corrected data according to F (see section 6.4.3.3). Data are displayed as mean ± SD. **(C)** A rod photoreceptor cell on top of a Müller cell appeared to be displaced passively by local Müller glia morphological plasticity (boxed region of interest). **(D)** Cells in Müller glia primary cultures alone were covered with particles of cellular (green arrow head) or debris-like (purple) appearance. **(E)** Coefficient of movement standard curve derived from AvMSD values of particles found on Müller glia cultured for 1-5 weeks. Data are displayed as mean ± SD. **(F)** Comparison of coefficient of movement values before and after arithmetic correction using the standard curve in (E). (Figure legend continues on following page)

←

(Figure 6.4.4 figure legend continued). The dotted line indicates the coefficient of movement value displayed by rod photoreceptors located next to a Müller cell rather than on top of it (see Figure 6.4.2D, G, H); such cells were considered to be stationary (Figure 6.4.1). Scale bars, 10 µm.

0.041 ± 0.012 $\mu m^2 min^{-1}$), whereas it was reduced for P14 cells (0.015 $\mu m^2 min^{-1}$) (Figure 6.4.4Bi; all not significant, 1-way ANOVA with Dunn's post test).

In isolation, these results suggest that rod photoreceptors obtained from P4- P11 mice are similarly capable of migrating along cultured Müller glia, while rod cells obtained from older animals are less motile.

6.4.3.3. The rod-Müller glia co-culture migration assay – an imperfect model for the analysis of potential Müller glia guided rod migration

Upon first inspection, the results presented in the previous section, suggested that the co-culture migration assay combined with the semi-automated rod tracking methodology can be used to describe the kinetics of Müller glia-guided rod photoreceptor migration *in vitro*. However, this experimental model was confronted with two major obstacles: 1) it proved to be difficult to time-coordinate the age of freshly isolated rod photoreceptor cells with the optimal *in vitro* age of cultured Müller glia (approximately 2-3 weeks, according to Warre-Cornish (PhD thesis, 2013)). At the expense of having optimally aged Müller glia, it was considered more important to have rod photoreceptors obtained from mice at accurately timed developmental stages. 2) during the course of this study an updated live cell imager with superior optic resolving power became available (JuLi™FL, BR; NanoEnTek Inc., Korea). With this superior imaging capability, it became apparent that apparent rod photoreceptors seemingly migrating along Müller glia were frequently accompanied by morphometric changes in the underlying Müller glia (Figure 6.4.4C, boxed region of interest). In other words, rod photoreceptor motility within this co-culture model may, to some extent, be a passive phenomenon, driven by plastic changes of Müller glia shape and form.

To investigate this further, there first needed to be a way to accurately quantify how dynamic cultured Müller glia cells were. When Müller glia primary cells were cultured in isolation, small cellular or debris-like particles were often detected on the surface of the glia even without the addition of rod photoreceptors (green and purple arrow heads in Figure 6.4.4D). Just like photoreceptors, these particles were motile and their movements could be tracked using the semi-automated tracking method developed within this study. Assuming that the motility of such particles is completely due to Müller glia morphometric changes, this provided a measure of the plastic behaviour of Müller cells, which would have to be subtracted when quantifying true rod photoreceptor movements. A coefficient of movement versus culture age standard curve was produced using MSD analysis on time-lapse recordings of Müller glia between 1 to 5 weeks of *in vitro* culture (Figure 6.4.4E; 1 week: N = 3, n = 599; 2 weeks: N = 3, n = 437; 3 weeks: N = 3, n = 242; 4 weeks: N = 2, n = 143; 5 weeks: N = 2, n = 148). This covers the whole range of Müller cell culture ages used in the co-culture experiments. The obtained coefficients of movement between the individual time points were variable but appeared to reduce, from a starting value of 0.033 ± 0.010 $\mu m^2 min^{-1}$ at 1 week, down to 0.012 ± 0.010 $\mu m^2 min^{-1}$ by 5 weeks of culture. The data points were fitted with a third order polynomial non-linear regression curve (Müller cells did visibly appear more plastic at week 4 compared to weeks 3 and 5), which served as the base line standard curve to arithmetically correct the perceived rod photoreceptor motility for Müller glia plasticity.

As can be seen in Figure 6.4.4F, all uncorrected, individual co-culture time-lapse recordings exhibited coefficient of movement values that were well above the coefficient of movement value recorded for rod photoreceptor cells considered to be stationary, represented by the dotted line (located on the culture dish surface of Müller glia primary cultures; see Figure 6.4.3G). P14 rod photoreceptors were the only cell population with a coefficient indicative of near stationary behaviour. However, following base line correction with the standard curve in Figure 6.4.4E, the coefficient of movement values calculated for many of the co-culture time-lapse recordings were now close or below the stationary threshold, with P14 rod cells now even exhibiting a negative coefficient (individual co-culture data shown in Figure 6.4.3G.; pooled co-culture data shown in Figure 6.4.3Bii). Few of the individual time-lapse recordings had coefficients that surpassed the stationary threshold by a respectable margin. No photoreceptor age related changes in kinetic behaviour were apparent between P4 and P11. Conversely, individual co-cultures containing rod photoreceptors obtained from mice at identical developmental

stages sometimes had quite different coefficients even though the Müller glia substrate cells were of comparable age: for instance, time-lapse recording ‘P8, 191113 (13d)’ (P8 rod photoreceptors, date, Müller glia culture age) had a greater coefficient of movement than time-lapse recording ‘P8, 101214 (11d)’ or ‘P8, 261113 (14d)’.

These data raise significant concerns regarding the robustness of the co-culture assay for studying photoreceptor movement. It may be possible to determine a time window, during which Müller glial morphometric changes are sufficiently small that changes in rod motility can be detected reliably but this does not appear to be possible with the current data sets.

6.5. Conclusion

The transplantation of postnatally derived rod photoreceptors into the subretinal space of recipient animals results in the presence of donor reporter labelled cells within the host ONL. These cells are functional and can contribute to the functional restoration of vision in various pre-clinical studies (MacLaren et al., 2006; Gust and Reh, 2011; Lakowski et al., 2011; Pearson et al., 2012; Barber et al., 2013; Gonzalez-Cordero et al., 2013; Decembrini et al., 2014; Warre-Cornish et al., 2014). It was inferred that these cells arose by a process whereby rod cells migrate from the sub-retinal space through the IPM, across the OLM and into the neural retina (Warre-Cornish *et al.*, 2014). This last phase of migration has been proposed to involve a component of Müller glia guidance (Warre-Cornish, PhD thesis, 2013). More recently, and during the time course of this thesis, a second mechanism, material transfer, has come to light, whereby protein and/or mRNA is transferred between transplanted cells in the sub-retinal space and photoreceptors of the recipient retina, was recently uncovered (Santos-Ferreira *et al.*, 2016; Pearson *et al.*, 2016). Although the mechanism underlying material transfer is yet to be determined, what is known is that it is at least as prevalent as true photoreceptor integration. In the light of these issues, monitoring, by time-lapse live imaging, the processes that occur following photoreceptor transplantation into the recipient eye could provide valuable new insight into how transplanted rod photoreceptors migrate into the recipient neural retina following transplantation, or conversely, how material transfer between non-integrated and resident photoreceptor cells is achieved.

The first half of this chapter was concerned with obtaining time-lapse recordings of the events that occur in the first few days after photoreceptor transplantation. This was followed by addressing directly whether rod photoreceptors can migrate along Müller glia during the post-transplantation integration process in an *in vitro* co-culture migration assay.

For successful real time imaging of the migration/integration of rod photoreceptors into the neural retina, robust labelling of the recipient tissue was essential. Two strategies for the labelling of the neural retina were pursued: i) viral administration of Müller glia targeting AAV ShH10 particles encapsidating a *DsRed* expression construct in order to selectively label Müller glia with DsRed (Klimczak *et al.*, 2009), and ii) exposing acutely explanted retinae to the vital dye Mitotracker® Orange CMTMRos with the prospect of

labelling both Müller glia and photoreceptor outer segments, as reported by others (Uckermann *et al.*, 2004; Franze *et al.*, 2007; Panfoli *et al.*, 2009; Agte *et al.*, 2011; Bianchini *et al.*, 2014). Following intra-vitreal administration of AAV ShH10 *CAG.DsRed* into P10 mice, robust cellular labelling, which was almost completely restricted to Müller glia, was achieved (Figure 6.3.2). Conversely, Mitotracker® Orange CMTMRos did not selectively label Müller glia within this current study despite published works claiming exactly that (Uckermann *et al.*, 2004; Franze *et al.*, 2007; Agte *et al.*, 2011). Rather, vital dye labelling was evident in photoreceptor somata as well as the other cellular layers of the neural retina (Figure 6.3.1). It was, however, possible to label photoreceptor outer segments (located within the IPM layer), as previously demonstrated elsewhere (Panfoli *et al.*, 2009; Bianchini *et al.*, 2014). In combination, viral administration and vital dye treatment promised to visualise all structures of the recipient neural retina where critical steps of photoreceptor migration/integration following their transplantation were most likely to occur: the IPM, which includes the segment region, the OLM and the ONL.

Despite robust reporter labelling, it proved extremely difficult to obtain images with sufficiently good signal-to-noise ratio using upright 2-photon fluorescence microscopy, it was impossible to generate images with a good signal-to-noise ratio (Figure 6.3.4B & 6.3.4C). This was most likely due to substantial light scattering and optical aberration occurring at the level of the membrane rich outer segments. Several strategies to circumvent this issue were explored, but ultimately the *Prph2*$^{rd2/rd2}$ retinal degeneration mouse model proved to be the most viable option, due to its inability to form outer segments to any meaningful extent (Travis *et al.*, 1991). In a previous rod photoreceptor transplantation study, *Prph2*$^{rd2/rd2}$ recipient mice exhibited robust photoreceptor integration levels, perhaps also related to a compromised OLM (Barber et al., 2013). When rod photoreceptors were transplanted into *Prph2*$^{rd2/rd2}$ mice in the present study, both the transplanted photoreceptors as, well as the labelled neural retina, could be imaged with unprecedented quality (Figure 6.3.5-6.3.7). For the first time, the dynamic behaviour of rod photoreceptors transplanted into the sub-retinal space could be observed. Grafted rod cells dynamically extended and retracted processes towards the OLM (Figure 6.3.5). More importantly, somatic rod movements were also observed as rod cell bodies migrated radially through the IPM and towards the OLM, in some instances even penetrating through the presumptive OLM into the underlying ONL (Figure 6.3.4-6.3.5). Somal movements were frequently preceded by the extension of a leading process, which the

trailing nucleus could then migrate into (Figure 6.3.7). Kinetically, such rod somal movements were directed and rapid, occurring on a time scale of 20 minutes or less, during which relatively short distances were covered (< 10 µm). Photoreceptor migration into the ONL appeared to be restricted to the first row of photoreceptor nuclei, at least within the relatively short time frame of this experiment. However, following rod migration into the ONL, all recorded cells lost detectable GFP signal within 1-2 hours, for reasons that are currently not well understood. In combination, this resulted in the inability to truly investigate whether rod migration within the ONL was guided by Müller glia or some other mode of migration. Nonetheless, this study provides the first observation of rod photoreceptor migration into the neural retina following sub-retinal transplantation. It should be kept in mind, however, that using *Prph2*$^{rd2/rd2}$ mice as transplantation recipients may have introduced unknown variables that boosted the likelihood of observing integration. Events that might be indicative of material transfer were not be observed, although given our current lack of a mechanistic description of this process, it is not completely clear how these would manifest when observed through live imaging.

The issue of the relevance of Müller glia guided rod photoreceptor migration was addressed in the co-culture *in vitro* transplantation model and migration assay, which had been previously developed within the group to study the migration of rod photoreceptors along Müller glia (Warre-Cornish, PhD thesis, 2013). In this model, Müller glia primary cultures were first established, following their isolation from P8 *Rlbp.GFP*$^{+/+}$ reporter mice, by plating them on a laminin coated dish and by culturing them ideally for 2-3 weeks. During this period, Müller glia elongated and matured, expressing various mature Müller glia markers. Once this stage was reached, freshly isolated *Nrl.GFP*$^{+/+}$ rod photoreceptors were added to the Müller cells, thus setting up the co-culture. Following time-lapse live imaging of such cultures, the position of rod photoreceptors during the recordings was manually tracked *in silico* in the original study (Warre-Cornish, PhD thesis, 2013). In order to make the tracking of rod cells more systematic and less subjective, the first objective was to develop an at least partially automated tracking tool. Such a tool would also facilitate future investigations into the mechanisms that underlie Müller glia guided rod migration using different gain or loss of function approaches.

A semi-automated tracking methodology, largely built around the Mosaic Particle Tracker 2D and 3D plugin in Fiji (Sbalzarini and Koumoutsakos, 2005), was developed that allowed the movement of rod photoreceptors to be accurately tracked (Figure 6.4.2

& 6.4.3). It also required a series of image processing steps aimed at enhancing the signal-to-noise ratio specifically of the imaged rod photoreceptors, similar to what was described by Chenouard *et al.* (2014). With the help of this new tracking tool, the detection of rod photoreceptor movements was made more systematic, less dependent on user manipulation, as well as more amenable to higher throughput analysis, compared to the manual tracking used previously (Warre-Cornish, PhD thesis, 2013). At the same time, the results produced with the new tracking methodology were consistent with the results produced by manual tracking: As demonstrated by MSD analysis, the movement of rod cells along Müller glia was significantly increased compared to the movement of rod cells on the tissue culture dish, as well as increased compared with the motility on the retinal neuron substrate. Rod photoreceptors cultured on the Müller glia substrate produced an MSD profile with positive curvature, which indicates directed and actively driven motions (Ruthardt *et al.*, 2011). Rod photoreceptors, which were located on the surface of the co-culture dish, produced a relatively shallow and linear MSD profile, consistent with stationary behaviour. Rod cells located on retinal neurons produced an MSD profile with negative curvature, which is a sign of retarded motion. Furthermore, a considerable proportion of instantaneous velocities measured on the Müller glia substrate fell within the previously reported range of cortical neuronal migration velocities when guided by radial glia (0.1-0.25 µm/min; according to Chen *et al.*, 2008 & Franco *et al.*, 2011). Conversely, the majority of instantaneous velocity measurements recorded from the culture dish surface or the retinal neuron substrate were indicative of stationary rod cells (~ 0 µm/min). Thus, not only could the semi-automated rod tracking methodology quantify rod motility on Müller glia in a manner that was consistent with visual observations, it could also quantitatively describe that directed rod motility is specifically observed on Müller glia but not on other retinal neurons or on laminin alone.

However, due to upgrades in the live imaging set-up, it became apparent that Müller glia dynamically changed in shape over time. Thus, rather than rod cells actively migrating via cell intrinsic mechanisms, their motility might be attributable to a large extent to the plasticity of Müller glia (Figure 6.4.4). Although it was attempted to arithmetically derive true rod motility by subtracting base line Müller glia plasticity, what remained were kinetic rod profiles that were highly variable, ranging from near stationary to quite fast movements but with little correlation between donor cell age and/or across preparations. Together, these findings indicate that rod-Müller glia co-culture model in its current form

does not represent a sufficiently robust *in vitro* transplantation model to study rod photoreceptor/glial cell interactions, at least not without significant optimisation.

In conclusion, the *in vivo/ex vivo* work presented within this chapter proved for the first time that transplanted rod photoreceptors can migrate into the neural retina following their injection into the sub-retinal space, indicating that true integration events are possible. Material transfer was not observed within the used experimental set-up. The *in vitro* arm of this chapter led to the development of a powerful semi-automated particle tracking tool, which unfortunately revealed inherent shortcomings of the rod-Müller glia co-culture migration assay.

CHAPTER VII. DISCUSSION

The main aim of this study was to provide a detailed description and characterisation of rod photoreceptor motility in development and after transplantation. In the adult retina, photoreceptors are exclusively located within the ONL, a cellular arrangement that is established during development. The experiments described in this thesis sought to increase our understanding of how the mature retinal architecture and associated neuronal circuitry required for normal vision are established, specifically by investigating how rod photoreceptors become enriched within the ONL.

Another scenario where rod photoreceptor migration likely plays an important role is following photoreceptor transplantation as part of cell replacement therapy to combat the effects of otherwise irreversible injury and/or disease-related photoreceptor degeneration. Here, photoreceptors are injected into the sub-retinal space but apparently become integrated within the ONL of the host animal. The presiding hypothesis was that donor cells must undergo some form of migration to relocate from the sub-retinal space into the ONL of the neural retina.

The work carried out as part of this thesis made significant advances in elucidating the kinetic and mechanistic details of rod photoreceptor motility during murine retinal development. Furthermore, it was possible for the first time to capture the hitherto hypothesised migration of transplanted rod photoreceptors from the sub-retinal space into the ONL of the host retina in real time.

7.1. Rod photoreceptor motility during development

Unpublished data from a previous study by the group has shown that rod photoreceptor somata are motile along their apico-basal axes during retinogenesis (Warre-Cornish, PhD thesis, 2013). However, it was initially assumed that rod cells carry out this radial motion only once en route to their final location within the ONL. The findings presented in this thesis demonstrate that rod motility manifests as a novel mode of neuronal migration: morphologically, kinetically, as well as at the level of molecular motors involved, it exhibits characteristics of somal translocation and IKNM (named oscillatory somal translocation). During this motion, rod somata oscillate between apical and basal positions within the neural retina, by cycling through kinetically uniform and rapid motions in the apical direction and more kinetically variable basally-directed motions; these motions may be interspersed with periods of stochastic movements where rod somata undergo only little or no net displacement. To my knowledge, this is the first report of an oscillatory apico-basal motion exhibited by a post-mitotic neuron en route to its final destination within neural tissue. Oscillatory somal translocation thus constitutes a novel mode of neuronal (progenitor) cell motility that is to be added to the existing list consisting of IKNM, somal translocation, multipolar migration, tangential migration, and glial-guided migration.

7.1.1. The purpose of oscillatory rod somal translocation

The discovery of this novel mechanism immediately evokes the question as to why it has never been reported before. When looking at the retina or other CNS tissues where neuronal motility has been observed, recently born neurons typically migrate away from their place of birth, at the mitotically active ventricular zone, towards their target location, which (usually) lacks mitotic activity. Rod photoreceptors, just like virtually all retinal cells generated from RPCs, are born near the apical limit (at the ventricular zone) of the neural retina. This already places them into their target stratum, the (presumptive) ONL and, the reasonable assumption has been that there would be no requirement for active migration. However, since the (presumptive) ONL is in such close vicinity to, and to some extent part of, the mitotically active ventricular zone at the apical limit, recently born rod

photoreceptors likely have to compete with neighbouring RPCs for space within the (presumptive) ONL. As part of IKNM, RPCs undergo rapid apical migrations and cell duplications, both symmetric and asymmetric, that increase steric crowding at the ventricular zone. Given that the apical margin presents a physical barrier to these cells, this crowding could be accommodated by pushing the somata of other cells (e.g. rod photoreceptors) in the basal direction. Computer simulations have indeed demonstrated that cells in pseudostratified and mitotically active epithelia are passively displaced in the basal direction exclusively due to rapid apical translocations of neighbouring, G2 stage epithelial progenitor cells (Kosodo *et al.*, 2011). Rod photoreceptors may thus display translocation in the *apical* direction to avoid being pushed into ectopically basal positions and to remain within the ONL. As will be discussed in the following section however, basal movement of rod photoreceptors may not be exclusively passive in nature. Nonetheless, based on the results in this thesis, it is more than likely that rapid apical translocation occurs to enrich rod somata within the forming ONL.

Early studies on fixed mammalian retinae have shown that rod photoreceptors are occasionally found basal to the ONL following its separation from the INL at P5 and sometimes even at early, but not later, adult stages (Spira *et al.*, 1984; Young, 1984). Based on morphological assessments, it was proposed that these ectopic rod photoreceptors must either return to the ONL, or initiate apoptosis if they fail to do so. The current study presents time-lapse evidence to support this hypothesis. However, rather than rapid apical translocation being triggered exclusively by reaching a certain depth threshold, e.g. the (presumptive) OPL, it can be initiated from virtually anywhere along the apico-basal axis. Oscillatory rod photoreceptor somal translocation was detected from as early as P1 (embryonic stages were not examined in this study) and up until approximately P10. The prolonged need for, especially the rapid apically directed aspect of, oscillatory rod somal translocation might be explained by the immense neurogenic potential of the neural retina during early development and the concomitant requirement for rod photoreceptors to remain within the (presumptive) ONL. In mice, there appears to be a developmental-stage dependent, roughly normal distribution of total neurogenesis, which peaks at around birth, a time when the majority of the rod photoreceptors are born (Young, 1985; Akimoto *et al.*, 2006). Evidence provided within this thesis suggests that the extent of oscillatory rod somal motility roughly mirrors the kinetics of retinal neurogenesis (especially rod neurogenesis) at post-natal stages as both gradually become attenuated towards P10-11. Likewise, a pre-natal increase in rod somal

motility corresponding to the increase in neurogenesis may be expected, but would need to be formally investigated. However, even in absence of neurogenic cell divisions, RPCs engage in non-neurogenic, symmetric cell divisions, which likely also increase steric crowding at the apical margin of the neural retina. It should thus also be investigated, whether non-neurogenic RPC divisions influence rod somal motility differently compared to rod-neurogenic divisions.

7.1.2. The mechanisms behind oscillatory rod somal translocation

Mechanistically, the rapid apical somal translocation aspect of oscillatory rod somal translocation in mice is actively driven by the microtubule associated dynein I motors, as demonstrated here by the absence of any rod rapid apical somal movements in retinal explants following exposure to the dynein I selective antagonist ciliobrevin D. The effect of the drug was rapid, but reversible, since rapid apical translocation of rod somata was partially restored following drug wash-off experiments. In other systems, dynein I cargoes the nucleus (the main occupant of the rod photoreceptor soma in terms of volume) along microtubules towards the microtubule minus ends (Schroer *et al.*, 1989; Roberts *et al.*, 2013). In keeping with the proposed role of this movement (enrichment of rod cells in the ONL), dynein I complex LOF (mediated via RNAi) resulted in the basal displacement of rod cells, frequently beyond the ONL domain (this was assessed at a developmental stage, P8, where the ONL had already separated from the INL; see Figure 4.3.7). This displacement towards ectopically basal positions within the retina is prevented by the activity of dynein I motors.

The idea that cytoplasmic dynein is required for photoreceptor nuclear positioning is not entirely new. In other model organisms, such as Drosophila and zebrafish, photoreceptors were also basally displaced in dynein/dynactin LOF studies (Fan and Ready, 1997; Whited *et al.*, 2004; Insinna *et al.*, 2010). However, in the zebrafish retina, which is more similar to the mouse retina compared with the Drosophila compound eye, although it is undoubtedly much thinner and comprised largely of cones, the somata of photoreceptors with functionally impaired dynein/dynactin were only basally displaced within, rather than beyond, the ONL (Insinna *et al.*, 2010). Even outside of the eye, dynein motors are prominent key components of cellular migration. Analysis of human patients has revealed

that mutations in *DYNC1H1* (the gene encoding the cytoplasmic dynein 1 heavy chain), can lead to neuronal migration defects in the brain associated with intellectual disability (Willemsen *et al.*, 2012). One of the novel conclusions of the present study is the fact that rod photoreceptors appear to be exposed to forces that push them in the basal direction and that rod cells utilise dynein I activity to prevent ectopically basal locations. For this to happen, dynein I motors need to dock onto the nucleus, which is presumably mediated by the linker of nucleoskeleton and cytoskeleton (LINC) complex located across the nuclear membranes (Crisp *et al.*, 2006; Zhang *et al.*, 2009; Yu *et al.*, 2011). Sun domain containing Sun1/2 and KASH domain containing SYNE proteins are part of the LINC complex. Several studies have demonstrated that loss of function of LINC complex components (e.g. SYNE2 or Sun1) leads to the basal displacement of photoreceptors, often accompanied by impaired axon and synapse formation, although the phenotype severity was variable (Yu *et al.*, 2011; Razafsky *et al.*, 2012; Maddox *et al.*, 2015). Given that dynein I motors can interact with the LINC complex, it would seem reasonable that the phenotypes associated with the LOF of either part of this interaction are similar.

Kinesin family microtubule-associated motor proteins generally transport cargo towards the microtubule plus end. Within neural progenitor cells of the developing rat cortex undergoing IKNM, kinesin motors have been reported to mediate nucleokinesis towards the microtubule plus ends (basally directed, within this context) (Tsai et al., 2010; Carabalona et al., 2016). Given similar tissue and intracellular microtubule cytoskeleton polarities, it was hypothesised that kinesin motors could equally drive basally-directed nucleokinesis in photoreceptors. However, rather than being actively driven by kinesins, the present study has demonstrated that basal movement of rod somata is most likely a matter of passive displacement caused by the apical movement of neighbouring cells or actomyosin constrictions, as will be explained below. LOF of the kinesin family member *Kif1a* did not result in apical crowding of rod somata as initially anticipated. Rather, ectopically basal mislocalisation, similar to what was observed following dynein I LOF, was detected. However, this only manifested at acute stages of *Kif1a* LOF (4 days of RNAi) and was resolved at prolonged stages (7 days of RNAi). The simplest explanation for this is that KIF1A functions as a basally acting brake. In its absence, rod somata might be at greater risk of ending up in ectopically basal locations outside of the ONL, but, due to the action of dynein I, most do eventually return apically into the ONL even when basally acting brake function of KIF1A is compromised. A kinesin mediated brake function on cargo transport has so far only been demonstrated for the *Kif5* isoform, which,

in the presence of syntaphilin, stopped the anterograde transport of mitochondria within axons in a neuronal activity-dependent manner (Chen and Sheng, 2013). It may be speculated whether *Kif1a*, perhaps in conjunction with some co-factor, can be similarly put into brake mode within rod photoreceptors.

This is in striking contrast to what is known to occur during true IKNM in rodent cortical neural progenitor cells, in which basal movement of the nucleus is actively driven by KIF1A (Tsai *et al.*, 2010; Carabalona *et al.*, 2016). It was, however, also pointed out that the kinesin family of motor proteins consists of many isoforms, many of which have been implicated in cortical neuronal migration (Tsai *et al.*, 2010). Due to its proven role during IKNM of rodent neural progenitor cells, the KIF1A isoform was also at the focus of the present study. However, in addition to fully understanding the role of KIF1A in rod somal translocation, the role of other kinesins should also be investigated in future experiments. Time lapse imaging studies will likely be able to resolve whether LOF of *Kif1a* (or the other kinesin isoforms), for instance by RNAi specifically in rod cells, increases the prevalence of basally-directed rod somal motions.

During neuronal migration, the nucleus is often physically coupled to the centrosome via microtubules. These microtubules are extended from the centrosome to enwrap the nucleus in a fork-like perinuclear cage structure (Tanaka *et al.*, 2004). In this way, centrosomal motions are linked to nuclear motions, although they may not always be tightly coordinated (Umeshima *et al.*, 2007). In the present study, it was determined that the centrosomes of rod photoreceptors within the early developing retina are located exclusively at the apical margin of the tissue, even at stages where the nuclei/somata displayed apico-basal motility. Later on during retinogenesis, the apically located centrosomes most likely transform into basal bodies, which nucleate a bipolar microtubule network extending in the basal (towards the nucleus) and in the apical directions (towards the segment region) (Troutt and Burnside, 1988). Since rod centrosomes are, therefore, relatively stationary at all times, oscillatory rod somal translocation during development is not kinetically coupled to centrosomal motility. Mouse rod photoreceptors share this feature with RPCs in the zebrafish retina undergoing true IKNM, which is also independent of centrosomal motility (Strzyz *et al.*, 2015).

IKNM in zebrafish RPCs is heavily dependent on actomyosin constrictions (Norden *et al.*, 2009). There, activated actomyosin accumulates basal to the nucleus just before the onset of rapid apical translocation events. As the actomyosin cytoskeleton constricts, the

nucleus is pushed in the apical direction. In murine rod photoreceptors, functional inhibition of NMII (the motor protein responsible for actomyosin constrictions) by RNAi for a prolonged (7 days) but not for an acute period (3-4 days) resulted in the accumulation of rod photoreceptor somata closer to the apical margin. The delayed phenotypic onset would imply that actomyosin constrictions play only a minor, possibly indirect role, in rod somal motility: acute application of pharmacological blockers of NMII (Blebbistatin) had no major effect on the kinetics of rod somal motility. It is unlikely, too, that the delayed phenotypic onset in the presence of LOF constructs is due to a long half-life of the NMII protein half-life, since a previous study reported significantly reduced NMMHC-IIB protein levels after 3 days of RNAi using the same target sequence (Shajia and Horowits, 2008). It is possible that, in contrast to zebrafish RPCs, actomyosin constrictions may thus drive basally, rather than apically, directed somal translocation in rod photoreceptors. While this is perhaps unlikely, NMII GOF experiments might help to confirm this, as increased NMII function would be predicted to lead to ectopically basal somal locations if there is an NMII-mediated active component to basal migration. Alternatively, since the constructs used here were under the control of ubiquitous promoters, and this applies to all the RNAi genetic targets investigated here, it is perhaps more plausible that the rod mislocalisation phenotypes may have arisen due to NMMHC-IIB gene silencing effects in other retinal cells, particularly RPCs still proliferation at these stages. Cytokinesis in dividing RPCs, the process, whereby the cytoplasm of a mitotic cell divides into two daughter cells, is known to be heavily dependent on actomyosin (reviewed by Heng and Koh, 2010). RNAi-mediated NMII ablation in RPCs may have thus resulted in reduced cell division rates and hence reduced forces pushing rod somata in the basal direction. However, it is unclear how likely this scenario is, given that there was no clear accumulation of M-phase arrested RPCs at the apical limit of the retina and no reduction in neural retinal thickness.

IKNM in zebrafish RPCs, especially the rapid apical aspect, relies heavily on actomyosin constrictions; so much so that it occurs even in complete absence of pharmacologically destabilised microtubules. Although not shown in this thesis, when complete microtubule destabilisation was pharmacologically induced in the mouse retina using high concentrations of the small molecule drug Demecolcine, this led to epithelial collapse and the apical extrusion of rod photoreceptors from the neural retina (data not shown). Consequently, it was difficult to draw any meaningful conclusions with respect to rod migration from this outcome, as also described by Lee and Norden, 2013. Conversely,

arresting microtubule dynamic behaviour in the mouse retina with low concentrations of Demecolcine did not significantly affect rod photoreceptor motility in the developing murine retina. This is probably because the microtubule-associated motor proteins are able to utilise sufficiently the microtubules established prior to microtubule arrest.

7.1.3. Oscillatory rod somal translocation in context

In parallel to the studies on developmental rod motility, the motility of cone photoreceptors was also explored by other members of the group (Waldron, PhD thesis, 2016). There, it was demonstrated that cone somata carry out oscillatory apico-basal motions during the second half of the first post-natal week that are kinetically very similar to the migratory behaviour exhibited by rod cells. Mechanistically, cone somal motility also appears to be largely driven by dynein I motors, based on pharmacological investigations. Previous analyses on fixed retinal sections do, however, suggest that cone photoreceptors, which are born predominantly at pre-natal stages, remain stationary at the apical margin of the neural retina up until ~P4 (Rich *et al.*, 1997; Smiley *et al.*, 2016). At similar time points (P1 & P3), rod photoreceptors already engage in oscillatory somal motility, presumably to avoid their excessive passive displacement to ectopically basal locations due to the radial motions of neighbouring cells. It is perhaps reasonable to assume that cone cells engage in oscillatory somal translocation between P4 and P11 for similar reasons to rods – to retain their location in the ONL during a period of high neurogenesis. However, how and why cone photoreceptors avoid being passively displaced prior to ~ P4 is not known. Morphologically, cone precursor cells have robust basal processes (Waldron, PhD thesis, 2016) that terminate in synaptic connections with horizontal cells from as early as P3 (Rich *et al.*, 1997), whereas rod cells form synaptic connections several days later (Blanks *et al.*, 1974). Cone somata are thus unlikely to end up more basal than their horizontal cell synaptic partners, effectively restricting cone locations to within the ONL. Wherever cone somata are located within the ONL, they eventually return to the apical limit of the retina by P12 (Rich *et al.*, 1997; Smiley *et al.*, 2016), most likely by performing a final rapid apical translocation motion. Their return to the apical retinal margin appears to be crucial for the correct visual function of the retina (Yu *et al.*, 2011). On the other hand, rod photoreceptors are found within, but frequently also basal to, the (presumptive) ONL during the first post-natal week. This

greater range of radial mobility compared with cone somata could be due to the later onset of synaptogenesis. Under normal conditions, the exact radial position where synaptogenesis occurs likely limits the basal most rod somal position possible. For rod photoreceptors in the mouse retina, the objective is thus not so much to find their way back to the apical retinal limit from any radial position within the (presumptive) ONL, but rather to become enriched within and/or to find their way back into the ONL from virtually any radial position within the neural retina.

How does the IKNM-like oscillatory rod somal translocation in the developing mouse retina compare to true IKNM of neuronal progenitor cells in other CNS tissues and/or species? Kinetically, rod somal apico-basal oscillations are virtually identical to true progenitor cell IKNM. As was recognised by Kosodo (2012) and Lee & Norden (2013), however, the mechanisms underlying true IKNM can be quite different depending on the model organism, tissue of interest and perhaps even the developmental stage. Presently, there are four described mechanisms that account for the apical movement during G2- and basal movement during G1-phase of the cell cycle: i) G2 - dynein I, G1 - KIF1A (Tsai *et al.*, 2010); ii) G2 - dynein I, G1 - NMII (Schenk *et al.*, 2009); iii) G2 - dynein I, G1 - passive displacement (Kosodo *et al.*, 2011); iv) G2 - NMII, G1 – stochastic (Norden *et al.*, 2009). Mechanisms i-iii were all observed in the developing rodent brain and they share the common feature that rapid apical translocation during G2 is driven by the microtubule associated dynein I motor complex. Basal movements during G1 have, however, been ascribed to a variety of different mechanisms, ranging from passive displacement to KIF1A (a microtubule associated, plus end directed kinesin motor protein family member) or NMII driven (responsible for actomyosin constrictions to push the nucleus). Conversely, in the zebrafish retina, IKNM was entirely dependent on NMII-mediated actomyosin constrictions. RPCs in the zebrafish neural retina are relatively short and wide. It may be possible, therefore, that actomyosin can accumulate near the nucleus at such high levels that NMII mediated actomyosin constrictions can push the nucleus within the radial extent of the RPC (Lee and Norden, 2013). By contrast, in the evolutionarily more advanced rodent cortex, neural progenitor cells form much longer and thinner apical and basal processes. These are possibly too narrow to contain an extended actomyosin mesh within the soma to create any meaningful push forces on the nucleus. Instead, microtubule associated motors transport the nucleus along the radially spanning microtubule filaments.

Where and how does the rod photoreceptor motility observed as part of this current, and a previous thesis (Warre-Cornish, PhD thesis, 2013), fit into the picture of known IKNM mechanisms? Although the IKNM-like, oscillatory somal motility exhibited by murine rod photoreceptors is mechanistically more similar to the IKNM of neural progenitor cells in the rodent brain rather than IKNM in the zebrafish retina, it does not fit completely with any of the mechanisms reported in the rodent brain. Dynein I-mediated apical movement of the nucleus does appear to have been conserved, however, basal movement of rod photoreceptor nuclei appears to be, to a large extent, a consequence of passive displacement caused by the apical movement of neighbouring cells (similar to the cortical neuronal progenitor cells described by Kosodo *et al.*, 2011), although NMII-mediated actomyosin constrictions may also contribute to some degree. At the same time, KIF1A, rather than mediating basal motions (Tsai *et al.*, 2010), appeared to exert a brake function that prevented ectopically basal rod somal positions, as has been reported KIF5 during mitosis and axonal transport (Saunders *et al.*, 2007; Chen and Sheng, 2013). The purpose behind rod somal motility is obviously completely different from that of true IKNM exhibited by epithelial progenitor cells. True IKNM in epithelial progenitor cells is intimately linked to the cell cycle and maintenance of tissue polarity (Frade, 2002; Baye and Link, 2008a; Spear and Erickson, 2012a). In fact, the link between interkinetic movement and cell cycle progression is so robust that blocking cell cycle progression also leads to the cessation of interkinetic motility (Ueno *et al.*, 2006; Leung *et al.*, 2011). Conversely, in the post-mitotic rod photoreceptor precursor cells of the developing mouse retina, the molecular machinery responsible for IKNM-like somal oscillations appears to have been uncoupled from cell cycle progression. This is the first report of an IKNM-like migration behaviour occurring within a post-mitotic neuronal cell population. It also constitutes a novel mode of migration (besides somal translocation, multipolar migration, tangential migration and glial-guided migration), by which post-mitotic neuronal precursor cells reach their target destinations.

7.1.4. Glial-guided rod photoreceptor migration during development?

Kinetically, aspects of the oscillatory rod somal translocation are also compatible with a glial-guided migration mechanism, at least according to the standards set by cortical glial-guided neuronal migration (Chen *et al.*, 2008; Franco *et al.*, 2011). Previous findings

following photoreceptor transplantation, which demonstrate a greater than chance physical association between donor labelled rod photoreceptors and their nearest neighbour Müller glial cell (Warre-Cornish, PhD thesis, 2013). Therefore, the present study also examined whether rod photoreceptors can migrate along retinal glial cells.

In years gone by, speculations and circumstantial evidence have fuelled the debate on whether glial-guided migration occurs to any relevant extent within the retina: Reichenbach and colleagues (1993) coined the term 'columnar unit' in reference to the often clonally related retinal neurons (especially rod photoreceptors) that cluster around a central, related Müller glia cell in the mature retina. These tight associations may have already existed during retinogenesis where rod photoreceptors display marked apico-basally directed somal motility (see chapter III). Furthermore, rod photoreceptors born from adult neurogenesis in the cichlid fish retina appear to move basally along Müller glia following their birth at the apical margin of the retina (Mack *et al.*, 2003). However, this study was based on analyses on fixed tissue rather than time-lapse microscopy, a technique, which was instrumental to the characterisation of glial-guided migration in the cortex (e.g. Edmondson and Hatten, 1987; Anton *et al.*, 1996; Franco *et al.*, 2011). In order to investigate whether developing rod photoreceptors migrate radially by employing glial-guidance mechanisms, time-lapse microscopy studies similar to those performed on cortical glial-guided migration will have to be performed (e.g. Franco *et al.*, 2011).

For retinal radial glia, the term NRSC has been coined within this thesis, which comprises a continuum of cells ranging from RPCs to its end stage Müller glia phenotype. RPCs to early Müller glia characteristically express *Nes* within the developing mouse retina. This feature was exploited by creating a *Nes* reporter construct (*pD10 TK.DsRed.eNestin714*) that was based on the reporter design from Lothian and Lendahl (1997), and which would make it possible to observe potential glial-guidance interactions by fluorescence microscopy. Late stage or fully differentiated Müller glia will have down-regulated their *Nes* expression levels to such an extent that no more reporter gene expression is detectable (Figure 5.3.2, 5.3.4, 5.3.5; Xue *et al.*, 2006; Lee *et al.*, 2012; Valamanesh *et al.*, 2013).

The original *Nes* reporter obtained from Lothian and Lendahl (1997) had a configuration of individual genetic elements where the *Nes* 2nd intronic enhancer element, which is important for *Nes* gene activity specifically in neuronal progenitor cells (*eNestin714*), was placed upstream of a ubiquitous gene expression module. The latter consisted of the thymidine kinase promoter and the *lacZ* reporter gene (*TK.lacZ*). When used in this same

configuration, the first version of the *Nes* reporter construct produced in this study (*pD10 eNestin714.TK.DsRed*) did not show reporter gene expression (note: *lacZ* was replaced with *DsRed*). The reason why the same configuration of genetic elements produced reporter gene expression in the study by Lothian and Lendahl (1997), but not here, is presently not known. It may be that the original configuration is functional only upon stable genomic integration, as was done by Lothian and Lendahl (1997), who produced transgenic reporter mice in this way. In the present study, the *Nes* reporter was introduced into retinal cells to be episomally maintained, rather than to be integrated into the genome. Perhaps the transcription machinery cannot be functionally assembled well enough in this case. However, when the *eNestin714* enhancer element was placed downstream of the *TK.DsRed* reporter gene expression module (*pD10 TK.DsRed.eNestin714*), to recapitulate a configuration of genetic elements more akin to the true *Nes* gene region, *Nes* reporter expression was unlocked in transfected cells of the mouse retina (compare Figure 5.3.7 & 5.3.9). Reporter expression was also spatio-temporally specific, meaning restricted to NRSCs ranging from RPCs to the early Müller glia state as well as restricted to early retinogenesis. It should be mentioned that the entire spectrum of NRSCs, including even fully differentiated Müller glia, can be labelled using a *Hes5* reporter strategy, e.g. the *Hes5-GFP* mouse (Nelson *et al.*, 2011). In fact, the ideal experimental design was thought to consist of labelling all NRSCs while having sparsely labelled rod photoreceptors. This would allow potential glial-guidance relationships between rod cells and NRSCs to be resolved most clearly.

The somata of some rod photoreceptors were indeed observed to move along labelled NRSCs in the post-natal mouse retina, sometimes displaying kinetics that were reminiscent of cortical glial-guided neuronal migration (see results in chapter V; Chen *et al.*, 2008; Franco *et al.*, 2011). It was intriguing, given these data, to confirm the existence of glial-guided rod migration during retinogenesis. However, such claims could ultimately not be upheld beyond reasonable doubt due to the pseudostratified nature of the neural retina and its cells, which can move in the apical and basal directions and to some extent even laterally. The boundaries between active/passive rod migration and rod-NRSC cell-cell adhesion versus 'involuntary' contact due to limited space simply became too difficult to define with confidence. By contrast, within the cortical plate layer of the developing brain, where glial-guided neuronal migration is accepted to occur, the neuroepithelium comprises mainly of neuronal precursors and only the processes (and not the cell bodies) of the radial glia, which provide guide rails for the neural precursors to

migrate unidirectionally along them towards the pial surface. This makes the case for cortical glial-guided neuronal migration considerably more clear cut. Another discrepancy from glial-guided neuronal migration in the cortex is the fact that rod photoreceptors always maintain a process that extends to the apical limit of the neural retina, whereas cortical neuronal precursor cells exhibit short processes devoid of contact with the apical/basal surface (Figure 5.3.1). It thus appears plausible that if glial-guidance exists between rod photoreceptors and NRSCs in the developing mouse retina, it is likely to markedly differ from cortical glial-guidance.

Cortical neuronal precursor cells, following their birth in the ventricular zone and subsequent multipolar migration through the subventricular and intermediate zones, often need to traverse large distances before reaching their target destinations in the cortical plate layers. This is especially the case in large animals like primates but also in smaller mammals, where the distance from ventricular zone to the pial surface overlying the cortical plate can span several millimetres. Given the long journey within the developing cortex, glial-guided migration represents an elegant solution to keeping the nascent neuronal precursors on track for their migration towards the cortical plate layers. In the developing retina, by contrast, photoreceptors are born in the ventricular zone at the apical edge of the retinal neuroepithelium, which is already part of / directly adjacent to the target destination of the photoreceptors. Compared with the brain, the distance between the place of rod birth and the final destination within the ONL is thus considerably shorter, begging the questions of whether glial-guidance would be required in this case. Although highly speculative, a conservation of neuronal migration mechanisms (including glial-guided neuronal migration) between brain and retina is a possibility since both share common neuroectodermal origins.

In order to find out whether glial-guided rod migration truly exists during retinogenesis, a different experimental approach will have to be undertaken, that manages to drastically reduce the image complexity imposed by the pseudostratified retina. It may also be worth exploring whether a cell-cell interface equivalent to the cortical interstitial junction (the cellular interface involving the surfaces of radial glia and neuronal precursors migrating along them) can be identified in the retina by ultrastructural or supra-resolution analyses. In the best-case scenario, putative interstitial junctions in the retina would be distinguishable from points of cell-cell contact that arose due to limited space.

7.2. Rod photoreceptor motility following transplantation

Pre-clinical mouse transplantation studies have demonstrated that rod photoreceptor cell replacement therapy holds the potential to become a viable clinical treatment option in the future (MacLaren et al., 2006; Bartsch et al., 2008; Eberle et al., 2011; Lakowski et al., 2011; Pearson et al., 2012; Gonzalez-Cordero et al., 2013; Homma et al., 2013). One of the main points of consideration with this technique is the fact that the degree of functional restoration of vision following transplantation is highly dependent on the number of rod cells within the recipient retina following transplantation (Pearson *et al.*, 2012). Observing and understanding the integration, and presumably also the preceding migration, of transplanted photoreceptors into the neural retina may thus help to enhance these processes in order to achieve consistently improved transplantation outcomes. However, more recent data from this group (Pearson *et al.*, 2016), and the group of Marius Ader (Santos-Ferreira *et al.*, 2016) have indicated that true integration events are likely to be relatively rare, compared to a much more prevalent mechanism, termed material transfer. The cellular mechanism underlying material transfer are not well understood although a working hypothesis in our group is that donor photoreceptors in the subretinal space release microvesicles containing a wide array of proteins and/or RNA, which are taken up by the photoreceptors of the recipient retina, thereby rendering them functional, at least for a period of time (Pearson and Kalargyrou, personal communication). For these reasons, it was important to attempt to capture the migration/integration and/or the material transfer events by real time live imaging.

7.2.1. The migration of transplanted rod photoreceptors into the host retina

7.2.1.1. Optimisation of the live imaging set-up

As part of this thesis, real-time imaging provided strong evidence for the migration of transplanted donor rod photoreceptors across the IPM and into the recipient neural retina. Several individual rod cells were observed to migrate following transplantation, both

within the IPM as well as into the neural retina. In order to successfully capture rod migration in real time following transplantation, a number of technical challenges had to be overcome first. The optical barrier imposed by the photoreceptor outer segments, which obstruct fluorescence imaging of the retina, proved to be especially challenging to circumvent. In the end, the *Prph2*$^{rd2/rd2}$ mouse, which lacks the ability to properly form outer segments (Travis *et al.*, 1991), was chosen as the most suitable recipient of rod photoreceptor transplantation to solve this problem. A previous report has shown that this model is able to support good transplantation outcomes, with robust numbers of donor reporter labelled cells found within the recipient retina post-transplantation (Barber *et al.*, 2013); implicit within this statement is the understanding that these may arise either by true integration and/or material transfer. In the present study, this model supported the migration of grafted rod photoreceptors, but not, apparently, material transfer. As noted above, the cellular mechanism underlying material transfer are unknown, but discussions within the group have suggested that material transfer may involve the outer segments of the resident photoreceptors as acceptors of the transfer. If correct, by using *Prph2*$^{rd2/rd2}$ mice as recipients of the rod transplantation, the balance between true integration and material transfer may have been shifted in favour of true integration. Another factor assisting migration may be the presence of serum in the live imaging medium, which was added in order to extend the life span of the tissue explant during the live recordings; previous reports have found that certain components present within serum (e.g. FGF-2) can stimulate the migration of neuronal and non-neuronal cells (Hossain *et al.*, 1996; Brink *et al.*, 2005).

7.2.1.1. Potential mechanisms underlying rod photoreceptor migration/integration following transplantation

While the explant retinal model has clear limitations, much of the structural integrity is maintained and the cellular movements exhibited by donor cells are probably representative of what rod photoreceptor migration following transplantation looks like, although the relative frequency, with which such events occurred, may be higher in this model than in outer segment bearing models. However, much larger numbers will be needed in future experiments to verify these assumptions. Notwithstanding, the movement of the soma of the transplanted rod photoreceptors usually only covered

relatively short distances of up to approximately 10 µm, and did so in ≤ 20 minutes. Such movements tended to be preceded by the extension of a short process in the direction of the subsequent somal movement. Frequently, these processes were extended towards the recipient neural retina, which could also be seen in a previous study on fixed, transplanted eyes (Warre-Cornish *et al.*, 2014). The extension of these processes was reminiscent of axonal growth (Dent and Gertler, 2003; Geraldo and Gordon-Weeks, 2009; Dent *et al.*, 2011). During axonogenesis, a highly dynamic growth cone is located at the tip of the extending axon, within which high concentrations of actin filaments are found. These, in return, underlie the highly dynamic nature of the lamellipodia and filopodia present on growth cones. They act as sensors of chemo-attractant or -repellent cues in the surroundings, in response to which they extend or retract in a direction-specific manner, thus guiding axon growth towards the target destination. The stalk of the axon mainly contains microtubule filaments that grow into the growth cone to consolidate growth cone advancements.

Just like growing axons, processes formed by transplanted rod photoreceptors appear to be extended towards certain target structures. Process extension towards the neural retina by transplanted rod photoreceptors may function in a very similar way to axonogenesis, since they appear to target specifically the apical margin of the neural retina rather than other structures of the recipient eye. If so, similar molecular regulators may mediate both axonal growth and rod photoreceptor process extension. Rho and Ras GTPases, such as RhoA, Rac, Cdc42 and R-Ras, are known key regulators of the actin and microtubule cytoskeleton during axonogenesis (Hall and Lalli, 2010). They coordinate the signal transduction pathways that have been elicited by extracellular axon guidance cues and translate them into appropriate growth cone and axonal responses (Dent and Gertler, 2003; Dent *et al.*, 2011). Depending on the detected cue(s), downstream effectors include, for instance, ADF/cofilin (via signalling through RhoA), an actin filament severing/recycling protein that promotes process extension by maintaining a pool of actin monomers that can be accessed for actin filament polymerisation (Meberg and Bamburg, 2000). Another effector is the microtubule destabilising protein stathmin, which is inhibited by signalling through R-Ras and Rac, thus leading to the stabilisation of microtubule filaments; this is likely important for the consolidation of axon growth (Watabe-Uchida *et al.*, 2006). Besides these effectors, a long list of other regulators of growth cone dynamics and axonogenesis exists (Dent and Gertler, 2003; Dent *et al.*,

2011). This list should be taken into consideration in order to address what mechanisms regulate process extension of transplanted rod photoreceptors.

As mentioned before, for migrating grafted rod photoreceptors, process extension was followed by nucleokinesis into the newly formed process. Conversely, neuronal axon growth does not usually invoke nuclear motility. In that respect, transplanted rod cells behaved more similar to neuronal precursor cells undergoing somal translocation, in that they first extend a process towards their target destination, which then allows the trailing nucleus to migrate into the new process in a grappling hook like manner (Nadarajah *et al.*, 2001, 2003; Cooper, 2013). In the cortex, somal translocation is dependent on the reelin signalling pathway (Rice and Curran, 2001; Franco *et al.*, 2011). The gene encoding the secreted protein reelin (*Reln*) is expressed by Cajal-Retzius cells close to the target destination of the somal translocation movement towards the pial surface and is recognised by somally translocating neurons. This leads to the stabilisation of the leading process as it extends towards the pia and increases the cell surface levels of the homophilic cell adhesion molecule N-Cadherin (*Cdh2*), both of which are required for terminal somal translocation.

In the (healthy) mature retina, however, *Reln* is only strongly expressed in the OPL and IPL (Rice *et al.*, 2001), consistent with the discovery of its role in retinal circuit assembly, but not in the ONL/OLM, where expression would be expected if it played a role in guiding transplanted rod cells towards the neural retina. Following retinal laceration, however, *Reln* expression also becomes detectable in the ONL, indicating that *Reln* upregulation could be an injury/disease response to facilitate repair mechanisms in the retina (Pulido *et al.*, 2007). Reelin signalling leads to increased N-Cadherin cell surface levels in the cortex (Franco *et al.*, 2011). This may also be the case in the retina. Indeed, the retinal detachment injury model exhibited increased N-Cadherin immunoreactivity specifically at the level of the RPE, ONL and OLM within the detachment area (Chen and Ma, 2007). It is thus possible that injury and disease can stimulate *Reln* expression in the ONL, which in turn increases N-Cadherin levels in cells contributing to the sub-retinal space. The very act of photoreceptor sub-retinal injection, or more generally, the act of introducing retinal detachment, stimulates *Cdh2* (N-Cadherin) expression in the retina (Chen and Ma, 2007), but whether this is reelin-dependent is yet to be determined. Process extension by the transplanted rod cells towards the neural retina could thus be mediated by homophilic N-cadherin interactions. This would also require *Cdh2* to be expressed in the transplanted rod cells. Indeed, rod cells freshly isolated from P8 mice – the currently

preferred donor cell population – also expressed *Cdh2* according to qPCR and immunocytochemistry (data not shown). The relevance of N-cadherin during process extension of transplanted rod photoreceptors should thus be explored in the future.

During the migration of transplanted photoreceptors harvested from P8 retinae, process extension from within the sub-retinal space towards the recipient neural retina was followed by nucleokinesis. Data presented in this thesis have shown that rod nucleokinesis/somal motility during early post-natal development is mainly dependent on microtubule associated motor proteins, with dynein I leading the way, but with the kinesin family member KIF1A being involved, to a lesser degree, as well. It is very likely, therefore, that these microtubule motors also play a role during rod photoreceptor precursor nucleokinesis following transplantation. Dynein and kinesin type microtubule motors generally possess processivity only towards the microtubule minus end or plus end respectively. It will be of significant interest to determine the organisation and potential polarity of the microtubule cytoskeleton during rod migration after transplantation and, related to that, the exact location of the centrosome since it is the main MTOC in rod precursor cells. This will help to narrow down whether rod nucleokinesis, in this situation, is based on kinesin activity towards microtubule plus ends or dynein activity towards the minus ends. Whether actomyosin constrictions are involved in developmental rod somal motility has not fully been resolved in the present study and should also be investigated in future rod photoreceptor transplantation experiments.

The mechanisms that make the whole rod photoreceptor cell migrate towards the recipient neural retina are likely to be chemotactic in nature. However, as addressed by Unachukwu *et al.* (2016), virtually nothing is presently known about the chemotactic signalling mechanisms involved in the migration of transplanted rod cells from within the sub-retinal space towards the retina. In their study, Unachukwu and colleagues (2016), have identified, following *in silico* prediction, the chemotactic ligand-receptor pair SDF-1α–CXCR4 as a putative mediator of rod photoreceptor chemotaxis following transplantation. Furthermore, they could verify SDF-1α–CXCR4 based chemotaxis in cultured mouse photoreceptors. Chemotactic signalling should thus be further explored for a better characterisation of the mechanisms underlying rod photoreceptor migration following transplantation.

It is also worth considering the possibility that the observed apparent movement of rod photoreceptors into the recipient neural retina might have occurred due to photoreceptors

being engulfed by microglia. This may explain why the GFP signal was rapidly reduced in rod photoreceptors following their (apparent) migration. The *Prph2*$^{rd2/rd2}$ mouse model does indeed exhibit sub-retinal microglia (Hughes *et al.*, 2003), which would be ideally positioned for such a process. Furthermore, the engulfment process by CNS microglia can occur on a similar timescale as the migration of transplanted rod photoreceptors (Neumann *et al.*, 2008). Arguing against this notion, however, is the fact that the sub-retinal microglia should have been labelled by Mitotracker® Orange CMTMRos much in the same way as the transplanted photoreceptors, as well as the photoreceptors of the recipient retina, yet Mitotracker® Orange CMTMRos labelling that could be clearly attributed to photoreceptor-engulfing microglia was not detected in this present study.

7.2.1.2. Apparent rod photoreceptor integration by material transfer

Taken together, the data presented in this thesis strongly support the occurrence of true donor photoreceptor migration and integration following transplantation. However, very recent evidence also points towards the existence of a second mechanisms, that of material transfer, between donor and host photoreceptors, which can give rise to numerous apparently integrated cells within the host (Pearson *et al.*, 2016; Santos-Ferreira *et al.*, 2016). Material transfer in the context of photoreceptor transplantation describes a process whereby transplanted cells injected into the sub-retinal space share cytoplasmic components such as protein or mRNA with resident photoreceptors of the recipient retina, but without undergoing classic cell-cell fusion accompanied by polyploidy (Pearson *et al.*, 2016; Santos-Ferreira *et al.*, 2016). The mechanisms underlying material transfer have not been elucidated yet and it is possible that the settings used in the current study for studying cellular movements in real time were not optimal for capturing material transfer events. In the study by Pearson and colleagues, the number of events accounted for by material transfer far exceeded that of true integration (Pearson *et al.*, 2016).

Material transfer is not restricted to XFPs, as many different proteins (including numerous phototransduction components and even structural proteins) appear to be transferred. At present, it is unclear whether the mechanism involves the transfer of proteins and/or RNA. Material transfer is also not unidirectional; in addition to occurring from donor to

recipient photoreceptor, it can also occur between donor photoreceptors residing in the subretinal space, and from host photoreceptor to donor photoreceptor, albeit at much lower frequency than from donor to host. Physical connections between sub-retinal and resident photoreceptors would, perhaps, be one way to account for this phenomenon. Previous works as well as data presented in the present study, have shown that sub-retinal photoreceptors extend processes towards the recipient neural retina (Figure 6.3.5 & 6.3.6; Warre-Cornish *et al.*, 2014). However, there are also numerous examples of host photoreceptors, which appeared to have been the recipients of material transfer, that lack any visible physical connection to a donor cell in the over-lying sub-retinal space (see Pearson *et al.*, 2016). In the absence of a sustained physical connection, communication via the release and uptake of microvesicles, which may carry protein and/or RNA, may present an alternative mechanistic hypothesis. Work carried out by others in the group has demonstrated that photoreceptor precursors do indeed produce and release microvesicles and that these carry relevant RNA and/or proteins (Kalargyrou and Pearson, personal communication). Whether these account for material transfer, however, has yet to be determined.

The time-lapse recordings presented in this thesis showed the migration of transplanted rod photoreceptors into the first two rows of ONL photoreceptor nuclei (Figure 6.3.7). Consistent with this was confocal analysis data of GFP positive donor cells within transgenic recipients that ubiquitously expressed DsRed; the soma of GFP positive/DsRed negative cells (i.e. true integration events, in contrast to GFP/DsRed double positive, which arise from material transfer) were almost always found within the first wo rows on ONL photoreceptor nuclei, whereas photoreceptor somata that were the recipients of material transfer were evenly distributed throughout the radial extent of the ONL (Pearson *et al.*, 2016). Whether true integration events are permanently restricted to the apical most portion of the ONL or whether gradual basal movement occurs later on in the post-transplantation period is currently not known.

7.2.2. The migration of rod photoreceptors on Müller glia primary cells

Based on previous works, transplanted rod photoreceptors have been proposed to migrate along resident Müller glia during the migration/integration process (Warre-Cornish, PhD thesis, 2013). As part of that study, a primary Müller glia & rod cell co-culture system was developed as an *in vitro* transplantation model and rod photoreceptor migration assay. Following time-lapse microscopy, the movement of rod cells relative to Müller glia was manually tracked *in silico*. In this present study, a reliable and time-efficient semi-automated rod tracking methodology was developed that could detect the movements of cultured rod photoreceptors. Importantly, it produced quantifications of rod motility that were very similar to previous descriptions based on manual cell tracking. However, during the course of this experiment, it was discovered that the substrate Müller glia primary cells retain a not insignificant degree of motility and constantly change shape and form. Altogether, this was determined to be too great, but most importantly, too variable, in order to be able to clearly distinguish rod motility from Müller cell plasticity.

By contrast, the *in vitro* migration of cerebellar neuronal precursor cells along Bergman radial glia – the classic *in vitro* glial-guided neuronal migration system – was, apparently, easier to demonstrate (Edmondson and Hatten, 1987; Gregory *et al.*, 1988; Anton *et al.*, 1997; Figure 7.2.1A). This classic experiment could in fact be replicated without difficulty within this study and the migration of neuronal precursor cells along radial glia was readily apparent (Figure 7.2.1B). Cultured Bergman radial glia are a lot thinner, while still being elongated, than the pre-established mature Müller glia cultures, which, by contrast, exhibit a flattened and wider appearance. With these widened cellular borders, plastic changes in Müller cell morphology may be a lot more pronounced compared with the Bergmann radial glia and they may have a much greater potential to push overlying cells around. If sufficiently large, these plastic changes could easily mask any intrinsic motility displayed by the overlying rod cell.

To circumvent this, it was attempted to arithmetically subtract the motility associated with Müller glia plastic behaviour from the perceived, apparent rod photoreceptor motility in this co-culture system. However, this proved to be too variable to arrive at a reliable conclusion. Another way to circumvent this could be to arrest all plastic changes in Müller cell shape and morphology prior to adding the freshly isolated rod photoreceptors. Pre-established Müller glia primary cell cultures may, for instance, be fixed prior to the

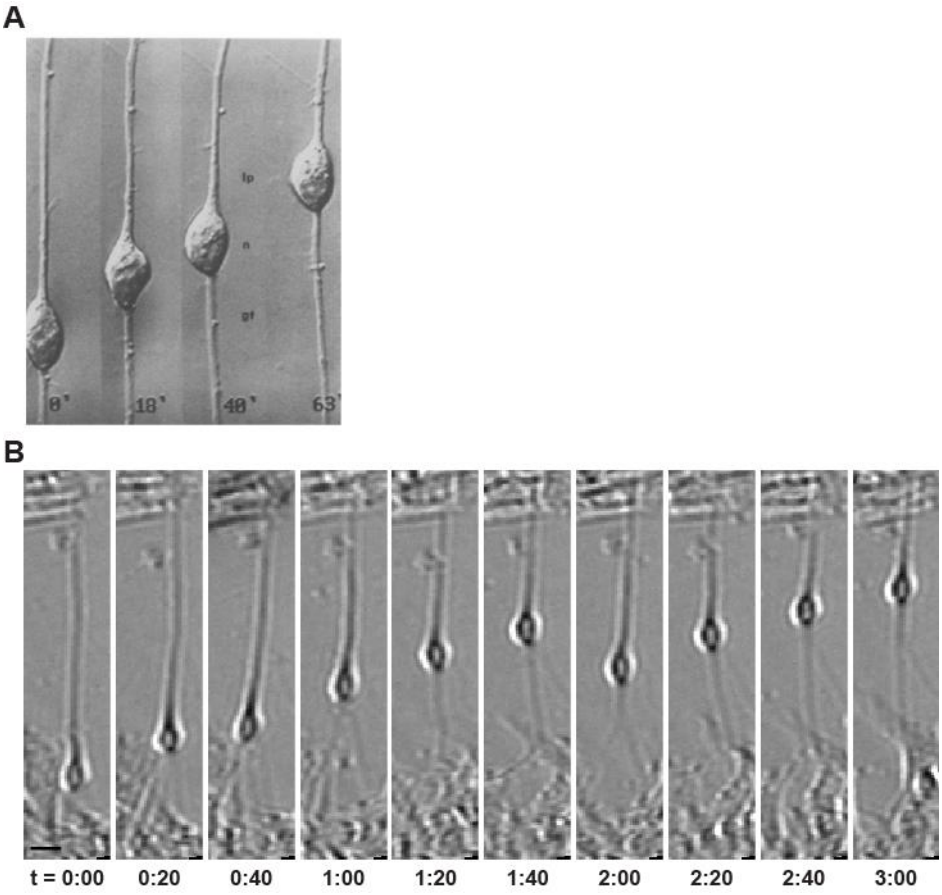

Figure 7.2.1 Glial-guided neuronal migration in the cortex – an i*n vitro* model. **(A)** Embryonic stage rodent hippocampal neurons migrate along cerebellar Bergmann radial glia in an *in vitro* co-culture system (reproduced, with permission, from Hatten and Mason, 1990). **(B)** Cortical glial-guided neuronal migration as reproduced as part of the present study. E13.5 (*Nrl.GFP*$^{+/+}$) mouse cerebellar cultures were prepared by enzymatic (trypsin) and mechanical dissociation and by plating onto a laminin coated dish. Cerebellar neurons were observed migrating along fibres (presumably Bergmann radial glia) from 24 hours after plating. Scale bar, 10 µm.

addition of freshly isolated rod photoreceptors. If the fixative is not well tolerated by the rod cells, pharmacological or genetic tools could be alternatively used in order to arrest the plastic changes in Müller cell morphology. Provided all Müller glia plastic changes can be arrested without affecting rod photoreceptors, the following are possible outcomes: a) rod photoreceptors migrate along arrested Müller glia; b) rod cells become stationary. The latter outcome would suggest that rod motilities detected in the co-culture model up to this point may have all been due to plastic changes in Müller cell morphology and shape, while the former suggests that rod cells possess intrinsic motility along their glial culture partner after all.

Should rod photoreceptors fail to migrate along Müller glia to any meaningful extent, how else might we explain the apparent physical interaction between rod photoreceptors and Müller cells? The evidence shown in this and previous studies has shown a strikingly close apposition between the rods and their nearest neighbouring Müller glial cell, often along the entire length of the rod photoreceptor (this thesis; Warre-Cornish, PhD thesis, 2013; Mack *et al.*, 2003). Müller glia have been shown in the past to be the preferred substrate for rod photoreceptor process/neurite extension (Kljavin and Reh, 1991) – a finding that has been replicated within the group previously (Warre-Cornish, PhD thesis, 2013), as well as within the present study (data not shown). Besides rod photoreceptors, Müller glia have been shown to directly support the *in vitro* neurite outgrowth of at least one other type of retinal neuron, the RGC (García *et al.*, 2002). This effect was increased by adding exogenous BDNF, suggesting that both cell-cell contact and soluble factors contribute to this process. Evidence suggests that the direct cell-cell contacts between Müller glia and RGCs are mediated by the cell adhesion molecules NCAM, N-cadherin and L1 (Drazba and Lemmon, 1990). Interestingly, amacrine cells were also able to produce neurites in culture when plated on dishes coated with either of the same three adhesion molecules, while rod photoreceptors grew neurites only on NCAM (Kljavin *et al.*, 1994). Müller glia thus likely support the neuritogenesis of various retinal neurons via cell-adhesion molecules expressed on both the retinal neurons and the glial partner. Homophilic NCAM is a strong candidate to mediate neurite outgrowth of rod cells along Müller glia. Post-translational modification of NCAM by poly-sialylation (PSA-NCAM) is known to increase the potential for neuronal migration and neurite outgrowth in general and PSA-NCAM is indeed expressed throughout the developing retina (hypo-sialylated NCAM, on the other hand, has a stabilising function in the nervous system and predominates in adulthood) (Bartsch *et al.*, 1990). The importance of NCAM, as well as

its sialylation state, for rod neuritogenesis and/or migration should thus be explored in future experiments.

Following neurite outgrowth, rod photoreceptors need to form synapses with bipolar and horizontal cells to establish the desired mature retinal circuitry. According to studies in the zebrafish, direct cellular contact with Müller glia at the level of the OPL is not required for synaptogenesis since the Müller cell branches are elaborated within the OPL only after synaptic contacts are formed (Williams *et al.*, 2010). Rather, paracrine signalling by the Müller glia seems to be required for the proper organisation and maturation of the photoreceptor ribbon synapse (Phillips *et al.*, 2011).

Considering all the points addressed within this section, it would seem reasonable to propose a role for Müller cells in rod photoreceptor neuritogenesis and synaptogenesis, while testing the role as a migration conduit will need robust further studies.

7.3. Future directions

Rod photoreceptors in the murine retina exhibit a high degree of motility along their radial axes during retinal development, displaying oscillatory apico-basal movements. These were collectively called oscillatory somal translocation, exhibiting morphological, kinetic and mechanistic similarities to IKNM and somal translocation. Future works will have to substantiate the findings that have already been generated here with the help of pharmacology and RNAi, using a refined genetic approach. The genetic tools available at the time of completion of this thesis did not target rod photoreceptors selectively/specifically. Using a different method of delivery or rod-specific promoters to drive the expression of the GOF/LOF constructs only in rods will both be explored. The primary goal will then be to perform time-lapse live imaging experiments on retinae where the expression levels of the genes of interest determined within this thesis are altered specifically in rod photoreceptors. This will be done in order to hopefully corroborate the time-lapse live imaging results generated here by means of pharmacological antagonists. Hence, RNAi of dynein I motor components is expected to attenuate rapid apical somal translocation in a similar way as the dynein I selective antagonist Ciliobrevin D. Overexpression may accelerate migration, as has been demonstrated for cultured mouse cerebellar granule neurons (Tanaka *et al.*, 2004). The other microtubule-associated motor protein KIF1A, which is currently hypothesised to function as a brake that acts to prevent excessively basal rod somal positions, could be addressed in a similar manner. It should be kept in mind, however, that the kinesin family of motor proteins consists of many isoforms and others may also contribute to rod somal motility (Tsai *et al.*, 2010). In order for dyneins and kinesins to cargo the rod nucleus along microtubule filaments, they need to associate with nuclear envelope binding partners – a role that is likely filled by the LINC complex and its constituent members (Sun1/2 and SYNE). The LINC complex has in fact already been implicated in photoreceptor somal positioning within the retina (Yu *et al.*, 2011; Razafsky *et al.*, 2012; Maddox *et al.*, 2015). However, a direct link to microtubule-associated motor proteins was so far only implied, but not fully demonstrated, and should thus be addressed in future experiments.

It is presently not well understood, whether actomyosin constrictions play a role in driving rod somal translocation in the developing retina, even after the LOF experiments

(pharmacological antagonist and RNAi) performed in the present study. To further investigate whether NMII, the motor protein responsible for actomyosin constrictions, mediates rod somal motility, it should be tested whether NMII GOF strategies (e.g. over-expression of constitutively active NMII) results in an increase in ectopically basal rod somata, since RNAi led to a slight apical crowding phenotype. More importantly, the focus should also be on targeting RNAi to rod photoreceptors specifically to avoid potential false positive due to non-specific RNAi targeting to non-rod cells. Given the content and extent of the mechanistic characterisation of developmental rod photoreceptor motility already achieved, it will be interesting to see if glial-guidance mechanisms are of any relevance. As discussed, however, an improved methodology will have to be designed that bypasses the complex nature of retinal pseudostratification in order to be able to unambiguously establish whether a clear links exists between rod motility and glial-guidance during retinogenesis. Currently, it was too difficult to distinguish active from passive rod somal movements and to establish whether contact between rod cells and NRSCs was deliberate or just due to space constraints.

It was hypothesised in this thesis that rod photoreceptors undergo apico-basal somal oscillations during retinal development in order for them to become enriched within the (presumptive) ONL and to prevent them for ending up in ectopically basal locations, which would otherwise lead to their apoptosis (Young, 1984). This hypothesis will need to be more thoroughly tested. For instance, this could be achieved by attenuating dynein I motor function by RNAi specifically in rod photoreceptors starting from neonatal stages and by subsequently monitoring the radial position of targeted rod somata throughout a fixed time point series. It will be especially interesting to find out whether those rod somata that find themselves within the OPL or INL rather than the ONL are more likely to undergo apoptosis. This can be easily achieved by checking for the presence of early and/or late apoptotic markers such as annexin V and cleaved caspase-3 respectively (Zhang *et al.*, 1997; Holubec *et al.*, 2005). Alternatively, they may remain in these ectopic locations and it will be particularly interesting to determine whether they can subsequently form correct synaptic connections with their appropriate postsynaptic partners.

Regarding the migration and integration of transplanted rod photoreceptors, further experiments will be required in order to conclude whether or not Müller glia are involved in the migration/integration process of photoreceptors. The *ex vivo* time lapse imaging of retinae from transplanted eyes will thus have to be optimised and repeated to permit

imaging of Müller glia labelled with a fluorescent marker such as DsRed, rather than Mitotracker® CMTMRos labelling. It will be of significant interest to examine the chemotaxis, neuritogenesis and nucleokinesis aspects of rod photoreceptor migration/integration into the recipient neural retina. There is a clear need to elucidate the cellular mechanism underlying material transfer, to determine whether or not material transfer from transplanted photoreceptors to resident photoreceptors could also constitute a novel therapeutic strategy; on the strength of the evidence presented thus far, it does appear sufficiently robust for fully functional gene products (mRNA and/or protein) of genes defective in the recipient to be exogenously resupplied (Pearson *et al.*, 2016; Santos-Ferreira *et al.*, 2016). Indirect evidence for this has been delivered in past studies where stationary night blind *Gnat1*$^{-/-}$ mice exhibited restored rod-mediated vision under scotopic light conditions following rod photoreceptor transplantation (Pearson *et al.*, 2012). More immediately, however, the transplantation field is already examining the potential for photoreceptor cell replacement therapy in disease stages with complete or near-complete loss of all photoreceptors, as is likely to be the case for most clinical presentations requiring treatment. In absence of a recipient ONL, the issue of material transfer becomes more academic.

REFERENCES

Adams NC, Tomoda T, Cooper M, Dietz G, Hatten ME (2002) Mice that lack astrotactin have slowed neuronal migration. Development 129:965–972.

Agathocleous M, Harris W a (2009) From progenitors to differentiated cells in the vertebrate retina. Annu Rev Cell Dev Biol 25:45–69.

Agte S, Junek S, Matthias S, Ulbricht E, Erdmann I, Wurm A, Schild D, Käs J a, Reichenbach A (2011) Müller glial cell-provided cellular light guidance through the vital guinea-pig retina. Biophys J 101:2611–2619.

Ahnelt K (1998) The photoreceptor mosaic. Nat Eye 12:531–540.

Akagi T, Inoue T, Miyoshi G, Bessho Y, Takahashi M, Lee JE, Guillemot F, Kageyama R (2004) Requirement of multiple basic helix-loop-helix genes for retinal neuronal subtype specification. J Biol Chem 279:28492–28498.

Akimoto M, Cheng H, Zhu D, Brzezinski JA, Khanna R, Filippova E, Oh ECT, Jing Y, Linares J-L, Brooks M, Zareparsi S, Mears AJ, Hero A, Glaser T, Swaroop A (2006) Targeting of GFP to newborn rods by Nrl promoter and temporal expression profiling of flow-sorted photoreceptors. Proc Natl Acad Sci U S A 103:3890–3895.

Alexandre P, Reugels AM, Barker D, Blanc E, Clarke JDW (2010) Neurons derive from the more apical daughter in asymmetric divisions in the zebrafish neural tube. Nat Neurosci 13:673–679.

Altman J (1969) Autoradiographic and Histological Studies of Postnatal Neurogenesis. J Comp Neur 137:433–458.

Anton ES, Cameron RS, Rakic P (1996) Role of neuron-glial junctional domain proteins in the maintenance and termination of neuronal migration across the embryonic cerebral wall. J Neurosci 16:2283–2293.

Anton ES, Kreidberg JA, Rakic P (1999) Distinct Functions of a3 and aV Integrin Receptors in Neuronal Migration and Laminar Organization of the Cerebral Cortex. Neuron 22:277–289.

Anton ES, Marchionni MA, Lee K, Rakic P (1997) Role of GGF / neuregulin signaling in interactions between migrating neurons and radial glia in the developing cerebral cortex. Development 124:3501–3510.

Aoki Y, Huang Z, Thomas SS, Bhide PG, Huang I, Moskowitz M a, Reeves S a (2000) Increased susceptibility to ischemia-induced brain damage in transgenic mice overexpressing a dominant negative form of SHP2. FASEB J 14:1965–1973.

Araque A, Carmignoto G, Haydon PG, Oliet SHR, Robitaille R, Volterra A (2014) Gliotransmitters travel in time and space. Neuron 81:728–739.

Arshavsky VY, Burns ME (2012) Photoreceptor Signaling: Supporting Vision across a Wide Range of Light Intensities. J Biol Chem 287:1620–1626.

Assadi AH, Zhang G, Beffert U, Mcneil RS, Renfro AL, Niu S, Quattrocchi CC, Antalffy BA, Sheldon M, Armstrong DD, Wynshaw-boris A, Herz J, Arcangelo GD, Clark GD (2003) Interaction of reelin signaling and Lis1 in brain development. Nat Genet 35:270–276.

Assawachananont J, Mandai M, Okamoto S, Yamada C, Eiraku M, Yonemura S, Sasai Y, Takahashi M (2014) Transplantation of embryonic and induced pluripotent stem cell-derived 3D retinal sheets into retinal degenerative mice. Stem Cell Reports 2:662–674.

Bae S, Bessho Y, Hojo M, Kageyama R (2000) The bHLH gene Hes6, an inhibitor of Hes1, promotes neuronal differentiation. Development 127:2933–2943.

Baehr W, Devlin MJ, Applebury ML (1979) Isolation and Characterisation of cGMP Phosphodiesterase from Bovine Rod Outer Segments. J biol Chem 254:11669–11667.

Baffet AD, Hu DJ, Vallee RB (2015) Cdk1 Activates Pre-mitotic Nuclear Envelope Dynein Recruitment and Apical Nuclear Migration in Neural Stem Cells. Dev Cell 33:703–716.

Bainbridge JWB, Mehat MS, Sundaram V, Robbie SJ, Barker SE, Ripamonti C (2015) Long-Term Effect of Gene Therapy on Leber's Congenital Amaurosis. N Engl J Med 372:1887–1897.

Bainbridge JWB, Smith AJ, Barker SS, Robbie S, Henderson R, Balaggan K, Viswanathan A, Holder GE, Stockman A, Tyler N, Petersen-Jones S, Bhattacharya SS, Thrasher AJ, Fitzke FW, Carter BJ, Rubin GS, Moore AT, Ali RR (2008) Effect of gene therapy on visual function in Leber's congenital amaurosis. N Engl J Med 358:2231–2239.

Banin E, Obolensky A, Idelson M, Hemo I, Reinhardtz E, Pikarsky E, Ben-Hur T, Reubinoff B (2006) Retinal

Incorporation and Differentiation of Neural Precursors Derived from Human Embryonic Stem Cells. Stem Cells 24:246–257.

Barber AC, Hippert C, Duran Y, West EL, Bainbridge JWB, Warre-cornish K, Luhmann UFO, Lakowski J, Sowden JC, Ali RR, Pearson RA (2013) Repair of the degenerate retina by photoreceptor transplantation. Proc Natl Acad Sci 110:354–359.

Barnea-Cramer AO, Wang W, Lu S-J, Singh MS, Luo C, Huo H, McClements ME, Barnard AR, MacLaren RE, Lanza R (2016) Function of human pluripotent stem cell-derived photoreceptor progenitors in blind mice. Sci Rep 6:29784.

Bartsch U, Kirchhoff F, Schachner M (1990) Highly sialylated N-CAM is expressed in adult mouse optic nerve and retina. J Neurocytol 19:550–565.

Bartsch U, Oriyakhel W, Kenna PF, Linke S, Richard G, Petrowitz B, Humphries P, Farrar GJ, Ader M (2008) Retinal cells integrate into the outer nuclear layer and differentiate into mature photoreceptors after subretinal transplantation into adult mice. Exp Eye Res 86:691–700.

Basak O, Taylor V (2007) Identification of self-replicating multipotent progenitors in the embryonic nervous system by high Notch activity and Hes5 expression. Eur J Neurosci 25:1006–1022.

Bassett EA, Wallace VA (2012) Cell fate determination in the vertebrate retina. Trends Neurosci 35:565–573.

Baye LM, Link BA (2007) Interkinetic nuclear migration and the selection of neurogenic cell divisions during vertebrate retinogenesis. J Neurosci 27:10143–10152.

Baye LM, Link BA (2008a) Nuclear migration during retinal development. Brain Res 1192:29–36.

Baye LM, Link B a (2008b) Nuclear migration during retinal development. Brain Res 1192:29–36.

Baylor BYDA, Lamb TD, Yau K (1979) Responses of Retinal Rods To Single Photons. J Physiol 288:613–634.

Bellion A, Baudoin J-P, Alvarez C, Bornens M, Métin C (2005) Nucleokinesis in tangentially migrating neurons comprises two alternating phases: forward migration of the Golgi/centrosome associated with centrosome splitting and myosin contraction at the rear. J Neurosci 25:5691–5699.

Belvindrah R, Graus-porta D, Goebbels S, Nave K, Muller U (2007) b1 Integrins in Radial Glia But Not in Migrating Neurons Are Essential for the Formation of Cell Layers in the Cerebral Cortex. J Neurosci 27:13854–13865.

Bianchini P, Calzia D, Ravera S, Candiano G, Bachi A, Morelli A, Bruschi M, Pepe IM, Diaspro A, Panfoli I (2014) Live imaging of mammalian retina: rod outer segments are stained by conventional mitochondrial dyes. J Biomed Opt 13:54017.

Biedermann B, Bringmann A, Reichenbach A (2002) High-affinity GABA uptake in retinal glial (Müller) cells of the guinea pig: Electrophysiological characterization, immunohistochemical localization, and modeling of efficiency. Glia 39:217–228.

Blackshaw S, Harpavat S, Trimarchi J, Cai L, Huang H, Kuo WP, Weber G, Lee K, Fraioli RE, Cho S-H, Yung R, Asch E, Ohno-Machado L, Wong WH, Cepko CL (2004) Genomic analysis of mouse retinal development. PLoS Biol 2:E247.

Blanchoin L, Boujemaa-paterski R, Sykes C, Plastino J (2014) Actin dynamics, architecture, and mechanics in cell motility. Physiol Rev 94:235–263.

Blanks JC, Adinolfi AM, Lolley RN (1974) Synaptogenesis in the Photoreceptor Terminal of the Mouse Retina. J Comp Neurol 156:81–94.

Boije H, Edqvist P-HD, Hallböök F (2009) Horizontal cell progenitors arrest in G2-phase and undergo terminal mitosis on the vitreal side of the chick retina. Dev Biol 330:105–113.

Borghesani PR, Peyrin JM, Klein R, Rubin J, Carter AR, Schwartz PM, Luster A, Corfas G, Segal RA (2002) BDNF stimulates migration of cerebellar granule cells. Development 129:1435–1442.

Bornens M (2008) Organelle positioning and cell polarity. Nat Rev Mol Cell Biol 9:874–886.

Borrell V, Kaspar BK, Gage FH, Callaway EM (2006) In vivo Evidence for Radial Migration of Neurons by Long-Distance Somal Translocation in the Developing Ferret Visual Cortex. Cereb cortex 16:1571–1583.

Bort R, Signore M, Tremblay K, Barbera JPM, Zaret KS (2006) Hex homeobox gene controls the transition of the endoderm to a pseudostratified, cell emergent epithelium for liver bud development. Dev Biol 290:44–56.

Boye SE, Boye SL, Lewin AS, Hauswirth WW (2013) A comprehensive review of retinal gene therapy. Mol Ther 21:509–519.

Brew H, Attwell D (1987) Electrogenic glutamate uptake is a major current carrier in the membrane of axolotl retinal glial cells. Nature 327:707–709.

Bringmann A, Iandiev I, Pannicke T, Wurm A, Hollborn M, Wiedemann P, Osborne NN, Reichenbach A (2009a)

Cellular signaling and factors involved in Müller cell gliosis: Neuroprotective and detrimental effects. Prog Retin Eye Res 28:423–451.

Bringmann A, Pannicke T, Biedermann B, Francke M, Iandiev I, Grosche J, Wiedemann P, Albrecht J, Reichenbach A (2009b) Role of retinal glial cells in neurotransmitter uptake and metabolism. Neurochem Int 54:143–160.

Bringmann A, Pannicke T, Grosche J, Francke M, Wiedemann P, Skatchkov SN, Osborne NN, Reichenbach A (2006) Müller cells in the healthy and diseased retina. Prog Retin Eye Res 25:397–424.

Brink HE, Stalling SS, Nicoll SB (2005) Influence of serum on adult and fetal dermal fibroblast migration, adhesion, and collagen expression. In Vitro Cell Dev Biol Anim 41:252–257.

Brown NL, Kanekar S, Vetter ML, Tucker PK, Gemza DL (1998) Math5 encodes a murine basic helix-loop-helix transcription factor expressed during early stages of retinal neurogenesis. Development 125:4821–4833.

Brzezinski JA, Park KU, Reh TA (2013) Blimp1 (Prdm1) prevents re-specification of photoreceptors into retinal bipolar cells by restricting competence. Dev Biol 384:194–204.

Bunr-Milam AH, Saari JC, Klock IB, Garwin GG (1985) Zonulae Adherentes Pore Size in the Externol Limiting Membrone of the Rabbit Retina. Invest Ophthalmol Vis Sci 26:1377–1380.

Burmeister M, Novak J, Liang MY, Basu S, Ploder L, Hawes NL, Vidgen D, Hoover F, Goldman D, Kalnins VI, Roderick TH, Taylor B a, Hankin MH, McInnes RR (1996) Ocular retardation mouse caused by Chx10 homeobox null allele: impaired retinal progenitor proliferation and bipolar cell differentiation. Nat Genet 12:376–384.

Calegari F, Huttner WB (2003) An inhibition of cyclin-dependent kinases that lengthens, but does not arrest, neuroepithelial cell cycle induces premature neurogenesis. J Cell Sci 116:4947–4955.

Calvert PD, Krasnoperova N V, Lyubarsky a L, Isayama T, Nicoló M, Kosaras B, Wong G, Gannon KS, Margolskee RF, Sidman RL, Pugh EN, Makino CL, Lem J (2000) Phototransduction in transgenic mice after targeted deletion of the rod transducin alpha -subunit. Proc Natl Acad Sci U S A 97:13913–13918.

Carabalona A, Hu DJ-K, Vallee RB (2016) KIF1A inhibition immortalizes brain stem cells but blocks BDNF-mediated neuronal migration. Nat Neurosci 19.

Carter-Dawson LD, LaVail MM (1979) Rods and Cones in the Mouse Retina - Autoradiographic Analysis of Cell Generation using Tritiated Thymidine. J Comp Neur 188:263–272.

Causeret F, Hidalgo-Sanchez M, Fort P, Backer S, Popoff M-R, Gauthier-Rouvière C, Bloch-Gallego E (2004) Distinct roles of Rac1/Cdc42 and Rho/Rock for axon outgrowth and nucleokinesis of precerebellar neurons toward netrin 1. Development 131:2841–2852.

Cepko C (2014) Intrinsically different retinal progenitor cells produce specific types of progeny. Nature 15:615–627.

Cepko CL (2015) The Determination of Rod and Cone Photoreceptor Fate. Annu Rev Vis Sci 1:211–234.

Cepko CL, Austin CP, Yang X, Alexiades M, Ezzeddine D (1996) Cell fate determination in the vertebrate retina. Proc Natl Acad Sci U S A 93:589–595.

Chaitin MH, Ankrum MT, Wortham HS (1996) Distribution of CD44 in the retina during development and the rds degeneration. Dev Brain Res 94:92–98.

Chebabo SR, Hester M a., Aitken PG, Somjen GG (1995) Hypotonic exposure enhances synaptic transmission and triggers spreading depression in rat hippocampal tissue slices. Brain Res 695:203–216.

Chen CK, Burns ME, Spencer M, Niemi G a, Chen J, Hurley JB, Baylor D a, Simon MI (1999) Abnormal photoresponses and light-induced apoptosis in rods lacking rhodopsin kinase. Proc Natl Acad Sci U S A 96:3718–3722.

Chen G, Sima J, Jin M, Wang K-Y, Xue X-J, Zheng W, Ding Y-Q, Yuan X-B (2008) Semaphorin-3A guides radial migration of cortical neurons during development. Nat Neurosci 11:36–44.

Chen HJ, Ma ZZ (2007) N-cadherin expression in a rat model of retinal detachment and reattachment. Investig Ophthalmol Vis Sci 48:1832–1838.

Chen J, Rattner A, Nathans J (2005) The Rod Photoreceptor-Specific Nuclear Receptor Nr2e3 Represses Transcription of Multiple Cone-Specific Genes. J Neurosci 25:118–129.

Chen Y, Sheng ZH (2013) Kinesin-1-syntaphilin coupling mediates activity-dependent regulation of axonal mitochondrial transport. J Cell Biol 202:351–364.

Cheng H, Aleman TS, Cideciyan A V., Khanna R, Jacobson SG, Swaroop A (2006) In vivo function of the orphan nuclear receptor NR2E3 in establishing photoreceptor identity during mammalian retinal development. Hum Mol Genet 15:2588–2602.

Cheng H, Khanna H, Oh ECT, Hicks D, Mitton KP, Swaroop A (2004a) Photoreceptor-specific nuclear receptor

NR2E3 functions as a transcriptional activator in rod photoreceptors. Hum Mol Genet 13:1563–1575.

Cheng L, Jin Z, Liu L, Yan Y, Li T, Zhu X, Jing N (2004b) Characterization and promoter analysis of the mouse nestin gene. FEBS Lett 565:195–202.

Chenouard N et al. (2014) Objective comparison of particle tracking methods. Nat Methods 11:281–289.

Chow RL, Lang RA (2001) Early Eye Development in Vertebrates. Annu Rev cell Dev Biol 17:255–296.

Chow RW-Y, Almeida AD, Randlett O, Norden C, Harris WA (2015) Inhibitory neuron migration and IPL formation in the developing zebrafish retina. Development 142:2665–2677.

Cicero MT (46BC) Orator.

Cina C, Maass K, Theis M, Willecke K, Bechberger JF, Naus CC (2009) Involvement of the cytoplasmic C-terminal domain of connexin43 in neuronal migration. J Neurosci 29:2009–2021.

Clarke GM, Anderson C a, Pettersson FH, Cardon LR, Andrew P (2011) Basic statistical analysis in genetic case-control studies. Nat Protoc 6:121–133.

Cooper JA (2008) A mechanism for inside-out lamination in the neocortex. Trends Neurosci:113–119.

Cooper JA (2014) Molecules and mechanisms that regulate multipolar migration in the intermediate zone. Front Cell Neurosci 8:1–11.

Cooper J a (2013) Mechanisms of cell migration in the nervous system. J Cell Biol 202:725–734.

Cooper N, Liu L, Yoshida A, Pozdnyakov N, Margulis A, Sitaramayya A (1995) The bovine rod outer segment guanylate cyclase, ROS-GC, is present in both outer segment and synaptic layers of the retina. J Mol Neurosci 6:211–222.

Corish P, Tyler-Smith C (1999) Attenuation of green fluorescent protein half-life in mammalian cells. Protein Eng 12:1035–1040.

Crisp M, Liu Q, Roux K, Rattner JB, Shanahan C, Burke B, Stahl PD, Hodzic D (2006) Coupling of the nucleus and cytoplasm: Role of the LINC complex. J Cell Biol 172:41–53.

Curcio CA, Medeiros NE, Millican CL (1996) Photoreceptor loss in age-related macular degeneration. Invest Ophthalmol Vis Sci 37:1236–1249.

Curcio CA, Sloan KR, Packer O, Hendrickson AE, Kalina RE (1985) Distribution of Cones in Human and Monkey Retina : Individual Variability and Radial Asymmetry. Science (80-) 236:579–582.

da Cruz L, Coley BF, Dorn J, Merlini F, Filley E, Christopher P, Chen FK, Wuyyuru V, Sahel J, Stanga P, Humayun M, Greenberg RJ, Dagnelie G (2013) The Argus II epiretinal prosthesis system allows letter and word reading and long-term function in patients with profound vision loss. Br J Ophthalmol 97:632–636.

Daiger SP, Sullivan LS, Bowne SJ (2013) RetNet - Retinal Information Network. Lab Mol Diagnosis Inherit Eye Dis Available at: https://sph.uth.edu/Retnet/home.htm.

Das SR, Bhardwaj N, Kjeldbye H, Gouras P (1992) Muller cells of chicken retina synthesize 11-cis-retinol. Biochem J 285 (Pt 3:907–913.

Das A V., Mallya KB, Zhao X, Ahmad F, Bhattacharya S, Thoreson WB, Hegde G V., Ahmad I (2006) Neural stem cell properties of Müller glia in the mammalian retina: Regulation by Notch and Wnt signaling. Dev Biol 299:283–302.

de Melo J, Blackshaw S (2011) In vivo electroporation of developing mouse retina. J Vis Exp:2–6.

Decembrini S, Koch U, Radtke F, Moulin A, Arsenijevic Y (2014) Derivation of traceable and transplantable photoreceptors from mouse embryonic stem cells. Stem Cell Reports 2:853–865.

Del Bene F, Wehman AM, Link B a, Baier H (2008) Regulation of neurogenesis by interkinetic nuclear migration through an apical-basal notch gradient. Cell 134:1055–1065.

Del Debbio CB, Balasubramanian S, Parameswaran S, Chaudhuri A, Qiu F, Ahmad I (2010) Notch and wnt signaling mediated rod photoreceptor regeneration by müller cells in adult mammalian retina. PLoS One 5:e12425.

Dent EW, Gertler FB (2003) Cytoskeletal Dynamics and Review Transport in Growth Cone Motility and Axon Guidance. Neuron 40:209–227.

Dent EW, Gupton SL, Gertler FB (2011) The Growth Cone Cytoskeleton in Axon Outgrowth and Guidance. Cold Spring Harb Perspect Biol 3:1–39.

Deterre P, Bigay J, Forquet F, Robert M, Chabre M (1988) cGMP phosphodiesterase of retinal rods is regulated by two inhibitory subunits. Proc Natl Acad Sci U S A 85:2424–2428.

Dimidschstein J, Passante L, Dufour A, Ameele J Van Den, Tiberi L, Hrechdakian T, Adams R, Lie DC, Jossin Y,

Vanderhaeghen P (2013) Ephrin-B1 Controls the Columnar Distribution of Cortical Pyramidal Neurons by Restricting Their Tangential Migration. Neuron 79:1123–1135.

Distel M, Hocking JC, Volkmann K, Köster RW (2010) The centrosome neither persistently leads migration nor determines the site of axonogenesis in migrating neurons in vivo. J Cell Biol 191:875–890.

Dmitriev A V, Govardovskii VI, Schwahn HN, Steinberg RH (1999) Light-induced changes of extracellular ions and volume in the isolated chick retina-pigment epithelium preparation. Vis Neurosci 16:1157–1167.

Domesick VB, Morest DK (1977) Migration and differentiation of ganglion cells in the optic tectum of the chick embryo. Neuroscience 2:459–475.

Dorn JD, Ahuja AK, Caspi A, Da Cruz L, Dagnelie G, Sahel JA, Greenberg RJ, McMahon MJ, Group AIS (2013) The Detection of Motion by Blind Subjects with the Epiretinal 60-Electrode (Argus II) Retinal Prosthesis. JAMA Ophthalmolgoy 131:183–189.

Drazba J, Lemmon V (1990) The role of cell adhesion molecules in neurite outgrowth on Muller cells. Dev Biol 138:82–93.

Dudek FE, Obenaus a, Tasker JG (1990) Osmolality-induced changes in extracellular volume alter epileptiform bursts independent of chemical synapses in the rat: importance of non-synaptic mechanisms in hippocampal epileptogenesis. Neurosci Lett 120:267–270.

Eberle D, Schubert S, Postel K, Corbeil D, Ader M (2011) Increased integration of transplanted CD73-positive photoreceptor precursors into adult mouse retina. Invest Ophthalmol Vis Sci 52:6462–6471.

Edmondson JC, Hatten ME (1987) Glial-Guided Granule Neuron Migration Video Microscopic Study in vitro : A High-Resolution Time-Lapse Video Microscopic Study. J Neurosci 7:1926–1934.

Edqvist P-HD, Hallböök F (2004) Newborn horizontal cells migrate bi-directionally across the neuroepithelium during retinal development. Development 131:1343–1351.

Eglen SJ, van Ooyen A, Willshaw DJ (2000) Lateral cell movement driven by dendritic interactions is sufficient to form retinal mosaics. Network 11:103–118.

Eichler W, Yafai Y, Keller T, Wiedemann P, Reichenbach A (2004a) PEDF derived from glial Müller cells: A possible regulator of retinal angiogenesis. Exp Cell Res 299:68–78.

Eichler W, Yafai Y, Wiedemann P, Reichenbach A (2004b) Angiogenesis-related factors derived from retinal glial (Müller) cells in hypoxia. Neuroreport 15:1633–1637.

Eiraku M, Takata N, Ishibashi H, Kawada M, Sakakura E, Okuda S, Sekiguchi K, Adachi T, Sasai Y (2011) Self-organizing optic-cup morphogenesis in three-dimensional culture. Nature 472:51–56.

Elias LAB, Wang DD, Kriegstein AR (2007) Gap junction adhesion is necessary for radial migration in the neocortex. Nature 448:901–907.

Evsyukova I, Plestant C, Anton ES (2013) Integrative mechanisms of oriented neuronal migration in the developing brain. Annu Rev Cell Dev Biol 29:299–353.

Fain GL, Gerschenfeld HM, Quandt FN (1980) Calcium Spikes in Toad Rods. J Physiol 303:495–513.

Fan SS, Ready DF (1997) Glued participates in distinct microtubule-based activities in Drosophila eye development. Development 124:1497–1507.

Ferreira TS, Postel K, Stutzki H, Zeck G, Ader M (2015) Daylight Vision Repair by Cell Transplantation. Stem Cells 33:79–90.

Fesenko EE, Kolesnikov SS, Lyubarsky AL (1985) Induction by cyclic GMP of cationic conductance in plasma membrane of retinal rod outer segment. Nature 313:310–313.

Firestone AJ, Weinger JS, Maldonado M, Barlan K, Langston LD, O'Donnell M, Gelfand VI, Kapoor TM, Chen JK (2012) Small-molecule inhibitors of the AAA+ ATPase motor cytoplasmic dynein. Nature 484:125–129.

Fishell G, Hatten ME (1991) Astrotactin provides a receptor system for CNS neuronal migration. Development 113:755–765.

Fletcher DA, Mullins RD (2010) Cell mechanics and the cytoskeleton. Na 463:485–492.

Frade JM (2002) Interkinetic nuclear movement in the vertebrate neuroepithelium: encounters with an old acquaintance. Prog Brain Res 136:67–71.

Franco SJ, Martinez-Garay I, Gil-Sanz C, Harkins-Perry SR, Müller U (2011) Reelin Regulates Cadherin Function via Dab1/Rap1 to Control Neuronal Migration and Lamination in the Neocortex. Neuron 69:482–497.

Franze K, Grosche J, Skatchkov SN, Schinkinger S, Foja C, Schild D, Uckermann O, Travis K, Reichenbach A, Guck J (2007) Müller cells are living optical fibers in the vertebrate retina. Proc Natl Acad Sci U S A 104:8287–8292.

Fuerst PG, Burgess RW (2009) Adhesion molecules in establishing retinal circuitry. Curr Opin Neurobiol 19:389–394.

Fuerst PG, Koizumi A, Masland RH, Burgess RW (2008) Neurite arborization and mosaic spacing in the mouse retina require DSCAM. Nature 451:470–474.

Furukawa T, Morrow EM, Li T, Davis FC, Cepko CL (1999) Retinopathy and attenuated circadian entrainment in Crx-deficient mice. Nat Genet 23:466–470.

Furukawa T, Mukherjee S, Bao Z, Morrow EM, Cepko CL (2000) rax , Hes1 , and notch1 Promote the Formation of Müller Glia by Postnatal Retinal Progenitor Cells. Neuron 26:383–394.

Gaiano N, Nye JS, Fishell G (2000) Radial Glial Identity Is Promoted by Notch1 Signaling in the Murine Forebrain. Neuron 26:395–404.

Gambello MJ, Darling DL, Yingling J, Tanaka T, Gleeson JG, Wynshaw-Boris A (2003) Multiple dose-dependent effects of Lis1 on cerebral cortical development. J Neurosci 23:1719–1729.

Gao G, Lu F, Sanmiguel JC, Tran PT, Abbas Z, Lynd KS, Marsh J, Spinner NB, Wilson JM (2002) Rep/Cap gene amplification and high-yield production of AAV in an A549 cell line expressing Rep/Cap. Mol Ther 5:644–649.

García M, Forster V, Hicks D, Vecino E (2002) Effects of Müller glia on cell survival and neuritogenesis in adult porcine retina in vitro. Investig Ophthalmol Vis Sci 43:3735–3743.

Geraldo S, Gordon-Weeks PR (2009) Cytoskeletal dynamics in growth-cone steering. J Cell Sci 122:3595–3604.

Godinho L, Link BA (2012) Cell migration. In: Retinal Development, 1st ed. (Sernagor E, Eglen S, Harris B, Wong R, eds), pp 74. Cambridge: Cambridge University Press.

Godinho L, Mumm JS, Williams PR, Schroeter EH, Koerber A, Park SW, Leach SD, Wong ROL (2005) Targeting of amacrine cell neurites to appropriate synaptic laminae in the developing zebrafish retina. Development 132:5069–5079.

Godinho L, Williams PR, Claassen Y, Provost E, Leach SD, Kamermans M, Wong ROL (2007) Nonapical symmetric divisions underlie horizontal cell layer formation in the developing retina in vivo. Neuron 56:597–603.

Goldman D (2014) Müller glial cell reprogramming and retina regeneration. Nat Rev Neurosci 15:431–442.

Gomes FL a F, Zhang G, Carbonell F, Correa J a, Harris W a, Simons BD, Cayouette M (2011) Reconstruction of rat retinal progenitor cell lineages in vitro reveals a surprising degree of stochasticity in cell fate decisions. Development 138:227–235.

Gonzalez-Cordero A, West EL, Pearson R a, Duran Y, Carvalho LS, Chu CJ, Naeem A, Blackford SJI, Georgiadis A, Lakowski J, Hubank M, Smith AJ, Bainbridge JWB, Sowden JC, Ali RR (2013) Photoreceptor precursors derived from three-dimensional embryonic stem cell cultures integrate and mature within adult degenerate retina. Nat Biotechnol 31:741–747.

Gouras P, Du J, Gelanze M, Kwun R, Kjeldbye H, Lopez R (1991a) Transplantation of photoreceptors labeled with tritiated thymidine into RCS rats. Invest Ophthalmol Vis Sci 32:1704–1707.

Gouras P, Du J, Gelanze M, Lopez R, Kwun R, Kjeldbye H, Krebs W (1991b) Survival and synapse formation of transplanted rat rods. J Neural Transplant Plast 2:91–100.

Gouras P, Du J, Kjeldbye H, Kwun R, Lopez R, Zack DJ (1991c) Transplanted photoreceptors identified in dystrophic mouse retina by a transgenic reporter gene. Investig Ophthalmol Vis Sci 32:3167–3174.

Gouras P, Du J, Kjeldbye H, Yamamoto S, Zack DJ (1992) Reconstruction of degenerate rd mouse retina by transplantation of transgenic photoreceptors. Investig Ophthalmol Vis Sci 33:2579–2586.

Gouras P, Du J, Kjeldbye H, Yamamoto S, Zack DJ (1994) Long-term photoreceptor transplants in dystrophic and normal mouse retina. Investig Ophthalmol Vis Sci 35:3145–3153.

Gouras P, Tanabe T (2003) Survival and integration of neural retinal transplants in rd mice. Graefe's Arch Clin Exp Ophthalmol 241:403–409.

Graw J (2010) Eye development. Curr Top Dev Biol 90:343–386.

Gregory A, Edmondson C, Hatten ME, Mason CA (1988) Cytology and Neuron-Glial Granule Cells in vitro Apposition of Migrating Cerebellar Granule Cells in vitro. J Neurosci 8:1728–1738.

Guo J, Anton ES (2014) Decision Making during Interneuron Migration in the Developing Cerebral Cortex. Trends Cell Biol 24:342–351.

Gust J, Reh TA (2011) Adult donor rod photoreceptors integrate into the mature mouse retina. Invest Ophthalmol Vis Sci 52:5266–5272.

Hagins WA, Penn RD, Yoshikami S (1970) Dark current and photocurrent in retinal rods. Biophys J 10:380–412.

Halfter W, Dong S, Balasubramani M, Bier ME (2001) Temporary disruption of the retinal basal lamina and its effect on retinal histogenesis. Dev Biol 238:79–96.

Hall A, Lalli G (2010) Rho and Ras GTPases in axon growth, guidance, and branching. Cold Spring Harb Perspect Biol 2:1–18.

Hamel C (2006) Retinitis pigmentosa. Orphanet J Rare Dis 1:40.

Hamon A, Roger JE, Yang X-J, Perron M (2015) Müller glial cell-dependent regeneration of the neural retina: An overview across vertebrate model systems. Dev Dyn:n/a-n/a.

Hartong DT, Berson EL, Dryja TP (2006) Retinitis pigmentosa. Lancet 368:1795–1809.

Hashimoto T, Zhang X-M, Chen BY, Yang X-J (2006) VEGF activates divergent intracellular signaling components to regulate retinal progenitor cell proliferation and neuronal differentiation. Development 133:2201–2210.

Hatakeyama J, Tomita K, Inoue T, Kageyama R (2001) Roles of homeobox and bHLH genes in specification of a retinal cell type. Development 128:1313–1322.

Hatanaka Y, Hisanaga S, Heizmann CW, Murakami F (2004) Distinct Migratory Behavior of Early- and Late-Born Neurons Derived from the Cortical Ventricular Zone. J Comp Neurol 479:1–14.

Hatten ME (1999) Central Nervous System Neuronal Migration. Annu Rev Neurosci 22:511–539.

Hatten ME, Mason CA (1990) Mechanisms of glial-guided neuronal migration in vitro and in vivo. Experientia 46:907–916.

Hawkins BS, Bressler NM, Miskala PH, Bressler SB, Holekamp NM, Marsh MJ, Redford M, Schwartz SD, Sternberg P, Thomas MA, Wilson DJ (2004) Surgery for subfoveal choroidal neovascularization in age-related macular degeneration: Ophthalmology 111:1967–1980.

He W, Cowan CW, Wensel TG (1998) RGS9, a GTPase accelerator for phototransduction. Neuron 20:95–102.

Hecht S, Shlaer S, Pirenne MH (1942) Energy, Quanta and Vision. J Gen Physiol 25:819–840.

Heck M, Hofmann KP (1993) G-protein-effector coupling: a real-time light-scattering assay for transducin-phosphodiesterase interaction. Biochemistry 32:8220–8227.

Heidelberger R, Thoreson WB, Witkovsky P (2006) Synaptic transmission at retinal ribbon synapses. Prog Retin Eye Res 24:682–720.

Heng JE, Vorwerk CK, Lessell E, Zurakowski D, Levin LA, Dreyer EB (1999) Ethambutol is toxic to retinal ganglion cells via an excitotoxic pathway. Investig Ophthalmol Vis Sci 40:190–196.

Heng JIT, Chariot A, Nguyen L (2010) Molecular layers underlying cytoskeletal remodelling during cortical development. Trends Neurosci 33:38–47.

Heng Y-W, Koh C-G (2010) Actin cytoskeleton dynamics and the cell division cycle. Int J Biochem Cell Biol 42:1622–1633.

Hennig AK, Peng G-H, Chen S (2008) Regulation of photoreceptor gene expression by Crx-associated transcription factor network. Brain Res 1192:114–133.

Henrique D, Hirsinger E, Adam J, Le Roux I, Pourquié O, Ish-Horowicz D, Lewis J (1997) Maintenance of neuroepithelial progenitor cells by Delta-Notch signalling in the embryonic chick retina. Curr Biol 7:661–670.

Hinds JW, Hinds PL (1978) Early development of amacrine cells in the mouse retina: an electron microscopic, serial section analysis. J Comp Neurol 179:277–300.

Hinds JW, Hinds PL (1979) Differentiation of photoreceptors and horizontal cells in the embryonic mouse retina: an electron microscopic, serial section analysis. J Comp Neurol 187:495–512.

Hippert C, Graca AB, Barber AC, West EL, Smith AJ, Ali RR, Pearson RA (2015) Müller glia activation in response to inherited retinal degeneration is highly varied and disease-specific. PLoS One 10:1–27.

Ho AC et al. (2015) Long-Term Results from an Epiretinal Prosthesis to Restore Sight to the Blind. Ophthalmology 122:1547–1554.

Hodgkin AL, McNaughton PA, Nunn BJ (1985) The Ionic Selectivity and Calcium Dependence of the Light-Sensitive Pathway in Toad Rods. J Physiol 358:447–468.

Hojo M, Ohtsuka T, Hashimoto N, Gradwohl G, Guillemot F, Kageyama R (2000) Glial cell fate specification modulated by the bHLH gene Hes5 in mouse retina. Development 127:2515–2522.

Hollyfield JG (1999) Hyaluronan and the functional organization of the interphotoreceptor matrix. Investig Ophthalmol Vis Sci 40:2767–2769.

Holt E, Bertsch W, Harris A (1988) Cellular Determination in the Xenopus Retina Is Independent of Lineage and Birth Date division. 1:15–26.

Holubec H, Payne CM, Bernstein H, Dvorakova K, Bernstein C, Waltmire CN, Warneke JA, Garewal H (2005) Assessment of Apoptosis by Immunohistochemical Markers Compared to Cellular Morphology in Ex Vivo-stressed Colonic Mucosa. J Histochem Cytochem 53:229–235.

Homma K, Okamoto S, Mandai M, Gotoh N, Rajasimha HK, Chang Y-S, Chen S, Li W, Cogliati T, Swaroop A, Takahashi M (2013) Developing rods transplanted into the degenerating retina of Crx-knockout mice exhibit neural activity similar to native photoreceptors. Stem Cells 31:1149–1159.

Hong SE, Shugart YY, Huang DT, Shahwan S Al, Grant PE, Jonathan OB, Martin NDT, Walsh CA (2000) Autosomal recessive lissencephaly with cerebellar hypoplasia is associated with human RELN mutations. Nature 26:93–96.

Hossain W a, Zhou X, Rutledge a, Baier C, Morest DK (1996) Basic fibroblast growth factor affects neuronal migration and differentiation in normotypic cell cultures from the cochleovestibular ganglion of the chick embryo. Exp Neurol 138:121–143.

Hsiau TH-C, Diaconu C, Myers C a, Lee J, Cepko CL, Corbo JC (2007) The cis-regulatory logic of the mammalian photoreceptor transcriptional network. PLoS One 2:e643.

Hu DJK, Baffet AD, Nayak T, Akhmanova A, Doye V, Vallee RB (2013) Dynein recruitment to nuclear pores activates apical nuclear migration and mitotic entry in brain progenitor cells. Cell 154:1300–1313.

Huang S, Moody SA (1997) Three types of serotonin-containing amacrine cells in tadpole retina have distinct clonal origins. J Comp Neurol 387:42–52.

Huckfeldt RM, Schubert T, Morgan JL, Godinho L, Di Cristo G, Huang ZJ, Wong ROL (2009) Transient neurites of retinal horizontal cells exhibit columnar tiling via homotypic interactions. Nat Neurosci 12:35–43.

Hughes EH, Schlichtenbrede FC, Murphy CC, Sarra GM, Luthert PJ, Ali RR, Dick AD (2003) Generation of activated sialoadhesin-positive microglia during retinal degeneration. Investig Ophthalmol Vis Sci 44:2229–2234.

Hyatt GA, Schmitt EA, Fadool JM, Dowling JE, Hyatt GA, Schmitt EA, Fado JM, Dowling JE (1996) Retinoic Acid Alters Photoreceptor Development in vivo. Proc Natl Acad Sci 93:13298–13303.

Ikeda H, Osakada F, Watanabe K, Mizuseki K, Haraguchi T, Miyoshi H, Kamiya D, Honda Y, Sasai N, Yoshimura N, Takahashi M, Sasai Y (2005) Generation of Rx+/Pax6+ neural retinal precursors from embryonic stem cells. Proc Natl Acad Sci U S A 102:11331–11336.

Inoue T, Hojo M, Bessho Y, Tano Y, Lee JE, Kageyama R (2002) Math3 and NeuroD regulate amacrine cell fate specification in the retina. Development 129:831–842.

Insinna C, Baye LM, Amsterdam A, Besharse JC, Link B a (2010) Analysis of a zebrafish dync1h1 mutant reveals multiple functions for cytoplasmic dynein 1 during retinal photoreceptor development. Neural Dev 5:12.

Izumi Y, Kirby CO, Benz a M, Olney JW, Zorumski CF (1999) Müller cell swelling, glutamate uptake, and excitotoxic neurodegeneration in the isolated rat retina. Glia 25:379–389.

Izumi Y, Shimamoto K, Benz AM, Hammerman SB, Olney JW, Zorumski CF (2002) Glutamate transporters and retinal excitotoxicity. Glia 39:58–68.

Jablonski MM, Iannaccone A (2000) Targeted disruption of Müller cell metabolism induces photoreceptor dysmorphogenesis. Glia 32:192–204.

Jadhav AP, Mason HA, Cepko CL (2006) Notch 1 inhibits photoreceptor production in the developing mammalian retina. Development 133:913–923.

Jadhav AP, Roesch K, Cepko CL (2009) Development and Neurogenic Potential of Müller Glial Cells in the Vertebrate Retina. Prog Retin Eye Res 28:249–262.

Jager RD, Mieler WF, Miller JW (2015) Age-Related Macular Degeneration. N Engl J Med 358:2606–2617.

Jefferys JGR (1995) Nonsynaptic Modulation of Neuronal Activity in the Brain : Electric Currents and Extracellular Ions. Physiol Rev 75:689–723.

Jia L, Oh ECT, Ng L, Srinivas M, Brooks M, Swaroop A, Forrest D (2009) Retinoid-related orphan nuclear receptor RORbeta is an early-acting factor in rod photoreceptor development. Proc Natl Acad Sci U S A 106:17534–17539.

Jiang C, Klassen H, Zhang X, Young M (2010) Laser injury promotes migration and integration of retinal progenitor cells into host retina. Mol Vis 16:983–990.

Jossin Y, Cooper J a (2011) Reelin, Rap1 and N-cadherin orient the migration of multipolar neurons in the developing neocortex. Nat Neurosci 14:697–703.

Jusuf PR, Harris W a (2009) Ptf1a is expressed transiently in all types of amacrine cells in the embryonic zebrafish retina. Neural Dev 4:34.

Kappeler C, Saillour Y, Baudoin J, Phan Dinh Tuy F, Alvarez C, Houbron C, Gaspar P, Hamard G, Chelly J, Metin C, Francis F (2006) Branching and nucleokinesis defects in migrating interneurons derived from doublecortin knockout mice. Hum Mol Genet 15:1387–1400.

Katoh K, Omori Y, Onishi A, Sato S, Kondo M, Furukawa T (2010) Blimp1 Suppresses Chx10 Expression in Differentiating Retinal Photoreceptor Precursors to Ensure Proper Photoreceptor Development. J Neurosci 30:6515–6526.

Kawaguchi A, Miyata T, Sawamoto K, Takashita N, Murayama A, Akamatsu W, Ogawa M, Okabe M, Tano Y, Goldman SA, Okano H (2001) Nestin-EGFP transgenic mice: visualization of the self-renewal and multipotency of CNS stem cells. Mol Cell Neurosci 17:259–273.

Kawai F, Horiguchi M, Suzuki H, Miyachi E-I (2001) Na+ Action Potentials in Human Photoreceptors. Neuron 30:451–458.

Kawamura S, Tachibanaki S (2008) Rod and cone photoreceptors: Molecular basis of the difference in their physiology. Comp Biochem Physiol Part A Mol Integr Physiol 150:369–377.

Kawauchi D, Taniguchi H, Watanabe H, Saito T, Murakami F (2006a) Direct visualization of nucleogenesis by precerebellar neurons: involvement of ventricle-directed, radial fibre-associated migration. Development 133:1113–1123.

Kawauchi T, Chihama K, Nabeshima Y, Hoshino M (2006b) Cdk5 phosphorylates and stabilizes p27 kip1 contributing to actin organization and cortical neuronal migration. 8.

Kawauchi T, Sekine K, Shikanai M, Chihama K, Tomita K, Kubo K, Nakajima K, Nabeshima Y-I, Hoshino M (2010) Rab GTPases-dependent endocytic pathways regulate neuronal migration and maturation through N-cadherin trafficking. Neuron 67:588–602.

Kelley MW, Williams RC, Turner JK, Creech-Kraft JM, Reh TA (1999) Retinoic acid promotes rod photoreceptor differentiation in rat retina in vivo. Neuroreport 10:2389–2394.

Kennedy B, Malicki J (2009) What drives cell morphogenesis: a look inside the vertebrate photoreceptor. Dev Dyn 238:2115–2138.

Khan RS, Fonseca-Kelly Z, Callinan C, Zuo L, Sachdeva MM, Shindler KS (2012) SIRT1 activating compounds reduce oxidative stress and prevent cell death in neuronal cells. Front Cell Neurosci 6:63.

Klassen HJ, Ng TF, Kurimoto Y, Kirov I, Shatos M, Coffey P, Young MJ (2004) Multipotent retinal progenitors express developmental markers, differentiate into retinal neurons, and preserve light-mediated behavior. Investig Ophthalmol Vis Sci 45:4167–4173.

Klimczak RR, Koerber JT, Dalkara D, Flannery JG, Schaffer D V (2009) A novel adeno-associated viral variant for efficient and selective intravitreal transduction of rat Müller cells. PLoS One 4:e7467.

Kljavin IJ, Legenaur C, Bixby JL, Reh TA (1994) Cell Adhesion Molecules Regulating Neurite Growth from Amacrine and Rod Photoreceptor Cells. J Neurosci 14:5035–5049.

Kljavin IJ, Reh TA (1991) Mueller Cells Are a Preferred Substrate by Rod Photoreceptor for in vitro Neurite Extension by Rod Photoreceptor Cells. J Neurosci 11:2985–2994.

Knöll B, Weinl C, Nordheim A, Bonhoeffer F (2007) Stripe assay to examine axonal guidance and cell migration. Nat Protoc 2:1216–1224.

Kofuji P, Biedermann B, Siddharthan V, Raap M, Iandiev I, Milenkovic I, Thomzig A, Veh RW, Bringmann A, Reichenbach A (2002) Kir potassium channel subunit expression in retinal glial cells: Implications for spatial potassium buffering. Glia 39:292–303.

Kosodo Y (2012) Interkinetic nuclear migration: Beyond a hallmark of neurogenesis. Cell Mol Life Sci 69:2727–2738.

Kosodo Y, Suetsugu T, Suda M, Mimori-Kiyosue Y, Toida K, Baba S a, Kimura A, Matsuzaki F (2011) Regulation of interkinetic nuclear migration by cell cycle-coupled active and passive mechanisms in the developing brain. EMBO J 30:1690–1704.

Krispel CM, Chen D, Melling N, Chen Y-J, Martemyanov KA, Quillinan N, Arshavsky VY, Wensel TG, Chen C-K, Burns ME (2006) RGS Expression Rate-Limits Recovery of Rod Photoresponses. Neuron 51:409–416.

Kwok-Keung Fung B, Stryer L (1980) Photolyzed rhodopsin catalyzes the exchange of GTP for bound GDP in retinal rod outer segments. Proc Natl Acad Sci U S A 77:2500–2504.

Labin AM, Safuri SK, Ribak EN, Perlman I (2014) Müller cells separate between wavelengths to improve day vision with minimal effect upon night vision. Nat Commun 5:4319.

Lakowski J, Baron M, Bainbridge J, Barber AC, Pearson RA, Ali RR, Sowden JC (2010) Cone and rod photoreceptor transplantation in models of the childhood retinopathy Leber congenital amaurosis using flow-sorted Crx-positive donor cells. Hum Mol Genet 19:4545–4559.

Lakowski J, Han Y-T, Pearson RA, Gonzalez-Cordero A, West EL, Gualdoni S, Barber AC, Hubank M, Ali RR, Sowden JC (2011) Effective Transplantation of Photoreceptor Precursor Cells Selected Via Cell Surface Antigen Expression. Stem Cells 29:1391–1404.

Lamba DA, McUsic A, Hirata RK, Wang P, Russell D, Reh TA (2010) Generation, Purification and Transplantation of Photoreceptors Derived from Human Induced Pluripotent Stem Cells. PLoS One 5:e8763.

Lange C, Huttner WB, Calegari F (2009) Cdk4/cyclinD1 overexpression in neural stem cells shortens G1, delays neurogenesis, and promotes the generation and expansion of basal progenitors. Cell Stem Cell 5:320–331.

Lee HO, Norden C (2013) Mechanisms controlling arrangements and movements of nuclei in pseudostratified epithelia. Trends Cell Biol 23:141–150.

Lee HY, Wroblewski E, Philips GT, Stair CN, Conley K, Reedy M, Mastick GS, Brown NL (2005) Multiple requirements for Hes1 during early eye formation Hae. Dev Biol 284:464–478.

Lee J-H, Park H-S, Shin JM, Chun M-H, Oh S-J (2012) Nestin expressing progenitor cells during establishment of the neural retina and its vasculature. Anat Cell Biol 45:38–46.

Lendahl U, Zimmerman LB, McKay RD (1990) CNS stem cells express a new class of intermediate filament protein. Cell 60:585–595.

Leskov IB, Klenchin V a, Handy JW, Whitlock GG, Govardovskii VI, Bownds MD, Lamb TD, Pugh EN, Arshavsky VY (2000) The gain of rod phototransduction: reconciliation of biochemical and electrophysiological measurements. Neuron 27:525–537.

Leung L, Klopper A V, Grill SW, Harris W a, Norden C (2011) Apical migration of nuclei during G2 is a prerequisite for all nuclear motion in zebrafish neuroepithelia. Development 138:5003–5013.

Linser PJ, Sorrentino M, Moscona AA (1984) Cellular compartmentalization of carbonic anhydrase-C and glutamine synthetase in developing and mature mouse neural retina. Dev Brain Res 13:65–71.

Lipshutz GS, Gruber C a, Cao Y, Hardy J, Contag CH, Gaensler KM (2001) In utero delivery of adeno-associated viral vectors: intraperitoneal gene transfer produces long-term expression. Mol Ther 3:284–292.

Liu JS, Antypa M, Rakic S, Walsh CA, Parnavelas JG (2007) Both Doublecortin and Doublecortin-Like Kinase Play a Role in Cortical Interneuron Migration. J Neurosci 27:3875–3883.

Liu JS, Schubert CR, Fu X, Fourniol FJ, Jaiswal JK, Houdusse A, Stultz CM, Moores CA, Walsh CA (2012) Molecular Basis for Specific Regulation of Neuronal Kinesin-3 Motors by Doublecortin Family Proteins. Mol Cell 47:707–721.

Liu W, Mo Z, Xiang M (2001) The Ath5 proneural genes function upstream of Brn3 POU domain transcription factor genes to promote retinal ganglion cell development. Proc Natl Acad Sci U S A 98:1649–1654.

Liu W, Wang JH, Xiang M (2000) Specific expression of the LIM/homeodomain protein Lim-1 in horizontal cells during retinogenesis. Dev Dyn 217:320–325.

Liu X, Seno K, Nishizawa Y, Hayashi F, Yamazaki A, Matsumoto H, Wakabayashi T, Usukura J (1994) Ultrastructural localization of retinal guanylate cyclase in human and monkey retinas. Exp Eye Res 59:761–768.

Livesey FJ, Young TL, Cepko CL (2004) An analysis of the gene expression program of mammalian neural progenitor cells. Proc Natl Acad Sci U S A 101:1374–1379.

Logan MA, Steele MR, Van Raay TJ, Vetter ML (2005) Identification of shared transcriptional targets for the proneural bHLH factors Xath5 and XNeuroD. Dev Biol 285:570–583.

London A, Benhar I, Schwartz M (2012) The retina as a window to the brain - from eye research to CNS disorders. Nat Rev Neurol 9:44–53.

Long KO, Fisher SK, Fariss RN, Anderson DH (1986) Disc shedding and autophagy in the cone-dominant ground squirrel retina. Exp Eye Res 43:193–205.

Lothian C, Lendahl U (1997) An evolutionarily conserved region in the second intron of the human nestin gene directs gene expression to CNS progenitor cells and to early neural crest cells. Eur J Neurosci 9:452–462.

Lowe DG, Dizhoor a M, Liu K, Gu Q, Spencer M, Laura R, Lu L, Hurley JB (1995) Cloning and expression of a second photoreceptor-specific membrane retina guanylyl cyclase (RetGC), RetGC-2. Proc Natl Acad Sci U S A 92:5535–5539.

Luo J et al. (2014) Human Retinal Progenitor Cell Transplantation Preserves Vision. J Biol Chem 289:6362–6371.

MacDonald RB, Randlett O, Oswald J, Yoshimatsu T, Franze K, Harris W a. (2015) Müller glia provide essential tensile strength to the developing retina. J Cell Biol 210:1075–1083.

Mack AF, Papanikolaou D, Lillo C (2003) Investigation of the migration path for new rod photoreceptors in the adult cichlid fish retina. Exp Neurol 184:90–96.

MacLaren RE, Pearson RA, MacNeil A, Douglas RH, Salt TE, Akimoto M, Swaroop A, Sowden JC, Ali RR (2006) Retinal repair by transplantation of photoreceptor precursors. Nature 444:203–207.

Maddox DM, Collin GB, Ikeda A, Pratt CH, Ikeda S, Johnson BA, Hurd RE, Shopland LS, Naggert JK, Chang B, Krebs MP, Nishina PM (2015) A mutation in Syne2 causes early retinal defects in photoreceptors, secondary neurons, and Müller Glia. Investig Ophthalmol Vis Sci 56:3776–3787.

Magalhães MM, Coimbra A (1972) The rabbit retina Müller cell. A fine structural and cytochemical study. J Ultrastruct Res 39:310–326.

Maguire AM et al. (2009) Age-dependent effects of RPE65 gene therapy for Leber's congenital amaurosis: a phase 1 dose-escalation trial. Lancet 374:1597–1605.

Malicki J (2004) Cell fate decisions and patterning in the vertebrate retina: the importance of timing, asymmetry, polarity and waves. Curr Opin Neurobiol 14:15–21.

Marín-Teva JL, Cuadros M a, Calvente R, Almendros a, Navascués J (1999) Naturally occurring cell death and migration of microglial precursors in the quail retina during normal development. J Comp Neurol 412:255–275.

Marín O, Rubenstein JLR (2001) A Long, Remarkable Journey: Tangential Migration in the Telencephalon. Nat Rev Neurosci 2:780–790.

Marín O, Rubenstein JLR (2003) Cell Migration in the Forebrain. Annu Rev Neurosci 26:441–483.

Marín O, Valdeolmillos M, Moya F (2006) Neurons in motion: same principles for different shapes? Trends Neurosci 29:655–661.

Marín O, Valiente M, Ge X, Tsai L (2010a) Guiding Neuronal Cell Migrations. Cold Spring Harb Perspect Biol 2:1–21.

Marín O, Valiente M, Ge X, Tsai L-H (2010b) Guiding neuronal cell migrations. Cold Spring Harb Perspect Biol 2:1–20.

Marín O, Yaron A, Bagri A, Tessier-Lavigne M, Rubenstein JLR (2001) Sorting of Striatal and Cortical Interneurons Regulated by Semaphorin-Neuropilin Interactions. Science (80-) 293:872–876.

Marquardt T, Gruss P (2002) Generating neuronal diversity in the retina: one for nearly all. Trends Neurosci 25:32–38.

Martinez-Morales JR, Wittbrodt J (2009) Shaping the vertebrate eye. Curr Opin Genet Dev 19:511–517.

Martini FJ, Valiente M, Bendito GL, Szabó G, Moya F, Valdeolmillos M, Marín O (2009) Biased selection of leading process branches mediates chemotaxis during tangential neuronal migration. Development 136:41–50.

Martini S, Bernoth K, Main H, Ortega GDC, Lendahl U, Just U, Schwanbeck R (2013) A critical role for Sox9 in Notch-induced astrogliogenesis and stem cell maintenance. Stem Cells 31:741–751.

Marvin MJ, Dahlstrand J, Lendahl U, McKay RD (1998) A rod end deletion in the intermediate filament protein nestin alters its subcellular localization in neuroepithelial cells of transgenic mice. J Cell Sci 111 (Pt 1:1951–1961.

Matsuda N, Lu H, Fukata Y, Noritake J, Gao H, Mukherjee S, Nemoto T, Fukata M, Poo M-M (2009) Differential activity-dependent secretion of brain-derived neurotrophic factor from axon and dendrite. J Neurosci 29:14185–14198.

Matsuda T, Cepko CL (2004) Electroporation and RNA interference in the rodent retina in vivo and in vitro. Proc Natl Acad Sci U S A 101:16–22.

Matter-Sadzinski L, Matter JM, Ong MT, Hernandez J, Ballivet M (2001) Specification of neurotransmitter receptor identity in developing retina: the chick ATH5 promoter integrates the positive and negative effects of several bHLH proteins. Development 128:217–231.

Matthews BJ, Kim ME, Flanagan JJ, Hattori D, Clemens JC, Zipursky SL, Grueber WB (2007) Dendrite self-avoidance is controlled by Dscam. Cell 129:593–604.

McGill TJ, Cottam B, Lu B, Wang S, Girman S, Tian C, Huhn SL, Lund RD, Capela A (2012) Transplantation of human central nervous system stem cells - neuroprotection in retinal degeneration. Eur J Neurosci 35:468–477.

McLoon SC, Barnes RB (1989) Early differentiation of retinal ganglion cells: an axonal protein expressed by premigratory and migrating retinal ganglion cells. J Neurosci 9:1424–1432.

Mears a J, Kondo M, Swain PK, Takada Y, Bush R a, Saunders TL, Sieving P a, Swaroop a (2001) Nrl is required for rod photoreceptor development. Nat Genet 29:447–452.

Meberg PJ, Bamburg JR (2000) Increase in neurite outgrowth mediated by overexpression of actin depolymerizing factor. J Neurosci 20:2459–2469.

Meller K, Tetzlaff W (1976) Cell and Tissue Electron Microscopic Studies on the Development of the Chick Retina. Cell Tissue Res 170:145–159.

Meyer EJ, Ikmi A, Gibson MC (2011) Interkinetic Nuclear Migration Is a Broadly Conserved Feature of Cell Division in Pseudostratified Epithelia. Curr Biol 21:485–491.

Meyer JS, Shearer RL, Capowski EE, Wright LS, Wallace K a, McMillan EL, Zhang S-C, Gamm DM (2009) Modeling early retinal development with human embryonic and induced pluripotent stem cells. Proc Natl Acad Sci U S A 106:16698–16703.

Michalczyk K, Ziman M (2005) Nestin structure and predicted function in cellular cytoskeletal organisation. Histol Histopathol 20:665–671.

Mignone JL, Kukekov V, Chiang A-S, Steindler D, Enikolopov G (2004) Neural stem and progenitor cells in nestin-GFP transgenic mice. J Comp Neurol 469:311–324.

Miyata T (2008) Development of three-dimensional archi- tecture of the neuroepithelium: role of pseudostratification and cellular "community." Dev Growth Differ 50:S105-112.

Miyata T, Kawaguchi A, Okano H, Ogawa M (2001) Asymmetric Inheritance of Radial Glial Fibers by Cortical Neurons. Neuron 31:727–741.

Miyata T, Ogawa M (2007) Twisting of neocortical progenitor cells underlies a spring-like mechanism for daughter-cell migration. Curr Biol 17:146–151.

Morest DK (1970a) A study of neurogenesis in the forebrain of opossum pouch young. Z Anat Entwicklungsgesch 130:265–305.

Morest DK (1970b) The Pattern of Neurogenesis in the Retina of the Rat. Z Anat Entwicklungsgesch 131:45–67.

Morgan JL, Dhingra A, Vardi N, Wong ROL (2006) Axons and dendrites originate from neuroepithelial-like processes of retinal bipolar cells. Nat Neurosci 9:85–92.

Morrow EM, Furukawa T, Cepko CL (1998) Vertebrate photoreceptor cell development and disease. Trends Cell Biol 8:353–358.

Morrow EM, Furukawa T, Lee JE, Cepko CL (1999) NeuroD regulates multiple functions in the developing neural retina in rodent. Development 126:23–36.

Mortimer D, Fothergill T, Pujic Z, Richards LJ, Goodhill GJ (2008) Growth cone chemotaxis. Trends Neurosci 31:90–98.

Mruthyunjaya P, Stinnett SS, Toth CA (2004) Change in visual function after macular translocation with 360deg; retinectomy for neovascular age-related macular degeneration. Ophthalmology 111:1715–1724.

Muniz A, Villazana-Espinoza ET, Hatch AL, Trevino SG, Allen DM, Tsin ATC (2007) A novel cone visual cycle in the cone-dominated retina. Exp Eye Res 85:175–184.

Muranishi Y, Terada K, Inoue T, Katoh K, Tsujii T, Sanuki R, Kurokawa D, Aizawa S, Tamaki Y, Furukawa T (2011) An essential role for RAX homeoprotein and NOTCH-HES signaling in Otx2 expression in embryonic retinal photoreceptor cell fate determination. J Neurosci 31:16792–16807.

Murciano A, Zamora J, Lopezsanchez J, Frade J (2002) Interkinetic Nuclear Movement May Provide Spatial Clues to the Regulation of Neurogenesis. Mol Cell Neurosci 21:285–300.

Muto A, Iida A, Satoh S, Watanabe S (2009) The group E Sox genes Sox8 and Sox9 are regulated by Notch signaling and are required for Müller glial cell development in mouse retina. Exp Eye Res 89:549–558.

Nadarajah B, Alifragis P, Wong ROL, Parnavelas JG (2003) Neuronal migration in the developing cerebral cortex: observations based on real-time imaging. Cereb cortex 13:607–611.

Nadarajah B, Brunstrom JE, Grutzendler J, Wong RO, Pearlman a L (2001) Two modes of radial migration in early development of the cerebral cortex. Nat Neurosci 4:143–150.

Nadarajah B, Parnavelas JG (2002a) Modes of neuronal migration in the developing cerebral cortex. Nat Rev Neurosci 3:423–432.

Nadarajah B, Parnavelas JG (2002b) Modes of neuronal migration in the developing cerebral cortex. Nat Rev Neurosci 3:423–432.

Nagelhus E a, Horio Y, Inanobe A, Fujita A, Haug F-M, Nielsen S, Kurachi Y, Ottersen OP (1999) Transport in Rat Retinal Müller Cells Is Mediated by a Coenrichment Of Kir4.1 and AQP4 in Specific Membrane Domains.

Glia 26:47–54.

Nagelhus E a, Veruki ML, Torp R, Haug FM, Laake JH, Nielsen S, Agre P, Ottersen OP (1998) Aquaporin-4 water channel protein in the rat retina and optic nerve: polarized expression in Müller cells and fibrous astrocytes. J Neurosci 18:2506–2519.

National Eye Institute (2015) Facts About Age-Related Macular Degeneration. Available at: https://nei.nih.gov/health/maculardegen/armd_facts.

Nelson BR, Ueki Y, Reardon S, Karl MO, Georgi S, Hartman BH, Lamba D a, Reh T a (2011) Genome-wide analysis of Müller glial differentiation reveals a requirement for Notch signaling in postmitotic cells to maintain the glial fate. PLoS One 6:e22817.

Neumann J, Sauerzweig S, Ronicke R, Gunzer F, Dinkel K, Ullrich O, Gunzer M, Reymann KG (2008) Microglia Cells Protect Neurons by Direct Engulfment of Invading Neutrophil Granulocytes: A New Mechanism of CNS Immune Privilege. J Neurosci 28:5965–5975.

Neves J, Zhu J, Sousa-Victor P, Konjikusic M, Riley R, Chew S, Qi Y, Jasper H, Lamba DA (2016) Immune modulation by MANF promotes tissue repair and regenerative success in the retina. Science (80-) 353:aaf3646-1-10.

Newman EA (1994) A Physiological Measure of Carbonic Anhydrase in Muller Cells. Glia 11:291–299.

Newman EA (2004a) Glial Modulation of Synaptic Transmission in the Retina. Glia 47:268–274.

Newman EA (2004b) A Dialogue between Glia and Neurons in the Retina: Modulation of Neuronal Excitability. Neuron Glia Biol 1:245–252.

Newman EA, Frambach DA, Odette LL (1984) Control of extracellular potassium levels by retinal glial cell K+ siphoning. Science 225:1174–1175.

Nieuwkoop PD (1963) Pattern Formation in Artificially Activated Ectoderm (Rana pipiens and Ambystoma puctatum. Dev Biol 7:255–279.

Nishida A, Furukawa A, Koike C, Tano Y, Aizawa S, Matsuo I, Furukawa T (2003) Otx2 homeobox gene controls retinal photoreceptor cell fate and pineal gland development. Nat Neurosci 6:1255–1263.

Nóbrega-pereira S, Kessaris N, Du T, Kimura S, Anderson SA, Marín O (2008) Postmitotic Nkx2-1 controls the migration of telencephalic interneurons by direct repression of guidance receptors. Neuron 59:733–745.

Noctor SC, Flint AC, Weissman T, Dammerman RS, Kriegstein AR (2001) Neurons derived from radial glial cells establish radial units in neocortex. Nature 409:714–720.

Noctor SC, Martínez-Cerdeño V, Ivic L, Kriegstein AR (2004) Cortical neurons arise in symmetric and asymmetric division zones and migrate through specific phases. Nat Neurosci 7:136–144.

Norden C, Young S, Link BA, Harris WA (2009) Actomyosin is the main driver of interkinetic nuclear migration in the retina. Cell 138:1195–1208.

O'Donnell M, Chance RK, Bashaw GJ (2009) Axon growth and guidance: receptor regulation and signal transduction. Annu Rev Neurosci 32:383–412.

Ogilvie JM, Speck JD, Lett JM, Fleming TT (1999) A reliable method for organ culture of neonatal mouse retina with long-term survival. J Neurosci Methods 87:57–65.

Oh ECT, Cheng H, Hao H, Jia L, Khan NW, Swaroop A (2008) Rod differentiation factor NRL activates the expression of nuclear receptor NR2E3 to suppress the development of cone photoreceptors. Brain Res 1236:16–29.

Oh ECT, Khan N, Novelli E, Khanna H, Strettoi E, Swaroop A (2007) Transformation of cone precursors to functional rod photoreceptors by bZIP transcription factor NRL. Proc Natl Acad Sci 104:1679–1684.

Ohsawa R, Kageyama R (2008) Regulation of retinal cell fate specification by multiple transcription factors. Brain Res 1192:90–98.

Ohtsuka T, Ishibashi M, Gradwohl G, Nakanishi S, Guillemot F, Kageyama R (1999) Hes1 and Hes5 as notch effectors in mammalian neuronal differentiation. EMBO J 18:2196–2207.

Omri S, Omri B, Savoldelli M, Jonet L, Thillaye-Goldenberg B, Thuret G, Gain P, Jeanny JC, Cristanti P, Behar-Cohen F (2010) The outer limiting membrane (OLM) revisited : clinical implications. Clin Ophthalmol 4:183–195.

Osakada F, Ikeda H, Mandai M, Wataya T, Watanabe K, Yoshimura N, Akaike A, Akaike A, Sasai Y, Takahashi M (2008) Toward the generation of rod and cone photoreceptors from mouse, monkey and human embryonic stem cells. Nat Biotechnol 26:215–224.

Osakada F, Ikeda H, Sasai Y, Takahashi M (2009) Stepwise differentiation of pluripotent stem cells into retinal cells.

Nat Protoc 4:811–824.

Ozeki Y, Tomoda T, Kleiderlein J, Kamiya A, Bord L, Fujii K, Okawa M, Yamada N, Hatten ME, Snyder SH, Ross CA, Sawa A (2003) Disrupted-in-Schizophrenia-1 (DISC-1): Mutant truncation prevents binding to NudE-like (NUDEL) and inhibits neurite outgrowth. Proc Natl Acad Sci 100:289–294.

Palczewski K (2006) G Protein–Coupled Receptor Rhodopsin. Annu Rev Biochem 75:743–767.

Panda D, Daijo JE, Jordan M a, Wilson L (1995) Kinetic stabilization of microtubule dynamics at steady state in vitro by substoichiometric concentrations of tubulin-colchicine complex. Biochemistry 34:9921–9929.

Panfoli I, Calzia D, Ravera S, Candiano G, Bachi A, Bianchini P, Diaspro A (2009) A new protocol for live imaging of mammalian retina ex vivo by confocal laser scanning microscopy. Nat Protoc Exch.

Park D, Xiang AP, Mao FF, Zhang L, Di CG, Liu XM, Shao Y, Ma BF, Lee JH, Ha KS, Walton N, Lahn BT (2010) Nestin is required for the proper self-renewal of neural stem cells. Stem Cells 28:2162–2171.

Parslow A, Cardona A, Bryson-Richardson RJ (2014) Sample drift correction following 4D confocal time-lapse imaging. J Vis Exp 86.

Pearson RA (2014) Advances in repairing the degenerate retina by rod photoreceptor transplantation. Biotechnol Adv 32:485–491.

Pearson RA, Barber AC, Rizzi M, Hippert C, Xue T, West EL, Duran Y, Smith AJ, Chuang JZ, Azam SA, Luhmann UFO, Benucci A, Sung CH, Bainbridge JW, Carandini M, Yau K-W, Sowden JC, Ali RR (2012) Restoration of vision after transplantation of photoreceptors. Nature 485:99–103.

Pearson RA, Barber AC, West EL, MacLaren RE, Duran Y, Bainbridge JW, Sowden JC, Ali RR (2010) Targeted disruption of outer limiting membrane junctional proteins (Crb1 and ZO-1) increases integration of transplanted photoreceptor precursors into the adult wild-type and degenerating retina. Cell Transplant 19:487–503.

Pearson RA, Catsicas M, Becker D, Mobbs P (2002) Purinergic and muscarinic modulation of the cell cycle and calcium signaling in the chick retinal ventricular zone. J Neurosci 22:7569–7579.

Pearson RA, Catsicas M, Becker DL, Bayley P, Lüneborg NL, Mobbs P (2004) Ca(2+) ‡ signalling and gap junction coupling within and between pigment epithelium and neural retina in the developing chick. Eur J Neurosci 19:2435–2445.

Pearson RA, Dale N, Llaudet E, Mobbs P (2005a) ATP released via gap junction hemichannels from the pigment epithelium regulates neural retinal progenitor proliferation. Neuron 46:731–744.

Pearson RA, Gonzalez-Cordero A, West EL, Claudio Ribeiro JR, Aghaizu N, Goh D, Sampson R, Georgiaids A, Waldron P, Duran Y, Naeem A, Kloc M, Cristante E, Kruczek K, Warre-Cornish K, Sowden JC, Smith AJ, Ali RR (2016) Donor and host photoreceptors engage in material transfer following transplantation of postmitotic photoreceptor precursors. Nat Commun 7.

Pearson RA, Lüneborg NL, Becker DL, Mobbs P (2005b) Gap Junctions Modulate Interkinetic Nuclear Movement in Retinal Progenitor Cells. J Neurosci 25:10803–10814.

Pellissier LP, Hoek RM, Vos RM, Aartsen WM, Klimczak RR, Hoyng S a, Flannery JG, Wijnholds J (2014) Specific tools for targeting and expression in Müller glial cells. Mol Ther — Methods Clin Dev 1:14009.

Pfeiffer-Guglielmi B, Francke M, Reichenbach A, Fleckenstein B, Jung G, Hamprecht B (2005) Glycogen phosphorylase isozyme pattern in mammalian retinal Müller (glial) cells and in astrocytes of retina and optic nerve. Glia 49:84–95.

Phillips JB, Blanco-Sanchez B, Lentz JJ, Tallafuss a., Khanobdee K, Sampath S, Jacobs ZG, Han PF, Mishra M, Titus T a., Williams DS, Keats BJ, Washbourne P, Westerfield M (2011) Harmonin (Ush1c) is required in zebrafish Muller glial cells for photoreceptor synaptic development and function. Dis Model Mech 4:786–800.

Picone R, Ren X, Ivanovitch KD, Clarke JDW, McKendry RA, Baum B (2010) A polarised population of dynamic microtubules mediates homeostatic length control in animal cells. PLoS Biol 8.

Pilaz L-J, Patti D, Marcy G, Ollier E, Pfister S, Douglas RJ, Betizeau M, Gautier E, Cortay V, Doerflinger N, Kennedy H, Dehay C (2009) Forced G1-phase reduction alters mode of division, neuron number, and laminar phenotype in the cerebral cortex. Proc Natl Acad Sci U S A 106:21924–21929.

Poché R a, Furuta Y, Chaboissier M-C, Schedl A, Behringer RR (2008) Sox9 is expressed in mouse multipotent retinal progenitor cells and functions in Müller glial cell development. J Comp Neurol 510:237–250.

Poché R a, Kwan KM, Raven M a, Furuta Y, Reese BE, Behringer RR (2007) Lim1 is essential for the correct laminar positioning of retinal horizontal cells. J Neurosci 27:14099–14107.

Poggi L, Vitorino M, Masai I, Harris W a (2005) Influences on neural lineage and mode of division in the zebrafish retina in vivo. J Cell Biol 171:991–999.

Poitry-yamate C, Tsacopoulos M (1991) Glial (Müller) cells take up and phosphorylate [3H]2-deoxy-D-glucose in a mammalian retina. Neurosci Lett 122:241–244.

Poitry-Yamate CL, Poitry S, Tsacopoulos M (1995) Lactate released by Müller glial cells is metabolized by photoreceptors from mammalian retina. J Neurosci 15:5179–5191.

Poitry-Yamate CL, Tsacopoulos M (1992) Glucose metabolism in freshly isolated Müller glial cells from a mammalian retina. J Comp Neurol 320:257–266.

Poitry S, Poitry-Yamate C, Ueberfeld J, MacLeish PR, Tsacopoulos M (2000) Mechanisms of glutamate metabolic signaling in retinal glial (Müller) cells. J Neurosci 20:1809–1821.

Polleux F, Whitford KL, Dijkhuizen P a, Vitalis T, Ghosh A (2002) Control of cortical interneuron migration by neurotrophins and PI3-kinase signaling. Development 129:3147–3160.

Pow D V, Barnett NL, Penfold P (2000) Are neuronal transporters relevant in retinal glutamate homeostasis? Neurochem Int 37:191–198.

Pow D V, Crook DK (1995) Immunocytochemical evidence for the presence of high levels of reduced glutathione in radial glial cells and horizontal cells in the rabbit retina. Neurosci Lett 193:25–28.

Pow D V, Crook DK (1996) Direct immunocytochemical evidence for the transfer of glutamine from glial cells to neurons: use of specific antibodies directed against the d-stereoisomers of glutamate and glutamine. Neuroscience 70:295–302.

Pow D V, Robinson SR (1994) Glutamate in some retinal neurons is derived solely from glia. Neuroscience 60:355–366.

Powell EM, Mars WM, Levitt P (2001) Hepatocyte Growth Factor / Scatter Factor Is a Motogen for Interneurons Migrating from the Ventral to Dorsal Telencephalon. Neuron 30:79–89.

Pozas E, Ibáñez CF (2005) GDNF and GFRa1 Promote Differentiation and Tangential Migration of Cortical GABAergic Neurons. Neuron 45:701–713.

Prada C, Genis-gfilvez LPJM, Ramirez G (1987) Two modes of free migration of amacrine cell neuroblasts in the chick retina. Anat 175:281–287.

Prada C, Puelles L, Jos MG (1981) A Golgi Study on the Early Sequence of Differentiation of Ganglion Cells in the Chick Embryo Retina. Anat Embryol (Berl) 161:305–317.

Prada FA, Magalhaes MM, Coimbra A, Genis-Galvez JM (1989) Morphological differentiation of the Müller cell: Golgi and electron microscopy study in the chick retina. J Morphol 201:11–22.

Preibisch S, Saalfeld S, Schindelin J, Tomancak P (2010) Software for bead-based registration of selective plane illumination microscopy data Partitioning biological data with transitivity clustering. Nat Publ Gr 7:418–419.

Pugacheva EN, Jablonski SA, Hartman TR, Henske EP, Golemis EA (2007) HEF1-Dependent Aurora A Activation Induces Disassembly of the Primary Cilium. Cell 129:1351–1363.

Pulido JS, Sugaya I, Comstock J, Sugaya K (2007) Reelin expression is upregulated following ocular tissue injury. Graefe's Arch Clin Exp Ophthalmol 245:889–893.

Qian H, Sheetz MP, Elson EL (1991) Single particle tracking. Analysis of diffusion and flow in two-dimensional systems. Biophys J 60:910–921.

Radtke ND, Aramant RB, Petry HM, Green PT, Pidwell DJ, Seiler MJ (2008) Vision Improvement in Retinal Degeneration Patients by Implantation of Retina Together with Retinal Pigment Epithelium. Am J Ophthalmol 146:172–182.

Radtke ND, Aramant RB, Seiler M, Petry HM (1999) Preliminary report: Indications of improved visual function after retinal sheet transplantation in retinitis pigmentosa patients. Am J Ophthalmol 128:384–387.

Rakic P (1971a) Guidance of neurons migrating to the fetal monkey neocortex Autoradiographic studies of the past decade have confirmed that neurons arise. Brain Res 33:471–476.

Rakic P (1971b) Neuron-glia relationship during granule cell migration in developing cerebellar cortex. A Golgi and electronmicroscopic study in Macacus Rhesus. J Comp Neurol 141:283–312.

Rakic P (1972) Mode of Cell Migration to the Superficial Layers of Fetal Monkey Neocortex. J Comp Neurol 145:61–83.

Rakic P (2003) Elusive Radial Glial Cells: Historical and Evolutionary Perspective. Glia 43:19–32.

Ramsey DJ, Arden GB (2015) Rods, Dark Adaptation, and the Development of Diabetic Retinopathy. Enliven Clin Ophthalmol Res 1:1–12.

Randlett O, Norden C, Harris W a (2011a) The vertebrate retina: a model for neuronal polarization in vivo. Dev Neurobiol 71:567–583.

Randlett O, Poggi L, Zolessi FR, Harris WA (2011b) The Oriented Emergence of Axons from Retinal Ganglion Cells Is Directed by Laminin Contact In Vivo. Neuron 70:266–280.

Rapaport DH, Wong LL, Wood ED, Yasumura D, LaVail MM (2004) Timing and Topography of Cell Genesis in the Rat Retina. J Comp Neurol 474:304–324.

Rauen T, Taylor WR, Kuhlbrodt K, Wiessner M (1998) High-affinity glutamate transporters in the rat retina: A major role of the glial glutamate transporter GLAST-1 in transmitter clearance. Cell Tissue Res 291:19–31.

Raymond PA, Rivlin PK (1987) Germinal cells in the goldfish retina that produce rod photoreceptors. Dev Biol 122:120–138.

Razafsky D, Blecher N, Markov A, Stewart-Hutchinson PJ, Hodzic D (2012) LINC Complexes Mediate the Positioning of Cone Photoreceptor Nuclei in Mouse Retina. PLoS One 7.

Ready DF, Hanson TE, Benzer S (1976) Development of the Drosophila Retina , a Neurocrystalline Lattice. Dev Biol 53:217–240.

Reese BE (2011) Development of the retina and optic pathway. Vision Res 51:613–632.

Reese BE, Galli-Resta L (2002) The role of tangential dispersion in retinal mosaic formation. Prog Retin Eye Res 21:153–168.

Reese BE, Harvey a R, Tan SS (1995) Radial and tangential dispersion patterns in the mouse retina are cell-class specific. Proc Natl Acad Sci U S A 92:2494–2498.

Reese BE, Necessary BD, Tam PP, Faulkner-Jones B, Tan SS (1999) Clonal expansion and cell dispersion in the developing mouse retina. Eur J Neurosci 11:2965–2978.

Reese BE, Tan SS (1998) Clonal boundary analysis in the developing retina using X-inactivation transgenic mosaic mice. Semin Cell Dev Biol 9:285–292.

Reh TA, Kljavin IJ (1989) Age of differentiation determines rat retinal germinal cell phenotype: induction of differentiation by dissociation. J Neurosci 9:4179–4189.

Reichelt W, Stabel-Burow J, Pannicke T, Weichert H, Heinemann U (1997) The glutathione level of retinal Müller glial cells is dependent on the high-affinity sodium-dependent uptake of glutamate. Neuroscience 77:1213–1224.

Reichenbach A, Bringmann A (2013) New functions of Müller cells. Glia 61:651–678.

Reichenbach A, Reichelt W (1986) Postnatal development of radial glial (Müller) cells of the rabbit retina. Neurosci Lett 71:125–130.

Reichenbach A, Stolzenburg JU, Eberhardt W, Chao TI, Dettmer D, Hertz L (1993) What do retinal müller (glial) cells do for their neuronal "small siblings"? J Chem Neuroanat 6:201–213.

Rice DS, Curran T (2001) Role of the Reelin Signalling Pathway in Central Nervous System Development. Annu Rev Neurosci 24:1105–1039.

Rice DS, Nusinowitz S, Azimi a M, Martínez a, Soriano E, Curran T (2001) The reelin pathway modulates the structure and function of retinal synaptic circuitry. Neuron 31:929–941.

Rich K a, Zhan Y, Blanks JC (1997) Migration and synaptogenesis of cone photoreceptors in the developing mouse retina. J Comp Neurol 388:47–63.

Rio C, Rieff HI, Qi P, Corfas G (1997) Neuregulin and erbB Receptors Play a Critical Role in Neuronal Migration. Neuron 19:39–50.

Rivas RJ, Hatten ME (1995) Motility and Cytoskeletal Organization of Migrating Cerebellar Granule Neurons. J Neurosci 15:981–989.

Roberts AJ, Kon T, Knight PJ, Sutoh K, Burgess SA (2013) Functions and mechanics of dynein motor proteins. Nat Rev Mol Cell Biol 14:713–726.

Roesch K, Jadhav AP, Trimarchi JM, Stadler MB, Roska B, Sun BB, Cepko CL (2008) The transcriptome of retinal Müller glial cells. J Comp Neurol 509:225–238.

Rompani SB, Cepko CL (2008) Retinal progenitor cells can produce restricted subsets of horizontal cells. Proc Natl Acad Sci U S A 105:192–197.

Rosenfeld PJ, Heier JS, Hantsbarger G, Shams N (2006) Tolerability and Efficacy of Multiple Escalating Doses of Ranibizumab (Lucentis) for Neovascular Age-Related Macular Degeneration. Ophthalmology 113:623–633.

Ruthardt N, Lamb DC, Bräuchle C (2011) Single-particle tracking as a quantitative microscopy-based approach to unravel cell entry mechanisms of viruses and pharmaceutical nanoparticles. Mol Ther 19:1199–1211.

Sahlender DA, Savtchouk I, Volterra A (2014) What do we know about gliotransmitter release from astrocytes?

Philos Trans R Soc Lond B Biol Sci 369:20130592.

Saito K, Kawaguchi A, Kashiwagi S, Yasugi S, Ogawa M, Miyata T (2003) Morphological asymmetry in dividing retinal progenitor cells. Dev Growth Differ 45:219–229.

Santos-Ferreira T, Llonch S, Borsch O, Postel K, Haas J, Ader M (2016) Retinal transplantation of photoreceptors results in donor–host cytoplasmic exchange. Nat Commun 7:13028.

Santos-Ferreira T, Postel K, Ader M (2014) Photoreceptor transplantation into the mammalian retina. Curr Ophthalmol Rep 2:91–99.

Sauer FC (1935) Mitosis in the Neural Tube. J Comp Neurol 62:377–405.

Sauer ME, Chittenden AC (1959) Deoxyribonucleic acid content of cell nuclei in the neural tube of the chick embryo: evidence for intermitotic migration of nuclei. Exp Cell Res 16:1–6.

Saunders AM, Powers J, Strome S, Saxton WM (2007) Kinesin-5 acts as a brake in anaphase spindle elongation. Curr Biol 17:453–454.

Sbalzarini IF, Koumoutsakos P (2005) Feature point tracking and trajectory analysis for video imaging in cell biology. J Struct Biol 151:182–195.

Schaar BT, Mcconnell SK (2005) Cytoskeletal coordination during neuronal migration. Proc Natl Acad Sci 102:13652–13657.

Schaper AA (1897) The Earliest Differentiation in the Central Nervous System of Vertebrates. Science (80-) 5:430–431.

Scheer N, Groth A, Hans S, Campos-Ortega J a (2001) An instructive function for Notch in promoting gliogenesis in the zebrafish retina. Development 128:1099–1107.

Schenk J, Wilsch-Bräuninger M, Calegari F, Huttner WB (2009) Myosin II is required for interkinetic nuclear migration of neural progenitors. Proc Natl Acad Sci U S A 106:16487–16492.

Schindelin J, Arganda-carreras I, Frise E, Kaynig V, Longair M, Pietzsch T, Preibisch S, Rueden C, Saalfeld S, Schmid B, Tinevez J, White DJ, Hartenstein V, Eliceiri K, Tomancak P, Cardona A (2012) Fiji : an open-source platform for biological-image analysis. Nat Methods 9:676–682.

Schmid RS, Anton ES (2003) Role of integrins in the development of the cerebral cortex. Cereb Cortex 13:219–224.

Schmid RS, Shelton S, Stanco A, Yokota Y, Kreidberg J a, Anton ES (2004) Alpha3Beta1 Integrin Modulates Neuronal Migration and Placement During Early Stages of Cerebral Cortical Development. Development 131:6023–6031.

Schroer TA, Steuer ER, Sheetz MP (1989) Cytoplasmic dynein is a minus end-directed motor for membranous organelles. Cell 56:937–946.

Schütte M, Werner P (1998) Redistribution of glutathione in the ischemic rat retina. Neurosci Lett 246:53–56.

Seiler MJ, Aramant RB (1998) Intact sheets of fetal retina transplanted to restore damaged rat retinas. Invest Ophthalmol Vis Sci 39:2121–2131.

Seiler MJ, Aramant RB, Thomas BB, Peng Q, Sadda SR, Keirstead HS (2010) Visual restoration and transplant connectivity in degenerate rats implanted with retinal progenitor sheets. Eur J Neurosci 31:508–520.

Shajia L, Horowits R (2008) Role of Nonmuscle Myosin IIB and N-RAP in Cell Spreading and Myofibril Assembly in Primary Mouse Cardiomyocytes. Cell Motil Cytoskelet 65:747–761.

Shikanai M, Nakajima K, Kawauchi T (2011) N-cadherin regulates radial glial fiber-dependent migration of cortical locomoting neurons. Commun Integr Biol 4:326–330.

Shinoe T, Kuribayashi H, Saya H, Seiki M, Aburatani H, Watanabe S (2010) Identification of CD44 as a cell surface marker for Müller glia precursor cells. J Neurochem 115:1633–1642.

Shu T, Ayala R, Nguyen M, Xie Z, Gleeson JG, Tsai L (2004) Ndel1 Operates in a Common Pathway with LIS1 and Cytoplasmic Dynein to Regulate Cortical Neuronal Positioning. Neuron 44:263–277.

Sidman RL, Rakic P (1973) Neuronal Migration, with Special Reference to Developing Human Brain: A Review. Brain Res 62:1–35.

Singh MS, Charbel Issa P, Butler R, Martin C, Lipinski DM, Sekaran S, Barnard AR, MacLaren RE (2013) Reversal of end-stage retinal degeneration and restoration of visual function by photoreceptor transplantation. Proc Natl Acad Sci U S A 110:1101–1106.

Singhal S, Lawrence JM, Bhatia B, Ellis JS, Kwan AS, Macneil A, Luthert PJ, Fawcett JW, Perez M-T, Khaw PT, Limb GA (2008) Chondroitin sulfate proteoglycans and microglia prevent migration and integration of grafted Müller stem cells into degenerating retina. Stem Cells 26:1074–1082.

Sinn R, Wittbrodt J (2013) An eye on eye development. Mech Dev 130:347–358.

Smart IH (1972) Proliferative characteristics of the ependymal layer during the early development of the mouse diencephalon, as revealed by recording the number, location, and plane of cleavage of mitotic figures. J Anat 113:109–129.

Smiley S et al. (2016) Establishment of a cone photoreceptor transplantation platform based on a novel cone-GFP reporter mouse line. Sci Rep 6:22867.

Smith AJ, Bainbridge JW, Ali RR (2009) Prospects for retinal gene replacement therapy. Trends Genet 25:156–165.

Smith JL SG (1987) Cell cycle and neuroepithelial cell shape during bending of the chick neural plate. Anat Rec 218: 196–2:196–206.

Snow RL, Robson JA (1994) Ganglion cell neurogenesis, migration and early differentiation in the chick retina. Neuroscience 58:399–409.

Snow RL, Robson JA (1995) Migration and differentiation of neurons in the retina and optic tectum of the chick. Exp Neurol 134:13–24.

Solecki DJ, Model L, Gaetz J, Kapoor TM, Hatten ME (2004) Par6alpha signaling controls glial-guided neuronal migration. Nat Neurosci 7:1195–1203.

Solecki DJ, Trivedi N, Govek E-E, Kerekes R a, Gleason SS, Hatten ME (2009) Myosin II motors and F-actin dynamics drive the coordinated movement of the centrosome and soma during CNS glial-guided neuronal migration. Neuron 63:63–80.

Solomon SG, Lennie P (2007) The machinery of colour vision. Nat Rev Neurosci 8:276–286.

Spaide RF, Laud K, Fine HF, Klancnik JM, Meyerle CB, Yannuzzi LA, Sorenson J, Slakter J, Fisher YL, Cooney MJ (2006) Intravitreal bevacizumab treatment of choroidal neovascularization secondary to age-related macular degeneration. Retina 26:383–390.

Spear PC, Erickson C a (2012a) Interkinetic nuclear migration: a mysterious process in search of a function. Dev Growth Differ 54:306–316.

Spear PC, Erickson C a. (2012b) Apical movement during interkinetic nuclear migration is a two-step process. Dev Biol 370:33–41.

Spira A, Hudy S, Hannah R (1984) Ectopic photoreceptor cells and cell death in the developing rat retina. Anat Embryol (Berl) 169:293–301.

Steinecke A, Gampe C, Nitzsche F, Bolz J (2014) DISC1 knockdown impairs the tangential migration of cortical interneurons by affecting the actin cytoskeleton. Front Biosci a J virtual Libr 8:1–13.

Steinert PM, et al. (1999) A High Molecular Weight Intermediate Filament-associated Protein in BHK-21 Cells Is Nestin, a Type VI Intermediate Filament Protein. J Biol Chem 274:9881–9890.

Stettler EM, Galileo DS (2004) Radial glia produce and align the ligand fibronectin during neuronal migration in the developing chick brain. J Comp Neurol 468:441–451.

Stingl K, Bartz-Schmidt KU, Besch D, Braun A, Bruckmann A, Gekeler F, Greppmaier U, Hipp S, Hörtdörfer G, Kernstock C, Koitschev A, Kusnyerik A, Sachs H, Schatz A, Stingl KT, Peters T, Wilhelm B, Zrenner E (2013) Artificial vision with wirelessly powered subretinal electronic implant alpha-IMS. Proc Biol Sci 280:20130077.

Strzyz PJ, Lee HO, Sidhaye J, Weber IP, Leung LC, Norden C (2015) Interkinetic Nuclear Migration Is Centrosome Independent and Ensures Apical Cell Division to Maintain Tissue Integrity. Dev Cell 32:203–219.

Sultan KT, Brown KN, Shi S (2013) Production and organization of neocortical interneurons. Front Cell Neurosci 7:1–14.

Sun W, Kim H, Moon Y (2010) Control of neuronal migration through rostral migratory stream in mice. Anat Cell Biol 43:269–279.

Surzenko N, Crowl T, Bachleda A, Langer L, Pevny L (2013) SOX2 maintains the quiescent progenitor cell state of postnatal retinal Muller glia. Development 140:1445–1456.

Suzuki SC, Bleckert A, Williams PR, Takechi M, Kawamura S, Wong ROL (2013) Cone photoreceptor types in zebrafish are generated by symmetric terminal divisions of dedicated precursors. Proc Natl Acad Sci U S A 110:15109–15114.

Suzuki T, Akimoto M, Imai H, Ueda Y, Mandai M (2007) Chondroitinase ABC Treatment Enhances Synaptogenesis Between Transplant and Host Neurons in Model of Retinal Degeneration. 16:493–503.

Swaroop a, Xu JZ, Pawar H, Jackson a, Skolnick C, Agarwal N (1992) A conserved retina-specific gene encodes a basic motif/leucine zipper domain. Proc Natl Acad Sci U S A 89:266–270.

Swaroop A, Kim D, Forrest D (2010) Transcriptional regulation of photoreceptor development and homeostasis in the mammalian retina. Nat Rev Neurosci 11:563–576.

Tabata H, Nakajima K (2003) Multipolar migration: the third mode of radial neuronal migration in the developing cerebral cortex. J Neurosci 23:9996–10001.

Tah V, Orlans HO, Hyer J, Casswell E, Din N, Sri Shanmuganathan V, Ramskold L, Pasu S (2015) Anti-VEGF therapy and the retina: An update. J Ophthalmol 2015:627674.

Takahashi K, Yamanaka S (2006) Induction of Pluripotent Stem Cells from Mouse Embryonic and Adult Fibroblast Cultures by Defined Factors. Cell 126:663–676.

Takatsuka K, Hatakeyama J, Bessho Y, Kageyama R (2004) Roles of the bHLH gene Hes1 in retinal morphogenesis. Brain Res 1004:148–155.

Tamamaki N, Nakamura K, Okamoto K, Kaneko T (2001) Radial glia is a progenitor of neocortical neurons in the developing cerebral cortex. Neurosci Res 41:51–60.

Tanaka T, Serneo FF, Higgins C, Gambello MJ, Wynshaw-Boris A, Gleeson JG (2004) Lis1 and doublecortin function with dynein to mediate coupling of the nucleus to the centrosome in neuronal migration. J Cell Biol 165:709–721.

Tanenbaum ME, Akhmanova A, Medema RH (2011) Bi-directional transport of the nucleus by dynein and kinesin-1. Commun Integr Biol 4:21–25.

Taranova O V., Magness ST, Fagan BM, Wu Y, Surzenko N, Hutton SR, Pevny LH (2006) SOX2 is a dose-dependent regulator of retinal neural progenitor competence. Genes Dev 20:1187–1202.

Thompson D a., Gal A (2003) Vitamin A metabolism in the retinal pigment epithelium: Genes, mutations, and diseases. Prog Retin Eye Res 22:683–703.

Torii M, Hashimoto-torii K, Levitt P, Rakic P (2009) Integration of neuronal clones in the radial cortical columns by EphA and ephrin-A signalling. Nature 461:524–528.

Tout S, Chan-Ling T, Holländer H, Stone J (1993) The role of Müller cells in the formation of the blood-retinal barrier. Neuroscience 55:291–301.

Townes-Anderson E, Dacheux RF, Raviola E (1988) Rod photoreceptors dissociated from the adult rabbit retina. J Neurosci 8:320–331.

Travis GH, Sutcliffe JG, Bok D (1991) The Retinal Degeneration Slow (rds) Gene Product Is a Photoreceptor Disc Membrane-Associated Glycoprotein. Neuron 6:61–70.

Trimarchi JM, Stadler MB, Cepko CL (2008) Individual retinal progenitor cells display extensive heterogeneity of gene expression. PLoS One 3:e1588.

Trivedi N, Solecki DJ (2011) Neuronal migration illuminated: A look under the hood of the living neuron. Cell Adh Migr 5:42–47.

Troutt L, Burnside B (1988) Microtubule polarity and distribution in teleost photoreceptors. J Neurosci 8:2371–2380.

Tsai J-W, Bremner KH, Vallee RB (2007) Dual subcellular roles for LIS1 and dynein in radial neuronal migration in live brain tissue. Nat Neurosci 10:970–979.

Tsai J-W, Chen Y, Kriegstein AR, Vallee RB (2005) LIS1 RNA interference blocks neural stem cell division, morphogenesis, and motility at multiple stages. J Cell Biol 170:935–945.

Tsai J-W, Lian W-N, Kemal S, Kriegstein AR, Vallee RB (2010) Kinesin 3 and cytoplasmic dynein mediate interkinetic nuclear migration in neural stem cells. Nat Neurosci 13:1463–1471.

Tsai L-H, Gleeson JG (2005) Nucleokinesis in neuronal migration. Neuron 46:383–388.

Turner DL, Cepko CL (1987) A common progenitor for neurons and glia persists in rat retina late in development. Nature 328:131–136.

Uckermann O (2004) Glutamate-Evoked Alterations of Glial and Neuronal Cell Morphology in the Guinea Pig Retina. J Neurosci 24:10149–10158.

Uckermann O, Iandiev I, Francke M, Franze K, Grosche J, Wolf S, Kohen L, Wiedemann P, Reichenbach A, Bringmann A (2004) Selective staining by vital dyes of Müller glial cells in retinal wholemounts. Glia 45:59–66.

Ueki Y, Wilken MS, Cox KE, Chipman L, Jorstad N, Sternhagen K, Simic M, Ullom K, Nakafuku M, Reh TA (2015) Transgenic expression of the proneural transcription factor Ascl1 in Müller glia stimulates retinal regeneration in young mice. Proc Natl Acad Sci U S A 112:13717–13722.

Ueno M, Katayama K, Yamauchi H, Nakayama H, Doi K (2006) Cell cycle progression is required for nuclear migration of neural progenitor cells. Brain Res 1088:57–67.

Umeshima H, Hirano T, Kengaku M (2007) Microtubule-based nuclear movement occurs independently of centrosome positioning in migrating neurons. Proc Natl Acad Sci 104:16182–16187.

Unachukwu UJ, Warren A, Li Z, Mishra S, Zhou J, Sauane M, Lim H, Vazquez M, Redenti S (2016) Predicted molecular signaling guiding photoreceptor cell migration following transplantation into damaged retina. Sci Rep 6:22392.

Unger VM, Hargrave P a, Baldwin JM, Schertler GF (1997) Arrangement of rhodopsin transmembrane alpha-helices. Nature 389:203–206.

Valamanesh F, Monnin J, Morand-Villeneuve N, Michel G, Zaher M, Miloudi S, Chemouni D, Jeanny J-C, Versaux-Botteri C (2013) Nestin expression in the retina of rats with inherited retinal degeneration. Exp Eye Res 110:26–34.

Valiente M, Marín O (2010) Neuronal migration mechanisms in development and disease. Curr Opin Neurobiol 20:68–78.

Vazquez-Chona FR, Clark AM, Levine EM (2009) Rlbp1 Promoter Drives Robust Müller Glial GFP Expression in Transgenic Mice. 50:3996–4003.

Vecino E, Hernández M, García M (2004) Cell death in the developing vertebrate retina. Int J Dev Biol 48:965–974.

Villar-Cervino V, Kappeler C, Nobrega-Pereira S, Henkemeyer M, Rago L, Niete MA, Marín O (2015) Molecular Mechanisms Controlling the Migration of Striatal Interneurons. J Neurosci 35:8718–8729.

Vitorino M, Jusuf PR, Maurus D, Kimura Y, Higashijima S-I, Harris W a (2009) Vsx2 in the zebrafish retina: restricted lineages through derepression. Neural Dev 4:14.

Walcott JC, Provis JM (2003) Müller cells express the neuronal progenitor cell marker nestin in both differentiated and undifferentiated human foetal retina. Clin Exp Ophthalmol 31:246–249.

Wald G (1935) Vitamin A in Eye Tissues. J Gen Physiol 18:905–915.

Wald G, Durell J, George RCC St. (1950) The Light Reaction in the Bleaching of Rhodopsin. Science (80-) 111:179–181.

Walker AS, Goings GE, Kim Y, Miller RJ, Chenn A, Szele FG (2010) Nestin reporter transgene labels multiple central nervous system precursor cells. Neural Plast 2010.

Wang J, Kefalov VJ (2012) The Cone-specific Visual Cycle. Prog Retin Eye Res 30:115–128.

Wang S, Cepko CL (2016) Photoreceptor Fate Determination in the Vertebrate Retina. Investig Opthalmology Vis Sci 57:ORSFe1.

Wang X, Tsai J-W, LaMonica B, Kriegstein AR (2011) A new subtype of progenitor cell in the mouse embryonic neocortex. Nat Neurosci 14:555–561.

Warre-Cornish K, Barber AC, Sowden JC, Ali RR, Pearson RA (2014) Migration, Integration and Maturation of Photoreceptor Precursors Following Transplantation in the Mouse Retina. Stem Cells Dev 23:941–954.

Watabe-Uchida M, John KA, Janas JA, Newey SE, Van Aelst L (2006) The Rac Activator DOCK7 Regulates Neuronal Polarity through Local Phosphorylation of Stathmin/Op18. Neuron 51:727–739.

Watanabe K, Kamiya D, Nishiyama A, Katayama T, Nozaki S, Kawasaki H, Watanabe Y, Mizuseki K, Sasai Y (2005) Directed differentiation of telencephalic precursors from embryonic stem cells. Nat Neurosci 8:288–296.

Watterson RL, Veneziano P, Bartha A (1956) Absence of a true germinal zone in neural tubes of young chick embryos as demonstrated by the colchicine technique. Anat Rec 124:379–380.

Weber IP, Ramos AP, Strzyz PJ, Leung LC, Young S, Norden C (2014) Mitotic Position and Morphology of Committed Precursor Cells in the Zebrafish Retina Adapt to Architectural Changes upon Tissue Maturation. Cell Rep 7:386–397.

Weir BS, Hill WG, Cardon LR (2004) Allelic association patterns for a dense SNP map. Genet Epidemiol 27:442–450.

West EL, Pearson RA, Tschernutter M, Sowden JC, MacLaren RE, Ali RR (2008) Pharmacological disruption of the outer limiting membrane leads to increased retinal integration of transplanted photoreceptor precursors. Exp Eye Res 86:601–611.

Wetts R, Fraser SE (1988) Multipotent Precursors Can Give Riste to All Major Cell Types of the Frog Retina. Science (80-) 239:1142–1145.

Whited JL, Cassell A, Brouillette M, Garrity PA (2004) Dynactin is required to maintain nuclear position within postmitotic Drosophila photoreceptor neurons. Development 131:4677–4686.

Willbold E, Mansky P, Layer PG (1996) Lateral and radial growth uncoupled in reaggregated retinospheroids of

embryonic avian retina. Int J Dev Biol 40:1151–1159.

Willbold E, Reinicke M, Lance-jones C, Lagenaur C, Lemmon V, Layer PG (1995) Muller Glia Stabilizes Cell Columns During Retinal Development : Lateral Cell Migration but not Neuropil Growth is Inhibited in Mixed Chick-Quail Retinospheroids. Eur J Neurosci 7:2277–2284.

Willbold E, Rothermel a, Tomlinson S, Layer PG (2000) Müller glia cells reorganize reaggregating chicken retinal cells into correctly laminated in vitro retinae. Glia 29:45–57.

Willemsen MH, Vissers LEL, Willemsen M a. a. P, van Bon BWM, Kroes T, de Ligt J, de Vries BB, Schoots J, Lugtenberg D, Hamel BCJ, van Bokhoven H, Brunner HG, Veltman J a., Kleefstra T (2012) Mutations in DYNC1H1 cause severe intellectual disability with neuronal migration defects. J Med Genet 49:179–183.

Williams PR, Suzuki SC, Yoshimatsu T, Lawrence OT, Waldron SJ, Parsons MJ, Nonet ML, Wong RO (2010) In vivo development of outer retinal synapses in the absence of glial contact. J Neurosci 30:11951–11961.

Wilson L, Jordan MA (1995) Microtubule dynamics: taking aim at a moving target. Chem Biol 2:569–573.

Wilson PM, Fryer RH, Fang Y, Hatten ME (2010) Astn2, a novel member of the astrotactin gene family, regulates the trafficking of ASTN1 during glial-guided neuronal migration. J Neurosci 30:8529–8540.

Wolburg H, Willbold E, Layer PG (1991) Müller glia endfeet, a basal lamina and the polarity of retinal layers form properly in vitro only in the presence of marginal pigmented epithelium. Cell Tissue Res 264:437–451.

Wurm A, Lipp S, Pannicke T, Linnertz R, Krügel U, Schulz A, Färber K, Zahn D, Grosse J, Wiedemann P, Chen J, Schöneberg T, Illes P, Reichenbach A, Bringmann A (2010) Endogenous purinergic signaling is required for osmotic volume regulation of retinal glial cells. J Neurochem 112:1261–1272.

Wurm A, Pannicke T, Wiedemann P, Reichenbach A, Bringmann A (2008) Glial cell-derived glutamate mediates autocrine cell volume regulation in the retina: Activation by VEGF. J Neurochem 104:386–399.

Xie Z, Sanada K, Samuels BA, Shih H, Tsai L (2003) Serine 732 Phosphorylation of FAK by Cdk5 Is Important for Microtubule Organization , Nuclear Movement , and Neuronal Migration. Cell 114:469–482.

Xu J, Dodd RL, Makino CL, Simon MI, Baylor D a, Chen J (1997) Prolonged photoresponses in transgenic mouse rods lacking arrestin. Nature 389:505–509.

Xue LP, Lu J, Cao Q, Kaur C, Ling E (2006) Nestin expression in Müller glial cells in postnatal rat retina and its upregulation following optic nerve transection. Neuroscience 143:117–127.

Xue XJ, Yuan XB (2010) Nestin is essential for mitogen-stimulated proliferation of neural progenitor cells. Mol Cell Neurosci 45:26–36.

Yamaguchi M, Saito H, Suzuki M, Mori K (2000) Visualization of neurogenesis in the central nervous system using nestin promoter-GFP transgenic mice. Neuroreport 11:1991–1996.

Yau KW (1994) Phototransduction mechanism in retinal rods and cones. The Friedenwald Lecture. Invest Ophthalmol Vis Sci 35:9–32.

Young RW (1984) Cell death during differentiation of the retina in the mouse. J Comp Neurol 229:362–373.

Young RW (1985) Cell differentiation in the retina of the mouse. Anat Rec 212:199–205.

Yu J, Lei K, Zhou M, Craft CM, Xu G, Xu T, Zhuang Y, Xu R, Han M (2011) KASH protein Syne-2/Nesprin-2 and SUN proteins SUN1/2 mediate nuclear migration during mammalian retinal development. Hum Mol Genet 20:1061–1073.

Zarbin M (2016) Cell-Based Therapy for Degenerative Retinal Disease. Trends Mol Med 22:115–134.

Zhang G, Assadi AH, Mcneil RS, Beffert U, Wynshaw-boris A, Herz J, Clark GD, D'Arcangelo G (2007) The Pafah1b Complex Interacts with the Reelin Receptor VLDLR. PLoS One 2:e252.

Zhang G, Gurtu V, Kain SR, Yan G (1997) Early detection of apoptosis using a fluorescent conjufate of annexin V. Apoptosis 23:525–531.

Zhang X, Lei K, Yuan X, Wu X, Zhuang Y, Xu T, Xu R, Han M (2009) SUN1/2 and Syne/Nesprin-1/2 Complexes Connect Centrosome to the Nucleus during Neurogenesis and Neuronal Migration in Mice. Neuron 64:173–187.

Zheng C, Heintz N, Hatten ME (1996) CNS Gene Encoding Astrotactin, Which Supports Neuronal Migration Along Glial Fibers. Science (80-) 272:417–419.

Zhou XE, Melcher K, Xu HE (2012) Structure and activation of rhodopsin. Acta Pharmacol Sin 33:291–299.

Zimmer G, Garcez P, Rudolph J, Niehage R, Weth F, Lent R, Bolz J (2008) Ephrin-A5 acts as a repulsive cue for migrating cortical interneurons. Eur J Neurosci 28:62–73.

Zolessi FR, Poggi L, Wilkinson CJ, Chien C-B, Harris W a (2006) Polarization and orientation of retinal ganglion

cells in vivo. Neural Dev 1:1–21.

Zuber ME, Gestri G, Viczian AS, Barsacchi G, Harris W a (2003) Specification of the vertebrate eye by a network of eye field transcription factors. Development 130:5155–5167.